Organic/Carbon Nanotubes Hybrid Thin Films for Chemical Detection

Hikmat Adnan Banimuslem

A thesis submitted in partial fulfilment of the requirements of
Sheffield Hallam University
for the degree of Doctor of Philosophy

April 2015

DECLARATION

I hereby declare that this thesis submitted for the degree of PhD is the result of my own research and that this thesis has not been submitted for higher degree to any other university or institution.

Hikmat Adnan Banimuslem

DEDICATION

To the memory of my daughter, Ryaheen

You left fingerprints of grace on our lives

You shan't be forgotten

ABSTRACT

Metallophthalocyanines (MPcs) are classified as an important class of conjugated materials and they possess several advantages attributed to their unique chemical structure. Carbon nanotubes (CNT), on the other hand, are known to enhance the properties of nano-composites in the conjugated molecules, due to their one dimensional electronic skeleton, high surface area and high aspect ratio. In this thesis, work has been carried out on the investigation of different substituted metal-phthalocyanines with the aim of developing novel hybrid film structures which incorporates these phthalocyanines and single-walled carbon nanotubes (SWCNT) for chemical detection applications.

Octa-substituted copper phthalocyanines ($CuPcR_8$) have been characterised using UV-visible absorption spectroscopy. Obtained spectra have yielded an evidence of a thermally induced molecular reorganization in the films. Influence of the nature of substituents in the phthalocyanine molecule on the thin films conductivity was also investigated. Octa-substituted lead (II) phthalocyanines ($PbPcR_8$) have also been characterized using UV-visible spectroscopy. Sandwich structures of ITO/$PbPcR_8$/In were prepared to investigate the electronic conduction in $PbPcR_8$. The variation in the J(V) behavior of the films as a result of heat treatment is expected to be caused by changes in the alignment inside the columnar stacking of the molecules of the films.

Thin films of non-covalently hybridised SWCNT and tetra-substituted copper phthalocyanine ($CuPcR_4$) molecules have been produced. FTIR, DC conductivity, SEM and AFM results have revealed the π-π interaction between SWCNTs and $CuPcR_4$ molecules and shown that films obtained from the acid-treated SWCNTs/$CuPcR_4$ hybrids demonstrated more homogenous surface. Thin films of pristine $CuPcR_4$ and $CuPcR_4$/SWCNT were prepared by spin coating onto gold-coated glass slides and applied as active layers for the detection of benzo[a]pyrene, pentachlorophenol (PCP), 2-chlorophenol, diuron and simazine in water as well as amines vapours in ambient air utilizing total internal reflection spectroscopic ellipsometry (TIRE) as an optical detection method.

Different concentrations of pesticides in water ranging from 1 to 25 μg/L have been examined. It was revealed that the shifts in $\Delta(\lambda)$ spectra of $CuPcR_4$/SWCNT films were evidently larger than those produced by the pristine $CuPcR_4$ films, indicating largely improved films' sensitivity of the hybrid films.

Adsorption of amines onto films' surfaces has been realised by monitoring changes in the phase shift ($\Delta(\lambda)$) of TIRE. Methylamine has shown higher sensitivity and lower response time among the studied amines. For all amines vapours, the sensitivity of SWCNT/$CuPcR_4$ hybrid films was higher than the sensitivity of pristine $CuPcR_4$ films.

Further work has been carried out on hybrids of SWCNT with zinc phthalocyanines (ZnPc). Thin films of pristine SWCNT and SWCNT/ZnPc hybrids were prepared by drop casting onto interdigitated electrodes and applied as active layers to detect ammonia vapor by measuring electrical resistance changes. Influence of pyrene substituent in the phthalocyanine ring on the hybrid formation and their sensor response has also been verified.

ACKNOWLEDGEMENT

Without the guidance and knowledge of my director of studies, supervisors and colleagues this work would not have been possible. I would therefore like to thank them individually.

Firstly, I am grateful to my director of studies Dr. Aseel Hassan for providing excellent support and expert knowledge throughout the work. I greatly enjoyed the learning process and worthwhile research studies under him. Secondly, thanks to my second supervisor Dr Alexei Nabok for the kind support and ideas that made this work meaningful.

My sincere gratitude belongs to Dr Tamara Basova for many words of advice during my study.

Thanks to PhD colleagues and friends for making life interesting during many hours underground in the laboratory. Thanks are also due to all MERI staff and technicians who were always of assistance.

Sincere thanks to my parents and family in Iraq who encouraged and supported me throughout the work.

I would also like to thank my financial sponsor, the Higher Committee for Education Development in Iraq (HCED) for the support during my PhD

Finally, special thanks to my wife, Ola, and my children, Ishaq, Ryaheen and Mohammed for their loving support, patience and understanding throughout the course of my studies. Your sacrifices allowed me to pursue this effort.

LIST OF ABBREVIATION

CNT	Carbon nanotube
SWCNT	Single-walled carbon nanotube
MWCNT	Multi-walled carbon nanotube
PCNT	Pristine carbon nanotube
ATCNT	Acid-treated carbon nanotube
Pc	Phthalocyanine
MPc	Metal phthalocyanine
MPcR	Substituted metal phthalocyanine
CuPc	Copper phthalocyanine
PbPc	Lead phthalocyanine
ZnPc	Zinc phthalocyanine
$CuPcR_8$	Octa-substituted copper phthalocyanine
$CuPcR_4$	Tetra- substituted copper phthalocyanine
$PbPcR_8$	Octa- substituted lead phthalocyanine
$PbPcR_4$	Tetra- substituted lead phthalocyanine
3a	2,3,9,10,16,17,23,24-Octakis(octyloxy)phthalocyaninato copper (II)
3b	2,3,9,10,16,17,23,24-Octakis(hexadecyloxy)phthalocyaninato copper (II)
3c	2,3,9,10,16,17,23,24-Octakis-[2-(2-(2-methoxyethoxy)ethoxy)ethoxy]phthalocyaninato copper (II)
4a	2,3,9,10,16,17,23,24-Octakis(octylthio)phthalocyaninato copper (II)
4b	2,3,9,10,16,17,23,24-Octakis(hexadecylthio)phthalocyaninato copper (II)
4c	2,3,9,10,16,17,23,24-Octakis-[2-(2-(2-methoxyethoxy)ethoxy)ethylthio]phthalocyaninato copper (II)
3g	2,3,9,10,16,17,23,24-Octakis(octyloxy)phtalocyaninato lead (II)
3h	2,3,9,10,16,17,23,24-Octakis(hexadecyloxy)phtalocyaninato lead (II)
4g	2,3,9,10,16,17,23,24-Octakis(octylthio)phtalocyaninato lead (II)
4h	2,3,9,10,16,17,23,24-Octakis(n-hexadecylthio)phtalocyaninato lead (II)
Pc1	1(4),8(11),15(18),22(25)-Tetrakis-[2-(2-(2-methoxyethoxy)ethoxy)ethoxy] phtalocyaninato Copper (II)
Pc2	2(3),9(10),16(17),23(24)-Tetrakis-[2-(2-(2-methoxyethoxy)ethoxy)ethoxy] phthalocyaninato Copper (II)
Pc3	1(4),8(11),15(18),22(25)-Tetrakis-[2-(2-(2-methoxyethoxy)ethoxy)ethylthio] phthalocyaninato Copper (II)
Pc4	2(3),9(10),16(17),23(24)-Tetrakis-[2-(2-(2-methoxyethoxy)ethoxy)ethylthio] phthalocyaninato Copper (II)

Pc5	2(3),9(10),16(17),23(24)-Tetrakis(hexadecylthio) phthalocyaninato Copper (II)
Pc6	2,3,9,10,16,17-Hexakis(4,7,10-trioxaundecan-1-sulfanyl)-23(24)-(1-pyrenylmethoxy) phthalocyaninato zinc (II) [Asymetrical]
Pc7	2,3,9,10,16,17-Hexakis(4,7,10-trioxaundecan-1-sulfanyl)-23(24)-(1-pyrenylmethoxy) phthalocyaninato zinc (II) [Symetrical]
LC	Liquid crystalline
TIRE	Total internal reflection ellipsometry
SPR	Surface Plasmon resonance
HOMO	Higher occupied molecular orbital
LUMO	Lower unoccupied molecular orbital
FTIR	Fourier transform infrared
AFM	Atomic force microscopy
SEM	Scanning electron microscopy
TEM	Transmission electron microscopy
DCM	Dichloromethane
DMF	Dimethylformamide
PCP	Pentachlorophenol
2CP	2-Chlorophenol
ITO	Indium-doped tin oxide
R_a	Main roughness
RMS	Standard deviation
R_{max}	Maximum height
DL	Detection limit
$\overline{S}$	Sensitivity

LIST OF PUBLICATION

Journal Publications

[1] H. Banimuslem, A. Hassan, T. Basova, A.A. Esenpınar, S. Tuncel, M. Durmuş, A.G. Gürek, V. Ahsen, Dye-modified carbon nanotubes for the optical detection of amines vapours, *Sensors Actuators B: Chemical.* 207 (2015) 224-234.

[2] H. Banimuslem, A. Hassan, T. Basova, M. Durmus, S. Tuncel, A.A. Esenpınar, A.G. Gürek, V. Ahsen, Copper Phthalocyanine Functionalized Single-Walled Carbon Nanotubes: Thin Films for Optical Detection, *Journal of Nanoscience and Nanotechnology.* 15 (2015) 2157-2167.

[3] H. Banimuslem, A. Hassan, T. Basova, A.D. Gülmez, S. Tuncel, M. Durmus, A.G. Gürek, V. Ahsen, Copper phthalocyanine/single walled carbon nanotubes hybrid thin films for pentachlorophenol detection, *Sensors and Actuators, B: Chemical.* 190 (2014) 990-998.

[4] S. Tuncel, E.N. Kaya, M. Durmuş, T. Basova, A.G. Gürek, V. Ahsen, H. Banimuslem, A. Hassan, Distribution of single-walled carbon nanotubes in pyrene containing liquid crystalline asymmetric zinc phthalocyanine matrix, *Dalton Transactions.* 43 (2014) 4689-4699.

[5] E. Kaya, S. Tuncel, T. Basova, H. Banimuslem, A. Hassan, A. Gurek, V. Ahsen, Effect of pyrene substitution on the formation and sensor properties of phthalocyanine-single walled carbon nanotube hybrid, *Sensors and Actuators, B: Chemical.* 199 (2014) 277-283.

[6] T. Basova, A. Berezin, V. Nadolinny, H. Peisert, T. Chassé, H. Banimuslem, A. Hassan, Formation of ordered films of axially bridged aluminum phthalocyanine [(tBu) 4PcAl] 2O via magnetic field-induced reaction, *Journal of Chemical Physics.* 139 (2013) 204710.

[7] T.V. Basova, M. Çamur, A.A. Esenpınar, S. Tuncel, A. Hassan, A. Alexeyev, H. Banimuslem, M. Durmuş, A.G. Gürek, V. Ahsen, Effect of substituents on the orientation of octasubstituted copper (II) phthalocyanine thin films, *Synthetic Metal.* 162 (2012) 735-742.

[8] S. Tuncel, H.A.J. Banimuslem, M. Durmuş, A.G. Gürek, V. Ahsen, T.V. Basova, A.K. Hassan, Liquid crystalline octasubstituted lead(ii) phthalocyanines: Effects of alkoxy and alkylthio substituents on film alignment and electrical properties, *New Journal of Chemistry*. 36 (2012) 1665-1672.

Conferences

[1] H. Banimuslem, A. Hassan, T. Basova, Electrical and structural properties of copper-phthalocyanine functionalized single-walled carbon nanotubes. 14th International Conference on Organized Molecular Films (ICOMF14) - LB14, Paris, France; 06/2012.

[2] H. Banimuslem, A. Hassan, T. Basova, Morphology and electrical properties of lead- and copper-phthalocyanines. UKSemiconductors 2012, The University of Sheffield, Sheffield, UK; 07/2012

[3] H. Banimuslem, A. Hassan, T. Basova, Tetra-substituted copper phthalocyanine (CuPcR4)/single-walled carbon nanotube hybrid structures: thin films' properties and potential applications. Third International Conference on Multifunctional, Hybrid and Nanomaterials (Hybrid 2013), Sorrento, Italy; 03/2013.

[4] H. Banimuslem, A. Hassan, T. Basova, Copper phthalocyanine functionalised single-walled carbon nanotubes: Thin films deposition and sensing properties. Key Engineering Materials. 605 (2014) 461-464. 3rd International Conference on Materials and Applications for Sensors and Transducers, Prague, Czech Republic; 09/2013.

[5] H. Banimuslem, A. Hassan, T. Basova, Optical Detection of Herbicides in Water using Dye-Modified Single Walled Carbon Nanotubes. Proceedings of the 8th international conference on sensing technology, Sep. 2-4, 2014, Liverpool, UK

[6] H. Banimuslem, A. Hassan, T. Basova, The smart integration of carbon nanotube with phthalocyanines for chemical detection. Fourth International Conference on Multifunctional, Hybrid and Nanomaterials (Hybrid 2015), Sitges, Barcelona, Spain; 03/2015

CONTENTS

List of Figures

List of Tables

Chapter 1

Introduction

1.1 Background

In order to satisfy the demands for the fast growing development of nanotechnology, it is essential to improve the variety of materials possessing electrical, optical, or mechanical properties. Amongst these, hybrid materials are rapidly finding their way in these new technologies, due to the efficient interaction between two or more components [1-3]. In recent decades, research relating to the interaction between carbon nanotubes (CNTs) and conjugated organic molecules, especially metallophthalocyanine (MPc) complexes, has been attracting increasing interest as a new topic of fundamental research with various potential applications ranging from sensing [4-8], which is the main theme of this thesis to photovoltaic [9-11] applications. Combining the remarkable electrical, thermal and mechanical properties of CNTs with the optoelectronic properties of MPcs is a promising path to realizing composite materials which are expected to be more efficient in improving the relative responses compared to the individual CNTs or MPc species [12-14].

In the sensor area, a range of materials has been employed to construct transducers, such as variety types of transition metal oxides [15], conducting polymers [16] and organic complexes like phthalocyanines [17-20]. Phthalocyanines (Pcs) in general and their metallo-derivatives (MPcs) in particular, hold a great promise for the development of many non-linear optical devices because of their activity as basis for optical limiting [21], fast response time, unique electronic adsorption properties and extensively delocalised π-π electron skeleton. Another advantage of MPcs is their process-ability in thin films structure, which means the possibility to deposit these compounds utilizing different methods, such as spin-coating, drop-casting, thermal evaporation and Langmuir-Blodgett techniques [22]. Application of substituted-MPcs as active membranes in surface plasmon resonance (SPR) and total internal reflection ellipsometry (TIRE) sensors has been demonstrated in the literature [6,23].

Metal Phthalocyanines (MPcs) are π-electron conjugated macrocyclic compounds, exhibiting outstanding performance in the field of chemical and bio sensors [20,24], liquid crystals [25-28], field effect transistors [29,30], electrochromic devices [31], and memory applications [32,33]. The structure of MPcs strongly affects their properties, such as specific surface area, electron transfer properties and thermal stability, therefore affecting their performance in device applications [34]. The major advantages of MPcs over other organic analogous are [35,36]: (i) their tuneable structure with high flexibility in having large variety of substitution on the periphery of the molecule's rim, as well as their ability to coordinate almost every metallic element in the centre of their macrocycle; (ii) an exceptional thermal and chemical stability compared with most of molecular materials; (iii) an excellent process-ability, resulting in the construction of a large variety of thin films by different deposition methods. Although the MPc-based devices have been studied for long time, there are still some specific restrictions which need to be overcome; these include, (i) the improvement of the reproducibility of the organic thin film devices due to the difficult control of the crystallite orientation of the polycrystalline film of MPc, (ii) the improvement of the selectivity and sensitivity of the MPc thin film sensors, (iii) more homogenous films are required for the manufacturing of semiconducting devices to avoid pin-holes and thus short circuit problems, (iv) the improvement of charge carrier mobility of the organic thin film diodes and transistors, which is determined by several key factors such as the type, orientation and structure of the MPcs, as well as the film thickness and the nature of interface between the organic film and the electrodes, (v) miniature, portable, robust, energy saving and low cost devices need to be fabricated, in order to satisfy the rapid development of nano-devices together with several other kinds of particular applications .

CNTs, on the other hand, demonstrating a high aspect ratio, are π-conjugated nanoscale materials. This kind of carbon family possess a unique combination of mechanical, thermal and electrical properties [37-39], making this type of carbon structure a highly attractive material for applications as a reinforcing filler in polymers [40], heat management components [41], and nanoelectronic devices [42]. Carbon nanotubes (CNTs) have been found to be extremely sensitive to their local chemical environment. This chemical sensitivity, due to their extraordinary one-dimentional carbon nanostructure, has made them ideal building blocks for chemical

detection [43]. Since Kong and co-researchers have demonstrated the potential of single walled carbon nanotubes (SWCNTs) in NO_2 and NH_3 gas detection [44], CNTs have been considered as promising candidates as sensing materials that can detect toxic gases such as NO_2, NH_3, O_2, H_2, CO_2, and CO [45-48]. The high sensitivity of CNTs towards chemical vapours can be assigned to the excellent electrical properties, small size, extremely high surface to volume ratio and large gas adsorption capacity. However, the poor solubility and dispersity of CNTs in conventional solvents has restricted their use as active layers processed by simple methods like spin coating. Acid-treatment as well as other modification methods can be employed to overcome the disadvantage of poor dispersity of CNTs [1,49-52]. The other downside is that CNTs are optically inert and almost unsuitable to use as active layers utilising optical detection techniques such as surface plasmon resonance (SPR) and total internal reflection spectroscopic ellipsometry (TIRE). Further surface modification of CNTs through hybridising with MPcs enhances their optical performance as well as their gas sensing activity arising from the mutual π-π interaction between CNTs and MPc resulting in enhanced detection effectiveness compared to the individual CNTs or MPcs species [6,53].

1.2 Aim and objectives

The principle aim of this research is the characterization of novel substituted metal-phthalocyanines (MPcs) and development of new methods to produce hybrids combining these MPcs and single-wall carbon nanotubes (SWCNTs) and to study the optical, structural, and electron transport properties and to place more emphasis on their sensing applications using TIRE method.

In order to satisfy the above stated aim the proposed research will have to achieve the following objectives:

- To study thin films of MPc molecules with different substituents on the periphery of the molecule ring. The research is mainly focused to look into films of tetra- and octa-substitued MPcs with different alkyl chain lengths.
- To develop a simple method for the hybridisation of MPcs, mainly having copper as the central atom, with SWCNT.

- To produce thin films of the new hybrid structures and to examine the formation of bonds between the MPc molecules and the CNT molecules as well as the films' morphology using Fourier Transform Infra-red (FTIR), Scanning Electron Microscopy (SEM), UV-visible spectroscopy and Atomic Force Microscopy (AFM) techniques.
- To apply several other methods of hybridisation in order to compare the quality of composite films formed between the MPcs and CNT molecules.
- Perform electrical measurements in order to investigate the electron transport properties of MPcs films and their new hybrids through the evaluation of their I(V) characteristics.
- To examine the use of the new hybrid films in chemical sensor applications using spectroscopic ellipsometry in total internal reflection ellipsometry (TIRE) as the optical transduction method. Various environmental pollutants, both in ambient air and in water, are examined; these include volatile organic compounds (VOCs), amines in air and different pesticides as water pollutants. The effect of SWCNTs on the sensing properties of MPcs/SWCNT hybrid films are investigated and compared to pristine MPc films.

Reference List

[1] H. Banimuslem, A. Hassan, T. Basova, M. Durmus, S. Tuncel, A.A. Esenpınar, A.G. Gürek, V. Ahsen, Copper Phthalocyanine Functionalized Single-Walled Carbon Nanotubes: Thin Films for Optical Detection, J. Nanosci. Nanotechnol. 15 (2015) 2157-2167.

[2] V. Parra, M. Rei Vilar, N. Battaglini, A.M. Ferraria, A.M.B. Do Rego, S. Boufi, M.L. Rodríguez-Méndez, E. Fonavs, I. Muzikante, M. Bouvet, New hybrid films based on cellulose and hydroxygallium phthalocyanine. Synergetic effects in the structure and properties, Langmuir. 23 (2007) 3712-3722.

[3] T.M. McEvoy, J.W. Long, T.J. Smith, K.J. Stevenson, Nanoscale conductivity mapping of hybrid nanoarchitectures: Ultrathin poly(o-phenylenediamine) on mesoporous manganese oxide ambigels, Langmuir. 22 (2006) 4462-4466.

[4] H. Banimuslem, A. Hassan, T. Basova, A.A. Esenpınar, S. Tuncel, M. Durmuş, A.G. Gürek, V. Ahsen, Dye-modified carbon nanotubes for the optical detection of amines vapours, Sensors Actuators B: Chem. (2014).

[5] H. Banimuslem, A. Hassan, T. Basova, I. Yushina, M. Durmuş, S. Tuncel, A.A. Esenpınar, A.G. Gürek, V. Ahsen, Copper phthalocyanine functionalized single-walled carbon nanotubes: thin film deposition and sensing properties, Key Eng. Mater. 605 (2014) 461-464.

[6] H. Banimuslem, A. Hassan, T. Basova, A.D. Gülmez, S. Tuncel, M. Durmus, A.G. Gürek, V. Ahsen, Copper phthalocyanine/single walled carbon nanotubes hybrid thin films for pentachlorophenol detection, Sensors Actuators B: Chem. 190 (2014) 990-998.

[7] E.N. Kaya, S. Tuncel, T.V. Basova, H. Banimuslem, A. Hassan, A.G. Gürek, V. Ahsen, M. Durmuş, Effect of pyrene substitution on the formation and sensor properties of phthalocyanine-single walled carbon nanotube hybrids, Sensors Actuators B: Chem. 199 (2014) 277-283.

[8] Y. Wang, N. Hu, Z. Zhou, D. Xu, Z. Wang, Z. Yang, H. Wei, E.S. Kong, Y. Zhang, Single-walled carbon nanotube/cobalt phthalocyanine derivative hybrid material: Preparation, characterization and its gas sensing properties, J. Mater. Chem. 21 (2011) 3779-3787.

[9] R.A. Hatton, N.P. Blanchard, A.J. Miller, S.R.P. Silva, A multi-wall carbon nanotube-molecular semiconductor composite for bi-layer organic solar cells, Physica E: Low-Dimensional Systems and Nanostructures. 37 (2007) 124-127.

[10] W. Feng, Y. Li, Y. Feng, J. Wu, Enhanced photoresponse from the orderedmicrostructure of naphthalocyanine-carbon nanotube composite film, Nanotechnology. 17 (2006) 3274-3279.

[11] U. Hahn, S. Engmann, C. Oelsner, C. Ehli, D.M. Guldi, T. Torres, Immobilizing water-soluble dendritic electron donors and electron acceptors - Phthalocyanines and perylenediimides - Onto single wall carbon nanotubes, J. Am. Chem. Soc. 132 (2010) 6392-6401.

[12] J. Pillay, K.I. Ozoemena, Layer-by-layer self-assembled nanostructured phthalocyaninatoiron(II)/SWCNT-poly(m-aminobenzenesulfonic acid) hybrid system on gold surface: Electron transfer dynamics and amplification of H2O2 response, Electrochim. Acta. 54 (2009) 5053-5059.

[13] F.C. Moraes, D.L.C. Golinelli, L.H. Mascaro, S.A.S. MacHado, Determination of epinephrine in urine using multi-walled carbon nanotube modified with cobalt phthalocyanine in a paraffin composite electrode, Sensors Actuators B: Chem. 148 (2010) 492-497.

[14] Z. Yang, H. Pu, J. Yuan, D. Wan, Y. Liu, Phthalocyanines-MWCNT hybrid materials: Fabrication, aggregation and photoconductivity properties improvement, Chem. Phys. Lett. 465 (2008) 73-77.

[15] G.S.V. Coles, G. Williams, Effects of high-temperature sintering on SnO2 sensor response to reducing gases, J. Mater. Chem. 2 (1992) 23-29.

[16] T.C. Pearce, J.W. Gardner, S. Friel, P.N. Bartlett, N. Blair, Electronic nose for monitoring the flavour of beers, Analyst. 4 (1993) 371-377.

[17] R. De Saja, J. Souto, M.L. Rodríguez-Méndez, J.A. De Saja, Array of lutetium bisphthalocyanine sensors for the detection of trimethylamine, Mater. Sci. Eng. C. 8-9 (1999) 565-568.

[18] M.J. Jafari, M.E. Azim-Araghi, S. Barhemat, S. Riyazi, Effect of post-deposition annealing on surface morphology and gas sensing properties of palladium phthalocyanine thin films, Surf. Interface Anal. 44 (2012) 601-608.

[19] R. Jaisutti, T. Osotchan, An investigation of molecular interactions between zinc phthalocyanine thin film and various oxidizing gases for sensor applications, Adv. Mater. Res. 403-408 (2012) 48-51.

[20] T. Basova, A. Tsargorodskaya, A. Nabok, A.K. Hassan, A.G. Gurek, G. Gumus, V. Ahsen, Investigation of gas-sensing properties of copper phthalocyanine films, Mater. Sci. Eng. C. 29 (2009) 814-818.

[21] D. Dini, M. Barthel, M. Hanack, Phthalocyanines as active materials for optical limiting, Euro. J. Organ. Chem. (2001) 3759-3769.

[22] R. Rella, J. Spadavecchia, G. Ciccarella, P. Siciliano, G. Vasapollo, L. Valli, Optochemical vapour detection using spin coated thin films of metal substituted phthalocyanines, Sensors Actuators B: Chem. 89 (2003) 86-91.

[23] T. Basova, A. Hassan, F. Yuksel, A.G. Gürek, V. Ahsen, Optical detection of pentachlorophenol in water using thin films of octa-tosylamido substituted zinc phthalocyanine, Sensors Actuators B: Chem. 150 (2010) 523-528.

[24] T. Basova, I. Jushina, A.G. Gürek, V. Ahsen, A.K. Ray, Use of the electrochromic behaviour of lanthanide phthalocyanine films for nicotinamide adenine dinucleotide detection, J. Royal Soc. Interface. 5 (2008) 801-806.

[25] D. Atilla, A.G. Gurek, T.V. Basova, V.G. Kiselev, A. Hassan, L.A. Sheludyakova, V. Ahsen, The synthesis and characterization of novel mesomorphic octa- and tetra-alkylthio-substituted lead phthalocyanines and their films, Dyes Pigm. 88 (2011) 280-289.

[26] T.V. Basova, A. Hassan, M. Durmus, A.G. Gurek, V. Ahsen, Orientation of the liquid crystalline nickel phthalocyanine films confined between electrodes, Synth. Met. 161 (2011) 1996-2000.

[27] S. Dong, H. Tian, D. Song, Z. Yang, D. Yan, Y. Geng, F. Wang, The first liquid crystalline phthalocyanine derivative capable of edge-on alignment for solution processed organic thin-film transistors, Chem. Commun. (2009) 3086-3088.

[28] N. Kilinc, A.S. Ahsen, D. Atilla, A.G. Gurek, S.E. San, Z.Z. Ozturk, V. Ahsen, Electrical properties of mesomorphic phthalocyanine-carbon nanotube composites, American Scientific Publishers, 25650 North Lewis Way, Stevenson Ranch 6 (2008) 607-612.

[29] H.U. Khan, M.E. Roberts, W. Knoll, Z. Bao, Pentacene based organic thin film transistors as the transducer for biochemical sensing in aqueous media, Chem. Mater. 23 (2011) 1946-1953.

[30] S. Liu, W.M. Wang, A.L. Briseno, S.C.B. Mannsfeld, Z. Bao, Controlled deposition of crystalline organic semiconductors for field-effect-transistor applications, Adv Mater. 21 (2009) 1217-1232.

[31] P.R. Somani, S. Radhakrishnan, Electrochromic materials and devices: Present and future, Mater. Chem. Phys. 77 (2003) 117-133.

[32] S. Tuncel, H.A.J. Banimuslem, M. Durmuş, A.G. Gürek, V. Ahsen, T.V. Basova, A.K. Hassan, Liquid crystalline octasubstituted lead(ii) phthalocyanines: Effects of alkoxy and alkylthio substituents on film alignment and electrical properties, New J. Chem. 36 (2012) 1665-1672.

[33] B. Mukherjee, A.K. Ray, A.K. Sharma, M.J. Cook, I. Chambrier, A simply constructed lead phthalocyanine memory diode, J. Appl. Phys. 103 (2008) 074507.

[34] H. Li, Z. Xu, K. Li, X. Hou, G. Cao, Q. Zhang, Z. Cao, Modification of multi-walled carbon nanotubes with cobalt phthalocyanine: Effects of the templates on the assemblies, J. Mater. Chem. 21 (2011) 1181-1186.

[35] J. Brunet, A. Pauly, C. Varenne, B. Lauron, On-board phthalocyanine gas sensor microsystem dedicated to the monitoring of oxidizing gases level in passenger compartments, Sensors Actuators B: Chem. 130 (2008) 908-916.

[36] N.L. Tran, F.I. Bohrer, W.C. Trogler, A.C. Kummel, A density functional theory study of the correlation between analyte basicity, ZnPc adsorption strength, and sensor response, J. Chem. Phys. 130 (2009) 20.

[37] S.E. Khadem, M. Rasekh, A. Toghraee, Design and simulation of a carbon nanotube-based adjustable nano-electromechanical shock switch, Appl. Math. Model. 36 (2012) 2329-2339.

[38] J. Liu, Y. Wang, Z. Qu, X. Fan, 2 μm passive Q-switched mode-locked Tm 3+:YAP laser with single-walled carbon nanotube absorber, Opt. Laser Technol. 44 (2012) 960-962.

[39] Y. Ji, Y.Y. Huang, E.M. Terentjev, Dissolving and aligning carbon nanotubes in thermotropic liquid crystals, Langmuir. 27 (2011) 13254-13260.

[40] P.M. Ajayan, L.S. Schadler, C. Giannaris, A. Rubio, Single-walled carbon nanotube-polymer composites: Strength and weakness, Adv. Mater. 12 (2000) 750-753.

[41] S. Shenogin, A. Bodapati, L. Xue, R. Ozisik, P. Keblinski, Effect of chemical functionalization on thermal transport of carbon nanotube composites, Appl. Phys. Lett. 85 (2004) 2229-2231.

[42] A.N. Cleland, Carbon nanotubes tune up, Nature. 431 (2004) 251-252.

[43] E. Llobet, Gas sensors using carbon nanomaterials: A review, Sensors Actuators B: Chem. 179 (2013) 32-45.

[44] J. Kong, N.R. Franklin, C. Zhou, M.G. Chapline, S. Peng, K. Cho, H. Dai, Nanotube molecular wires as chemical sensors, Science. 287 (2000) 622-625.

[45] D.R. Kauffman, A. Star, Carbon nanotube gas and vapor sensors, Angewandte Chemie - International Edition. 47 (2008) 6550-6570.

[46] T. Zhang, S. Mubeen, N.V. Myung, M.A. Deshusses, Recent progress in carbon nanotube-based gas sensors, Nanotechnology. 19 (2008) 332001.

[47] E.S. Snow, F.K. Perkins, E.J. Houser, S.C. Badescu, T.L. Reinecke, Chemical detection with a single-walled carbon nanotube capacitor, Science. 307 (2005) 1942-1945.

[48] J. Li, Y. Lu, Q. Ye, M. Cinke, J. Han, M. Meyyappan, Carbon nanotube sensors for gas and organic vapor detection, Nano Letters. 3 (2003) 929-933.

[49] S.B. Yang, B. Kong, D. Jung, Y. Baek, C. Han, S. Oh, H. Jung, Recent advances in hybrids of carbon nanotube network films and nanomaterials for their potential applications as transparent conducting films, Nanoscale. 3 (2011) 1361-1373.

[50] J.L. Blackburn, T.M. Barnes, M.C. Beard, Y.-. Kim, R.C. Tenent, T.J. McDonald, B. To, T.J. Coutts, M.J. Heben, Transparent conductive single-walled carbon nanotube networks with precisely tunable ratios of semiconducting and metallic nanotubes, ACS Nano. 2 (2008) 1266-1274.

[51] J.T. Han, S.Y. Kim, J.S. Kim, H.J. Jeong, S.Y. Jeong, G.-. Lee, Enhanced electrical properties of transparent carbon nanotube/binder hybrid thin films: Effects of the silane sol and the bundle size of the carbon nanotubes, Ind. Eng. Chem. Res. 49 (2010) 6416-6421.

[52] E. Kymakis, G.A.J. Amaratunga, Photovoltaic cells based on dye-sensitisation of single-wall carbon nanotubes in a polymer matrix, Solar Energy Mater. Solar Cells. 80 (2003) 465-472.

[53] L. Cao, H. Chen, H. Zhou, L. Zhu, J. Sun, X. Zhang, J. Xu, M. Wang, Carbon-nanotube-templated assembly of rare-earth phthalocyanine nanowires, Adv. Mater. 15 (2003) 909-913.

Chapter 2

Literature Review

Chapter overview

This chapter provides an extensive analysis of the literature as related to the proposed work and gives an overview of the contents of the remaining chapters of this thesis. The features of carbon nanotubes and why this material has gained significant interest from researchers are also discussed. Furthermore, a general discussion of phthalocyanines and their applications are also introduced. Finally, the smart integration between phthalocyanines and carbon nanotubes has been reviewed with particular emphasis on their sensing application.

2.1 Carbon Nanotubes (CNTs)

A sheet of paper may be rolled up with its edges connected to make a tube. Carrying out this experiment hypothetically with a graphene layer results in a carbon tube. Such structures actually exist; they are entirely made up from carbon atoms and accommodate a cylindrical cavity. When different diameters are provided, several of these tubes may fit one into another to make a multi-walled carbon tubes. The diameter of both single- and multi-walled species measures on the nanometer scale, therefore the name carbon nanotubes (CNTs) [1].

The first discovery of multi-walled carbon nanotubes (MWCNTs) [2] and single-walled carbon nanotubes (SWCNTs) [3] was made by Iijama in 1991 and 1993 respectively (Figure 2.1a). The diameters are approximately 1-2nm for SWCNTs and 2-100nm for MWCNTs, which consist of more than one concentrically rolled layer of graphene, and their length are roughly between 1-10μm. Therefore, the aspect ratio (ratio of length to diameter) becomes 1000 or more [4-6]. Based on the unique structure of the parent material (graphene), carbon nanotubes are suggested to have novel properties that make them potentially beneficial in many applications. These include high performance nanocomposites which are conductive and of natural high strength [7], nanosized semiconductor devices [8], nano-probes [9], energy conversion devices [10], sensors [11,12], field emission displays [13], radiation sources [14] and drug delivery systems [15,16]; however these applications still remain in the "possible" stage. Lack of availability of bulk quantities of high quality and low cost, as well as processing difficulties are the main obstacles in expanding the technological applications of carbon nanotubes.

As a member of the fullerene structural family, the carbon atoms in carbon nanotubes are sp^2-bonded. Due to the extended electron system, the surface electrons are highly polarizable, and so are subject to large attractive inter-tubular van der Waals forces [17]. In addition, carbon nanotubes are smooth-sided compounds with attractive interactions of 0.5 eV per nanometer of tube-to-tube contact. These extreme cohesive forces could account for the bundled structure of SWCNTs. The size of bundles has been shown to be judged by distortions of van der Waals bonds between nanotubes in the surrounding area of a catalytic particle and the degree of nanotube bending in the bundle [18]. The typical bundle size of as-produced SWNTs varies between

nanometers to microns. Figure 2.1b shows a Transmission Electron Microscopy (TEM) image of a nanotube bundles [19].

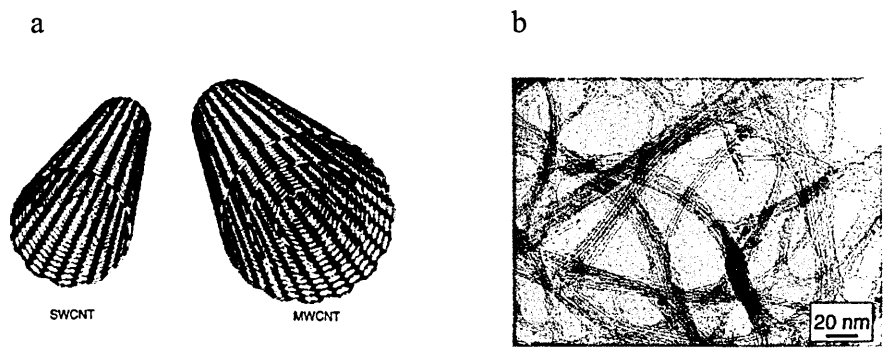

Figure 2.1: (a) Conceptual diagram of SWCNT and MWCNT, (b) TEM image of SWCNTs [19]

Although the chemical reactivity of carbon nanotubes, compared with graphene, is enhanced as a result of the surface curvature, carbon nanotubes tend to aggregate together when exposed to most solvents, aqueous or organic due to their hydrophobic nature [20]. Therefore, the studies and applications of CNTs are hindered by processing and manipulation difficulties owing to their insolubility or poor dispersion in common solvents and polymeric matrices [21].

2.1.1 CNTs' structure

The structure of CNTs depends on the different angles and curvatures in which the graphene sheet could be rolled into a tube and is determined by a single vector. This vector is called chiral vector, which discriminate CNTs into three forms; zigzag, armchair and chiral (Figure 2.2). The electronic properties of CNTs vary according to their structure. Armchair nanotubes are metallic, while zigzag and chiral are either metallic or semiconducting nanotubes. SWCNTs, in general, can be a mixture of metallic and semiconducting tubes, depending sensitively on the structure, however, MWCNTs are considered to be metallic material [1,22].

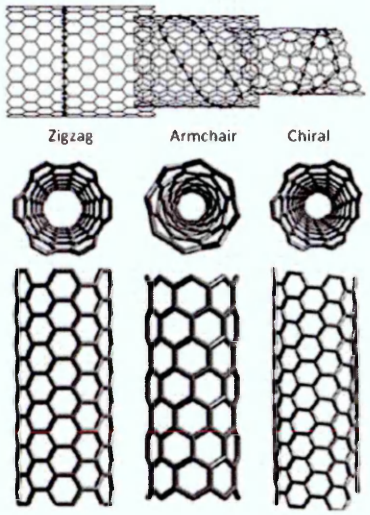

Figure 2.2: Classification of carbon nanotubes according to the chiral vector [23]

2.1.2 Production of CNTs

Major progress has been seen in recent years in the field of carbon nanotubes production since their excellent properties and potential applications were identified (see table 2.1 for review). In general, SWCNTs always grow from carbon plasma in the presence of directing agents which are usually transition metal nanoparticals such as Co, Fe, Ni, V, etc [24,25]. The most important differences between the available methods could be summarised as:

- the method of plasma generation,
- the technique of introducing the catalyst metal,
- CNTs yield,
- the quality of CNTs, and
- commercialization and up-scaling possibilities.

Table 2.1: A summary of production techniques of SWCNTs [25]

Short name	Technology of preparation [reference]	Typical mean diameter (nm)	product description
Laser ablation (PLV)	Ablation from graphite doped with (Fe, Co, Ni, ...) catalyst [26].	1.4 (1-1.8)	High quality, good diameter control, bundled tubes, commercial.
DC arc discharge	First reported production. Modified Kratschmer reactor [2].	1.5 (0.9-3.1)	Lesser quality, carbonaceous impurities abundant, bundled.
Gas phase decomposition	Decomposition in an oxygen-free environment. Typical: HiPco® (high pressure CO decoposition) [27].	1 (0.9-1.3)	Easy purification, good quality, commercial.
CCVD	Catalytic chemical vapour deposition. Supported metal catalysts are used [28].	1.5 (1.3-2)	Cheapest, up-scalable, commercial, most feasible from the application point of view.
Flame pyrolysis	Carbon source + metallocene catalyst. Conventional low pressure pyrolysis reactor [29].	2-3	Low yield, bad quality, still under development, plant technology available, large commercialization potential.
Solar furnace	Solar rays focused on a metal doped graphite target. Growth dynamics similar to PLV [30].	1.4	Good quality, little amorphous carbon, spreading is limited.
Zeolite grown	CNTs grow by thermal decomposition of template molecules within zealite channels [31].	0.45	Monodisperse diameter distribution, oriented tubes, CNTs metastable outside the channels.

2.1.3 Modification of CNTs

In addition to its promising properties, CNTs, as produced, possess a variety of diameters, length distribution, and structure within the same sample [22]. The most important property that severely disadvantages the applications of CNTs is their insolubility in any solvent and polymeric matrices due to strong van der Waals interaction that tightly hold them together, forming bundles [32]. CNTs can undergo chemical functionalization to enhance their solubility, broaden their properties and to produce novel hybrid materials potentially suitable for applications. The main approaches for functionalization of CNTs can be classified into two major groups (Figure 2.3); (1) the covalent attachment of chemical molecule [33-35], through the reaction on the conjugated structure of CNTs, and (2) the non-covalent molecular adsorption or wrapping of variety functional groups onto the nanotube [36-38].

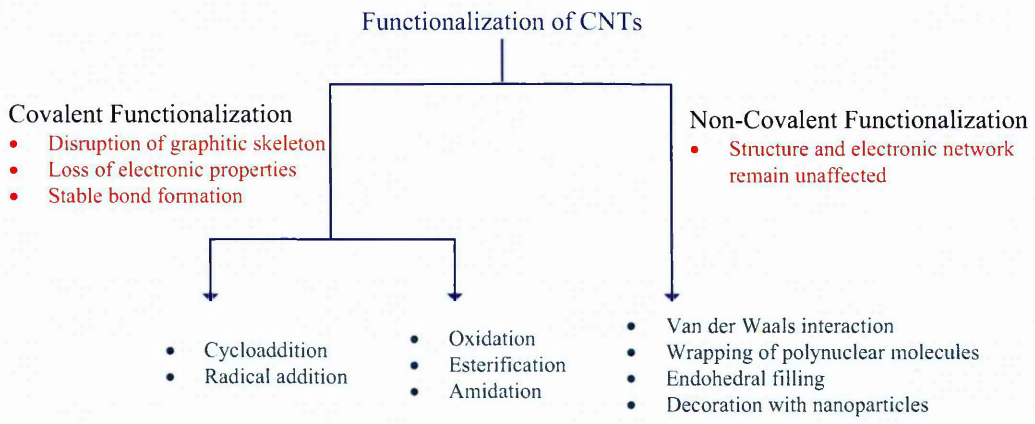

Figure 2.3: Overview scheme of the functionalization of CNTs

Before being grafted with polymeric, bio, or any other functional molecules, CNTs need to be pre-treated to open the end caps, eliminate the residual metal catalysts, generate functional groups at the defects, shorten the nanotubes and provide de-bundling and exfoliation effect to the CNTs aggregates [39], as shown in Figure 2.4.

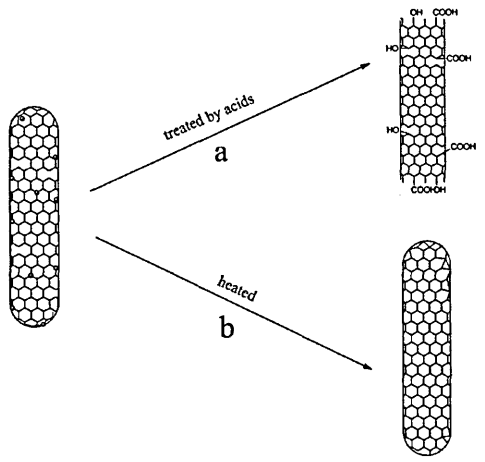

Figure 2.4: A sketch of CNTs pre-treated by different methods; (a) acid treatment can effectively purify CNTs, open their caps and generate the functional groups, (b) heat treatment can purify and integrate the CNTs.

Among the different surface treatment methods, acid oxidation is perhaps the most commonly studied. Acids, such as nitric or sulphuric, or any other oxidizing agent is used for this purpose. The oxygenated functional groups can be held to the side-wall of CNT after the oxidation process [40-42], meanwhile, the residual amorphous carbon and catalysts can be also removed. Bower and co-workers [43] were the first research group who found that the NHO_3 can be inserted into the CNTs bundles, resulting in bundle exfoliation. Following this work, similar procedure has been explored later on including the work presented in the current thesis, [44,45].

Keeping the building skeleton of CNTs during the acid treatment develops a serious problem because covalent sidewall functionalization creates sp^3 carbon sites on CNTs, which disrupt the electronic structure, and leads to loss of the novel characteristics of CNTs, such as their high conductivity and extraordinary mechanical properties [22]. With increasing functionalization degree, the nanotubes can finally change into insulating material. Therefore, to reduce damaging effect of acid treatment, low concentration of oxidizing agents are used [46]. In addition to the non-damaging effect, the low concentration treatment allows further π-π interaction between CNTs and several other molecules such as phthalocyanines as reported

recently [47,48]. The further functionalization of carbon nanotubes could be classified into two types according to the modifiers: organic (organic functional groups, small organic molecules, polymers, DNA, protein, etc.) and inorganic (metal nanoparticals, metal oxides, etc.) [32].

Oxygen containing groups can be generated on the sidewall of CNTs not only by chemical modification such as acids treatment [49], O_2-plasma-oxidization method has also been reported to achieve sidewall oxygenated group attachments [50]. It is known that the amount and type of oxygen containing groups depends on the treatment method. In the case of nitric acid treatment, formation of acid groups such as carboxyl, phenol and lactol have been reported [51,52]. Nevertheless, carbonyl and lactone are observed in oxygen plasma functionalization method [50]. Among these oxygen-containing groups, carboxyl group (COOH) is very attractive, since it can be readily used for further covalent or non-covalent functionalization [21]. Non-covalent functionalization, compared with covalent functionalization, does not lead to substantial changes in the chemical, structural, electronic and mechanical properties of CNTs [53] as shown in Figure 2.3. Therefore, CNTs functionalized with organic molecules via non-covalent interactions is quite appealing and has important consequences for their electrochemical activities. The realization of non-covalent functionalization is mainly ascribed to the adsorption ability of organic modifiers on the carbon nanotube surface or through π-π conjugation between aromatic molecules and CNTs. In addition to oxygen containing groups, as organic functional groups, nitrogen containing groups such as amines [54,55], hydrocarbons such as alkyl [56] and sulfur containing groups [57] have been used to modify CNTs.

Polymers, which can disrupt the van der Waals interactions between the walls of CNTs, have gained increasing attention due to their quite efficient dispersity [58]. Owing to their native electron trans-mediation, good environmental stability and specific organic groups [59], tremendous efforts have been made over the past few decades to prepare polymer-CNTs composites. These polymers include polypyrrole [60], poly(methylene blue) [61], poly(neutral red) [62], poly(acrylic acid) [63,64] and poly(3-methylthiophene) [65].

Among organic materials modified CNTs, DNA [66] and enzymes [67] have received great attention due to their high selectivity and sensitivity to analytical reagents.

Similar to organic modification, inorganic nanomaterial functionalized CNTs have also received great attention. Generally, two types of inorganic nanomaterials have been employed to modify CNTs, one is noble metal nanoparticles, including Au [68], Ag [69], and Pt [70], and the other is metal oxide nanostructures such as ZnO [71], CuO [72] and SnO_2 [73]. In addition, many different compounds have also been proposed to modify CNTs surfaces to enhance their performance. However, owing to the effect of size and dispersion of noble metal particles and poor electrical conductivity of metal oxides, the sensing activity of CNTs has been inhibited. In order to decrease their particle size and improve electron transport especially in the modified electrode surfaces in electrochemical sensors, CNTs as a good carrier and conducting pathways have been widely employed [74].

2.2 Phthalocyanines (Pcs)

2.2.1 History

Phthalocyanines (Pcs) represent without doubt the most important chromophoric system developed during the 20th century. Historically, the most important event was probably their accidental discovery around 1928 by a dye manufacturing company in Scotland. The first synthesis of phthalocyanine was reported in 1907 [75] when Braun and Tcherniac engaged in a study of the chemistry of o-cyanobenzamide. When this compound was heated, a trace amount of a blue substance was obtained which undoubtedly was metal-free phthalocyanine. The structure of this metal-free, unsubstituted phthalocyanine was determined only about a quarter of a century later by the comprehensive studies of Dent and Linstead [76] and the X-ray diffraction analyses of Robertson [77] while examining both metal-free phthalocyanines (Figure 2.5a) and metallophthalocyanines (Figure 2.5b). In 1927, de Diesbach and co-workers [78] reported that when 1,2-dibromobenzene was treated with copper(I) cyanide in boiling quinoline for eight hour, a blue product was obtained. This was almost certainly the first preparation of copper phthalocyanine (CuPc). The molecular formula was determined from elemental analysis and the compound was remarkably stable against alkali, concentrated acids and heat, but they were unable to suggest the structure. In 1928, in the manufacture of phthalimide by Scottish Dyes (later to become part of ICI) from the reaction of phthalic anhydride with ammonia

in a reactor, the formation of a blue impurity was observed in certain production batches. This contaminant was isolated as a dark-blue, insoluble crystalline substance. Ultimately, the compound proved to be iron phthalocyanine (FePc), the source of the iron being the wall of the reactor. An independent synthesis involving passing ammonia gas through molten phthalic anhydride in the presence of iron filings confirmed the findings.

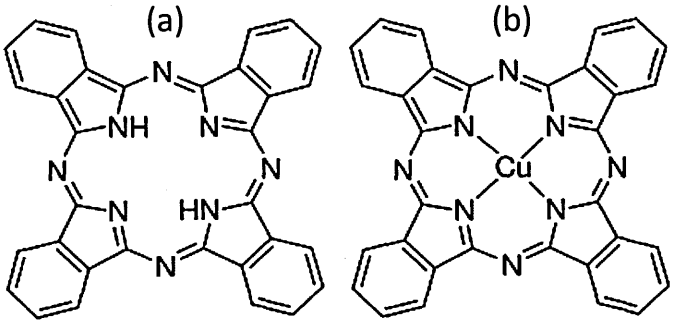

Figure 2.5: The molecular structure of (a) metal-free phthalocyanine and (b) metalophthalocyanine

2.2.2 Emerging material

Following this discovery, the colour manufacturing industry was quick to recognize the unique properties of the compound and to exploit their commercial potential. Phthalocyanine have emerged as one of the most extensively studied classes of compounds, because of their intense, bright colours, their high stability and their unique molecular structure [79,80].

Phthalocyanines are two-dimensional 18 π-electron aromatic porphyrin synthetic analogues, consisting of four isoindole subunits linked together through nitrogen atoms. Phthalocyanines and their metallo derivatives (MPcs) have recently attracted an increasing interest not only for the preparation of dyes and pigments but also as building blocks for the construction of new molecular materials for electronics and optoelectronics. These arise from their electronic delocalization, which makes them valuable in different fields of science and technology [81]. The chemical flexibility of

this class of compounds allows the preparation of a large variety of related structures and, consequently, the tailoring of the physical, electronic, and optical properties, as well as the improvement of processability. Therefore, peripheral substitution of phthalocyanines with bulky groups or hydrocarbon chains enhances their solubility and permits the deposition onto substrate, using spin-coating or LB deposition techniques [82].

The possibility of incorporating a broad range of metal atoms into the Pc cavity offers additional features to optimize the physical responses. On the other hand, their thermal and environmental stability are important characteristics that make them promising candidates to be incorporated into devices. To achieve this goal, an important point must be addressed which is the control of the supramolecular arrangement of these macrocycles in the solid state [83]. Liquid crystalline (LC) discotic mesophase materials can self-organise their molecules from organic solution into columnar stacks and develop potential solution processed molecular electronic materials. The columnar aggregates of discotic phthalocyanine molecules with effective overlap of π-orbitals along the stacking direction and low reformation energy [84] provide efficient anisotropic electronic transport networks along the molecular columns in the liquid crystalline mesophases with hole mobilities in the order of 10^{-1} cm^2/Vs [85]. Disk-like molecules, comprising a flat rigid aromatic core and flexible peripheral substituents, self-organize into one-dimensional supramolecular columns providing efficient anisotropic electronic transport channels [86]. Such self assembled columns in organic discotic molecules can adopt two types of characteristic orientations on surfaces: (i) homogeneous alignment, where the edge-on orientation of molecules and the columns parallel to the substrate surface is observed and (ii) homeotropic alignment, where the molecules are aligned face-on to the substrate and the columnar axes perpendicularly arranged with respect to the substrate surface [87]. Usually, homeotropic alignment can be generated by thermal annealing, that is slow cooling of the isotropic melt confined between two substrates [88].

In the last few decades, phthalocyanines have been extensively studied as targets for optical switching and limiting devices [89], organic field effect transistors [90], sensors [91-93], light emitting devices [94], molecular solar cells [95], data storage media [96],

photosensitizers [97] and electronic nose for cancer detection [98]. There are significant number of studies that were concerned with insoluble unsubstituted-phthalocyanines and their application employing their unique ability to evaporate without decomposition [99]. However, peripherally substituted soluble metallophthalocyanines facilitate films fabrication and their investigation using wet-deposition techniques.

2.2.3 Electrical properties of Pcs

Studies on organic semiconducting thin films have become increasingly significant for electronic applications. These materials are chemically and thermally quite stable and therefore, efforts have been made to utilize thin films of these materials as molecular modules in a number of electronic and optoelectronic devices [100]. Among these organic materials are the metal free phthalocyanines (H_2Pcs) and metal substituted phthalocyanines (MPcs) such as FePc, MgPc, PbPc, ZnPc, CuPc, and CoPc. These materials are generally p-type semiconductors and can be simply deposited resulting in pure and homogeneous thin films [101] either by vacuum sublimation or any other wet techniques in the case of peripherally substituted derivatives. The wide ranges of the conductivity of phthalocyanines, which result from their versatile chemical and physical systems, encourage researchers to achieve the best property required. During the last three decades, the semiconducting properties of phthalocyanines have been investigated in details. [89,95,96,100,102-104]. The conductivity phenomenon in phthalocyanine compounds can be due to either the intrinsic properties of a specific phthalocyanine or generally to the group of molecules at supramolecular level with an extended orbital overlapping along the conducting pathway.

Phthalocyanines could be self-assembled in columns at a supramolecular level leading to increased conductivity character. The co-facial stacking of phthalocyanine molecules enables electron delocalization within the axis of the column through π-π orbital overlap. Metallophthalocyanines mainly crystalise in an inclined stacked insulating arrangements called α and β modifications that do not allow an appropriate overlap of π-orbitals and hence no formation of a conduction band. Among the different methods used for organizing metallophthalocyanines with semiconducting properties are chemical methods such as oxidative doping or the so-called "shish-

kebab" approach as well as physical ones like the preparation of discotic liquid crystals and organized films by thermal treatment [82]. Basova and co-workers [88] have reported that the orientation of liquid crystalline nickel phthalocyanine molecules does not only depend on thermal treatment but it depends also on the interface between the film and the top contact (Figure 2.6). While thermal treatment of the film maintained between bottom and top electrodes induces homeotropic alignment, it strongly modifies the orientation of the columns from homeotropic to planar (homogeneous) when the top electrode is air.

In addition, substitutions of long alkyl, alkoxy and alkylthio substituents on the aromatic ring lead to the enhancement of liquid-crystalline behaviour in which the aromatic rings assembled into columnar stacks [105].

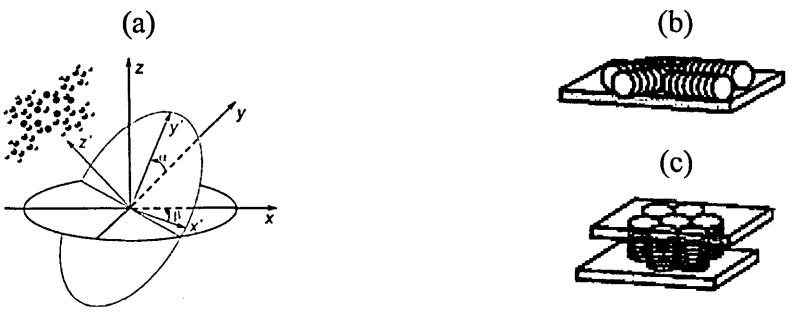

Figure 2.6: The orientation of Phthalocyanine molecule; (a) the coordinate axes of phthalocyanine molecule (x', y', z'; red colour) with respect to the substrate surface coordinate system (x, y, z; black colour), (b) and (c) schematic diagrams of the orientation of phthalocyanine molecule as top layer, and confined between two electrodes, respectively, after heat treatment [88]

Columnar liquid crystals, which are high ordered materials, are good candidates as organic semiconductors for electronic devices due to their potential to possess high mobility of charge carriers as well as the anisotropic property of conduction along the columns [106,107]. Therefore, the alignment of discotic liquid crystalline materials becomes a crucial point for high conductivity in different semiconducting applications.

It has been concluded from the literatures [87,103,108] that the intercolumnar packing dimensions of the polycyclic aromatic hydrocarbons are strongly dependent on the aromatic core size, the side chain length and the number of side chains. The effect of different substituents on the orientation and hence on the conductivity of the films of octasubstituted copper (II) phthalocyanines with alkylthio-, alkyloxy-, (trioxyethylene)thio- and (trioxyethylene)oxy-substituents in peripheral positions has been extensively studied by our research group [103]. It has been found that the lateral conductivity decreases slightly with the increase of alkyl chain length and the presence of sulphur in the alkylthio group resulting in higher conductivity in comparison with those containing alkyloxy groups in the substituent. Many other studies have previously reported that alkylthio-substituted phthalocyanines display higher conductivities than their alkyloxy-substituted phthalocyanines in their mesophase [86].

For unsubstituted phthalocyanines, the electrical switching effect has been reported for films of lead phthalocyanine (PbPc) in monoclinic phase. Switching effect was observed only in films consisting of a mixture of monoclinic grains and amorphous phase but not in films having triclinic phase structure [109]. In this connection, there have been some works that were devoted to structural studies of evaporated PbPc films [109,110]. However, the nature of switching effect has not been clearly understood yet. Some works have also explored the potential of some octasubstituted lead phthalocyanines as an active material for memory devices [111]. The electrical switching effect or the electrical bistable phenomenon of the metal-insulator-metal devices with organic layer as the insulator was first reported in 1968 [112]. Due to the promise of a new generation memory devices, interest has rapidly increased in the organic bistable devices (OBD). The main advantages of OBD are low power and low cost, their qualities of simple device structure, and simple production process [96]. The basic principle of an organic switching device is to demonstrate bistable behaviour showing two different conductivity states at the same applied voltage. When the voltage exceeds a particular value, the OBD unexpectedly switched from a low conduction state to a high conduction state with conductivity change of some orders of magnitude [113]. To explain this phenomenon, several mechanisms have been suggested such as formation of charge transfer complexes, charge trapping defect states in the band gap [114], formation of conducting filaments, and change of

molecular orientation [115]. In a previous work, which has been published by our research group [102], switching behaviour has been observed in octa-substituted lead phthalocyanine film spin-coated between two metal electrodes. In this study, the switching disappeared after heat treatment. The switching effect in the freshly deposited films was ascribed to the presence of potential barriers, which result from polycrystalline structure of phthalocyanine before heat-treatment. Bistable behaviour has been reported for other substituted lead-phthalocyanine in earlier work [111,116] and for insoluble copper-phthalocyanine using thermal deposition [96].

2.2.4 Optical properties of Pcs

Pcs complexes, with extended two dimensional π-electron delocalisation system, have been extensively reported regarding their nonlinear optical properties (NLOP). The tailor ability and architectural flexibility of Pcs molecules, results in the possibility of the variation of the chemical structure and therefore the modification of NLOP. Moreover the small absorption losses and thermal stability make Pcs promising candidate for nonlinear optical applications [81].

As detailed in the above section, the wide conjugative aromatic system of Pcs creates intense bands in the absorption spectra. The very well resolved and strongest absorption band in a variety number of Pcs is known as Q-band. The high absorptivity of Q-band is the source of purity and depth of the colour of Pcs pigments [117]. This band usually lies in the visible wavelength region at 650-670nm for free base phthalocyanine [118]. The incorporation of metal ions inside the central cavity of Pcs results in thermodynamically stable in delocalised ions and therefore, higher symmetry is achieved. Thus, the absorption spectra of such complexes show only one absorption peak for the corresponding Q-band. At this point, it is essential to mention that this fact is only valid in the case of symmetrically substituted Pcs; otherwise, the breaking of the symmetry gives rise to split of the Q-band [82].

There are several factors that influence the absorption spectra of Pcs leading to a shift of Q-band within the range of ca. 100nm between 620 and 720nm as a function of the metal size, coordination and oxidation state [119,120]. In the comparison to the free base phthalocyanine, the species with closed shell metal, for example; lithium(I), zinc(II) or magnesium(II) exhibit maximum wavelength value around 670nm. The

species with open shell metal ions that interact strongly with phthalocyanine ring such as cobalt(II), ruthenium(II) or iron(II) have Q-band shifted to the blue with absorption at around 630 to 650nm [121]. Moreover, a bigger shift through metal incorporation has been reported for vanadyl and lead(II) to reach the values up to 700nm. Recently, deep red manganese phthalocyanine has been reported with Q-band peaks at strongly shifted values of 808 and 828nm [122].

Another factor, which is substitutions, can possibly modify the molecular structure allow for considerable control over the physical, electronic and optical properties. Functionalities can in general be divided into electron-withdrawing and electron-releasing species. The former group is represented by chemical units such as carboxyl, sulfonyl or flour groups, while the latter compromises functions like amino, alkyle or alkoxy groups [82].

In principle, there are three types of substitutions according to the position of substituents; peripheral functionalisation (β- or meta-position), nonperipheral in the α-position (ortho-position) and hexadeca substitution, which compromise both peripheral and nonperipheral (Figure 2.7) [82]. Functionalisation at nonperipheral parts of Pcs results in more significant impact in the absorption spectra in comparison to β-substituted (peripheral) Pcs [123-125].

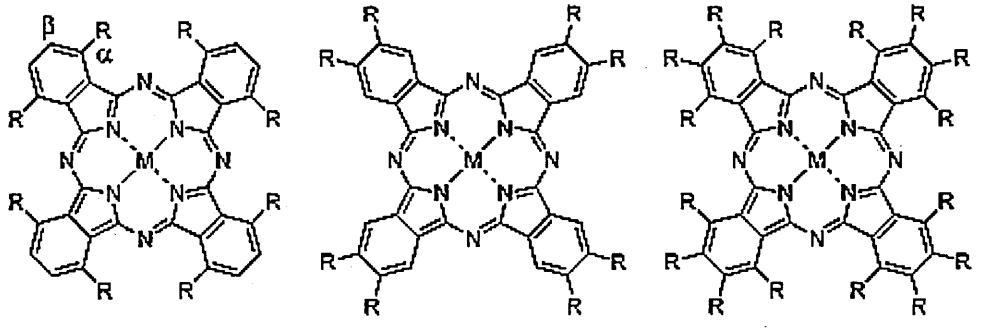

Figure 2.7: Structure and substitution patterns in metallophthalocyanine; nonperipheral (left), peripheral (middle) and hexadeca substitution (right) [82]

2.3 Carbon nanotube-Phthalocyanine conjugated hybrid

The formation of supramolecular architectures in which organic material present a high degree of order, which spans from the nano-scopic to macro-scopic level across multiple length scales, is highly required and represents a key issue within the fast developing fields of nanoscience and nanotechnology [126]. In this context, the use of self-assembly appears as an attractive and efficient approach for the construction of such ordered structure as it can allow preparation of complex, and multi-functional systems in a capable and controlled manner through the utilization of non-covalent interactions. Among the organic compounds, π-conjugated systems are the perfect candidates for the production of such supramolecular structures due to their excellent self-organization ability [127].

Several studies have been reported on the MPcs-CNTs hybrid thin films utilized as optoelectronic devices [128-132] electro-catalytical devices [133,134] and sensing devices [135-137]. It has been observed that MPc-CNT complexes retain the excellent catalytic properties of phthalocyanines without losing any of the electronic properties of the carbon nanotubes [138].

The non-covalent functionalization is particularly attractive since the electronic structure of the nanotubes remains essentially unaffected and therefore enhances the electro-catalytic properties of phthalocyanine. However, the thermo-gravimetric analysis [33] suggests that the SWCNTs-ZnPc-covalently-linked hybrid shows more chemical stability than SWCNTs-ZnPc-adsorbed hybrid since the ratios of ZnPc functional group to carbon atoms were 1:1430 and 1:482 for covalent complex and adsorbed complex respectively. In addition, Mugadza and Nyokong [133] reported that the non-covalently linked SWCNT-CoPc shows lower sensitivity and selectivity to 2-mercaptoethanol (2-ME) than the covalently linked hybrid.

It is essential to highlight the criteria of the association nature between CNTs and Pcs and the conditions that make covalent or adsorption (π-π interaction) bonds occur between these compounds or just a composite of the two. This actually depends not only on the modification procedure of CNTs but also on the central atom of MPc, substitution groups, chain length and the site of substituents. For instance, although it tends to covalently bond with dicyclohexylcarbodiimide (DCC)-treated substituted-zinc (II) phthalocyanine (ZnPc), amine functionalized SWCNTs non-covalently

adsorbs untreated-ZnPc [33]. Furthermore, it depends on the type of CNTs whether single or multi-walled, the large diameter to length ratio of multi-walled CNTs may adjust the electronic structure which may be significantly different from that of single-walled CNTs [139].

2.3.1 Enhancement of electrical properties

The extraordinary electronic properties of CNTs in general and SWCNTs in particular suggest many possible applications and bridge those of the bulk and molecules [140,141], since they readily accept electrons which can then be transported under nearly ideal conditions along the axis [142]. In addition, the orientation possibilities of nanotubes enable the conductivity control of carbon nanotubes doped liquid crystal composite hybrids and therefore offer wide range of nano-electronic applications [143,144]. The DC-conductivity of thin films of SWCNTs-tetrakis(alkylthio)-substituted lutetium(III)bisphthalocyanines prepared by jet-spraying chloroform suspension is found to be higher than that of only phthalocyanine films in both cases of as coated films and ordered (annealed to liquid crystalline temperature) films [145]. However, larger increase in conductivity was observed in the ordered films indicating the orientation of SWCNTs in liquid crystalline phase of the phthalocyanine. In contrast, it is important here to reveal that carbon nanotubes tend to make bundles and aggregations in chloroform [11]. Brito and co-workers [146] have ascribed the increase in the hybrid materials conductivity to the impurities, when they studied the structural and electrical properties of layer-by-layer thin films of MWCNT/NiPc and MWCNT/chitosan+NiPc. The increase in the impurities concentration leads to the formation of localized states (traps) where the charge carriers can move by the hopping mechanism [147]. Self-assembled monolayer nano-composite films of SWCNT-FePc and FePc have been formed onto gold electrodes [148] to study the electron transfer dynamics using electrochemical impedance spectroscopy and cyclic voltammetry. The high electrical conductivity of SWCNT, coupled with enhanced electron density of the nano-composite confirmed by TEM images, may have facilitated better electron transport in the SWCNT-FePc film, resulting in lowest charge transfer resistance [148]. In the field of photovoltaic application the photocurrent of poly(3-hexylthiophene)-NaPc/MWCNTs film is

found to be much larger than that of poly(3-hexylthiophene)-NaPc in all the visible and near-infrared wavelength regions [149]. Similar behaviour has been observed in the work of Yang et al [150] where the photosensitivity in CuPc-MWCNTs hybrid material was 1.6 and 1.46 larger than that of pristine CuPc material and just blended CuPc/MWCNTs material. The π-stacking between the phthalocyanine molecules and carbon nanotubes can reduce the activation energies for charge transfer and therefore high charge mobility is expected from these hybrids that are interesting as a photo-active layer in photovoltaic devices [149]. To study the interface between carbon nanotubes and metal phthalocyanines, very thin film of copper phthalocyanine has been grown by thermal evaporation onto supported MWCNTs layer, previously deposited by chemical vapour deposition onto silicon substrate [129]. The presence of organic nanocrystals decorating the nanotubes was confirmed using several microscopic techniques and XRD data have shown the presence of both α and β crystalline phases of CuPc . A shift of the highest occupied molecular level towards the Fermi level was observed for very thin films, together with a small shift of the nitrogen and copper core level peak position and the interaction between the organic molecules and nanotubes is found to be quite weak, determining very small effects on the photoemission spectra [129].

2.3.2 Senor applications

Phthalocyanine complexes have been recognised to exhibit substantial changes in optical, electrical and magnetic properties on interaction with wide range of reducing and oxidizing agents [151-157]. These characteristics can be employed for a several kinds of chemical detection applications. The crystalline structure of phthalocyanines is such that they can easily accommodate dopant molecules in channels adjacent to the phthalocyanine stacks. When dopant molecule such as NO_2 is adsorbed onto phthalocyanine surface, charge transfer interaction takes place, which results in very large increase in surface conduction [93]. The process is somehow similar to the doping of intrinsic silicon to produce p-type semiconductor. In addition, phthalocyanine thin films conductivity has been shown to be sensitive to low concentrations of various gases [158]. Both the sensitivity and the reversibility of the Pc-based detectors are, in most cases, acceptable [159]. Much work has been carried

out in order to understand the influence of the morphology, the temperature, the central metal and the peripheral substituents on the sensing ability of the phthalocyanine thin films.

The most promising candidates as far as applications are concerned are based on double-decker phthalocyanines [160]. Efforts are being made to transform the present laboratory devices into real-world sensors especially with the development of phthalocyanine-based electronic noses [160]. Many groups of researchers have been engaged in the synthesis of novel phthalocyanines for sensing applications to detect different types of agents such as halogens [157], phenols [91], different types of herbicides, and pesticides and organic vapours [92,159,161].

Recent reports have shown that CNTs-MPcs hybrids exhibited enhanced responses in comparison to the use of CNTs or MPcs alone. Work carried out on these hybrids included the detection of important molecules such as benzo[a]pyrine [38], amines [48], pesticides [44], asulam [162], hydrolysis products of V-type nerve agents [163], mercaptoethanol and nitric oxide [164], and epinephrine [165].

To date the research effort in hybrid carbon nanotube-conjugatd molecule systems has largely focused on the use of single-walled carbon nanotubes [33,134,148,166,167]. A major complication with SWCNTs is that they are a mixture of metallic and semiconducting tubes, complicating the interpretation of experimental data. Conversely, as a result of their larger diameter and more complex multilayered structure, multi-walled carbon nanotubes (MWCNTs) are invariably metallic, offering far more predictable functionality. Notably, both types of carbon nanotubes exhibit poor solubility in common solvents unless chemically functionalized or stabilized by a physical interaction with a soluble molecule [130].

SWCNTs-CoPc derivative hybrid thin film chemiresistor sensor has been synthesized by using dip-dropping method and confirmed employing infrared spectroscopy, Raman spectroscopy, UV-Vis spectroscopy and X-ray photoelectron spectroscopy [167]. The results revealed that CoPc derivatives have been successfully anchored on the surfaces of carbon nanotubes through π-π stretching and the resistance variation of the hybrid film was investigated by introducing different concentrations of organic solvent vapors. The hybrid sensors have shown higher sensitivity and selectivity for Dimethyl methylphosphonate (DMMP) compared with

other vapors and with bare SWCNTs based sensors, showing a sudden and significant increase in resistance. The source of the resistance responses of the hybrid sensors might be attributed to the large SWCNT-CoPc derivative conjugated π structure [167]. As the vapor molecules being chemisorbed onto the surface of MPc derivatives in the hybrids, surface charge transfer interactions happen [168], followed by charge moving between MPcs and SWCNTs. Since SWCNTs-MPcs could form a brilliant charge transfer composite [33,132], the charge can well-travel from MPc derivatives to SWCNTs causing a very large and fast variation in the electrical properties and therefore the resistance. In the work of Wang and co-workers [167] the resistance has increased because DMMP is a strong electron donor. In contrast, the resistance of CuPc-MWCNT hybrid film has shown a completely different behavior from others prepared from CoPc-MWCNTs and VPc-MWCNTs when they are exposed to hydrogen peroxide (H_2O_2) vapor [137]. While the resistance of CoPc-MWCNTs and VPc-MWCNTs sensors exhibit an obvious increase when exposed to H_2O_2 and other vapors, only CuPc-MWCNTs film show a significant decrease in resistance over wide range of concentrations. However, CuPc-MWCNTs device behave similar to other phthalocyanines-MWCNTs hybrids when exposed to vapors except H_2O_2. The electrical conductivity of thin films of the composites made from MPc and CNTs can be modulated by interactions with different gases. Such effects can be interpreted within the framework of the band theory if we consider the adsorbed gases to produce appropriate donor or accepter level within the band gap of the organic materials at the film surface. Thin films of pure MPc are p-type semiconductors. Upon exposure to oxidizing agents (electron acceptors) like NO_2 [93], SO_2 [169], and halogens [157] show an increase in electrical conductivity by generating extra charge carriers (holes), while reducing agents (electron donors) like NH_3 [170], CH_3OH [171], CO_2 [20], and DMMP [155,167] trap charge carriers and decrease electrical conductivity.

It is important to mention that CNTs-MPc derivative hybrids are not only used in toxic chemical detection, MWCNTs-CoPc composite is found to be very sensitive and selective to ascorbic acid (AA) which is one of the most important vitamins that exist widely in fruits and vegetables [172]. Rapid increase in current was observed corresponding to presence of AA on the surface of the hybrid electrodes. Nonetheless, no significant increase in the catalytic current was obtained when the

concentration of the AA solution was less than 5μM. Shah and co-workers [135] on the other hand have prepared humidity sensors by blending poly-N-epoxypropylcarbazol (PEPC) together with nickel phthalocyanine NiPc and CNTs in benzol and the mixture was drop-casted on different types of electrodes initially evaporated on glass substrates. In a self-made humidity chamber the capacitance increased with increasing humidity for all synthesized electrodes and this increase can be ascribed to the absorption of water by the composite molecules. The dielectric constant of the material is changed with absorption of water vapor, leading to the formation of charge transfer complexes and doping of the nanocomposite by H_2O and thus results in capacitance increase [135].

Several research efforts have employed the unique sensing properties of the CNTs-MPcs conjugated system in the detection of a diverse range of environmental pollutants such as amitrol herbicide [173], duiron herbicide [55], glyphosate (GLY) herbicide [174], organophosphours pesticide [175], asulam pesticide [176], phenolic compounds after benzene oxidation [177], and determination of epinephrine in urine [178].

2.4 Total Internal Reflection Ellipsometry (TIRE)

Several methods used to determine chemical compounds imply measuring the variation of physical properties of an active layer induced by the adsorption of a chemical molecule on its surface. This active layer becomes the transducer that transforms the interaction with the environment in an optical or electrical signal. Among these methods are; high performance liquid chromatography [179-181], electrochemical [182-185], electrical based sensors [47] and optical detection methods [92]. Sensors and measurement tools based on optical phenomena have always been of special interest, mostly because they usually do not require any physical or electrical contact with the materials under investigation and therefore they are not destructive. Some techniques, such as surface plasmon resonance (SPR) [159] and UV-visible absorption spectroscopy [186] are quite well recognised, and widely used. However, others like total internal reflection ellipsometry (TIRE), where ellipsometry can be used in total internal reflection mode and in combination with the surface plasmon resonance phenomenon [187], are still underexploited in the sensor area.

The main task for all electrical, mechanical and optical sensors is to detect low concentration chemical and biological analytes under extremely dilute conditions. SPR sensors are the most commonly used optical sensors due to their unique ability for real-time monitoring. However, their sensitivities are unsatisfactory to detect trace amounts of small molecular weight molecules such as cancer biomarkers, hormones, antibiotics, insecticides, which are respectively important for early-stage disease diagnosis, explosive materials, food quality control, environmental monitoring, and homeland security protection. With the fast development of nanotechnology in the past few years, nanomaterials-enhanced surface plasmon resonance sensors have been developed and used as effective tools to detect molecules in a much diluted solutions [188].

Ellipsometry is an analytical tool which is well established for thin films and surface characterisation. This method relies on two parameters, the light intensity ratio (ψ) and phase shift (Δ) of p and s components of the polarized light. Regarding organic materials, ellipsometry were extensively utilized to study polymer thin films [189,190], self-organised layers [191,192], LB films [193] and liquid crystal [194,195]. The majority of these applications however focuses on the surface properties. Ellipsometry is well known in thin films industry for in-situ monitoring of film deposition to control layer thickness, growth rate and layer quality. However, the method of ellipsometry in general is recognised as an optical measurement tool but not as a sensor.

Due to the high sensitivity to the thickness increment, in the range of 0.01 nm, this technique has been recently adapted for the measurement of molecular layer adsorbed on solid surfaces, which naturally leads to sensor applications [161,196].

Further advances of spectroscopic ellipsometry for sensing application have been achieved in its total internal reflection mode. The idea of using ellipsometry in internal reflection mode was first realised experimentally by Westphal [197] where the prism was used to couple the light beam into a thin metal film thus combining the ellipsometic principle of detection with the phenomenon of SPR. The increased sensitivity has been achieved and the method was originally called as surface plasmon enhanced ellipsometry. The method was further explored and theoritically explained by Arwin [199] and got the current name of total internal reflection ellipsometry (TIRE). Later on, Nabok and co-workers [196] developed detailed

modelling that showed 10 fold gain of the sensitivity by using of Δ spectra instead of ψ and traditional SPR measurements.

There has been a number of research studies where TIRE can be used for monitoring of thin layers on surfaces [199]. Examples are given in the literature [200] of some probable applications of TIRE, where it has been established that TIRE is used for the monitoring of corrosion. TIRE technique has also been exploited in the biomolecules detection [201], however, it still seems to be not fully recognised in the chemical vapour detection. A detailed theoretical background of TIRE technique is found in Chapter 3. The main advantage of TIRE technique over standard ellipsometry is the possibility of performing measurements in opaque media. The ability of spectroscopic measurements of two ellipsometric parameters (Ψ and Δ) constitutes the main advantage over the conventional Kretschman SPR, where only one parameter (reflection intensity) can be measured. In addition to the above-mentioned advantages of optical detection methods, particularly TIRE technique, based on CNTs active layer, there is another advantage of incorporating CNTs into the TIRE technique. The problem in the well-known electrochemical and electrical methods based CNTs sensors caused by the differences in Fermi level positions in metallic-CNTs and semiconducting-CNTs [202] can be avoided in TIRE method because it depends on the variation of the optical parameters before and after exposure to contaminated media. This optical response is related to the modifier only and CNTs work as adsorbent material in the system because CNTs are optically inert whether metallic or semiconducting tubes.

2.5 Theory of Ellipsometry

Ellipsometry is a non-destructive optical method used to determine the optical properties of materials. The idea of Ellipsometry lies in measurements of changes of polarized light upon its reflection from a sample. As light reflects from a sample surface the state of polarized light changes from linear to elliptical, as in Figure 2.8.

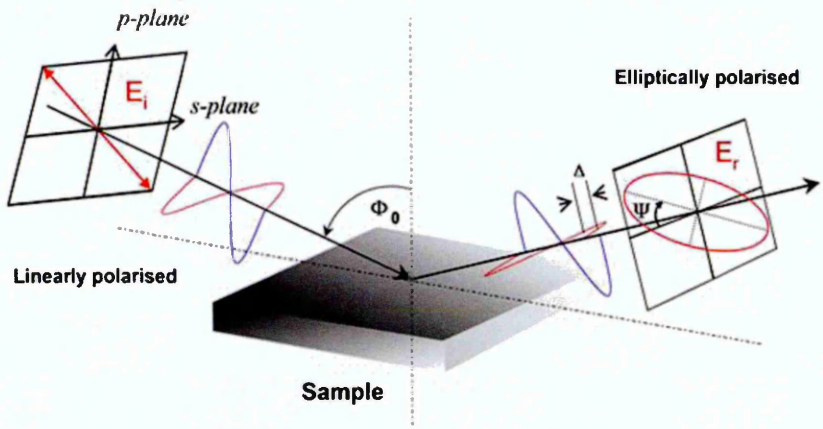

Figure 2.8: The changes in polarization of light reflected from the surface

Ellipsometry technique does not measure directly the optical properties of the material but the angles of (ψ) and (Δ). Psi (ψ) and delta (Δ) are defined as the ratio (ρ) of complex reflection coefficients r_p and r_s for electric vectors, p (parallel) and s (normal) to the plane of incidence [198].

$$\rho = \frac{r_p}{r_s} = \frac{|r_p|\exp(i\delta_p)}{|r_s|\exp(i\delta_s)} = \tan\psi \exp(i\Delta) \qquad (2.1)$$

In eq. 2.1, ψ represents the amplitude ratio of p and s components of polarized light while Δ is the phase difference between p and s components.

$$\tan\psi = \frac{|r_p|}{|r_s|}, \ \Delta = \delta_p - \delta_s \qquad (2.2)$$

In the case of reflection / transmission at the interface between two media with respective indices N_0 and N_1, the reflection and transmission coefficients are described by Fresnel's formula [203];

$$r_s = \left(\frac{E_{0r}}{E_{0i}}\right)_s = \frac{n_i \cos\theta_i - n_t \cos\theta_t}{n_i \cos\theta_i + n_t \cos\theta_t} \qquad r_p = \left(\frac{E_{0r}}{E_{0i}}\right)_p = \frac{n_t \cos\theta_i - n_i \cos\theta_t}{n_i \cos\theta_t + n_t \cos\theta_i} \tag{2.3}$$

$$t_s = \left(\frac{E_{0t}}{E_{0i}}\right)_s = \frac{2n_i \cos\theta_i}{n_i \cos\theta_i + n_t \cos\theta_t} \qquad t_p = \left(\frac{E_{0t}}{E_{0i}}\right)_p = \frac{2n_i \cos\theta_i}{n_i \cos\theta_t + n_t \cos\theta_i} \tag{2.4}$$

Substitution of r_p and r_s in equation (2.2), their values from (2.3) and Snell's Law, $N_0 \sin\theta_0 = N_1 \sin\theta_1$, yields;

$$N_1 = N_0 \tan\theta_0 \left[1 - \frac{4\rho}{(1+\rho^2)} \sin^2\theta_0\right]^{1/2} \tag{2.5}$$

For the three layer systems, consisting of a substrate, films and ambient (Figure 2.9), the total reflectance can be calculated as

$$R = r_{01} + t_{01}t_{10}r_{12}e^{-i2\beta} + t_{01}t_{10}r_{10}r_{12}^{\ 2}e^{-i4\beta} + \ldots \tag{2.6}$$

Where r_{01}, r_{12}, t_{01} and t_{10} are Fresnel reflection and transmission coefficients at the 0/1, 1/0 and 1/2 interfaces respectively and β is the phase thickness of the film;

$$\beta = 2\pi\left(\frac{d_1}{\lambda}\right)N_1\cos\theta_1 = 2\pi\left(\frac{d_1}{\lambda}\right)\left(N_1^{\ 2} - N_0^{\ 2}\sin^2\theta_0\right)^{1/2} \tag{2.7}$$

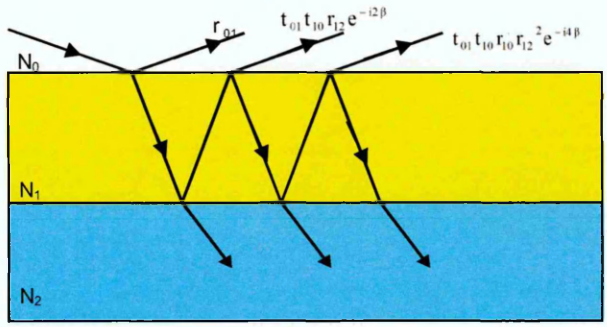

Figure 2.9: Optical model for an ambient – thin film – substrate structure

The summation of equation 6 for the p and s reflectance components is given by;

$$R_p = \frac{r_{01p} + r_{12p}e^{-i2\beta}}{1 + r_{01p}r_{12p}e^{-i2\beta}} \quad \text{and} \quad R_s = \frac{r_{01s} + r_{12s}e^{-i2\beta}}{1 + r_{01s}r_{12s}e^{-i2\beta}} \qquad (2.8)$$

The main ellipsometric equation depends on a number of parameters of the system through Fresnel's formula;

$$\tan\psi e^{i\Delta} = \rho(N_{0,}N_1, N_2, d_1, \theta_0, \lambda) \qquad (2.9)$$

Solving the main ellipsometric equation is quite a difficult task. Two approaches are typically used, namely, forward and reverse ellipsometry problems. In forward ellipsometry problems, the values of ψ and Δ can be found from known parameters $N_0, N_1, N_2, d_1, \theta_0, \lambda$ and by solving Fresnel equations analytically, which is a rather straightforward procedure. Solving the reverse ellipsometric problem, i.e. finding the parameters of the reflective system such as refractive index (N_1) and thickness (d_1) of the film, can be obtained from the experimental values of ψ_{exp} and Δ_{exp} and is much more complex. It can be tackled using some of the least square techniques which involve solving a forward problem (Fresnel equation) several times and

finding the theoretical values (ψ_{the} and Δ_{the}) and subsequent minimizations of the error function. The approach is based on finding the mean square error (MSE) between the experimental values of $\psi_i^{\exp}$ and $\Delta_i^{\exp}$ and theoretical (modelled) ones ψ_i^{mod} and Δ_i^{mod} as given, for example, in [204];

$$MSE = \frac{1}{2N-M}\sum_{i=1}^{N}\left[\left(\frac{\Psi_i^{\mathrm{mod}} - \Psi_i^{\exp}}{\sigma_{\Psi,i}^{\exp}}\right)^2 + \left(\frac{\Delta_i^{\mathrm{mod}} - \Delta_i^{\exp}}{\sigma_{\Delta,i}^{\exp}}\right)^2\right] = \frac{1}{2N-M}\chi^2 \qquad (2.10)$$

A smaller MSE implies a better fit. MSE is weighted by the error bars of each measurement, so noisy data are weighted less. There are several types of ellipsometry instrumentation developed within the last 4 – 5 decades ranging from simple fixed angle, single wavelength units to modern spectroscopic ellipsometric instruments. Spectroscopic ellipsometers can be split into two major categories: instruments that use rotating optical elements (analyzer or compensator) and instruments that use a photoelastic modulator. For example, the J. A. Woollam M2000 spectroscopic ellipsometric instrument exploits the principle of a rotating compensator, which consists of a wide spectral range of light source (350 – 1000 nm), polarizer, rotating compensator, analyzer and a photodetector, as shown in Figure 2.10.

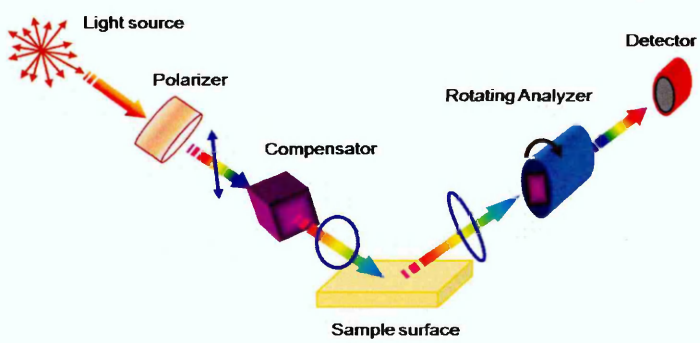

Figure 2.10: The schematic of rotating analyzer spectroscopic ellipsometry

Reference List

[1] a. krueger, Carbon Materials and Nanotechnology, wily-vch, germany, 2010.

[2] S. Iijima, Helical microtubules of graphitic carbon, Nature. 354 (1991) 56-58.

[3] S. Iijima, T. Ichihashi, Single-shell carbon nanotubes of 1-nm diameter, Nature. 363 (1993) 603-605.

[4] N. Nakashima, Soluble carbon nanotubes: Fundamentals and applications, Inter. J. Nanosci. 4 (2005) 119-137.

[5] N. Nakashima, T. Fujigaya, Fundamentals and applications of soluble carbon nanotubes, Chem. Lett. 36 (2007) 692-697.

[6] R.H. Baughman, A.A. Zakhidov, W.A. De Heer, Carbon nanotubes - The route toward applications, Science. 297 (2002) 787-792.

[7] W. Wang, K.A.S. Fernando, Y. Lin, M.J. Meziani, Metallic single-walled carbon nanotubes for conductive nanocomposites, J. Am. Chem. Soc. 130 (2008) 1415-1419.

[8] P.L. McEuen, M.S. Fuhrer, H. Park, Single-walled carbon nanotube electronics, IEEE Transactions on Nanotechnology. 1 (2002) 78-84.

[9] C.V. Nguyen, Q. Ye, M. Meyyappan, Carbon nanotube tips for scanning probe microscopy: Fabrication and high aspect ratio nanometrology, Measur. Sci. Tech. 16 (2005) 2138-2146.

[10] N.M. Gabor, Z. Zhong, K. Bosnick, J. Park, P.L. McEuen, Extremely efficient multiple electron-hole pair generation in carbon nanotube photodiodes, Science. 325 (2009) 1367-1371.

[11] A.L. Ndiaye, C. Varenne, P. Bonnet, E. Petit, et al. Elaboration of single wall carbon nanotubes-based gas sensors: Evaluating the bundling effect on the sensor performance, Thin Solid Films. 520 (2012) 4465-4469.

[12] M.D. Shirsat, T. Sarkar, J. Kakoullis Jr., N.V. Myung, B. Konnanath, A. Spanias, A. Mulchandani, Porphyrin-functionalized single-walled carbon nanotube chemiresistive sensor arrays for VOCs, Journal of Physical Chemistry C. 116 (2012) 3845-3850.

[13] S.C. Lim, D.S. Lee, H.K. Choi, I.H. Lee, Y.H. Lee, Field emission of carbon-nanotube point electron source, Diamond and Related Materials. 18 (2009) 1435-1439.

[14] P.J. Boul, K. Turner, J. Li, M.X. Pulikkathara, R.C. Dwivedi, E.D. Sosa, Y. Lu, O.V. Kuznetsov, P. Moloney, R. Wilkins, M.J. O'Rourke, Single wall carbon nanotube response to proton radiation, Journal of Physical Chemistry C. 113 (2009) 14467-14473.

[15] A.P. Terzyk, A. Pacholczyk, M. Wiśniewski, P.A. Gauden, Enhanced adsorption of paracetamol on closed carbon nanotubes by formation of nanoaggregates: Carbon nanotubes as potential materials in hot-melt drug deposition-experiment and simulation, J. Colloid Interface Sci. 376 (2012) 209-216.

[16] N.M. Bandaru, N.H. Voelcker, Glycoconjugate-functionalized carbon nanotubes in biomedicine, Journal of Materials Chemistry. 22 (2012) 8748-8758.

[17] L. Henrard, E. Hernández, et al. Van der Waals interaction in nanotube bundles: Consequences on vibrational modes, Physical Review B - Cond. Mat. Mater. Phys.. 60 (1999) R8521-R8524.

[18] N.I. Alekseev, N.A. Charykov, The characteristic size of carbon nanotube bundles, Russian Journal of Physical Chemistry A. 83 (2009) 1176-1181.

[19] S. Chiashi, Y. Murakami, Y. Miyauchi, S. Maruyama, Cold wall CVD generation of single-walled carbon nanotubes and in situ Raman scattering measurements of the growth stage, Chemical Physics Letters. 386 (2004) 89-94.

[20] E.P. Dillon, C.A. Crouse, A.R. Barron, Synthesis, characterization, and carbon dioxide adsorption of covalently attached polyethyleneimine-functionalized single-wall carbon nanotubes, ACS Nano. 2 (2008) 156-164.

[21] S. Chen, W. Shen, G. Wu, D. Chen, M. Jiang, A new approach to the functionalization of single-walled carbon nanotubes with both alkyl and carboxyl groups, Chem. Phys. Lett. 402 (2005) 312-317.

[22] N. Karousis, N. Tagmatarchis, D. Tasis, Current progress on the chemical modification of carbon nanotubes, Chem. Rev. 110 (2010) 5366-5397.

[23] L. Nasdala, A. Kempe, R. Rolfes, Are finite elements appropriate for use in molecular dynamic simulations? Composites Sci. Technol. 72 (2012) 989-1000.

[24] D. Lashmore, B. White, M. Schauer, J. Mann, Synthesis and electronic properties SWCNT sheets, Materials Research Society Symposium Proceedings. 1081 (2008) 107-112.

[25] H. Kuzmany, A. Kukovecz, F. Simon, M. Holzweber, C. Kramberger, T. Pichler, Functionalization of carbon nanotubes, Synth. Met. 141 (2004) 113-122.

[26] T. Guo, P. Nikolaev, A. Thess, D.T. Colbert, R.E. Smalley, Catalytic growth of single-walled manotubes by laser vaporization, Chemical Physics Letters. 243 (1995) 49-54.

[27] P. Nikolaev, M.J. Bronikowski, R.K. Bradley, F. Rohmund, D.T. Colbert, K.A. Smith, R.E. Smalley, Gas-phase catalytic growth of single-walled carbon nanotubes from carbon monoxide, Chemical Physics Letters. 313 (1999) 91-97.

[28] J. Colomer, C. Stephan, S. Lefrant, G. Van Tendeloo, I. Willems, Z. Kónya, A. Fonseca, C. Laurent, J.B. Nagy, Large-scale synthesis of single-wall carbon nanotubes by catalytic chemical vapor deposition (CCVD) method, Chemical Physics Letters. 317 (2000) 83-89.

[29] R.L. Vander Wal, T.M. Ticich, et al. Directed Synthesis of Metal-Catalyzed Carbon Nanofibers and Graphite Encapsulated Metal Nanoparticles, J. Phys. Chem. B. 104 (2000) 11606-11611.

[30] D. Laplaze, P. Bernier, W.K. Maser, G. Flamant, T. Guillard, A. Loiseau, Carbon nanotubes: The solar approach, Carbon. 36 (1998) 685-688.

[31] Z.K. Tang, H.D. Sun, J. Wang, J. Chen, G. Li, Mono-sized single-wall carbon nanotubes formed in channels of AlPO4-5 single crystal, Appl. Phys. Lett. 73 (1998) 2287-2289.

[32] C. Gao, Z. Guo, J. Liu, X. Huang, The new age of carbon nanotubes: An updated review of functionalized carbon nanotubes in electrochemical sensors, Nanoscale. 4 (2012) 1948-1963.

[33] W. Chidawanyika, T. Nyokong, Characterization of amine-functionalized single-walled carbon nanotube-low symmetry phthalocyanine conjugates, Carbon. 48 (2010) 2831-2838.

[34] C.A. Dyke, J.M. Tour, Covalent functionalization of single-walled carbon nanotubes for materials applications, Journal of Physical Chemistry A. 108 (2004) 11151-11159.

[35] A. Gasnier, J.M. González-Domínguez, A. Ansón-Casaos, J. Hernández-Ferrer, M.L. Pedano, M.D. Rubianes, M.T. Martínez, G. Rivas, Single-wall carbon nanotubes covalently functionalized with polylysine: Synthesis, characterization and analytical applications for the development of electrochemical (Bio)sensors, Electroanalysis. (2014).

[36] J. Ryu, M. Han, Improvement of the mechanical and electrical properties of polyamide 6 nanocomposites by non-covalent functionalization of multi-walled carbon nanotubes, Composites Sci. Technol. 102 (2014) 169-175.

[37] G. De Filpo, F.P. Nicoletta, L. Ciliberti, P. Formoso, G. Chidichimo, Non-covalent functionalisation of single wall carbon nanotubes for efficient dye-sensitised solar cells, J. Power Sources. 274 (2015) 274-279.

[38] H. Banimuslem, A. Hassan, T. Basova, M. Durmus, S. Tuncel, A.A. Esenpınar, A.G. Gürek, V. Ahsen, Copper Phthalocyanine Functionalized Single-Walled Carbon Nanotubes: Thin Films for Optical Detection, Journal of Nanoscience and Nanotechnology. 15 (2015) 2157-2167.

[39] F. Ren, H. Yu, L. Wang, M. Saleem, Z. Tian, P. Ren, Current progress on the modification of carbon nanotubes and their application in electromagnetic wave absorption, RSC Advances. 4 (2014) 14419-14431.

[40] S. Barreto, D. Suleiman, Effect of single-walled carbon nanotubes on the transport properties of sulfonated poly(styrene-isobutylene-styrene) membranes, J. Membr. Sci. 474 (2015) 92-102.

[41] J. Liu, A.G. Rinzler, H. Dai, J.H. Hafner, R.K. Bradley, P.J. Boul, A. Lu, T. Iverson, K. Shelimov, C.B. Huffman, F. Rodriguez-Macias, Y. Shon, T.R. Lee, D.T. Colbert, R.E. Smalley, Fullerene pipes, Science. 280 (1998) 1253-1256.

[42] H. Banimuslem, A. Hassan, T. Basova, I. Yushina, M. Durmuş, S. Tuncel, A.A. Esenpınar, A.G. Gürek, V. Ahsen, Copper phthalocyanine functionalized single-walled carbon nanotubes: thin film deposition and sensing properties, Key Eng Mat. 605 (2014) 461-464.

[43] C. Bower, A. Kleinhammes, Y. Wu, O. Zhou, Intercalation and partial exfoliation of single-walled carbon nanotubes by nitric acid, Chemical Physics Letters. 288 (1998) 481-486.

[44] H. Banimuslem, A. Hassan, T. Basova, A.D. Gülmez, S. Tuncel, M. Durmus, A.G. Gürek, V. Ahsen, Copper phthalocyanine/single walled carbon nanotubes hybrid thin films for pentachlorophenol detection, Sensors and Actuators, B: Chemical. 190 (2014) 990-998.

[45] H. Banimuslem, A. Hassan, T. Basova, A.D. Gülmez, M. Durmuş, A.G. Gürek, V. Ahsen, Optical Detection of Herbicides in Water using Dye-Modified Single Walled Carbon Nanotubes, Proceedings of the 8th international conference on sensing technology, Sep. 2-4, 2014, Liverpool, UK.

[46] T. Park, S. Banerjee, T. Benny, S.S. Wong, Purification strategies and purity visualization techniques for single-walled carbon nanotubes, Journal of Materials Chemistry. 16 (2006) 141-154.

[47] B. Wang, Y. Wu, X. Wang, Z. Chen, C. He, Copper phthalocyanine noncovalent functionalized single-walled carbon nanotube with enhanced NH_3 sensing performance, Sensors Actuators B: Chem. 190 (2014) 157-164.

[48] H. Banimuslem, A. Hassan, T. Basova, A.A. Esenpınar, et al. Dye-modified carbon nanotubes for the optical detection of amines vapours, Sensors Actuators B: Chem. (2014).

[49] S.A. Girei, S.P. Thomas, M.A. Atieh, K. Mezghani, S.K. De, S. Bandyopadhyay, A. Al-Juhani, Effect of -COOH functionalized carbon nanotubes on mechanical, dynamic mechanical and thermal properties of polypropylene nanocomposites, J. Thermoplast. Compos. Mater. 25 (2012) 333-350.

[50] T. Xu, J. Yang, J. Liu, Q. Fu, Surface modification of multi-walled carbon nanotubes by O 2 plasma, Appl. Surf. Sci. 253 (2007) 8945-8951.

[51] M.A. Montes-Morán, D. Suárez, J.A. Menéndez, E. Fuente, On the nature of basic sites on carbon surfaces: An overview, Carbon. 42 (2004) 1219-1224.

[52] Y. Li, S. Wang, Z. Luan, J. Ding, C. Xu, D. Wu, Adsorption of cadmium(II) from aqueous solution by surface oxidized carbon nanotubes, Carbon. 41 (2003) 1057-1062.

[53] D. Tuncel, Non-covalent interactions between carbon nanotubes and conjugated polymers, Nanoscale. 3 (2011) 3545-3554.

[54] P. Tambe, A. Bhattacharyya, S.S. Kamath, A.R. Kulkarni, T.V. Sreekumar, A. Srivastav, K.U.B. Rao, Y. Liu, S. Kumar, Structure-property relationship studies in amine functionalized multiwall carbon nanotubes filled polypropylene composite fiber, Polym. Eng. Sci. 52 (2012) 1183-1194.

[55] T. Mugadza, T. Nyokong, Electrochemical, microscopic and spectroscopic characterization of benzene diamine functionalized single walled carbon nanotube-cobalt (II) tetracarboxy-phthalocyanine conjugates, J. Colloid Interface Sci. 354 (2011) 437-447.

[56] Y. Shen, J.S. Reparaz, M.R. Wagner, A. Hoffmann, C. Thomsen, J. Lee, S. Heeg, B. Hatting, S. Reich, A. Saeki, S. Seki, K. Yoshida, S.S. Babu, H. Möhwald, T. Nakanishi, Assembly of carbon nanotubes and alkylated fullerenes: Nanocarbon hybrid towards photovoltaic applications, Chemical Science. 2 (2011) 2243-2250.

[57] R.D.K. Misra, B. Girase, D. Depan, J.S. Shah, Hybrid nanoscale architecture for enhancement of antimicrobial activity: Immobilization of silver nanoparticles on thiol-functionalized polymer crystallized on carbon nanotubes, Advanced Engineering Materials. 14 (2012) B93-B100.

[58] P.-. Ma, N.A. Siddiqui, G. Marom, J.-. Kim, Dispersion and functionalization of carbon nanotubes for polymer-based nanocomposites: A review, Composites Part A: Applied Science and Manufacturing. 41 (2010) 1345-1367.

[59] W. Cheung, P.L. Chiu, R.R. Parajuli, Y. Ma, S.R. Ali, H. He, Fabrication of high performance conducting polymer nanocomposites for biosensors and flexible electronics: Summary of the multiple roles of DNA dispersed and functionalized single walled carbon nanotubes, Journal of Materials Chemistry. 19 (2009) 6465-6480.

[60] C. Hsueh, A. Brajter-Toth, Electrochemical preparation and analytical applications of ultrathin overoxidized polypyrrole films, Anal. Chem. 66 (1994) 2458-2463.

[61] J. Wang, P. Nien, C. Chen, L. Chen, K. Ho, A glucose bio-battery prototype based on a GDH/poly(methylene blue) bioanode and a graphite cathode with an iodide/tri-iodide redox couple, Bioresour. Technol. 116 (2012) 502-506.

[62] U. Yogeswaran, S. Chen, Electrocatalytic properties of electrodes which are functionalized with composite films of f-MWCNTs incorporated with poly(neutral red), J. Electrochem. Soc. 154 (2007) E178-E186.

[63] A. Liu, I. Honma, H. Zhou, Simultaneous voltammetric detection of dopamine and uric acid at their physiological level in the presence of ascorbic acid using poly(acrylic acid)-multiwalled carbon-nanotube composite-covered glassy-carbon electrode, Biosensors and Bioelectronics. 23 (2007) 74-80.

[64] A. Liu, T. Watanabe, I. Honma, J. Wang, H. Zhou, Effect of solution pH and ionic strength on the stability of poly(acrylic acid)-encapsulated multiwalled carbon nanotubes aqueous dispersion and its application for NADH sensor, Biosensors and Bioelectronics. 22 (2006) 694-699.

[65] D.P. Quan, D.P. Tuyen, T.D. Lam, P.T.N. Tram, N.H. Binh, P.H. Viet, Electrochemically selective determination of dopamine in the presence of ascorbic and uric acids on the surface of the modified Nafion/single wall carbon nanotube/poly(3-methylthiophene) glassy carbon electrodes, Colloids and Surfaces B: Biointerfaces. 88 (2011) 764-770.

[66] S. Daniel, T.P. Rao, K.S. Rao, S.U. Rani, G.R.K. Naidu, H.-. Lee, T. Kawai, A review of DNA functionalized/grafted carbon nanotubes and their characterization, Sensors and Actuators, B: Chemical. 122 (2007) 672-682.

[67] F. Patolsky, Y. Weizmann, I. Willner, Long-range electrical contacting of redox enzymes by SWCNT connectors, Angewandte Chemie - International Edition. 43 (2004) 2113-2117.

[68] Y. Guo, S. Guo, Y. Fang, S. Dong, Gold nanoparticle/carbon nanotube hybrids as an enhanced material for sensitive amperometric determination of tryptophan, Electrochim. Acta. 55 (2010) 3927-3931.

[69] C. Xue, R. Zhou, M. Shi, Y. Gao, G. Wu, X. Zhang, H. Chen, M. Wang, A green route to water soluble carbon nanotubes and in situ loading of silver nanoparticles, Nanotechnology. 19 (2008) 325605-325613.

[70] G. Wei, F. Xu, Z. Li, K.D. Jandt, Protein-promoted synthesis of Pt nanoparticles on carbon nanotubes for electrocatalytic nanohybrids with enhanced glucose sensing, Journal of Physical Chemistry C. 115 (2011) 11453-11460.

[71] C. Zhang, G. Wang, M. Liu, Y. Feng, Z. Zhang, B. Fang, A hydroxylamine electrochemical sensor based on electrodeposition of porous ZnO nanofilms onto carbon nanotubes films modified electrode, Electrochim. Acta. 55 (2010) 2835-2840.

[72] J. Yang, L. Jiang, W. Zhang, S. Gunasekaran, A highly sensitive non-enzymatic glucose sensor based on a simple two-step electrodeposition of cupric oxide (CuO) nanoparticles onto multi-walled carbon nanotube arrays, Talanta. 82 (2010) 25-33.

[73] F. Zhang, X. Wang, C. Li, X. Li, Q. Wan, Y. Xian, L. Jin, K. Yamamoto, Assay for uric acid level in rat striatum by a reagentless biosensor based on functionalized multi-wall carbon nanotubes with tin oxide, Analytical and Bioanalytical Chemistry. 382 (2005) 1368-1373.

[74] M. Shamsipur, M. Najafi, M. M. Hosseini, Highly improved electrooxidation of glucose at a nickel(II) oxide/multi-walled carbon nanotube modified glassy carbon electrode, Bioelectrochemistry. 77 (2010) 120-124.

[75] A. Braun, J. Tcherniac, Ãœber die Produkte der Einwirkung von Acetanhydrid auf Phthalamid, Ber. Dtsch. Chem. Ges. 40 (1907) 2709-2714.

[76] C.E. Dent, R.P. Linstead, 215. Phthalocyanines. Part IV. Copper phthalocyanines, Journal of the Chemical Society (Resumed). (1934) 1027.

[77] J. Robertson, 136. An *X*-ray study of the structure of the phthalocyanines. Part I. The metal-free, nickel, copper, and platinum compounds, Journal of the Chemical Society (Resumed). DOI: 10.1039/JR9350000615 (1935) 615-621.

[78] H. deDiesbach, E. Von der weid, Some complex salts of o- dinitrile with copper and pyridine Helvetica Chimica Acta. 10 (1927) 886.

[79] R. Christie, Colour Chemistry, The Royal Society of Chemistry, Cambridge CB4 0WF, UK, 2001.

[80] C.C. Leznoff, A.B.P. Lever, Phthalocyanines: Properties and Applications, (1989).

[81] G. Torre, C.G. Claessens, T. Torres, Phthalocyanines: old dyes, new materials. Putting color in nanotechnology, Chemical Communications. DOI: 10.1039/B614234F (Feature Article) (2007) 2000-2015.

[82] C.G. Claessens, U. Hahn, T. Torres, Phthalocyanines: From outstanding electronic properties to emerging applications, Chemical Record. 8 (2008) 75-97.

[83] S. Kumar, Chemistry of Discotic Liquid Crystals: From Monomers to Polymers, Taylor and Francis Group, LLC, USA, 2011.

[84] J. Brédas, D. Beljonne, V. Coropceanu, J. Cornil, Charge-transfer and energy-transfer processes in p-conjugated oligomers and polymers: A molecular picture, Chem. Rev. 104 (2004) 4971-5003.

[85] A.M. Van De Craats, J.M. Warman, Core-size effect on the mobility of charge in discotic liquid crystalline materials, Adv Mater. 13 (2001) 130-133.

[86] K. Ban, K. Nishizawa, K. Ohta, A.M. Van de Craats, J.M. Warman, I. Yamamoto, H. Shirai, Discotic liquid crystals of transition metal complexes 29: Mesomorphism and charge transport properties of alkylthio-substituted phthalocyanine rare-earth metal sandwich complexes, Journal of Materials Chemistry. 11 (2001) 321-331.

[87] S. Sergeyev, W. Pisula, Y.H. Geerts, Discotic liquid crystals: A new generation of organic semiconductors, Chem. Soc. Rev. 36 (2007) 1902-1929.

[88] T.V. Basova, A. Hassan, M. Durmus, A.G. Gurek, V. Ahsen, Orientation of the liquid crystalline nickel phthalocyanine films confined between electrodes, Synth. Met. 161 (2011) 1996-2000.

[89] P. Mineo, F. Lupo, I. Fragalà, E. Scamporrino, A. Gulino, Properties of uncharged water-soluble tetra(ω-methoxypolyethyleneoxy) phthalocyanine free base: Viable switching of the optical response by means of H_3O^+ ions, J. Lumin. 132 (2012) 409-413.

[90] S. Liu, W.M. Wang, A.L. Briseno, S.C.B. Mannsfeld, Z. Bao, Controlled deposition of crystalline organic semiconductors for field-effect-transistor applications, Adv Mater. 21 (2009) 1217-1232.

[91] G. Giancane, T. Basova, A. Hassan, G. Gümüş, A.G. Gürek, V. Ahsen, L. Valli, Investigations and application in piezoelectric phenol sensor of Langmuir-Schäfer films of a copper phthalocyanine derivative functionalized with bulky substituents, J. Colloid Interface Sci. 377 (2012) 176-183.

[92] A. Hassan, T. Basova, F. Yuksel, G. Gümüş, A.G. Gürek, V. Ahsen, Study of the interaction between simazine and metal-substituted phthalocyanines using spectral methods, Sensors and Actuators, B: Chemical. (2012).

[93] M.J. Jafari, M.E. Azim-Araghi, S. Barhemat, S. Riyazi, Effect of post-deposition annealing on surface morphology and gas sensing properties of palladium phthalocyanine thin films, Surf. Interface Anal. 44 (2012) 601-608.

[94] Y. Chen, Q. Wang, J. Chen, D. Ma, D. Yan, L. Wang, Organic semiconductor heterojunction as charge generation layer in tandem organic light-emitting diodes for high power efficiency, Organic Electronics: physics, materials, applications. 13 (2012) 1121-1128.

[95] T. Torres, D.M. Guldi, J.J. Cid, C.G. Claessens, M. Garcia-Iglesias, I. Lopez-Duarte, M. Martinez-Diaz, D. Mate, A. Medina, M. Rodriguez-Morgade, I. Sanchez, P. Vazquez, Phthalocyanines and subphthalocyanines for solar cell applications, ECS. 2 (2008) 1115.

[96] K. Onlaor, B. Tunhoo, P. Keeratithiwakorn, T. Thiwawong, J. Nukeaw, Electrical bistable properties of copper phthalocyanine at different deposition rates, Solid-State Electronics. 72 (2012) 60-66.

[97] J.F. Zhao, J. Wang, J. Chen, W. Chidawanykia, T. Nyokong, K. Ishii, N. Kobayashi, Gallium phthalocyanine photosensitizers: Carboxylation enhances the cellular uptake and improves the photodynamic therapy of cancers, Anti-Cancer Agents in Medicinal Chemistry. 12 (2012) 604-610.

[98] A. D'Amico, C. Di Natale, C. Falconi, E. Martinelli, R. Paolesse, G. Pennazza, M. Santonico, P.J. Sterk, Detection and identification of cancers by the electronic nose, Expert Opinion on Medical Diagnostics. 6 (2012) 175-185.

[99] T. Basova, P. Semyannikov, V. Plyashkevich, A. Hassan, I. Igumenov, Volatile phthalocyanines: Vapor pressure and thermodynamics, Critical Reviews in Solid State and Materials Sciences. 34 (2009) 180-189.

[100] S. Karan, B. Mallik, Thickness dependent surface electrical conductivity in copper (II) phthalocyanine thin films, Thin Solid Films. 520 (2012) 2343-2350.

[101] H.S. Soliman, A.A.M. Farag, N.M. Khosifan, M.M. El-Nahass, Electrical transport mechanisms and photovoltaic characterization of cobalt phthalocyanine on silicon heterojunctions, Thin Solid Films. 516 (2008) 8678-8683.

[102] S. Tuncel, H.A.J. Banimuslem, M. Durmuş, A.G. Gürek, V. Ahsen, T.V. Basova, A.K. Hassan, Liquid crystalline octasubstituted lead(ii) phthalocyanines: Effects of alkoxy and alkylthio substituents on film alignment and electrical properties, New Journal of Chemistry. 36 (2012) 1665-1672.

[103] T.V. Basova, M. Çamur, A.A. Esenpinar, S. Tuncel, A. Hassan, A. Alexeyev, H. Banimuslem, M. Durmu, A.G. Gürek, V. Ahsen, Effect of substituents on the orientation of octasubstituted copper(II) phthalocyanine thin films, Synth. Met. 162 (2012) 735-742.

[104] G. Cardenas-Jiron, P. Leon-Plata, D. Cortes-Arriagada, J.M. Seminario, Electrical characteristics of cobalt phthalocyanine complexes adsorbed on graphene, Journal of Physical Chemistry C. 115 (2011) 16052-16062.

[105] J.F. Van Der Pol, E. Neeleman, J.C. Van Miltenburg, J.W. Zwikker, R.J.M. Nolte, W. Drenth, A polymer with the mesomorphic order of liquid crystalline phthalocyanines, Macromolecules. 23 (1990) 155-162.

[106] J. Piris, M.G. Debije, N. Stutzmann, A.M. Van de Craats, M.D. Watson, K. Müllen, J.M. Warmam, Anisotropy in the Mobility and Photogeneration of Charge Carriers in Thin Films of Discotic Hexabenzocoronenes, Columnarly Self-Assembled on Friction-Deposited Poly(tetrafluoroethylene), Adv Mater. 15 (2003) 1736-1740.

[107] R.E. Hughes, S.P. Hart, D.A. Smith, B. Movaghar, R.J. Bushby, N. Boden, Exciton dynamics in a one-dimensional self-assembling lyòtropic discotic liquid crystal, J Phys Chem B. 106 (2002) 6638-6645.

[108] D. Atilla, A.G. Gurek, T.V. Basova, V.G. Kiselev, A. Hassan, L.A. Sheludyakova, V. Ahsen, The synthesis and characterization of novel mesomorphic octa- and tetra-alkylthio-substituted lead phthalocyanines and their films, Dyes and Pigments. 88 (2011) 280-289.

[109] A. Miyamoto, K. Nichogi, A. Taomoto, T. Nambu, M. Murakami, Structural control of evaporated lead-phthalocyanine films, Thin Solid Films. 256 (1995) 64-67.

[110] L. Ottaviano, L. Lozzi, A.R. Phani, A. Ciattoni, S. Santucci, S. Di Nardo, Thermally induced phase transition in crystalline lead phthalocyanine films investigated by XRD and atomic force microscopy, Appl. Surf. Sci. 136 (1998) 81-86.

[111] B. Mukherjee, A.K. Ray, A.K. Sharma, M.J. Cook, I. Chambrier, A simply constructed lead phthalocyanine memory diode, J. Appl. Phys. 103 (2008).

[112] L.V. Gregor, Electrical conductivity of polydivinylbenzene films, Thin Solid Films. 2 (1968) 235-246.

[113] M.H. Tang, Z.Q. Zeng, J.C. Li, Z.P. Wang, X.L. Xu, G.Y. Wang, L.B. Zhang, S.B. Yang, Y.G. Xiao, B. Jiang, Resistive switching behavior of La-doped ZnO films for nonvolatile memory applications, Solid-State Electronics. 63 (2011) 100-104.

[114] A. Beck, J.G. Bednorz, C. Gerber, C. Rossel, D. Widmer, Reproducible switching effect in thin oxide films for memory applications, Appl. Phys. Lett. 77 (2000) 139-141.

[115] B.J. Choi, D.S. Jeong, S.K. Kim, C. Rohde, S. Choi, J.H. Oh, H.J. Kim, C.S. Hwang, K. Szot, R. Waser, B. Reichenberg, S. Tiedke, Resistive switching mechanism of TiO 2 thin films grown by atomic-layer deposition, J. Appl. Phys. 98 (2005).

[116] T.V. Basova, A.G. Gürek, D. Atilla, A.K. Hassan, V. Ahsen, Synthesis and characterization of new mesomorphic octakis(alkylthio)-substituted lead phthalocyanines and their films, Polyhedron. 26 (2007) 5045-5052.

[117] K. Kadish, K. Smith, R. Guilard, The Porphyrin Handbook,Vol.7, theoritical and physical characterisation, Academic Press USA. 2000.

[118] C.C. Leznoff, A.B.P. Lever, Phthalocyanine: Properties and Applications, VCH Publishers (LSK)Ltd: cambridge, 1989, 1993, 1996.

[119] K. Ishii, N. Kobayashi, K. Kadish, K. Smith, R. Guilard, The Porphyrin Handbook, Elsevier Science, New York. (2003).

[120] M. Stillman, T. Nyokong, Phthalocyanines: Properties and Applications, VCH, NEW York, Vol. I. (1989).

[121] T. Rawling, A. McDonagh, Ruthenium phthalocyanine and naphthalocyanine complexes: Synthesis, properties and applications, Coord. Chem. Rev. 251 (2007) 1128-1157.

[122] C.C. Leznoff, L.S. Black, A. Hiebert, P.W. Causey, D. Christendat, A.B.P. Lever, Red manganese phthalocyanines from highly hindered hexadecaalkoxyphthalocyanines, Inorg. Chim. Acta. 359 (2006) 2690-2699.

[123] T. Fukuda, S. Homma, N. Kobayashi, Deformed phthalocyanines: Synthesis and characterization of zinc phthalocyanines bearing phenyl substituents at the 1-, 4-, 8-, 11-, 15-, 18-, 22-, and/or 25-positions, Chemistry - A European Journal. 11 (2005) 5205-5216.

[124] Y. Chen, M. Hanack, W.J. Blau, D. Dini, Y. Liu, Y. Lin, J. Bai, Soluble axially substituted phthalocyanines: Synthesis and nonlinear optical response, J. Mater. Sci. 41 (2006) 2169-2185.

[125] M.J. Cook, M.J. Heeney, Phthalocyaninodehydroannulenes, Chemistry - A European Journal. 6 (2000) 3958-3967.

[126] G. Bottari, J.A. Suanzes, O. Trukhina, T. Torres, Phthalocyanine-carbon nanostructure materials assembled through supramolecular interactions, Journal of Physical Chemistry Letters. 2 (2011) 905-913.

[127] F.J.M. Hoeben, P. Jonkheijm, E.W. Meijer, A.P.H.J. Schenning, About supramolecular assemblies of p-conjugated systems, Chem. Rev. 105 (2005) 1491-1546.

[128] U. Hahn, S. Engmann, C. Oelsner, C. Ehli, D.M. Guldi, T. Torres, Immobilizing water-soluble dendritic electron donors and electron acceptors - Phthalocyanines and perylenediimides - Onto single wall carbon nanotubes, J. Am. Chem. Soc. 132 (2010) 6392-6401.

[129] L. Lozzi, S. Santucci, F. Bussolotti, S. La Rosa, Investigation on copper phthalocyanine/multiwalled carbon nanotube interface, J. Appl. Phys. 104 (2008).

[130] R.A. Hatton, N.P. Blanchard, V. Stolojan, A.J. Miller, S.R. Silva, Nanostructured copper phthalocyanine-sensitized multiwall carbon nanotube films, Langmuir. 23 (2007) 6424-6430.

[131] B. Ballesteros, S. Campidelli, G. De La Torre, C. Ehli, D.M. Guldi, M. Prato, T. Torres, Synthesis, characterization and photophysical properties of a SWNT-phthalocyanine hybrid, Chemical Communications. 28 (2007) 2950-2952.

[132] B. Ballesteros, G. De La Torre, C. Ehli, G.M.A. Rahman, F. Agulló-Rueda, D.M. Guidi, T. Torres, Single-wall carbon nanotubes bearing covalently linked phthalocyanines - Photoinduced electron transfer, J. Am. Chem. Soc. 129 (2007) 5061-5068.

[133] T. Mugadza, T. Nyokong, Covalent linking of ethylene amine functionalized single-walled carbon nanotubes to cobalt (II) tetracarboxyl-phthalocyanines for use in electrocatalysis, Synth. Met. 160 (2010) 2089-2098.

[134] T. Mugadza, T. Nyokong, Synthesis and characterization of electrocatalytic conjugates of tetraamino cobalt (II) phthalocyanine and single wall carbon nanotubes, Electrochim. Acta. 54 (2009) 6347-6353.

[135] M. Shah, Z. Ahmad, K. Sulaiman, K.S. Karimov, M.H. Sayyad, Carbon nanotubes' nanocomposite in humidity sensors, Solid-State Electronics. 69 (2012) 18-21.

[136] Y. Ji, Y.Y. Huang, E.M. Terentjev, Dissolving and aligning carbon nanotubes in thermotropic liquid crystals, Langmuir. 27 (2011) 13254-13260.

[137] A.L. Verma, S. Saxena, G.S.S. Saini, V. Gaur, V.K. Jain, Hydrogen peroxide vapor sensor using metal-phthalocyanine functionalized carbon nanotubes, Thin Solid Films. 519 (2011) 8144-8148.

[138] X. Wang, Y. Liu, W. Qiu, D. Zhu, Immobilization of tetra-tert-butylphthalocyanines on carbon nanotubes: A first step towards the development of new nanomaterials, Journal of Materials Chemistry. 12 (2002) 1636-1639.

[139] N. He, Y. Chen, J. Bai, J. Wang, W.J. Blau, J. Zhu, Preparation and optical limiting properties of multiwalled carbon nanotubes with -conjugated metal-free phthalocyanine moieties, Journal of Physical Chemistry C. 113 (2009) 13029-13035.

[140] A.A. Mamedov, N.A. Kotov, M. Prato, D.M. Guldi, J.P. Wicksted, A. Hirsch, Molecular design of strong single-wall carbon nanotube/polyelectrolyte multilayer composites, Nature Materials. 1 (2002) 190-194.

[141] A.B. Dalton, S. Collins, E. Muñoz, J.M. Razal, V.H. Ebron, J.P. Ferraris, J.N. Coleman, B.G. Kim, R.H. Baughman, Super-tough carbon-nanotube fibres, Nature. 423 (2003) 703.

[142] D.C. Sorescu, K.D. Jordan, P. Avouris, Theoretical study of oxygen adsorption on graphite and the (8,0) single-walled carbon nanotube, J Phys Chem B. 105 (2001) 11227-11232.

[143] I. Dierking, S.E. San, Magnetically steered liquid crystal-nanotube switch, Appl. Phys. Lett. 87 (2005) 1-3.

[144] I. Dierking, G. Scalia, P. Morales, D. LeClere, Aligning and reorienting carbon nanotubes with nematic liquid crystals, Adv Mater. 16 (2004) 865-869.

[145] N. Kilinc, A.S. Ahsen, D. Atilla, A.G. Gurek, S.E. San, Z.Z. Ozturk, V. Ahsen, Electrical properties of mesomorphic phthalocyanine-carbon nanotube composites, Sensor. Lett. 6 (2008) 607-612.

[146] J.B. Brito, D.J.C. Gomes, V.D. Justina, A.M.F. Lima, C.A. Olivati, J.R. Silva, N.C. de Souza, Nanostructured films from phthalocyanine and carbon nanotubes: Surface morphology and electrical characterization, J. Colloid Interface Sci. 367 (2012) 467-471.

[147] B.S. Shim, Z. Tang, M.P. Morabito, A. Agarwal, H. Hong, N.A. Kotov, Integration of conductivity, transparency, and mechanical strength into highly homogeneous layer-by-layer composites of single-walled carbon nanotubes for optoelectronics, Chemistry of Materials. 19 (2007) 5467-5474.

[148] I. Adebayo Akinbulu, T. Nyokong, Fabrication and characterization of single walled carbon nanotubes-iron phthalocyanine nano-composite: Surface properties and electron transport dynamics of its self assembled monolayer film, New Journal of Chemistry. 34 (2010) 2875-2886.

[149] W. Feng, Y. Li, Y. Feng, J. Wu, Enhanced photoresponse from the orderedmicrostructure of naphthalocyanine-carbon nanotube composite film, Nanotechnology. 17 (2006) 3274-3279.

[150] Z. Yang, H. Pu, J. Yuan, D. Wan, Y. Liu, Phthalocyanines-MWCNT hybrid materials: Fabrication, aggregation and photoconductivity properties improvement, Chemical Physics Letters. 465 (2008) 73-77.

[151] F. Aziz, K. Sulaiman, K.S. Karimov, M.R. Muhammad, M.H. Sayyad, B.Y. Majlis, Investigation of optical and humidity-sensing properties of vanadyl phthalocyanine-derivative thin films, Molecular Crystals and Liquid Crystals. 566 (2012) 22-32.

[152] D.D. Erbahar, I. Gürol, G. Gümüş, E. Musluoglu, Z.Z. Öztürk, V. Ahsen, M. Harbeck, Pesticide sensing in water with phthalocyanine based QCM sensors, Sensors and Actuators, B: Chemical. 173 (2012) 562-568.

[153] N. Kilinç, S. Öztürk, D. Atilla, A.G. Gürek, V. Ahsen, Z.Z. Öztürk, Electrical and NO_2 sensing properties of liquid crystalline phthalocyanine thin films, Sensors and Actuators, B: Chemical. 173 (2012) 203-210.

[154] A. Singh, S. Samanta, A. Kumar, A.K. Debnath, R. Prasad, P. Veerender, V. Balouria, D.K. Aswal, S.K. Gupta, Implication of molecular orientation on charge transport and gas sensing characteristics of cobalt-phthalocyanine thin films, Organic Electronics: physics, materials, applications. 13 (2012) 2600-2604.

[155] D.C. Tiwari, R. Sharma, K.D. Vyas, M. Boopathi, V.V. Singh, P. Pandey, Electrochemical incorporation of copper phthalocyanine in conducting polypyrrole for the sensing of DMMP, Sensors and Actuators, B: Chemical. 151 (2010) 256-264.

[156] S. Singh, S.K. Tripathi, G.S.S. Saini, Optical and infrared spectroscopic studies of chemical sensing by copper phthalocyanine thin films, Mater. Chem. Phys. 112 (2008) 793-797.

[157] A. Altindal, Z.Z. Öztürk, S. Dabak, O. Bekaroğlu, Halogen sensing using thin films of crosswise-substituted phthalocyanines, Sensors and Actuators, B: Chemical. 77 (2001) 389-394.

[158] T. Basova, E. Kol'tsov, A.K. Ray, A.K. Hassan, A.G. Gurek, V. Ahsen, Liquid crystalline phthalocyanine spun films for organic vapour sensing, Sensors and Actuators, B: Chemical. 113 (2006) 127-134.

[159] T. Basova, A. Tsargorodskaya, A. Nabok, A.K. Hassan, A.G. Gurek, G. Gumus, V. Ahsen, Investigation of gas-sensing properties of copper phthalocyanine films, Materials Science and Engineering C. 29 (2009) 814-818.

[160] G. De La Torre, C.G. Claessens, T. Torres, Phthalocyanines: Old dyes, new materials. Putting color in nanotechnology, Chemical Communications. (2007) 2000-2015.

[161] A. Hassan, T. Basova, S. Tuncel, F. Yuksel, A.G. Gürek, V. Ahsen, Phthalocyanine films as active layers of optical sensors for pentachlorophenol and simazine detection, Procedia Engineering. 25 (2011) 272-275.

[162] M.P. Siswana, K.I. Ozoemena, T. Nyokong, Electrocatalysis of asulam on cobalt phthalocyanine modified multi-walled carbon nanotubes immobilized on a basal plane pyrolytic graphite electrode, Electrochim. Acta. 52 (2006) 114-122.

[163] J. Pillay, K.I. Ozoemena, Single-walled carbon nanotube-induced crystallinity on the electropolymeric film of tetraaminophthalocyaninatonickel(II) complex: Impact on the rate of heterogeneous electron transfer, Chemical Physics Letters. 441 (2007) 72-77.

[164] J. Francisco Silva, S. Griveau, C. Richard, J.H. Zagal, F. Bedioui, Glassy carbon electrodes modified with single walled carbon nanotubes and cobalt phthalocyanine and nickel tetrasulfonated phthalocyanine: Highly stable new hybrids with enhanced electrocatalytic performances, Electrochemistry Communications. 9 (2007) 1629-1634.

[165] K.I. Ozoemena, D. Nkosi, J. Pillay, Influence of solution pH on the electron transport of the self-assembled nanoarrays of single-walled carbon nanotube-cobalt tetra-aminophthalocyanine on gold electrodes: Electrocatalytic detection of epinephrine, Electrochim. Acta. 53 (2008) 2844-2851.

[166] J. Liu, Y. Wang, Z. Qu, X. Fan, 2 μm passive Q-switched mode-locked Tm 3+:YAP laser with single-walled carbon nanotube absorber, Opt. Laser Technol. 44 (2012) 960-962.

[167] Y. Wang, N. Hu, Z. Zhou, D. Xu, Z. Wang, Z. Yang, H. Wei, E.S. Kong, Y. Zhang, Single-walled carbon nanotube/cobalt phthalocyanine derivative hybrid material: Preparation, characterization and its gas sensing properties, Journal of Materials Chemistry. 21 (2011) 3779-3787.

[168] T.A. Temofonte, K.F. Schoch, Phthalocyanine semiconductor sensors for room-temperature ppb level detection of toxic gases, J. Appl. Phys. 65 (1989) 1350-1355.

[169] M.R. Tarasevich, V.S. Tyurin, K.A. Radyushkina, Electrochemical reactions of sulfur dioxide on organic complexes in aqueous solutions and a sensor for assaying sulfur dioxide, Russian J. Electrochem. 35 (1999) 366-369.

[170] S. Maldonado, E. García-Berríos, M.D. Woodka, B.S. Brunschwig, N.S. Lewis, Detection of organic vapors and NH3(g) using thin-film carbon black-metallophthalocyanine composite chemiresistors, Sensors and Actuators, B: Chemical. 134 (2008) 521-531.

[171] S. Singh, G.S.S. Saini, S.K. Tripathi, Effect of chemical on conductivity of iron phthalocyanine pyridine thin films, AIP Conference Proceedings. 1393 (2011) 333-334.

[172] X. Zuo, N. Li, H. Zhang, Direct electrochemical determination of ascorbic acid by a cobalt(II) tetra-neopentyloxy phthalocyanine-multi-walled carbon nanotubes glassy carbon electrode, J. Mater. Sci. 47 (2012) 2731-2735.

[173] T. Mugadza, Y. Arslanolu, T. Nyokong, Characterization of 2,(3)-tetra-(4-oxo-benzamide) phthalocyaninato cobalt (II) - Single walled carbon nanotube conjugate platforms and their use in electrocatalysis of amitrole, Electrochim. Acta. 68 (2012) 44-51.

[174] F.C. Moraes, L.H. Mascaro, S.A.S. Machado, C.M.A. Brett, Direct electrochemical determination of glyphosate at copper phthalocyanine/multiwalled carbon nanotube film electrodes, Electroanalysis. 22 (2010) 1586-1591.

[175] A.N. Ivanov, R.R. Younusov, G.A. Evtugyn, F. Arduini, D. Moscone, G. Palleschi, Acetylcholinesterase biosensor based on single-walled carbon nanotubes - Co phtalocyanine for organophosphorus pesticides detection, Talanta. 85 (2011) 216-221.

[176] M.P. Siswana, K.I. Ozocmcna, D.A. Geraldo, T. Nvokong, Nanostructured nickel (II) phthalocyanine-MWCNTs as viable nanoeomposite platform for electrocatalvtic detection of asulam pesticide at neutral pH conditions, Journal of Solid State Electrochemistry. 14 (2010) 1351-1358.

[177] I. Cesarino, F.C. Moraes, T.C.R. Ferreira, M.R.V. Lanza, S.A.S. MacHado, Real-time electrochemical determination of phenolic compounds after benzene oxidation, J Electroanal Chem. 672 (2012) 34-39.

[178] F.C. Moraes, D.L.C. Golinelli, L.H. Mascaro, S.A.S. MacHado, Determination of epinephrine in urine using multi-walled carbon nanotube modified with cobalt phthalocyanine in a paraffin composite electrode, Sensors and Actuators, B: Chemical. 148 (2010) 492-497.

[179] M. Mattarozzi, F. Lambertini, M. Suman, M. Careri, Liquid chromatography-full scan-high resolution mass spectrometry-based method towards the comprehensive analysis of migration of primary aromatic amines from food packaging, Journal of Chromatography A. 1320 (2013) 96-102.

[180] H. Pan, X. Zeng, B. Zhu, L. He, T. Liao, W. Zhe, S. Wang, B. Jiang, M. Wang, Determination of biogenic amines in cheese by nanofiber solid phase extraction-reversed phase high performance liquid chromatography with pre-column derivatization, Journal of Food, Agriculture and Environment. 11 (2013) 115-118.

[181] I.G. Casella, M. Gatta, E. Desimoni, Determination of histamine by high-pH anion-exchange chromatography with electrochemical detection, Food Chem. 73 (2001) 367-372.

[182] R. Ziólkowski, L. Górski, P. Prokaryn, M. Zaborowski, A. Kutyla-Olesiuk, P. Ciosek, W. Wróblewski, E. Malinowska, Development of silicon-based electrochemical transducers, Analytical Methods. 5 (2013) 5464-5470.

[183] X. Wang, S. Reisberg, N. Serradji, G. Anquetin, M.-. Pham, W. Wu, C.-. Dong, B. Piro, E-assay concept: Detection of bisphenol A with a label-free electrochemical competitive immunoassay, Biosensors and Bioelectronics. 53 (2014) 214-219.

[184] J.H. Chen, X. Zhang, S. Cai, D. Wu, J. Lin, C. Li, J. Zhang, Label-free electrochemical biosensor using home-made 10-methyl-3-nitro-acridone as indicator for picomolar detection of nuclear factor kappa B, Biosensors and Bioelectronics. 53 (2014) 12-17.

[185] J. Kang, A.T. Hussain, M. Catt, M. Trenell, B. Haggett, E.H. Yu, Electrochemical detection of non-esterified fatty acid by layer-by-layer assembled enzyme electrodes, Sensors and Actuators, B: Chemical. 190 (2014) 535-541.

[186] C. Liu, W. Lu, Optical amine sensor based on metallophthalocyanine, J Chin Inst Chem Eng. 38 (2007) 483-488.

[187] H. Arwin, Is ellipsometry suitable for sensor applications? Sensors Actuators A Phys. 92 (2001) 43-51.

[188] S. Zeng, D. Baillargeat, H. Ho, K. Yong, Nanomaterials enhanced surface plasmon resonance for biological and chemical sensing applications, Chem. Soc. Rev. 43 (2014) 3426-3452.

[189] T. Mutschler, B. Kieser, R. Frank, G. Gauglitz, Characterization of thin polymer and biopolymer layers by ellipsometry and evanescent field technology, Analytical and Bioanalytical Chemistry. 374 (2002) 658-664.

[190] S. Yukioka, T. Inoue, Ellipsometric analysis on the in situ reactive compatibilization of immiscible polymer blends, Polymer. 35 (1994) 1182-1186.

[191] S. Lee, K. Lee, J. Hong, Evidence for spin coating electrostatic self-assembly of polyelectrolytes, Langmuir. 19 (2003) 7592-7596.

[192] M.A. Hempenius, M. Péter, N.S. Robins, E.S. Kooij, G.J. Vancso, Water-soluble poly (ferrocenylsilanes) for supramolecular assemblies by layer-by-layer deposition, Langmuir. 18 (2002) 7629-7634.

[193] A.V. Nabok, N.V. Lavrik, Z.I. Kazantseva, B.A. Nesterenko, L.N. Markovskiy, V.I. Kalchenko, A.N. Shivaniuk, Complexing properties of calix[4]resorcinolarene LB films, Thin Solid Films. 259 (1995) 244-247.

[194] P. Alliprandini Filho, G.G. Dalkiranis, R.A.S.Z. Armond, E.M. Therézio, I.H. Bechtold, A.A. Vieira, R. Cristiano, H. Gallardo, A. Marletta, O.N. Oliveira, Emission ellipsometry used to probe aggregation of the luminescent 2,1,3-benzothiadiazole dyes and ordering in an E7 liquid crystal matrix, Physical Chemistry Chemical Physics. 16 (2014) 2892-2896.

[195] R.P. Richter, K.B. Rodenhausen, N.B. Eisele, M. Schubert, Coupling Spectroscopic Ellipsometry and Quartz Crystal Microbalance to Study Organic Films at the Solid-Liquid Interface, Springer Series in Surface Sciences. 52 (2014) 223-248.

[196] A. Nabok, A. Tsargorodskaya, The method of total internal reflection ellipsometry for thin film characterisation and sensing, Thin Solid Films. 516 (2008) 8993-9001.

[197] P. Westphal, A. Bornmann, Biomolecular detection by surface plasmon enhanced ellipsometry, Sensors and Actuators, B: Chemical. 84 (2002) 278-282.

[198] H. Arwin, M. Poksinski, K. Johansen, Total internal reflection ellipsometry: Principles and applications, Appl. Opt. 43 (2004) 3028-3036.

[199] M. Poksinski, H. Arwin, Protein monolayers monitored by internal reflection ellipsometry, Thin Solid Films. 455-456 (2004) 716-721.

[200] M. Poksinski, H. Dzuho, H. Arwin, Copper corrosion monitoring with total internal reflection ellipsometry, J. Electrochem. Soc. 150 (2003) B536-B539.

[201] P. Westphal, A. Bornmann, Biomolecular detection by surface plasmon enhanced ellipsometry, Sensors and Actuators, B: Chemical. 84 (2002) 278-282.

[202] E. Llobet, Gas sensors using carbon nanomaterials: A review, Sensors and Actuators, B: Chemical. 179 (2013) 32-45.

[203] H. Fujiwara, Spectroscopic Ellipsometry: Principles and Applications, John Wiley & Sons, 2007.

[204] J A Woollam Co. Inc, Guide to using WVASE32, Software for Spectroscopic Ellipsometry Data Acquisition and Analysis. Wex Tech Systems Inc., new york, 2001.

Chapter 3

Experimental Details

Chapter overview

In this chapter experimental procedures and measurement techniques used throughout this study are described in sufficient details. First experimental methods used in this study are described with further emphasis placed on Total Internal Reflection Ellipsometry (TIRE) as the optical detection method employed in the study of interaction between several chemical analytes and MPc/SWCNTs hybrid films. Materials under investigation, mainly novel substituted metal phthalocyanines (MPcs) and commercially purchased single-walled carbon nanotubes (SWCNTs) and the methods applied to produce thin films for application in optical detection are fully described.

3.1 Experimental techniques

In this study significant work was carried out using TIRE as the main method to study the interaction of a range of chemical pollutants with the sensing MPc/SWCNTs hybrid layers prepared in this work. UV-Visible spectroscopy, Fourier Transform Infrared (FTIR) and Raman Spectroscopy have been used for films' optical characterisation. Morphology measurements have been carried out using Atomic Force Microscopy (AFM) and Scanning Electron Microscopy (SEM). DC electrical measurements on films were performed using Semiconductor Characterisation System (Keithly 4200). These methods are described in sections 3.1.1-3.1.7.

3.1.1 Total Internal Reflection Ellipsometry (TIRE)

3.1.1.1 Theoretical background

A comprehensive theoretical background on ellipsometry in general is presented in chapter 2. TIRE employs a prism coupler technique which combines the advantages of spectroscopic ellipsometry and the experimental convenience of surface plasmon resonsnace (SPR) based on Kretschmann's configuration [1]. The angle of incidence between the incident polarised light beam and the prism is selected such that it is close to the angle of total internal reflection, which is determined by the nature of media used. This angle determines the use of the appropriate prism, and it can be calculated by the following relation [1];

$$\theta = \arcsin\left[\frac{1}{N_1}\sqrt{\frac{\varepsilon_m N_2^{\,2}}{\varepsilon_m + N_2^{\,2}}}\right] \qquad (3.1)$$

where N_1 and N_2 are the complex refractive indices of glass and dielectric film respectively, ε_m is the real part of dielectric constant of metal film.

In contrast to the conventional sensing analytical tool of SPR based upon monitoring the intensity of reflected p-polarised light, the TIRE method detects two ellipsometric parameters ψ and Δ which are related, respectively, to the amplitude

ratio and the phase shift of the p and s components of polarised light. Basically, the more light interacts with the sample, the more accurate the measurements.

The spectra of two ellipsometric parameters ψ and Δ, representing, respectively, the amplitude ratio $tg(\psi) = A_p / A_s$ and phase shift $\Delta = \varphi_p - \varphi_s$ between the p and s components of polarised light, were recorded with the M2000V instrument in the 350–1000nm spectral range using the rotating analyzer principle. The typical ψ and Δ spectra from a single spectroscopic measurement are shown in Figure 3.1. The ψ spectrum resembles typical SPR spectra with the maximum intensity corresponding to the conditions of total internal reflection while the minimum is due to surface plasmon resonance. At the same time, the Δ spectrum experiences a sharp drop from 270° to 90° near the plasmon resonance. From the spectra given in Figure 3.1 it is quite obvious that Δ spectrum is more sensitive than ψ spectrum to small variations in films' optical constants and/or their thickness caused by molecular binding. The comparison of ψ and Δ spectra for TIRE in different media shows that TIRE is about 10 times more sensitive towards changes in both, thickness d and refractive index, n of thin films as compared to conventional ellipsometry [2].

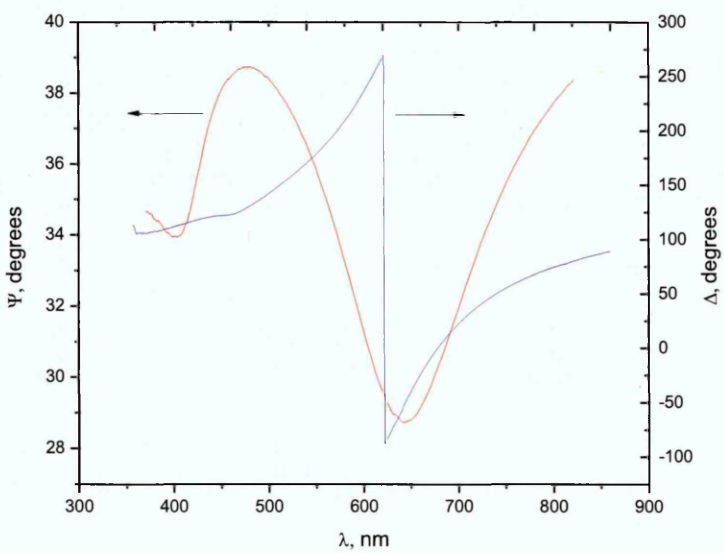

Figure 3.1: TIRE single spectroscopic spectra

Optical parameters of the reflection system, i.e. thicknesses, refractive indices and extinction coefficients of the substrate and adsorbed layers, can be obtained by solving the reverse ellipsometric problem numerically:

$$tg(\psi)\exp(i\Delta) = {R_p}/{R_s} \qquad (3.2)$$

where R_p and R_s are Fresnel reflection coefficients for the p and s components of polarised light related to the parameters of reflection system, particularly the thickness (*d*) and refractive index (*n*) of the adsorbed layers, via Fresnel equations [3].

3.1.1.2 TIRE experimental set-up

The TIRE experiment setup used in the current study is based on the commercial M2000 J. A. Woollam Spectroscopic Ellipsometry operating in 350–1000 nm spectral range and exploiting the rotating compensator principle (Figure 3.2 (a)).

In order to use the instrument as a sensor operating in liquid or gaseous media, a special 200µl volume TIRE cell, constructed from polytetrafluoroethylene (PTFE) material, was used. A silicon O-ring was used to seal the gold-coated glass slide against the cell, as shown in Figure 3.2 (b). The cell contains inlet and outlet tubes to allow injection of different gases or liquids into the cell in order to perform different chemical interactions with hybrid films.

Another key element of TIRE is the glass prism, which couples the light beam into a thin gold film. Figure 3.2 (c) shows the TIRE cell with a 68° prism attached to the J. A. Woollam sample stage. The choice of the 68° prism was made to provide the condition of total internal reflection on a glass–water interface. For gas detection experiments a 45° prism has been used instead. A gold (Au)-coated glass slide was brought into optical contact with the prism via index matching liquid to exclude the presence of an air gap.

Other elements of the TIR set-up are explained in a schematic diagram of TIRE presented in Figure 3.3. The set-up comprises a white light source (1), monochromator (2), polarizer (3), analyzer (4) and a photodetector array (5). Elements 6–9 were fixed on the ellipsometer sample stage using vacuum suction [2,4].

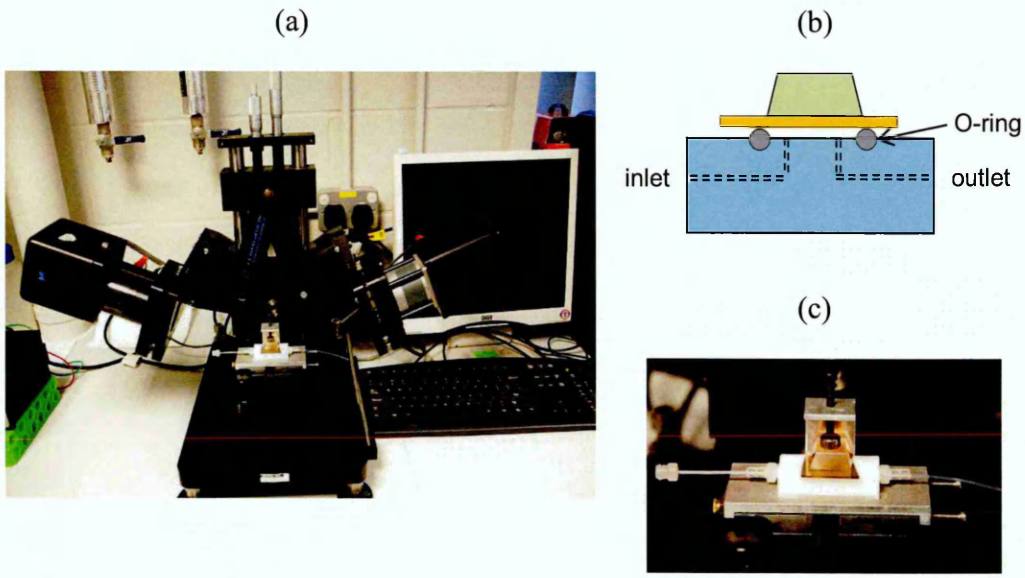

Figure 3.2: (a) J.A.Woollam M2000 Ellipsometer (b) A home-made TIRE cell (c) an image showing zoomed-in TIRE cell attached to the prism on ellipsometer stage.

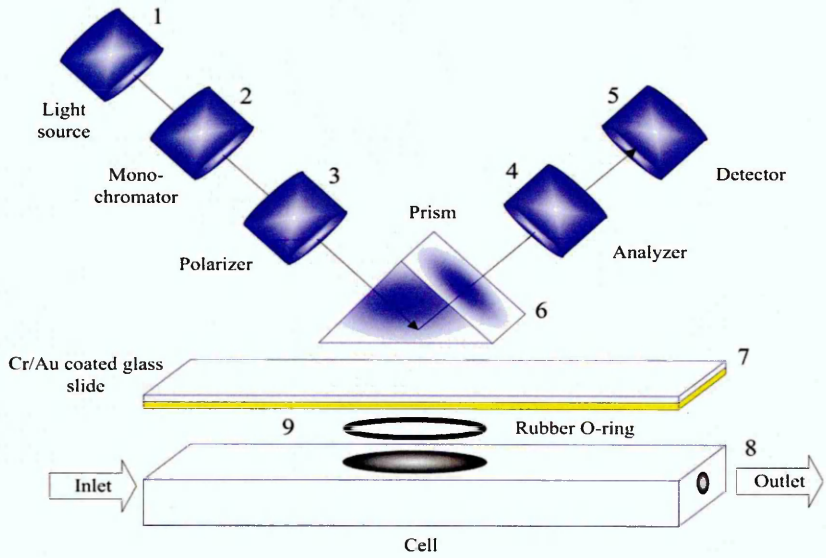

Figure 3.3: A schematic diagram illustrating the total internal reflection ellipsometry experimental set-up.

3.1.1.3 Experimental data fitting

In order to determine the films' thickness as well as its optical constants, data fitting is performed on the measured ψ and Δ spectra by solving Fresnel equations many times for different values of n and d and subsequently minimizing the error function of the experimental and theoretical (calculated) values of ψ and Δ using one of least-square techniques. Commercial WVASE32® software is provided by J.A. Woollam Co., Inc. for this task.

Data processing requires building an optical model, which corresponds to the sample under investigation. Dielectric functions of some layers (namely; BK7 glass, gold, water or gas) are known and can be selected from the WVASE software library [5]. Parameters of unknown layers (i.e. thickness and dispersion of n and k) can be found by fitting the experimental data to the model layer which can be selected from the WVASE library. The most common model for adsorbed molecular layers is Cauchy.

Figure 3.4 shows the TIRE measurement protocol, which typically starts with a single spectroscopic scan of the sample of a bare gold film in water or fresh air to obtain the effective thickness and dispersion curves for optical parameters $n(\lambda)$ and $k(\lambda)$ of the chromium-gold layer (a thin chromium adhesion layer, typically 3-5nm, is first deposited on the glass slide to minimise gold film delamination). A three-layer model consisting of ambient (BK7 glass), gold, and fluid (water or gas) was used, where the parameters for glass and fluid are fixed but the thickness and optical constants of the metal layer are varied. The dispersion spectra of $n(\lambda)$ and $k(\lambda)$ as well as the thickness of evaporated gold layer were taken as initial guess values. The effective parameters for the Cr/Au layer obtained by fitting for that particular sample were then used as fixed parameters for further fitting of data obtained on the same sample.

Ellipsometry data fitting requires a great deal of experience and the outcomes depend on the selection of a physically adequate model as well as the choice of initial parameter fitting routine, i.e. the use of 'normal fit', or 'point by point fit' option, limiting the range of variable parameters, and removing 'anomalous' data points, and so. In order to achieve reliable results, the fitting procedure needs to be repeated several times (preferably from different initial conditions) until consistent values of

thickness (d), refractive index (n) and extinction coefficient (k) are achieved. In some cases a good fit cannot be achieved due to the following reasons [6]:

(i) the measurements of (Ψ, Δ) spectra are inaccurate.

(ii) inappropriate functions selected in data analysis

(iii) the optical model applied for data analysis is not suitable, and

(iv) depolarization effect from the sample

3.1.2 UV-Visible Absorption Spectroscopy

3.1.2.1 Theoretical background

UV-Vis absorption spectroscopy is the measurement of light absorption by a sample in the ultraviolet-visible spectral region of the electromagnetic spectrum. This absorption or attenuation can occur when light passes through a translucent liquid sample, or when light is reflected from a sample surface. The difference in the incident light and the transmitted light is used to determine the actual absorbance. When an atom or molecule absorbs energy, electrons are promoted from their ground state to an excited state. Molecules can only absorb radiant energy in definite units, or quanta, which correspond to the energy difference between the ground and excited states. The energy, E, carried by any one quantum is proportional to its frequency of oscillation, that is:

$$E = h\vartheta = {}^{hc}/_{\lambda} \qquad (3.3)$$

where ϑ is the frequency, λ is the related wavelength and h is Plank's constant (6.626×10^{-34} m^2.kg/s).

In addition to electronic excitation, the atoms within a molecule can rotate and vibrate with respect to each other. These vibrations and rotations also have discrete energy levels, which can be considered as being packed on top of each electronic level.

Experimental Measurements

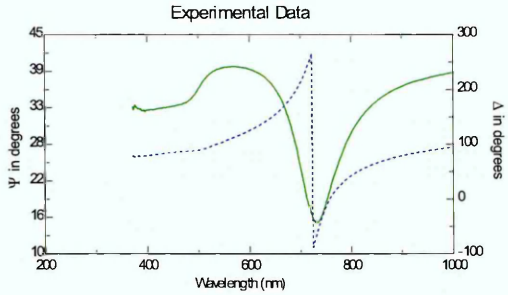

Creating a Model

Estimation for the layers' thicknesses

AMBIENT: bk7		
2	au-cr-nk	25.000 nm
1	cauchy	0.000 nm
0	my-water-fit	1 mm

Data Generation and Fitting

Repeating the model estimated data and fitting enhances the results

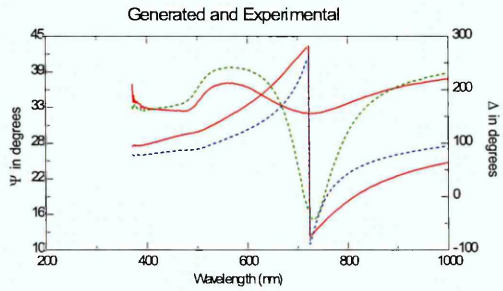

Results

Close fit between theoretical and experimental

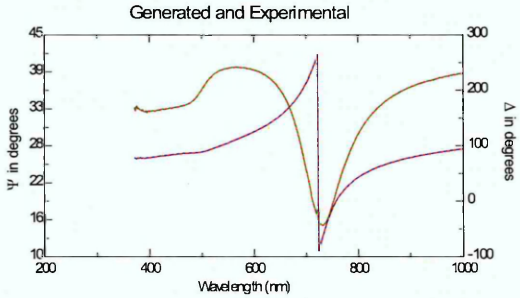

Results

The actual data

AMBIENT: bk7		
2	au-cr-nk	29.439 nm
1	cauchy	0.000 nm
0	my-water-fit	1 mm

Figure 3.4: A flow chart summarising TIRE experimental procedure

Absorption of ultraviolet and visible radiation in organic molecules is restricted to certain functional groups (chromophores) that contain valence electrons of low excitation energy. The spectrum of a molecule containing these chromophores is complex as the superposition of atomic rotational and vibrational transitions on the electronic transitions gives a combination of overlapping lines. This appears as a continuous absorption band [7].

The UV-Visible spectral region is divided into three sub-domains termed near UV (185-400 nm), visible (400-700 nm) and near infrared (700-1100 nm). Most commercial spectrophotometers cover the spectral range between 185 to 900 nm. The principle of absorption is the interaction of ions or molecules of the sample with the photons of an incident beam produced by a source. When a molecule interacts with a photon, this photon is absorbed and one or more of the molecule's outer electrons will capture its energy. Consequently, total electronic energy increases and promotion of an electron from a higher occupied molecular orbital (HOMO) to a lower unoccupied molecular orbital (LUMO) takes place. The electronic transitions of organic compounds represent the majority of studies made in the UV-Vis. The observed transitions involve electrons engaged in σ, π or non-bonding n electron orbitals which might happen according to transitions explained in Figure 3.5.

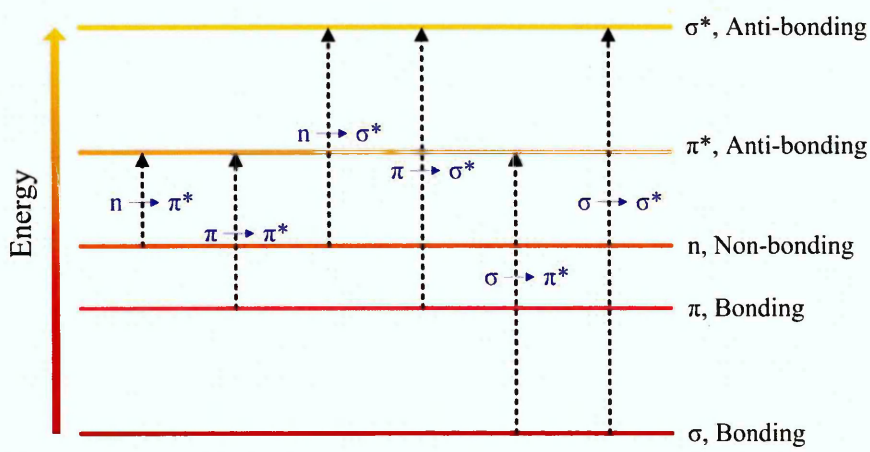

Figure 3.5: Possible electronic transitions in organic materials

3.1.2.2 Instrumentation

UV-Visible absorption spectra have been recorded on Varian 50 scan UV-Visible spectrophotometer. A spectrophotometer is designed around three fundamental parts: the source, the monochromater, which constitute the optical section and the detection system (Figure 3.6). These components are typically integrated in a unique framework to make spectrometers [8,9].

All the samples have been measured in the form of solution. First, the cuvette has been washed and filled with solvent to measure the baseline. The cuvette then was filled with the sample solution to record the spectra.

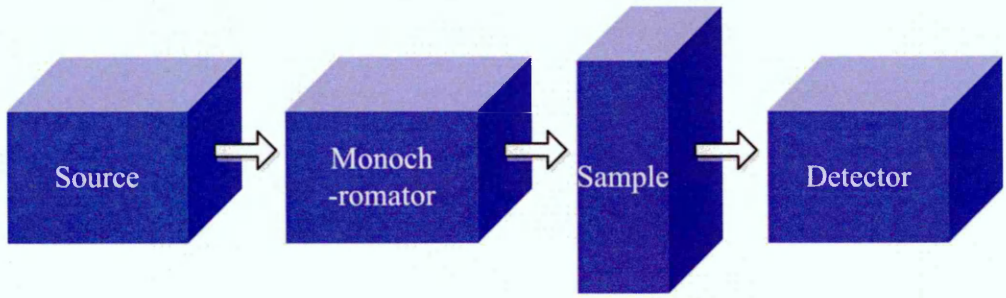

Figure 3.6: Instrumentations in UV-Vis. Spectrophotometer

3.1.3 Fourier Transform Infrared (FTIR)

When molecules are irradiated with IR, the IR with the same wavelength resulting from the frequency of the vibration or other modes of the molecular bonds will be absorbed, and an absorption peak will appear at this wavelength or wave number. If we consider that the characteristic bonds of molecules are wavelength absorber, each absorber can absorb a characteristic wavelength to show an absorbance peak at the corresponding wavelength when an IR wave passes through the sample. Therefore, IR spectroscopy can be used to

1. Identify a known component present in an unknown sample.
2. Study the formation of new chemical bonds or substitutions.
3. Perform quantitative analysis for a component of interest.

A nexus FTIR spectrometer operating in the range of 400-4000 cm^{-1} has been used in this study. In a classic dispersive IR spectrometer, an IR spectrum is measured by scanning the sample with a continuous wavelength range of IR. The setup of Fourier transform infrared (FTIR) spectrometer does not record the spectral intensity directly as a function of wavelength, but an interferogram (interfered waves) is taken instead. In an interferometer, a beam of light is split into two beams, beam 1 and 2 in Figure 3.7 by a beam splitter [10].

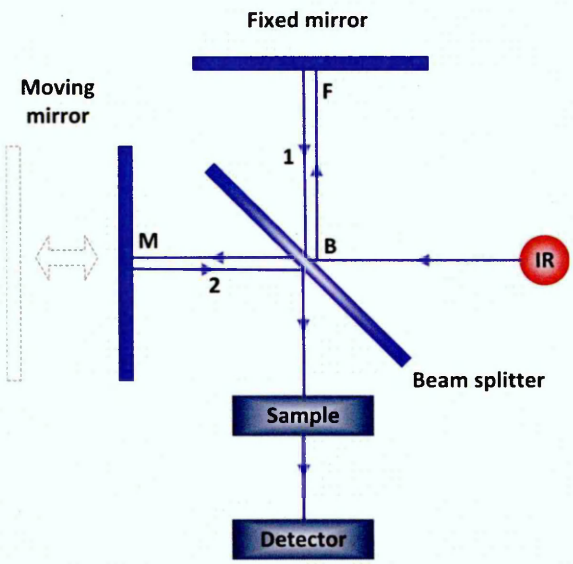

Figure 3.7: Interferometer: IR, infrared radiation source; B, beam splitter; F, fixed mirror; M, moving mirror

The beam splitter is designed to transmit half of the radiation and reflect the other half. Beam 1 travels a distance of 2FB, while beam 2 travels a distance of 2MB. Due to the movement of the moving mirror, the distance FB is different from the distance MB. This difference is called the optical path difference. Phase shift will occur depending on the optical path difference resulting in an interference pattern, or interferogram. The interference pattern varies with the displacement of the moving mirror resulting in constructive and destructive interface. This makes FTIR more powerful and faster than the conventional IR spectrometer because more energy will

reach the sample than that possible with a dispersive spectrometer. As a result, the signal to noise ratio can be increased [11].

3.1.4 Raman Spectroscopy

Raman spectrum is the shift in wavelength of the inelastically scattered radiation that provides the chemical and structural information. Raman shifted photons can be of either higher or lower energy, depending upon the vibrational state of the molecule under study. A simplified energy diagram that illustrates these concepts is shown in Figure 3.8.

Stokes radiation occurs at lower energy (longer wavelength) than the Rayleigh radiation, and anti-Stokes radiation has greater energy. The energy increase or decrease is related to the vibrational energy levels in the ground electronic state of the molecule, and as such, the observed Raman shift of the Stokes and anti-Stokes features are a direct measure of the vibrational energies of the molecule [12].

Raman spectra were recorded with a Triplemate, SPEX spectrometer equipped with CCD detector in back-scattering geometry. The 488 nm, 40 mW line of an Ar-laser was used for the spectral excitation.

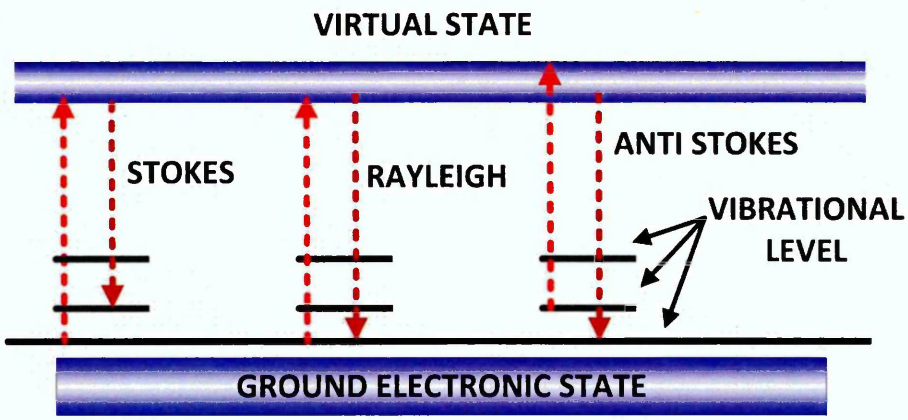

Figure 3.8: Simplified energy diagram

3.1.5 Atomic Force Microscopy (AFM)

3.1.5.1 Theoretical background

The atomic force microscope (AFM) was invented in 1986 by Binning et al [13]. AFM, like all other scanning probe microscopes, utilizes a sharp probe moving over the surface of a sample in a raster scan. In the case of AFM, the probe is a tip on the end of a cantilever, which bends in response to the force between the tip and the sample. Unlike traditional microscopes, scanned-probe systems do not use lenses, so the size of the probe determines the resolution limit. In AFM the cantilever is treated as a Hookean spring, and hence a simple relationship may be assumed between the deflection of the lever, x, and the force F acting on the tip [14]:

$$F = -kx \qquad (3.4)$$

The constant of proportionality k is the spring constant, which, is strongly dependent on the physical dimensions of the cantilever (width-w, length-l, thickness-t) and the elasticity of material [5].

3.1.5.2 Distance between sample surface and tip

Three different primary imaging modes are possible according to the distance (d) between sample surface and the tip, contact mode ($d < 0.5\ nm$), non-contact mode ($0.5\ nm < d < 10$), and tapping mode ($d \sim 0.5\text{-}2\ nm$), as shown in Figure 3.9, which illustrates the relation between force and distance.

In contact mode, the tip scans the sample surface by being pushed against the surface. Contact mode is suitable for hard surfaces where the tip cannot damage the surface [15]. In non-contact mode, the separation of the tip from sample surface is large, that the interaction between tip and sample surface is small and mostly in the range of the damped forces in ambient conditions. Therefore, non-contact mode is appropriate for measurement mostly under vacuum, and even sub-molecular resolution could be achieved [16].

In tapping mode, the cantilever oscillates and the tip taps the surface slightly during scanning. Thus the surface is less damaged than in the case of contact mode while the lateral forces are eliminated. The feedback loop maintains a constant oscillation amplitude by maintaining a constant tip-sample intraction during scan [17]. Tapping mode tends to be more applicable to general imaging in air, particularly for soft surfaces, as the resolution is similar to or even better than contact mode, while the forces applied to the sample are lower. In fact, the only disadvantage of tapping mode is that the scan speed is slightly slower than in contact mode and the AFM operation is a bit more coplex, but these disadvantages are outweighed by the advantages.

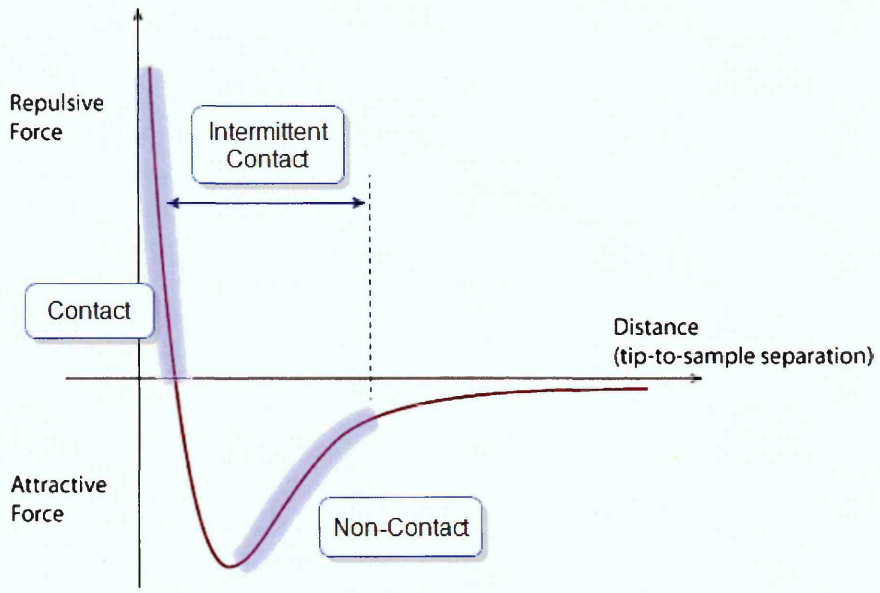

Figure 3.9: Van der Waals force against distance [18]

In this work tapping mode has been used for measuring the topography of thin films surfaces, which allows a higher resolution and does not destroy the organic layers.

3.1.5.3 Instrumntations

The AFM instrument used in this study is NanoScope IIIa Multimode 8 AFM (Figure 3.10a); the microscope itself rests on an anti-vibration platform (Figure 3.10b and c), which can be spring suspended on a tripod to reduce further noise. The NanoScope IIIa Multimode 8 instrument gives the opportunity to take images of the sample surface with nano-meter resolution and to determine their characteristics, such as; sample features' height and distribution.

(a)

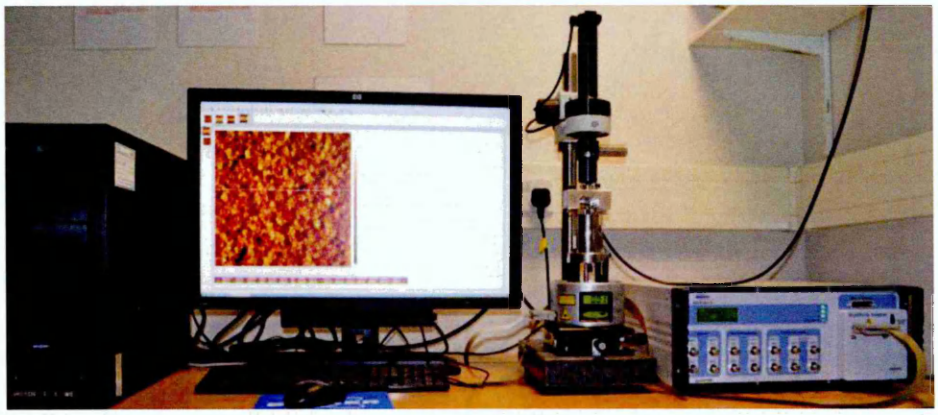

(b)

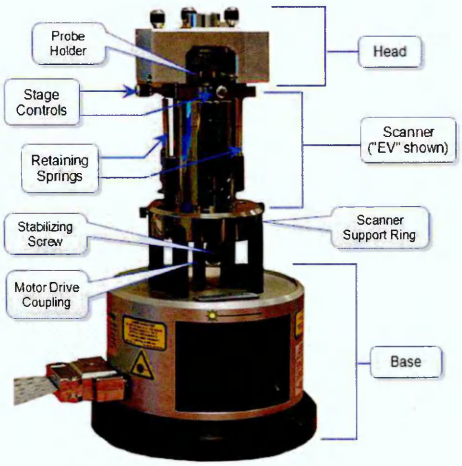

(c)

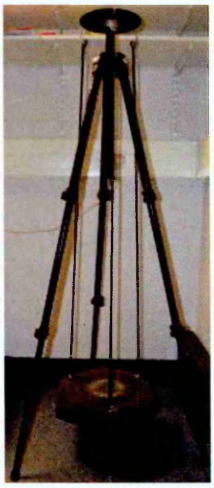

Figure 3.10: (a) NanoScope IIIa Multimode 8 SPM system components and (b) a zoomed in SPM and (c) vibration reduction tripod

The software provided with this system (NanoScope Analysis 1.50) can analyse the section, roughness, particle size, etc. and create pseudo 3D images of the sample surface.

Changes in the tip-sample interaction are monitored using an optical cantilever detection system (Figure 3.11), where a laser beam is reflected back from the cantilever and collected by a position sensitive detector consisting of two closely spaced photodiodes connected to a differential amplifier. Angular displacement of the cantilever results in one photodiode collecting more light than the other photodiode, producing an output signal (the difference between the photodiode signals is normalised by their sum), which is proportional to the deflection of the cantilever. The accuracy of the detection of cantilever deflections is less than 1Å (thermal noise limited). The long beam path (several centimetres) amplifies changes in the beam angle [18].

Probes used are Antimony (*n*) doped silicon (TESP-SS) and silicon nitride (SCANASYST-AIR); these probes are primarily used for tapping mode applications. The tip and cantilever are an integrated assembly of single crystal silicon, produced by etching technique. The characteristics of TESP-SS and SCANASYST-AIR probes are summarised in tables 3.1 and 3.2.

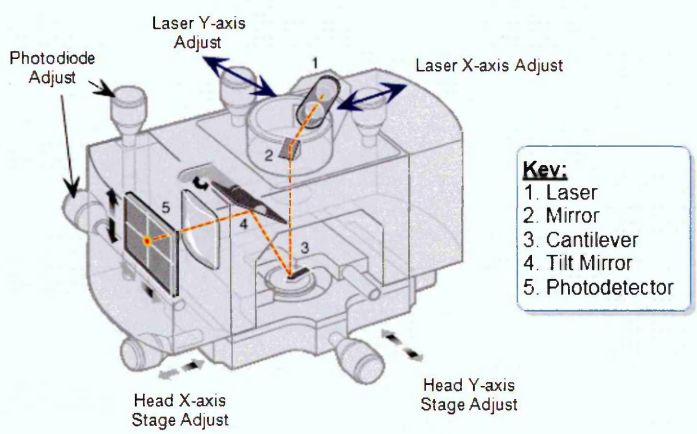

Figure 3.11: NanoScope IIIa beam deflection detection system [18]

Table 3.1: TESP-SS probe characteristics [19].

Material	0.01-0.025 Ωcm Antimony (n) doped Si.
Resonant frequency, *kHz*	230-410
Spring constant, *N/m*	20-80
Length, μm	125
Tip geometry	Super Sharp (ss)
Cantilever geometry	Rectangular

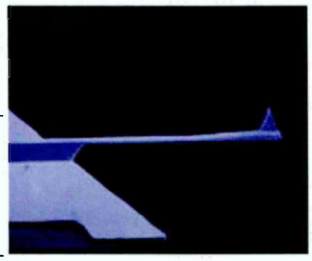

Table 3.2: SCANASYST-air probe characteristics [19].

Material	Silicon Nitride
Resonant frequency, *kHz*	45-95
Spring constant, *N/m*	0.2-0.8
Length, μm	115
Tip geometry	Rotated (symmetric)
Cantilever geometry	Triangular

3.1.6 Scanning Electron Microscopy (SEM)

3.1.6.1 Theoretical background

The SEM was invented soon after the transmission electron microscope (TEM) but took longer to be developed into a practical tool for scientific research. Today, SEM is used in many fields, such as medical and materials research, semiconductor industry, and forensic-science labs. It is not completely clear who first proposed the principle of scanning the surface of a specimen with a finely focused beam of electrons to produce an image of the surface. The first published description appeared in 1935 in a paper by Knoll [20]. In 1942 Zworykin and co-workers [21] first described a true SEM with a resolution of 50 nm and magnification of 8000x.

3.1.6.2 Instrumentations

FEI-nova nanosem 200 SEM (Figure 3.12a) is used in this research. The scheme of SEM operation is illustrated in Figure 3.12b, which consists of electron gun as electron source, two condenser lenses, scanning coils, which facilitates the deflection of electron beam in x and y directions, objective lens, and detectors for backscattered and secondary electrons. SEM operates inside vacuum chamber with high-energy electron source (2-25kV). Condenser lenses focus the electron beam into a nano-meter size. The reflected electron from the sample, backscattered or secondary electrons, are collected by the detector to provide an image of the sample. In many cases, the backscattered electrons reflected from the sample are used in analytical SEM due to the relation of intensity and atomic number of materials [22].

3.1.6.3 Secondary and backscattered electron

Two imaging modes are available in SEM; Secondary Electron Imaging (SEI) or Backscattered Electron Imaging (BEI). In the former, low energy secondary electrons (typically < 50 eV) emitted from the interaction between the incident beam of high energy electrons with the atoms of the sample via inelastic collisions are detected and used to build an image of the surface topography of the sample. Due to the relatively low energies of these secondary electrons, only those from the surface (a very thin layer of tens of nanometres) are able to emerge from the sample. In the

case of BEI, the image is derived from scattered or reflected electrons from elastic collisions of the high energy electron beam with the nuclei of the atoms at high angles approaching 180° (Figure 3.13).

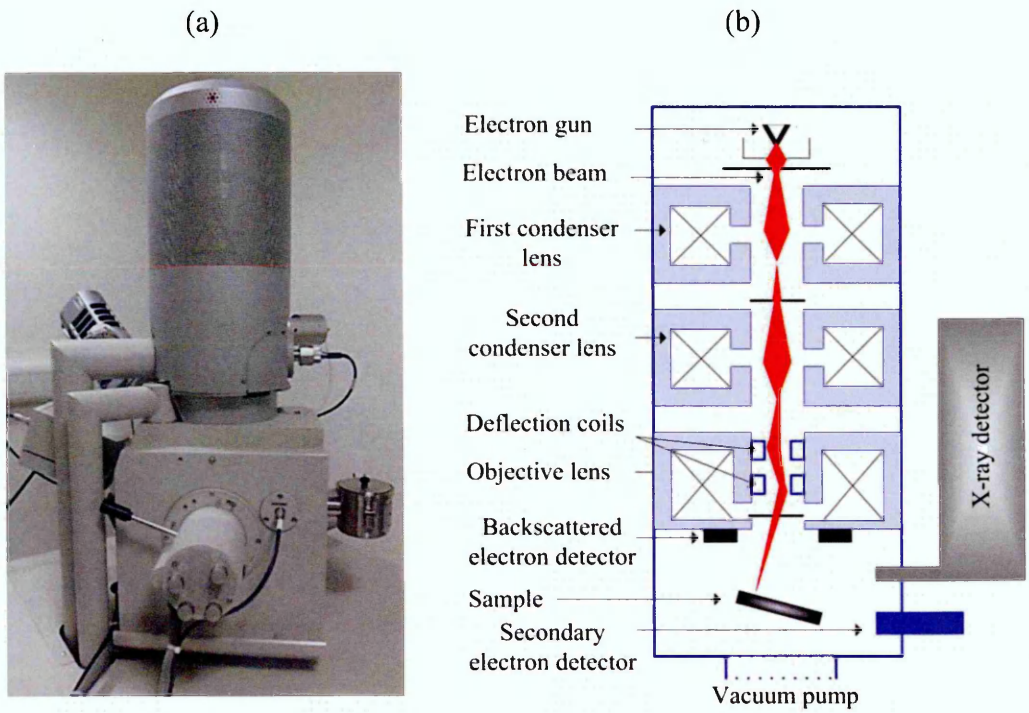

Figure 3.12: (a) SEM system and (b) Schematic illustration of the operation of SEM

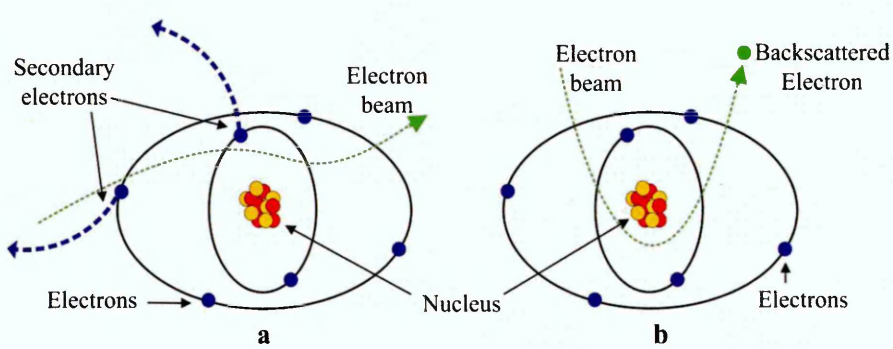

Figure 3.13: Interaction between electrons beam and sample producing (a) secondary electrons and (b) backscattered electrons

The yield of backscattered electrons is a function of atomic number. Heavier elements, i.e. those with higher atomic number, reflect a greater proportion of electrons and so appear brighter, and lighter elements with a low atomic number reflect a lower proportion of electrons and appear darker. The contrast indicates the average atomic number of the elements present within the microstructure and is indicative of the varying elemental compositions [21,23].

3.1.7 Semiconductor Characterisation (I-V Characteristics)

According to Ohm's low the current *I (in amperes)* in a sample is proportional directly to the potential difference *V (in volts)* across two points on this sample [24]:

$$I = {}^{V}/_{R} \qquad (3.5)$$

where R is the sample resistance measured in *ohms*.

Consider that the current passes through a peace of material with length *l (m)* and a cross section area *A* (m^2) as in Figure 3.14. The electrical resistivity ρ can be defined as:

$$\rho = R\,{}^{A}/_{l} \qquad (3.6)$$

Conductivity σ *(S/m)* is the inverse of the resistivity; $\sigma = 1/\rho$.

Therefore, we can write Ohm's low in the following expression:

$$J = \sigma E \qquad (3.7)$$

where *J* is the current density *(I/A) (in ampere/cm*^{2}*)* and *E* is the magnitude of the electric field *(V/l) (in volt/m)*.

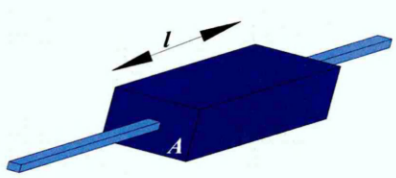

Figure 3.14: A piece of resistive material with electrical contacts on the ends

3.1.7.1 Structure of studied devices

Two types of device configurations were studied in the current work; sandwich film structure and planar structure using intedigitated electrodes. For sandwich structures (Figure 3.15a), Indium Tin Oxide (ITO) coated glass substrates were used. ITO substrates were washed in chloroform for 15 minutes using ultrasonic path, rinsed with water and then left to dry in a desiccator. Active layers have been deposited from diluted solutions onto the ITO substrates using spin-coating method. Top electrodes were evaporated through shadow mask under vacuum with pressure of about $2x10^{-5}$ mbar using vacuum thermal deposition. The rate of film deposition was controlled by a film thickness monitor at the rate 0.1 $nm.s^{-1}$, and the obtained thickness was 40 nm. In such kind of devices, to calculate conductivity from I-V curves, the cross section area (*A*) will be the device active area as determined by the overlap area between the active layer and the top electrode and *l* is the film thickness which can be determined utilizing spectroscopic ellipsometry.

In the planar structure (Figure 3.15b), the interdigitated electrode geometry is used to determine the conductivity based on equations 3.5 and 3.6:

$$\sigma = {}^{L}/_{RHWn} \qquad (3.8)$$

where H is the film thickness, L is the gap between fingers, W is the overlap distance between the electrodes and n is the number of fingers (n=10-15).

3.1.7.2 Instrumentations

The Model 4200 Kiethely Semiconductor Characterisation System (4200-SCS) (Figure 3.16) has been used for the DC electrical characterisation of MPc thin films utilising the two types of device configurations. The system is specified to work at the 1pA-1A current range with the maximum voltage of 21-210 V, and 200mV-200V voltage range with the maximum current of 10.5-105mA. This system can automatically perform IV and CV measurements of semiconductor devices and test structures, using up to eight Source-Measure Units (SMUs). A variety of supported external components enhance the capabilities of this machine.

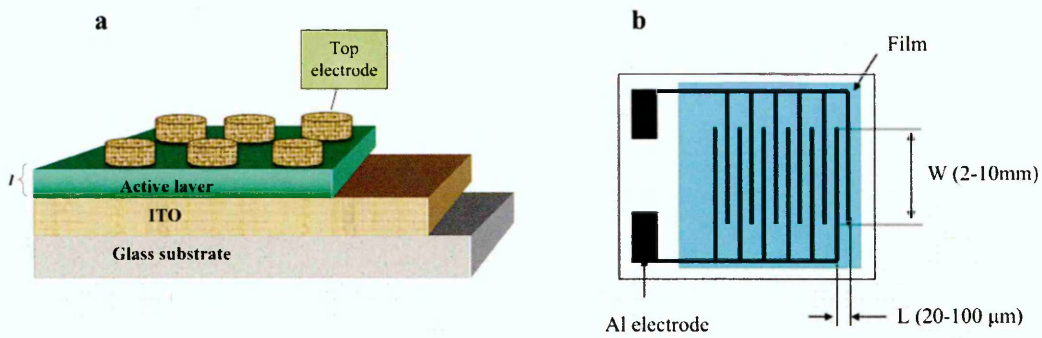

Figure 3.15: Schematic illustration of devices structure used in this study, (a) sandwich structure and (b) interdigitated electrodes

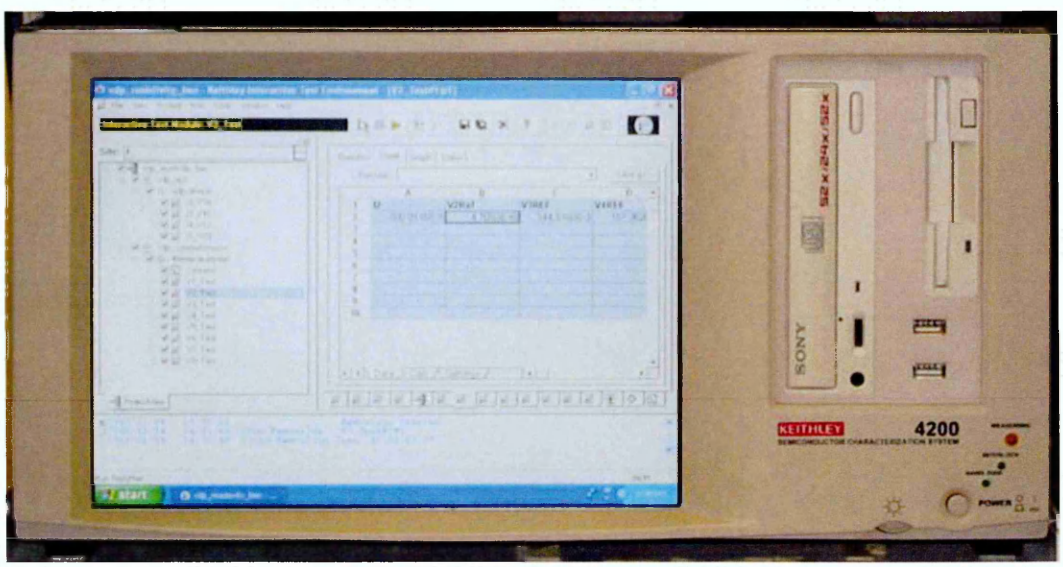

Figure 3.16: Keithley 4200 semiconductor characterisation system

3.2 Materials

In this work, novel substituted metal phthalocyanines (MPcR) were used to prepare thin films from their solutions and also investigated as hybrid components to enhance the solubility and thus the optical activity of single walled carbon nanotubes (SWCNTs). The MPc/SWCNTs composite films prepared thereafter have been used as optical active layers for chemical detection applications using TIRE method. All investigated MPcs were synthesised and chemically characterised by our co-researcher in Gebze Technical University, Turkey. A brief description of chemical synthesis will be explained where important in later chapters. SWCNT and other materials used in this work were obtained from commercial suppliers and presented in table 3.3.

3.3 Samples preparation

3.3.1 Spin coating

Spin coating is a fast and easy method to generate thin and homogeneous organic films out of solutions. Spin coating is a procedure used to apply uniform thin films to flat substrates. In short, an excess amount of a solution is placed on the substrate, which is then rotated at high speed in order to spread the fluid by centrifugal force. This method was first described by Emslie et al. (1958) [25] and Meyerhofer et al. (1978) [26].

In the early stages of spin coating the rate of thinning by centrifugal forces is much larger than by evaporation. After spin-off, the thinning of the film is just due to evaporation and occurs constantly. The transition point between the spin-off and evaporation is the point where the rate of thinning due to centrifugal forces is the same as that due to evaporation. Figure 3.17 represents the stages of spin coating. Film thickness at the transition is defined as $h_{\circ}$. The time after reaching the transition point is called drying time t_d, when, saturation, nucleation and growth take place. The liquid film becomes supersaturated due to evaporation of the solvent (Figure 3.17c). After complete evaporation, a solid film is formed on the substrate (figure 3.17d).

Table 3.3: List of materials and their supplier.

	Material	Abbreviation	Purity (%)	Density, g/cm^3	Supplier	
	Raw materials					
1.	Single-walled carbon nanotube	SWCNT	77	1.7-1.9	Sigma Aldrich	d, 0.7-1.1nm L, 300-2300nm
	Solvents					
2.	Chloroform		99.9	1.492	Sigma Aldrich	
3.	Dichloromethane	DCM	99.8	1.235	Sigma Aldrich	
4.	Dimethylformamide	DMF	99.8	0.944	Sigma Aldrich	
	Acids					
5.	Nitric acid	HNO_3	70	1.413	Fisher Scientific	
6.	Sulfuric acid	H_2SO_4	99.999	1.840	Fisher Scientific	
	Analyts					
7.	Benzo[a]pyrene		96	1.24	Fluka	Powder
8.	Pentachlorophenol	PCP	97	1.978	Sigma Aldrich	Powder
9.	Simazine				Fluka	Powder
10.	Atrazine				Fluka	Powder
11.	2-chlorophenol	2CP	99	1.241	Sigma Aldrich	Powder
12.	Isoproturon				Fluka	Powder
13.	Diuron		98		Sigma Aldrich	Powder

14.	Methylamine	-	0.897	Sigma Aldrich	40% in H_2O
15.	Dimethylamine	-	0.89	Sigma Aldrich	40% in H_2O
16.	Trimethylamine	-	0.88	Sigma Aldrich	45% in H_2O

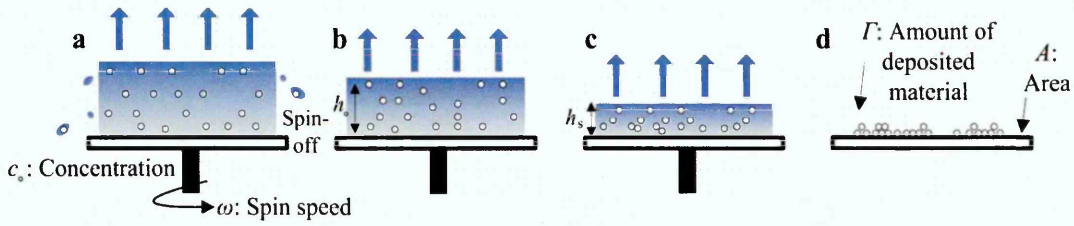

Figure 3.17: Schematic figure of spin-coating indicating the dominant process at the beginning of spin-coating (spin-off) and later after the equilibrium liquid film thickness is reached

The film thinning for an ideal Newtonian liquid is described by Meyerhofer as [26]:

$$\frac{dh}{dt} = -2kh^2 - E \qquad (3.9)$$

where h is the film thickness; E evaporation rate and k spin-off coefficient, which is defined as:

$$k = \frac{\omega^2}{3\nu} \qquad (3.10)$$

where ω is the spinning speed; υ is the kinetic viscosity of the liquid. Karpitschka and co-workers solved the equation analytically, for the case of constant evaporation rate. The amount of material deposited at the end of the spinning process is [27]:

$$\Gamma = \frac{N(h \to 0)}{A} \simeq 0.8c_o\left(\frac{E}{k}\right)^{\frac{1}{3}} \simeq c_o\left(\frac{E}{3\upsilon}\right)^{\frac{1}{3}}\omega^{-\frac{2}{3}} \qquad (3.11)$$

According to equation 3.11, the amount of deposited material can be controlled by the initial concentration, evaporation rate and speed of spinning.

In the present work a photo resist spinner model 4000 (Electronic Micro Systems Ltd.) has been used to spin cast thin films of MPc and its hybrids with SWCNTs. A drop of the materials solution is deposited using adjustable micro-syringe (Eppendorf 10-100 μl) onto a rotating substrate.

3.3.2 Thermal evaporation

Vacuum deposition via thermal evaporation includes two simple processes; evaporation and condensation. It brings to mind the familiar process by which liquid water appears on the lid of a boiling pan but, the situation and heat source are quite different.

Evaporation process occurs in vacuum, where gases other than the source material are almost completely removed before the evaporation begins. Therefore, particles can travel straight to the deposition target avoiding collision with the background vapor. Hot objects inside the evaporation chamber, such as heating filaments, creates an unwanted vapors that limit the quality of the vacuum. Generally, other unwanted gases collide with the evaporated material may react with them. For example, if aluminium is deposited in the presence of oxygen, it will form aluminium oxide. They also reduce the amount of vapor that reaches the substrate, which makes the thickness difficult to control [28].

Edwards E306A Thermal Evaporator has been used to evaporate a metal film onto a substrate. The metal source to be evaporated, typically gold and aluminium, is placed in a suitable filament or crucible, in which a large current is passed. The metal melts, and evaporates onto the target substrate above the source, producing a film. The thickness of the metal film is monitored in-situ using a quartz crystal thickness monitor (Model Edward FTM5) Even though the turret can accommodate up to four different materials, and changed via manual rotation, the most common practice was to evaporate single material during one pump-down cycle.

The major components of the Edwards E306A Thermal Evaporator are :

- A diffusion pump supported by a rotary pumping system.
- Chamber.
- An electrical system, which incorporates the Edwards E306A Thermal Evaporator Controller.

3.3.3 Substrates

All substrates have been washed thoroughly using chloroform for 15 minutes in ultrasonic bath, followed by thorough rinsing with deionized water and then left to dry in a desiccator

For chemical detection research gold-coated glass slides were used for light coupling using TIRE method as described in section 3.1.1. The samples were prepared by the evaporation of 3-5 nm of chromium onto pre-cleaned microscopic glass slides followed by the evaporation of 25-30 nm of gold layer using thermal evaporator. Thin films of MPc as well as MPc/SWCNT hybrids were deposited from diluted solution on the gold-coated substrate by spin-coating technique.

Silicon substrates of $1x1cm^2$ in area were used for morphology studies. First, the substrate was cut using diamond cutter, washed with chloroform in ultrasonic bath for 15 minutes, rinsed with deionised water and left to dry in a desiccator. Thin films were deposited from diluted solutions onto the silicon substrates by spin-coating method. Thin layer ~ 1 nm in thickness of gold was deposited on top of the organic film as well as its hybrids with SWCNTs to allow more interaction of electrons with the film surface in the case of SEM study.

Indium-doped tin oxide (ITO)-coated glass substrates are used as conductive bottom electrodes in electrical measurements in the case of sandwich device structure.

Reference List

[1] H. Arwin, M. Poksinski, K. Johansen, Total internal reflection ellipsometry: Principles and applications, Appl. Opt. 43 (2004) 3028-3036.

[2] A. Nabok, A. Tsargorodskaya, The method of total internal reflection ellipsometry for thin film characterisation and sensing, Thin Solid Films. 516 (2008) 8993-9001.

[3] R.M.A. Azzam, The intertwined history of polarimetry and ellipsometry, Thin Solid Films. 519 (2011) 2584-2588.

[4] A.V. Nabok, A. Tsargorodskaya, A.K. Hassan, N.F. Starodub, Total internal reflection ellipsometry and SPR detection of low molecular weight environmental toxins, Appl. Surf. Sci. 246 (2005) 381-386.

[5] A. Tsargorodska, Research and development in optical biosensors for determination of toxic environmental pollutants. PhD thesis, Sheffield Hallam University (2007).

[6] H. Fujiwara, Spectroscopic Ellipsometry: Principles and Applications, John Wiley & Sons, 2007.

[7] Laurier research instrumentation, user guidlines and standard operating procedure for the UV-Vis spectrophotometer, July 2007.

[8] W. Schnabel, Polymers and Light: Fundamentals and Technical Applications, Wiley-VCH, Weinheim, 2007.

[9] Chemical Analysis: Modern Instrumentation Methods and Techniques, Wiley, Chichester, 2007.

[10] Y. Leng, Materials Characterization: Introduction to Microscopic and Spectroscopic Methods, John Wiley & Sons (Asia) Pte Ltd, Singapore, 2008.

[11] S. Zhang, L. Li, A. Kumar, Materials Characterization Techniques, CRC, Boca Raton, Fla, 2009.

[12] P. Vandenabeele, Raman spectroscopy, Analytical and Bioanalytical Chemistry. 397 (2010) 2629-2630.

[13] G. Binnig, C.F. Quate, C. Gerber, Atomic force microscope, Phys. Rev. Lett. 56 (1986) 930-933.

[14] J.C. Vickerman, I.S. Gilmore, Surface Analysis: The Principal Techniques, Wiley, Chichester, 2009.

[15] I. Schmitz, M. Schreiner, G. Friedbacher, M. Grasserbauer, Tapping-Mode AFM in Comparison to Contact-Mode AFM as a Tool for in Situ Investigations of Surface Reactions with Reference to Glass Corrosion, Anal. Chem. 69 (1997) 1012-1018.

[16] R. Pawlak, S. Kawai, S. Fremy, T. Glatzel, E. Meyer, High-resolution imaging of C 60 molecules using tuning-fork-based non-contact atomic force microscopy, Journal of Physics Condensed Matter. 24 (2012) 84005-84015

[17] F. Ghani, Nucleation and growth of unsubstituted metal phthalocyanine films from solution on planar substrates, PhD thesis, Max plank institute of colloid and interfaces (2012).

[18] Bruker Corporation, Multimode 8 with Scan Asyst Instruction Manual 004-1033-000, Bruker, UK, 2009, 2010, 2011.

[19] Bruker Corporation, www.bruker.co.uk, 2014

[20] M . Knoll, Aufladepotentiel und sekundaremission elektronenbestrahlung, Korper. Z. Tech. Phys. 16 (1935) 467-475.

[21] Zworykin V, Hiller J, Snyder R, scanning electron microscope, ASTM Bulletin. 117 (1942) 15-23.

[22] R.F. Egerton, Physical Principles of Electron Microscopy: An Introduction to TEM, SEM, and AEM, Springer, New York, NY, 2007.

[23] Basal Science Clarified, www.bsclarified.wordpress.com, Scanning Electron Microscopy Part 1: Imaging, May 2011

[24] L. Solymar, D. Walsh, Electrical Properties of Materials, Oxford University Press, Oxford, 2010.

[25] A.G. Emslie, F.T. Bonner, L.G. Peck, Flow of a viscous liquid on a rotating disk, J. Appl. Phys. 29 (1958) 858-862.

[26] D. Meyerhofer, Characteristics of resist films produced by spinning, J. Appl. Phys. 49 (1978) 3993-3997.

[27] S. Karpitschka, C.M. Weber, H. Riegler, Physics of Spin Casting Dilute Solutions, (2012).

[28] Edwards Vacuum, https://www.edwardsvacuum.com/Support/Reference/Documentation.aspx, (2014).

Chapter 4

Octa-Substituted Copper and Lead Phthalocyanines: Electrical, structural and optical studies

Chapter overview

This chapter studies the effect of different substituents on the characteristics of thin films of octasubstituted copper (II) phthalocyanines ($CuPcR_8$) and lead phthalocyanines ($PbPcR_8$). The first part of this chapter focuses on the effect of alkylthio-, alkyloxy-, (trioxyethylene)thio- and (trioxyethylene)oxy- substituents in peripheral positions on the properties of $CuPcR_8$ while the second part studies the properties of novel octasubstituted lead(II) phthalocyanines with octylthio, octyloxy and hexadecyloxy groups. The investigation of thin films of these complexes by UV-visible absorption spectroscopy is reported using Varian 50 scan UV-Visible spectrophotometer. The current-voltage characteristics and electrical switching behaviour of $PbPcR_8$ in sandwich structure of ITO/$PbPcR_8$/In are also studied using Keithley 4200 semiconductors characterization system.

4.1 Octa-substituted copper phthalocyanines ($CuPcR_8$)

Synthesis procedures of all copper phthalocyanine derivatives have been carried out by co-researchers and is summarised in Figure 4.1 and Table 4.1. Further details on the synthesis of these phthalocyanines are found in the literature [1]. All other reagents used in this chapter were purchased from commercial supplier.

Table 4.1: $CuPcR_8$ derivatives used in this chapter

Symbol	Compound	Formula	Initial decomposition temp. °C	Main decomposition temp. °C
3a	2,3,9,10,16,17,23,24-Octakis(octyloxy)phthalocyaninato copper (II)	$C_{96}H_{144}CuN_8O_8$	300	420
3b	2,3,9,10,16,17,23,24-Octakis(hexadecyloxy)phthalocyaninato copper (II)	$C_{160}H_{272}CuN_8O_8$	300	424
3c	2,3,9,10,16,17,23,24-Octakis-[2-(2-(2-methoxyethoxy)ethoxy)ethoxy] phthalocyaninato copper (II)	$C_{88}H_{128}CuN_8O_{32}$	300	406
4a	2,3,9,10,16,17,23,24-Octakis(octylthio)phthalocyaninato copper (II)	$C_{96}H_{144}CuN_8S_8$	330	378
4b	2,3,9,10,16,17,23,24-Octakis(hexadecylthio)phthalocyaninato copper (II)	$C_{160}H_{272}CuN_8S_8$	330	384
4c	2,3,9,10,16,17,23,24-Octakis-[2-(2-(2-methoxyethoxy)ethoxy)ethylthio]phthalocyaninato copper (II)	$C_{88}H_{128}CuN_8O_{24}S_8$	285	337

4.1.1 Film preparation

Small volume (3-4μL) of solutions of $CuPcR_8$ derivatives in chloroform (10mg/ml) was dispensed via microsyringe on to an ultrasonically cleaned substrate held onto photoresist spinner. The speed of substrate rotation was 2000rpm. Spinning was continued for 30s during which time the solvent had evaporated to generate a film of phthalocyanine derivatives. The films were then heated to a temperature 10-20°C above the isotropic transition temperature or to the maximal possible temperature lower than temperature of decomposition (Table 4.1) and slowly cooled down to room temperature at the rate of 10°C min^{-1} for comparison with as deposited layers. Glass slides, silicon wafers and interdigitated electrodes have been used as substrates to perform UV-Vis absorption, ellipsometry and IV measurements respectively.

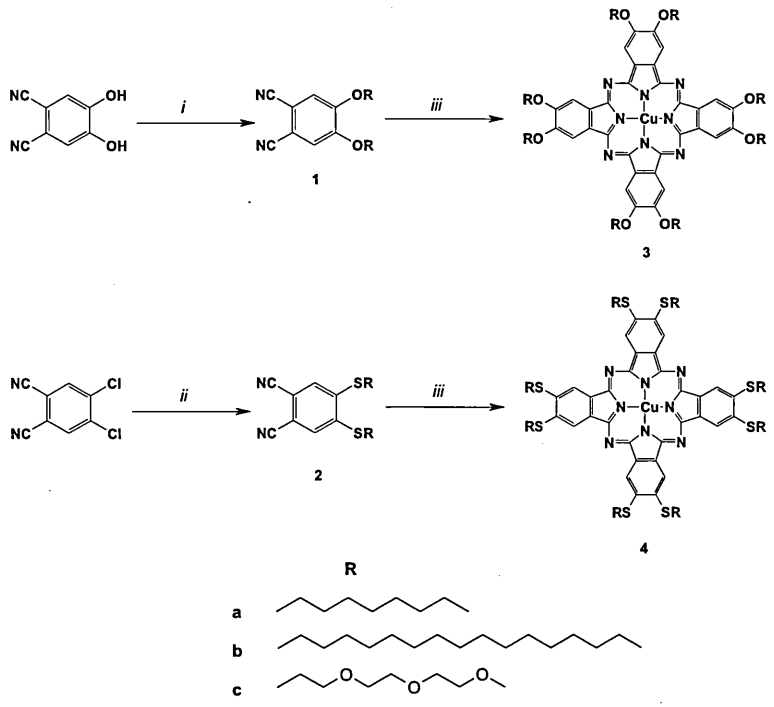

Figure 4.1: Synthesis of octa-substituted copper (II) phthalocyanines. Reagents and conditions: (*i*) RBr (1-bromooctane, 1-bromohexadecane or triethylene glycol 2-bromoethyl methyl ether), potassium carbonate, DMF, room temperature, 3 days; (*ii*) RSH (1-octanethiol, 1-hexadecanethiol or 2-[2-(2-methoxyethoxy)ethoxy]ethanethiol), potassium carbonate, DMF, room temperature, 3 days; (*iii*) $CuCl_2$ (anhydrous), DBU (1,8-diazabicyclo[5.4.0] undec-7-ene), hexanol, reflux, 24 h.

4.1.2 UV-visible absorption spectra

UV-visible absorption spectra were recorded on Varian 50 scan UV-Visible spectrophotometer. It was shown earlier that the spin-coating method provides a simple and convenient procedure for preparing ordered films of the phthalocyanines which can be heated to form thin liquid-crystalline films [2,3]. The electronic absorption spectra of the films of $CuPcR_8$ before and after heating are presented in Figure 4.2.

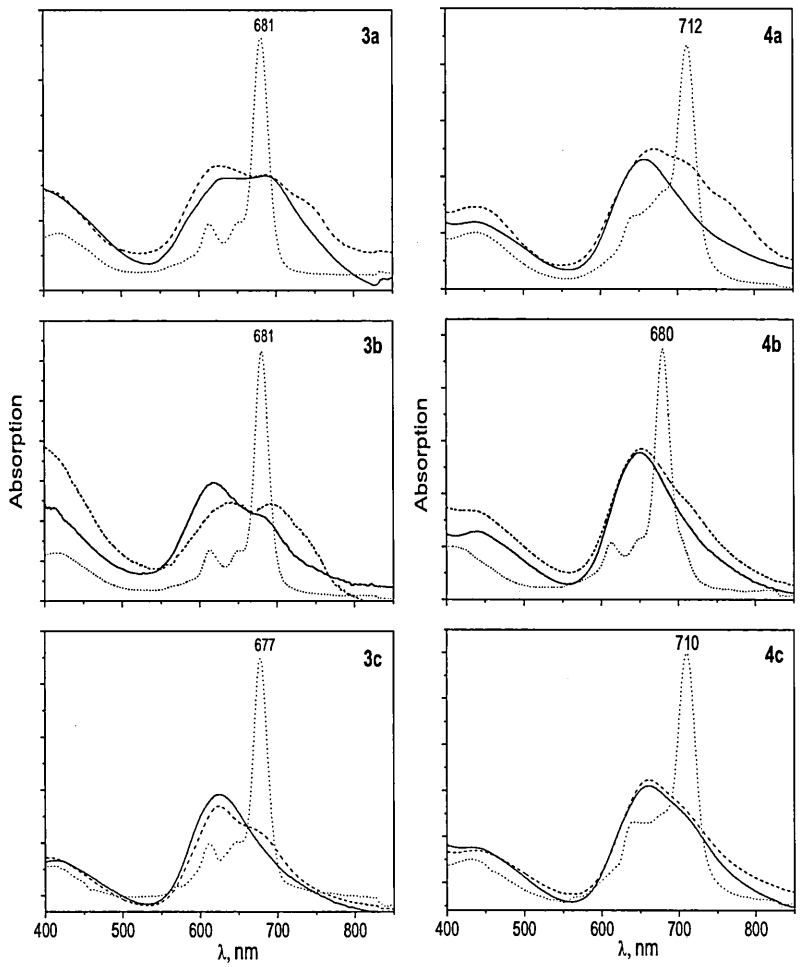

Figure 4.2: The electronic absorption spectra of **3a**, **3b**, **3c**, **4a**, **4b** and **4c** solution in chloroform (dotted lines); as-deposited films on glass (dashed lines); films after heating (solid lines)

The Q-band structure is more complex than that observed in the solution phase where non-aggregated phthalocyanines give rise to a single main band assigned to the doubly degenerate transition a_{1u}-e_g. In the optical spectra of $CuPcR_8$ films the main absorption bands are broadened through exciton coupling effects which also lead to shifts in the band positions. These are dependent upon molecular packing [4]. Splitting of Q-band in the spectra of the films of **3a, 3b, 3c** and **4a** before heating indicate the herring-bone arrangement of phthalocyanine molecules which is typical for many crystalline phthalocyanines [5]. Films give rise to both a red- and a blue-shifted band consistent with exciton splitting arising from the presence of translationally non-equivalent molecules in the 'unit cell', as in a herringbone arrangement of molecules within adjacent columns. After heating the spectra of films **3a** and **3b** change, however the Q-band splitting does not disappear confirming the persistence of herring-bone arrangement.

The spectra of the films of **3c** and **4a** after heating are blue shifted relative to the spectra of the monomers. From these spectral changes it can be deduced that on passing from crystal to mesophase, changes into parallel (face-to-face) dimer stacking are observed. This type of re-organization is analogous to that undergone by the octaalkyl analogues upon transition from the crystal phase to the hexagonal discotic mesophase [6]. The Q-bands in the spectra of **4b** and **4c** films are blue-shifted both before and after thermal treatment.

4.1.3 Current-Voltage (I-V) Characteristics

DC conductivity measurements were carried out using Keithley 4200 semiconductors characterisation system. The current-voltage (I-V) characteristics of $CuPcR_8$ films were measured in the direction parallel to the films plane using interdigitated electrode structures. Film thicknesses were determined using a Woolam $M-2000V^{TM}$ rotating analyser spectroscopic ellipsometer in the spectral range of 350-1000 nm and were used in the calculation of conductivities of $CuPcR_8$ complexes; the results are summarized in Table 4.2. The lateral conductivity tends to decrease slightly with the increase of chain length (films **3a** and **3b**; **4a** and **4b**). A similar behaviour was observed by Nakahara and co-workers for in-plane conductivity as a result of increasing chain length in phthalocyanine molecules [7].

The observed decrease in conductivity with increasing length of the alkyl chain was related to an increase in the hopping distance between localised sites [8,9]. The conductivity of alkylthio-substituted phthalocyanines (**4a-4c**) is higher than that of alkyloxy-substituted derivatives (**3a-3c**). The Q-bands of alkylthio-substituted phthalocyanines are red-shifted, compared with the Q-bands of alkyl- and/or alkyloxy-substituted phthalocyanines. The red-shift means that the energy gap between the HOMO and LUMO narrows on changing from alkyl or alkyloxy groups to alkylthio groups [10]. This was found to result in an increased electroconductivity, as was previously reported by van de Craats and his co-workers for alkylthio-substituted phthalocyanines, both for the metal free and copper complexes [9].

Furthermore, it was suggested that the larger size of the sulphur atom which is bridging the Pc macrocycle to the alkyl chain is the cause for hindering the structural disorder in the molecular stacks during the melting of the hydrocarbon chain when transition from crystalline to hexagonal mesophase (D_h) takes place [11]. This was found to enhance the electron mobility of charge carriers between stacks by one order of magnitude and thus leading to higher conductivity as compared to the alkyloxy-substituted derivatives.

Table 4.2: Film thickness and calculated conductivity of $CuPcR_8$ films

Compound	**3a**	**3b**	**3c**	**4a**	**4b**	**4c**
Thickness, nm	198	150	139	120	116	156
$\sigma_{//}$, Ω^{-1} m^{-1}	5.1×10^{-9}	2.6×10^{-9}	4.2×10^{-8}	6.7×10^{-8}	5.0×10^{-8}	2.0×10^{-7}

4.2 Octa-substituted lead phthalocyanines ($PbPcR_8$)

Synthesis procedures of lead phthalocyanine derivatives used in this section have been carried out by co-researchers and is summarised in Figure and Table 4.3. Further details on the synthesis of these phthalocyanines are found in the literature [12]. All other reagents used in this section were purchased from commercial supplier.

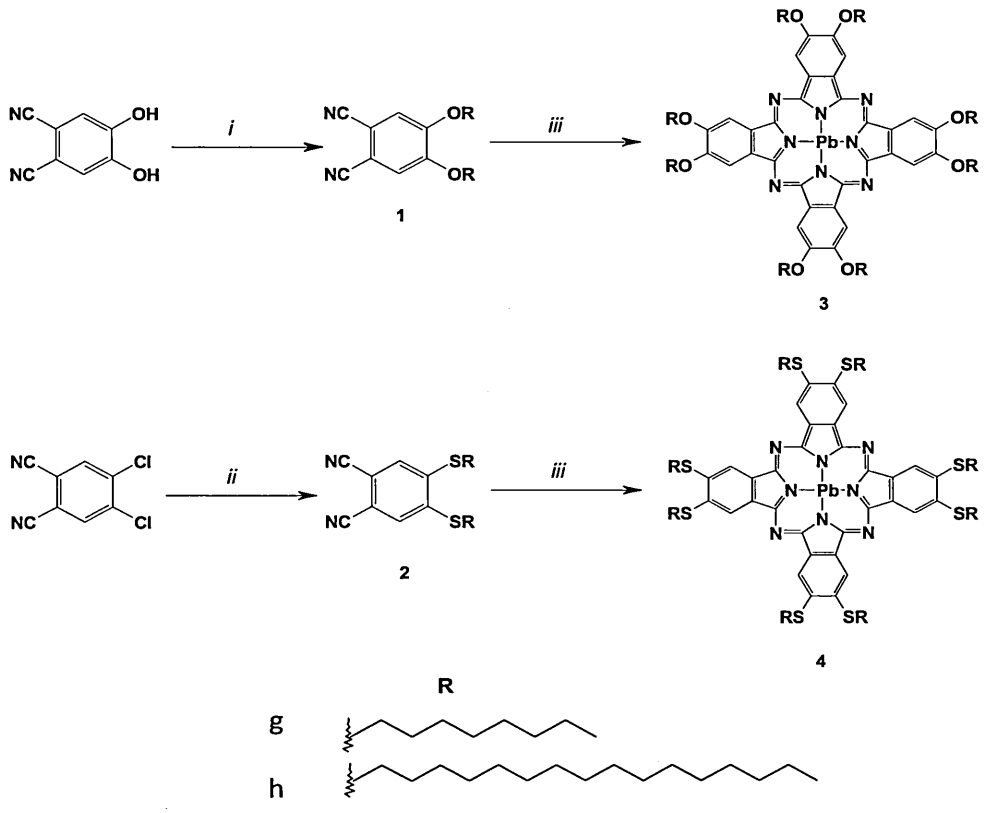

Figure 4.3: Synthesis of octa-substituted lead (II) phthalocyanines. Reagents and conditions: (*i*) RBr(1-bromooctane, 1-bromohexadecane or triethylene glycol 2-bromoethyl methyl ether), potassium carbonate, DMF, room temperature, 3 days; (*ii*) RSH (1-octanethiol, 1-hexadecanethiol or 2-[2-(2-methoxyethoxy)ethoxy]ethanethiol), potassium carbonate, DMF, room temperature, 3 days; (*iii*) PbO (anhydrous), 210^{0}C, solvent-free, 5 hours

Table 4.3: $PbPcR_8$ used in this chapter

Symbol	Compound	Formula
3g	2,3,9,10,16,17,23,24-Octakis(octyloxy)phtalocyaninato lead (II)	$C_{96}H_{144}N_8O_8Pb$
3h	2,3,9,10,16,17,23,24-Octakis(hexadecyloxy)phtalocyaninato lead (II)	$C_{160}H_{272}N_8O_8Pb$
4g	2,3,9,10,16,17,23,24-Octakis(octylthio)phtalocyaninato lead (II)	$C_{96}H_{144}N_8PbS_8$
4h	2,3,9,10,16,17,23,24-Octakis(n-hexadecylthio)phtalocyaninato lead (II)	$C_{160}H_{272}N_8PbS_8$

4.2.1 UV-Vis. Absorption spectra

The electronic absorption spectra of compounds **3g, 3h, 4g and 4h** in THF ($1x10^{-5}$ M) are presented in Figure 4.4. In common with other Pc derivatives, PbPc complexes have two intensive bands in the UV–vis spectra: the Soret band (B-band) and the Q-band. The Q-band absorption has been assigned to a π–π * transition from the highest occupied molecular orbital (HOMO) of a_{1u} symmetry to the lowest unoccupied molecular orbital (LUMO) of e_g symmetry. In THF, the Q bands maxima were observed at 707 nm for **3g**, 708 nm for **3h**, 739 nm for **4g** and 740 nm for **4h**.

The red-shift ca. 30 nm in the spectra of alkylthio-substituted derivatives (**4g, 4h**) compared to alkyloxy-substituted derivatives (**3g, 3h**) can be ascribed to the greater electron donating nature of SR groups in comparison with OR groups; this is due to the higher electron donating ability of sulphur atom compared to that of oxygen atom. The increase of electron density in the phthalocyanine ring results in the narrowing of the HOMO–LUMO gap [13]. Furthermore, the presence of Pb ion leads to additional shift to longer wavelengths in comparison with planar Pc analogues. For instance, the Q bands of Pb(II) phthalocyanine complexes (**3g-h** and **4g-h**) were red-shifted by ~ 30 nm compared to Cu(II) counterparts in Chloroform [1]. The observed red spectral shift is due to the non-planar structure of Pb(II) phthalocyanine complexes (Figure 4.5).

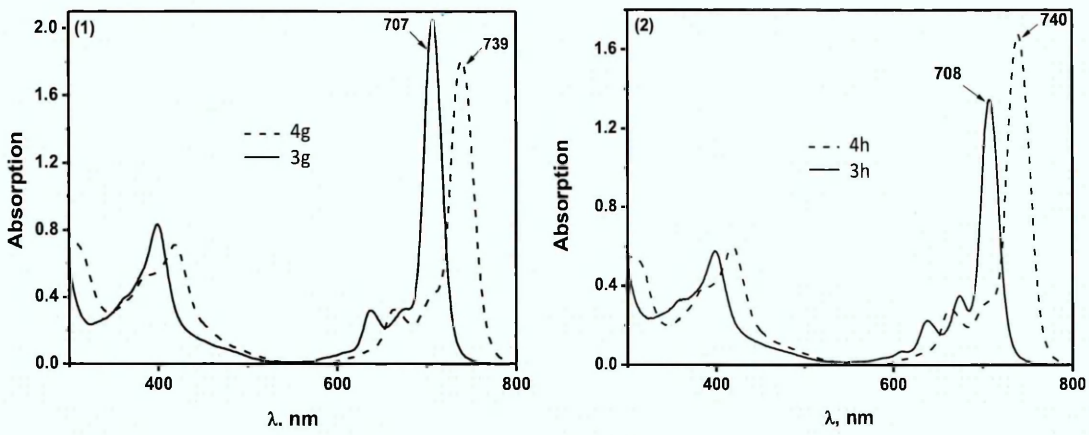

Figure 4.4: Electronic absorption spectra of **3g-4g** (1) and **3h-4h** (2) in tetrahydrofuran (THF) (C=1x10^{-5} M)

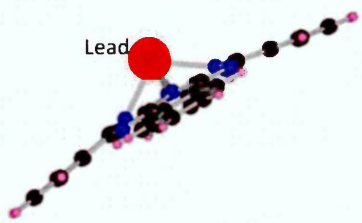

Figure 4.5: The non-plannar structur of PbPc

4.2.2 Films preparation and characterisation.

Thin films of $PbPcR_8$ were prepared in sandwich forms using spin coating. Solutions in dichloromethane in the concentration 10 mg/mL were spun at 2000 rpm onto ITO coated slides and were left to dry for a few hours. Two sandwich structures (ITO/PbPc/In, Al/PbPc/Al) were prepared to investigate the current density-voltage (J(V)) characteristics of thin films of these molecules. Indium and aluminum as electrodes were evaporated under vacuum with pressure of about 2x10^{-5} mbar using vacuum thermal deposition. The rate of film deposition was controlled by a film thickness monitor at the rate 0.1 nm.s^{-1}, and the obtained thickness was 40 nm.

Thickness of the spin coated $PbPcR_8$ films was measured by spectroscopic ellipsometry. The measurements were performed on films deposited on silicon substrates using a Woolam *M-2000V*^{TM} rotating analyser spectroscopic ellipsometer

in the spectral range of 350-1000 nm.

The J(V) characteristics of the devices produced in this work were investigated before and after heat treatment at 70°C using semiconductor characterisation system (Keithly 4200). The measurements were performed by applying a cyclic bias regime in the range ±2V (starting from -2V up to +2V and then back to -2V). All electrical measurements were performed in air and at room temperature.

4.2.3 Electrical and optical properties

Spectroscopic ellipsometry measurements were carried out for the characterization of thickness, refractive index (n) and extinction coefficient (k) of the $PbPcR_8$ films. Using Levenberg-Marquardt multivariate regression algorithm, the measured ellipsometric data were fitted to the model for organic films.

The variation of refractive index and extinction coefficient of **4g** film deposited at 2000 r.p.m. with incident photon wavelength are shown in Figure 4.6 as an example. The thicknesses, refractive indices and extinction coefficients (at λ=633 nm) obtained from ellipsometry data fitting for the other lead phthalocyanines are listed in Table 4.4.

The current-voltage characteristics of thin films of **4g** are presented in Figure 4.7. As shown in the inset to Figure 4.7, the conduction was found to be ohmic at low voltages due to thermal generation of charge carriers, but exhibits power-law dependence at higher voltages (V>0.5V). The room temperature conductivities are summarized in Table 4.4. The conductivity was determined from the linear (Ohmic) region of the measured I(V) curves, i.e., in the voltage range 0-0.5V. The obtained results demonstrate an increase in electronic conduction after heat treatment. Increase of conductivity is found to be larger for **4g** and **4h** films compared to **3g** and **3h.**

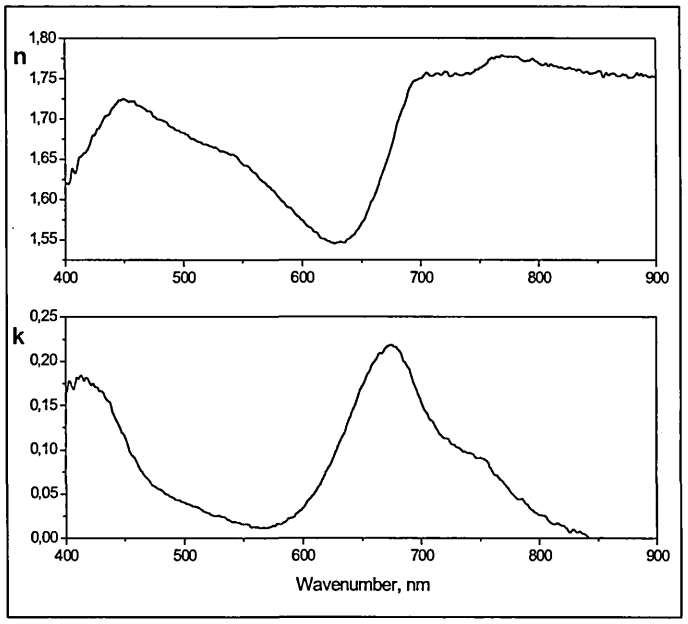

Figure 4.6: Variation of refractive index and extinction coefficient of **4g** film deposited at 2000 r.p.m. with incident photon wavelength

Table 4.4: Thicknesses, refractive indices and extinction coefficients (at λ=633 nm) obtained from ellipsometry data fitting and DC conductivity for $PbPcR_8$ films deposited at 2000 r.p.m

				DC conductivity (σ) $\Omega^{-1}m^{-1}$	
	n	k	Thickness, *nm*	Before heating	After heating
3g	1.50	0.15	38.4	$1.7\cdot10^{-10}$	$5.5\cdot10^{-8}$
3h	1.44	0.08	40.12	$1.9\cdot10^{-10}$	$4.1\cdot10^{-9}$
4g	1.55	0.12	46.66	$2.5\cdot10^{-10}$	$7.8\cdot10^{-7}$
4h	1.51	0.09	47.73	$3.3\cdot10^{-10}$	$2.3\cdot10^{-7}$

The J(V) characteristics are shown to be mainly dependant on the type of electrodes used. In the case of the Al bottom and top electrodes, all junctions have shown open-circuit, probably due to a naturally grown insulating Al_2O_3 layer formed onto the surface of bottom Al electrode[14]. Evaporation of gold electrodes has always led to short circuit in all of our produced samples. AFM micrographs have revealed rough surface morphology of evaporated gold film[15]. This confirms aggregation of Au atoms leading to formation of large grains on both, the organic film and on the glass substrate. Furthermore, due to the high melting point of Au it appears to cause damage to the $PbPcR_8$ which is in liquid crystalline form at about room temperature. The ITO/PbPc/In structures on the other hand have exhibited interesting J(V) behavior. Figure 4.7 shows the J(V) curves of **4g** before and after heat treatment as an example. Both curves demonstrate asymmetric characteristics over the two bias polarities, however, after heat treatment; the studied structure demonstrates clear rectification characteristics, typical of diode behavior. Similar characteristics were observed for the other PbPc analogues studied here.

The dissimilar behavior before and after heat-treatment can be explained by the effect of thermal annealing on the films, which is expected to result in changing the alignment inside the columnar stacking of the molecules in the films. $PbPcR_8$ derivatives exhibit a hexagonal columnar structure over a wide temperature range. It was shown in previous works [3,6] that the ordered films of liquid crystalline metal phthalocyanines can be obtained upon slow cooling from isotropic melt or by heating at the temperature of liquid crystalline phase for some time. Moreover, it has been shown earlier that the heat treatment of films of LC nickel phthalocyanines deposited between two electrodes is found to result in hexagonal homeotropic alignment of molecules in the films [15].

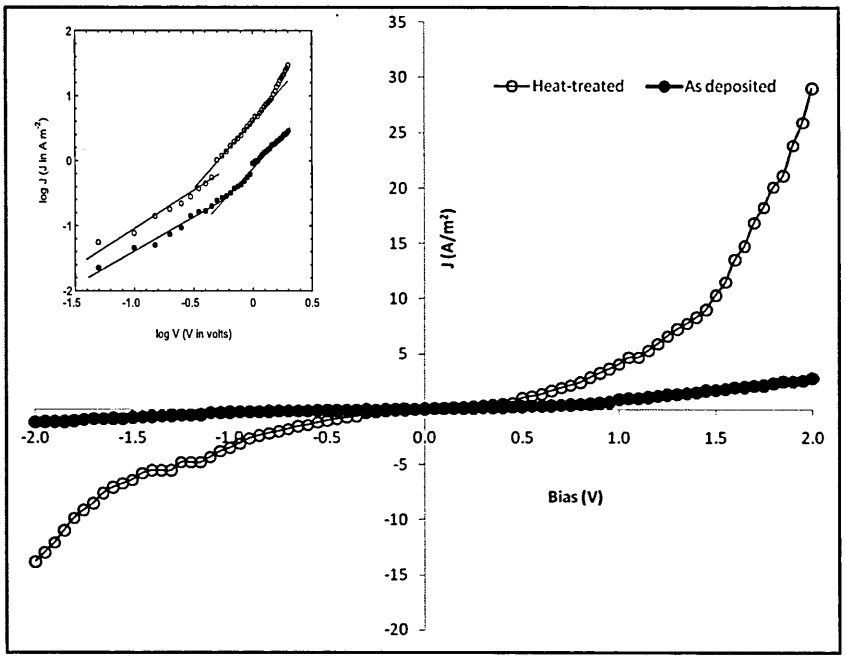

Figure 4.7: J(V) characteristics of thin films of **4g** deposited between ITO and In electrodes. The inset shows the same data of the forward bias characteristics plotted on a log-log scale

The obvious increase of the conductivity for heat-treated **4g** and **4h** films can be ascribed to the increasing π-π interaction in the columnar homeotropic alignment as opposed to the disordered structure of as deposited films [16]. Sulphur atoms in **4g** and **4h** positively affect the electrical conductivity in comparison with oxygen in the substituent chains of **3g** and **3h** (see Table 4.4). As the sulphur is larger than oxygen, the rotational and translational movements of the molecules are hindered within the cores of the columns. Consequently, the structural disorder will be reduced in the stacked alkylthio molecules leading to rapid charge transport [11]. The lowest value of conductivity for **3h** films may also be explained by the formation of crystalline phase at room temperature. According to the published literature [5], the molecules in the crystal are arranged in tilted stacks, which are widely spaced, with the contacts between the aromatic cores bigger than in mesogenic phase.

Among all studies $PbPcR_8$ analogues only **4g** and **4h** have exhibited switching behavior, as shown in Figure 4.8. The films of these compounds have shown

switching loop of memory cell, which can be utilised in applications as memory or logic elements [17]. This effect however was found to degrade after a few cycles of I(V) tests, and has completely disappeared after the samples were subjected to heat treatment. On the first measured I(V) loop, the on state current was found to be larger than the off state by nearly three orders of magnitude giving a high ON/OFF ratio (see inset to Figure 4.8). The possible explanation of this molecular switching effect is that the freshly deposited PbPc film is composed of clusters of different structures within the column stacks before heating. The variation in the film substructure may result in the occurrence of potential barriers, which have to be surmounted by the charge carriers, and thus gives rise to the highly conducting ON state. Furthermore, in the ON state, the external electric field is possibly able to turn some of the stacks into equal orientations resulting in equal lead ion separation which would enhance the highly conductive channels [18]. Several other metal phthalocyanines, both substituted [10,20] and unsubstituted [21] have demonstrated electrical switching which was explained by the existence of potential barriers that control charge transport and thus switching between the ON and OFF states. Thin films of unsubstituted PbPc of the monoclinic structure have shown switching behaviour which was explained by an electric field-induced order–disorder transition mechanism in the stacking direction [22]. In a printed memory device which utilises a water soluble CuPc derivative and a conductive polymer layers sandwiched between two metal electrodes, switching from the OFF state to the ON state was ascribed to increased crystallinity of the CuPc film [23]. This change in crystallinity was confirmed by SEM study, and was found to be responsible for the conductivity after switching. Mukherjee and co-workers [20] have attributed the bistable effect in ITO/PbPc/Al devices to a combination of the presence of a hole-injection barrier at the ITO/PbPc interface and space charge limited hole transport across the undepleted region of the PbPc film to the counter electrode. Thermally deposited thin films of unsubstituted copper phthalocyanine (CuPc) have exhibited bistable effects with an increased ON/OFF ratio when film deposition rate was increased [21]. It was argued that the conductive switching behaviour of the CuPc bistable devices involve bulk trap-controlled space charge limited mechanism and that the carrier transport could be ascribed to a field-induced arrangement of structural defects [21].

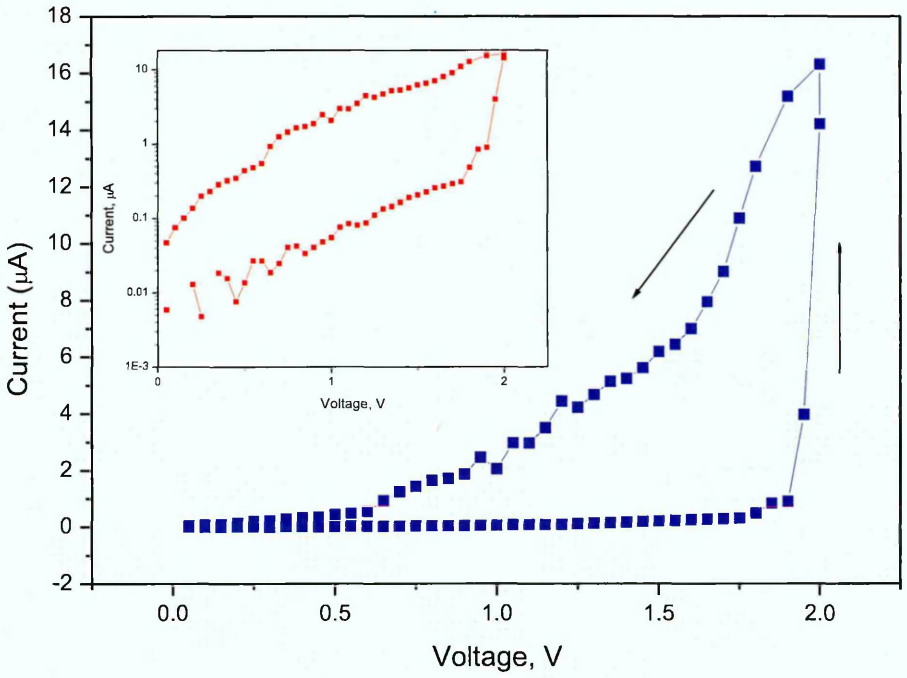

Figure 4.8: Switching characteristics of **4g** films deposited between ITO and In electrodes. The inset shows the same data produced on a log-linear scale for clarity

In the current study the disappearance of the switching effect in heat-treated samples can be further supported by the POM images (Figure 4.9) which clearly reveal film transformation to hexagonal homeotropic phase which results in the disappearance of the potential barriers between clusters within the stacks that were thought to be present in the freshly prepared samples. The **4g** and **4h** films deposited between ITO and metal electrodes do not exhibit any birefringence over a large area when observed between cross-polarizers during POM measurements. The lack of birefringence is characteristic of the hexagonal homeotropic phase, which has a face-on arrangement of discs, as illustrated schematically in Figure below. In other words, the molecules rotate in the direction of face-on to the substrate plane after thermal treatment.

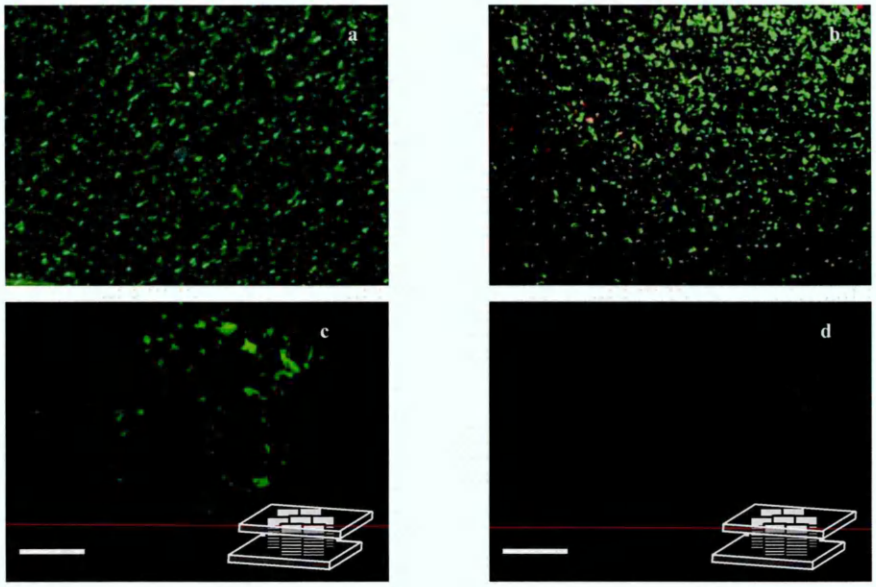

Figure 4.9: Polarizing optical microscopy images with cross polarizers of the **3g** (a), **3h** (b), **4g** (c), **4h** (d) films deposited between ITO and metal electrode. Schematic illustrations of the macroscopic alignments are also given

Summary

In this chapter, thin films of $CuPcR_8$ and $PbPcR_8$ have been prepared. The films were then studied using UV-Vis absorption spectroscopy, ellipsometry and semiconductor characterisation system. The splitting of Q-band in the UV-Vis spectra of $CuPcR_8$ in both cases; solution and film, comfirming the hearing-bone arrangment. The higher conductivity values were found for the films of phthalocyanines with the molecules oriented perpendicular to the substrate surface. The lateral conductivity tends to dicrease slightely with the increasing of chain length, and the higher conductivity in the alkylithio-derivatives is thought to be caused by the reduced structural disorder during phase transition which is caused by the presence of sulphur atoms.Films of $PbPcR_8$ exhibited an increase in the electronic conduction after heat treatment. A typical switching effect was also observed with high ON/OFF ratio, making this kind of material as promising candidates for memory applications.

Reference List

[1] T.V. Basova, M. Çamur, A.A. Esenpınar, S. Tuncel, A. Hassan, A. Alexeyev, H. Banimuslem, M. Durmuş, A.G. Gürek, V. Ahsen, Effect of substituents on the orientation of octasubstituted copper (II) phthalocyanine thin films, Synth. Met. 162 (2012) 735-742.

[2] T. Basova, E. Kol'tsov, A.G. Gürek, D. Atilla, V. Ahsen, A.K. Hassan, Investigation of liquid-crystalline behaviour of copper octakisalkylthiophthalocyanine and its film properties, Mater. Sci. Eng. C. 28 (2008) 303-308.

[3] T.V. Basova, M. Durmus, A. Gü l Gürek, V. Ahsen, A. Hassan, Effect of interface on the orientation of the liquid crystalline nickel phthalocyanine films, J. Phys. Chem. C. 113 (2009) 19251-19257.

[4] B.M. Hassan, H. Li, N.B. McKeown, The control of molecular self-association in spin-coated films of substituted phthalocyanines, J. Mater. Chem. 10 (2000) 39-45.

[5] K. Hatsusaka, K. Ohta, I. Yamamoto, H. Shirai, Discotic liquid crystals of transition metal complexes, part 30: Spontaneous uniform homeotropic alignment of octakis(dialkoxyphenoxy)phthalocyaninatocopper(II) complexes, J. Mater. Chem.11 (2001) 423-433.

[6] T.V. Basova, A.G. Gürek, V. Ahsen, Investigation of liquid-crystalline behavior of nickel octakisalkylthiophtahlocyanines and orientation of their films, Mater. Sci. Eng. C. 22 (2002) 99-104.

[7] H. Nakahara, K.Z. Sun, K. Fukuda, N. Azuma, H. Nishi, H. Uchida, T. Katsube, Molecular orientation and electrical behaviour of Langmuir-Blodgett films of phthalocyanine derivatives containing eight alkyl chains, J. Mater. Chem. 5 (1995) 395-399.

[8] D. Atilla, N. Kilinç, F. Yuksel, A.G. Gürek, Z.Z. Öztürk, V. Ahsen, Synthesis, characterization, mesomorphic and electrical properties of tetrakis(alkylthio)-substituted lutetium(III) bisphthalocyanines, Synth. Met. 159 (2009) 13-21.

[9] A.M. Van de Craats, P.G. Shouten, J.M. Warman, Fundamental phthalocyanine molecular material, The Japanese Liquid Crystal Society. 2 (1998) 12-27.

[10] K. Ban, N. Kaoru, K. Ohta, H. Shirai, Discotic liquid crystals of transition metal complexes 27: Supramolecular structure of liquid crystalline octakisalkylthiophthalocyanines and their copper complexes, J. Mater. Chem. 10 (2000) 1083-1090.

[11] K. Ban, K. Nishizawa, K. Ohta, A.M. Van de Craats, J.M. Warman, I. Yamamoto, H. Shirai, Discotic liquid crystals of transition metal complexes 29: Mesomorphism and charge transport properties of alkylthio-substituted phthalocyanine rare-earth metal sandwich complexes, J. Mater. Chem. 11 (2001) 321-331.

[12] S. Tuncel, H.A.J. Banimuslem, M. Durmuş, A.G. Gürek, V. Ahsen, T.V. Basova, A.K. Hassan, Liquid crystalline octasubstituted lead(ii) phthalocyanines: Effects of alkoxy and alkylthio substituents on film alignment and electrical properties, New J. Chem. 36 (2012) 1665-1672.

[13] T. Nyokong, Electronic spectral and electrochemical behavior of near infrared absorbing metallophthalocyanines, Structure and Bonding. 135 (2010) 45-88.

[14] J. Koo, H. Lee, Y. Ha, Y. Choi, Y.K. Kim, Electrical properties of porphyrin-based switching devices, Thin solid films, 438-439 (2003) 123-127.

[15] T.V. Basova, A. Hassan, M. Durmus, A.G. Gurek, V. Ahsen, Orientation of the liquid crystalline nickel phthalocyanine films confined between electrodes, Synth. Met. 161 (2011) 1996-2000.

[16] K. Ohta, K. Hatsusaka, M. Sugibayashi, M. Ariyoshi, K. Ban, F. Maeda, R. Naito, K. Nishizawa, A.M. Van De Croats, J.M. Warman, Discotic liquid crystalline semiconductors, Molec. Cryst. Liquid Cryst. 397 (2003) 25/[325]-45/[345].

[17] C.P. Collier, J.O. Jeppesen, Y. Luo, J. Perkins, E.W. Wong, J.R. Heath, J.F. Stoddart, Molecular-based electronically switchable tunnel junction devices, J. Am. Chem. Soc. 123 (2001) 12632-12641.

[18] C. Hamann, A. Mrwa, Switching behaviour of lead phthalocyanine thin films, Int. J. Elect. 73 (1992) 1039-1040.

[19] T.V. Basova, A.G. Gürek, D. Atilla, A.K. Hassan, V. Ahsen, Synthesis and characterization of new mesomorphic octakis(alkylthio)-substituted lead phthalocyanines and their films, Polyhedron. 26 (2007) 5045-5052.

[20] B. Mukherjee, A.K. Ray, A.K. Sharma, M.J. Cook, I. Chambrier, A simply constructed lead phthalocyanine memory diode, J. Appl. Phys. 103 (2008).

[21] K. Onlaor, B. Tunhoo, P. Keeratithiwakorn, T. Thiwawong, J. Nukeaw, Electrical bistable properties of copper phthalocyanine at different deposition rates, Solid-State Elect. 72 (2012) 60-66.

[22] T. Frauenheim, C. Hamann, M. Mueller, Electric field-induced disorder-order transition in organic polycrystalline films of quasi-one-dimensional lead-phthalocyanine. Phys. Stat. Solidi (A) App.Res. 86 (1984) 735-747.

[23] K. Lian, R. Li, H. Wang, J. Zhang, D. Gamota, Printed flexible memory devices using copper phthalocyanine, Mater. Sci. Eng. B: Solid-State Materials for Advanced Technology. 167 (2010) 12-16.

Chapter 5

Modification of Single-Walled Carbon Nanotubes Using Optical Detection Method

Chapter overview

This chapter is dedicated to compare between two types of hybrid materials depending on the method followed for SWCNT modification. Tetra-substituted copper phthalocyanine ($CuPcR_4$) having different non-peripheral substitutions were prepared by co-researchers from Gebze Technical University, Turkey, and have been used in this part of the study. These are labelled according to the type of substituents as **Pc1** and **Pc2** for $R=O(C_7H_{15}O_3)$, **Pc3** and **Pc4** for $R=S(C_7H_{15}O_3)$, and **Pc5** for $R=S(C_{16}H_{33})$, as shown in Figure 5.1. Full details of synthesis and characterisation of $CuPcR_4$ is published in the literature [1,2]. FTIR and Raman spectroscopy have been utilized to address the nature of interaction between SWCNT and $CuPcR_4$. The UV-Visible spectra and morphology of the prepared hybrids are also discussed. DC-conductivity measurements were carried out to monitor the effect of acid treatment on the separation of metallic and semiconducting nanotubes. Finally, the suitability of hybrid films' structures for the optical detection method using total internal reflection ellipsometry (TIRE) technique has been examined.

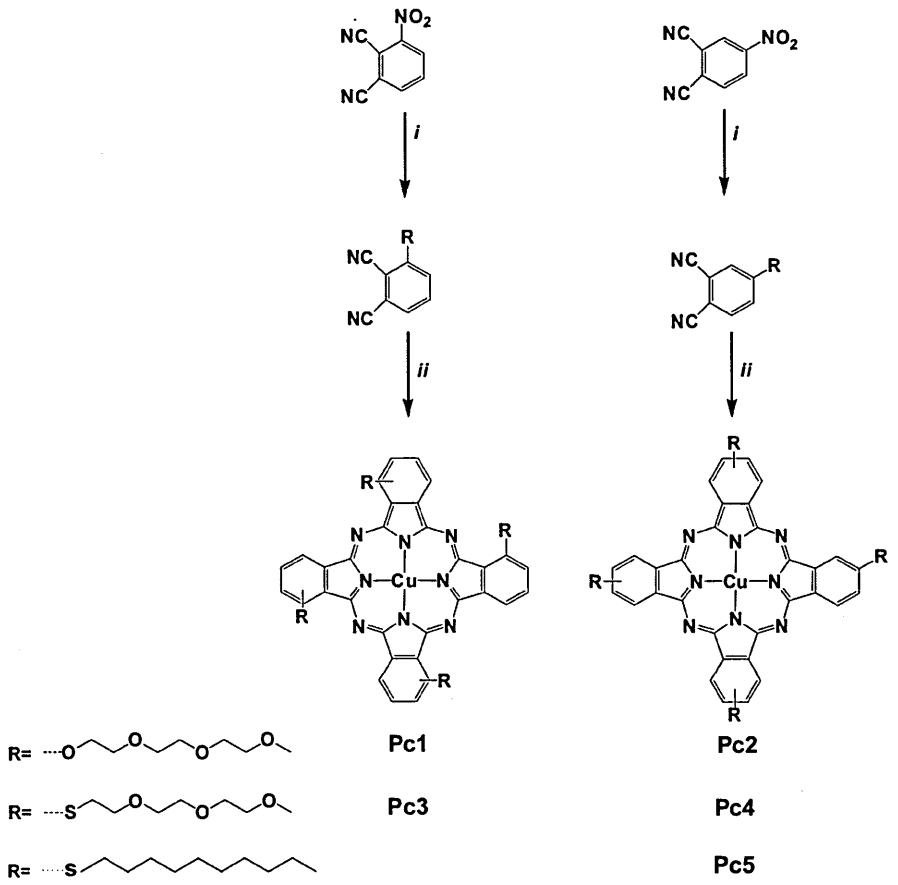

Figure 5.1: Synthesis route of $CuPcR_4$ derivatives

5.1 Experimental details

5.1.1 Preparation of SWCNT-$CuPcR_4$ Hybrids

Pristine SWCNT-$CuPcR_4$ hybrid (PCNT-Pc): The purpose of this part of the work is to further emphasise the effect of acid treatment on improving the binding between SWCNT and $CuPcR_4$ molecules and thus enhancing the solubility of the hybrid in conventional organic solvents. 5 mg of **Pc3** has been dissolved in 1 ml DMF and sonicated for 15 minutes. At the same time 1mg of pristine (untreated) SWCNT was suspended in 3 ml DMF and sonicated for 40 minutes. After sonication, the suspension was stirred and the **Pc3** solution was added drop wise to the CNTs suspension during stirring. The stirring was continued for another 5 hours before the mixture was centrifuged, washed with DMF several times, centrifuged again and finally dried.

Acid-treated SWCNT-CuPcR$_4$ hybrid (ATCNT-Pc): 25 mg SWCNT was stirred under 70 °C in concentrated 3:1 HNO_3 and H_2SO_4 for 2 hours. The mixture was then centrifuged, washed several times with water, centrifuged again and dried. 2 mg of the resultant powder was mixed with 5 mg of **Pc3** in 5 ml DMF and sonicated for 4 hours. The suspension was centrifuged, washed with DMF, centrifuged again and dried.

Figure 5.2 shows the solutions of **Pc3** and the suspensions of SWCNT, PCNT-**Pc3** and ATCNT-**Pc3** in DMF. It can be visibly appreciated that ATCNT-**Pc3** exhibited better solubility than PCNT-**Pc3** and for both hybrids the brownish colour indicates that π-π interaction took place between the two materials [3,4].

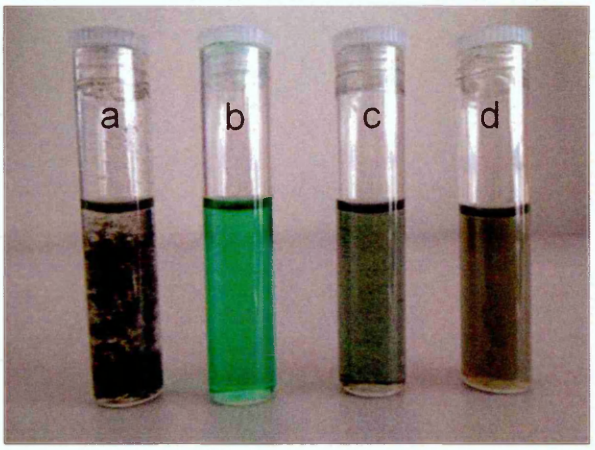

Figure 5.2: (a) pristine SWCNT, (b) **Pc3**, (c) PCNT-**Pc3**, and (d) ATCNT-**Pc3**

5.2 Characterisation of SWCNT-CuPcR$_4$ Hybrids

Pristine and acid treated SWCNT were used for the preparation of their hybrids with CuPcR$_4$ derivatives. Pristine SWCNT were oxidized by means of a mixture of sulfuric and nitric acid. This procedure introduces carboxylic acid functionalities and defects at the ends of the nanotubes as well as some carboxylic acid units at the sidewalls [5-7].

5.2.1 Foureir Transform Infrared Spectra (FTIR)

FTIR analysis was carried out in order to determine the interaction between $CuPcR_4$ and SWCNT. Figure 5.3 shows FTIR spectra of pure **Pc3**, PCNT-**Pc3** and ATCNT-**Pc3**. The bands at 2858 and 2921 cm^{-1} assigned to the C-H stretches of substitution groups in **Pc3** are present in all spectra. Another feature that should be given attention is the peaks at 1490, 1384, 1251 and 1078 cm^{-1}, which are characteristics of phthalocyanine macrocycles [8], and are present in all three spectra. All these observations suggest that the substituted copper phthalocyanine has successfully anchored onto SWCNT walls by means of noncovalent binding.

The spectra of the hybrids contain some bands which correspond to $CuPcR_4$ molecule vibrations. The largest shift in the peak position associated with the C=C stretching mode from 1635 cm^{-1} in the spectrum of pure **Pc3** to 1653 cm^{-1} is observed in the hybrids spectra. These shifts as well as different ratio of intensities may result from the electron delocalization due to the π-π interactions between SWCNT and $CuPcR_4$ molecules [3,9]. The spectrum of ATCNT-**Pc3** shows a band at around 1730 assigned to ν(C=O) vibration of carboxylic group, which results from the acidification of carbon nanotubes in ATCNT-**Pc3** [10,11].

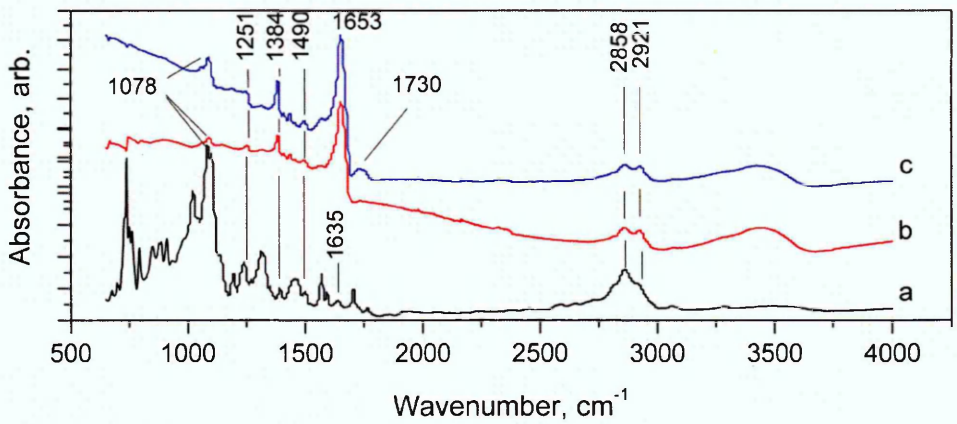

Figure 5.3: FTIR spectra of (a) pure **Pc3**, (b) PCNT-**Pc3** and (c) ATCNT-**Pc3**

5.2.2 Raman spectra

The non-covalent attachment can also be confirmed by Raman spectroscopy. Raman spectra for pristine SWCNT, acid treated SWCNT and both hybrids are shown in Figure 5.4. The radial breathing modes (RBM), disorder D mode and tangential/graphite mode (G-band) are monitored as indicators of functionalisation with **Pc3** [12]. The spectra were normalized to the tangential G band at ~1580cm^{-1}. Both spectra of pristine SWCNT before (Figure 5.4a) and after (Figure 5.4b) hybridization contained the following characteristic peaks: the D band located at about 1340 cm^{-1} (disorder mode), which is due to the breathing modes of sp^2 atoms [13-15] and the G band centred at 1590 cm^{-1} (tangential mode), due to bond stretching of all pairs of sp^2 atoms [16].

Comparing Figure 5.4a with Figure 5.4b, little variation of the ratio of the D band to the G band (I_D/I_G) can be observed, which suggests that $CuPcR_4$ derivatives are associated with the surface of SWCNT through non-covalent modification. Moreover, the multiple peaks observed in the radial breathing mode (RBM) of SWCNT (158-304 cm^{-1}) could be ascribed to a distribution of diameters in the SWCNT samples [17,18]. They correspond to nanotube diameters in the range from 0.7 to 1.4 nm.

The Raman spectra of PCNT-**Pc3** revealed significant shift on the peak positions located in the range 158-225 cm^{-1}. For example, the RBMs at 202, 227 and 258 cm^{-1} of SWCNT have a shift to 207, 230 and 262 cm^{-1} after adsorption of **Pc3**. It was shown [19] that the radial breathing modes of the Raman spectrum are sensitive to the adsorption coating of the nanotubes with polynuclear aromatic hydrocarbon molecules. The π-π stacking interaction between SWCNT and phthalocyanine aromatic rings induced a higher frequency shift of RBM and gave a kind of "mode hardening" effect [20].

In the Raman spectrum of the acid-treated SWCNT, the radial breathing modes have disappeared when compared to the spectrum of pristine SWCNT (Figure 5.4c). The decay of these modes is consistent with the disruption of the oscillator strength that gives rise to these modes. Similar results were reported by Fantini and co-workers [21] where spectral shifts, broadening, and reduction in RBM intensity were attributed to displacement of the Fermi level due to the added functional group on the CNT side-

wall. As shown in Figure 5.5c, the carboxylated SWCNTs showed the characteristic peaks with a disorder-induced D-band at 1348 cm^{-1} and a tangential stretch G-band at 1588 cm^{-1}.

The D/G peak intensity ratio increases from 0.04 for pristine SWCNT to 0.30 for acid treated SWCNT which indicates the formation of covalent bonds at the surface of the carbon nanotube through conversion of sp^2-hybridized carbon atoms to sp^3-hybridized carbons on the nanotube surface.

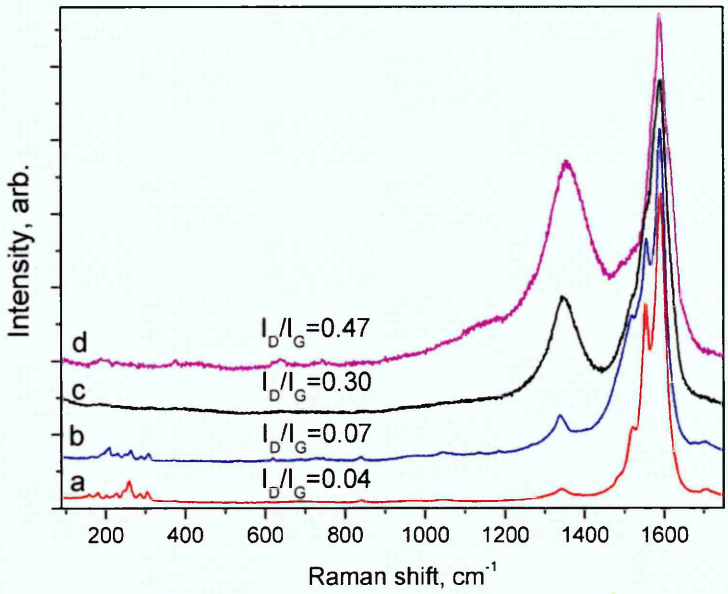

Figure 5.4: Raman spectra of pristine SWCNT (a), PCNT-**Pc3** (b), acid-treated SWCNT (c) and ATCNT-**Pc3** (d)

The relative decrease in the tangential mode (G-band) is consistent with the loss of electronic resonance as a result of the covalent attachment of the substituent. Further increase in the relative intensity of the D band vs. G band (I_D/I_G=0.47) was also observed in the spectrum of acid treated SWCNT hybrids with **Pc3** (Figure 5.4d). Raman spectra of the other functionalized SWCNT materials display similar modifications but to different degrees [22,23].

The Raman spectra of the hybrids with acid treated SWCNT are significantly affected by the interaction with **Pc3**, whereas those with pristine SWCNT do not vary so much upon the addition of the **Pc3** binder. The I_D/I_G ratios of the hybrids with pristine SWCNT increase only slightly with the addition of the phthalocyanine, whereas those with acid treated SWCNT increase significantly.

It might be that, in the bundled network structure of the hybrids with pristine SWCNT, the π-π interactions between nanotubes and **Pc3** are the dominant influence on the Raman spectrum.

However, in the case of the hybrids with acid treated SWCNT, not only π-π interaction but also van der Waals interaction of –COOH groups with the nitrogen atoms of phthalocyanine ring [24] and alkyl substituents of phthalocyanine ring [10] are the factors affecting the Raman spectra.

5.2.3 UV-Visible absorption spectra

Figure 5.5 shows the UV-visible absorption spectra of solutions of SWCNT, **Pc3**, PCNT-**Pc3** and ATCNT-**Pc3** in DMF. Figure 5.6 shows the spectra of the other phthalocyanines (**Pc1**, **Pc2**, **Pc4** and **Pc5**) and their hybrids with ATCNT in DMF. All the $CuPcR_4$ compounds used in this work exhibit typical electronic absorption spectra. The spectra are characterised with two strong absorption regions, one in the wavelength range of 650-720 nm (Q-band) arising from the electron transitions from highest occupied molecular orbital (HOMO) a_{1u} to the lowest unoccupied molecular orbital (LUMO) e_g and another in the range of 300-450 nm (B-band) which is attributed to the electron transitions from the (HOMO) a_{2u} to the (LUMO) e_g [2,25]. Furthermore, absorption within the Q-band is split into two absorption peaks, one with much higher intensity than the other. This can be ascribed to dominant monomer absorption with the lower intensity shoulder being ascribed to molecular aggregation in chloroform solution. The absorption spectrum of SWCNT is featureless as reported elsewhere [7,26,27].

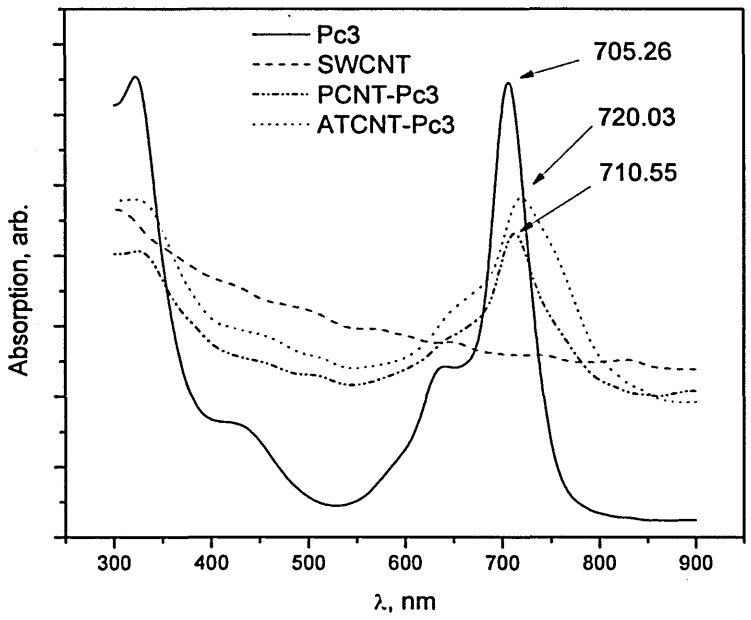

Figure 5.5: UV-Vis absorption spectra of **Pc3** (solid line), SWCNT (dashed line), PCNT-**Pc3** (dashed-dotted line) and ATCNT-**Pc3** (dotted line) solutions in DMF

In the absorption spectra of PCNT-Pc3 and ATCNT-Pc3, the maxima of the Q-bands are shifted to the red by $\Delta\lambda$ = 5.29 nm and $\Delta\lambda$ = 14.77 nm respectively. The maxima of the Q-bands in the absorption spectra of ATCNT-**Pc1**, ATCNT-**Pc2**, ATCNT-**Pc4** and ATCNT-**Pc5** hybrids shown in Figure 5.6a,b,c and d are broadened and red-shifted by 16.42, 10.59, 17.48 and 20 nm in comparison with **Pc1**, **Pc2**, **Pc4** and **Pc5** spectra, respectively.

It can also be seen that the Q-band splitting has either disappeared or became weaker in the absorption spectra of the hybrids, which indicates dominant monomer absorption. These changes are suggested to take place due to the strong π-π interaction between carbon nanotubes and phthalocyanine molecules, where phthalocyanines are usually considered as electron donors, while carbon nanotubes as acceptors [28].

This interaction has been frequently ascribed to the reduced aggregation in the MPc/CNT composites [29,30].

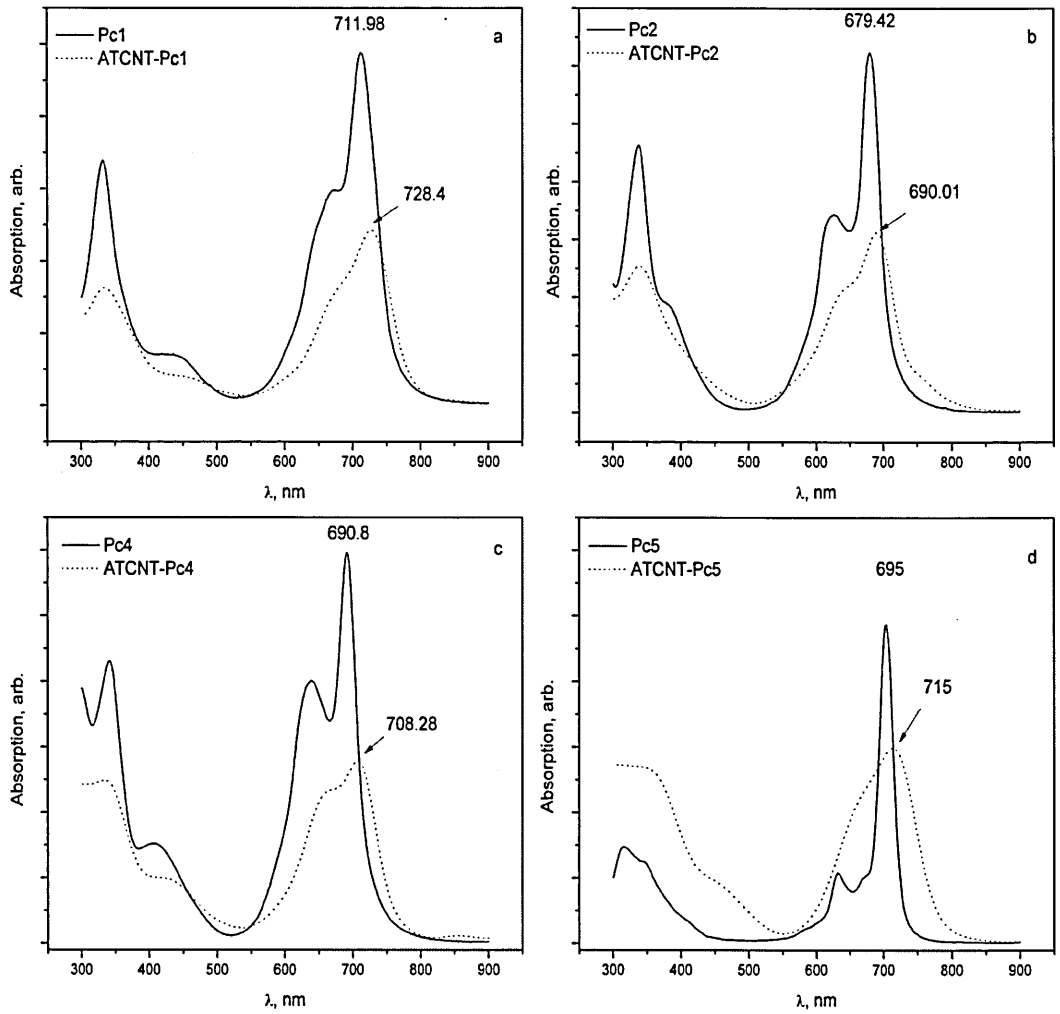

Figure 5.6: UV-Vis absorption spectra of (a) **Pc1**, (b) **Pc2**, (c) **Pc4** and (d) **Pc5** and their hybrids with ATCNT in DMF

5.2.4 Morphology

5.2.4.1 Atomic force microscopy (AFM)

Figures 5.7-5.18 show AFM images of $CuPcR_4$ and SWCNT/$CuPcR_4$ films spun onto silicon substrates with the roughness analysis presented at the bottom of the Figures and 3D images at the right.

AFM measurements in tapping mode have been performed on all samples in this study. Figure 5.7 shows typical fibre features of $CuPcR_4$ (**Pc3**) film, which is

different from the topology of its hybrids. Phthalocyanine and almost all organic dyes tend to make very dense aggregations in the solid state.

These aggregates are represented as a coplanar association of rings developing from monomer to dimer and higher order complexes and are driven by π-π interaction and van der Waals forces [31].

It can clearly be seen that surface of PCNT-**Pc3** film (Figure 5.8) is less homogeneous than that of ATCNT-**Pc3** (Figure 5.9) with significant decrease in main roughness of the latter; this is because ATCNT-**Pc3** exhibited improved solubility in organic solvents, resulting in smoother and more homogeneous films. This is because the de-bundling effect of the acid treatment, which results in better dispersion of the complex in organic solvents.

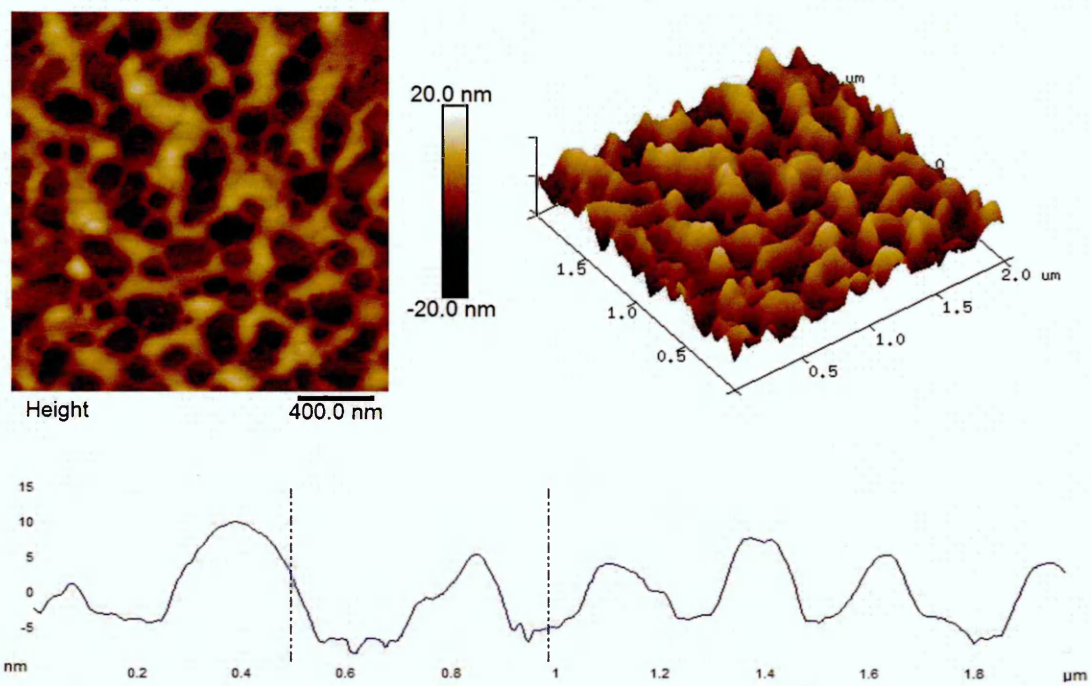

Figure 5.7: AFM image of **Pc3**; top and 3D view. Roughness analysis shown at the bottom

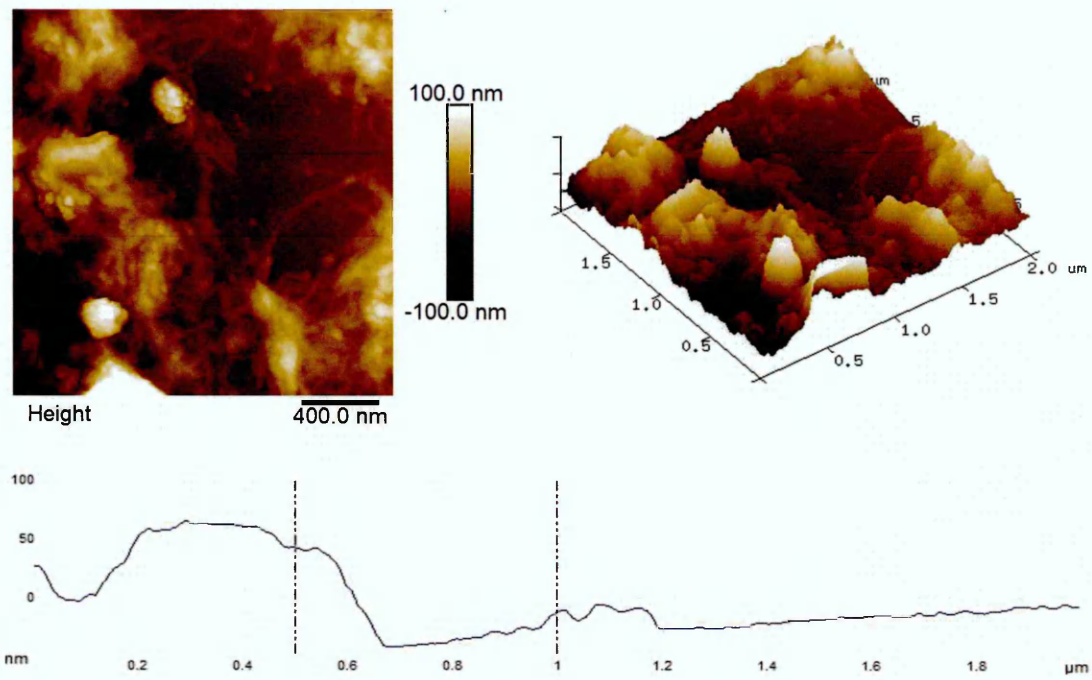

Figure 5.8: AFM image of PCNT-**Pc3**; top and 3D view. Roughness analysis shown at the bottom

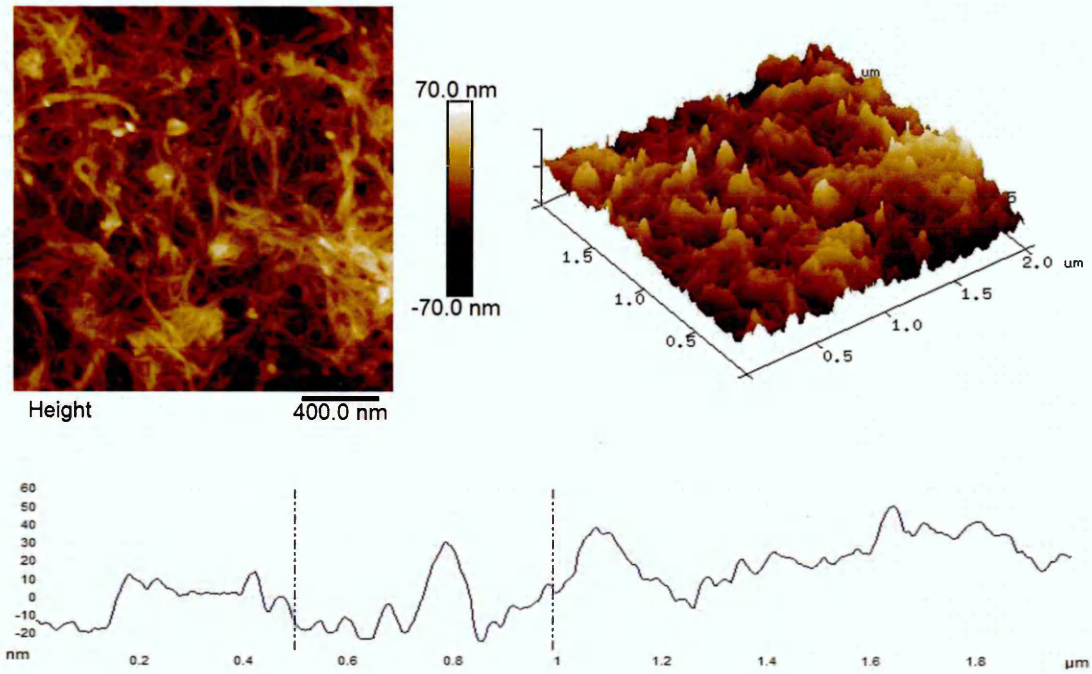

Figure 5.9: AFM image of ATCNT-**Pc3**; top and 3D view. Roughness analysis shown at the bottom

Films of other $CuPcR_4$ (**Pc1**, **Pc2**, **Pc4** and **Pc5**) demonstrate fibrous-like porous morphology in a similar manner as **Pc3** and presented in Figures 5.10,12,14 and 16. Figures 5.11, 5.13, 5.15 and 5.17, represent the AFM images of ATCNT-**Pc1**, ATCNT-**Pc2**, ATCNT-**Pc4** and ATCNT-**Pc5**, which show that the phthalocyanine molecules are attached to the surface of carbon nanotubes confirming the formation of networks of $CuPcR_4$ and SWCNT. Similar morphology was observed for poly(3-hexylthiophene) (P3HT)/multi-walled carbon nanotube (MWCNT) films [32] and MWCNTs and SWCNTs with lead tetra-iso-pentyloxyphthalocyanine (PbPc) [33].

The main roughness (R_a), standard deviation (RMS) and maximum height (R_{max}) for all phthalocyanines measured in this study and their hybrids with SWCNT are summarised in Table 5.1. Figure 5.18 represents an enlarged AFM image of ATCNT-**Pc5** deposited on silicon, showing individual and shortened nanotubes with approximate length of 250 nm surrounded by phthalocyanine molecules.

Table 5.1. Roughness parameters of all $CuPcR_4$ and their hybrids with SWCNT

	R_a, nm	**RMS, nm**	**R_{max}, nm**
Pc1	1.954	3.172	9.658
ATCNT-Pc1	4.921	8.751	19.102
Pc2	1.450	2.197	7.695
ATCNT-Pc2	3.312	6.935	17.613
Pc3	1.733	3.501	8.461
PCNT-Pc3	8.213	15.575	37.570
ATCNT-Pc3	5.811	9.550	20.275
Pc4	1.630	2.153	6.876
ATCNT-Pc4	4.153	7.877	18.252
Pc5	0.837	1.204	4.168
ATCNT-Pc5	4.727	6.812	16.906

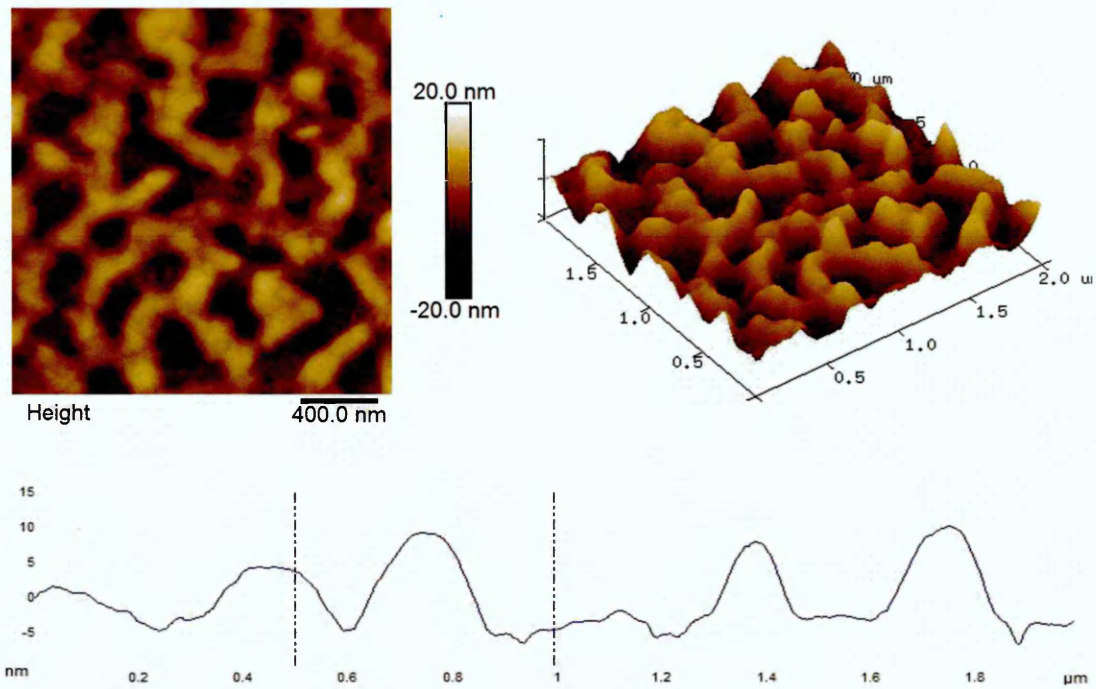

Figure 5.10: AFM image of **Pc1**; top and 3D view. Roughness analysis shown at the bottom

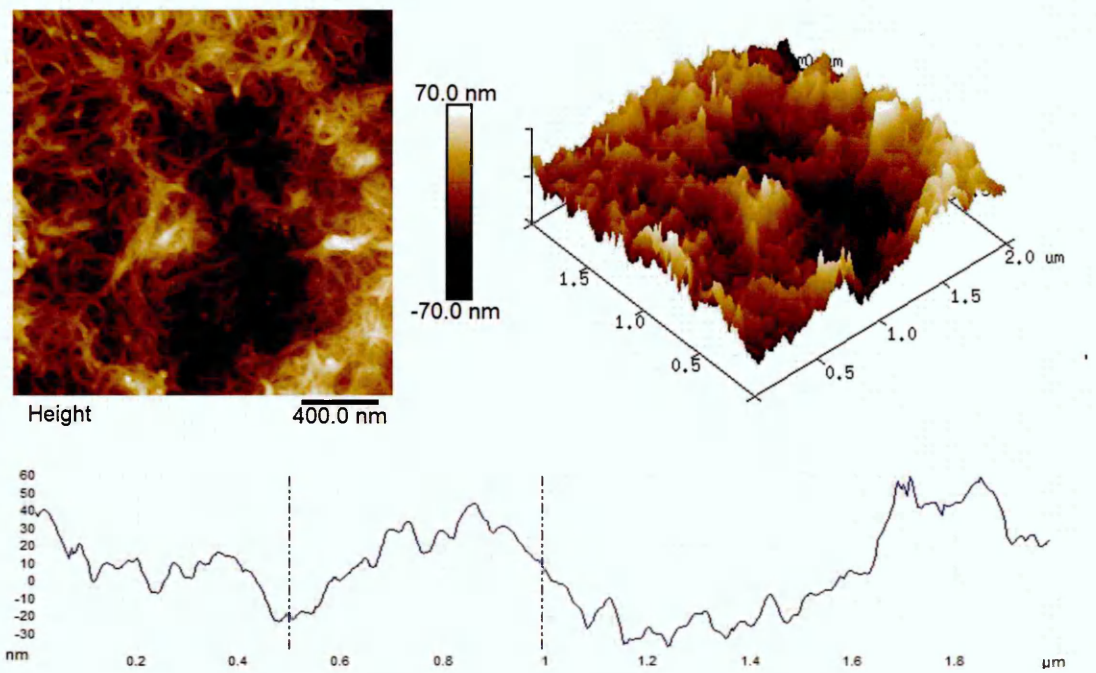

Figure 5.11: AFM image of ATCNT-**Pc1**; top and 3D view. Roughness analysis shown at the bottom

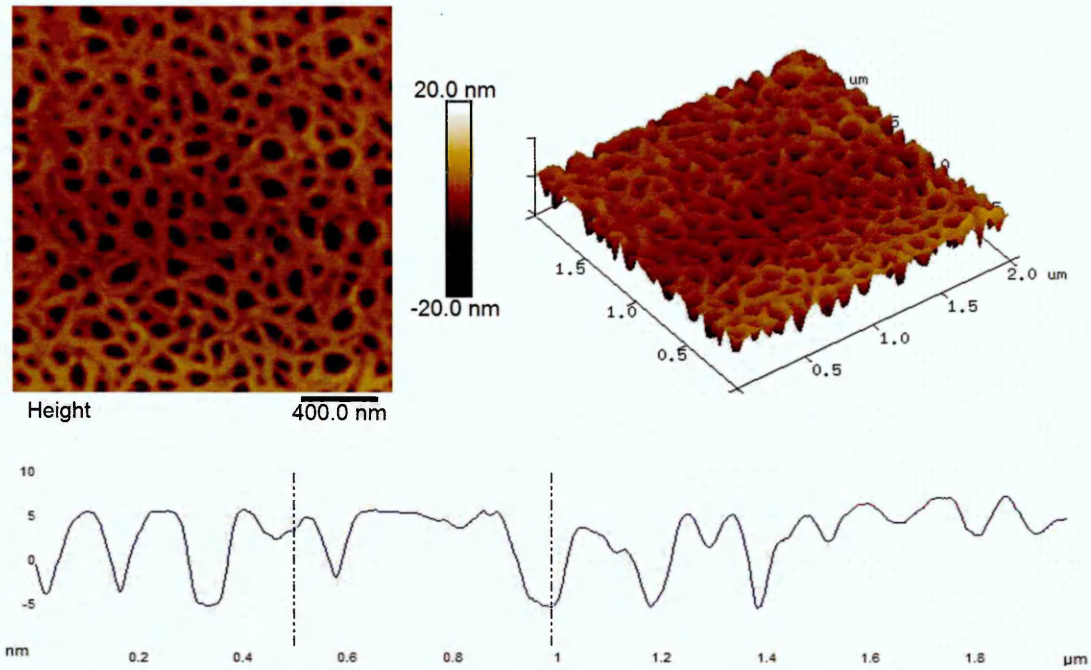

Figure 5.12: AFM image of **Pc2**; top and 3D view. Roughness analysis shown at the bottom

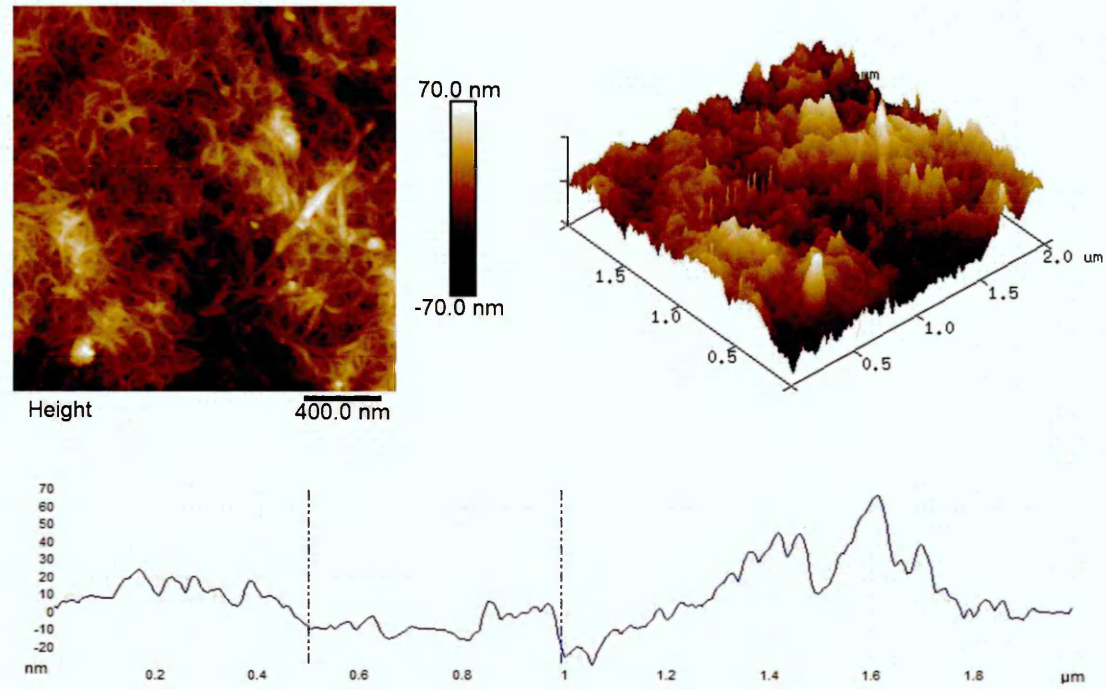

Figure 5.13: AFM image of ATCNT-**Pc2**; top and 3D view. Roughness analysis shown at the bottom

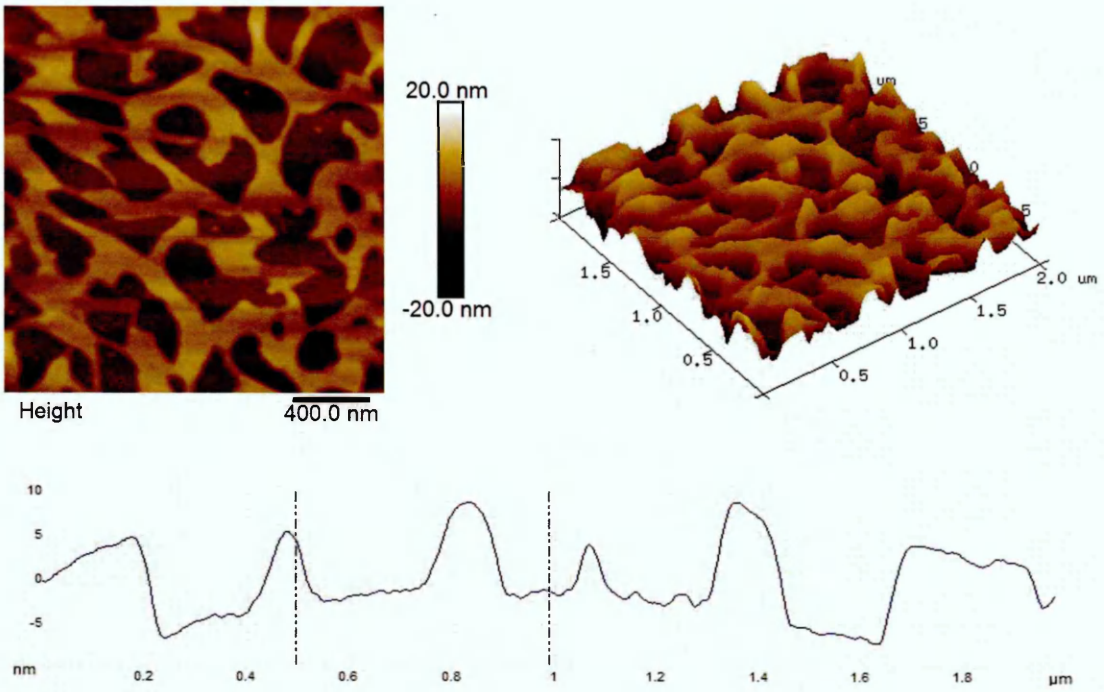

Figure 5.14: AFM image of **Pc4**; top and 3D view. Roughness analysis shown at the bottom

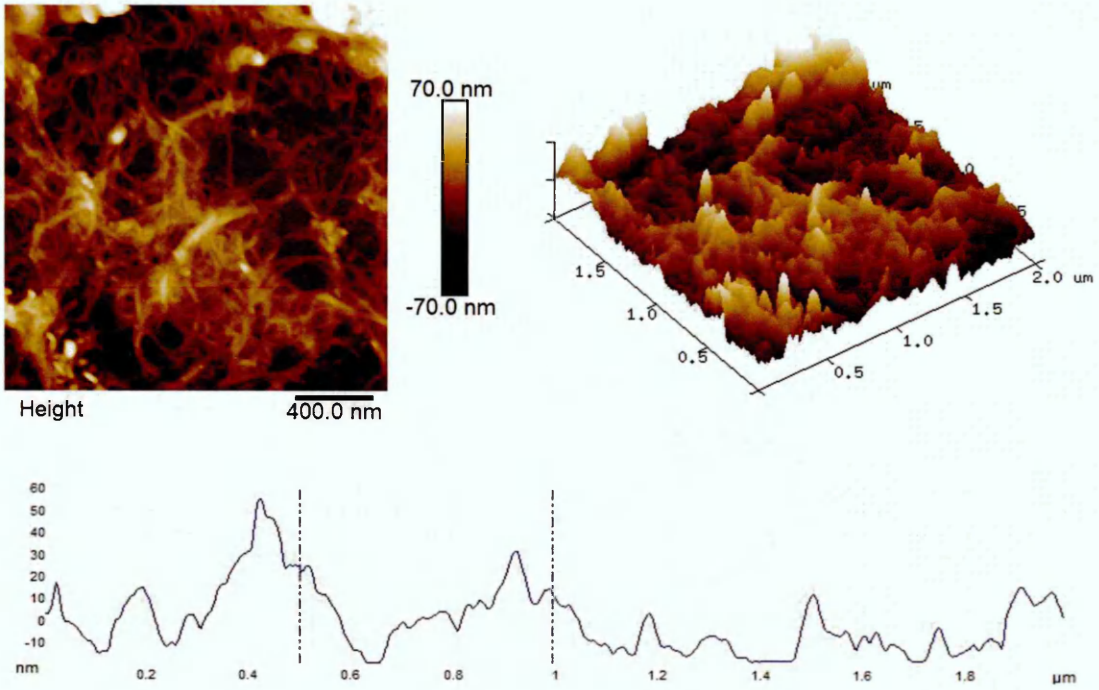

Figure 5.15: AFM image of ATCNT-**Pc4**; top and 3D view. Roughness analysis shown at the bottom

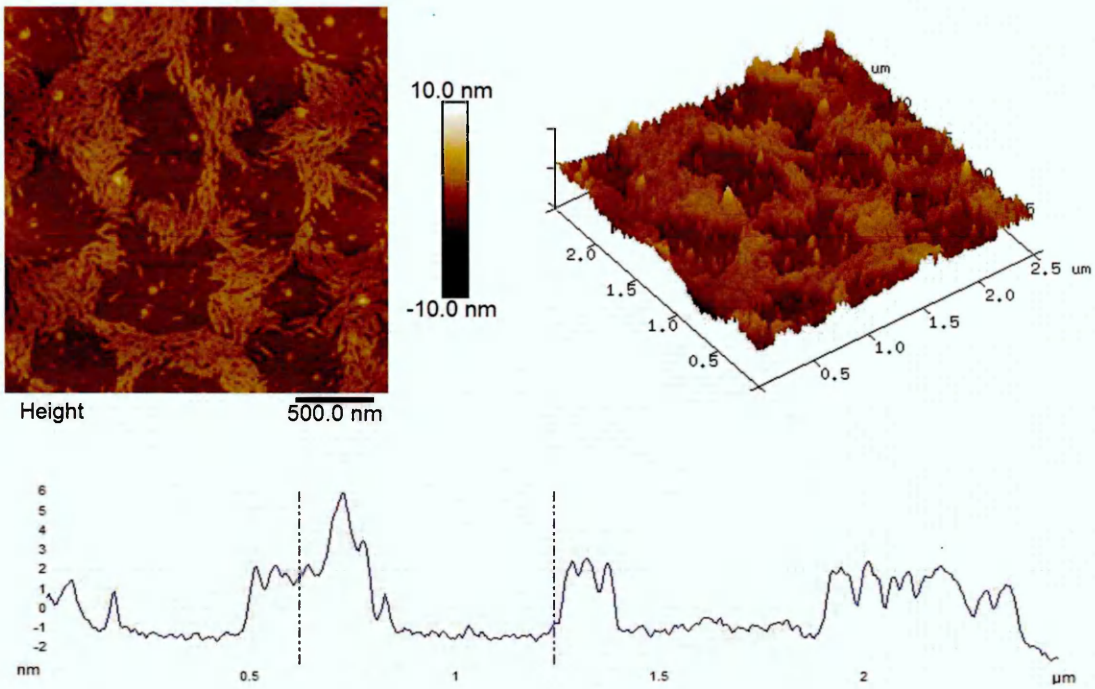

Figure 5.16: AFM image of **Pc5**; top and 3D view. Roughness analysis shown at the bottom

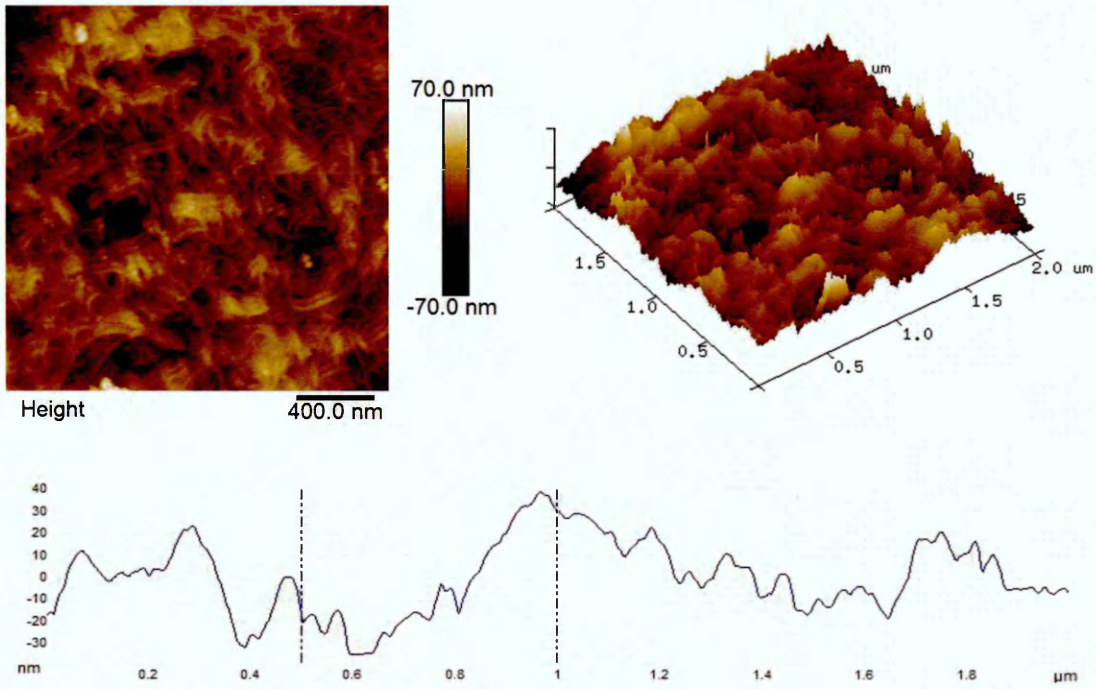

Figure 5.17: AFM image of ATCNT-**Pc5**; top and 3D view. Roughness analysis shown at the bottom

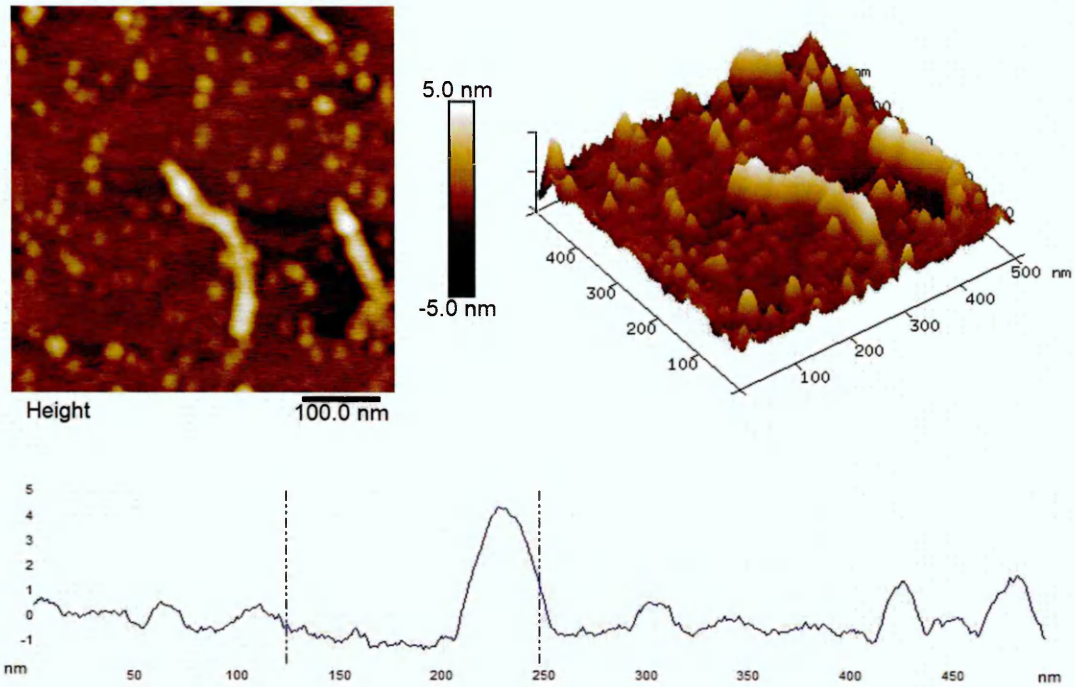

Figure 5.18: AFM image of ATCNT-**Pc5** in higher resolution; top and 3D view. Roughness analysis shown at the bottom

5.2.4.2 Scanning electron microscopy (SEM)

Pristine CNTs typically tend to bundle together (Figure 5.19) and to aggregate due to van der Waals attraction between individual tubes [34] as well as the high length to diameter ratio; this makes them hard to disperse in common organic solvents [7]. Figure 5.19 shows the SEM images of pristine SWCNT; (a and b) as powder, (c and d) as thin films drop-casted on silicon substrate from its DMF solution.

The intrinsic quality of SWCNTs structure is still preserved after mixing with phthalocyanines without acid treatment. This can obviously be seen in Figure 5.20a and b, which represent the image of PCNT-**Pc3** thin film. Figure 5.20c shows the random distribution of phthalocyanine molecules aggregations onto carbon nanotube bundles in a high magnification image of PCNT-**Pc3**.

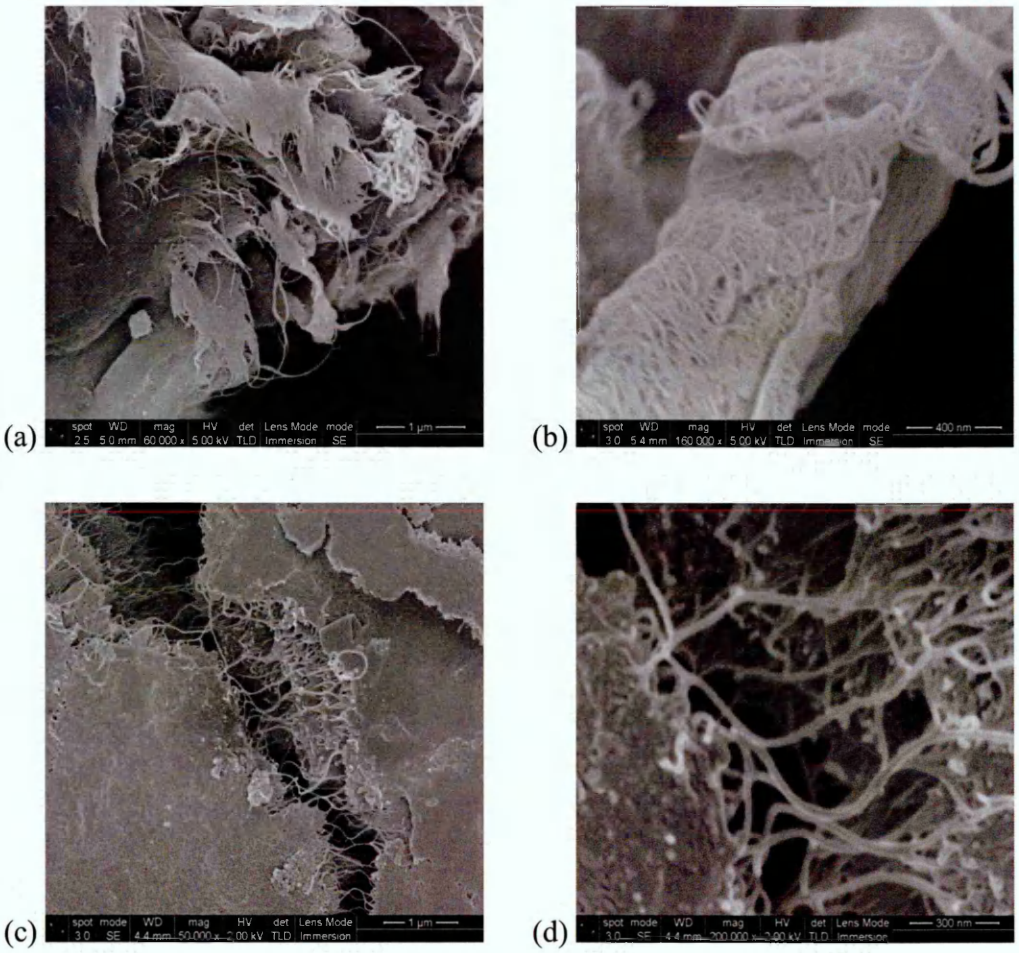

Figure 5.19: SEM images of pristine SWCNT; (a,b) in powder form and (c,d) in thin film form deposited on silicon substrate from solution of DMF.

Acid treatment of the nanotubes induces the de-bundling effect (Figure 5.21) disrupting the van der Waals interactions [2,35] and leading to the formation of carbon nanotubes network with much improved solubility in organic solvents.

This chemical modification has been performed to achieve enhanced interaction between SWCNT and $CuPcR_4$ molecules leading to the formation of a composite with much improved solubility in common organic solvents and hence smoother films were obtained to perform optical investigation.

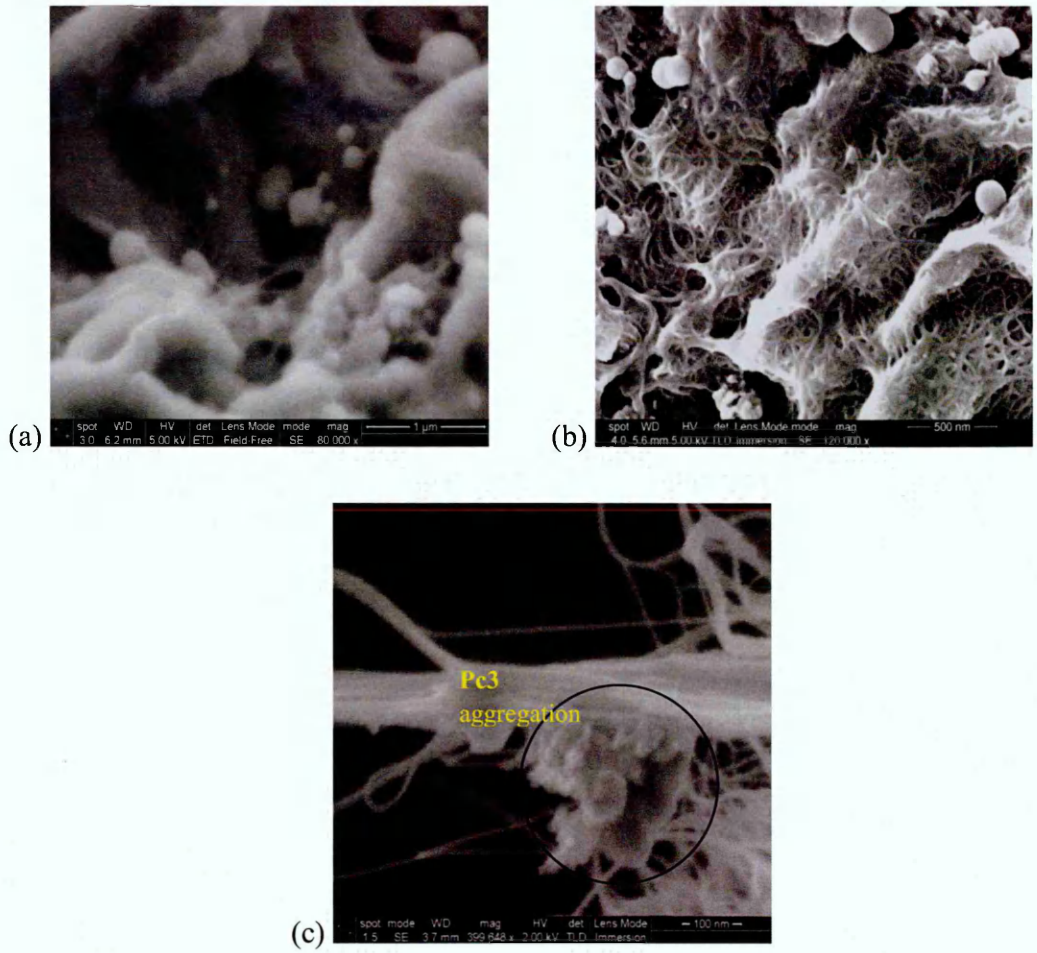

Figure 5.20: SEM images of PCNT-**Pc3** in thin film form deposited on silicon substrate from solution of DMF; (a) and (b): the intrinsic quality of SWCNT after mixing with phthalocyanine, (c) image: the aggregation of phthalocyanine attached the SWCNT bundle.

Figures 5.22a,b and c show SEM images of ATCNT-**Pc3** hybrid deposited as thin films from DMF solution onto silicon substrate. Similar results have been reported by Wang et al [35], where SWCNT was acidified and modified by mixing with lead phthalocyanine and Elouarzaki et al [36], where multi-walled carbon nanotubes have been modified using cobalt phthalocyanine.

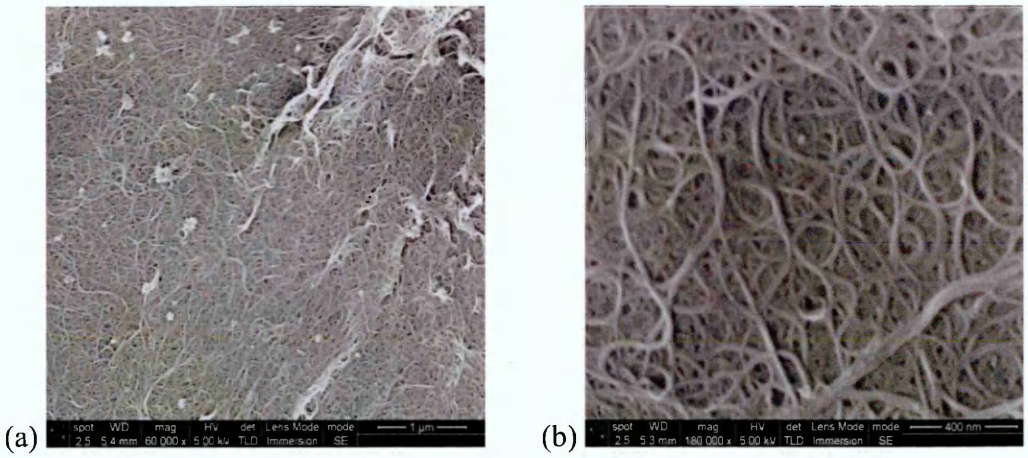

Figure 5.21: SEM images of acid treated SWCNT (ATCNT) in thin film form deposited on silicon substrate from solution of DMF

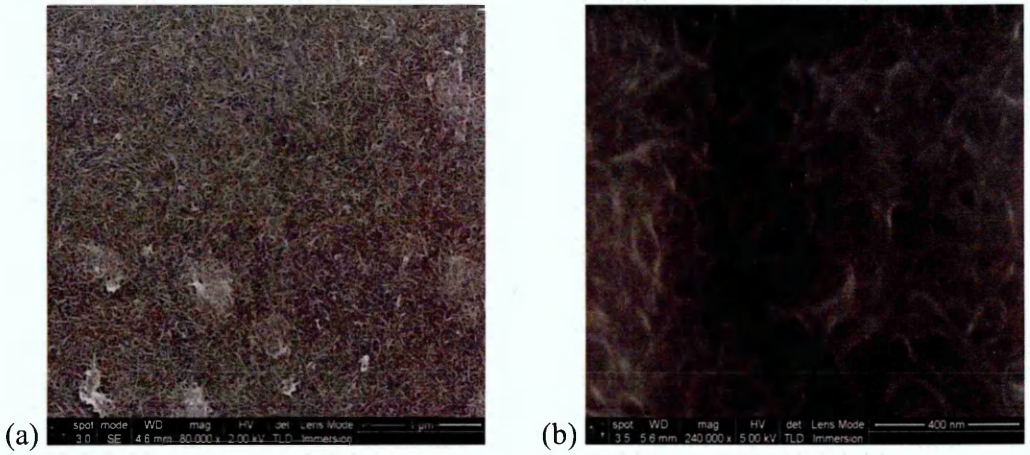

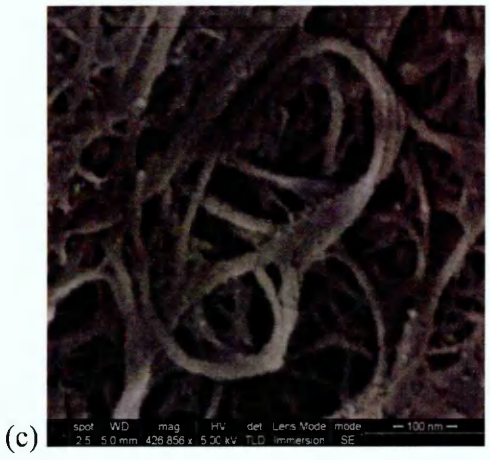

Figure 5.22: SEM images of ATCNT-**Pc3** in thin film form deposited on silicon substrate from solution of DMF; (a) and (b): smooth films obtained for optical detection, (c) image shows phthalocyanine molecules nicely covered the individual tubes

ATCNT-**Pc1**, ATCNT-**Pc2**, ATCNT-**Pc4** and ATCNT-**Pc5** have revealed similar SEM morphology features as ATCNT-**Pc3** and are presented in Figure 5.23.

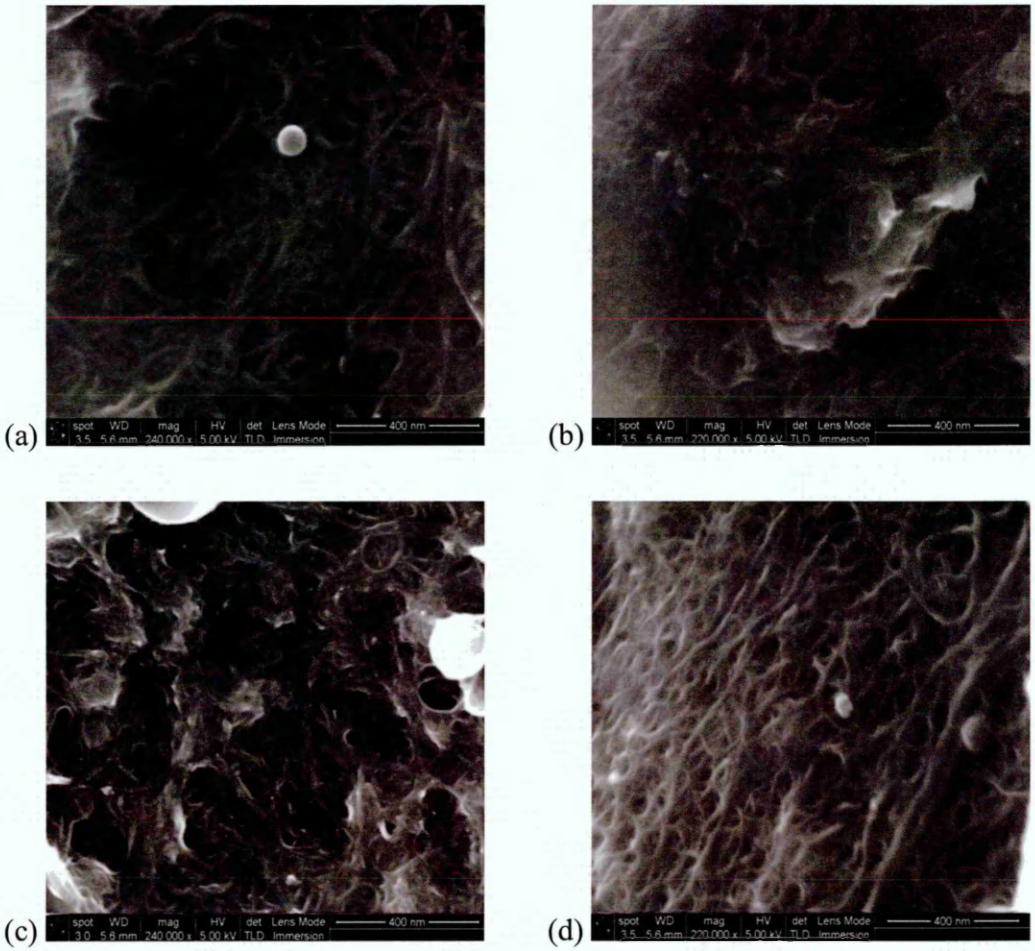

Figure 5.23: SEM images of (a) ATCNT-**Pc1**, (b) ATCNT-**Pc2**, (c) ATCNT-**Pc4** and (d) ATCNT-**Pc5** in thin film form deposited on silicon substrate from solution of DMF

5.2.5 Electrical conductivity

Thin films of PCNT-**Pc3** and ATCNT-**Pc3** as well as **Pc3** were deposited onto interdigitated electrods by drop-casting from their solutions in DMF (0.5 mg/ml). The I-V characteristics of the films were performed using Keithley 4200

semiconductor characterisation system in the voltage range ±2V. The conductivity (σ) was calculated using the following relation:

$$\sigma = \frac{L}{RHWn} \qquad (5.1)$$

This equation is the same as equation (3.18), where *L*, *W*, *H* and *n* are as defined in section 3.1.7. *R* is the film's resistance, which is derived from the liner fitting of the I-V characteristics of the films, as shown in Figure 5.24. Values of conductivity obtained are 1.67×10^{-4} for **Pc3** film and 7.54×10^{-1} for ATCNT-**Pc3** film, which shows an increase by more than three orders of magnitude in the case of ATCNT-**Pc3** film in comparison with the pure $CuPcR_4$ film. On the other hand thin film of PCNT-**Pc3** has shown short circuit, and therefore it was not possible to determine the conductivity for these composites.

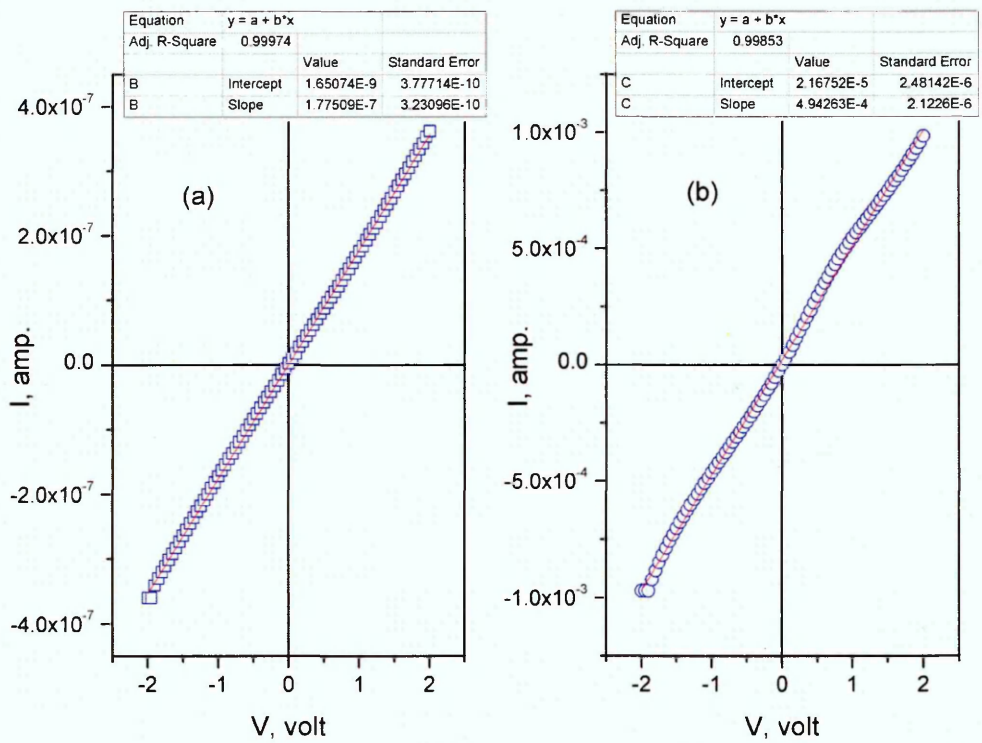

Figure 5.24: I(V) curves of (a) **Pc3** and (b) ATCNT-**Pc3**. The linear fitting parameters are shown above corresponding characteristics.

The large increase in conductivity of the hybrid films can be ascribed to the large SWCNT/CuPc conjugated π-π system [37,38]. Consequently, charge can favourably transfer from CuPc molecules to SWCNTs resulting in a large increase in conductivity. On the other hand, PCNT-**Pc3** exhibited very high conductivity (samples demonstrated short circuit in our measuring system) in almost all prepared samples. Pristine CNTs are typically composed of metallic and semiconducting nanotubes and their separation has been a serious obstacle in many applications and research [39,40]. Yang and co-workers [41] have reported that the acid treatment of SWCNT separates the semiconducting from the metallic phases. It has been shown that the majority of metallic CNTs with smaller diameters (typically $\leq$ 1.1 nm) will be etched way as a result of acid treatment, whereas those with larger diameters are significantly reduced leaving the semiconducting nanotubes intact [41].

5.3 Total Internal Reflection Ellipsometry (TIRE)

Using total internal reflection spectroscopic ellipsometry (TIRE), thin films of the new hybrids have been examined as an optical sensing membrane for the detection of benzo[a]pyrene in water to demonstrate the sensing properties of these hybrids. Polycyclic aromatic hydrocarbons (PAH), in general, are a class of fused-ring aromatic compounds which are found in air, natural waters, soil and in marine environments. PAH mainly arise in incomplete combustion from both anthropogenic and natural activities such as power production, petroleum refining or by automobile emissions and forest fires. Many PHA are concern for both human and environment health due to their acute toxicity, mutagenicity, or carcinogenicity. It is well known that certain metabolites of benzo[a]pyrene, e.g., epoxides and diol epoxides, bind with DNA to form stable adducts and are responsible for the mutagenic activity. Thus it is desirable to develop suitable technique for the detection of benzo[a]pyrene and all its related hazardous PHA compounds [42].

Figure 5.25 shows typical TIRE spectra of Cr/Au films used in the present work. The spectrum of $\Psi(\lambda)$, demonstrating the amplitude ratio of A_p/A_s, resembles very much the conventional surface plasmon resonance (SPR) curve, while the spectrum of $\Delta(\lambda)$ is associated with the phase shift between the p- and s-components of polarized light. The phase shift changes sharply from 270° down to -90° near the plasmon resonance.

According to Arwin's modelling [43], the position of the sharp drop in $\Delta(\lambda)$ spectrum is about 10 times more sensitive to analytes adsorption than $\Psi(\lambda)$ spectrum.

To examine the compatibility of the hybrids prepared in this work with TIRE technique, small volumes of solutions of **Pc3**, PCNT-**Pc3** and ATCNT-**Pc3** in DMF were drop-casted onto gold-coated glass substrates by using microcyrenge. Thereafter, the samples were exposed to deionized water and saturated solution of benzo[a]pyrene in water (6.2 μg/l) to demonstrate the changes of ellipsometry spectra and thus films' optical parameters induced by the adsorption of benzo[a]pyrene onto the films surfaces. It is worthwhile mentioning that the films of PCNT-**Pc3** were shown to be rough and inhomogeneous and therefore unsuitable for optical investigation, as it has not given well-resolved spectra when measured by spectroscopic ellipsometry.

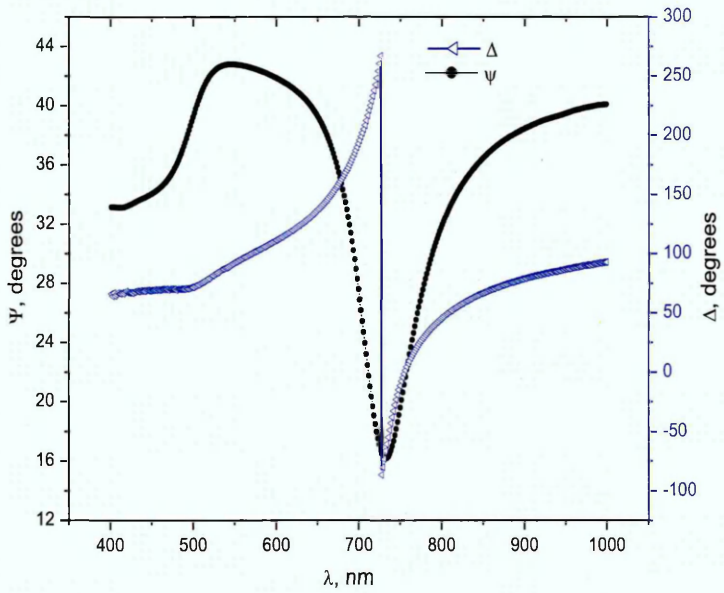

Figure 5.25: Typical TIRE spectra of Au/Cr layer in water

On the other hand, thin films prepared from ATCNT-**Pc3** exhibited much smoother surfaces and have therefore shown significant enhancement in the adsorption properties as active optical sensing layers. Figure 5.26 shows the spectra of $\Psi(\lambda)$ and $\Delta(\lambda)$ of **Pc3** and ATCNT-**Pc3** thin films before and after exposure to benzo[a]pyrene.

The initial response time of the studied layers was a fraction of minute but the spectra were measured 10 minutes after injection of contaminated water in order to achieve equilibrium.

During exposure to contaminated water, it was difficult to detect shifts in $\Psi(\lambda)$ because of the shape of the curve, however, significantly larger shifts have been observed in $\Delta(\lambda)$ spectra. These are typical features of TIRE method as reported earlier [44-46]. The spectra of $\Delta(\lambda)$ were further enlarged and shown at the bottom of Figure 5.26 to provide better assessment of the effect of benzo[a]pyrene exposures. It can clearly be seen that the adsorption of benzo[a]pyrene on ATCNT-**Pc3** film has resulted in larger shift (9.55 nm) than that shown by pure phthalocyanine (4.6 nm) under exposure to saturated benzo[a]pyrene solution in water. Carbon nanotubes in general are characterised with uniform surface with delocalised π-electrons of high density, which enhances their adsorption properties, especially for analytes with aromatic molecules [47].

It is necessary to mention that the aim of the present chapter is to investigate the suitability of functionalized CNTs as sensing active layers, which are compatible with optical techniques such as TIRE. Therefore the work does not examine effects of different concentrations of this analyte as well as different range of other related analytes. This is the subject of the next chapter. The parameters of organic films before and after exposure to benzo[a]pyrene solution in water were determined by fitting the experimental Ψ and Δ spectra to the theoretical organic model by fixing Cr/Au layer parameters. Table 5.2 summarises the thickness of all layers found from theoretical data fitting as well as the values of refractive index and extinction coefficients given at λ=633 nm. The data in Table 5.2 shows an increase in film thickness as well as in optical parameters n and k for both films. The increase in films' thickness in the case of **ATCNT-Pc3** was more significant which is probably due to the predominant surface interaction of the analyte with SWCNT/$CuPcR_4$ films. Further to the data summarised in Table 5.2 the variation in refractive index and extinction coefficient as a function of λ for both films in pure water and benzo[a]pyrene solution media are shown in Figure 5.27.

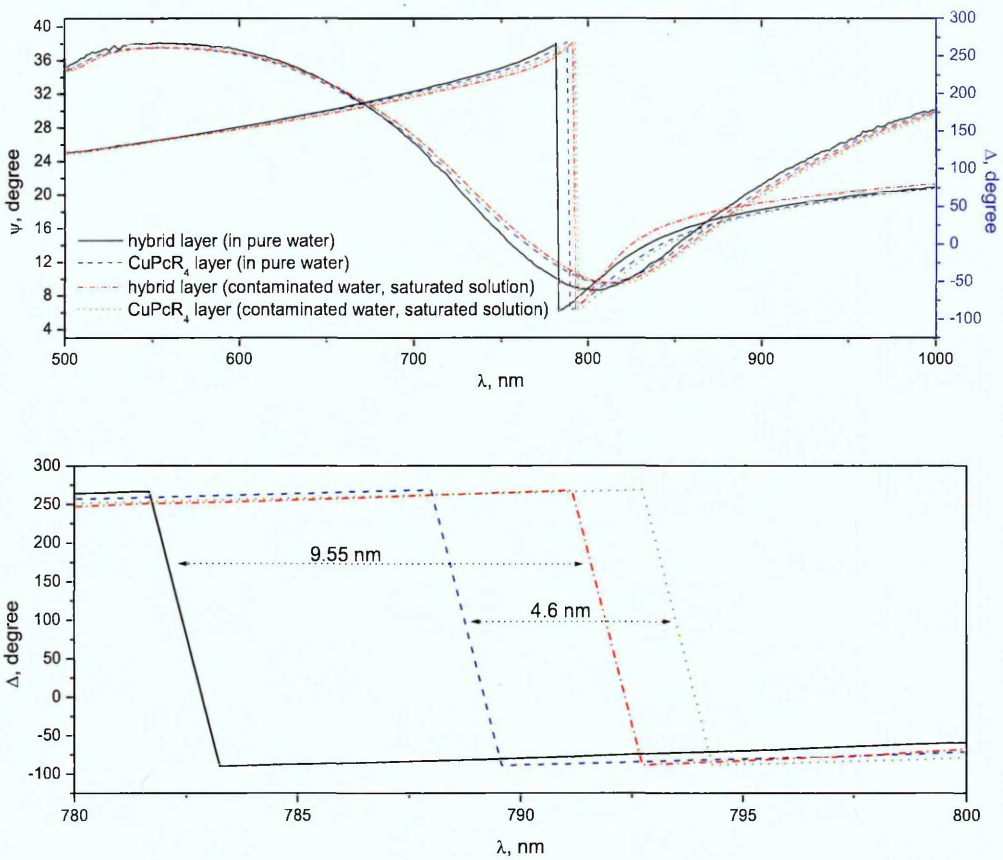

Figure 5.26: Ψ(λ) and Δ(λ) TIRE spectra of **Pc3** film in water (dashed line); after injection of benzo[a]pyrene saturated solution (dotted line). ATCNT-**Pc3** film in water (solid line); after injection of benzo[a]pyrene saturated solution (dashed-dotted line). An enlarged section of Δ(λ) spectra are shown at the bottom of the figure

Table 5.2: Experimental data fitting; film thickness (*d*), refractive index (*n*) and extinction coefficient (*k*) at 633nm wavelength.

	Before exposure			After exposure		
	d, nm	*k*	*n*	*d*, nm	*n*	*k*
Pc3	97.86	1.532	0.373	98.1	1.542	0.377
ATCNT-Pc3	147.73	1.334	0.133	149.49	1.359	0.135

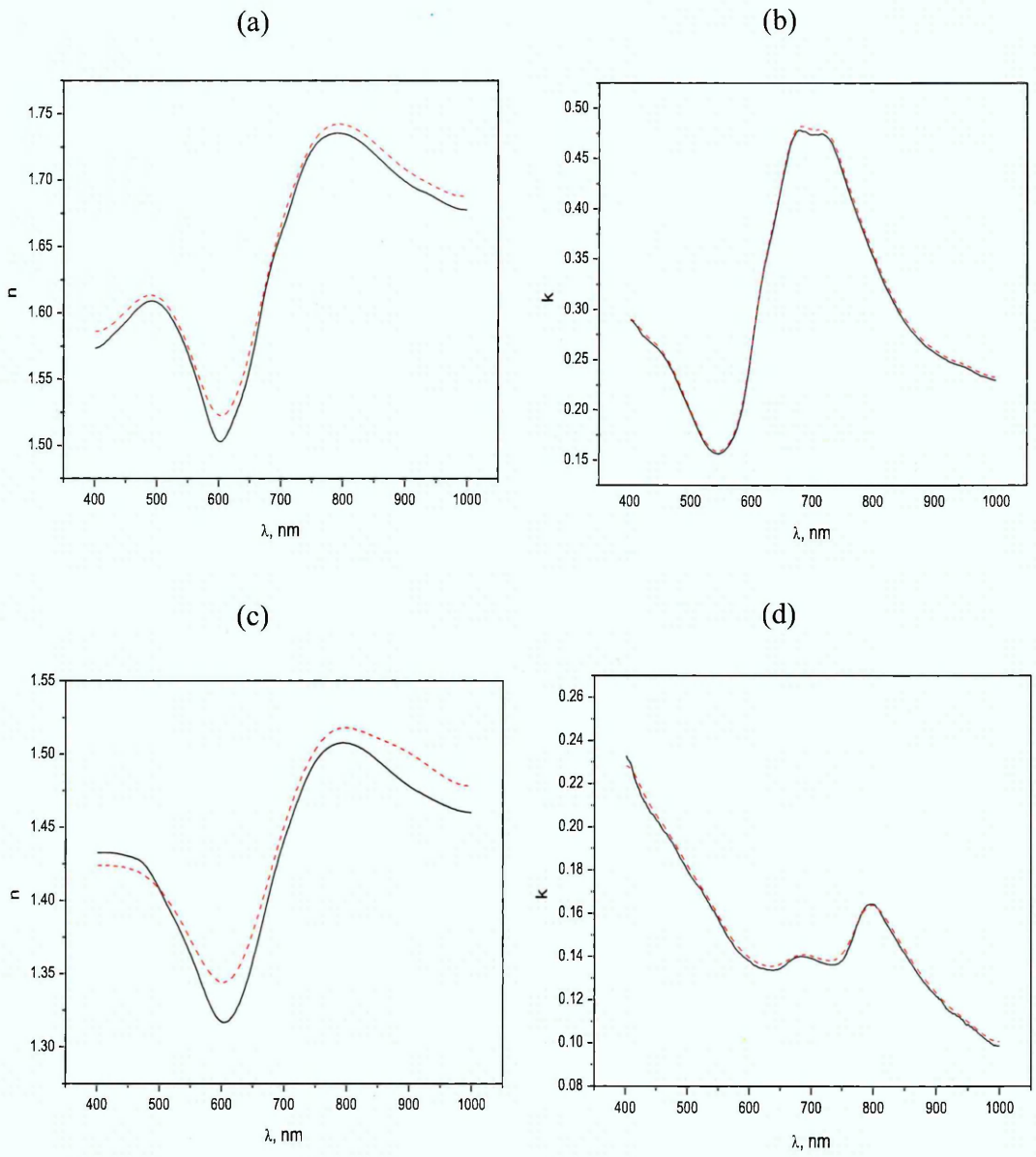

Figure 5.27: Refractive index (n) and extinction coefficient (k) of **Pc3** film (a and b) and ATCNT-**Pc3** film (c and d) in pure water (solid line) and benzo[a]pyrene solution (dashed line)

Summary

Hybrid structures of single-walled carbon nanotubes and $CuPcR_4$ have been prepared. FTIR and Raman spectra have shown that non-covalent binding between $CuPcR_4$ and SWCNTs has been significantly enhanced as a result of acid treatment of CNTs. Using SEM and AFM measurements morphology of the films is found to be highly dependent on the solubility of the hybrid which is determined by the method used to produce the hybrid structure. Thin films of acid-treated SWCNT/$CuPcR_4$ hybrid exhibited much higher conductivity than $CuPcR_4$ and improved films' homogeneity has enabled the use of such hybrids as optically active sensing layers for the detection of pollutants in water. The response of acid-treated SWCNT/$CuPcR_4$ hybrid films to the presence of benzo[a]pyrene in water was shown to be two times larger than that demonstrated by $CuPcR_4$ films.

Reference List

[1] H. Banimuslem, A. Hassan, T. Basova, A.D. Gülmez, S. Tuncel, M. Durmus, A.G. Gürek, V. Ahsen, Copper phthalocyanine/single walled carbon nanotubes hybrid thin films for pentachlorophenol detection, Sensor. Actuator. B: Chem. 190 (2014) 990-998.

[2] Hikmat Banimuslem, Aseel Hassan, Tamara Basova , Mahmut Durmuş, Sinem Tuncel, Aliye Aslı Esenpınar, Ayse Gül Gürek, Vefa Ahsen, Copper phthalocyanine functionalized single-walled carbon nanotubes: thin films for optical detection, J. Nanosci. Nanotechnol. 15 (2015) 2157-2167.

[3] Y. Wang, N. Hu, Z. Zhou, D. Xu, Z. Wang, Z. Yang, H. Wei, E.S. Kong, Y. Zhang, Single-walled carbon nanotube/cobalt phthalocyanine derivative hybrid material: Preparation, characterization and its gas sensing properties, J. Mater. Chem. 21 (2011) 3779-3787.

[4] W. Feng, Y. Li, Y. Feng, J. Wu, Enhanced photoresponse from the orderedmicrostructure of naphthalocyanine-carbon nanotube composite film, Nanotechnology. 17 (2006) 3274-3279.

[5] F. Patolsky, Y. Weizmann, I. Willner, Long-range electrical contacting of redox enzymes by SWCNT connectors, Angewandte Chemie - International Edition. 43 (2004) 2113-2117.

[6] P. Diao, Z. Liu, Electrochemistry at chemically assembled single-wall carbon nanotube arrays, J Phys. Chem. B. 109 (2005) 20906-20913.

[7] H. Banimuslem, A. Hassan, T. Basova, I. Yushina, M. Durmuş, S. Tuncel, A.A. Esenpınar, A.G. Gürek, V. Ahsen, Copper phthalocyanine functionalized single-walled carbon nanotubes: thin film deposition and sensing properties, Key. Eng. Mat. 605 (2014) 461-464.

[8] Z. Yang, H. Pu, J. Yuan, D. Wan, Y. Liu, Phthalocyanines-MWCNT hybrid materials: Fabrication, aggregation and photoconductivity properties improvement, Chem. Phys. Lett. 465 (2008) 73-77.

[9] S. Singh, S.K. Tripathi, G.S.S. Saini, Optical and infrared spectroscopic studies of chemical sensing by copper phthalocyanine thin films, Mater. Chem. Phys. 112 (2008) 793-797.

[10] L. Piao, Q. Liu, Y. Li, Interaction of Amino Acids and Single-Wall Carbon Nanotubes, J. Phys. Chem. C. 116 (2012) 1724-1731.

[11] B. Wang, X. Zhou, Y. Wu, Z. Chen, C. He, Lead phthalocyanine modified carbon nanotubes with enhanced NH3 sensing performance, Sensor. Actuator. B: Chem. 171-172 (2012) 398-404.

[12] K.A. Wepasnick, B.A. Smith, J.L. Bitter, D. Howard Fairbrother, Chemical and structural characterization of carbon nanotube surfaces, Analyt. Bioanalyt. Chem. 396 (2010) 1003-1014.

[13] B. Ballesteros, G. De La Torre, C. Ehli, G.M.A. Rahman, F. Agulló-Rueda, D.M. Guidi, T. Torres, Single-wall carbon nanotubes bearing covalently linked phthalocyanines - Photoinduced electron transfer, J. Am. Chem. Soc. 129 (2007) 5061-5068.

[14] T. Mugadza, T. Nyokong, Synthesis, characterization and the electrocatalytic behaviour of nickel (II) tetraamino-phthalocyanine chemically linked to single walled carbon nanotubes, Electrochim. Acta. 55 (2010) 6049-6057.

[15] C. Casiraghi, A. Hartschuh, H. Qian, S. Pliscanec, C. Georgia, A. Fasoli, K.S. Novoselov, D.M. Basko, A.C. Ferrari, Raman spectroscopy of graphene edges, Nano Lett. 9 (2009) 1433-1441.

[16] C. Dyke, J. Tour, Unbundled and highly functionalized carbon nanotubes from aqueous reactions, Nano Lett. 3 (2003) 1215-1218.

[17] L. Alvarez, G. de la Fuente, A. Righi, S. Rols, E. Anglaret, J. Sauvajol, E. Munoz, W. Maser, A. Benito, M. Martinez, Diameter dependence of Raman intensities for single-wall carbon nanotubes, Phys. Review B. 63 (2001).

[18] D. Huo, L. Yang, C. Hou, H. Fa, X. Luo, Y. Lu, X. Zheng, J. Yang, L. Yang, Molecular interactions of monosulfonate tetraphenylporphyrin (TPPS1) and meso-tetra(4-sulfonatophenyl)porphyrin (TPPS) with dimethyl methylphosphonate (DMMP), Spectrochimica Acta - Part A: Molecular and Biomolecular Spectroscopy. 74 (2009) 336-343.

[19] S. Gotovac, H. Honda, Y. Hattori, K. Takahashi, H. Kanoh, K. Kaneko, Effect of nanoscale curvature of single-walled carbon nanotubes on adsorption of polycyclic aromatic hydrocarbons, Nano Lett. 7 (2007) 583-587.

[20] Y. Zhang, J. Zhang, H. Son, J. Kong, Z. Liu, Substrate-induced Raman frequency variation for single-walled carbon nanotubes, J. Am. Chem. Soc. 127 (2005) 17156-17157.

[21] C. Fantini, M.L. Usrey, M.S. Strano, Investigation of electronic and vibrational properties of single-walled carbon nanotubes functionalized with diazonium salts, J. Phys. Chem. C. 111 (2007) 17941-17946.

[22] E. Jubete, K. Elechowska, O.A. Loaiza, P.J. Lamas, E. Ochoteco, K.D. Farmer, K.P. Roberts, J.F. Biernat, Derivatization of SWCNTs with cobalt phthalocyanine residues and applications in screen printed electrodes for electrochemical detection of thiocholine, Electrochim. Acta. 56 (2011) 3988-3995.

[23] J. Chao, W. Huang, J. Wang, S. Xiao, Y. Tang, J. Liu, Click-Chemistry-Conjugated oligo-angiomax in the Two-Dimensional DNA lattice and its interaction with thrombin, American Chem. Soc.10 (2009) 877-883.

[24] A. Jha, U.K. Ghorai, D. Banerjee, S. Mukherjee, K.K. Chattopadhyay, Surface modification of amorphous carbon nanotubes with copper phthalocyanine leading to enhanced field emission, RSC Advances. 3 (2013) 1227-1234.

[25] T.V. Basova, M. Çamur, A.A. Esenpınar, S. Tuncel, A. Hassan, A. Alexeyev, H. Banimuslem, M. Durmuş, A.G. Gürek, V. Ahsen, Effect of substituents on the orientation of octasubstituted copper (II) phthalocyanine thin films, Synth. Met. 162 (2012) 735-742.

[26] C.A. Dyke, J.M. Tour, Covalent functionalization of single-walled carbon nanotubes for materials applications, J. Phys. Chem. A. 108 (2004) 11151-11159.

[27] T. Mugadza, T. Nyokong, Synthesis and characterization of electrocatalytic conjugates of tetraamino cobalt (II) phthalocyanine and single wall carbon nanotubes, Electrochim. Acta. 54 (2009) 6347-6353.

[28] E. Llobet, Gas sensors using carbon nanomaterials: A review, Sensor. Actuator. B: Chemical. 179 (2013) 32-45.

[29] R. De Saja, J. Souto, M.L. Rodríguez-Méndez, J.A. De Saja, Array of lutetium bisphthalocyanine sensors for the detection of trimethylamine, Mater. Sci. Eng. C. 8-9 (1999) 565-568.

[30] X. Wang, S. Reisberg, N. Serradji, G. Anquetin, M.-. Pham, W. Wu, C.-. Dong, B. Piro, E-assay concept: Detection of bisphenol A with a label-free electrochemical competitive immunoassay, Biosens. Bioelectron. 53 (2014) 214-219.

[31] N. He, Y. Chen, J. Bai, J. Wang, W.J. Blau, J. Zhu, Preparation and optical limiting properties of multiwalled carbon nanotubes with -conjugated metal-free phthalocyanine moieties, J. Phys. Chem. C. 113 (2009) 13029-13035.

[32] F. Boon, S. Desbief, L. Cutaia, O. Douhéret, A. Minoia, B. Ruelle, S. Clément, O. Coulembier, J. Cornil, P. Dubois, R. Lazzaroni, Synthesis and characterization of nanocomposites based on functional regioregular poly(3-hexylthiophene) and multiwall carbon nanotubes, Macromol. Rapid Commun. 31 (2010) 1427-1434.

[33] B. Wang, X. Zhou, Y. Wu, Z. Chen, C. He, Lead phthalocyanine modified carbon nanotubes with enhanced NH3 sensing performance, Sensor. Actuator. B: Chem. 171-172 (2012) 398-404.

[34] J.J. Hernández, M.-. García-Gutiérrez, D.R. Rueda, T.A. Ezquerra, R.J. Davies, Influence of single wall carbon nanotubes and thermal treatment on the morphology of polymer thin films, Composites Sci. Technol. 72 (2012) 421-427.

[35] B. Wang, X. Zhou, Y. Wu, Z. Chen, C. He, Lead phthalocyanine modified carbon nanotubes with enhanced NH3 sensing performance, Sensor. Actuator. B: Chem. 171-172 (2012) 398-404.

[36] K. Elouarzaki, R. Haddad, M. Holzinger, A. Le Goff, J. Thery, S. Cosnier, MWCNT-supported phthalocyanine cobalt as air-breathing cathodic catalyst in glucose/O2 fuel cells, J. Power Sources. 255 (2014) 24-28.

[37] E.B. Barros, A.G.S. Filho, V. Lemos, J.M. Filho, S.B. Fagan, M.H. Herbst, J.M. Rosolen, C.A. Luengo, J.G. Huber, Charge transfer effects in acid treated single-wall carbon nanotubes, Carbon. 43 (2005) 2495-2500.

[38] M.D. Shirsat, T. Sarkar, J. Kakoullis Jr., N.V. Myung, B. Konnanath, A. Spanias, A. Mulchandani, Porphyrin-functionalized single-walled carbon nanotube chemiresistive sensor arrays for VOCs, J. Phys. Chem. C. 116 (2012) 3845-3850.

[39] D. Rossouw, G.A. Botton, E. Najafi, V. Lee, A.P. Hitchcock, Metallic and semiconducting single-walled carbon nanotubes: Differentiating individual SWCNTs by their carbon 1s spectra, ACS Nano. 6 (2012) 10965-10972.

[40] J.L. Blackburn, T.M. Barnes, M.C. Beard, Y.-. Kim, R.C. Tenent, T.J. McDonald, B. To, T.J. Coutts, M.J. Heben, Transparent conductive single-walled carbon nanotube networks with precisely tunable ratios of semiconducting and metallic nanotubes, ACS Nano. 2 (2008) 1266-1274.

[41] C. Yang, J.S. Park, K.H. An, S.C. Lim, K. Seo, B. Kim, K.A. Park, S. Han, C.Y. Park, Y.H. Lee, Selective removal of metallic single-walled carbon nanotubes with small diameters by using nitric and sulfuric acids, J. Phys. Chem. B. 109 (2005) 19242-19248.

[42] L.J. Casarett, J. Doull, C.D. Klaassen, M.O. Amdur, Casarett and Doull's Toxicology: The Basic Science of Poisons, Macmillan, 1986.

[43] H. Arwin, M. Poksinski, K. Johansen, Total internal reflection ellipsometry: Principles and applications, Appl. Opt. 43 (2004) 3028-3036.

[44] T. Basova, A. Tsargorodskaya, A. Nabok, A.K. Hassan, A.G. Gurek, G. Gumus, V. Ahsen, Investigation of gas-sensing properties of copper phthalocyanine films, Mater. Sci. Eng. C. 29 (2009) 814-818.

[45] A. Hassan, T. Basova, F. Yuksel, G. Gümüş, A.G. Gürek, V. Ahsen, Study of the interaction between simazine and metal-substituted phthalocyanines using spectral methods, Sensor. Actuator. B: Chem. (2012).

[46] A.V. Nabok, A. Tsargorodskaya, A.K. Hassan, N.F. Starodub, Total internal reflection ellipsometry and SPR detection of low molecular weight environmental toxins, Appl. Surf. Sci. 246 (2005) 381-386.

[47] M. Kragulj, J. Trickovic, B. Dalmacija, Á Kukovecz, Z. Kónya, J. Molnar, S. Roncevic, Molecular interactions between organic compounds and functionally modified multiwalled carbon nanotubes, Chem. Eng. J. 225 (2013) 144-152.

Chapter 6

Total Internal Reflection Ellipsometry (TIRE) for the Detection in Water and Ambient Air

Chapter overview

This chapter focuses towards studying the interaction between SWCNT-phthalocyanine thin films and some hazardous chemicals using TIRE method. TIRE has been applied to detect very small amount of contaminants both in water and in ambient air. Therefore, this chapter is divided into two parts; the first part will discuss the use of TIRE to detect some pesticides (pentachlorophenol, 2-chlorophenol, simazine and diuron) in water solution while the second part will be focused on the use of TIRE for amines (methylamine, dimethylamine and trimethylamine) vapour detection.

6.1 Detection of pesticides in water

6.1.1 Introduction

The worldwide use of pesticides and herbicides for agricultural issues is classified as a global environmental pollution problem. Pesticide used in agriculture can easily take way to surface or ground waters, possibly causing adverse ecotoxicological effects on aquatic life and changing drinking water quality [1]. Chlorophenols (Cps), in general, are a group of organochlorides of phenol that contains one or more covalently bonded chlorine atoms, which can be devided into five groups that; mono-chlorophenols (MCPs), dichlorophenols (DCPs), trichlorophenols (TCPs), tetrachlorophenols (TeCPs) and pentachlorophenols (PCPs). The physical properties of CPs vary in principle depending on the number of chlorine atoms and their position relative to OH group, which complicates their simultaneous determination [2].

CPs are chemical with high toxicity including estogenic, mutagenic and carcinogenic effects. Additionally, they have very high acute toxicity, interfering with oxidative phosphorylation and inhibiting adenosine triphosphate synthesis within body cells [3]. PCP is the most toxic representative of the chlorophenols. It can accumulate in living organisms and result in negative effects, including carcinogenicity. PCP has attracted great attention worldwide because of its common application in agriculture, industry, and commercial product synthesis. It has been widely detected in soils, sediments, water, plants and human breast milk due to its low biodegradability and chemical stability [4]. PCP concentrations in various surface waters from different countries ranging from trace levels to 10,500 μgL^{-1} have been reported by the World Health Organization [5]. Furthermore, it has been listed as priority pollutant by U.S. environmental protection agency [6]. Although PCP has been banned since 1984, it is still found in the environment [5].

Monitoring of pesticides and herbicides in comparatively low concentrations, especially in drinking and natural waters is a complicated and expensive task. The European Union has limited the maximum allowable concentration for a single pesticide to 0.1 μg/L [5], and their presence in different foods and drinks is limited by legislation.

Different analytical procedures based on liquid chromatography–mass spectrometry (LC–MS) [7-9], LC–tandem mass spectrometry (LC–MS/MS) [10], high performance liquid chromatography (HPLC) [11], gas chromatography–mass spectrometry (GC–MS) [12] and surface plasmon resonance [13] have been reported to provide efficient determination of these pesticides, according to the present legislation. However these methods, although highly sensitive and specific, are quite laborious, time-consuming, and expensive. There is therefore continuous demand for highly sensitive, cost-effective, rapid and portable detection methods which at the same time can meet international legislation allowed levels of the toxic compounds. Ellipsometry can be used in total internal reflection (TIRE) mode and in combination with the surface plasmon resonance phenomenon for sensing aspects [13-15]. There has been extensive work in applying TIRE as a technique for the detection of biomolecules [16,17]. It was established that TIRE is a more suitable technique than surface plasmon resonance (SPR) method for the registration of low molecular weight toxins such as simazine, atrazine and T2 mycotoxin [18]. TIRE technique has attracted substantial attention because of its fast response, simple instrumentation, being non-destructive method and its ability of performing measurements in non-transparent media [19].

6.1.2 Materials and sample preparation

Thin films of **Pc5** and ATCNT-**Pc5**, which were fully discussed in chapter 5, are used in this work as active layers to detect pentachlorophenol (PCP), 2-chlorophenol (2CP), simazine and diuron (Figure 6.1) solution in water in low concentrations ranging from 1 to 25μg/l. The choice of hybrids of **Pc5** with SWCNTs is random and they are considered as model sample representing the whole class of compounds studied in this thesis. The preparation of thin films for TIRE study has been discussed in chapter 3.

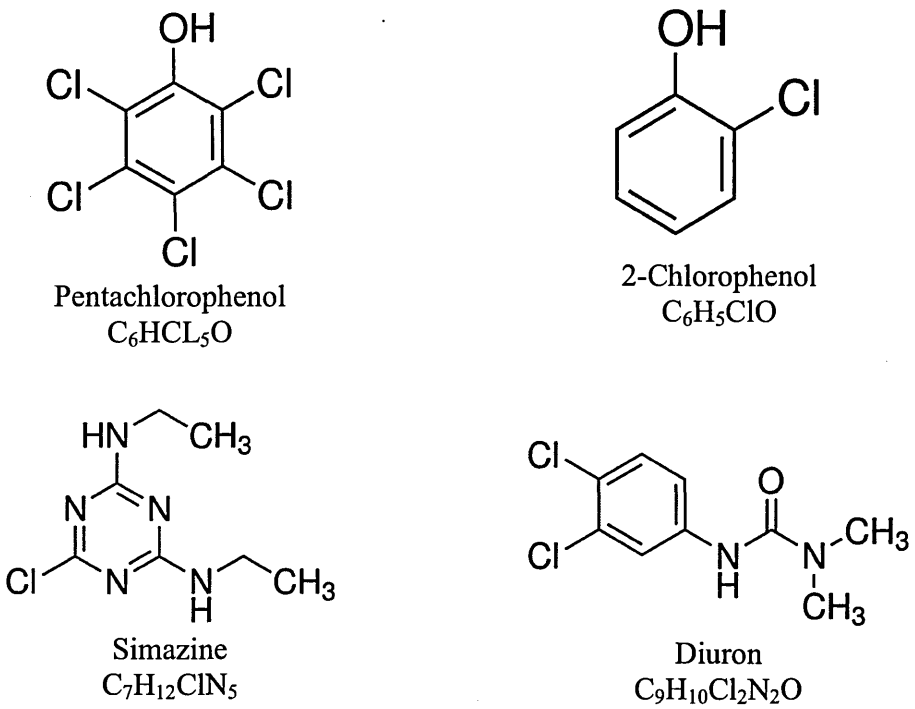

Figure 6.1: The chemical structure of the investigated analytes [20]

6.1.3 Spectral shift

The adsorption of pentachlorophenol (PCP), 2-chlorophenol (2CP), simazine and diuron onto the surface of **Pc5** and ATCNT-**Pc5** thin films in water solutions has been studied using TIRE method. **Pc5** and ATCNT-**Pc5** hybrid films were spun onto gold-coated glass substrates as described in chapter 3. Figure 6.2 shows the typical TIRE spectra of Cr/Au films used in the present work. The spectrum of $\Psi(\lambda)$, demonstrating the amplitude ratio of A_p/A_s, resembles very much the conventional surface plasmon resonance (SPR) curve, while the spectrum of $\Delta(\lambda)$ is associated with the phase shift between the p- and s-components of polarized light. The latter changes sharply from 270° down to -90° near the plasmon resonance. According to Arwin's modelling [15], the position of the sharp drop in $\Delta(\lambda)$ spectrum is about 10 times more sensitive to analytes adsorption than $\Psi(\lambda)$ spectrum. Further details about TIRE spectra can be found in chapter 3.

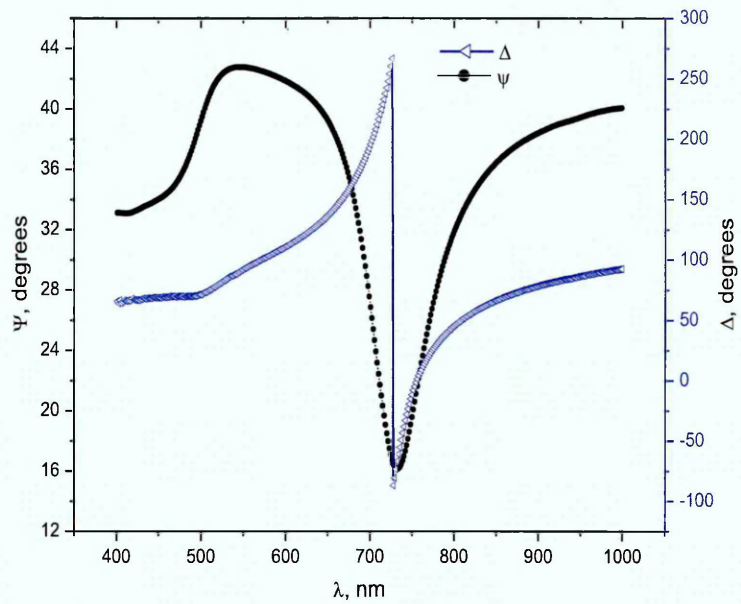

Figure 6.2: Typical TIRE spectra of Cr/Au film

Figure 6.3 represents the spectra of *Ψ(λ)* and *Δ(λ)* of **Pc5** and ATCNT-**Pc5** hybrid thin films before and after exposure to PCP, 2PC, diuron and simazine in two concentrations (2 and 15 μg/l). The initial response time of the sensors was fraction of a minute but the spectra were measured 10 minutes after injection of contaminated water or pure water to achieve the equilibrium response or recovery, respectively. During exposure to contaminated water, it was difficult to detect shifts in *Ψ(λ)* because of the shape of the curve, however, significantly larger shifts have been observed in *Δ(λ)* spectra. These are typical features of TIRE method as reported earlier [18,19,21-23]. The spectra of *Δ(λ)* were further enlarged and shown above in Figure 6.3a and Figure 6.3b to provide better assessment. It can clearly be seen that the adsorption of analytes on the hybrid film has resulted in larger shifts than on pure $CuPcR_4$. Carbon nanotubes in general are characterised with uniform surface with delocalised π-electrons of high density, which enhances their adsorption properties, especially for analytes with oxygen-containing aromatic molecules [23,24]. Complete recovery of *Δ(λ)* spectra are observed after flushing the cell with deionised water in the case of PCP and 2PC interaction as previously established for films of metal phthalocyanines with other types of substituents [25].

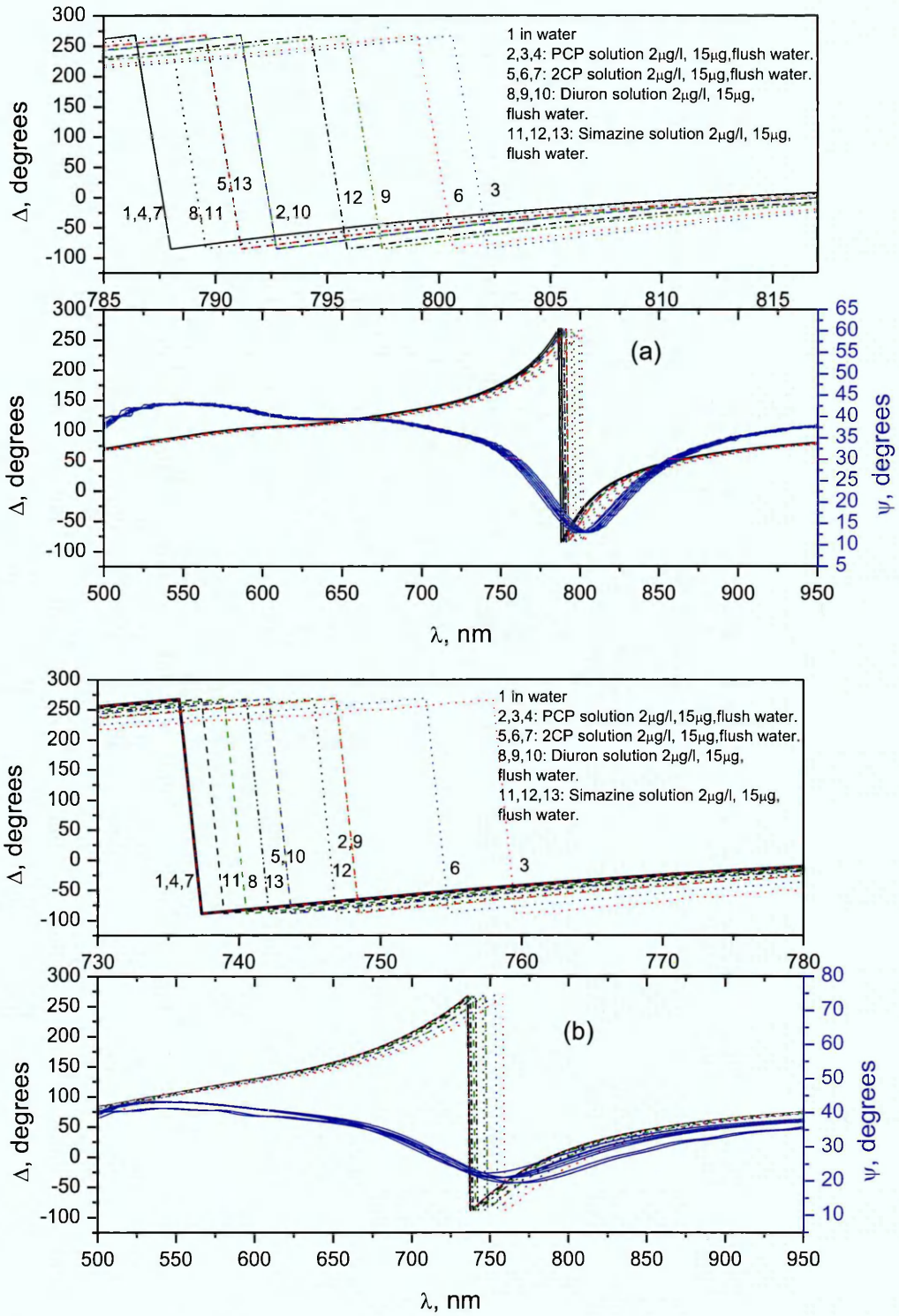

Figure 6.3: Ψ(λ) and Δ(λ) TIRE spectra of (a) **Pc5** coated Cr/Au and (b) ATCNT-**Pc5** hybrid films in water and after exposure to contaminated water

However, when exposed to simazine and diuron-contaminated water, films did not show complete recovery after flushing with water. The larger shift was observed for PCP exposure among all other analytes examined in this work. Therefore, PCP has been further studied to establish the recovery with longer exposure time. Figure 6.4 shows the spectra of $\Psi(\lambda)$ and $\Delta(\lambda)$ of **Pc5** and ATCNT-**Pc5** hybrid thin films before and after exposure to PCP in the concentrations of 1,2 and 5 μg/l. The higher adsorption of PCP than other pesticides can be ascribed to the π-π interactions between the π electrons of the aromatic ring of PCP and the π electron system of the aromatic rings of the SWCNTs [26]. Complete recovery of $\Delta(\lambda)$ spectra are observed after flushing the cell with deionised water. However, when exposure to 5 μg/l PCP-contaminated water continued for 30 minutes, **Pc5** exhibited further shift but did not show complete recovery after flushing with water; in contrast to ATCNT-**Pc5** layer which remained stable with time under repeated exposures to 5 μg/l PCP-contaminated water and exhibited complete reversibility. It is expected that the presence of SWCNT in the composite film inhibits the diffusion of PCP molecules inside the film and most interaction takes place on the surface of the film. Table 6.1 represents the dependence of phase shift change ($\delta\Delta$) on analytes concentration in the range 1-25 μg/l in water for **Pc5** and ATCNT-**Pc5** layers.

6.1.4 Experimental data fitting

Theoretical fitting to experimental Ψ and Δ spectra was carried out by applying a 4-layer model consisting of water solution, organic layer, Au layer and BK7 glass. The optical parameters (refractive index n and extinction coefficient k) and film thickness d, of all layers are summarised in Table 6.2.

The parameters of the organic films after exposure to PCP, 2-CP, diuron and simazine solutions in water were determined by fitting experimental Ψ and Δ spectra to the theoretical organic model by fixing Cr/Au layer parameters. Table 6.2 and Table 6.3 summarise the thickness of all layers found from theoretical data fitting as well as the values of refractive index and extinction coefficients given at λ=633nm. The data in Table 6.3 show an increase in film thickness as well as optical parameters (n and k) for both films. The increase in films' thickness in the case of ATCNT-**Pc5** composite was more significant which is probably due to the

predominant surface interaction of the analyte with ATCNT-**Pc5** films. Further to the data summarised in Table 6.3 the variation in refractive index and extinction coefficient as a function of λ for both films in pure water and PCP solution media (concentration of 10 μg/l) are shown in Figure 6.5.

Table 6.1: Changes in the phase shift spectra (δΔ) of ATCNT-**Pc5** hybrid and pristine **Pc5** films on exposure to PCP, 2PC, diuron and simazine in the concentration range 1-25 μg/L

Conc.	**δΔ(λ), nm**							
	Pc5				ATCNT-**Pc5**			
	PCP	2PC	Diur.	Sima.	PCP	2PC	Diur.	Sima.
1	3.2	1.93	0	0	6.27	4.11	1.31	0
2	4.77	3.21	1.61	1.5	11.12	6.32	3.16	1.56
5	7.9	5.98	3.87	3.22	16.22	12.47	7.17	4.31
10	11.2	9.87	6.63	5.69	19.5	15.1	9.13	7.73
15	14.2	12.64	9.51	7.92	22.21	17.37	11	9.46
20	16.1	14.06	10.14	8.66	24.84	18.84	13.14	10.14
25	17.8	16.14	11.54	10.12	26	20.1	14.23	10.73

Table 6.2: Parameters of four-layer model in TIRE spectra fitting

Layer	*n*	*k*	*d, nm*
BK7	1.51	0	10^6
Cr/Au	0.36	2.86	27.43
Active layer		See Table 6.3	
Aqueous solution	1.34	0	-

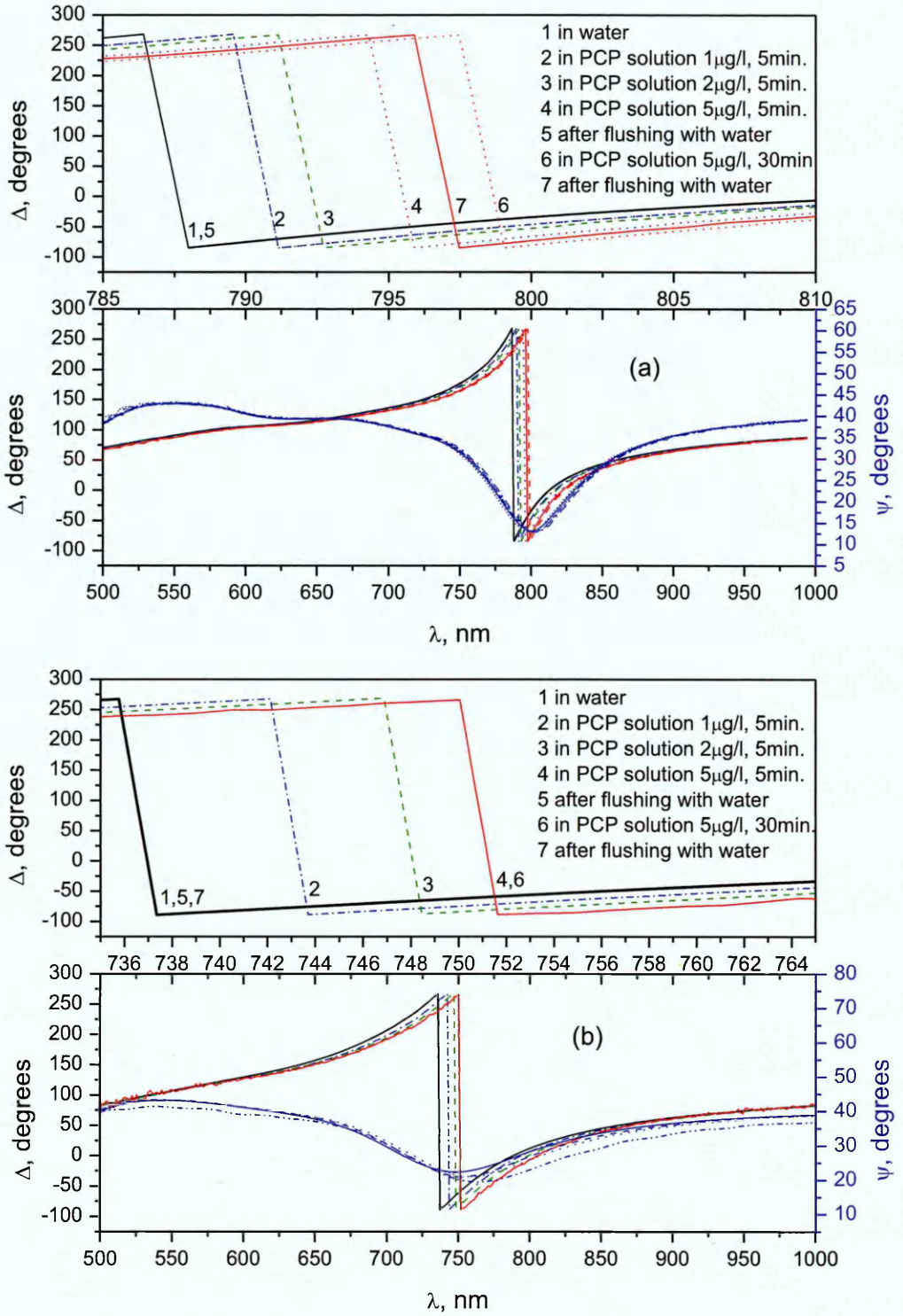

Figure 6.4: Ψ(λ) and Δ(λ) TIRE spectra of (a) **Pc5** coated Cr/Au and (b) ATCNT-**Pc5** hybrid films in water (1); after injection of PCP solution of 1μg/l (2); 2μg/l (3); 5μg/l (4) for 5 minutes; after flushing with water (5) and after injecting with PCP solution 5μg/l for 30 minutes (6); after flushing with water (7). An enlarged section of Δ(λ) spectra are shown above the figure

Table 6.3: Changes in the optical parameters of Pc5 and ATCNT-Pc5 films caused by adsorption of PCP, 2-CP, diuron and simazine from its solution with concentration of 10 μg/l at λ=633nm

		Pc5			ATCNT-**Pc5**		
		n	***k***	***d,nm***	***n***	***k***	***d,nm***
Initial film		1.56	0.32	37.4	1.41	0.28	54.9
Exposd films	PCP	1.59	0.31	38.1	1.47	0.29	56.5
	2PC	1.59	0.32	37.9	1.45	0.30	55.8
	Diuron	1.57	0.33	37.6	1.43	0.29	55
	Simazine	1.56	0.33	37.7	1.45	0.27	55.1

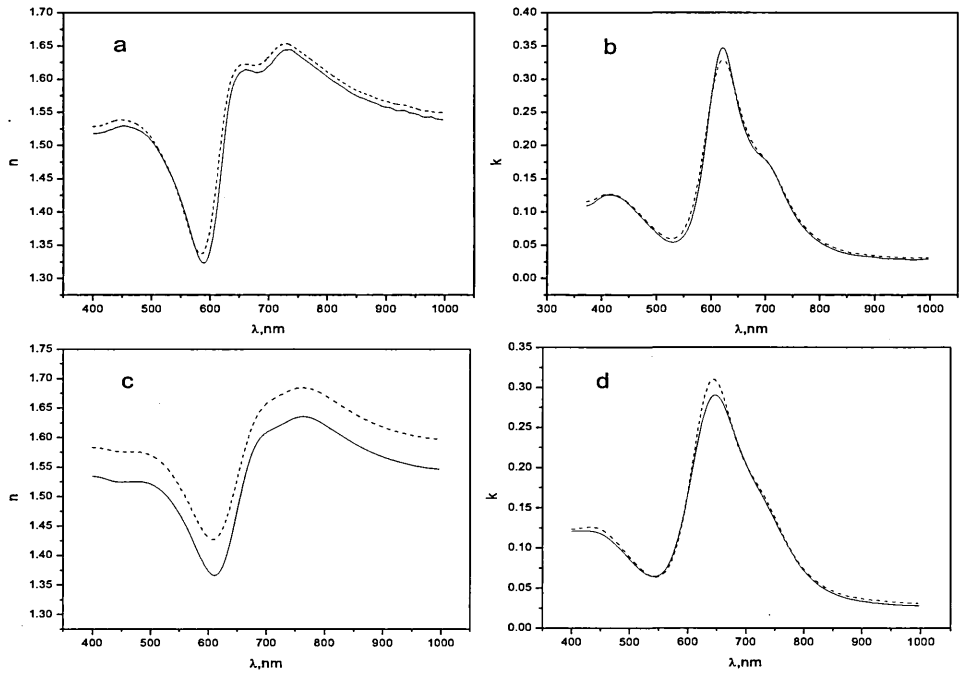

Figure 6.5: Refractive index (n) and extinction coefficient (k) of **Pc5** film (a and b) and ATCNT-**Pc5** film (c and d) in pure water (solid line) and PCP solution of 10 μg/l (dashed line)

6.1.5 Determination of films' sensitivity and detection limit

In order to evaluate the response of the two types of layers, the average sensitivity has been calculated based on changes in Δ spectra shifts (Table 6.1) using the following equation [23]:

$$\bar{S} = \frac{1}{\Delta_\circ}\frac{1}{m}\sum_{i=1}^{m}\frac{\delta\Delta}{C_i} \qquad (6.1)$$

where $\delta\Delta$ is the change in the Δ spectra under analyte concentration (C_i), m is the number of different concentrations used in the study, and $\Delta_\circ$ is the initial phase shift (before exposure).

The average sensitivities were presented in Figure 6.6. All films exhibited higher sensitivity for PCP compared to the other analytes where the highest sensitivity for PCP was found to be 0.00396/(μg/L) in the case of ATCNT-**Pc5** active layer. The lower sensitivity for simazine is suggested to be demonstrated because simazine is not oxygen containing.

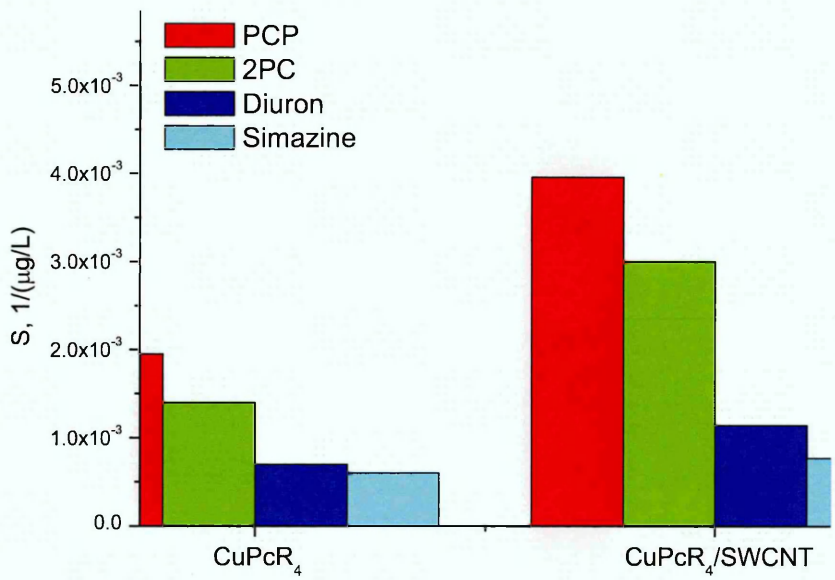

Figure 6.6: Sensitivity of Pc5 and ATCNT-Pc5 active layers estimated from equation 6.1 for PCP, 2PC, diuron and simazine

The lowest detectable concentration was calculated using the variation in the relative shift change in the baseline using the root-mean-square deviation (rmsd) [27].

A fifth order polynomial fit has been applied to the dynamic base line (Figure 6.7) over 305 point at the wavelength of 730nm, where Δ(λ) spectrum has shown a sharp drop in the gold layer. This gives not only the curve-fitting equation but also the statistical parameters of the polynomial fit.

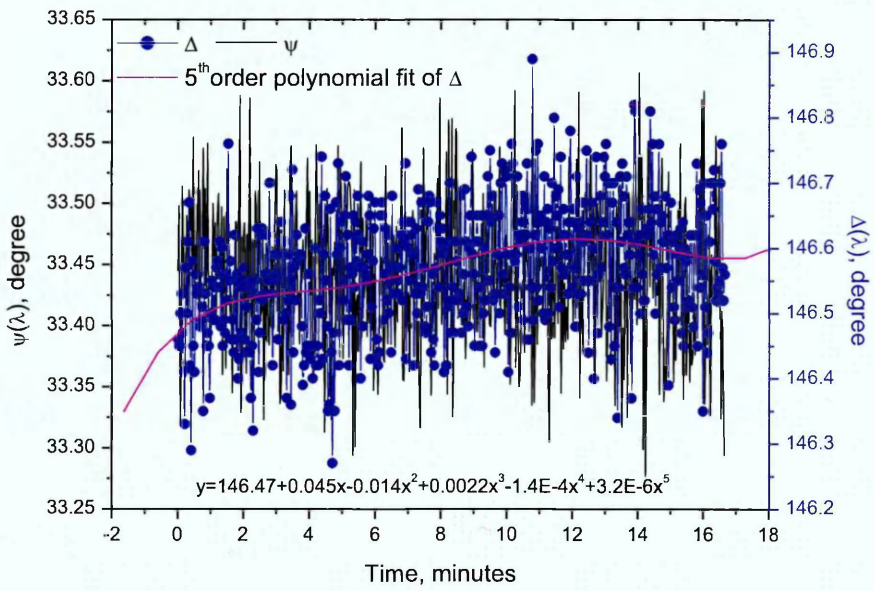

Figure 6.7: The dynamic spectra of base line of gold substrate at λ =730 nm. The fifth order polynomial fit has been extracted for the phase shift spectrum only and the equation has been presented

The root mean square noise can be calculated according to the following equation;

$$rms_{noise} = \sqrt{\frac{V_{x^2}}{N}} \qquad (6.2)$$

where

$V_{x^2} = \sum(y_i - y)^2$; yi is the measured data point and y is the corresponding value calculated from the curve-fitting equation (Figure 6.7). N is the number of data points used in the curve fitting. The average noise level was found to be 0.162.

Figure 6.8 to 6.11 show the changes in the phase shift versus analytes concentrations in the range of 1-25 μg/L, plotted from Table 6.1. According to the signal-to-noise ratio definition, when the signal-to-noise ratio equals 3, the signal is considered to be a true signal [28]. Therefore, the detection limit can be extrapolated from the linear calibration curve, presented in the insets to Figures 6.8 to 6.11, when the signal equals 3 times the noise.

$$DL\left(\frac{\mu g}{L}\right) = 3\frac{rms_{noise}}{slope} \qquad (6.3)$$

Using the above equation, and the slopes from Figures 6.8 to 6.11, the detection limits is calculated and summarised in table 6.4.

Table 6.4: The detection limits for studied sensors calculated according to equations 6.2 and 6.3.

	DL, μg/L			
	PCP	**2CP**	**Diuron**	**Simazine**
Pc5	0.2791	0.3812	0.646	0.832
ATCNT-**Pc5**	0.133	0.171	0.335	0.62

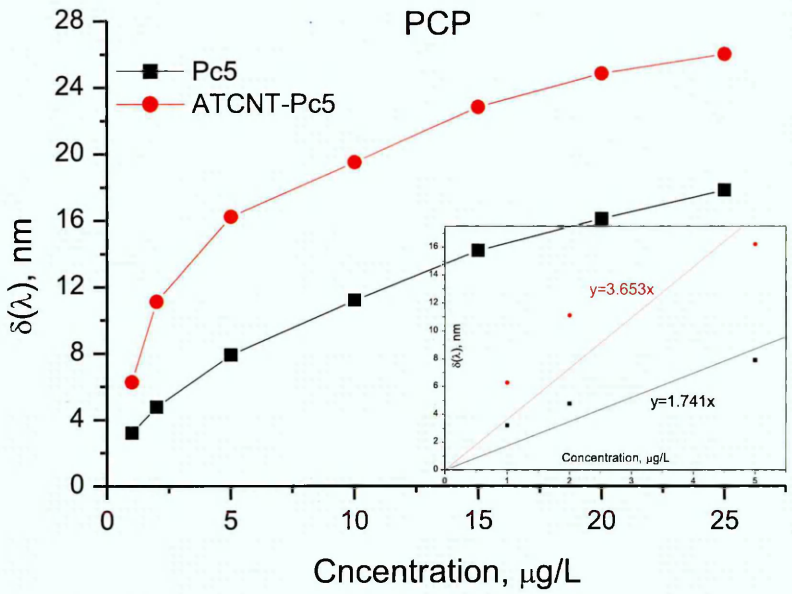

Figure 6.8 Changes in the phase shift depending on the concentrations of PCP. The inset represents the linear fitting for the first three points of each curve

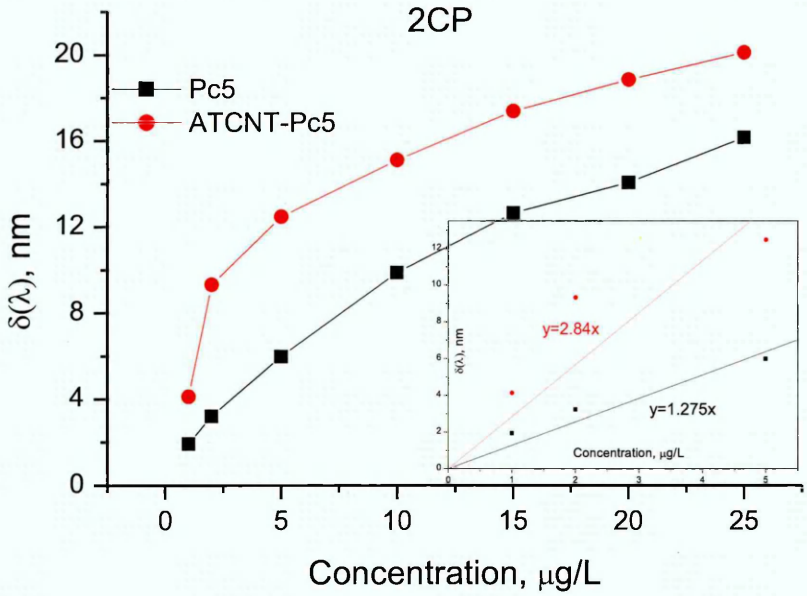

Figure 6.9 Changes in the phase shift depending on the concentrations of 2CP. The inset represents the linear fitting for the first three points of each curve

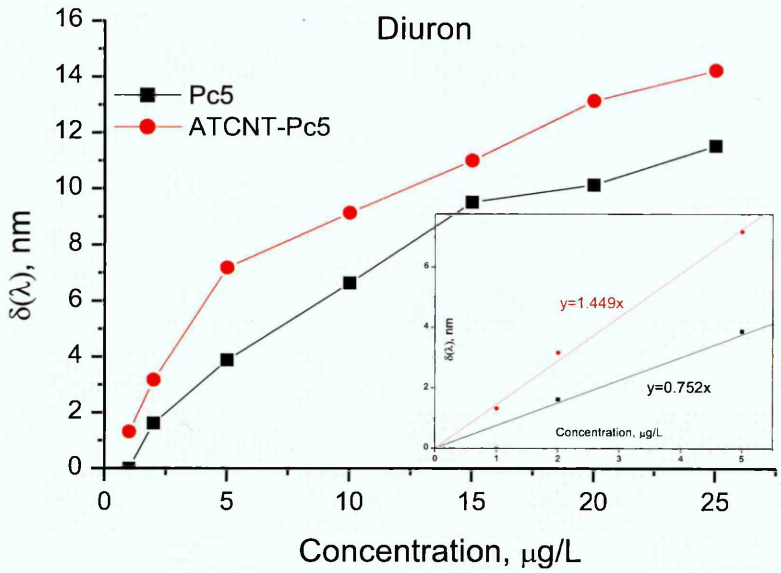

Figure 6.10 Changes in the phase shift depending on the concentrations of Diuron. The inset represents the linear fitting for the first three points of each curve

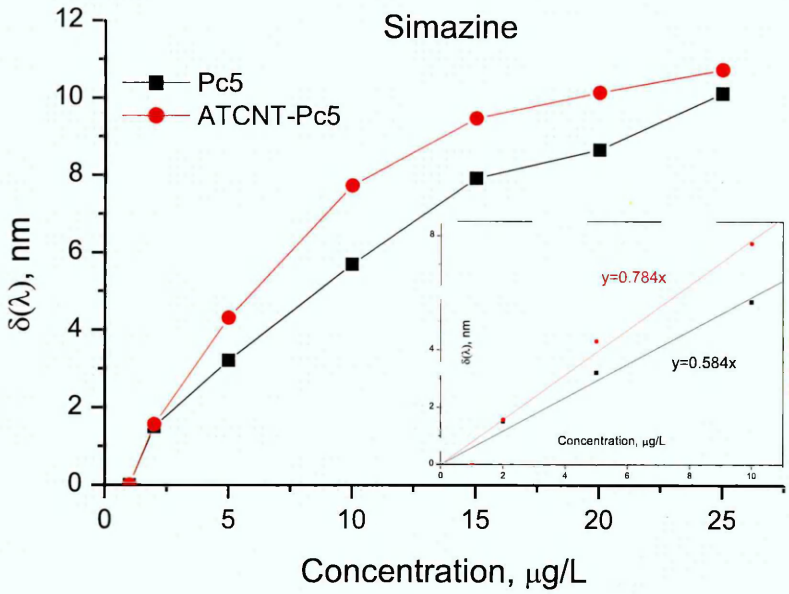

Figure 6.11 Changes in the phase shift depending on the concentrations of Simazine. The inset represents the linear fitting for the first three points of each curve

6.2 Detection of amine vapours in ambient air

6.2.1 Introduction

Over the past few years, there has been an increasing demand of simple and effective method to detect toxic odours that are produced by organic volatile compounds due to their damaging effects on biological system and environment in general [14,29-31]. Among these hazardous gases, amines complexes are commonly used in agriculture, pharmaceutical, dye manufacturing and food processing industries [32]. In addition, amines and their derivatives are considered as indicators of spoilage in food because they play a vital role in the degradation pathways of amino acids in living organisms [33]. In the case of fish and seafood, biogenic amines include methylamine, dimethylamine and trimethylamine, among others. The concentration of these decomposition products rises with time, so the determination of the freshness in fish and seafood is reliable with the quantification of these vapours [34].

Detection strategies based on gas chromatography or high performance liquid chromatography have proved to give good results but are complex to implement and require a lot of processing time [35]. Sensor based on electrochemical or optical devices have been researched over the last decades with good outcome [36-41]. These techniques are non-destructive and relatively straightforward, as well as having the added advantage of being less expensive than the separation procedures.

6.2.2 Materials and sample preparation

Thin films of pristine **Pc1,2,3,4** and ATCNT-**Pc1,2,3,4** hybrids, which were discussed in chapter 5, were used in this work as active layers to detect methylamine, dimethylamine and trimethylamine (Figure 6.12) vapours in ambient air in low concentrations ranging from 4 to 200ppm. The sample preparation for TIRE study has been explained in Chapter 3. Methylamine, dimethylamine and trimethylamine solutions in water (40%) were purchased from Sigma-Aldrich (see Chapter 3) and ambient air was used as the diluent gas. Small amounts of amine solutions were transferred into 2L glass bottle using micro syringe and were left to vaporize. The vapour concentration was calculated according to the following gas law:

$$c = \frac{22.4\rho T V_s}{273MV} \times 10^3 \qquad (6.4)$$

Where c is the concentration in ppm, ρ the density of the liquid sample in g/mL, T the temperature of container in Kelvin, V_s the volume of the liquid sample in μL, M the molecular weight of sample in grams, and V is the container volume in litre. The diluted gas has been further diluted in a 50 mL syringe to obtain amines concentrations of 4, 8, 20, 40, 80 and 200 ppm, which were injected into the gas cell that was fixed on the TIRE experiment set up. Table 6.5 the concentration calculations according to eq. 6.4. The films were degased by injecting fresh air into the gas cell following each gas exposure.

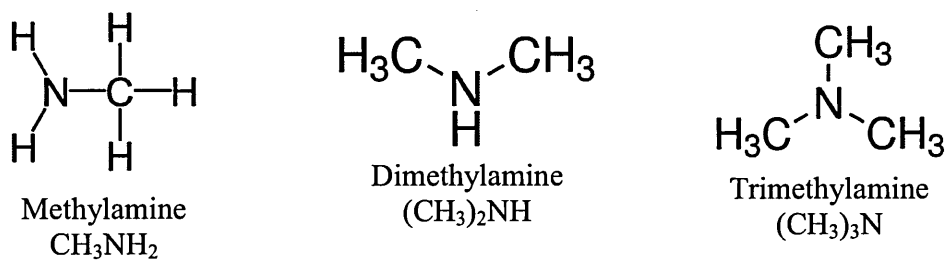

Figure 6.12: Chemical structure of the amines used in this work [20]

6.2.3 Spectral shift

The adsorption of amines vapours onto the surface of $CuPcR_4$ and SWCNT/$CuPcR_4$ hybrids has been studied using TIRE method. Phthalocyanines and their hybrids were spun onto gold-coated glass substrates as described in Chapter 5. Figure 6.13 shows typical TIRE spectra of Cr/Au films in air used in the present work; this was fully discussed in section 6.1.3.

Table 6.5: Amines concentrations as calculated using equation (6.4)

						Calculated concentration	Further dilution by 50cc syringe		The original solutions are 40% conc. in water
	V_s (µL)	ρ (g/mL)	V (L)	T (K)	M (g)	C1 (ppm)	C2=C1*X/50 (ppm)	X	C=C2*40%, (ppm)
Methylamine	1	0.89	2	291	31.7	335.1808	10.05542344	1.5	4
							20.11084688	3	8
							50.2771172	7.5	20
							100.5542344	15	40
							201.1084688	30	80
	2	0.89	2	291	31.7	670.3616	502.771172	37.5	200
Dimethylamine	2	0.89	2	291	42.08	505.0015	10.10002925	1	4
							20.2000585	2	8
							50.50014624	5	20
							101.0002925	10	40
							202.000585	20	80
	4	0.89	2	291	45.08	942.7889	499.6781107	26.5	200
Trimethylamine	2	0.83	2	291	59.11	335.2706	10.0581185	1.5	4
							20.116237	3	8
							50.29059251	7.5	20
							100.581185	15	40
							201.16237	30	80
	4	0.88	2	291	59.11	710.9353	504.7640514	35.5	200

Figure 6.14, 6.15, 6.16 and 6.17 present the spectra of $\Psi(\lambda)$ and $\Delta(\lambda)$ of **Pc1, Pc2, Pc3** and **Pc4** and their hybrids with the acid treated SWCNT thin films respectively before and after exposure to amines vapours; the shifts are summarised in Table 6.6. The concentrations of amines were varied from 4 to 200 ppm in air. The spectra were measured 10 minutes after injection of contaminated or fresh air to achieve the equilibrium response or recovery, respectively.

During exposure to contaminated air, it was difficult to detect shifts in $\Psi(\lambda)$ because of the shape of the curve, however, significantly larger shifts have been observed in $\Delta(\lambda)$ spectra. These are typical features of TIRE method as reported earlier [18,19,21]. The spectra of $\Delta(\lambda)$ were further enlarged and shown at the top of Figures 6.14, 6.15, 6.16 and 6.17 to provide better assessment of the effect of amines exposures.

It can clearly be seen that the adsorption of amines on hybrid films has resulted in larger shifts and these shifts have been summarised in Table 6.6.

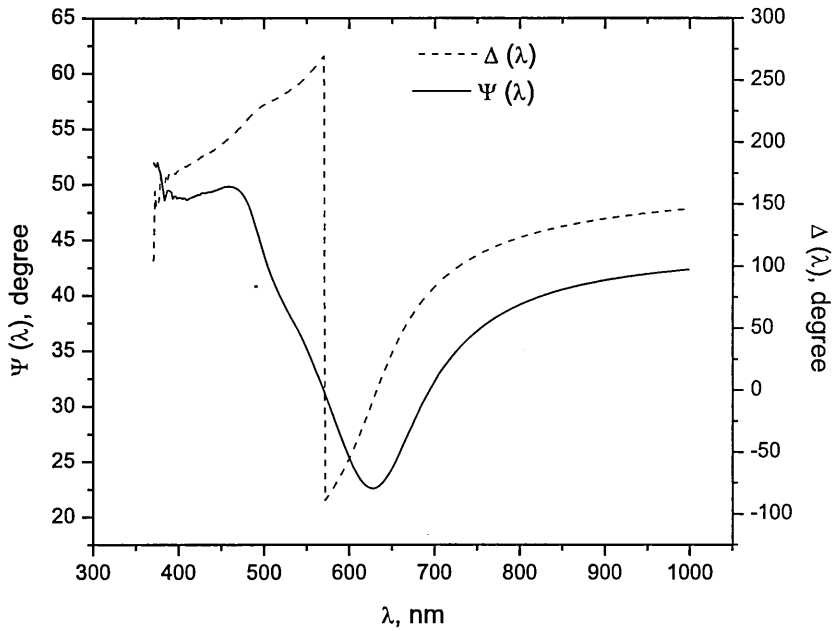

Figure 6.13: Typical TIRE spectra of Cr/Au film in air

Carbon nanotubes in general are characterised with uniform surface with delocalised π-electrons of high density, which enhances their adsorption properties. When hybrid films are exposed to amine vapours, larger numbers of molecules are adsorbed onto the surface resulting in larger changes in the optical properties of the films and hence larger shifts in $\Delta(\lambda)$ compared to pristine phthalocyanine films.

Complete recovery in the time range of 100-400s of $\Delta(\lambda)$ spectra was observed after flushing the cell with fresh air as previously established for films of metal phthalocyanines with other types of substituents [21]. Figure 6.18 shows the dependence of phase shift change on amines concentrations in the range of 4-200 ppm for phthalocyanine layers and their hybrids with SWCNTs.

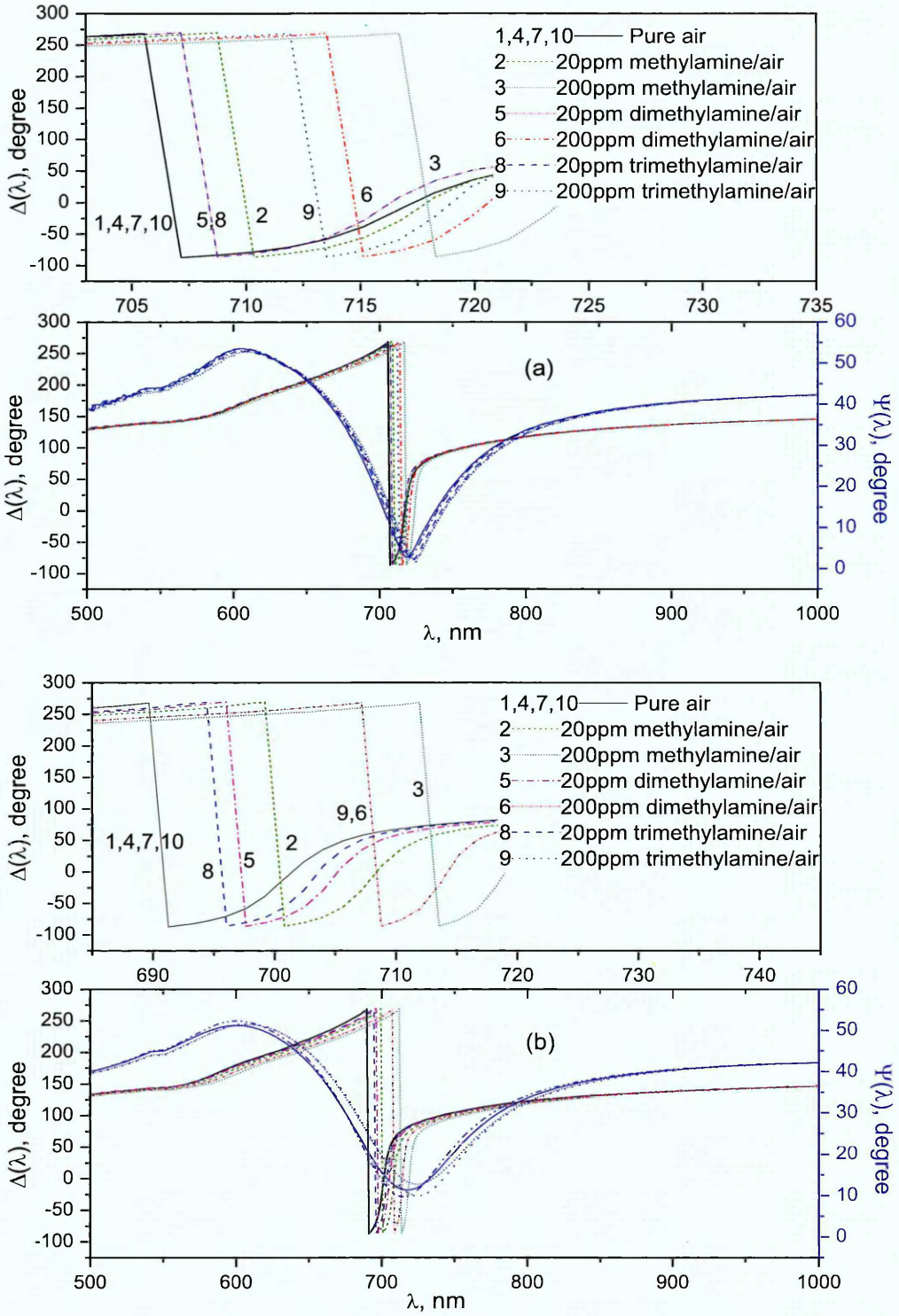

Figure 6.14: Ψ(λ) and Δ(λ) spectra of (a) **Pc1** and (b) ATCNT-**Pc1** coated Cr/Au in air (1,4,7 and 10); after injection of 20 and 200 ppm of methylamine (2,3), dimethylamine (5,6), trimethylamine (8,9). Enlarged section of Δ(λ) shown above

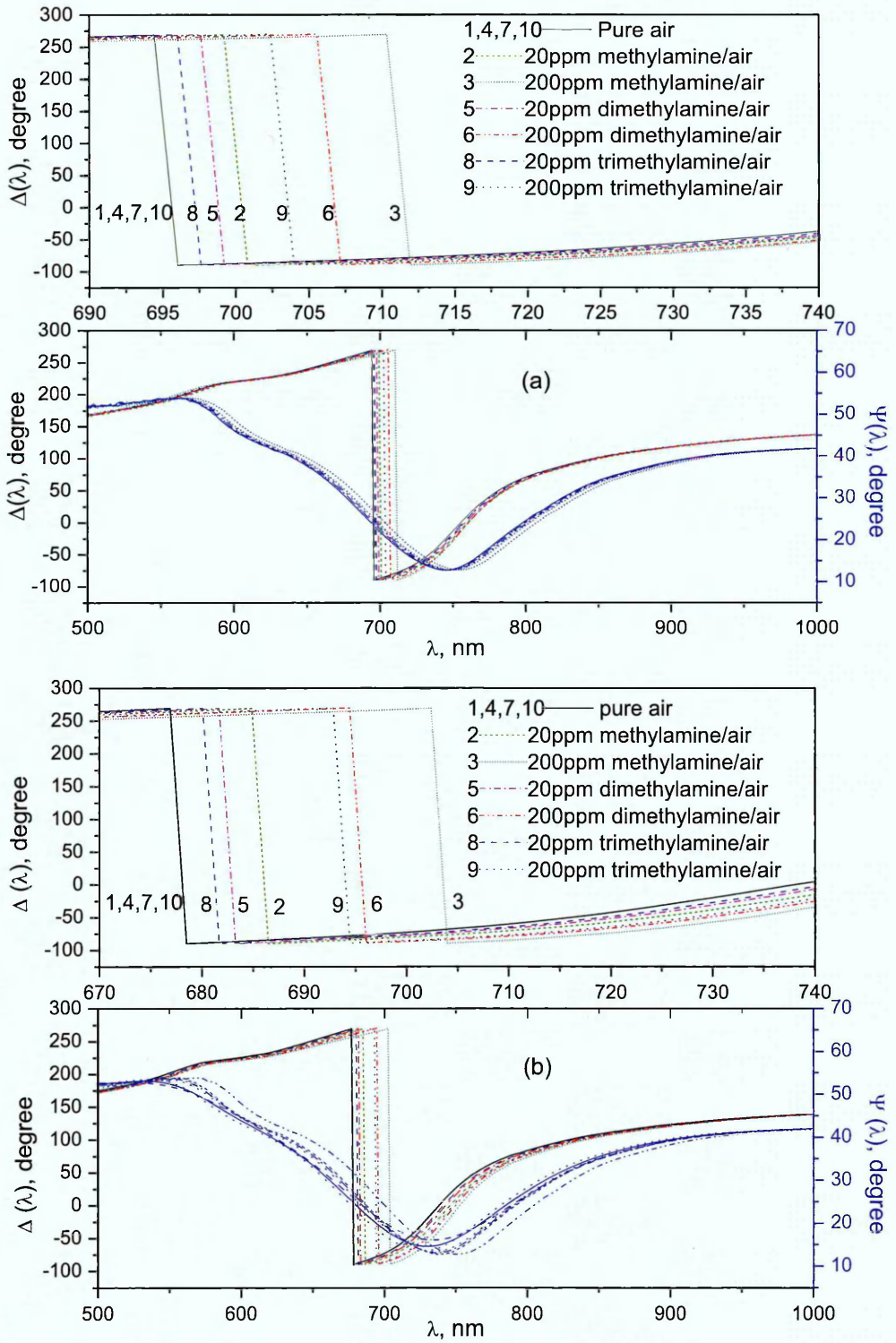

Figure 6.15: Ψ(λ) and Δ(λ) spectra of (a) **Pc2** and (b) ATCNT-**Pc2** coated Cr/Au in air (1,4,7 and 10); after injection of 20 and 200 ppm of methylamine (2,3), dimethylamine (5,6), trimethylamine (8,9). Enlarged section of Δ(λ) shown above

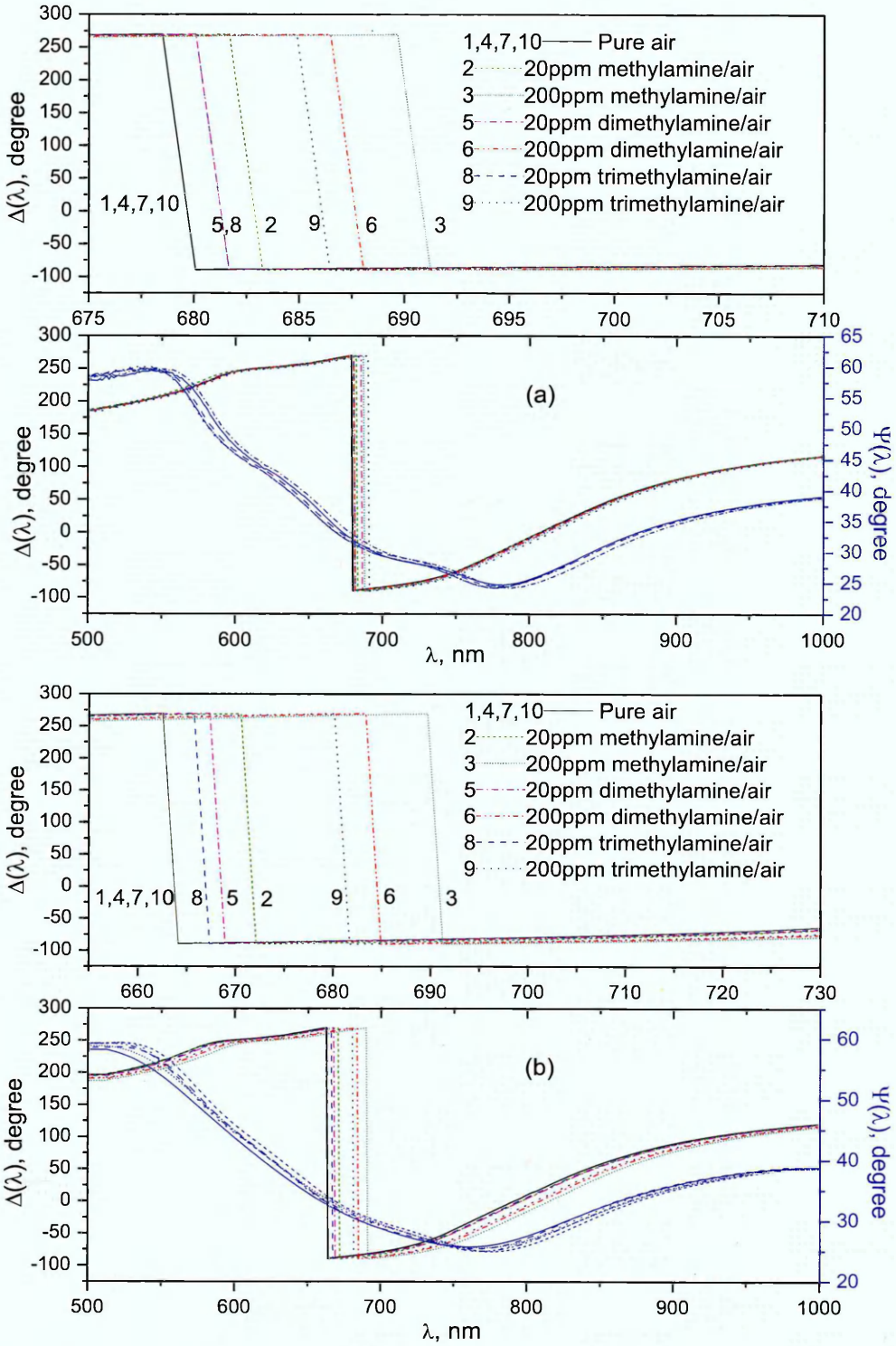

Figure 6.16: Ψ(λ) and Δ(λ) spectra of (a) **Pc3** and (b) ATCNT-**Pc3** coated Cr/Au in (1,4,7 and 10); after injection of 20 and 200 ppm of methylamine (2,3), dimethylamine (5,6), trimethylamine (8,9). Enlarged section of Δ(λ) shown above

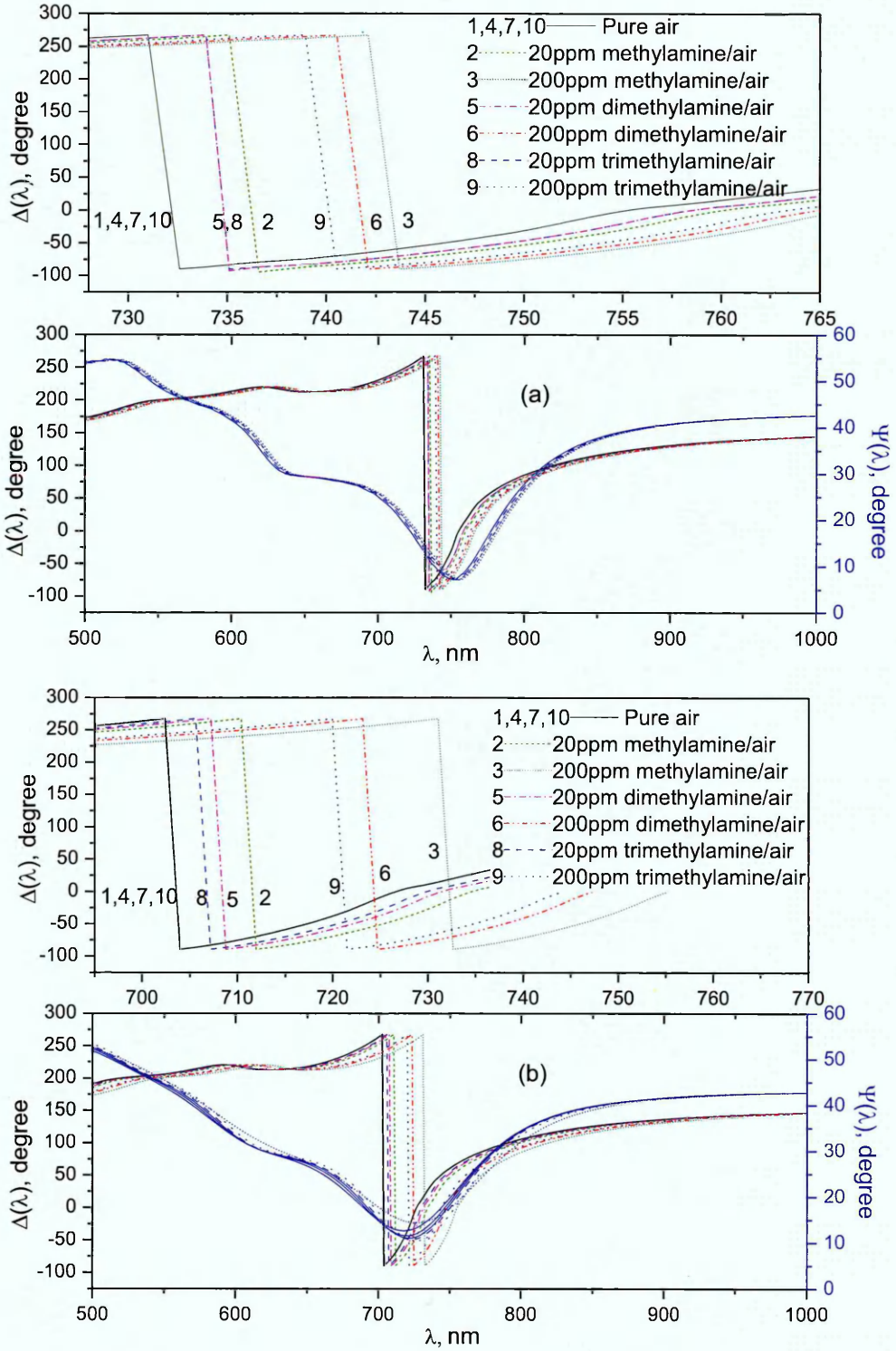

Figure 6.17: Ψ(λ) and Δ(λ) spectra of (a) **Pc4** and (b) ATCNT-**Pc4** coated Cr/Au in air (1,4,7 and 10); after injection of 20 and 200 ppm of methylamine (2,3), dimethylamine (5,6), trimethylamine (8,9). Enlarged section of Δ(λ) shown above

Table 6.6: The changes in the phase shifts Δ(λ) of phthalocyanines and their composites with carbon nanotubes active layers upon exposure to methylamine, dimethylamine and trimethylamine gases in different concentrations

		δΔ(λ), nm							
	Conc. , ppm	**Pc1**	ATCNT-**Pc1**	**Pc2**	ATCNT-**Pc2**	**Pc3**	ATCNT-**Pc3**	**Pc4**	ATCNT-**Pc4**
Methylamine	4	-	1.64	-	1.25	-	1.79	-	1.43
	8	1.31	4.19	1.9	3.51	-	3.2	1.25	3.1
	20	3.24	9.08	4.09	8.03	3.05	7.14	3.67	7.98
	40	6.9	15.81	7.51	15.16	6.02	13.63	6.87	13.91
	80	10	20.01	12.12	20.9	9.35	20.02	9.53	23.55
	200	11.19	22.57	15.97	25.39	11.11	27.22	11.32	28.58
Dimethylamine	4	-	-	-	-	-	-	-	-
	8	-	3.29	-	1.91	-	2.01	-	2
	20	1.78	6.35	3.05	4.97	1.59	4.74	2.25	4.79
	40	3.69	10.59	5.95	8.21	3.32	9.9	3.95	9.31
	80	6.78	15.03	9.34	13.32	6.01	15.5	7.45	16.61
	200	8.02	17.72	11.04	17.34	7.95	20.76	9.5	20.75
Trimethylamine	4	-	-	-	-	-	-	-	-
	8	-	2.21	-	-	-	1.98	-	1.68
	20	1.54	4.68	1.59	3.19	1.57	3.06	2.05	3.19
	40	2.89	8.58	3.82	6.38	3.12	6.8	3.42	6.95
	80	5.1	14.64	6.11	11.12	5.4	12.76	5.9	11.83
	200	6.4	17.43	7.97	15.77	6.3	17.7	7.82	17.56

Earlier studies have shown that water molecules are weakly physisorbed onto carbon nanotube surface [42-44]. Larger response to humidity has been reported in boron- and nitrogen-doped carbon nanotubes [45], which indicate strong interaction between water molecules and doped-CNTs, however, the recovery time of sensor based on these materials was achieved in about 2.5 h. In this work the baseline was measured using ambient air and therefore the humidity interaction resulting from the diluted gas can be negligible.

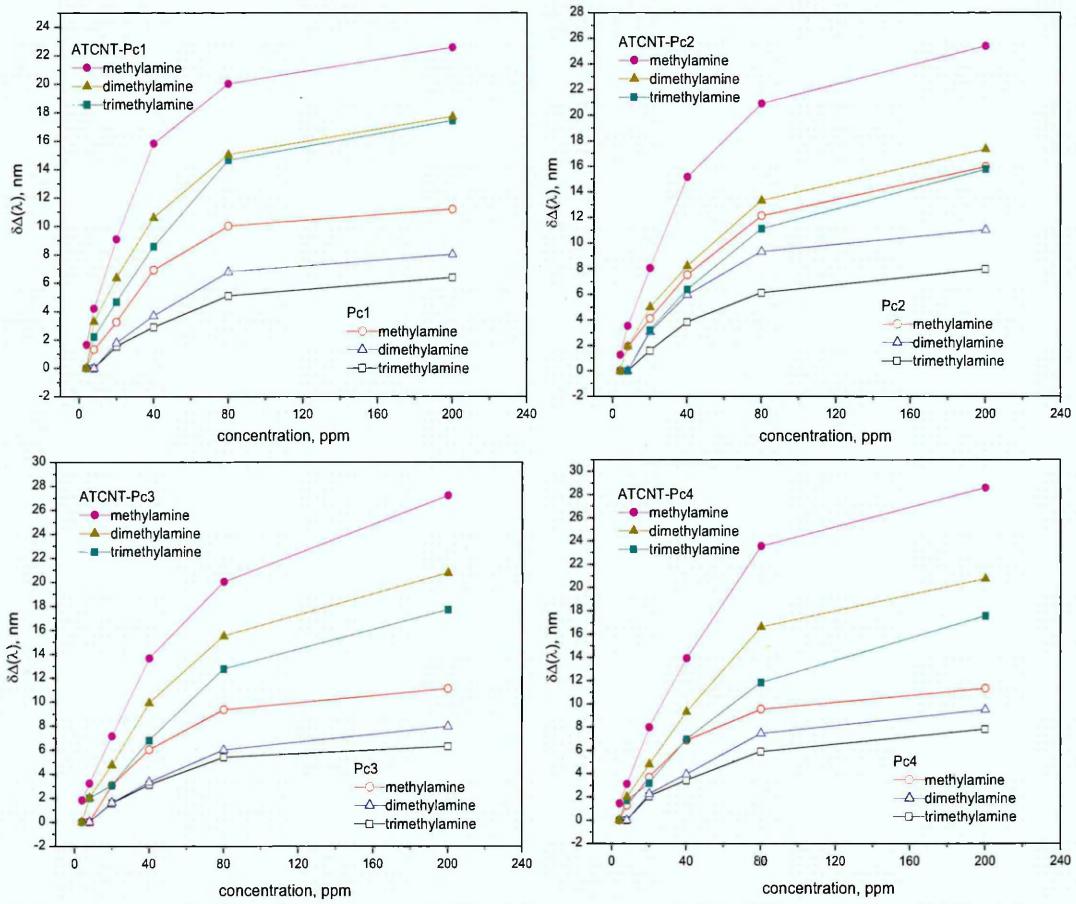

Figure 6.18: Phase shift changes (δΔ) in Δ(λ) spectra of studied Cu(II) phthalocyanines derivatives and their hybrids with acid treated SWCNT layers on treatment with amines vapours in the concentration range 4-200 ppm

6.2.4 Experimental data fitting

Theoretical fitting to experimental Ψ and Δ spectra was carried out by applying a 4-layer model consisting of air, organic layer, Au layer and BK7 glass. The parameters of organic films after exposure to amines vapours were determined by fitting experimental Ψ and Δ spectra to the theoretical organic model by fixing Cr/Au layer parameters. Table 6.7 summarises the thickness of all layers found from theoretical data fitting as well as the values of refractive index and extinction coefficients given at λ=633 nm. Further to the data summarised in Table 6.7 the variation in refractive index and extinction coefficient as a function of λ for **Pc1,2,3,4** and ATCNT-**Pc1,2,3,4** films in pure air and after exposure to amines vapours at the concentration of 40 ppm are shown in Figures 6.19, 6.20, 6.21 and 6.22.

6.2.5 Sensitivity and Response time

In order to evaluate the response of the two types of layers the average sensitivity has been calculated based on changes in Δ spectra shifts (Table 6.6) using equation 6.1. The average sensitivities were presented in Figure 6.23. All films exhibited higher sensitivity for methylamine than dimethylamine and trimethylamine, where the highest sensitivity for methylamine was found to be 0.000325 /ppm in the case of ATCNT-**Pc2** active layer. The lower sensitivity for secondary and tertiary amines can be explained by the steric hindrance that their molecular shapes provide which allows smaller number of these molecules to interact with films' surfaces as compared to methylamine [46]. Furthermore, the higher vapour temperature of dimethylamine and trimethylamine (7-9° C) in comparison to methylamine (-7°C) reduces the number density of these amines at room temperature. Therefore, the interaction probability with the film surface is reduced. It was recently found that changes in the intensity of the Q-band in the UV-visible spectra of thin films of metalloporphyrin were ~ 0.85 and 0.5 (a.u.) after exposure to low concentrations of dimethylamine and trimethylamine respectively [47]. This is found consistent with our observations where dimethylamine showed better interaction with the active layer than trimethylamine.

Table 6.7: Changes in the optical parameters and films' thicknesses of $CuPcR_4$ and SWCNT/$CuPcR_4$ films at λ=633 nm caused by adsorption of amines (40 ppm)

	Initial film			After exposure to 40 ppm								
				Methylamine			Dimethylamine			Trimethylamine		
	n	*k*	*d,nm*	*n*	*k*	*d,nm*	*n*	*k*	*d,nm*	*n*	*k*	*d,nm*
Pc1	1.633	0.192	40.6	1.639	0.198	40.9	1.638	0.198	40.7	1.636	0.194	40.8
ATCNT-**Pc1**	1.394	0.124	69.4	1.40	0.127	69.8	1.41	0.126	70.1	1.398	0.124	70
Pc2	1.573	0.270	32.2	1.590	0.273	32.6	1.576	0.276	32.3	1.581	0.268	32.2
ATCNT-**Pc2**	1.367	0.151	51	1.369	0.158	52.1	1.369	0.156	51.7	1.375	0.155	51.7
Pc3	1.580	0.254	36.3	1.591	0.265	37	1.583	0.257	37	1.586	0.253	36.4
ATCNT-**Pc3**	1.402	0.271	63.7	1.425	0.295	64.3	1.415	0.285	64.5	1.419	0.278	63.9
Pc4	1.522	0.369	33.1	1.530	0.373	33.4	1.524	0.372	33.6	1.526	0.370	33.4
ATCNT-**Pc4**	1.396	0.126	55.3	1.4	0.128	55.9	1.407	0.126	55.8	1.397	0.127	55.5

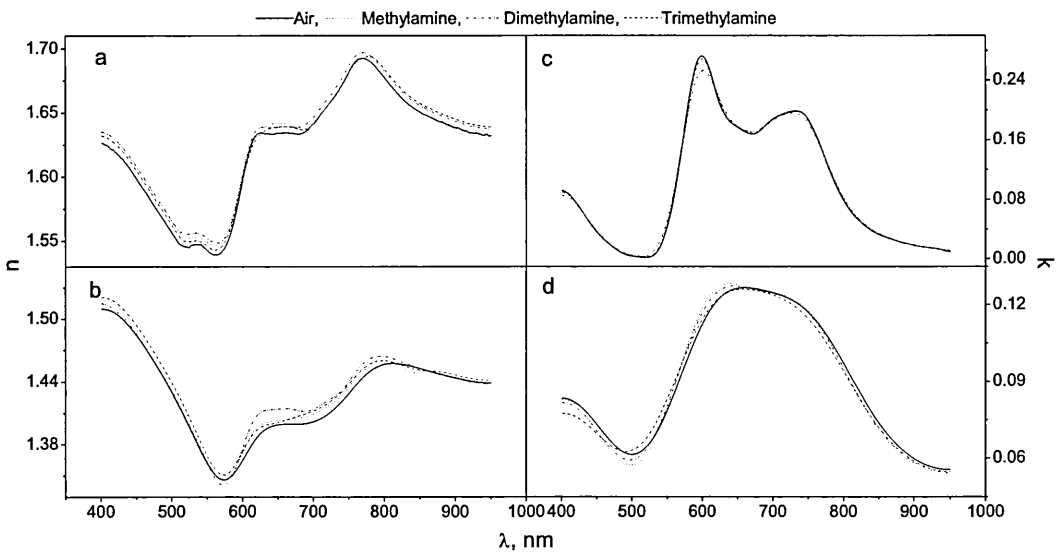

Figure 6.19: The variation in refractive index and extinction coefficient of (a and c) **Pc1** and (b and d) ATCNT-**Pc1** layers as exposed to air (solid lines), methylamine (dotted lines), dimethylamine (dashed-dotted lines) and trimethylamine (dashed lines) in the concentration of 40 ppm

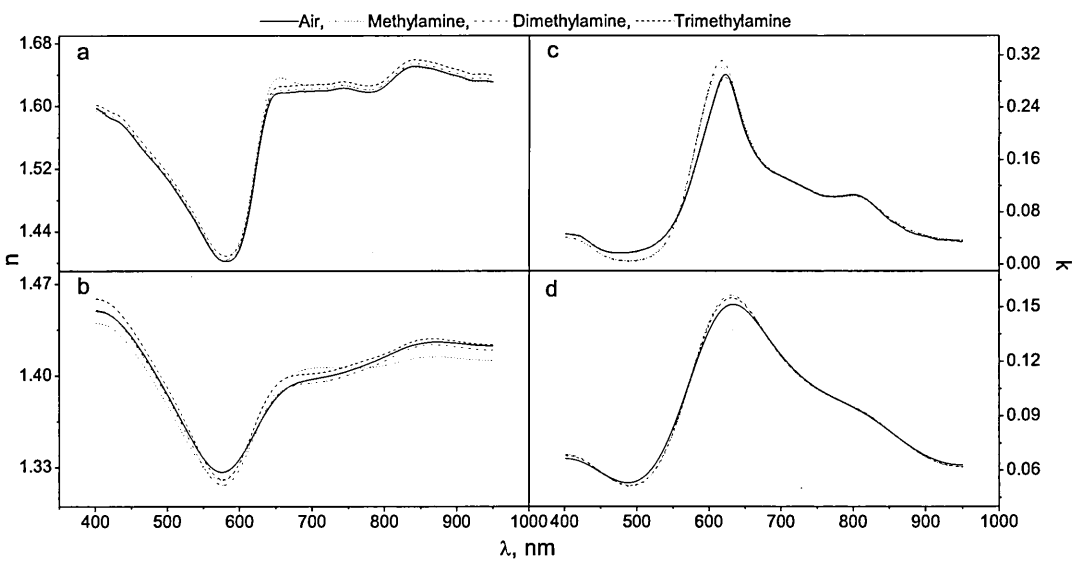

Figure 6.20: The variation in refractive index and extinction coefficient of (a and c) **Pc2** and (b and d) ATCNT-**Pc2** layers as exposed to air (solid lines), methylamine (dotted lines), dimethylamine (dashed-dotted lines) and trimethylamine (dashed lines) in the concentration of 40 ppm

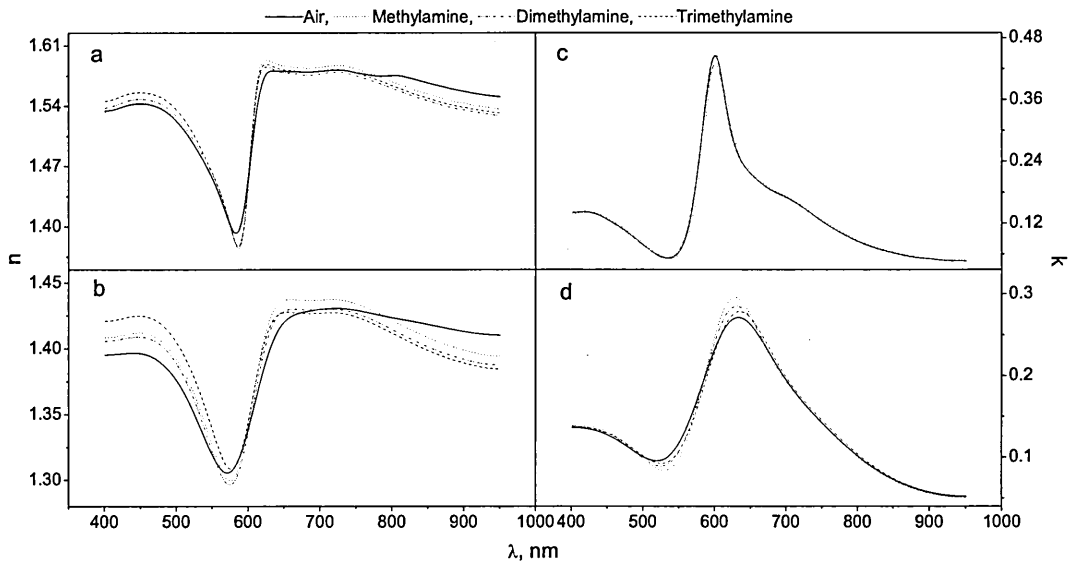

Figure 6.21: The variation in refractive index and extinction coefficient of (a and c) **Pc3** and (b and d) ATCNT-**Pc3** layers as exposed to air (solid lines), methylamine (dotted lines), dimethylamine (dashed-dotted lines) and trimethylamine (dashed lines) in the concentration of 40 ppm

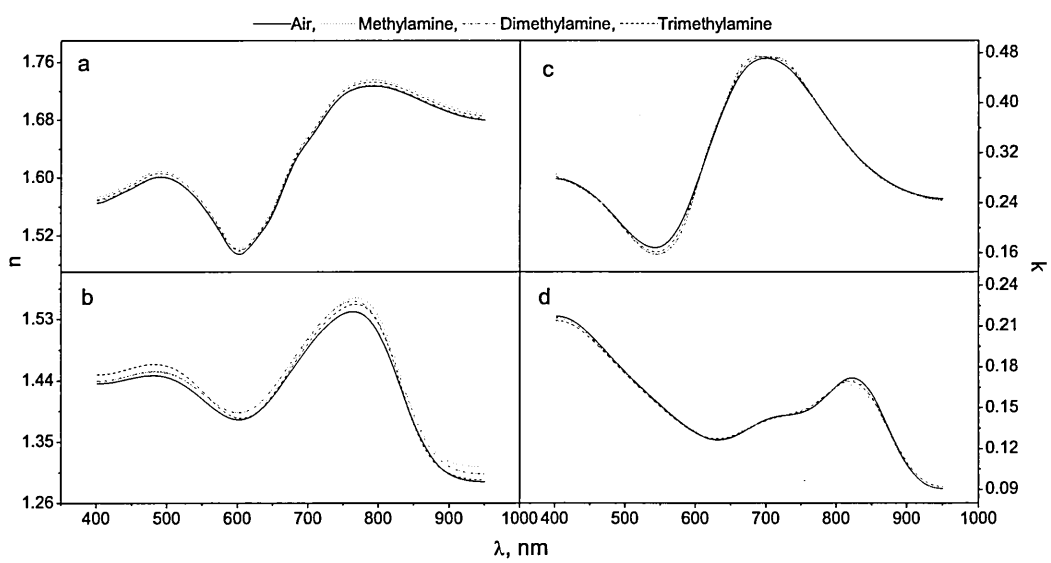

Figure 6.22: The variation in refractive index and extinction coefficient of (a and c) **Pc4** and (b and d) ATCNT-**Pc4** layers as exposed to air (solid lines), methylamine (dotted lines), dimethylamine (dashed-dotted lines) and trimethylamine (dashed lines) in the concentration of 40 ppm

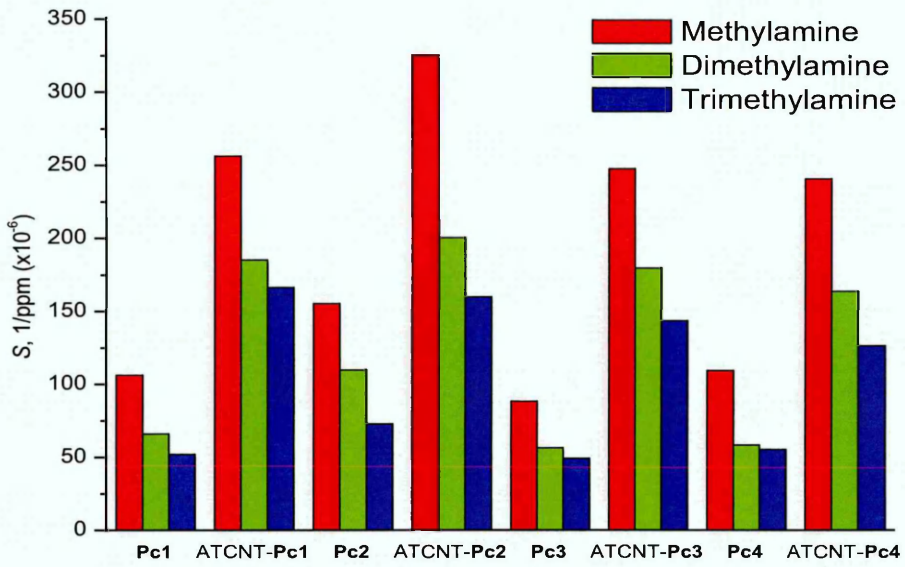

Figure 6.23: Sensitivity of phthalocyanines and their hybrids with SWCNTs active layers estimated from eq. 6.1 for methylamine, dimethylamine and trimethylamine

Pc2 and **Pc4** show higher sensitivity to analytes than **Pc1** and **Pc3**. The non-peripheral tetra substitution in **Pc1** and **Pc3** makes them less sensitive to the examined analytes due to their lower overall affinity [48].

To calculate the response time, **Pc2** and ATCNT-**Pc2** films were selected and exposed to methylamine, dimethylamine and trimethylamine at concentration of 40 ppm. For methylamine, the response time t_{80}, which is defined as the time it takes to reach 80% of the steady state shift, was measured to be 158 s in **Pc2** film and 66 s in ATCNT-**Pc2** film. This is much lower than the response time of 440 s and 270 s found by Liu et al [46] using zinc phthalocyanine film and Saini et al [32] using copper phthalocyanine film, respectively. The response time for dimethylamine was found to be 230 s and 101 s detected by **Pc2** and ATCNT-**Pc2** films respectively, while for trimethylamine, response times were found to be 267 s and 136 s. The recovery time t^*_{80}, which is defined as the time required to reach 80% of the base line were measured to be 393, 350 and 387 s for methylamine, dimethylamine and trimethylamine respectively as detected by **Pc2**, whereas ATCNT-**Pc2** hybrid film exhibited recovery times of 150, 191 and 138 s respectively.

Figure 6.24 shows the response and recovery times of **Pc2** and its SWCNTs hybrid films on exposures to methylamine at concentration of 40 ppm.

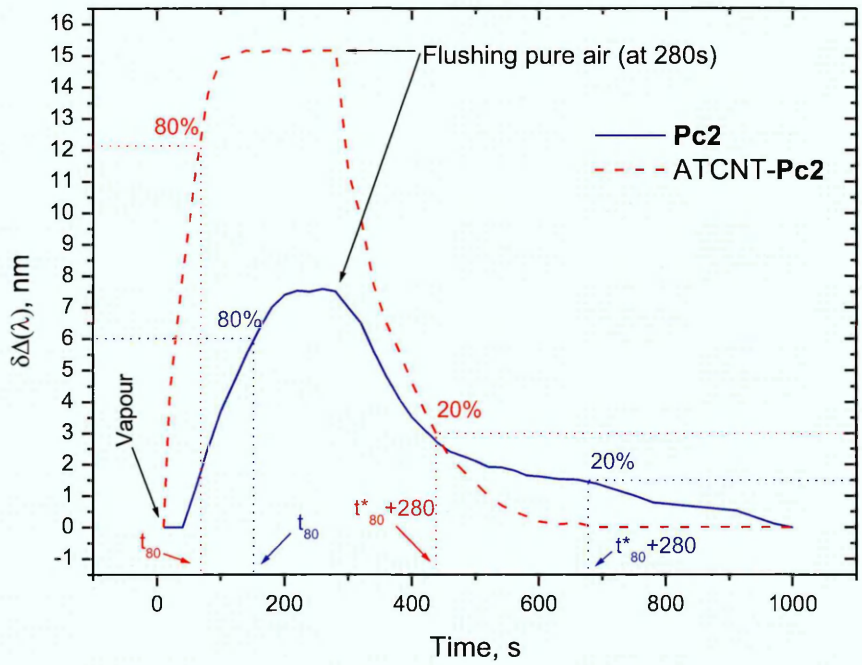

Figure 6.24: The rise and decay curves of the *δΔ(λ)* during the detection of 40 ppm methylamine vapour by **Pc2** and **Pc2-ATCNT** films

6.2.6 Detection limit

The lowest detectable concentration was calculated according to section 6.1.6 above in this chapter. Using gold-air interface experiment, a fifth order polynomial fit has been applied on the dynamic base line (Figure 6.25) over 305 point at the wave length 570nm, where Δ(λ) spectrum has shown a sharp drop in the gold layer. This gives not only the curve-fitting equation but also the statistical parameters of the polynomial fit.

The root mean square noise can be calculated according to eq. 6.2, where, *yi* is the measured data point and *y* is the corresponding value calculated from the curve-fitting equation (Figure 6.25). *N* is the number of data points used in the curve fitting. The average noise level was found to be 0.117.

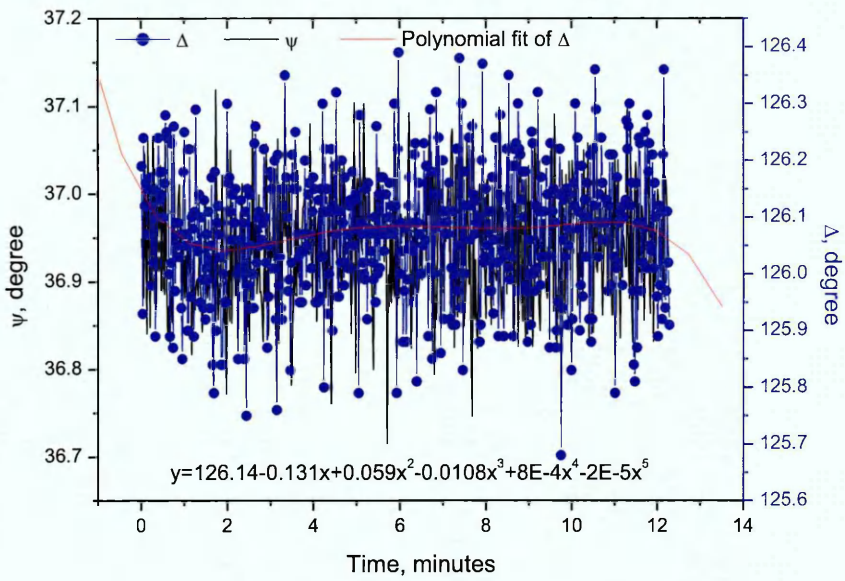

Figure 6.25: The dynamic spectra of base line of gold-air substrate at λ =570 nm. The fifth order polynomial fit has been extracted for the phase shift spectrum only and the equation has been presented

Figure 6.26 to 6.29 show the changes in the phase shift versus analytes concentrations for the first few linear points, plotted from Table 6.6.

According to eq. 6.3 with the replacement of units to ppm, the detection limits can be extrapolated from the linear calibration curves, presented in Figures 6.26 to 6.29. When the signal equals 3 times the noise, the detection limits have been calculated and presented in Table 6.8.

Several detection techniques for amines' vapours were reported in the literatures. When aqua(chloro)(5,10,15,20-tetraphenylporphyrinato)chromium(III) used as optical active layer based on UV-visible absorption technique, a detection limit of 10 ppm was reported [47] under dynamic conditions, while a limit of 24 ppm has been realized by using fiber-optic fluorescence sensor employing 2-naphtol bonded to polyethylene oxide [49].

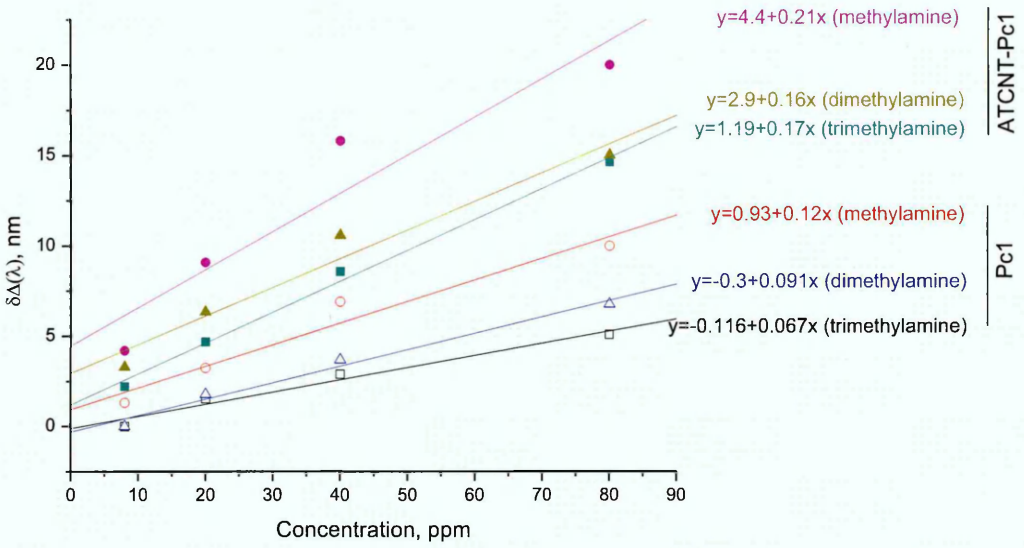

Figure 6.26: Changes in the phase shift of **Pc1** and ATCNT-**Pc1** spectra versus analytes concentrations for the first few linear points, plotted from Table 6.6

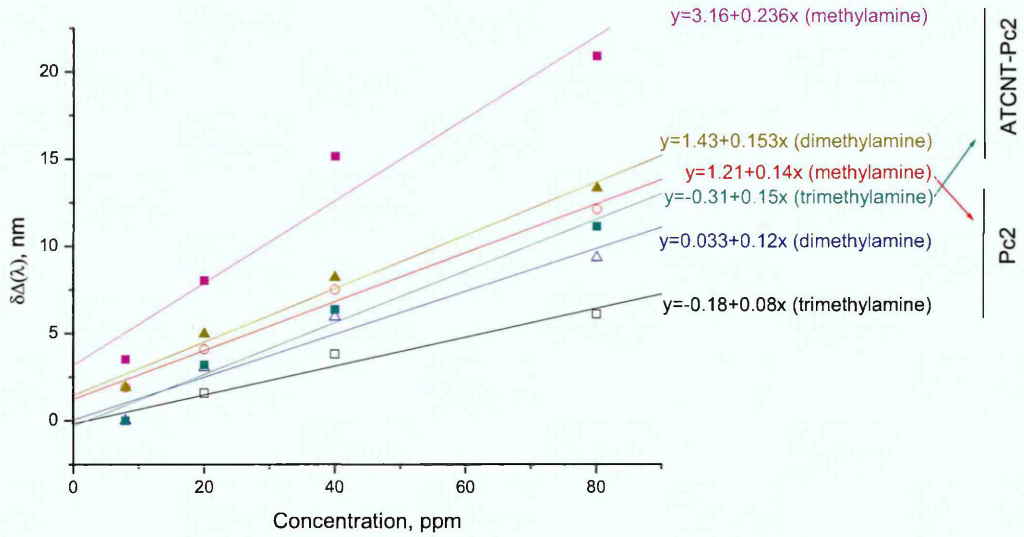

Figure 6.27: Changes in the phase shift of **Pc2** and ATCNT-**Pc2** spectra versus analytes concentrations for the first few linear points, plotted from Table 6.6

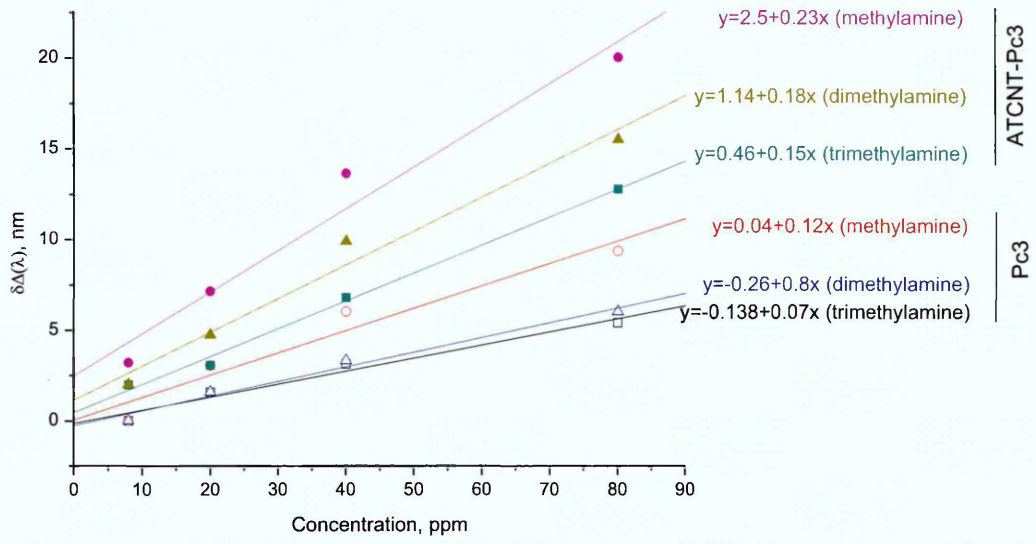

Figure 6.28: Changes in the phase shift of **Pc3** and ATCNT-**Pc3** spectra versus analytes concentrations for the first few linear points, plotted from Table 6.6

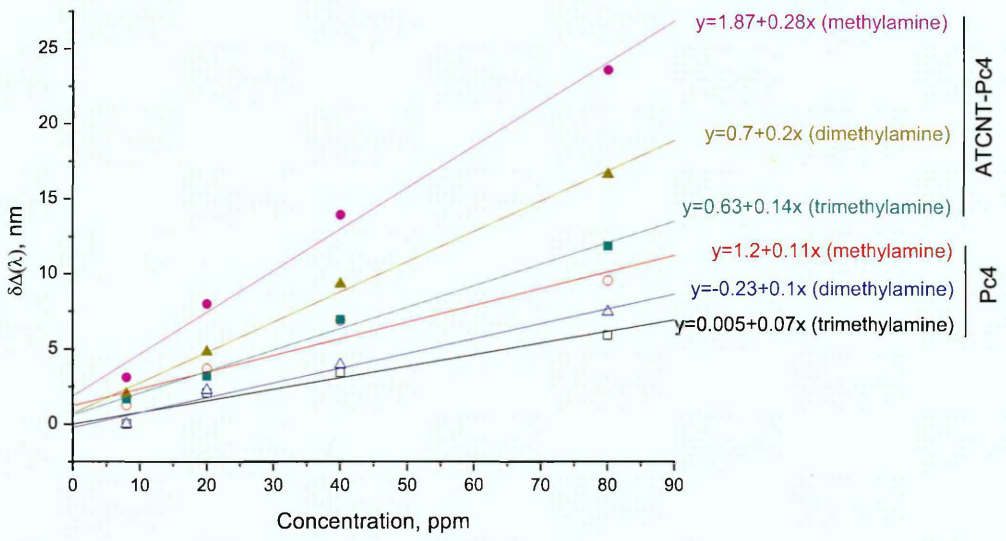

Figure 6.29: Changes in the phase shift of **Pc4** and ATCNT-**Pc4** spectra versus analytes concentrations for the first few linear points, plotted from Table 6.6

Table 6.8: The detection limits for amines sensors calculated according to equations 6.2 and 6.3

	DL(ppm)		
	Methylamine	**Dimethylamine**	**Trimethylamine**
Pc1	2.925	3.857143	5.238806
ATCNT-**Pc1**	1.671429	2.19375	2.064706
Pc2	2.507143	2.925	4.3875
ATCNT-**Pc2**	1.487288	2.294118	2.34
Pc3	2.925	4.3875	5.014286
ATCNT-**Pc3**	1.526087	1.95	2.34
Pc4	3.190909	3.51	5.014286
ATCNT-**Pc4**	1.253571	1.755	2.507143

Summary

Thin films of single-walled carbon nanotubes (SWCNT) hybridized with tetrasubstituted copper phthalocyanine ($CuPcR_4$) have been used as optical active layers to detect pentachlorophenol (PCP), 2-chlorophenol (2CP), diuron and simazine in water and methylamine, dimethylamine and trimethylamine in air using Total Internal Reflection Ellipsometry (TIRE) technique.

The produced films exhibited higher sensitivity for pentachlorophenol than other pesticides used in in the case of water ambient and higher sensitivity towards methylamine than dimethylamine and trimethylamine vapours. Hybrid films, in general, exhibited higher sensitivity and lower detection limit than pristine phthalocyanine films towards all the investigated analytes.

Reference List

[1] L.G. Freitas, H. Singer, S.R. Müller, R.P. Schwarzenbach, C. Stamm, Source area effects on herbicide losses to surface waters-A case study in the Swiss Plateau, Agriculture, Ecosystems and Environment. 128 (2008) 177-184.

[2] C. Fan, N. Li, X. Cao, Determination of chlorophenols in honey samples using in-situ ionic liquid-dispersive liquid-liquid microextraction as a pretreatment method followed by high-performance liquid chromatography, Food Chem. 174 (2015) 446-451.

[3] J. Ryczkowski, Application of IR spectroscopy for N_2O determination, Polish journal of environmental studies, Applied Catalysis A: General. 106 (1993) N3-N4.

[4] X. Li, Z. Lin, C. Luo, J. Bai, Y. Sun, Y. Li, Enhanced microbial degradation of pentachlorophenol from soil in the presence of earthworms: Evidence of functional bacteria using DNA-stable isotope probing, Soil Biol. Biochem. 81 (2015) 168-177.

[5] World Health Organization (WHO). *Pentachlorophenol*; Environmental Health Criteria 71; World Health Organization, International Programme on Chemical Safety: Geneva, Swizerland, 1987.

[6] L. Keith, W. Telliard, ES&T special report: priority pollutants: (I) a perspective view, Environ. Sci. Technol. 13 (1979) 416-423.

[7] A. Di Corcia, C. Crescenzi, E. Guerriero, R. Samperi, Ultratrace determination of atrazine and its six major degradation products in water by solid-phase extraction and liquid chromatography-electrospray/mass spectrometry, Environmental Science and Technology. 31 (1997) 1658-1663.

[8] R. Koeber, C. Fleischer, F. Lanza, K.-. Boos, B. Sellergren, D. Barcelót, Evaluation of a multidimensional solid-phase extraction platform for highly selective on-line cleanup and high-throughput LC-MS analysis of triazines in river water samples using molecularly imprinted polymers, Anal. Chem. 73 (2001) 2437-2444.

[9] S. Rodriguez-Mozaz, M.J. López De Alda, D. Barceló, Monitoring of estrogens, pesticides and bisphenol A in natural waters and drinking water treatment plants by solid-phase extraction-liquid chromatography-mass spectrometry, Journal of Chromatography A. 1045 (2004) 85-92.

[10] R. Jeannot, H. Sabik, E. Sauvard, E. Genin, Application of liquid chromatography with mass spectrometry combined with photodiode array detection and tandem mass spectrometry for monitoring pesticides in surface waters, Journal of Chromatography A. 879 (2000) 51-71.

[11] G. Gervais, S. Brosillon, A. Laplanche, C. Helen, Ultra-pressure liquid chromatography-electrospray tandem mass spectrometry for multiresidue determination of pesticides in water, Journal of Chromatography A. 1202 (2008) 163-172.

[12] T. Dagnac, S. Bristeau, R. Jeannot, C. Mouvet, N. Baran, Determination of chloroacetanilides, triazines and phenylureas and some of their metabolites in soils by pressurised liquid extraction, GC-MS/MS, LC-MS and LC-MS/MS, Journal of Chromatography A. 1067 (2005) 225-233.

[13] J.D. Wright, J.V. Oliver, R.J.M. Nolte, S.J. Holder, N.A.J.M. Sommerdijk, P.I. Nikitin, The detection of phenols in water using a surface plasmon resonance system with specific receptors, Sensors and Actuators, B: Chemical. 51 (1998) 305-310.

[14] T. Basova, A. Hassan, F. Yuksel, A.G. Gürek, V. Ahsen, Optical detection of pentachlorophenol in water using thin films of octa-tosylamido substituted zinc phthalocyanine, Sensors & Actuators: B.Chemical. 150 (2010) 523-528.

[15] H. Arwin, M. Poksinski, K. Johansen, Total internal reflection ellipsometry: Principles and applications, Appl. Opt. 43 (2004) 3028-3036.

[16] P. Westphal, A. Bornmann, Biomolecular detection by surface plasmon enhanced ellipsometry, Sensors and Actuators, B: Chemical. 84 (2002) 278-282.

[17] B. Lassen, M. Malmsten, Competitive protein adsorption studied with TIRF and ellipsometry, J. Colloid Interface Sci. 179 (1996) 470-477.

[18] A.V. Nabok, A. Tsargorodskaya, A.K. Hassan, N.F. Starodub, Total internal reflection ellipsometry and SPR detection of low molecular weight environmental toxins, Appl. Surf. Sci. 246 (2005) 381-386.

[19] A. Hassan, T. Basova, F. Yuksel, G. Gümüş, A.G. Gürek, V. Ahsen, Study of the interaction between simazine and metal-substituted phthalocyanines using spectral methods, Sensors and Actuators, B: Chemical. (2012).

[20] Sigma Aldrich, www.sigmaaldrich.co.uk. 2015.

[21] T. Basova, A. Tsargorodskaya, A. Nabok, A.K. Hassan, A.G. Gurek, G. Gumus, V. Ahsen, Investigation of gas-sensing properties of copper phthalocyanine films, Materials Science and Engineering C. 29 (2009) 814-818.

[22] H. Banimuslem, A. Hassan, T. Basova, I. Yushina, M. Durmuş, S. Tuncel, A.A. Esenpınar, A.G. Gürek, V. Ahsen, Copper phthalocyanine functionalized single-walled carbon nanotubes: thin film deposition and sensing properties, Key Eng Mat. 605 (2014) 461-464.

[23] H. Banimuslem, A. Hassan, T. Basova, A.D. Gülmez, S. Tuncel, M. Durmus, A.G. Gürek, V. Ahsen, Copper phthalocyanine/single walled carbon nanotubes hybrid thin films for pentachlorophenol detection, Sensors and Actuators, B: Chemical. 190 (2014) 990-998.

[24] M. Salam, Effect of oxidation treatment of multi-walled carbon nanotubes on the adsorption of pentachlorophenol from aqueous solution: Kinetics study, Arabian Journal of Chemistry. 5 (2012) 291-296.

[25] A. Hassan, T. Basova, S. Tuncel, F. Yuksel, A.G. Gürek, V. Ahsen, Phthalocyanine films as active layers of optical sensors for pentachlorophenol and simazine detection, Procedia Engineering. 25 (2011) 272-275.

[26] P.E. Diaz-Flores, R. Leyva-Ramos, R.M. Guerrero-Coronado, J. Mendoza-Barron, Adsorption of pentachlorophenol from aqueous solution onto activated carbon fiber, Industrial and Engineering Chemistry Research. 45 (2006) 330-336.

[27] H. Martens, Multivariate Calibration, John Wiley & Sons, 1989.

[28] J. Li, Y. Lu, Q. Ye, M. Cinke, J. Han, M. Meyyappan, Carbon nanotube sensors for gas and organic vapor detection, Nano letters. 3 (2003) 929-933.

[29] A.K. Diallo, J. Tardy, Z.Q. Zhang, F. Bessueille, N. Jaffrezic-Renault, M. Lemiti, Trimethylamine biosensor based on pentacene enzymatic organic field effect transistor, Appl. Phys. Lett. 94 (2009) 263302

[30] Y. Sun, J. Liu, G. Frye-Mason, S.-. Ja, A.K. Thompson, X. Fan, Optofluidic ring resonator sensors for rapid DNT vapor detection, Analyst. 134 (2009) 1386-1391.

[31] B. Geng, F. Zhan, H. Jiang, Z. Xing, C. Fang, Facile production of self-assembly hierarchical dumbbell-like COOH nanostructures and their room-temperature CO-gas-sensing properties, Crystal Growth and Design. 8 (2008) 3497-3500.

[32] R. Saini, A. Mahajan, R.K. Bedi, D.K. Aswal, Room temperature detection of amine vapours using copper phthalocyanine based thin films, Physica Status Solidi (A) Applications and Materials Science. 209 (2012) 1245-1250.

[33] M.L. Rodríguez-Méndez, M. Gay, C. Apetrei, J.A. De Saja, Biogenic amines and fish freshness assessment using a multisensor system based on voltammetric electrodes. Comparison between CPE and screen-printed electrodes, Electrochim. Acta. 54 (2009) 7033-7041.

[34] R. De Saja, J. Souto, M.L. Rodríguez-Méndez, J.A. De Saja, Array of lutetium bisphthalocyanine sensors for the detection of trimethylamine, Materials Science and Engineering C. 8-9 (1999) 565-568.

[35] A. Önal, A review: Current analytical methods for the determination of biogenic amines in foods, Food Chem. 103 (2007) 1475-1486.

[36] K.I. Oberg, R. Hodyss, J.L. Beauchamp, Simple optical sensor for amine vapors based on dyed silica microspheres, Sensors and Actuators, B: Chemical. 115 (2006) 79-85.

[37] B.R. Takulapalli, G.M. Laws, P.A. Liddell, J. Andréasson, Z. Erno, D. Gust, T.J. Thornton, Electrical detection of amine ligation to a metalloporphyrin via a hybrid SOI-MOSFET, J. Am. Chem. Soc. 130 (2008) 2226-2233.

[38] S. Brittle, T.H. Richardson, A.D.F. Dunbar, S. Turega, C.A. Hunter, Alkylamine sensing using langmuir-blodgett films of n-alkyl-N-phenylamide- substituted zinc porphyrins, J Phys Chem B. 112 (2008) 11278-11283.

[39] S. Lee, N. Takahara, S. Korposh, D. Yang, K. Toko, T. Kunltake, Nanoassembled thin film gas sensors. III. sensitive detection of amine odors using TiO2/ poly(acrylic acid) ultrathin film quartz crystal microbalance sensors, Anal. Chem. 82 (2010) 2228-2236.

[40] G. Giancane, L. Valli, State of art in porphyrin Langmuir-Blodgett films as chemical sensors, Adv. Colloid Interface Sci. 171-172 (2012) 17-35.

[41] J. Roales, J.M. Pedrosa, M.G. Guillén, T. Lopes-Costa, S.M.A. Pinto, M.J.F. Calvete, M.M. Pereira, Optical detection of amine vapors using ZnTriad porphyrin thin films, Sensors and Actuators, B: Chemical. 210 (2015) 28-35.

[42] P.S. Na, H. Kim, H. So, K.. Kong, H. Chang, B.H. Ryu, Y. Choi, J. Lee, B. Kim, J. Kim, J. Kim, Investigation of the humidity effect on the electrical properties of single-walled carbon nanotube transistors, Appl. Phys. Lett. 87 (2005).

[43] D. Sung, S. Hong, Y. Kim, N. Park, S. Kim, S.L. Maeng, K.. Kim, Ab initio study of the effect of water adsorption on the carbon nanotube field-effect transistor, Appl. Phys. Lett. 89 (2006).

[44] L. Liu, X. Ye, K. Wu, R. Han, Z. Zhou, T. Cui, Humidity sensitivity of multi-walled carbon nanotube networks deposited by dielectrophoresis, Sensors. 9 (2009) 1714-1721.

[45] J. Adjizian, R. Leghrib, A.A. Koos, I. Suarez-Martinez, A. Crossley, P. Wagner, N. Grobert, E. Llobet, C.P. Ewels, Boron- and nitrogen-doped multi-wall carbon nanotubes for gas detection, Carbon. 66 (2014) 662-673.

[46] C. J. Liu, W. Lu, Optical amine sensor based on metallophthalocyanine, J Chin Inst Chem Eng. 38 (2007) 483-488.

[47] N.D. Boscher, T. Bohn, P. Heier, F. Moisy, B. Untereiner, K. Heinze, P. Choquet, Optical sensing responses of CrIIICl(TPP)(H2O)-based coatings obtained by an atmospheric pressure plasma method – Application to the detection of volatile amines, Sensors Actuators B: Chem. 191 (2014) 553-560.

[48] M. Harbeck, C. Tasaltin, I. Gürol, E. Musluolu, V. Ahsen, Z.Z. Öztürk, Preferential sorption of polar compounds by fluoroalkyloxy substituted phthalocyanines for the use in sorption based gas sensors, Sensors and Actuators, B: Chemical. 150 (2010) 616-624.

[49] J.M. Charlesworth, C.A. McDonald, A fibre-optic fluorescing sensor for amine vapours, Sensors and Actuators: B.Chemical. 8 (1992) 137-142.

Chapter 7

Distribution of Single-Walled Carbon Nanotubes in Pyrene Containing Liquid Crystalline Zinc Phthalocyanine Matrix: Formation and Sensor Properties

Chapter overview

Composites of single walled carbon nanotubes (SWCNT) with a discotic zinc phthalocyanines and the distribution of SWCNT in the ordered matrix of hexagonal columnar mesophase of these derivatives is studied using Raman spectroscopy, UV-Vis. Absorption and Fluorescence microscopy, X-ray diffraction, Scanning electron microscopy and Transmission electron microscopy. Conductometric gas sensor devices have been synthesized based on the prepared composite. The fabricated devices have then been examined to detect ammonia gas in the concentration range 1 to 200ppm.

7.1 Introduction

This chapter is devoted to study the distribution of SWCNT in liquid crystalline asymmetrically (**Pc6**) and symmetrically (**Pc7**) substituted zinc phthalocyanine (ZnPc) bearing one pyrene and six polyoxy groups as side chains (Figure 7.1). Full details of the synthesis and chemical characterisation of 2,3,9,10,16,17-Hexakis (4,7,10-trioxaundecan-1-sulfanyl)-23(24)-(1-pyrenylmethoxy) phthalocyaninato zinc (asymmetic **Pc6** and symmetric **Pc7**) are found in the published work of Tuncel *et al.* and Kaya *et al.* [1,2]. The effects of nanotubes on the crystalline phase behaviour of this phthalocyanine derivative and on the structural and functional properties of the SWCNT-phthalocyanine composite thin films are investigated. The polyoxy groups are chosen to exhibit the liquid crystalline properties of this material. The pyrene group is also chosen to enhance the interaction of phthalocyanine with the SWCNT. The pyrenyl group is known to interact strongly with SWCNT via π-stacking interactions [3-5]. This has been used, for example, in the production of SWCNT-nanoparticle hybrids, the grafting of proteins and other biomolecules to SWCNT [3] and to immobilize light harvesting groups on the SWCNT, as well as in the design of new photoelectric devices [5]. To demonstrate the potential applications of the SWCNT-ZnPc hybrids towards gas sensing, a conductometric gas sensor device based on the hybrid material has been fabricated. A comparative analysis of sensor response of pristine SWCNT and SWCNT-ZnPc hybrid films to ammonia vapour (1-200 ppm) was carried out to demonstrate the synergetic effect between SWCNTs and ZnPc derivatives. Influence of pyrene group on the phthalocyanine ring on the hybrids formation and their sensor response is discussed. As ammonia is a low boiling point compound and volatile, it is very important to develop sensitive sensors to detect the gaseous NH_3 molecules. Chemical sensing application of SWCNTs for the detection of NO_2 and NH_3 gases was first reported by Kong et al [6]. Other studies have revealed that semiconducting SWCNTs could detect small concentrations of NH_3 and NO_2 with high sensitivity at room temperature [7].

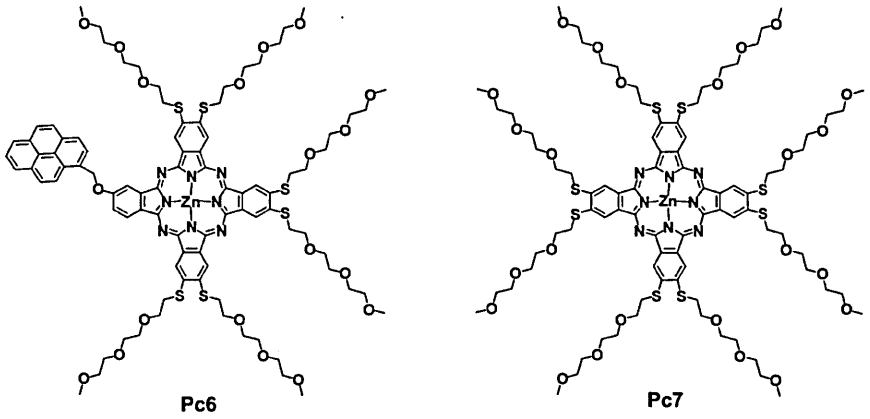

Figure 7.1: Asymmetrical (**Pc6**) and symmetrical (**Pc7**) zinc phthalocyanine derivatives

7.2 Experimental

7.2.1 Preparation of SWCNT-zinc phthalocyanine hybrids

5 mg of zinc phthalocyanines (**Pc6** or **Pc7**) have been dissolved in 1 mL DMF and sonicated for 15 minutes. At the same time 1.0 mg SWCNTs was suspended in 3 mL DMF and sonicated for 30 minutes. After sonication the suspension was stirred and the solution of **Pc6** or **Pc7** was added drop wise to the SWCNTs suspension during stirring to obtain the hybrids **SWCNT-Pc6** and **SWCNT-Pc7**, respectively. Addition of zinc phthalocyanine solution was stopped when the green phthalocyanine solution ceased to become colorless due to phthalocyanine adsorption to the SWCNT. The stirring was continued for another 1 hour before the mixture was centrifuged. The obtained solid washed with DMF several times, centrifuged again and finally dried in vacuum.

7.2.2 Sensor properties study

The sensing performance was studied at the relative humidity of 50%RH against low-concentration of NH_3 (1-200 ppm) diluted in air. Pure commercial NH_3 gas was used as the NH_3 source. Air was used as the diluent gas, and NH_3 was diluted by a syringe static volumetric method. Diluted NH_3 was injected into the container by a

microsyringe. In order to degas the test chamber, heating was immediately applied at 80 °C after turning off the NH_3 gas.

Thin films of hybrids **SWCNT-Pc6** and **SWCNT-Pc7** were deposited by drop-casting their solutions in DMF (0.5 mg/mL) onto interdigitated electrodes, which were used to examine the hybrid films' DC electrical conductivity. The electrical resistance of the sensors was measured with Keithley 236 by applying a constant dc voltage (3V). The response and recovery times of the films were defined as the times needed to reach 80% of the final or baseline resistance, respectively.

7.3 Characterisation of SWCNT-ZnPc (Pc6 and Pc7) complexes

7.3.1 Raman spectra

The non-covalent attachment of phthalocyanine molecules to SWCNT can be confirmed by Raman spectroscopy. Raman spectra for pristine SWCNT and both hybrids (**SWCNT-Pc6** and **SWCNT-Pc7**) are shown in Figure 7.2. The radial breathing modes (RBM), disorder (D) mode and tangential/graphite mode (G-band) are monitored as indicators of functionalisation with phthalocyanines [8]. The spectra were normalized to the tangential G band at ~1590 cm^{-1}. Both spectra of pristine SWCNT before and after hybridization contained the following characteristic peaks: the D band located at about 1340 cm^{-1} (disorder mode), which is due to breathing modes of sp^2 atoms [9-11] and the G band centred at 1590 cm^{-1} (tangential mode), due to bond stretching of all pairs of sp^2 atoms [12].

In Figure 7.2 (region III), which is an enlarged part of the spectrum from 400 to 1350 cm^{-1}, we can see that the characteristic vibrations of phthalocyanine macrocycle [1] have been affected noticeably by interaction with SWCNT. Comparing SWCNT and hybrid spectra, only little variation of the ratio of the D band to the G band (I_D/I_G) can be observed, which suggests that ZnPc derivatives are associated with the surface of SWCNT through a non-covalent modification. Moreover, the multiple peaks observed in the radial breathing mode (RBM) of SWCNT in the range 158-304 cm^{-1} (Figure 7.2 (region II)) could be ascribed to a distribution of diameters in the SWCNT samples [13,14]. They correspond to nanotube diameters in the range from 0.7 to 1.4 nm. The Raman spectra of the noncovalently functionalized SWCNT-**Pc6** and

SWCNT-**Pc7** revealed significant shift on the peak positions located in the range 158-225 cm^{-1}. For example, the RBMs at 158, 179, 200, 225 cm^{-1} of SWCNT have shifted to 165, 187, 205, 229 cm^{-1} and to 166, 189, 207, 232 cm^{-1} after the adsorption of **Pc7** and **Pc6**, respectively. It was shown that the radial breathing modes of the Raman spectrum are sensitive to the adsorption coating of the nanotubes with polynuclear aromatic hydrocarbon molecules [15].

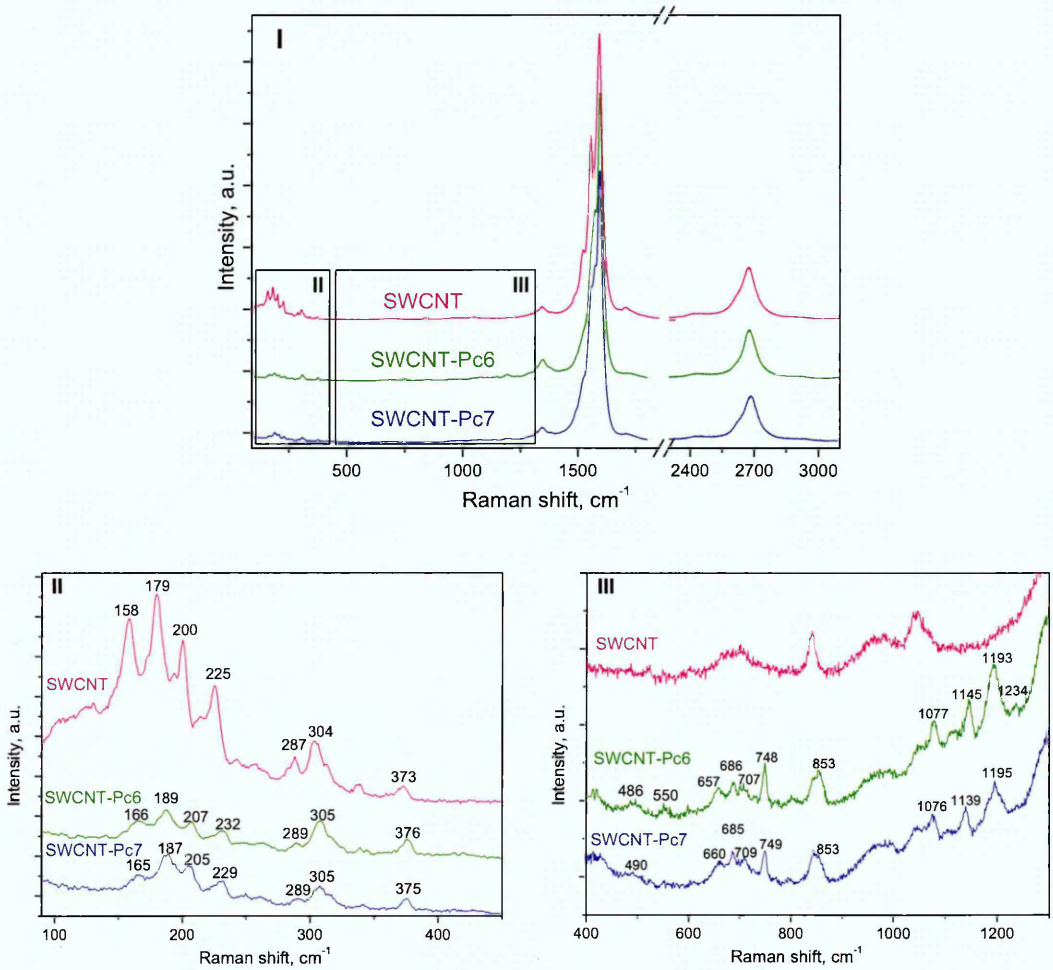

Figure 7.2: Raman spectra of pristine SWCNT, hybrids SWCNT-**Pc6** and SWCNT-**Pc7** in the range 90-3200 cm^{-1} (I), in the range of radial breathing modes 90-450 cm^{-1} (II), in the range of phthalocyanine vibrations 400-1300 cm^{-1} (III)

The π-π stacking interaction between SWCNT and phthalocyanine aromatic rings induced a higher frequency shift of RBM and gave a kind of mode "hardening effect" [16]. In particular, the higher frequency shift indicates that SWCNT becomes stiffer after coating with aromatic ring. Adsorption of **Pc6** containing an additional pyrene group is shown to induce a more remarkable shift in comparison with **Pc7** because of the better ZnPc molecule-SWCNT interaction.

7.3.2 Optical absorption and fluorescence emission spectra

The optical absorption and fluorescence emission spectra of the zinc phthalocyanines (**Pc6** and **Pc7**) solutions in DMF are shown in Figure 7.3 and 7.4 respectively. The absorption spectrum of **Pc7** in DMF consists of a Soret band at 372 nm and Q-band at 704 nm. Introduction of one pyrene moiety leads to a small shift of the Soret band to 371 nm and Q-band to 698 nm. The fluorescence emission peaks (excitation wavelength is 650 nm) were observed at 719 nm for **Pc6** and 721 nm for **Pc7** in DMF. Because of the pyrene substitution, **Pc6** showed higher emission intensity than **Pc7** as it can be seen in Figure 7.4.

The formation of the SWCNT-ZnPc hybrids can also be confirmed by the fluorescence measurements. The addition of sonicated SWCNT solution to a solution containing either **Pc6** or **Pc7** in DMF quenched the emission of both macrocycles as shown in Figures 7.5 and 7.6 respectively. However, the fluorescence intensity of **Pc6** was found to be more quenched than **Pc7** suggesting that pyrene substituted ZnPc (**Pc6**) has interacted with SWCNT more efficiently than **Pc7**.

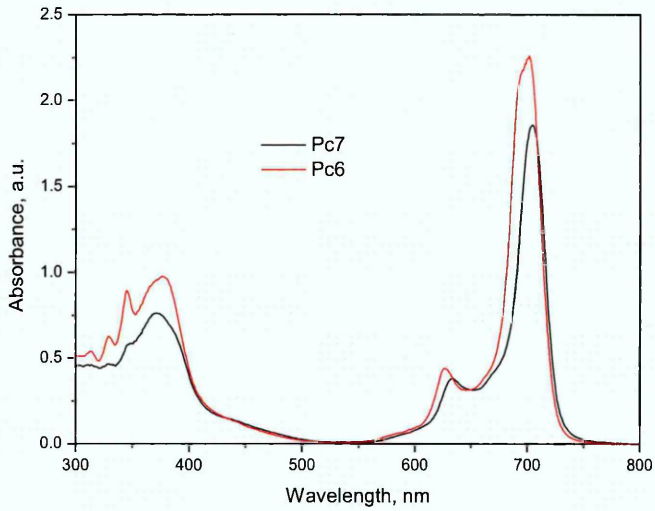

Figure 7.3: UV-vis optical absorption spectra of **Pc6** and **Pc7** in DMF

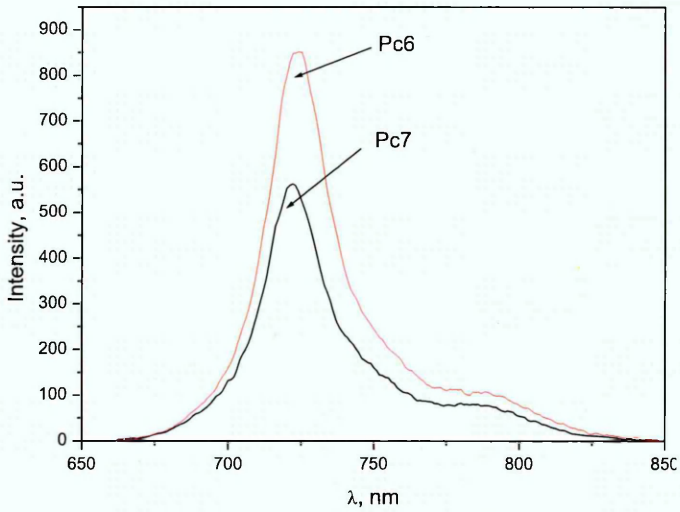

Figure 7.4: Fluorescence emission spectra of **Pc6** (λ_{em}=719) and **Pc7** (λ_{em}=721) in DMF (C=1×10^{-5} M). Excitation wavelength=650 nm

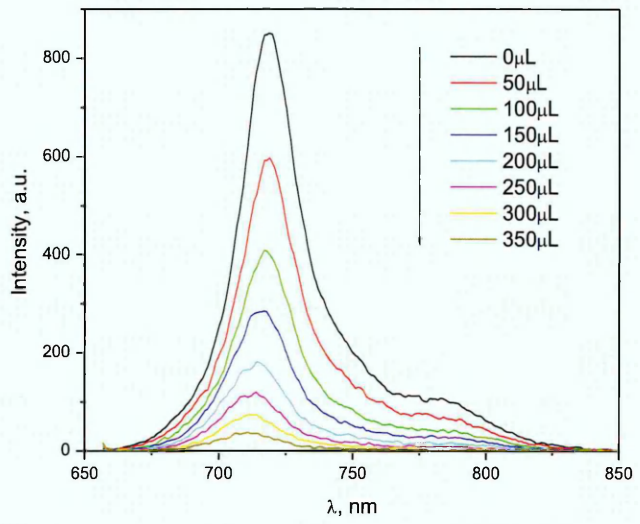

Figure 7.5: Fluorescence emission changes of **Pc6** observed during the titration of SWCNT (0-350μl) in DMF (C=1×10^{-5} M). Excitation wavelength=650 nm

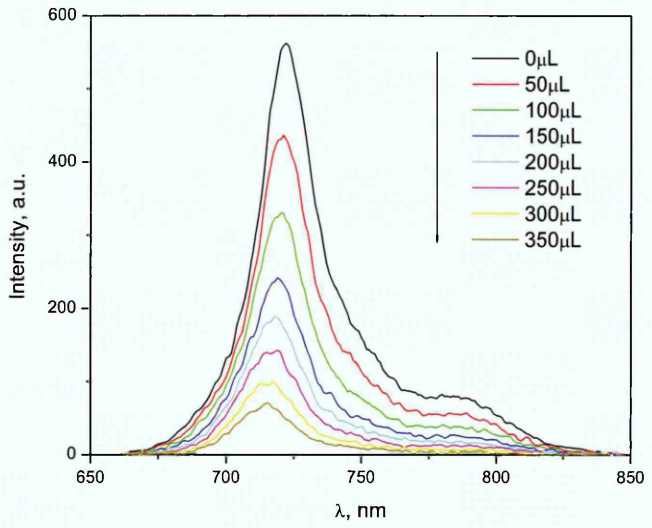

Figure 7.6: Fluorescence emission changes of **Pc7** observed during the titration of SWCNT (0-350μl) in DMF (C=1×10^{-5} M). Excitation wavelength=650 nm

7.3.3 X-Ray diffraction

The identification of mesophases was carried out by X-ray diffraction (XRD) measurements at room temperature. Dichloromethane solution of **Pc6** and **Pc7** were dropped onto glass slides and left the solvent to evaporate at room temperature. The powder diffraction patterns of **Pc6** and **Pc7** contain typical reflections of a columnar mesophase of substituted Pcs (Figures 7.7 and 7.8, and Table 7.1). In the low angle region (2θ = 4°-6°), the phthalocyanine derivatives produce a sharp peak with either a shoulder or a small additional peak. In the literature, it has been observed that, in the case of the rectangular columnar phase, the (10) peak of the Col_r mesophase splits in the (11) and (20) reflections of the Col_r phase [17].

Additionally, it is known that the lattice constants a and b can be calculated from the following equation:

$$\frac{1}{d_h^2} k_l = h^2/a^2 + k^2/b^2 \qquad (7.1)$$

Based on this information, possible indexation of the Col_r mesophase can be proposed as in Table 7.1. These results suggest a two-dimensional rectangular lattice with disc-like molecules stacked in columns in the rectangular arrangement. Both XRD patterns of **Pc6** and **Pc7** show a Col_r phase with *p2gg* symmetry.

The X-ray diffraction patterns of hybrids at room temperature shows similar features to those of compounds **Pc6** and **Pc7** confirming the rectangular columnar mesophase of the composites as shown in Figures 7.7 and 7.8. The columnar mesophase structure is not destroyed by the inclusion of SWCNTs, however the shift of the corresponding XRD peaks is observed. The XRD patterns of the compound **Pc6** at 20 °C display the most intensive diffraction peak at 2θ = 4.52° corresponding to intercolumnar distance of 19.53 Å (Figure 7.7). This peak shifts to 4.56° (d = 19.36 Å) in the XRD pattern of SWCNT-**Pc6**. This points out that the inclusion of carbon nanotubes into the columnar matrix leads to a decrease of the intercolumnar distance.

In the case of compound **Pc7** the corresponding diffraction peak at 2θ = 4.22° (d = 20.9 Å) shifts to 2θ = 4.54° (d = 19.45 Å) upon addition of SWCNT, however addition of more amount of SWCNT leads back to an increase of the intercolumnar distance to 20.44 Å which can be associated with the formation of inhomogeneous

material as was revealed by Polarised Optical Microscopy *(see section 7.3.4)*.

The XRD patterns of SWCNT-**Pc6** hybrid also show the Col_r phase with *p2gg* symmetry, however it is obvious that the number of diffraction peaks increases after the addition of SWCNT to compound **Pc6**. This appears to be explained by the formation of domains with different orientations. As opposed to the Col_r phase with *p2gg* symmetry in the case of pristine **Pc7**, the XRD patterns of SWCNT-**Pc7** show a Col_r phase with *C2mm* symmetry (*hk: h+k=2n, h0: h=2n, 0k: k=2n* for *C2mm*; *hk:* no conditions, *h0: h=2n, 0k: k=2n* for *p2gg*).

Table 7.1: X-Ray diffraction data for compounds **Pc6** and **Pc7** and their composites at room temperature

Compound	Phase	Observed spacings (Å)	Calculated spacings (Å)	Lattice parameters(Å)	Miller indices (h k)
Pc6	Col_r	21.2744	21.2744	a= 39.07	(1 1)
		19.5346	19.5346	b= 24.80	(2 0)
		11.5901	11.8231		(1 2)
		9.8400	9.7675		(4 0)
		7.1438	7.4531		(5 1)
SWCNT-**Pc6**	Col_r	21.5296	21.5296	a= 38.73	(1 1)
		19.3624	19.3624	b= 25.90	(2 0)
		12.2971	12.2721		(1 2)
		11.0661	10.7583		(2 2)
		9.8821	9.6824		(4 0)
		7.2490	7.1722		(3 3)
		5.5144	5.5329		(7 0)
		5.3312	5.4105		(7 1)
Pc7	Col_r	23.8566	23.8566	a= 41.84	(1 1)
		20.9197	20.9197	b= 29.04	(2 0)
		13.4669	13.7052		(1 2)
		12.0379	11.9203		(2 2)
		10.3243	10.4600		(4 0)
		6.0294	5.9772		(7 0)
SWCNT-**Pc7**	Col_r	22.2990	22.2990	a= 38.90	(1 1)
		19.4491	19.4491	b= 27.21	(2 0)
		10.9620	11.1553		(2 2)
		9.8643	9.7250		(4 0)
		7.2392	7.4369		(3 3)

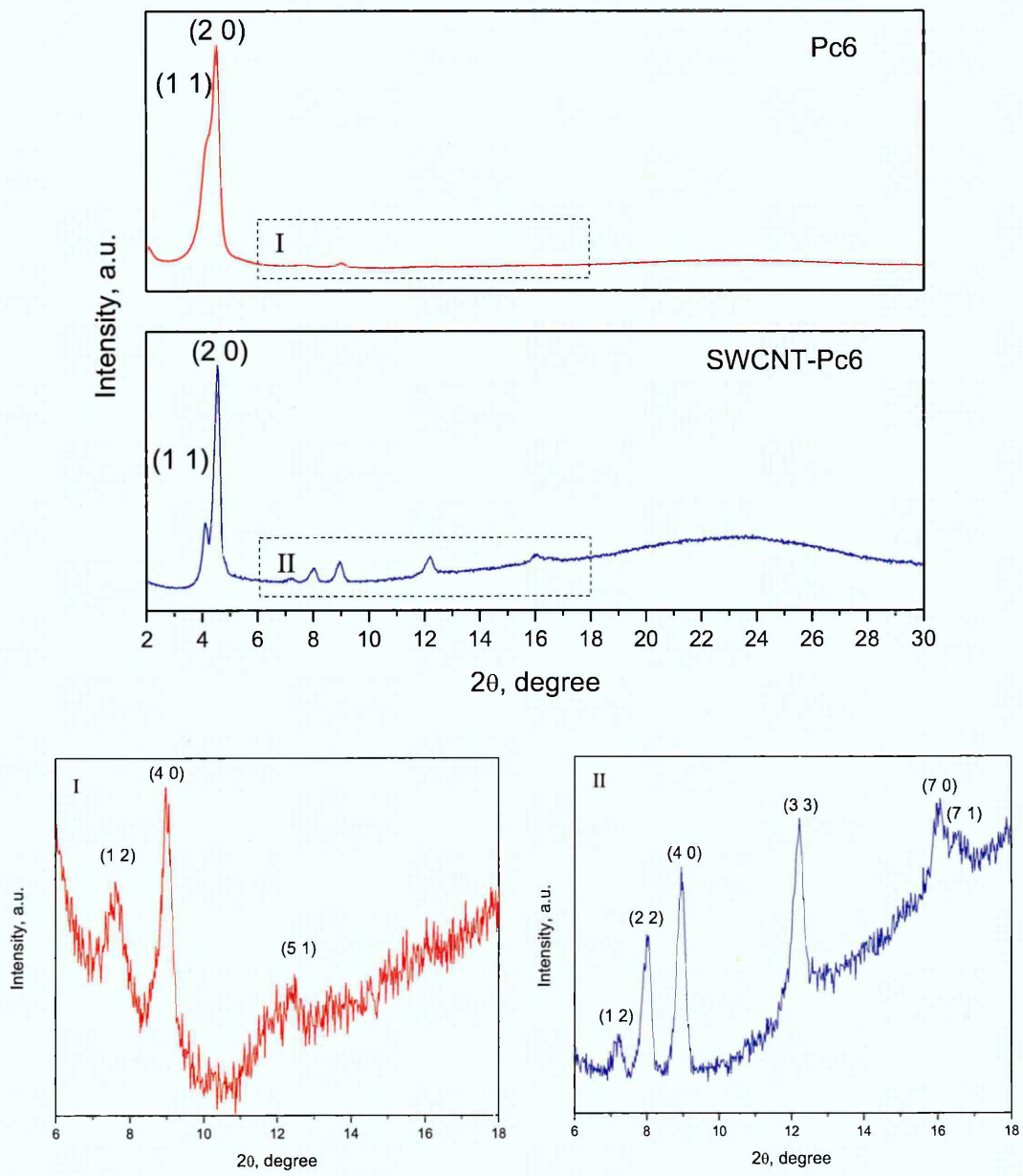

Figure 7.7: XRD patterns of **Pc6** and its hybrid at room temperature

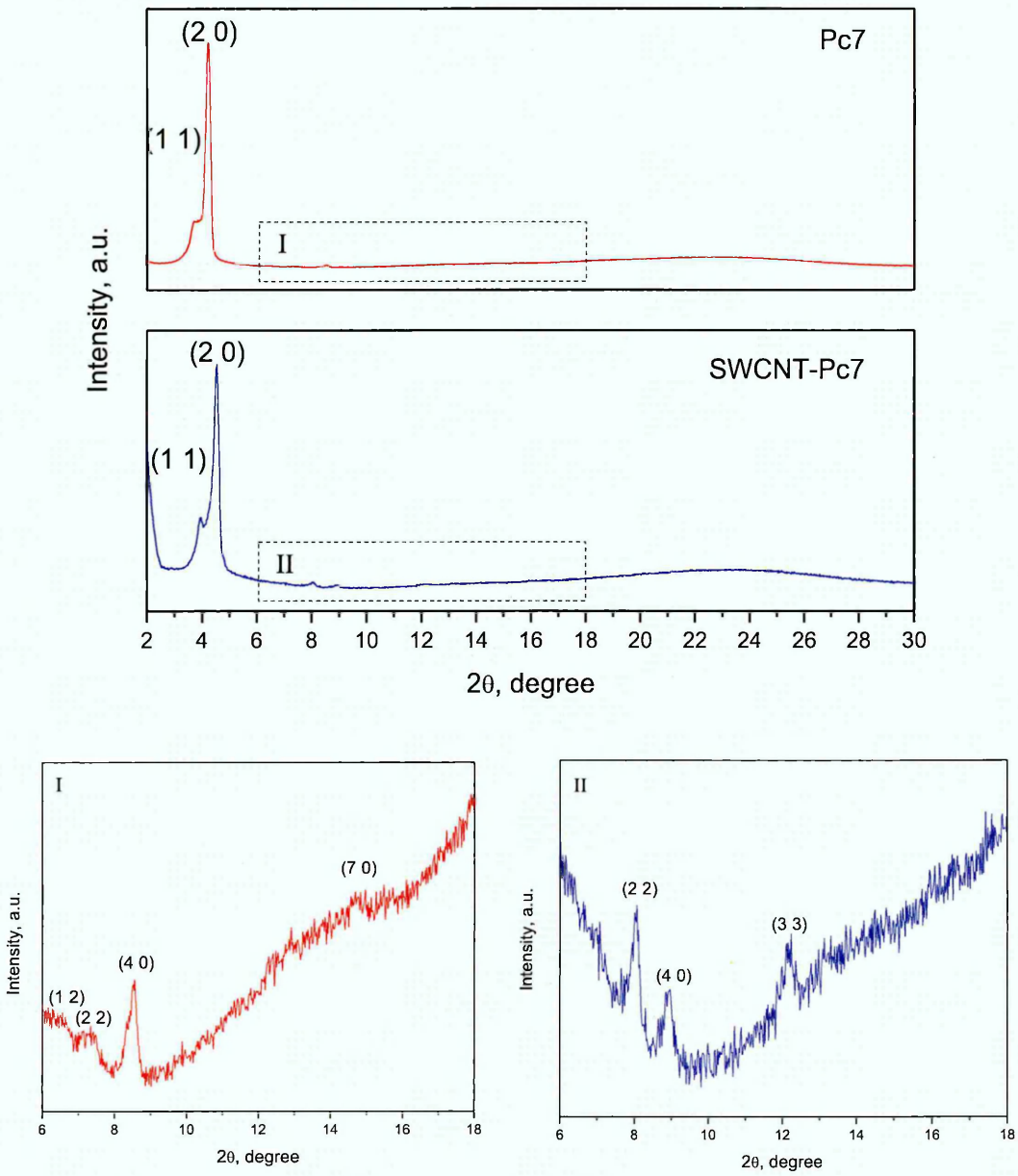

Figure 7.8: XRD patterns of **Pc7** and its hybrid at room temperature

7.3.4 Polarizing optical microscopy

Compound **Pc6** is isotropic liquid at about 230°C accompanying decomposition. When this sample was cooled from isotropic melt, typical hexagonal texture was formed at about 200 °C. This hexagonal texture remained constant until 130 °C during cooling. A fingerprint texture of rectangular phase was observed below 130 °C as can be seen in Figure 7.9 confirming the transition from hexagonal phase to rectangular phase. Similar transitions were observed in the literature [17].

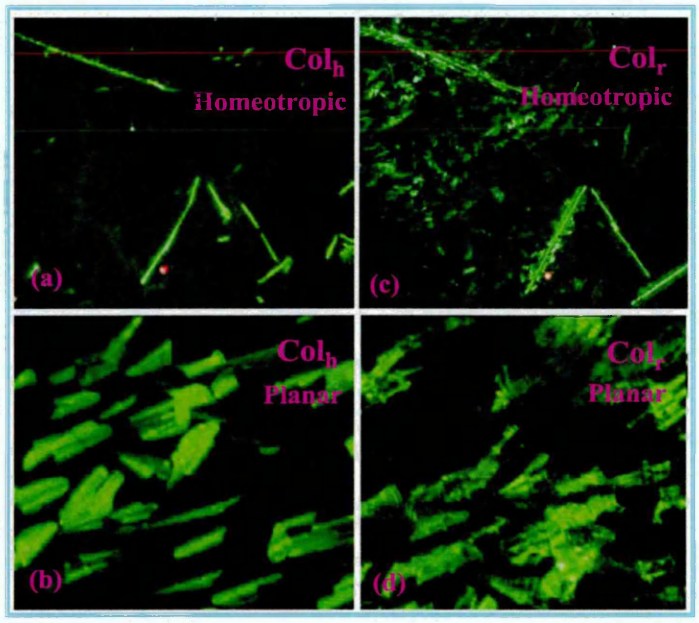

Figure 7.9: POM measurements for compound **Pc6**. (a) Homeotropic alignment in the Colh mesophase, 200°C (b) Planar alignment in the Colh mesophase, 200°C (c) Homeotropic alignment in the Colr mesophase, 25°C (d) Planar alignment in the Colr mesophase, 25°C. Magnification: 40X. Heating-cooling rate: 20°C.min^{-1}.

All SWCNT-ZnPc composites containing 1 and 2 wt.% were found to be liquid crystalline in nature. Similar to the pure ZnPcs, they show textures of columnar mesophases at room temperature (Figure 7.10). Figures 7.10a and 7.10d show typical mosaic textures of pure phthalocyanine derivatives. To the SWCNT composites (Figures 7.10 b,e), the texture is obviously different, especially in the case of

SWCNT-**Pc6** (Figures 7.10 b), from that of the pure materials. Inclusion of carbon nanotubes into the columnar matrix leads to an increase of the domains size, especially in the case of the composite SWCNT-**Pc6**. We can suggest that SWCNTs dispersed in LC matrix can act as seeds for oriented domain growth.

In the case of the composite SWCNT-**Pc6** the fan-shaped texture is still persistent whereas the star-like layered structure is clearly seen. It is necessary to mention that when we tried to insert more SWCNTs in the columnar liquid crystal we observe small black aggregates of CNTs under the polarizing microscope, which meant that the CNTs are not homogeneously dispersed in the liquid crystal matrix of the composites for such high CNT additive. In the case of the composite SWCNT-**Pc7** the formation of inhomogeneous films containing small amount of black aggregates of CNTs starts to observe already at lower percentage of SWCNTs.

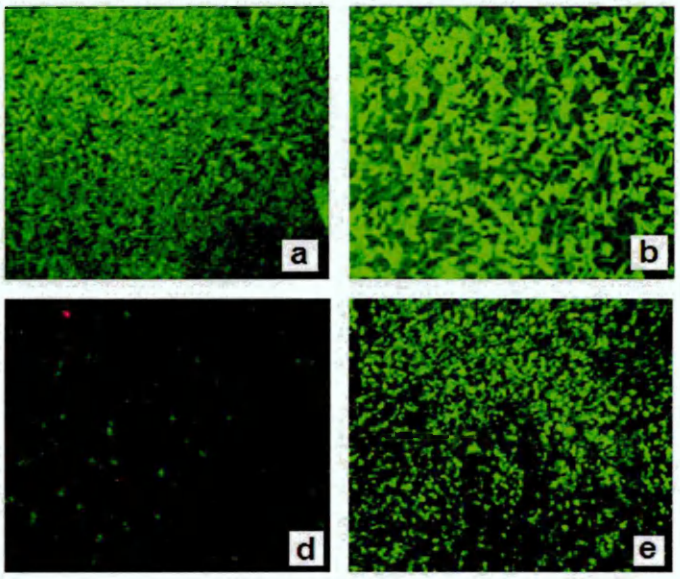

Figure 7.10: Polarizing optical microscopy images of the films of pure **Pc6** (a) and its composite (b); pure **Pc7** (d) and its composite (e), obtained under crossed polarized light

7.3.5 Microscopy characterisation

SEM images of thin films of the composites SWCNT-**Pc6** and SWCNT-**Pc7** are given in Figures 7.11 (a,b and c). The films consist of thicker nanotubes of 10-30 nm in diameter. These nanotubes appear to consist of bundles of SWCNTs wrapped by layers of LC phthalocyanine molecules. It can be suggested that the core part of phthalocyanine LC molecules anchors around the SWCNT walls, meanwhile the tail part repels sideway to enhance the π-π stacking by maximizing the hexagon–hexagon interactions between the two hybrid components. Similar scheme of interaction between porphyrin derivative $ZnP(alkyl)_4$ and the surface of semiconducting SWCNTs were visualized by performing DFT calculations [18].

In the case of SWCNT-**Pc6**, these thicker nanotubes have a tendency to lie stretched mainly in one direction in the LC matrix (Figure 7.11a), while in the SWCNT-**Pc7** they are more tangled and disordered (Figure 6.11c). The edge view of the SWCNT-**Pc6** film (Figure 7.11b) shows that the films of SWCNT-**Pc6** have layered structure with the layers align parallel to each other with the phthalocyanine molecules perpendicular to the layers according to the data of polarized Raman spectroscopy [1]. The more ordered structure of the SWCNT-**Pc6** films appears to be connected with the presence of the pyrene groups in compound **Pc6** which are known to interact strongly with SWCNTs via π-stacking interactions [3-5,19]. Meanwhile, discotic LCs derived from triphenylene have been reported to orient CNTs [20,21]. However, owing to their rather low miscibility with pristine CNTs, the use of triphenylene covalently modified CNTs was essential.

Inspecting the TEM images of pristine SWCNTs shows the presence of large aggregates of nanotubes. Figure 7.12 (a) and (b) show the TEM images of SWCNT-Pc6 and SWCNT-Pc7 hybrids, respectively. From these figures, we can observe the coverage of phthalocyanines on the sidewall of SWCNT. Furthermore the SWCNT-ZnPc nanohybrid appears to be made of bundles composed of tubes with specific rugged surface and a layer of thickness of about 1.5-2 nm immobilized onto the sidewall of SWCNT.

(a) (b)

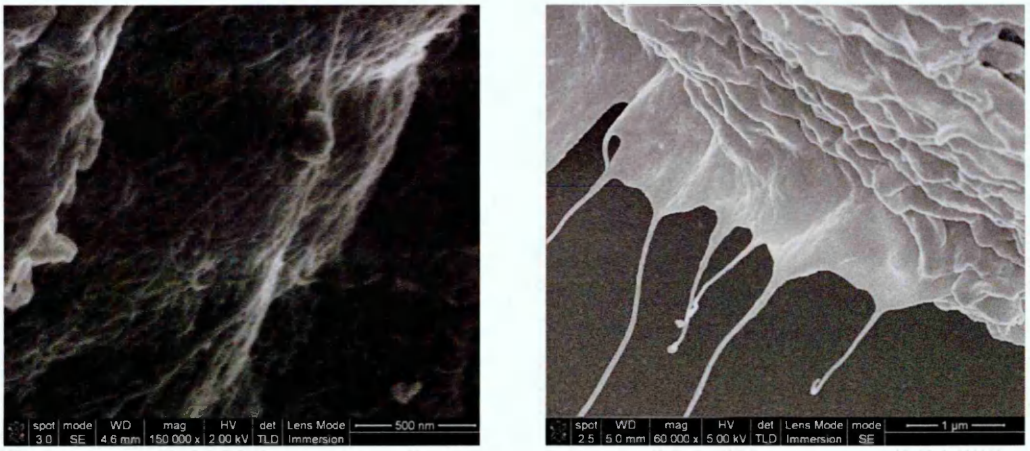

(c)

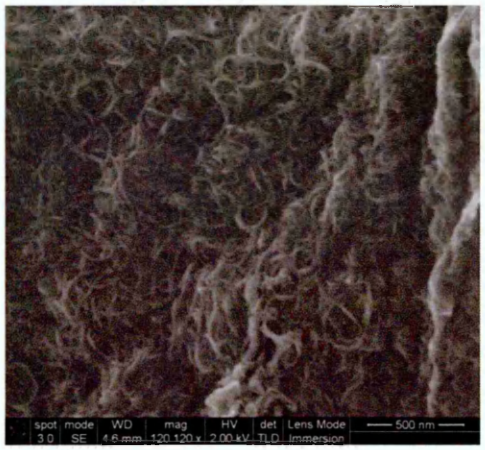

Figure 7.11: SEM images of thin films of SWCNT-**Pc6**; (a) surface view inside the film, (b) edge (at edge of the film) view and SWCNT-**Pc7**; (c) surface view

The intermolecular alkyl–π and π–π interactions and relative orientation of similar porphyrin derivative $ZnP(alkyl)_4$ on the surface of the semiconducting SWCNT were visualized by performing DFT calculations [18]. The results show that the aromatic macrocycle interacts with the surface of the nanotubes and that the alkyl chains also surround the nanotubes to some extent.

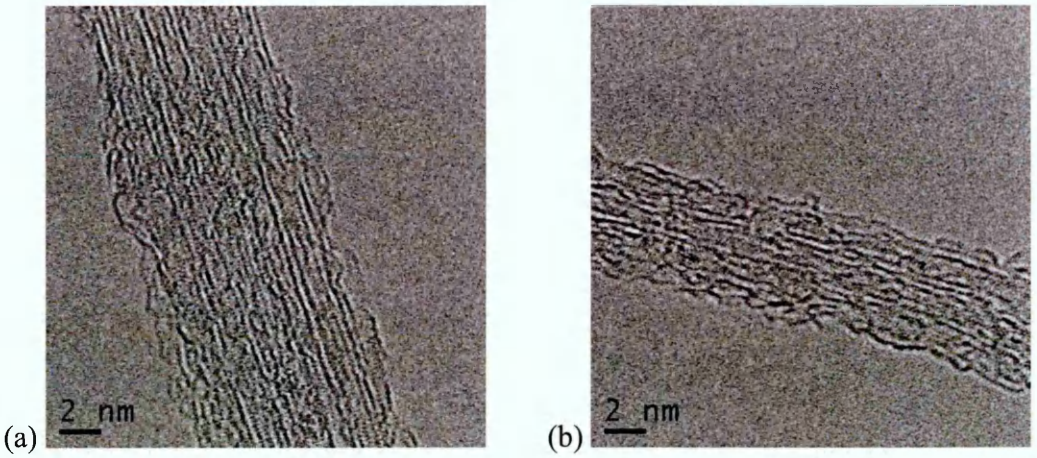

Figure 7.12: TEM images of SWCNT-**Pc6** hybrid (a) and SWCNT-**Pc7** hybrid (b)

7.4 Study of electrical and sensor properties of SWCNT-ZnPc hybrids

7.4.1 Lateral conductivity

The I(V) dependencies for the films deposited onto interdigitated electrodes were performed using Keithley 236 semiconductor characterisation system in the voltage range 0-10V. From equation 3.7, the conductivity (σ) can be defined as:

$$\sigma = \frac{L}{RHWn} \qquad (7.2)$$

where L, W, H and n are as defined in section 3.1.7, R is the film's resistance as derived from the I-V curves (Figures 7.13 and 7.14), which has been calculated from the liner fitting parameters that are shown as insets to Figures 7.13 and 7.14.

The calculated conductivities are 8.2×10^{-6}, 1.9×10^{-2}, 4.4×10^{-6} and 4.6×10^{-3} for **Pc6**, SWCNT-**Pc6**, **Pc7** and SWCNT-**Pc7** respectively. The lateral conductivity tends to increase with the presence of SWCNTs. For example, the conductivity of SWCNT-**Pc6** composite films is about 4 orders of magnitude higher than that of pure **Pc6** films. It is necessary to mention that the presence of SWCNTs leads to the formation of non-homogeneous composite films containing small particles of aggregated nanotubes. The larger electrical conductivity of the nanocomposites arises due to the highly delocalized π electron density of phthalocyanine molecules bonded to SWCNTs, which provides a facile path for electronic conduction. Increase of

conductivity in the region of 2-4 orders of magnitude in dependence on the orientations of the LC columns and SWCNTs has been observed in the case of discotic ionic liquid crystals of triphenylene derivatives bearing six imidazolium ion pendants [22].

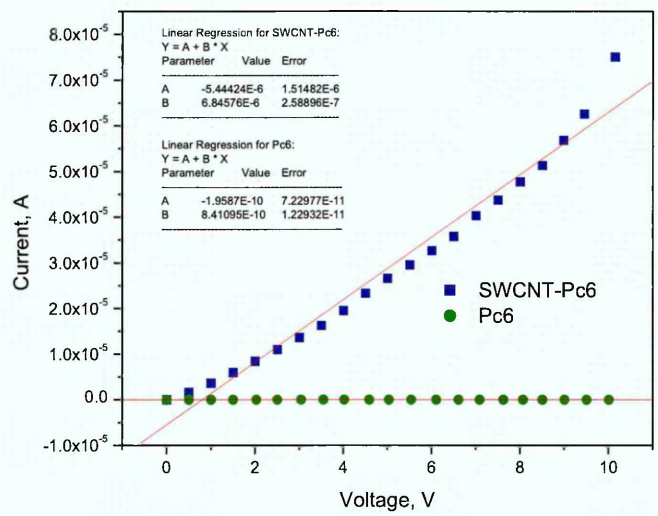

Figure 7.13: I(V) curves of **Pc6** and its hybrid with SWCNTs. The linear fitting parameters are shown as inset

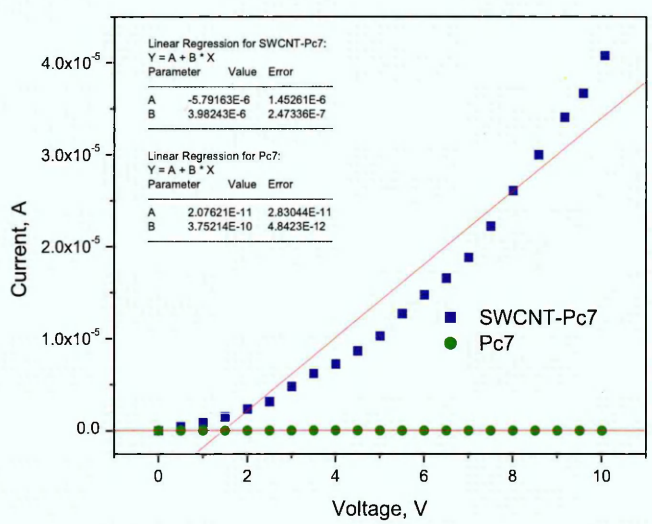

Figure 7.14: I(V) curves of **Pc7** and its hybrid with SWCNTs. The linear fitting parameters are shown as inset

7.4.2 Ammonia vapour detection

Figure 7.15 shows the normalized sensor response R ($R = (R_c - R_o)/R_o$; where R_c is the steady state resistance of the sensor at certain concentration of ammonia and R_o is the baseline resistance of the sensor) of the films of pristine SWCNT and SWCNT hybrids with **Pc6** and **Pc7** on exposure to ammonia of the concentrations 5, 20, 40, 60 and 80 ppm. In order to degas, heating was immediately applied at 80 °C after turning off the NH_3 gas. The temperature was chosen following published results in the literature, which demonstrated that the sensor resistance of SWCNT films did not return to baseline value for a long time after NH_3 was replaced by fresh air at room temperature [23,24].

The resistance of the sensor increased following 3 min exposure to NH_3; this is the result of adsorption of electron donating NH_3 molecules on pristine SWCNTs causing charge transfer between the SWCNTs and the analyte molecules. This result shows that pristine SWCNTs exhibit p-type conductivity. Similar results were observed for films of both studied hybrids.

The proposed mechanism of sensor response of the modified carbon nanotubes to ammonia and other reducing analytes has already been discussed in the literature [25,26]. Theoretical studies indicate a weak interaction between pristine SWCNTs and NH_3, with little charge transfer [27,28]. It is also known that surface charge transfer interaction occurs upon adsorption of strong electron donor molecules like ammonia [29] onto the surface of phthalocyanine derivative in hybrids leading to electron transfer from NH_3 to the phthalocyanine molecule; the formed charge transfer complexes trap holes leading to the observed increase in the resistance. Since SWCNTs/MPc conjugates can form an excellent charge transfer complexes [10,30], the charge can favourably travel from MPc to SWCNTs rapidly, resulting in a large and fast variation in the films' resistance. The combination of the useful properties of SWCNTs (namely, high conductivity and extremely high surface area), and the properties of MPc derivatives (specifically, appropriate binding sites for ammonia resulting in charge transfer complexes) provides ground for synergic effect between SWCNTs and ZnPc derivatives as active layers for sensor applications.

Both hybrids, SWCNT-**Pc6** and SWCNT-**Pc7**, exhibited an enhanced response to NH_3 compared to that of pristine SWCNT film, with the largest response observed in

the case of SWCNT-**Pc6** hybrid. The response of pristine SWCNT and SWCNT/ZnPc hybrid films towards different NH_3 concentrations is depicted in Figure 7.16. The results show that the SWCNT/ZnPc hybrids response is much higher than that of pristine SWCNTs sensor. The SWCNT-**Pc6** sensor can detect about 1 ppm of NH_3 gas, which indicates relativity higher sensitivity compared to that demonstrated by pristine SWCNTs. Meanwhile, the SWCNTs sensor can detect 10 ppm of NH_3.

Response linearity for all three films towards ammonia was observed for concentrations in range up to 100 ppm with a trend to saturate at concentrations higher than 100 ppm. The response value of SWCNT-**Pc6** film is higher than the SWCNT-**Pc7** hybrid films. This result can be explained by the presence of larger number of active sites (ZnPc and pyrene molecules) in SWCNT-**Pc6** hybrid since the derivative **Pc6** was shown to interact with SWCNTs more efficiently than **Pc7**.

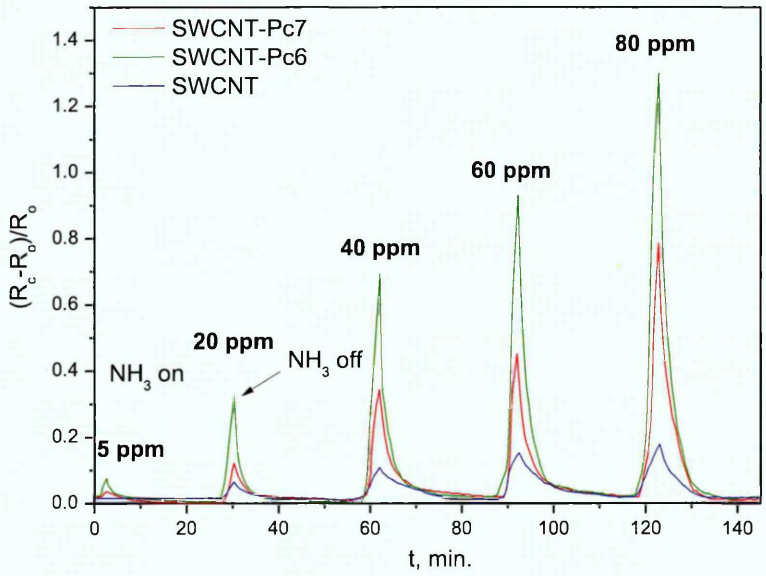

Figure 7.15: The response curve of pristine SWCNT, SWCNT-**Pc6** and SWCNT-**Pc7** films to ammonia vapour at concentrations of 5-80 ppm

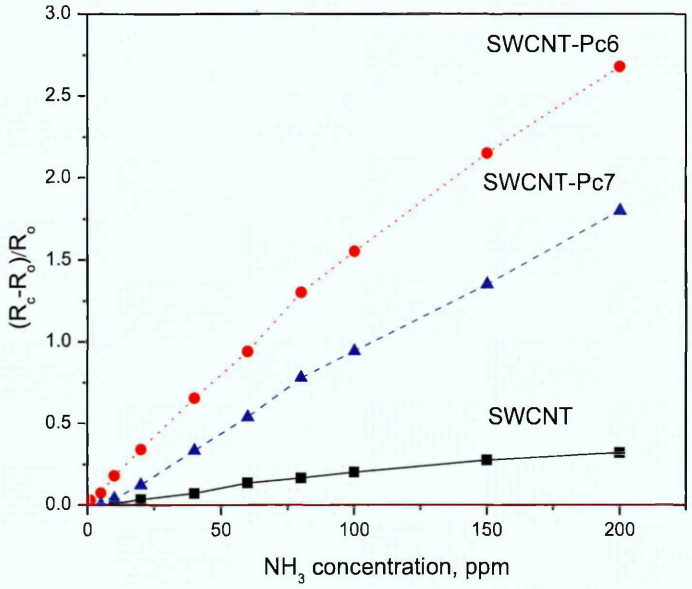

Figure 7.16: Response of pristine SWCNT, SWCNT-**Pc6** and SWCNT-**Pc7** films versus NH_3 concentration

Summary

Hybrid structures of single-walled carbon nanotubes with symmetrically octasubstituted ZnPc bearing eight polyoxy groups and asymmetrically substituted ZnPc bearing one pyrene and six polyoxy groups as side chains have been prepared and characterized by spectral methods and microscopy. Pyrene containing ZnPc has interacted with SWCNT more efficiently than zinc phthalocyanine without pyrene substituent. It has also been shown that the response of the hybrid films with pyrene containing ZnPc to the ammonia vapour is two times larger than that demonstrated by hybrid films with ZnPc without pyrene substituents.

Reference List

[1] S. Tuncel, E.N. Kaya, M. Durmuş, T. Basova, A.G. Gürek, V. Ahsen, H. Banimuslem, A. Hassan, Distribution of single-walled carbon nanotubes in pyrene containing liquid crystalline asymmetric zinc phthalocyanine matrix, Dalton Transactions. 43 (2014) 4689-4699.

[2] E.N. Kaya, S. Tuncel, T.V. Basova, H. Banimuslem, A. Hassan, A.G. Gürek, V. Ahsen, M. Durmuş, Effect of pyrene substitution on the formation and sensor properties of phthalocyanine-single walled carbon nanotube hybrids, Sensors Actuators B: Chem. 199 (2014) 277-283.

[3] L. Bogani, C. Danieli, E. Biavardi, N. Bendiab, A. Barra, E. Dalcanale, W. Wernsdorfer, A. Cornia, Single-Molecule-Magnet Carbon-Nanotube Hybrids, Angewandte Chemie. 121 (2009) 760-764.

[4] R.J. Chen, Y. Zhang, D. Wang, H. Dai, Noncovalent sidewall functionalization of single-walled carbon nanotubes for protein immobilization, J. Am. Chem. Soc. 123 (2001) 3838-3839.

[5] F. D'Souza, R. Chitta, A.S. Sandanayaka, N.K. Subbaiyan, L. D'Souza, Y. Araki, O. Ito, Supramolecular carbon nanotube-fullerene donor-acceptor hybrids for photoinduced electron transfer, J. Am. Chem. Soc. 129 (2007) 15865-15871.

[6] J. Kong, N.R. Franklin, C. Zhou, M.G. Chapline, S. Peng, K. Cho, H. Dai, Nanotube molecular wires as chemical sensors, Science. 287 (2000) 622-625.

[7] L. Valentini, I. Armentano, J. Kenny, C. Cantalini, L. Lozzi, S. Santucci, Sensors for sub-ppm NO_2 gas detection based on carbon nanotube thin films, Appl. Phys. Lett. 82 (2003) 961-963.

[8] K.A. Wepasnick, B.A. Smith, J.L. Bitter, D. Howard Fairbrother, Chemical and structural characterization of carbon nanotube surfaces, Analytical and Bioanalytical Chemistry. 396 (2010) 1003-1014.

[9] T. Mugadza, T. Nyokong, Synthesis, characterization and the electrocatalytic behaviour of nickel (II) tetraamino-phthalocyanine chemically linked to single walled carbon nanotubes, Electrochim. Acta. 55 (2010) 6049-6057.

[10] B. Ballesteros, G. De La Torre, C. Ehli, G.M.A. Rahman, F. Agulló-Rueda, D.M. Guidi, T. Torres, Single-wall carbon nanotubes bearing covalently linked phthalocyanines - Photoinduced electron transfer, J. Am. Chem. Soc. 129 (2007) 5061-5068.

[11] C. Casiraghi, A. Hartschuh, H. Qian, S. Pliscanec, C. Georgia, A. Fasoli, K.S. Novoselov, D.M. Basko, A.C. Ferrari, Raman spectroscopy of graphene edges, Nano Letters. 9 (2009) 1433-1441.

[12] C. Dyke, J. Tour, Unbundled and highly functionalized carbon nanotubes from aqueous reactions, Nano Letters. 3 (2003) 1215-1218.

[13] L. Alvarez, G. de la Fuente, A. Righi, S. Rols, E. Anglaret, J. Sauvajol, E. Munoz, W. Maser, A. Benito, M. Martinez, Diameter dependence of Raman intensities for single-wall carbon nanotubes, Physical Review B. 63 (2001).

[14] D. Huo, L. Yang, C. Hou, H. Fa, X. Luo, Y. Lu, X. Zheng, J. Yang, L. Yang, Molecular interactions of monosulfonate tetraphenylporphyrin (TPPS1) and meso-tetra(4-sulfonatophenyl)porphyrin (TPPS) with dimethyl methylphosphonate (DMMP), Spectrochimica Acta - Part A: Molecular and Biomolecular Spectroscopy. 74 (2009) 336-343.

[15] S. Gotovac, H. Honda, Y. Hattori, K. Takahashi, H. Kanoh, K. Kaneko, Effect of nanoscale curvature of single-walled carbon nanotubes on adsorption of polycyclic aromatic hydrocarbons, Nano Letters. 7 (2007) 583-587.

[16] Y. Zhang, J. Zhang, H. Son, J. Kong, Z. Liu, Substrate-induced Raman frequency variation for single-walled carbon nanotubes, J. Am. Chem. Soc. 127 (2005) 17156-17157.

[17] J. Tant, Y.H. Geerts, M. Lehmann, V. De Cupere, G. Zucchi, B.W. Laursen, T. Bjørnholm, V. Lemaur, V. Marcq, A. Burquel, Liquid crystalline metal-free phthalocyanines designed for charge and exciton transport, The Journal of Physical Chemistry B. 109 (2005) 20315-20323.

[18] F. D'Souza, S.K. Das, A.S.D. Sandanayaka, N.K. Subbaiyan, D.R. Gollapalli, M.E. Zandler, T. Wakahara, O. Ito, Photoinduced charge separation in three-layer supramolecular nanohybrids: Fullerene-porphyrin-SWCNT, Physical Chemistry Chemical Physics. 14 (2012) 2940-2950.

[19] R.O. Ogbodu, E. Antunes, T. Nyokong, Physicochemical properties of a zinc phthalocyanine-pyrene conjugate adsorbed onto single walled carbon nanotubes, Dalton Transactions. 42 (2013) 10769-10777.

[20] S. Kumar, H.K. Bisoyi, Aligned carbon nanotubes in the supramolecular order of discotic liquid crystals, Angewandte Chemie - International Edition. 46 (2007) 1501-1503.

[21] H.K. Bisoyi, S. Kumar, Carbon nanotubes in triphenylene and rufigallol-based room temperature monomeric and polymeric discotic liquid crystals, Journal of Materials Chemistry. 18 (2008) 3032-3039.

[22] J.J. Lee, A. Yamaguchi, M.A. Alam, Y. Yamamoto, T. Fukushima, K. Kato, M. Takata, N. Fujita, T. Aida, Discotic ionic liquid crystals of triphenylene as dispersants for orienting single-walled carbon nanotubes, Angewandte Chemie - International Edition. 51 (2012) 8490-8494.

[23] J. Li, Y. Lu, Q. Ye, M. Cinke, J. Han, M. Meyyappan, Carbon nanotube sensors for gas and organic vapor detection, Nano letters. 3 (2003) 929-933.

[24] K. Dong, D. Ham, B.H. Kang, K. Lee, J. Choi, J. Lee, H.H. Choi, B. Ju, Effect of plasma treatment on the gas sensor with single-walled carbon nanotube paste, Talanta. 89 (2012) 33-37.

[25] B. Wang, Y. Wu, X. Wang, Z. Chen, C. He, Copper phthalocyanine noncovalent functionalized single-walled carbon nanotube with enhanced NH_3 sensing performance, Sensors Actuators B: Chem. 190 (2014) 157-164.

[26] Y. Wang, N. Hu, Z. Zhou, D. Xu, Z. Wang, Z. Yang, H. Wei, E.S. Kong, Y. Zhang, Single-walled carbon nanotube/cobalt phthalocyanine derivative hybrid material: Preparation, characterization and its gas sensing properties, Journal of Materials Chemistry. 21 (2011) 3779-3787.

[27] C.W. Bauschlicher Jr, A. Ricca, Binding of NH_3 to graphite and to a (9, 0) carbon nanotube, Physical Review B. 70 (2004) 115409.

[28] S. Peng, K. Cho, Chemical control of nanotube electronics, Nanotechnology. 11 (2000) 57.

[29] B. Wang, X. Zhou, Y. Wu, Z. Chen, C. He, X. Zuo, Preparation, characterization and NH_3 sensing of 1, 8, 15, 22-tetra-iso-pentyloxyphthalocyanine copper, nickel and lead spin-coating films, Sensors Actuators B: Chem. 161 (2012) 498-503.

[30] W. Chidawanyika, T. Nyokong, Characterization of amine-functionalized single-walled carbon nanotube-low symmetry phthalocyanine conjugates, Carbon. 48 (2010) 2831-2838.

Chapter 8

Conclusion and Future work

8.1 Conclusion

In this work, copper phthalocyanine (CuPc) and lead phthalocyanine (PbPc) thin films have been characterized and studied for possible device applications. Hybrid structures of single walled carbon nanotubes (SWCNT) and CuPc and zinc phthalocyanine (ZnPc) were prepared as thin films and examined as a sensing element to detect different kinds of pollutants using optical and electrical detection techniques.

Octa-substituted copper(II) phthalocyanines ($CuPcR_8$), containing alkylthio-, alkyloxy-, (trioxyethylene)thio- and (trioxyethylene)oxy- substituents in peripheral positions have been investigated. It was shown that the type of substituent in the phthalocyanine molecule has a significant effect on the films' orientation and on its electrical properties. Higher surface conductivity values were found for films of phthalocyanines with the molecules oriented perpendicular to the substrate surface. The lateral conductivity tends to decrease slightly with the increase of chain length, and the higher conductivity in the alkylthio- derivatives is thought to be caused by the reduced structural disorder during phase transition which is caused by the presence of sulphur atoms in the chains.

Furthermore, Octa-substituted alkylthio- and alkoxy- lead (II) phthalocyanines ($PbPcR_8$) have also been invetigated and examined for electrical switching applications. Thin films prepared from these compounds have exhibited an increase in electronic conduction after heat treatment. Typical switching effect was also observed with high ON/OF ratios making them promising candidates for memory applications.

Hybrid structures of SWCNT and tetra-substituted copper phthalocyanine ($CuPcR_4$) have been prepared. FTIR and Raman spectra have shown that non-covalent binding between $CuPcR_4$ and SWCNTs has been significantly enhanced as a result of acid treatment of SWCNT. Using SEM and AFM measurements morphology of the films

was found to be highly dependent on the solubility of the hybrid which is determined by the method used to produce the hybrid structure. The acid-treatment of SWCNT is found to result in the separation of bundled carbon nanotubes, leading to enhanced π-π interaction formation in the SWCNT/$CuPcR_4$ system. Thin films of acid-treated SWCNT/$CuPcR_4$ hybrid exhibited much higher conductivity than $CuPcR_4$ and improved films' homogeneity has enabled the use of such hybrids as optically active sensing layers for the detection of pollutants in water utilizing Total Internal Reflection Ellipsometry technique (TIRE). The response of acid-treated SWCNT/$CuPcR_4$ hybrid films to the presence of benzo[a]pyrene in water was shown to be two times larger than that demonstrated by $CuPcR_4$ films.

Thin films of SWCT/$CuPcR_4$ with different substitutions have been prepared. The morphology and optical properties of the hybrid films were studied and the interaction between the two materials was ascribed to the π-π interaction as well as van der Waals forces. The prepared films were applied as an optical active layer to detect some pesticides in water in comparatively low concentrations, including pentachlorophenol, 2-chlorophenol, diuron and simazine using TIRE technique. Concentrations as low as 133 ng/L have been detected by spin coated active layers of SWCNT/$CuPcR_4$ hybrids with an average sensitivity of 0.00396/(μg/L). The produced films exhibited higher sensitivity for pentachlorophenol than other analytes used in this work. Hybrid films, in general, exhibited higher sensitivity and lower detection limit than pristine phthalocyanine films towards all the investigated pesticides.

In the case of gas sensing, concentrations as low as 3.6 ppm of methylamine have been detected by spun active layers of SWCNT/$CuPcR_4$ hybrids with an average sensitivity of 0.000325/ppm. The produced films exhibited higher sensitivity for methylamine than dimethylamine and trimethylamine due to the steric hindrance of secondary and tertiary amines which reduces the probability of being adsorbed by the sensor. Hybrid films, in general, show higher sensitivity, lower detection limit and shorter response time than bare phthalocyanine films towards all the investigated amines' vapours. The higher π-electron density in the carbon nanotubes is expected to result in larger number of adsorbed molecules onto the hybrid films' surfaces.

Hybrid structures of single-walled carbon nanotubes with symmetrically octasubstituted ZnPc bearing eight polyoxy groups and asymmetrically substituted ZnPc bearing one pyrene and six polyoxy groups as side chains have been prepared and characterized by spectral methods and microscopy. It was shown by the methods of Raman spectroscopy and fluorescence spectroscopy that pyrene containing ZnPc has interacted with SWCNT more efficiently than zinc phthalocyanine without pyrene substituent. To demonstrate the potential applications of the SWCNT/ZnPc hybrids towards gas sensing, a conductometric gas sensor device based on the hybrid materials has been fabricated. The comparative analysis of sensor response of pristine SWCNT and films of the SWCNT/ZnPc hybrids to ammonia vapour (1-200 ppm) was carried out to demonstrate the synergetic effect between SWCNTs and ZnPc derivatives. It has also been shown that the response of the hybrid films with pyrene containing ZnPc to the ammonia vapour is two times larger than that demonstrated by hybrid films with ZnPc without pyrene substituents.

8.2 Future work

The current investigation has focused on examining the copper derivatives of the substituted Pcs as chemical detection element. For future work however, all other metal Pcs studied here will need to be examined for similar application.

Some pesticides and amines have been investigated in this work. Further investigation will need to consider more analytes including CL_2, NO_2 and CO.

A comparative study can be performed to evaluate SWCNT/MPc hybrid layers' sensitivities towards all studied analytes using electrical-based sensing method and TIRE. Therefore, the design of a new cell for TIRE technique can be carried out to include two planar electrodes to measure the optical and electrical changes in the film caused by adsorption of analyte molecules at the same time.

This project has focused on the analysis of the studied layers sensitivity; however, less emphasis was placed on the selectivity of the films as a result of exposure to a broader range of pollutants. This could certainly be one essential objective of future studies of these hybrids.

Sensors and Actuators B 207 (2015) 224–234

Contents lists available at ScienceDirect

Sensors and Actuators B: Chemical

journal homepage: www.elsevier.com/locate/snb

-modified carbon nanotubes for the optical detection of amines ›ours☆

at Banimuslem[a,b], Aseel Hassan[a], Tamara Basova[c,d], Aliye Aslı Esenpınar[e], m Tuncel[f], Mahmut Durmuş[f,*], Ayşe Gül Gürek[f], Vefa Ahsen[f]

ials and Engineering Research Institute, Sheffield Hallam University, Sheffield S1 1WB, UK
ent of Physics, Faculty of Science, Babylon University, Babylon, Iraq
ev Institute of Inorganic Chemistry SB RAS, 3 Lavrentiev Ave., Russia
ibirsk State University, Pirogova Str. 2, Russia
eli University, Department of Chemistry, 39100 Kırklareli, Turkey
Institute of Technology, Department of Chemistry, Gebze 41400, Kocaeli, Turkey

ICLE INFO

istory:
d 11 June 2014
d in revised form 6 October 2014
d 10 October 2014
le online 23 October 2014

s:
hthalocyanine
alled Carbon Nanotubes

detection

ABSTRACT

Thin films of peripheral and non-peripheral tetra-substituted copper phthalocyanines [$CuPcR_4$, $R=-O(CH_2CH_2O)_3CH_3$ or $-S(CH_2CH_2O)_3CH_3$] and their hybrids with single walled carbon nanotubes (SWCNT) have been investigated as optical active layers for amines vapours detection. Adsorption of amines onto the films' surfaces has been realized by monitoring changes in the phase shift ($\Delta(\lambda)$) of total internal reflection ellipsometry spectra. Methylamine has shown higher sensitivity and lower response time among the studied three amines. The steric hindrance provided by the shapes of the secondary and tertiary amine molecules is thought to decrease the interaction with films' surfaces as compared to methylamine. For all active layers used in this study, the sensitivity of SWCNT/$CuPcR_4$ hybrid films was higher than the sensitivity of pristine $CuPcR_4$ films with clear recovery in the $\Delta(\lambda)$ spectra after flushing the cell with air. The lower response time at 40 ppm is found to be 66 s and the highest sensitivity is 0.000325/ppm towards methylamine vapour.

-oduction

er the past few years, there has been an increasing demand mple and effective method to detect toxic odours that are ced by organic volatile compounds due to their damaging s on biological system and environment in general [1–4]. g these hazardous gases, amine complexes are commonly n agriculture, pharmaceutical, dye manufacturing and food ssing industries [5]. In addition, amines and their derivatives nsidered as indicators of spoilage in foods because they play l role in the degradation pathways of amino acids in living isms [6]. In the case of fish and seafood, biogenic amines e ammonia, methylamine, dimethylamine, trimethylamine, cine, adaverine, dopamine, and histamine among others. ncentration of these decomposition products increases with time, therefore, the determination of freshness in fish and seafood is reliable with the quantification of these vapours [7].

Several methods used to determine chemical compounds imply measuring the variation of physical properties of an active layer induced by the adsorption of gas molecule on its surface. This active layer becomes the transducer that transforms the interaction with the environment in an optical or electrical signal. Among these methods are; high performance liquid chromatography [8–10], electrochemical sensors [11–14], electrical-based sensors [15] and optical detection methods [16]. Sensors and measurement tools based on optical phenomena have always been of special interest, mostly because they usually do not require any physical or electrical contact with the materials under investigation and therefore they are not destructive. Some techniques, such as surface plasmon resonance (SPR) [17] and UV–visible absorption spectroscopy [18] are quite well recognised, and widely used. However, some methods like total internal reflection ellipsometry (TIRE), where ellipsometry can be used in total internal reflection mode and in combination with the surface plasmon resonance phenomenon [19] are still underexploited in the sensor area. There have been a number of research studies where TIRE can be used for monitoring of thin layers on surfaces [20]. Studies in the literature

r presented at the 7th European conference on Optical Sensors and Biosen- hens, Greece, 13–16 April 2014.

esponding author. Tel.: +44 1142256904; fax: +44 114 2256930.
ail address: a.hassan@shu.ac.uk (A. Hassan).

dx.doi.org/10.1016/j.snb.2014.10.046
05/

e explored some possible applications of TIRE, which included se for the monitoring of corrosion [21] as well as its exploita- in biomolecules detection [22]. However, it still seems to be totally explored in the field of chemical vapour detection. A ailed theoretical background of TIRE technique is found in the rature [23].

range of sensitive materials has been employed to construct sensors; these include several types of transition metal oxides], conducting polymers [25] as well as organic complexes like halocyanines [7,17,26,27]. Phthalocyanines (Pcs) in general and ir metallo-derivatives (MPcs) in particular, hold a great promise the development of many non-linear optical devices because of ir activity as basis for optical limiting [28], fast response time, que electronic absorption properties and the extensively delo- sed π–π electron skeleton.

Carbon nanotubes (CNTs), on the other hand, have been found e extremely sensitive to their local chemical environment. This mical sensitivity, due to their extraordinary one-dimensional bon nanostructure, has made them ideal building blocks for mical detection [29]. CNTs have been demonstrated as promis- candidates for the detection of toxic gases such as NO_2, NH_3, H_2, CO_2, and CO [30–33]. However, the poor solubility and dis- sity of CNTs in conventional solvents has restricted their use as ive layers processed by simple methods like spin coating. Acid- tment as well as other modifications has been shown to assist vercoming the disadvantage of poor dispersity of CNTs [34–36]. other downside is that CNTs are optically inert and almost unsuitable to use as optically active layers utilising techniques h as SPR and TIRE. Further surface modification of CNTs through ridisation with MPcs enhances their optical performance as well as gas sensing activity. This arises from the mutual π interaction between CNTs and MPc resulting in more detection efficiency compared to the individual CNTs or MPcs species [37].

In this work, we report the use of single-walled carbon nanotubes (SWCNT) hybridized with tetra-substituted copper phthalocyanines $CuPcR_4$ (Fig. 1) as an optical active layer to detect methylamine, dimethylamine and trimethylamine in air using TIRE technique. The morphology and optical properties of the SWCNT/$CuPcR_4$ hybrid films are also discussed.

2. Experimental

2.1. Materials

3-nitrophthalonitrile [38], 4-nitrophthalonitrile [39], 3-(4,7,10-trioxaundecane-1-oxanonyl)phthalonitrile [40], 3-(4,7,10-trioxau ndecane-1-sulfanyl)phthalonitrile [41], 4-(4,7,10-trioxaundecane-1-oxanonyl)phthalonitrile [42], 4-(4,7,10-trioxaundecane-1-sulfa nyl)phthalonitrile [43] were synthesized and purified according to procedures described in the literatures. Dimethylformamide (DMF), n-hexanol, n-hexane, CH_2Cl_2 and tetrahydrofuran (THF) were dried as described by Perrin and Armarego [44] before use. $CuCl_2$, 1,8-diazabicyclo[5.4.0]undec-7-ene (DBU) and triethylene glycol monomethyl ether were purchased from Fluka. K_2CO_3 and neutral Al_2O_3 were purchased from Merck.

SWCNTs were commercially purchased from Sigma-Aldrich. Methylamine, dimethylamine and trimethylamine solutions in water (40%) were also obtained from Sigma–Aldrich. Air was used as the diluent gas. Small amounts of amine solutions have been transferred into 2 L glass bottle using micro syringe and were left

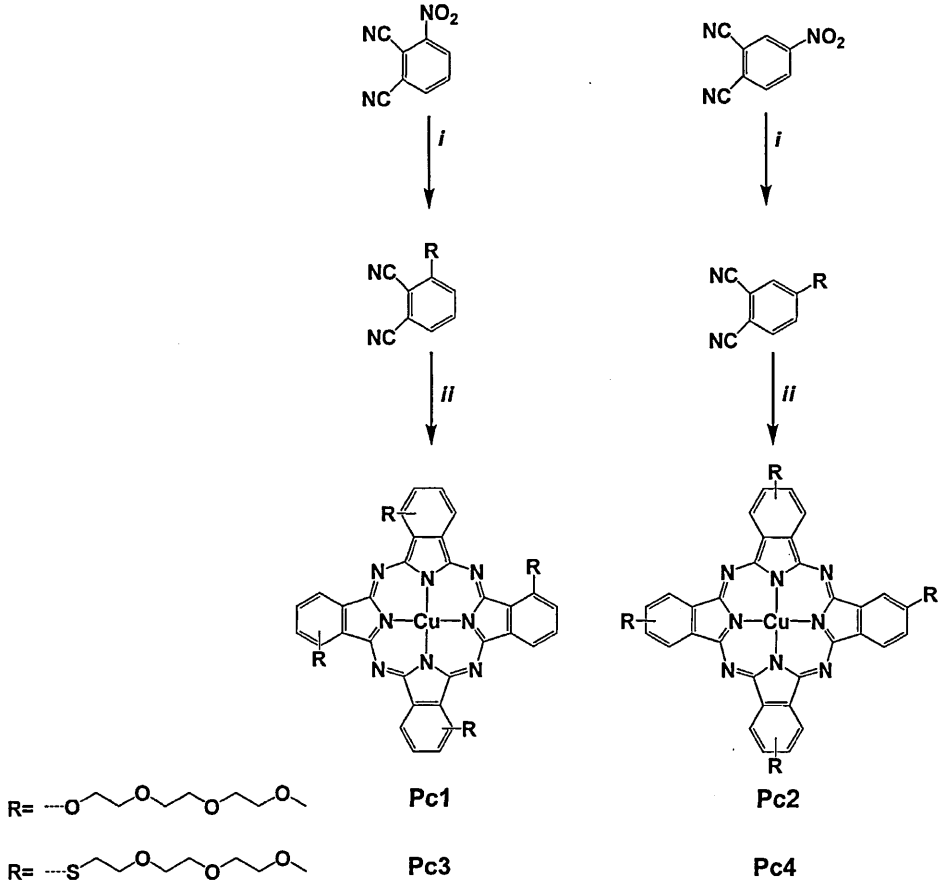

Fig. 1. Synthesis of $CuPcR_4$ derivatives. i: Corresponding ROH or RSH, anhydrous K_2CO_3, anhydrous DMF; ii: anhydrous $CuCl_2$, anhydrous n-hexanol, DBU.

orize. The vapour concentration was calculated according to lowing gas law [18]:

$$\frac{.4\rho TV_s}{73MV} \times 10^3 \quad (1)$$

c is the concentration in ppm, ρ the density of the liquid sam- /mL, T the temperature of container in Kelvin, V_s the volume liquid sample in μL, M the molecular weight of sample in , and V is the container volume in litre. The diluted gas has urther diluted in a 50 mL syringe to obtain amines concen- s of 4, 8, 20, 40, 80 and 200 ppm, which were injected into s cell, fixed on the experiment set up. Table 1 shows detailed tion of the gas concentrations of all examined amines. The ere degased by injecting fresh air into the gas cell.

easurements

pectra were recorded between 4000 and 650 cm^{-1} using a Elmer Spectrum 100 FT-IR spectrometer with an attenuated eflection (ATR) accessory, featuring a zinc selenide (ZnSe) . Optical spectra in the UV–visible region were recorded himadzu UV-Vis-2101 spectrophotometer using 1 cm path cuvette at room temperature. Matrix-assisted laser desorp- nization time-of-flight mass spectrometry (MALDI-TOF-MS) rements were performed on a Bruker Daltonics micrOTOF by ,3-dihydroxybenzoic acid as matrix. The surface morphol- the films was investigated by SEM and AFM using FEI-nova m 200 and Nanoscope IIIa multimode atomic force micro- respectively.

experimental set-up for TIRE measurements was built on V (J.A. Woollam Co., Inc.) spectroscopic ellipsometer, oper- the 350–1000 nm wavelength range. Details of TIRE method e experimental set-up are found in previous publications] The choice of the prism was dictated by conditions of total l reflection of light on the glass/air interface; the prism used case is a 45° BK7 glass prism with an index of refraction 5. The cell has a volume of 2 mL and contains inlet and out- es to allow injection of different gases or fluids into the cell r to perform different chemical interactions.

spectra of the two ellipsometric parameters Ψ and Δ, rep- ng, respectively, the amplitude ratio $tg(\Psi) = A_p/A_s$ and phase $= \varphi_p - \varphi_s$ between p- and s-components of polarised light, ecorded with the M2000 V instrument in the 350–1000 nm l range using the rotating analyzer principle. Optical param- f the reflection system, i.e. thicknesses, refractive indices and on coefficients of the substrate and adsorbed layers, can be d by solving the reverse ellipsometric problem numerically:

$$\mathrm{xp}(i\Delta) = R_p/R_s \quad (2)$$

R_p and R_s are Fresnel reflection coefficients for p- and onents of polarized light related to the parameters of reflec- stem, particularly the thickness (d) and refractive index (n) dsorbed layers, via Fresnel equations [47]. The fitting is per- by solving Fresnel equations many times for different values d d and subsequently minimizing the error function of the ental and theoretical (calculated) values of Ψ and Δ using east-square techniques. Commercial WVASE32® software is d by J.A. Woollam Co., Inc. for this task. The samples for TIRE ere prepared by the evaporation of 3–5 nm of chromium on opic glass slides followed by the evaporation of 25–30 nm layer.

thesis of $CuPcR_4$ derivatives

cR_4 derivatives (**Pc1**, **Pc2**, **Pc3** and **Pc4**) were obtained by lotetramerization of corresponding phthalonitriles in the presence of anhydrous $CuCl_2$ and DBU in anhydrous n-hexanol (Fig. 1). The compounds are soluble in CH_2Cl_2, chloroform, THF, ethanol and methanol and are characterized by MALDI-TOF mass spectroscopy, FT-IR and UV–Vis spectroscopy.

1(4),8(11),15(18),22(25)-Tetrakis-[2-(2-(2-methoxyethoxy) ethoxy)ethoxy] phtalocyaninato Copper (II) (Pc1)

A mixture of 3-(4,7,10-trioxaundecane-1-oxanonyl)phthalonitrile (0.5 g, 1.7 mmol), anhydrous $CuCl_2$ (0.11 g, 0.86 mmol), anhydrous n-hexanol (2 mL) and DBU (0.07 mL, 0.45 mmol) was heated and stirred at 170 °C for 24 h in a round-bottomed flask under argon atmosphere. The resulting green suspension was cooled and the product was extracted with n-hexane. The oily green product was purified by column chromatography on neutral Al_2O_3 using CH_2Cl_2 as eluent. Yield: 0.235 g (47%). Anal. calcd. for $C_{60}H_{72}N_8O_{16}Cu$: C, 58.84; H,5.92; N, 9.15%, found: C, 58.96; H, 5.73; N, 9.56%. IR (ATR) ν_{max} (cm^{-1}): 3036 (aromatic CH), 2872 (aliphatic CH), 1648, 1592, 1452, 1340, 1272, 1236, 1072. UV–Vis (THF) λ_{max} (log ε) (nm): 699 (4.98), 358 (4.14). MALDI-TOF-MS m/z: Calcd. for $C_{60}H_{72}N_8O_{16}Cu$: 1224.82, Found 1224.42 $[M]^+$.

2(3),9(10),16(17),23(24)-Tetrakis-[2-(2-(2-methoxyethoxy) ethoxy)ethoxy] phthalocyaninato Copper (II) (Pc2)

Pc2 was prepared according to the modified synthetic route previously reported by Erdem et al. [42]. This compound was synthesized by the same procedure used for the synthesis of **Pc1** starting with 4-(4,7,10-trioxaundecane-1-oxanonyl)phthalonitrile (0.5 g, 1.7 mmol), anhydrous $CuCl_2$ (0.11 g, 0.86 mmol), anhydrous n-hexanol (2 mL) and DBU (0.07 mL, 0.45 mmol) in this study. Yield: 0.380 g (76%). Anal. calcd. for $C_{60}H_{72}N_8O_{16}Cu$: C, 58.84; H,5.92; N, 9.15%, found: C, 59.01; H, 5.51; N, 9.42%. IR (ATR) ν_{max} (cm^{-1}): 3069 (aromatic CH), 2867 (aliphatic CH), 1607, 1510, 1483, 1406, 1343, 1273, 1242, 1196, 1091, 1060. UV-Vis (THF) λ_{max} (log ε) (nm): 682 (4.93), 340 (4.68). MALDI-TOF-MS m/z: Calcd. for $C_{60}H_{72}N_8O_{16}Cu$: 1224.82, Found 1225.29 $[M]^+$.

1(4),8(11),15(18),22(25)-Tetrakis-[2-(2-(2-methoxyethoxy) ethoxy)ethylthio] phthalocyaninato Copper (II) (Pc3) [48]

Pc3 was prepared by the same procedure used for the synthesis of **Pc1** starting with 3-(4,7,10-trioxaundecane-1-sulfanyl)phthalonitrile (0.5 g, 1.6 mmol), anhydrous $CuCl_2$ (0.11 g, 0.81 mmol), anhydrous n-hexanol (2 mL) and DBU (0.07 mL, 0.45 mmol). Yield: 0.370 g (74%). Anal. calcd. for $C_{60}H_{72}N_8O_{12}S_4Cu$: C, 55.90; H,5.63; N, 8.69%, found: C, 56.14; H, 5.23; N, 8.88%. IR (ATR) ν_{max} (cm^{-1}): 3060 (aromatic CH), 2912 (aliphatic CH), 1636, 1568, 1464, 1312, 1084, 1024. UV–Vis (THF) λ_{max} (log ε) (nm): 712 (4.93), 339 (4.64). MALDI-TOF-MS m/z: Calcd. for $C_{60}H_{72}N_8O_{12}S_4Cu$: 1289.09, Found 1288.75 $[M]^+$.

2(3),9(10),16(17),23(24)-Tetrakis-[2-(2-(2-methoxyethoxy) ethoxy)ethylthio] phthalocyaninato Copper (II) (Pc4)

Pc4 was prepared by the same procedure used for the synthesis of **Pc1** starting with 4-(4,7,10-trioxaundecane-1-sulfanyl)phthalonitrile (0.5 g, 1.6 mmol), anhydrous $CuCl_2$ (0.11 g, 0.81 mmol), anhydrous n-hexanol (2 mL) and DBU (0.07 mL, 0.45 mmol). Yield: 0.365 g (73%). Anal. calcd. for $C_{60}H_{72}N_8O_{12}S_4Cu$: C, 55.90; H,5.63; N, 8.69%, found: C, 56.05; H, 5.32; N, 8.99%. IR (ATR) ν_{max} (cm^{-1}): 3067 (aromatic CH), 2871–2864 (aliphatic CH), 1602, 1505, 1450, 1391, 1308, 1084, 1195, 1097, 1085. UV–Vis (THF) λ_{max} (log ε) (nm): 682 (4.91), 341 (4.59). MALDI-TOF-MS m/z: Calcd. for $C_{60}H_{72}N_8O_{12}S_4Cu$: 1289.08, Found 1289.41 $[M]^+$.

2.4. Preparation of SWCNTs-$CuPcR_4$ hybrids

SWCNTs were first acidified and cut into short and uncapped nanotubes according to a multi-step procedure developed by Smalley and co-workers [49]. This was carried out by stirring the nanotubes under 70 °C in a mixture of concentrated HNO_3 and H_2SO_4 (3:1, v:v) for 2 h. The mixture was centrifuged, washed thoroughly in deionised water and dried at 70 °C for 12 hours.

le 1
nes concentrations as calculated using Eq. (1). Decimal fractions of the final gas concentration values are rounded to the nearest one.

						Calculated concentration	Further dilution by 50 cc syringe		The original solutions are 40% conc. in water
	V_s (μL)	ρ (g/mL)	V (L)	T (K)	M (g)	C1 (ppm)	C2 = C1 × X/50 (ppm)	X	C = C2 × 40%, (ppm)
ethylamine	1	0.89	2	291	31.7	335.1808	10.05542344	1.5	4
							20.11084688	3	8
							50.2771172	7.5	20
							100.5542344	15	40
							201.1084688	30	80
	2	0.89	2	291	31.7	670.3616	502.771172	37.5	200
imethylamine	2	0.89	2	291	42.08	505.0015	10.10002925	1	4
							20.2000585	2	8
							50.50014624	5	20
							101.0002925	10	40
							202.000585	20	80
	4	0.89	2	291	45.08	942.7889	499.6781107	26.5	200
imethylamine	2	0.83	2	291	59.11	335.2706	10.0581185	1.5	4
							20.116237	3	8
							50.29059251	7.5	20
							100.581185	15	40
							201.16237	30	80
	4	0.88	2	291	59.11	710.9353	504.7640514	35.5	200

The acidified SWCNTs (0.5 mg) were added to a solution of , **Pc2**, **Pc3** or **Pc4** (1.5 mg/mL) in chloroform and ultrasonicated 15 min to get suspensions of **Pc1-CNT**, **Pc2-CNT**, **Pc3-CNT** and **–CNT**. Thin films were produced by spin-casting the obtained utions onto gold-coated slides and onto silicon substrates using hotoresist spinner (Microsystem model 4000) at 2000 rpm. Simi-y, thin films were produced from a solution of all pristine $CuPcR_4$ pounds in chloroform (2 mg/mL) for comparison.

Results and discussion

. *Characterization of SWCNT/$CuPcR_4$ hybrid films*

.1. *UV–Vis absorption spectra*

Fig. 2 shows the UV–visible absorption spectra of solutions of CNTs, CuPc (**Pc1**, **Pc2**, **Pc3** and **Pc4**) and SWCNT/CuPc (**Pc1-T**, **Pc2-CNT**, **Pc3-CNT** and **Pc4-CNT**) hybrids in chloroform. All $CuPcR_4$ compounds used in this work exhibit typical electronic orption spectra. The spectra are characterised with two strong orption regions, one in the wavelength range of 650–720 nm (Q-d) arising from the electron transitions from highest occupied lecular orbital (HOMO) a_{1u} to the lowest unoccupied molec-r orbital (LUMO) e_g and another in the range of 300–450 nm band) which is attributed to the electron transitions from the MO) a_{2u} to the (LUMO) e_g [50]. Furthermore, absorption within Q-band is split into two absorption peaks, one with much her intensity than the other. This can be ascribed to domi-t monomer absorption with the lower intensity shoulder being ribed to molecular aggregation in chloroform solution. The orption spectrum of SWCNT is featureless as reported elsewhere]

The maxima of the Q-bands in the absorption spectra of **Pc1-**, **Pc2-CNT**, **Pc3-CNT** and **Pc4-CNT** hybrids are broadened and -shifted by ≈12.45, 10.59, 16.42 and 17.48 nm in comparison h **Pc1**, **Pc2**, **Pc3** and **Pc4** spectra, respectively. It can also be seen t the Q-band splitting has either disappeared or became weaker the absorption spectra of hybrid, which indicates a dominant nomer absorption. These changes are suggested to take place to the strong π–π interaction between carbon nanotubes and halocyanine molecules, where phthalocyanines are usually con-ered as electron donors, while carbon nanotubes as acceptors]. This interaction has been frequently ascribed to the reduced egation in the MPc/CNT composites [53,54].

3.1.2. *Morphology*

Fig. 3 shows SEM images of pristine SWCNTs, acid-treated SWCNTs, **Pc1-CNT**, **Pc2-CNT**, **Pc3-CNT** and **Pc4-CNT** hybrids deposited as thin film from chloroform solution onto silicon substrate. Pristine CNTs typically tend to bundle together (Fig. 3a) and to aggregate

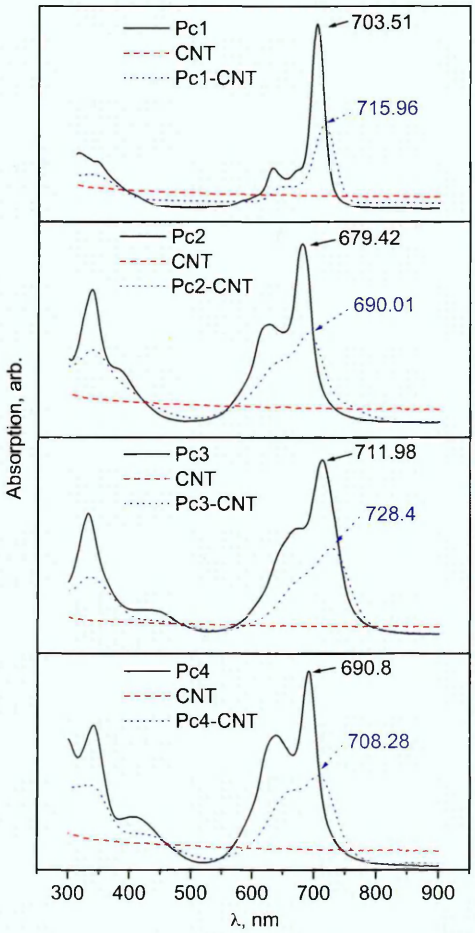

Fig. 2. Optical absorption spectra of pristine SWCNT (dashed lines), **Pc1**, **Pc2**, **Pc3** and **Pc4** (solid lines) and **Pc1-CNT**, **Pc2-CNT**, **Pc3-CNT** and **Pc4-CNT** hybrids (dotted lines) in chloroform.

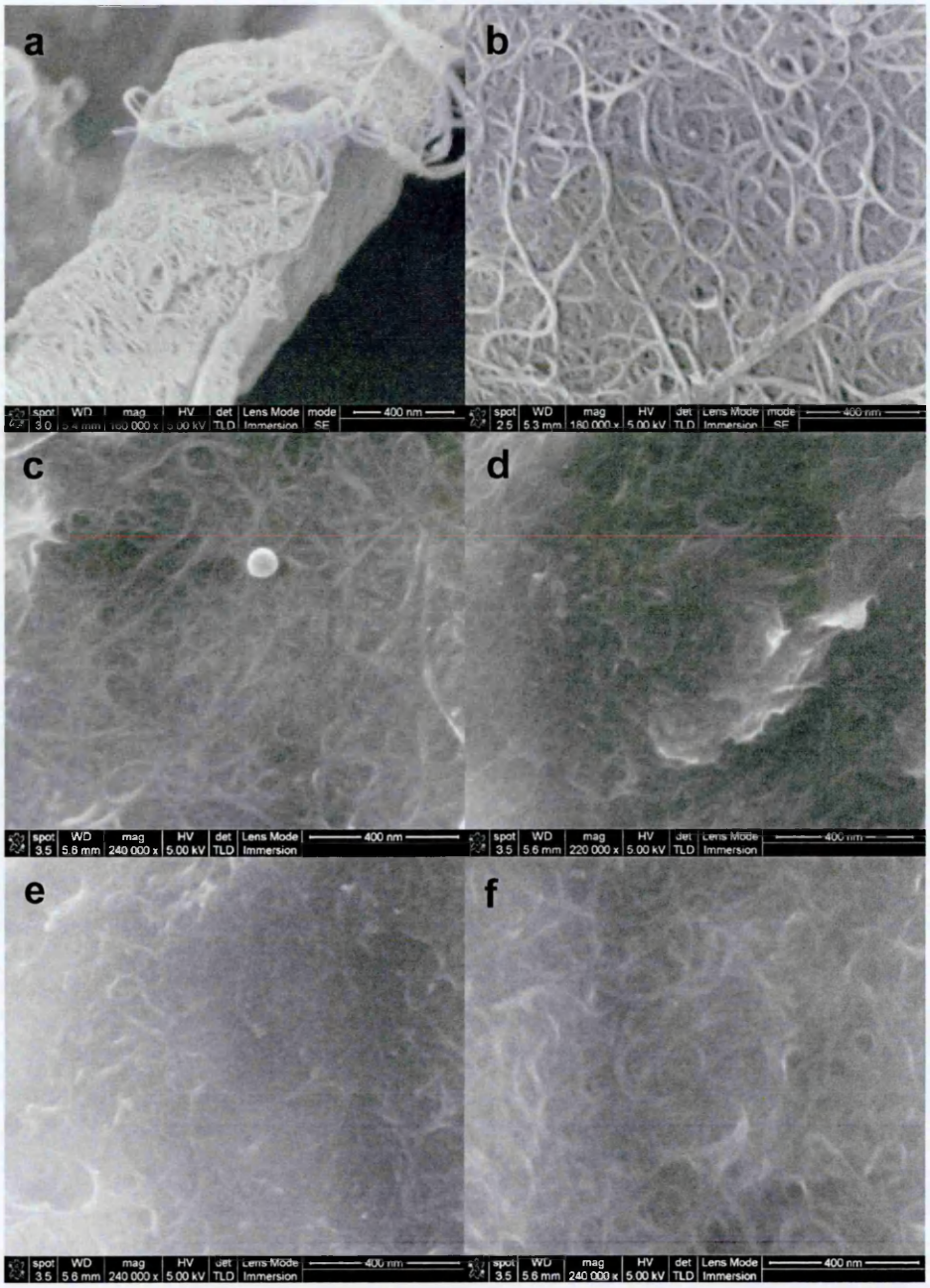

Fig. 3. SEM images of (a) pristine SWCNT, (b) acidified SWCNT, (c) **Pc1-CNT**, (d) **Pc2-CNT**, (e) **Pc3-CNT** and (f) **Pc4-CNT** hybrids.

van der Waals attraction between individual tubes [55] ll as the high length to diameter ratio; this makes them to disperse in common organic solvents. Chemical mod- n has been performed to achieve enhanced interaction en SWCNTs and $CuPcR_4$ molecules leading to the forma- f a composite with much improved solubility in chloroform. tained solution is conveniently used for thin film deposi- sing spin-coating technique. Fig. 3b shows that the intrinsic of SWCNTs structure is still preserved after the acid treat- However, after mixing with phthalocyanines (Fig. 3c–f), the site dispersion was significantly improved to form a uni- suspended solution in chloroform; hence smoother films btained to perform optical investigation, using TIRE experi-

Fig. 4a and b shows AFM images of **Pc2** and **Pc2-CNT**, as an example, spun onto silicon substrates with the roughness analysis presented at the bottom of the images. All other phthalocyanines and their hybrids with SWCNT exhibited the same surface morphology. The films of $CuPcR_4$ demonstrate fibrous-like porous morphology. Hybrids on the other hand show that phthalocyanine molecules are attached to the surface of carbon nanotubes confirming the formation of networks of $CuPcR_4$ and SWCNT. Similar morphology was observed for poly(3-hexylthiophene) (P3HT)/multi-walled carbon nanotube (MWCNT) films [56] and 2(3),9(10),16(17),23(24)-tetrakis(hexadecylthio) phthalocyaninato copper (II)/single-walled carbon nanotube (SWCNT) films [57]. The main roughness (R_a), standard deviation (RMS) and maximum height (R_{max}) are summarised in Table 2.

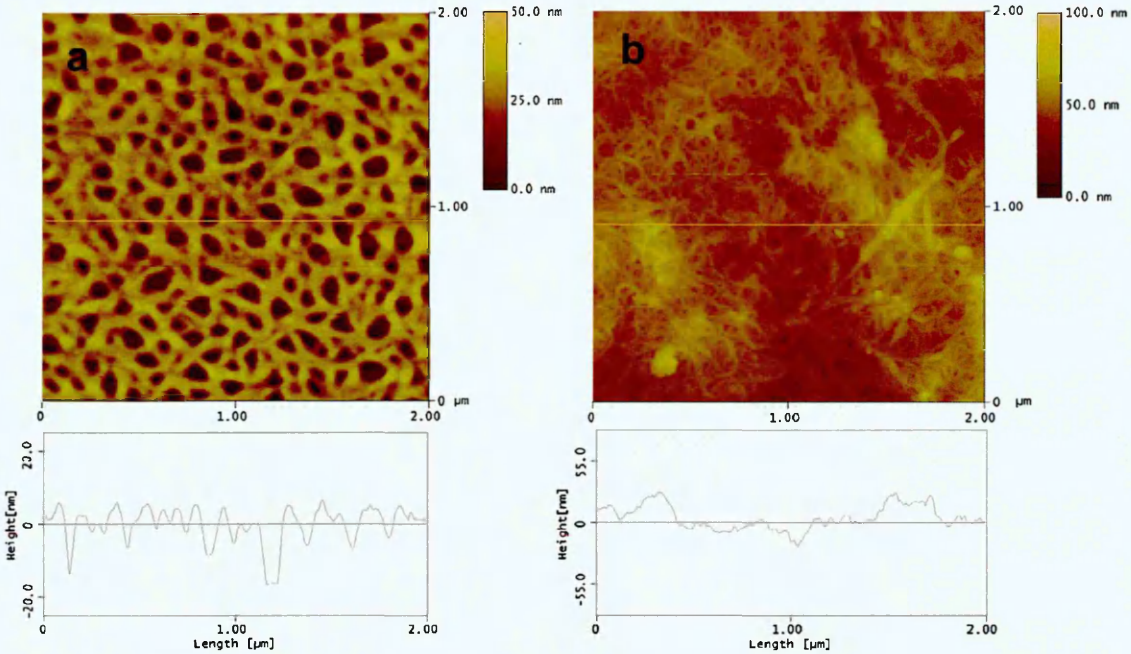

Fig. 4. AFM images of (a) **Pc2**, (b) **Pc2-CNT** in thin film form deposited on silicon. Roughness analyses are shown below.

. *Total internal reflection ellipsometry (TIRE)*

.1. *Spectral shifts*

The adsorption of amines vapours onto the surface of $CuPcR_4$ SWCNT/$CuPcR_4$ hybrids has been studied using TIRE method. halocyanines and their hybrids were spun onto gold-coated ss substrates as described in the experimental section. Fig. 5 ws typical TIRE spectra of Cr/Au films in air used in the present rk.

The spectrum of $\Psi(\lambda)$, demonstrating the amplitude ratio of A_s, resembles very much the conventional surface plasmon res- nce (SPR) curve, while the spectrum of $\Delta(\lambda)$ is associated with phase shift between p- and s-components of polarized light. latter changes sharply from 270° down to -90° near the plas- n resonance. According to Arwin's modelling [23] the position he sharp drop in $\Delta(\lambda)$ spectrum is about 10 times more sensi- to analytes adsorption than $\Psi(\lambda)$ spectrum. Fig. 6 presents the ctra of $\Psi(\lambda)$ and $\Delta(\lambda)$ of **Pc2** and its hybrid with SWCNT thin s respectively before and after exposure to amines vapours as example. The responses of the other three samples are given Table 3. The concentrations of amines were varied from 4 to ppm in air. The spectra were measured 10 min after injection ontaminated and fresh air to achieve the equilibrium response ecovery, respectively.

During exposure to contaminated air, it was difficult to detect fts in $\Psi(\lambda)$ because of the shape of the curve, however, significantly larger shifts have been observed in $\Delta(\lambda)$ spectra. These are typical features of TIRE method as reported earlier [16,17,46]. The spectra of $\Delta(\lambda)$ were further enlarged and shown at the top of Fig. 6 to provide better assessment of the effect of amines exposures. It can clearly be seen that the adsorption of amines on hybrid films has resulted in larger shifts and these shifts have been summarised in Table 3. The concentrations of amines has been further diluted below 4 ppm and the minimum detection limits of methylamine, dimethylamine and trimethylamine were found to be 3.6, 4.4 and 6.4 ppm respectively in the case **Pc2-CNT** hybrid films, while bare phthalocyanine (**Pc2**) shows minimum limits of 8, 9.6 and 13.2 ppm for methylamine, dimethylamine and trimethylamine, respectively. Similar trend was observed for all four prepared phthalocyanines and their hybrids.

Carbon nanotubes in general are characterised with uniform surface with delocalised π-electrons of high density, which enhances their adsorption properties. When hybrid films are exposed to amine vapours, larger numbers of molecules are

le 2
ghness analysis of $CuPcR_4$ and SWCNT/$CuPcR_4$ films.

lm	R_a, nm	RMS, nm	R_{max}, nm
1	1.954	3.172	9.658
1-CNT	4.921	8.751	19.102
	1.450	2.197	7.695
2-CNT	3.312	6.935	17.613
	1.733	3.501	8.461
--CNT	5.811	9.550	20.275
4	1.630	2.153	6.876
4-CNT	4.153	7.877	18.252

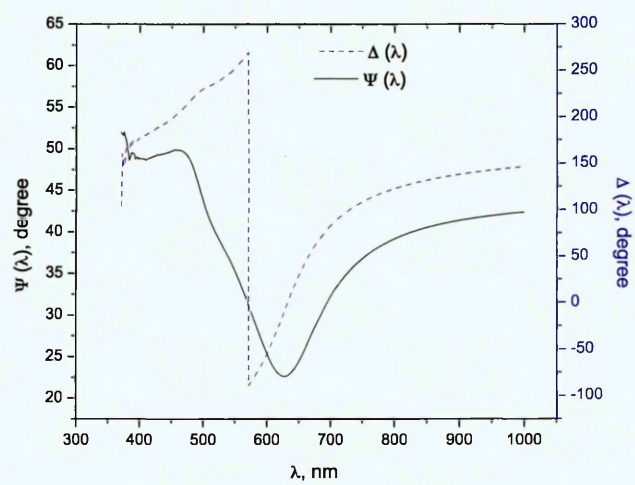

Fig. 5. Typical TIRE spectra of Cr/Au film in air.

nges in the phase shifts $\Delta(\lambda)$ of phthalocyanines and their composites with carbon nanotubes active layers upon exposure to methylamine, dimethylamine and ylamine gases in different concentrations.

	Conc., ppm	$\delta\Delta(\lambda)$, nm							
		Pc1	Pc1-CNT	Pc2	Pc2-CNT	Pc3	Pc3-CNT	Pc4	Pc4-CNT
lamine	4	–	1.64	–	1.25	–	1.79	–	1.43
	8	1.31	4.19	1.9	3.51	–	3.2	1.25	3.1
	20	3.24	9.08	4.09	8.03	3.05	7.14	3.67	7.98
	40	6.9	15.81	7.51	15.16	6.02	13.63	6.87	13.91
	80	10	20.01	12.12	20.9	9.35	20.02	9.53	23.55
	200	11.19	22.57	15.97	25.39	11.11	27.22	11.32	28.58
thylamine	4	–	–	–	–	–	–	–	–
	8	–	3.29	–	1.91	–	2.01	–	2
	20	1.78	6.35	3.05	4.97	1.59	4.74	2.25	4.79
	40	3.69	10.59	5.95	8.21	3.32	9.9	3.95	9.31
	80	6.78	15.03	9.34	13.32	6.01	15.5	7.45	16.61
	200	8.02	17.72	11.04	17.34	7.95	20.76	9.5	20.75
thylamine	4	–	–	–	–	–	–	–	–
	8	–	2.21	–	–	–	1.98	–	1.68
	20	1.54	4.68	1.59	3.19	1.57	3.06	2.05	3.19
	40	2.89	8.58	3.82	6.38	3.12	6.8	3.42	6.95
	80	5.1	14.64	6.11	11.12	5.4	12.76	5.9	11.83
	200	6.4	17.43	7.97	15.77	6.3	17.7	7.82	17.56

ed onto the surface resulting in larger changes in the l properties of the films and hence larger shifts in $\Delta(\lambda)$ red to bare phthalocyanines films. Several detection tech- s for amines' vapours were reported in the literatures. When

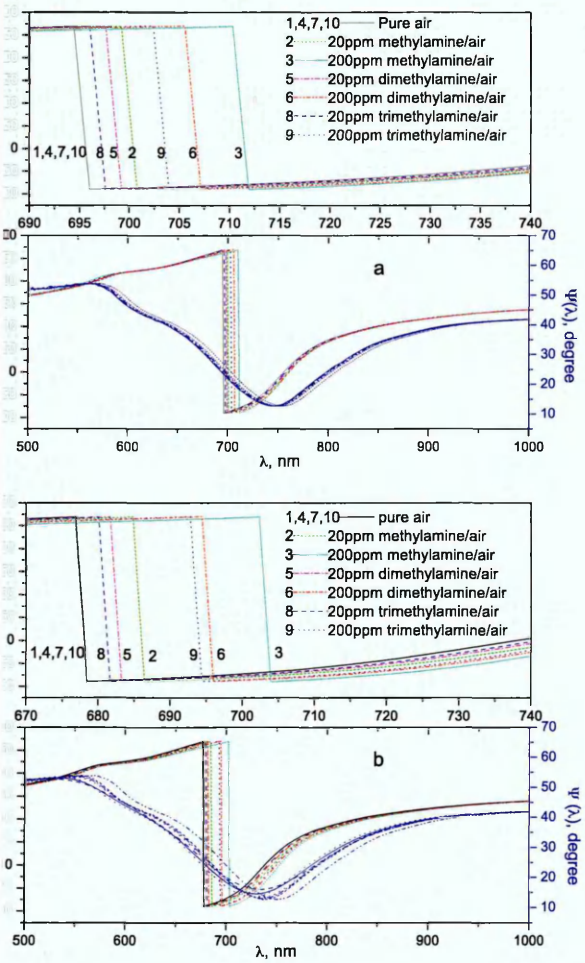

$\Psi(\lambda)$ and $\Delta(\lambda)$ TIRE spectra of (a) **Pc2** and (b) **Pc2-CNT** coated Cr/Au in fresh 7 and 10); after injection of 20 and 200 ppm of methylamine (2,3 respec- dimethylamine (5,6), trimethylamine (8,9). An enlarged section of $\Delta(\lambda)$ are shown above.

aqua(chloro)(5,10,15,20-tetraphenylporphyrinato)chromium(III) used as optical active layer based on UV-visible absorption technique, a detection limit of 10 ppm has been reported [58] under dynamic conditions, while a limit of 24 ppm has been realized by using fiber-optic fluorescence sensor employing 2-naphtol bonded to polyethylene oxide [59]

Complete recovery of $\Delta(\lambda)$ spectra was observed after flushing the cell with fresh air as previously established for films of metal phthalocyanines with other types of substituents [17]. Fig. 7 shows the dependence of phase shift change on amines concentrations in the range of 4–200 ppm for phthalocyanine layers and their hybrids with SWCNT.

Earlier studies have shown that water molecules are weakly physisorbed onto carbon nanotube surface [60–62]. Larger response to humidity has been reported in boron- and nitrogen-doped carbon nanotubes [63], which indicate strong interaction between water molecules and doped-CNTs, however, the recovery time of sensor based on these materials was achieved in about 2.5 h. In this work the baseline has been measured using ambient air and therefore the humidity interaction resulting from the diluted gas can be negligible.

3.2.2. Experimental data fitting

Theoretical fitting to experimental Ψ and Δ spectra was carried out by applying a 4-layer model consisting of air, organic layer, Au layer and BK7 glass. The parameters of organic films after exposure to amines vapours were determined by fitting experimental Ψ and Δ spectra to the theoretical organic model by fixing Cr/Au layer parameters. Table 4 summarises the thickness of all layers found from theoretical data fitting as well as the values of refractive index and extinction coefficients given at $\lambda = 633$ nm. Further to the data summarised in Table 4 the variation in refractive index and extinction coefficient as a function of λ for **Pc2** and **Pc2-CNT** films in pure air and after exposure to amines vapours at the concentration of 40 ppm are shown as an example in Fig. 8.

3.2.3. Sensitivity and response time

In order to evaluate the response of the two types of layers the average sensitivity has been calculated based on changes in Δ spectra shifts (Table 3) using the following equation:

$$\bar{S} = \frac{1}{\Delta_o}\frac{1}{m}\sum_{i=1}^{m}\frac{\delta\Delta}{C_i} \quad (3)$$

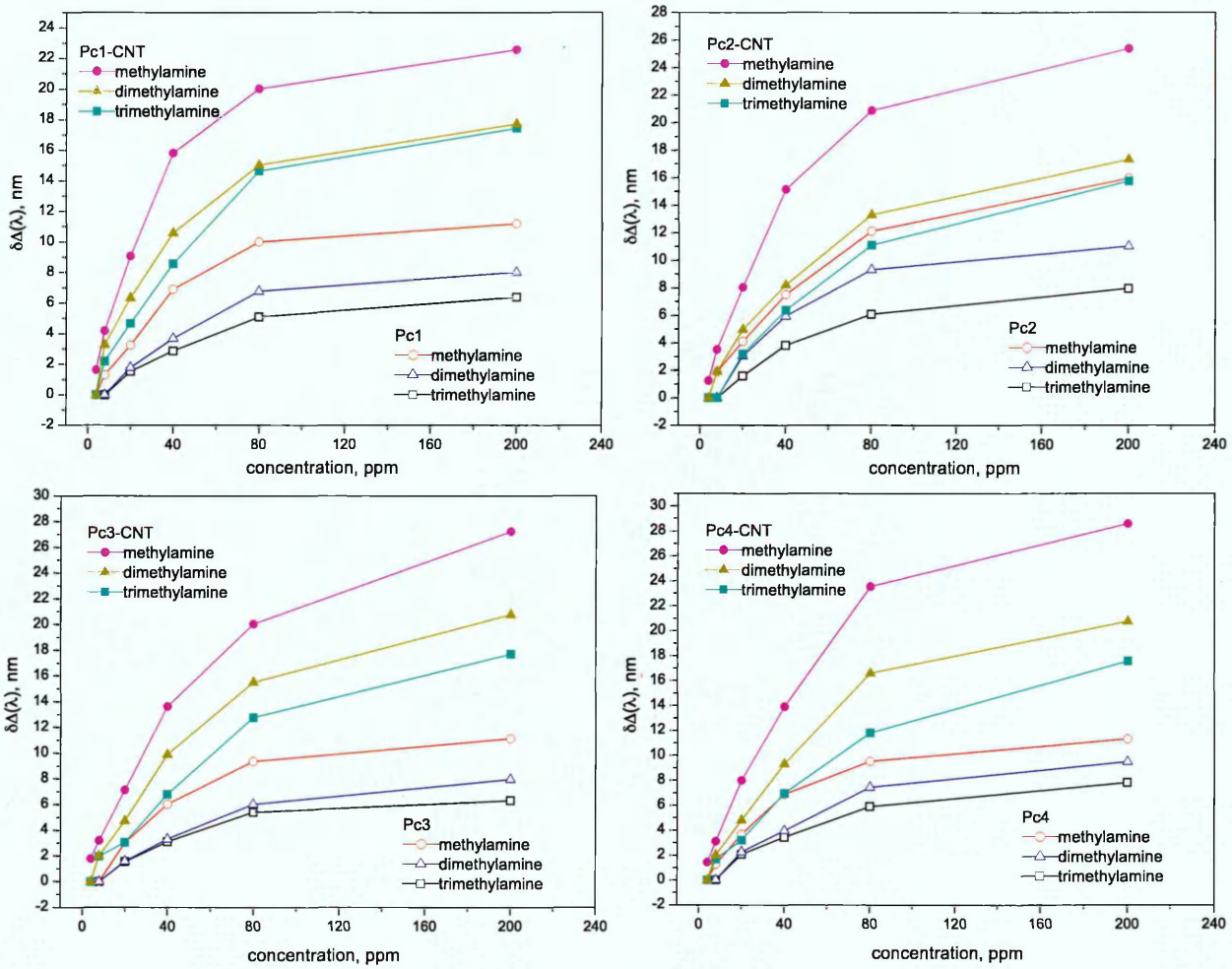

7. Phase shift changes (δΔ) in Δ(λ) spectra of Cu(II) phthalocyanines and their hybrids with SWCNT layers on treatments with amines vapours in the concentration 4-200 ppm.

re $\delta\Delta$ is the change in the Δ spectra under analyte concen- ion (C_i), m is the number of different concentrations used in study, and $\Delta_\circ$ is the initial change in the phase shift spec- before exposure to amines vapours). The average sensitivities e presented in Fig. 9. All films exhibited higher sensitivity for hylamine than dimethylamine and trimethylamine, where the est sensitivity for methylamine was found to be 0.000325/ppm he case of Pc2-CNT active layer. The lower sensitivity for sec- ary and tertiary amines can be explained by the steric hindrance their molecular shapes provide which allows smaller num- of these molecules to interact with films' surfaces as compared to methylamine [18]. Furthermore, the higher vapour temperature of dimethylamine and trimethylamine (7–9° C) in comparison to methylamine (−7° C) reduces the number density of these amines at room temperature. Therefore, the interaction probability with the film surface is reduced. It was recently found that changes in the intensity of the Q-band in the UV–visible spectra of thin films of metalloporphyrin were ~0.85 and 0.5 (a.u.) after exposure to low concentrations of dimethylamine and trimethylamine respectively [58]. This is found consistent with our observations where dimethylamine showed better interaction with the active layer than trimethylamine.

4

es in the optical parameters and films' thicknesses of $CuPcR_4$ and $SWCNT/CuPcR_4$ films at λ = 633 nm caused by adsorption of amines (40 ppm).

		After exposure to 40 ppm										
	Initial film			Methylamine			Dimethylamine			Trimethylamine		
	n	k	d,nm	n	k	d,nm	n	k	d,nm	n	k	d,nm
	1.633	0.192	40.6	1.639	0.198	40.9	1.638	0.198	40.7	1.636	0.194	40.8
-CNT	1.394	0.124	69.4	1.40	0.127	69.8	1.41	0.126	70.1	1.398	0.124	70
	1.573	0.270	32.2	1.590	0.273	32.6	1.576	0.276	32.3	1.581	0.268	32.2
-CNT	1.367	0.151	51	1.369	0.158	52.1	1.369	0.156	51.7	1.375	0.155	51.7
	1.580	0.254	36.3	1.591	0.265	37	1.583	0.257	37	1.586	0.253	36.4
-CNT	1.402	0.271	63.7	1.425	0.295	64.3	1.415	0.285	64.5	1.419	0.278	63.9
	1.522	0.369	33.1	1.530	0.373	33.4	1.524	0.372	33.6	1.526	0.370	33.4
-CNT	1.396	0.126	55.3	1.4	0.128	55.9	1.407	0.126	55.8	1.397	0.127	55.5

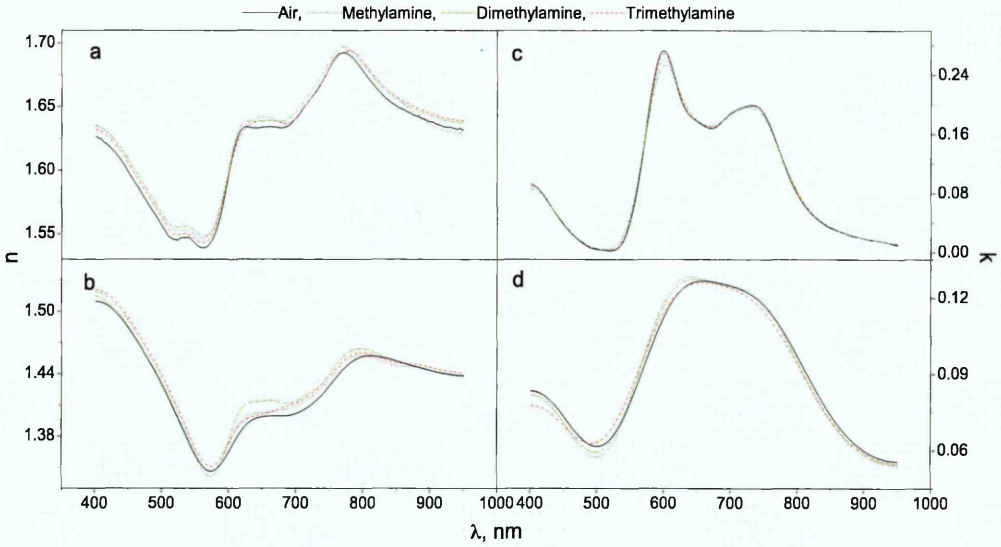

:e variation in refractive index and extinction coefficient of (a and c) **Pc2** and (b and d) **Pc2-CNT** layers as exposed to air (solid lines), methylamine (dotted lines), lamine (dashed-dotted lines) and trimethylamine (dashed lines) in the concentration of 40 ppm.

and **Pc4** show higher sensitivity to analytes than **Pc1** and :e non-peripheral tetra substitution in **Pc1** and **Pc3** makes ess sensitive to the examined analytes due to their lower l affinity [64].

calculate the response time, **Pc2** and **Pc2-CNT** films elected and exposed to methylamine, dimethylamine and hylamine at concentration of 40 ppm. For methylamine, ponse time t_{80}, which is defined as the time it takes to 80% of the steady state shift, was measured to be 158 2 film and 66 s in **Pc2-CNT** film. This is much lower he response time of 440 s and 270 s found by Liu and] using zinc phthalocyanine film and Saini et al. [5] using phthalocyanine film, respectively. The response time for ylamine was found to be 230 s and 101 s detected by d **Pc2-CNT** films respectively, while for trimethylamine, se times were found to be 267 s and 136 s. The recov- e t^*_{80}, which is defined as the time required to reach the base line were measured to be 393, 350 and 387 ethylamine, dimethylamine and trimethylamine respec- s detected by **Pc2**, whereas **Pc2-CNT** hybrid film exhibited

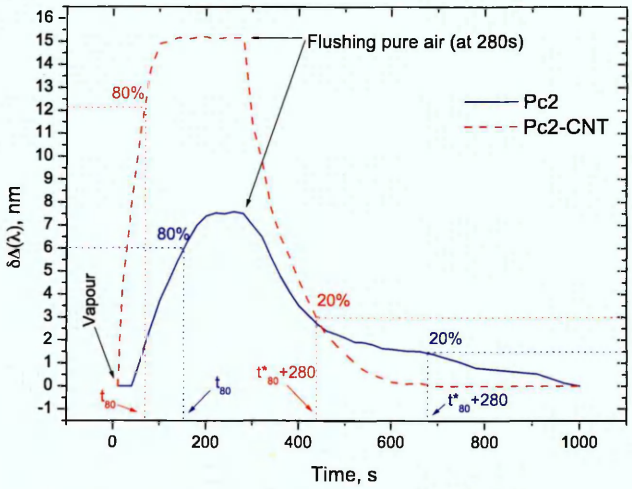

Fig. 10. The rise and decay curves of the $\delta\Delta(\lambda)$ during the detection of 40 ppm methylamine vapour by **Pc2** and **Pc2-CNT** films.

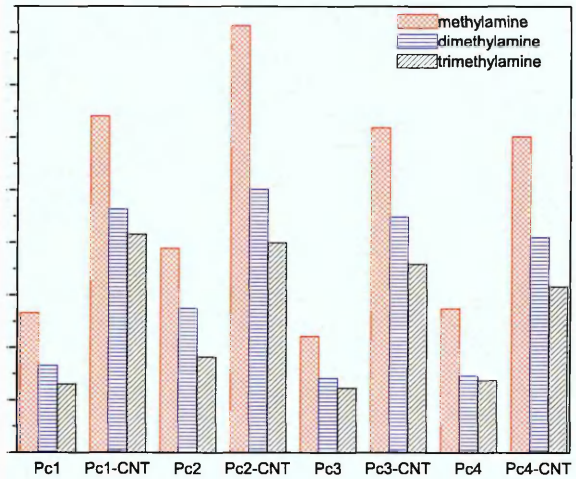

nsitivity of Cu(II) phthalocyanines and their hybrids with SWCNT active mated from Eq. (3) for methylamine, dimethylamine and trimethylamine.

recovery times of 150, 191 and 138 s respectively. Fig. 10 shows the response and recovery times of **Pc2** and its hybrid films on exposures to methylamine at concentration of 40 ppm as an example.

4. Conclusion

Concentrations as low as 3.6 ppm for methylamine have been detected by spun active layers of SWCNT/tetra-substituted copper phthalocyanine hybrids with an average sensitivity of 0.000325/ppm. The produced films exhibited higher sensitivity for methylamine than dimethylamine and trimethylamine due to the steric hindrance of secondary and tertiary amines which reduces the probability of being adsorbed by the sensor. Hybrid films, in general, show higher sensitivity, lower detection limit and shorter response time than bare phthalocyanine films towards all the investigated amines' vapours. The higher π-electron density in carbon nanotubes is expected to result in larger number of adsorbed molecules onto the hybrid films' surfaces.

⊏nowledgements

The authors acknowledge the financial support through the ⊏teral project between the Scientific and Technological Research ⊐ncil of Turkey (TUBITAK, Project number: 108M384) and the ⊏sian Foundation of Basic Research (RFBR, Project numbers: 12-91372-CT_a). Hikmat Banimuslem wishes to acknowledge the ⊐ncial support from the Higher Committee for Education Devel-ⁿent in Iraq (HCED). Tamara Basova acknowledges the financial ⊐port from the Ministry of Education and Science of the Russian ⊐eration.

⊐erences

A.K. Diallo, J. Tardy, Z.Q. Zhang, F. Bessueille, N. Jaffrezic-Renault, M. Lemiti, Trimethylamine biosensor based on pentacene enzymatic organic field effect transistor, Appl. Phys. Lett. 94 (2009) 263302.

T. Basova, A. Hassan, F. Yuksel, A.G. Gürek, V. Ahsen, Optical detection of pentachlorophenol in water using thin films of octa-tosylamido substituted zinc phthalocyanine, Sens. Actuators B. Chem. 150 (2010) 523–528.

B. Geng, F. Zhan, H. Jiang, Z. Xing, C. Fang, Facile production of self-assembly hierarchical dumbbell-like CoOOH nanostructures and their room-temperature CO-gas-sensing properties, Cryst. Growth Des. 8 (2008) 3497–3500.

Y. Sun, J. Liu, G. Frye-Mason, S. Ja, A.K. Thompson, X. Fan, Optofluidic ring resonator sensors for rapid DNT vapor detection, Analyst 134 (2009) 1386–1391.

R. Saini, A. Mahajan, R.K. Bedi, D.K. Aswal, Room temperature detection of amine vapours using copper phthalocyanine based thin films, Phys. Status Solidi A. 209 (2012) 1245–1250.

M.L. Rodríguez-Méndez, M. Gay, C. Apetrei, J.A. De Saja, Biogenic amines and fish freshness assessment using a multisensor system based on voltammetric electrodes. Comparison between CPE and screen-printed electrodes, Electrochim. Acta 54 (2009) 7033–7041.

R. De Saja, J. Souto, M.L. Rodríguez-Méndez, J.A. De Saja, Array of lutetium bis-phthalocyanine sensors for the detection of trimethylamine, Mater. Sci. Eng. C 8-9 (1999) 565–568.

M. Mattarozzi, F. Lambertini, M. Suman, M. Careri, Liquid chromatography-full scan-high resolution mass spectrometry-based method towards the comprehensive analysis of migration of primary aromatic amines from food packaging, J. Chromatogr. A 1320 (2013) 96–102.

H. Pan, X. Zeng, B. Zhu, L. He, T. Liao, W. Zhe, S. Wang, B. Jiang, M. Wang, Determination of biogenic amines in cheese by nanofiber solid phase extraction-reversed phase high performance liquid chromatography with pre-column derivatization, J. Food Agric. Environ. 11 (2013) 115–118.

I.G. Casella, M. Gatta, E. Desimoni, Determination of histamine by high-pH anion-exchange chromatography with electrochemical detection, Food Chem. 73 (2001) 367–372.

R. Ziółkowski, L. Górski, P. Prokaryn, M. Zaborowski, A. Kutyla-Olesiuk, P. Ciosek, W. Wróblewski, E. Malinowska, Development of silicon-based electrochemical transducers, Anal. Methods 5 (2013) 5464–5470.

X. Wang, S. Reisberg, N. Serradji, G. Anquetin, M.-. Pham, W. Wu, C.-. Dong, B. Piro, E-assay concept: detection of bisphenol A with a label-free electrochemical competitive immunoassay, Biosens. Bioelectron. 53 (2014) 214–219.

J.H. Chen, X. Zhang, S. Cai, D. Wu, J. Lin, C. Li, J. Zhang, Label-free electrochemical biosensor using home-made 10-methyl-3-nitro-acridone as indicator for picomolar detection of nuclear factor kappa B, Biosens. Bioelectron. 53 (2014) 12–17.

J. Kang, A.T. Hussain, M. Catt, M. Trenell, B. Haggett, E.H. Yu, Electrochemical detection of non-esterified fatty acid by layer-by-layer assembled enzyme electrodes, Sens. Actuators B. Chem. 190 (2014) 535–541.

B. Wang, X. Zhou, Y. Wu, Z. Chen, C. He, Lead phthalocyanine modified carbon nanotubes with enhanced NH_3 sensing performance, Sens. Actuators B. Chem. 171-172 (2012) 398–404.

A. Hassan, T. Basova, F. Yuksel, G. Gümüş, A.G. Gürek, V. Ahsen, Study of the interaction between simazine and metal-substituted phthalocyanines using spectral methods, Sens. Actuators B. Chem. 175 (2012) 73–77.

T. Basova, A. Tsargorodskaya, A. Nabok, A.K. Hassan, A.G. Gürek, G. Gümüs, V. Ahsen, Investigation of gas-sensing properties of copper phthalocyanine films, Mater. Sci. Eng. C 29 (2009) 814–818.

J. Liu, W. Lu, Optical amine sensor based on metallophthalocyanine, J. Chin. Inst. Chem. Eng. 38 (2007) 483–488.

H. Arwin, Is ellipsometry suitable for sensor applications? Sens. Actuators A. Phys. 92 (2001) 43–51.

M. Poksinski, H. Arwin, Protein monolayers monitored by internal reflection ellipsometry, Thin Solid Films 455-456 (2004) 716–721.

M. Poksinski, H. Dzuho, H. Arwin, Copper corrosion monitoring with total internal reflection ellipsometry, J. Electrochem. Soc. 150 (2003) B536–B539.

P. Westphal, A. Bornmann, Biomolecular detection by surface plasmon enhanced ellipsometry, Sens. Actuators B. Chem. 84 (2002) 278–282.

H. Arwin, M. Poksinski, K. Johansen, Total internal reflection ellipsometry: Principles and applications, Appl. Opt. 43 (2004) 3028–3036.

[24] G.S.V. Coles, G. Williams, Effects of high-temperature sintering on SnO_2 sensor response to reducing gases, J. Mater. Chem. 2 (1992) 23–29.

[25] T.C. Pearce, J.W. Gardner, S. Friel, P.N. Bartlett, N. Blair, Electronic nose for monitoring the flavour of beers, Analyst 4 (1993) 371–377.

[26] M.J. Jafari, M.E. Azim-Araghi, S. Barhemat, S. Riyazi, Effect of post-deposition annealing on surface morphology and gas sensing properties of palladium phthalocyanine thin films, Surf. Interface Anal. 44 (2012) 601–608.

[27] R. Jaisutti, T. Osotchan, An investigation of molecular interactions between zinc phthalocyanine thin film and various oxidizing gases for sensor applications, Adv. Mater. Res. 403–408 (2012) 48–51.

[28] D. Dini, M. Barthel, M. Hanack, Phthalocyanines as active materials for optical limiting, Eur. J. Org. Chem. 9 (2001) 3759–4376.

[29] E. Llobet, Gas sensors using carbon nanomaterials: a review, Sens. Actuators B. Chem. 179 (2013) 32–45.

[30] J. Kong, N.R. Franklin, C. Zhou, M.G. Chapline, S. Peng, K. Cho, H. Dai, Nanotube molecular wires as chemical sensors, Science 287 (2000) 622–625.

[31] D.R. Kauffman, A. Star, Carbon nanotube gas and vapor sensors, Angew. Chem. Int. Ed. 47 (2008) 6550–6570.

[32] T. Zhang, S. Mubeen, N.V. Myung, M.A. Deshusses, Recent progress in carbon nanotube-based gas sensors, Nanotechnology 19 (2008) 33201.

[33] E.S. Snow, F.K. Perkins, E.J. Houser, S.C. Badescu, T.L. Reinecke, Chemical detection with a single-walled carbon nanotube capacitor, Science 307 (2005) 1942–1945.

[34] M.H. Tang, Z.Q. Zeng, J.C. Li, Z.P. Wang, X.L. Xu, G.Y. Wang, L.B. Zhang, S.B. Yang, Y.G. Xiao, B. Jiang, Resistive switching behavior of La-doped ZnO films for nonvolatile memory applications, Solid-State Electron. 63 (2011) 100–104.

[35] J.L. Blackburn, T.M. Barnes, M.C. Beard, Y.-. Kim, R.C. Tenent, T.J. McDonald, B. To, T.J. Coutts, M.J. Heben, Transparent conductive single-walled carbon nanotube networks with precisely tunable ratios of semiconducting and metallic nanotubes, ACS Nano 2 (2008) 1266–1274.

[36] J.T. Han, S.Y. Kim, J.S. Kim, H.J. Jeong, S.Y. Jeong, G. Lee, Enhanced electrical properties of transparent carbon nanotube/binder hybrid thin films: effects of the silane sol and the bundle size of the carbon nanotubes, Ind. Eng. Chem. Res. 49 (2010) 6416–6421.

[37] L. Cao, H. Chen, H. Zhou, L. Zhu, J. Sun, X. Zhang, J. Xu, M. Wang, Carbon-nanotube-templated assembly of rare-earth phthalocyanine nanowires, Adv. Mater. 15 (2003) 909–913.

[38] R. George, A. Snow, Synthesis of 3-nitrophthalonitrile and tetra-alpha-substituted phthalocyanines, J. Heterocycl. Chem. 32 (1995) 495–498.

[39] J.G. Young, W. Onyebuagu, Synthesis and characterization of di-disubstituted phthalocyanines, J. Org. Chem. 55 (1990) 2155–2159.

[40] N. Kobayashi, R. Higashi, K. Ishii, K. Hatsusaka, K. Ohta, Aggregation, complexation with guest molecules, and mesomorphism of amphiphilic phthalocyanines having four-or eight tri (ethylene oxide) chains, Bull. Chem. Soc. Jpn. 72 (1999) 1263–1271.

[41] H. Yanik, D. Aydin, M. Durmuş, V. Ahsen, Peripheral and non-peripheral tetrasubstituted aluminium, gallium and indium phthalocyanines: Synthesis, photophysics and photochemistry, J. Photochem. Photobiol. A 206 (2009) 18–26.

[42] S.S. Erdem, I.V. Nesterova, S.A. Soper, R.P. Hammer, Solid-phase synthesis of asymmetrically substituted AB 3-Type phthalocyanines, J. Org. Chem. 73 (2008) 5003–5007.

[43] D. Atilla, N. Saydan, M. Durmuş, A.G. Gürek, T. Khan, A. Rück, H. Walt, T. Nyokong, V. Ahsen, Synthesis and photodynamic potential of tetra- and octa-triethyleneoxysulfonyl substituted zinc phthalocyanines, J. Photochem. Photobiol. A 186 (2007) 298–307.

[44] D. Perrin, W. Armarego (Eds.), Purification of Laboratory Chemicals, 192, 2nd ed., Pergamon Press, Oxford, 1989, p. 334.

[45] A. Nabok, A. Tsargorodskaya, The method of total internal reflection ellipsometry for thin film characterisation and sensing, Thin Solid Films 516 (2008) 8993–9001.

[46] A.V. Nabok, A. Tsargorodskaya, A.K. Hassan, N.F. Starodub, Total internal reflection ellipsometry and SPR detection of low molecular weight environmental toxins, Appl. Surf. Sci. 246 (2005) 381–386.

[47] R.M.A. Azzam, The intertwined history of polarimetry and ellipsometry, Thin Solid Films 519 (2011) 2584–2588.

[48] H. Banimuslem, A. Hassan, T. Basova, M. Durmuş, S. Tuncel, A. Esenpınar, A. Gürek, V. Ahsen, Copper phthalocyanine functionalized single-walled carbon nanotubes: thin films for optical detection, J. Nanosci. Nanotechnol. 15 (2015) 2157–2167.

[49] J. Liu, A.G. Rinzler, H. Dai, J.H. Hafner, R.K. Bradley, P.J. Boul, A. Lu, T. Iverson, K. Shelimov, C.B. Huffman, F. Rodriguez-Macias, Y. Shon, T.R. Lee, D.T. Colbert, R.E. Smalley, Fullerene pipes, Science 280 (1998) 1253–1256.

[50] T.V. Basova, M. Çamur, A.A. Esenpınar, S. Tuncel, A. Hassan, A. Alexeyev, H. Banimuslem, M. Durmuş, A.G. Gürek, V. Ahsen, Effect of substituents on the orientation of octasubstituted copper (II) phthalocyanine thin films, Synth. Met. 162 (2012) 735–742.

[51] T. Mugadza, T. Nyokong, Synthesis and characterization of electrocatalytic conjugates of tetraamino cobalt (II) phthalocyanine and single wall carbon nanotubes, Electrochim. Acta 54 (2009) 6347–6353.

[52] N. He, Y. Chen, J. Bai, J. Wang, W.J. Blau, J. Zhu, Preparation and optical limiting properties of multiwalled carbon nanotubes with -conjugated metal-free phthalocyanine moieties, J. Phys. Chem. C 113 (2009) 13029–13035.

[53] Z. Yang, H. Pu, J. Yuan, D. Wan, Y. Liu, Phthalocyanines-MWCNT hybrid materials: Fabrication, aggregation and photoconductivity properties improvement, Chem. Phys. Lett. 465 (2008) 73–77.

Wang, N. Hu, Z. Zhou, D. Xu, Z. Wang, Z. Yang, H. Wei, E.S. Kong, Y. Zhang, ngle-walled carbon nanotube/cobalt phthalocyanine derivative hybrid mate- l: Preparation, characterization and its gas sensing properties, J. Mater. em. 21 (2011) 3779–3787.
Hernández, M. García-Gutiérrez, D.R. Rueda, T.A. Ezquerra, R.J. Davies, Influ- ce of single wall carbon nanotubes and thermal treatment on the morphology polymer thin films, Composites Sci. Technol. 72 (2012) 421–427.
Boon, S. Desbief, L. Cutaia, O. Douhéret, A. Minoia, B. Ruelle, S. Clément, O. ulembier, J. Cornil, P. Dubois, R. Lazzaroni, Synthesis and characterization nanocomposites based on functional regioregular poly(3-hexylthiophene) d multiwall carbon nanotubes, Macromol. Rapid Commun. 31 (2010) 1427– 34.
Banimuslem, A. Hassan, T. Basova, A.D. Gülmez, S. Tuncel, M. Durmuş, . Gürek, V. Ahsen, Copper phthalocyanine/single walled carbon nanotubes brid thin films for pentachlorophenol detection, Sens. Actuators B. Chem. 0 (2014) 990–998.
D. Boscher, T. Bohn, P. Heier, F. Moisy, B. Untereiner, K. Heinze, P. Choquet, ptical sensing responses of $Cr^{III}Cl(TPP)(H_2O)$-based coatings obtained by an mospheric pressure plasma method–Application to the detection of volatile nines, Sens. Actuators B. Chem. 191 (2014) 553–560.
M. Charlesworth, C.A. McDonald, A fibre-optic fluorescing sensor for amine pours, Sens. Actuators B Chem. 8 (1992) 137–142.
G. Na, H. Kim, H. So, K. Kong, H. Chang, B.H. Ryu, Y. Choi, J. Lee, B. Kim, J. m, J. Kim, Investigation of the humidity effect on the electrical properties of ngle-walled carbon nanotube transistors, Appl. Phys. Lett. 87 (2005) 093101.
Sung, S. Hong, Y. Kim, N. Park, S. Kim, S.L. Maeng, K. Kim, Ab initio study of e effect of water adsorption on the carbon nanotube field-effect transistor, pl. Phys. Lett. 89 (2006) 243110.
Liu, X. Ye, K. Wu, R. Han, Z. Zhou, T. Cui, Humidity sensitivity of multi-walled rbon nanotube networks deposited by dielectrophoresis, Sensors. 9 (2009) 14–1721.
Adjizian, R. Leghrib, A.A. Koos, I. Suarez-Martinez, A. Crossley, P. Wagner, N. robert, E. Llobet, C.P. Ewels, Boron- and nitrogen-doped multi-wall carbon notubes for gas detection, Carbon 66 (2014) 662–673.
Harbeck, C. Tasaltin, I. Gürol, E. Musluolu, V. Ahsen, Z.Z. Öztürk, Preferential rption of polar compounds by fluoroalkyloxy substituted phthalocyanines r the use in sorption based gas sensors, Sens. Actuators B. Chem. 150 (2010) 6–624.

phies

t Banimuslem is a PhD student in the Material and Engineering research e, Sheffield Hallam University, UK. He is currently investigating func- aterials, which include the hybrids of CNT and substituted phthalocyanine les for sensor applications.

Aseel Hassan BSc, MSc, PhD in Physics, is a Senior Lecturer at the Faculty of Arts, Computing Engineering and Sciences of Sheffield Hallam University, UK. He carries out his research within the Materials and Engineering Research Institute and his interest lies in thin film technology mainly for application in chemical and biosensing, as well as for electronic device application. He uses optical techniques such as surface plasmon resonance and spectroscopic ellipsometry, as well as quartz crystal microbalance detection techniques, employing organic thin films such as metallophthalocyanines and calix-resorcinarenes as the sensing layers.

Tamara Basova received her PhD (1999) and DSc (2011) in Physical Chemistry from Nikolaev Institute of Inorganic Chemistry, Novosibirsk, Russia. Now, she is a leading researcher in the institute. Her research interests are mainly directed towards the synthesis and characterization of various phthalocyanines and the investigation of the sensor and electrical properties of their oriented films.

Aliye Aslı Esenpınar BSc, MSc, PhD is an Associated Professor at Kırklareli University, Department of Chemistry in Turkey. Her research interests are the synthesis, characterization, photochemical and photophysical properties of phthalocyanine, coumarin and crown ether compounds.

Sinem Tuncel BSc, MSc, PhD is a Research Assistant at Chemistry Department, Gebze Institute of Technology, Turkey. Her research interests are the synthesis and characterization of phthalocyanines and the investigation of their liquid crystalline, photophysical and photochemical properties.

Mahmut Durmuş BSc, MSc, PhD is an Professor at Gebze Institute of Technology, Department of Chemistry in Turkey. His research interests are the design, synthesis and characterization of advanced materials such as phthalocyanines, borondipyrromethenes (BODIPY), coumarins and phosphazenes for different applications including photodynamic therapy (PDT) of cancer, liquid crystals, energy transfer dyes, chemosensors etc.

Ayşe Gül Gürek BSc, MSc, PhD is a professor at Department of Chemistry of Gebze Institute of Technology Turkey. Her research interests are: the synthesis of stable ligands, e.g. phthalocyanines, *vic*-dioximes with such functional groups as crown ether, aza ether, and thia ether, the synthesis of transition metal complexes and the investigation of their liquid crystal, semiconductor, chemical sensor, NLO and photodynamic therapy properties by enlightening the structure of these macrocyclic compounds.

Vefa Ahsen BSc, MSc, PhD is a professor at the Chemistry Department of Science Faculty at Gebze Institute of Technology Turkey. His research interest lies in the synthesis of stable ligands, e.g. phthalocyanines, vic-dioximes with such functional group as crown ether, aza ether, and thia ether, the synthesis of their alkaline and transition metal complexes as nanomaterials. The main application areas of these materials (gas sensors, photodynamic therapy, catalysis, liquid crystals, semiconductors and NLO) are investigated.

Article

Journal of Nanoscience and Nanotechnology
Vol. 14, 1–11, 2014
www.aspbs.com/jnn

Copper Phthalocyanine Functionalized Single-Walled Carbon Nanotubes: Thin Films for Optical Detection

Hikmat Banimuslem[1], Aseel Hassan[1], Tamara Basova[2,*], Mahmut Durmuş[3], Sinem Tuncel[3], Aliye Aslı Esenpınar[4], Ayse Gül Gürek[3], and Vefa Ahsen[5]

[1] *Materials and Engineering Research Institute, Sheffield Hallam University, Sheffield S1 1WB, UK*
[2] *Nikolaev Institute of Inorganic Chemistry SB RAS, Russia*
[3] *Department of Chemistry, Gebze Institute of Technology, Gebze, Kocaeli, Turkey*
[4] *Department of Chemistry, Kırklareli University, 39100, Kırklareli, Turkey*
[5] *TUBITAK-Marmara Research Center, Materials Institute, Gebze, Kocaeli, Turkey*

Thin films of non-covalently hybridised single-walled carbon nanotubes (SWCNT) and tetra-substituted copper phthalocyanine ($CuPcR_4$) molecules have been produced from their solutions in dimethylformamide (DMF). FTIR spectra revealed the $\pi-\pi$ interaction between SWCNTs and $CuPcR_4$ molecules. DC conductivity of films of acid-treated SWCNT/$CuPcR_4$ hybrid has increased by more than three orders of magnitude in comparison with conductivity of $CuPcR_4$ films. Scanning electron microscopy (SEM) and atomic force microscopy (AFM) measurements have shown that films obtained from the acid-treated SWCNTs/$CuPcR_4$ hybrids demonstrated more homogenous surface which is ascribed to the highly improved solubility of the hybrid powder in DMF. Using total internal reflection ellipsometry spectroscopy (TIRE), thin films of the new hybrid have been examined as an optical sensing membrane for the detection of benzo[a]pyrene in water to demonstrate the sensing properties of the hybrid.

Keywords: Hybrid Materials, Single-Walled Carbon Nanotubes, Metal Phthalocyanine, Thin Films, Spectral Ellipsometry, Optical Detection, Microscopy.

1. INTRODUCTION

Since their discovery by Iijima in 1991,[1] carbon nanotubes (CNTs) have attracted significant interest by researchers around the globe due to their unique electronic, metallic and structural properties.[2–4] In particular single-walled carbon nanotubes (SWNT), having their special quasi-one-dimensional electronic structures and extremely high surface area, provide excellent grounds for unique sensing systems.[5–8] CNTs, both, single-walled (SWCNTs) and multi-walled (MWCNTs) are very important and interesting class of materials which have been mainly produced by chemical vapour deposition (CVD)[9] and were subjected to thorough investigation over the last two decades due to their potential use in commercial applications.[10] The modification of CNT network surface by subjecting them to different chemical treatment and through hybridization with various organic materials has enabled their use in applications such as photovoltaic application[11–14] and chemical detection.[15,16] Their inclusion in composites as well as in hybrid materials has enabled the development of new functional materials with significantly improved mechanical, optical and electronic properties. Among these hybrids, the smart integration of carbon nanotubes (CNT) with metallophthalocyanine (MPc) complexes has gained increasing attention over the past few years. This is currently receiving thorough investigation by several research groups around the world in order to enhance the opto-electronic, electro-catalytic and sensing properties of MPc films.[17–24] The evidence so far has shown that these hybrids are expected to be more efficient in improving the relative response of hybrid films compared to the individual CNT or MPc species.[25–27] The main problem with using CNTs in device fabrication is their insolubility in conventional solvents, which makes them difficult to process as thin films. For instance, thin films incorporating CNTs are optically inert and are dominated by rough surfaces and therefore are not suitable for chemical detection applications using optical transduction methods such as SPR and TIRE.[28,29]

*Author to whom correspondence should be addressed.

Phthalocyanines (Pcs), on the other hand, are two-dimentional 18 π-electron aromatic analogues, having four isoindole subunits connected together through nitrogen atoms.[30,31] Due to their excellent thermal and chemical stability, as well as the high flexibility in having large variety of substitution on the periphery of the molecule's rim, phthalocyanines and their metallo derivatives (MPcs) have attracted strong interest and have been used in a wide range of applications. These include chemical and bio sensors,[29,32] liquid crystals,[24,33,34] photovoltaic cells,[35] field effect transistors,[36,37] electrochromic devices,[38] and memory applications.[39] The opportunity of incorporating about 70 different metal atoms into Pc cavity offers additional features to enhance the physical responses.[40] Furthermore, Pcs are very simple to process in producing homogeneous thin films, mainly using wet technology such as spin coating.[41–44] Application of different phthalocyanine films as active layers in surface plasmon resonance (SPR)[45] and total internal reflection ellipsometry (TIRE)[46] techniques have been widely reported in the literatures.

It is expected that functionalization of SWCNTs with metallophthalocyanine derivatives may overcome the problem of poor optical properties of SWCNTs as well as improving the reversibility and reproducibility of phthalocyanine active layers. The development of CNT/MPc hybrids by noncovalent functionalization is proving to be a promising approach to feasibly incorporating carbon nanotubes into different devices without compromising the electronic structure of the nanotubes.[47]

In this work hybrid thin films have been prepared by combining SWCNT and tetra-substituted copper phthalocyanine $CuPcR_4$ with $R = S(CH_2CH_2O)_3CH_3$ (Fig. 1) molecules. The interaction between the two materials was investigated by using different characterisation methods including SEM, AFM, UV-visible, FTIR and Raman spectroscopy. The phthalocyanines with long alkyl–$X(CH_2)_nCH_3$ or polyoxyalkyl $-X(CH_2)_nCH_3$ (X = S, O) substituents are widely used as chemically sensitive coating materials, and are particularly suitable for detecting various organic compounds by both optical and electrical techniques.[45,48–51] The main aim of current study is to examine the compatibility of thin films produced from SWCNT/MPc hybrids with optical detection techniques, using TIRE method for the detection of analytes dissolved in water.

2. EXPERIMENTAL DETAILS

2.1. Materials

3-nitrophthalonitrile[52] and 3-(4,7,10-trioxaundecane-1-sulfanyl)phthalonitrile[53] were synthesized and purified according to procedures described in the literature. Dimethylformamide (DMF), hexanol, *n*-hexane and dichloromethane (DCM) were dried as described by Perrin and Armarego[54] before use. $CuCl_2$, 1,8-diazabicyclo[5.4.0]undec-7-ene (DBU) and polyethylene glycol monomethyl ether were purchased from Fluka and K_2CO_3 was obtained from Merck. Column chromatography was performed on neutral Al_2O_3. SWCNT (0.7–1.4 nm in diameter) used in this work was purchased from Sigma-Aldrich.

2.2. Preparation of Copper Phthalocyanine

1(4), 8(11), 15(18),22(25)-Tetrakis-[2-(2-(2-methoxyetoxy) ethoxy)ethylthio]phthalocyaninato copper (II) (Fig. 1) was synthesized as following: A mixture of 3-(4,7,10-trioxaundecane-1-sulfanyl)phthalonitrile (0.5 g, 1.6 mmol), anhydrous $CuCl_2$ (0.11 g, 0.81 mmol), dry hexanol (2 ml) and 0.07 ml (0.45 mmol) 1,8-diazabicyclo-[5.4.0]-undec-7-ene (DBU) was stirred and heated at 170 °C for 24 h under argon in a round-bottomed flask. The resulting green suspension was cooled and the product was extracted with *n*-hexane. The waxy green product was purified by column chromatography (neutral Al_2O_3, CH_2Cl_2). The compound is soluble in CH_2Cl_2, $CHCl_3$, tetrahydrofuran (THF), ethanol and methanol. Yield: 0.370 g (74%), IR (ATR) ν_{max} (cm^{-1}): 3060 (aromatic CH), 2912 (aliphatic CH), 1636, 1568, 1464, 1312, 1084, 1024. UV-Vis (THF)

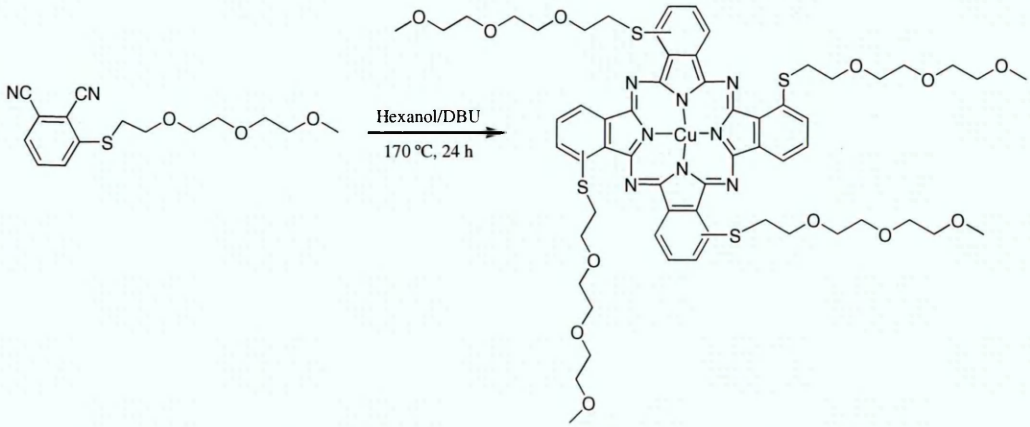

Figure 1. Synthesis route of 1(4),8(11),15(18),22(25)-tetrakis-[2-(2-(2-metoxyetoxy)etoxy)ethylthio]phthalocyaninato copper(II).

λ_{max} (log ε) (nm): 712 (4.93), 339 (4.64). MALDI-TOF-MS m/z: Calcd. for $C_{60}H_{72}N_8O_{12}S_4Cu$: 1289.09, Found 1288.75 $[M]^+$. Thermal stability of the $CuPcR_4$ complex has been investigated by TGA. Decomposition starts at about 250 °C and the main decomposition temperature is 466 °C.

2.3. Preparation of SWCNT-$CuPcR_4$ Hybrids

2.3.1. 1-Pristine SWCNT-$CuPcR_4$ Hybrid (Hybrid 1)

The purpose of this part of the work is to further clarify the effect of acid treatment on improving the binding between SWCNT and $CuPcR_4$ molecules and thus enhancing the solubility of the hybrid in conventional organic solvents such as DMF. 5 mg of $CuPcR_4$ has been dissolved in 1 ml DMF and sonicated for 15 min. At the same time 1mg of pristine (untreated) SWCNTs was suspended in 3 ml DMF and sonicated for 40 min. After sonication, the suspension was stirred and the $CuPcR_4$ solution was added drop wise to the CNTs suspension during stirring. The stirring was continued for another 5 h before the mixture was centrifuged, washed with DMF several times, centrifuged again and finally dried.

2.3.2. 2-Acid-Treated SWCNT-$CuPcR_4$ Hybrid (Hybrid 2)

25 mg SWCNTs was stirred under 70 °C in concentrated 3:1 HNO_3 and H_2SO_4 for 2 h. The mixture was then centrifuged, washed several times with water, centrifuged again and dried. 2 mg of the resultant powder was mixed with 5 mg of $CuPcR_4$ in 5 ml DMF and sonicated for 4 h. The suspension was centrifuged, washed with DMF, centrifuged again and dried. Figure 2 shows the solution of $CuPcR_4$ and the suspensions of SWCNT, SWCNT-$CuPcR_4$ hybrid (hybrid 1) and acid-treated SWCNT-$CuPcR_4$ hybrid (hybrid 2) in DMF. It can be visibly appreciated that hybrid 2 exhibited better solubility than hybrid 1 and for both hybrids the brownish colour indicates that π–π interaction took place between the two materials.[20,55]

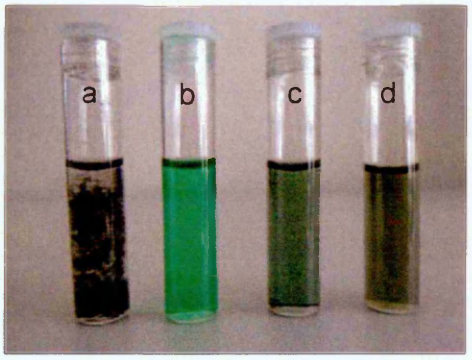

Figure 2. (a) pristine SWCNTs, (b) $CuPcR_4$, (c) hybrid 1, and (d) hybrid 2 in DMF.

2.4. Thin Film Deposition

Silicon substrates were used to deposit thin films to carry out AFM, SEM and ellipsometry measurements. Conductivity measurements on the other hand were performed on films deposited onto interdigitated electrodes with the dimensions L, W and n of 20 μm, 2 mm and 10 respectively, where L is the gap between electrodes, W is the overlapping distance and n is the number of electrodes. For TIRE experiment, gold-coated glass substrate has been prepared by sequentially evaporating 3–5 nm of chromium onto the microscopic slides followed by the evaporation of 25–30 nm of gold layer under vacuum of about 3×10^{-5} mbar. All substrates were washed thoroughly with deionized water and chloroform using ultrasonic bath and finally blown dry using nitrogen gun before use. Thin films of SWCNT-$CuPcR_4$ hybrids as well as $CuPcR_4$ were produced by drop-casting solutions of these materials in DMF using a microsyringe and left to dry in a desiccator for 24 h.

2.5. Characterisation

Thermogravimetric analysis (TGA) of $CuPcR_4$ was carried out on a Mettler Toledo Stare Thermal Analysis System at a rate of 10 °C · min^{-1} in a nitrogen flow (50 ml · min^{-1}). Fourier transform infrared (FTIR) spectra have been recorded using Nexus FTIR for powders over the range of 400–4000 cm^{-1}. Raman spectra were recorded with a Triplemate, SPEX spectrometer equipped with CCD detector in back-scattering geometry. The 488 nm, 40 mW line of an Ar-laser was used for the spectral excitation. UV-Vis absorption spectra were recorded on Varian 50 scan UV-Visible spectrophotometer. Scanning electron microscopy (SEM) images were obtained using FEI-nova nanosem 200, while atomic force microscope (AFM) images were obtained using Nanoscope IIIa multimode atomic force microscope. The experimental set-up for TIRE measurements was built on M2000V (J.A. Woollam Co., Inc.) spectroscopic ellipsometer, operating in the wavelength range 370–1000 nm. Full details of TIRE method and the experimental set-up are found in previous publications.[56,57] The measured ellipsometric data were fitted to the model for organic films. DC-conductivity measurements were carried out using Keithley 4200 semiconductors characterization system.

3. RESULTS AND DISCUSSION

3.1. Characterisation of SWCNT-$CuPcR_4$ Hybrids

Pristine and acid treated SWCNT were used for hybrids preparation. Pristine SWCNTs were oxidized by means of a mixture of sulfuric and nitric acid. This procedure introduces carboxylic acid functionalities and defects at the ends of the nanotubes as well as some carboxylic acid units at the sidewalls.[58–60]

FTIR analysis was carried out in order to determine the interaction between $CuPcR_4$ and SWCNTs. Figure 3 shows

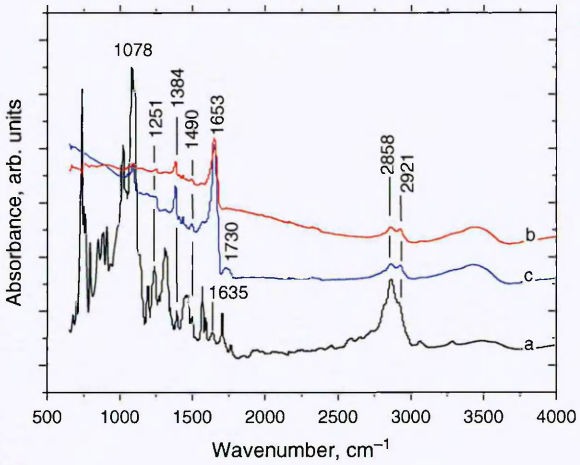

Figure 3. FTIR spectra of (a) pure $CuPcR_4$, (b) hybrid 1 and (c) hybrid 2.

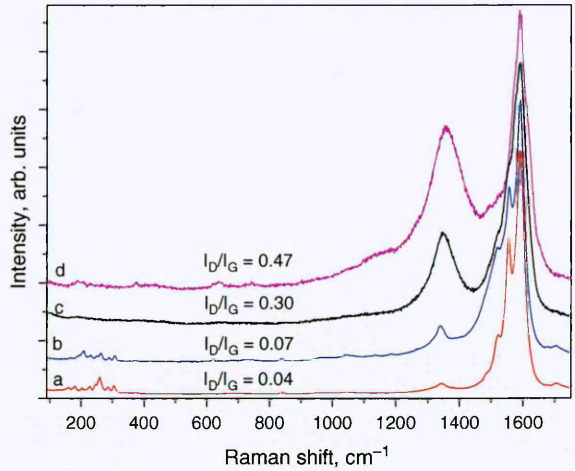

Figure 4. Raman spectra of pristine SWCNT (a), hybrid 1 (b), acid-treated SWCNT (c) and hybrid 2 (d).

FTIR spectra of pure $CuPcR_4$, SWCNT-$CuPcR_4$ (hybrid 1) and acid treated SWCNT-$CuPcR_4$ (hybrid 2). The bands at 2858 and 2921 cm^{-1} assigned to the C—H stretches of substitution groups in $CuPcR_4$ are present in all spectra. Another feature that should be given attention is the peaks at 1490, 1384, 1251 and 1078 cm^{-1}, which are characteristics of phthalocyanine macrocycles,[27] and are present in all three spectra. All these observations suggest that the substituted copper phthalocyanine has successfully anchored onto SWCNT walls by means of noncovalent binding. The spectra of the hybrids contain some bands which correspond to $CuPcR_4$ molecule vibrations. The largest shift in the peak position associated with the C=C stretching mode from 1635 cm^{-1} in the spectrum of pure $CuPcR_4$to 1653 cm^{-1} is observed in the hybrids spectra. These shifts as well as different ratio of intensities may result from the electron delocalization due to the π–π interactions between SWCNTs and $CuPcR_4$ molecules.[20,61] The spectrum of hybrid 2 shows a band at around 1730 assigned to ν(C=O) vibration of carboxylic group, which results from the acidification of carbon nanotubes in hybrid 2.[16,62]

The non-covalent attachment can be also confirmed by Raman spectroscopy. Raman spectra for pristine SWCNT, acid treated SWCNT and both hybrids are shown in Figure 4. The radial breathing modes (RBM), disorder D mode and tangential/graphite mode (G-band) are monitored as indicators of functionalisation with $CuPcR_4$.[63] The spectra were normalized to the tangential G band at ~1580 cm^{-1}. Both spectra of pristine SWCNT before (Fig. 4(a)) and after (Fig. 4(b)) hybridization contained the following characteristic peaks: the D band located at about 1340 cm^{-1} (disorder mode), which is due to breathing modes of sp^2 atoms in rings[64–66] and the G band centered at 1590 cm^{-1} (tangential mode), due to bond stretching of all pairs of sp^2 atoms in both rings and chains.[67]

Comparing Figure 4(a) with Figure 4(b), little variation of the ratio of the D band to the G band (I_D/I_G) can be observed, which suggested that $CuPcR_4$ derivatives associated with the surface of SWCNT through non-covalent modification. Moreover, the multiple peaks observed in the radial breathing mode (RBM) of SWCNT (158–304 cm^{-1}) could be ascribed to a distribution of diameters in the SWCNT samples.[68,69] They correspond to nanotube diameters in the range from 0.7 to 1.4 nm.

The Raman spectra of the noncovalently functionalized SWCNT-$CuPcR_4$ revealed significant shift on the peak positions located in the range 158–225 cm^{-1}. For example, the RBMs at 202, 227 and 258 cm^{-1} of SWCNT have a shift to 207, 230 and 262 cm^{-1} after of $CuPcR_4$ adsorption. It was shown[70] that the radial breathing modes of the Raman spectrum are sensitive to the adsorption coating of the nanotubes with polynuclear aromatic hydrocarbon molecules. The π–π stacking interaction between SWNTs and phthalocyanine aromatic rings induced a higher frequency shift of RBM and give a kind of mode "hardening effect."[71]

In the Raman spectrum of the acid-treated SWCNTs, the radial breathing modes have disappeared when compared to the spectrum of pristine SWCNTs (Fig. 4(c)). The decay of these modes is consistent with the disruption of the oscillator strength that gives rise to these modes. Similar results were reported by Fantini et al.,[72] where spectral shifts, broadening, and reduction in RBM intensity were attributed to displacement of the Fermi level due to the added functional group on the CNT side-wall.

As shown in Figure 4(c), the carboxylated SWCNT showed the characteristic peaks with a disorder-induced D-band at 1348 cm^{-1} and a tangential stretch G-band at 1588 cm^{-1}. The D/G peak intensity ratio increases from 0.04 for pristine SWCNT to 0.30 for acid treated SWCNT which indicates the formation of covalent bonds at the surface of the carbon nanotube through conversion of sp^2-hybridized carbon atoms to sp^3-hybridized carbons

on the nanotube surface. The relative decrease in the tangential mode (G-band) is consistent with the loss of electronic resonance as a result of the covalent attachment of the substituent. Further increase in the relative intensity of the D band versus G band ($I_D/I_G = 0.47$) was also observed in the spectrum of acid treated SWCNT hybrids with $CuPcR_4$ (Fig. 4(d)). Raman spectra of the other functionalized SWCNT materials display similar modifications but to different degrees.[73,74]

The Raman spectra of the hybrids with acid treated SWCNT are significantly affected by the interaction with $CuPcR_4$, whereas those with pristine SWCNT do not vary so much upon the addition of the $CuPcR_4$ binder. The I_D/I_G ratios of the hybrids with pristine SWCNT increase only slightly with the addition of the phthalocyanine, whereas those with acid treated SWCNT increase significantly. It might be that, in the bundled network structure of the hybrids with pristine SWCNT, the π–π interactions between nanotubes and $CuPcR_4$ are the dominant influence on the Raman spectrum. However, in the case of the hybrids with acid treated SWCNT, not only π–π interaction but also van der Waals interaction of –COOH groups with the nitrogen atoms of phthalocyanine ring[75] and alkyl substituents of phthalocyanine ring[62] are the factors affecting the Raman spectra.

The interaction between the $CuPcR_4$ and the SWCNTs can also be inferred from the analysis of optical absorption spectra. UV-Vis absorption spectra of solutions of pure $CuPcR_4$, pristine SWCNT, hybrid 1 and hybrid 2 in DMF are shown in Figure 5. The spectrum of SWCNT is featureless as it was frequently reported in the literature.[23,76] On the other hand, the $CuPcR_4$ exhibited typical electronic absorption spectra with two characteristic regions of peaks: the Q-band in the wavelength range 600–750 nm and the Soret (B) band in the wavelength range of 300–450 nm. The Q-band, which results from HOMO–LUMO transitions, is split into two peaks: one at 705 nm is associated with the monomer absorption and the second at 631 nm is resulting from aggregates absorption.[29,77] The aggregates absorption can be attributed to absorption by dimers or even higher aggregation.[78] In the absorption spectra of hybrid 1 and hybrid 2, the peak maxima of the Q-bands shifted to the red by $\Delta\lambda = 5$ nm and $\Delta\lambda = 11$ nm, respectively. As a consequence of the electronic interactions with SWCNTs, Pc is usually regarded as the electron donor, while CNTs as electron acceptor.[22] The absorption band in the spectra of hybrid 2 is broadened; this change might account for the strong π–π interaction between SWCNTs and $CuPcR_4$ derivative, which significantly reduces the aggregation of the hybrid and hence changes the absorption.[27]

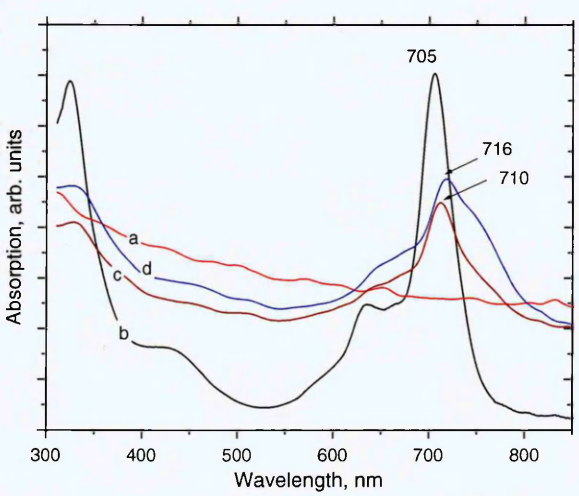

Figure 5. UV-Vis absorption spectra of (a) SWCNTs, (b) $CuPcR_4$, (c) hybrid 1 and (d) hybrid 2 in DMF.

3.2. Investigation of SWCNT-$CuPcR_4$ Films

3.2.1. Morphology

Figures 6(a)–(d) shows the SEM images of pristine SWCNT, acid-treated SWCNT, hybrid 1 and hybrid 2, respectively. Pristine CNTs typically tend to bundle together (Figs. 6(a) and (c)) and to aggregate due to van der Waals attraction between individual tubes[79] as well as the high length to diameter ratio; this makes them hard to disperse in common organic solvents. Acid treatment of the nanotubes provides the de-bundling effect (Figs. 6(b) and (d)) disrupting the van der Waals interactions and leading to the formation of a composite with much improved solubility in DMF and hence smoother films were obtained to perform optical investigation.

AFM measurements in tapping mode have been performed on all samples in this study. Figure 7(a) shows typical fibre features of $CuPcR_4$ film, which is different from the topology of its hybrids. Phthalocyanine and almost all organic dyes tend to make very dense aggregations in the solid state. These aggregates are represented as a coplanar association of rings developing from monomer to dimer and higher order complexes and are driven by π–π interaction and van der Waals forces.[22] It can clearly be seen that surface of hybrid 1 film (image b) is less homogeneous than that of hybrid 2 (images c) with significant decrease in main roughness of the latter; this is because hybrid 2 exhibited improved solubility in DMF, resulting in more homogeneous films. Roughness analysis of AFM images is summarized in Table I.

3.2.2. Electrical Conductivity

The films of hybrid 1 and hybrid 2 as well as $CuPcR_4$ were deposited onto interdigitated electrods by drop-casting from their solutions in DMF (0.5 mg/ml). The I–V characteristics of the films were performed using Keithley 4200 semiconductor characterisation system in the voltage range 0–5 V. The conductivity (σ) was calculated using the following relation:

$$\sigma = L/RtWn \quad (1)$$

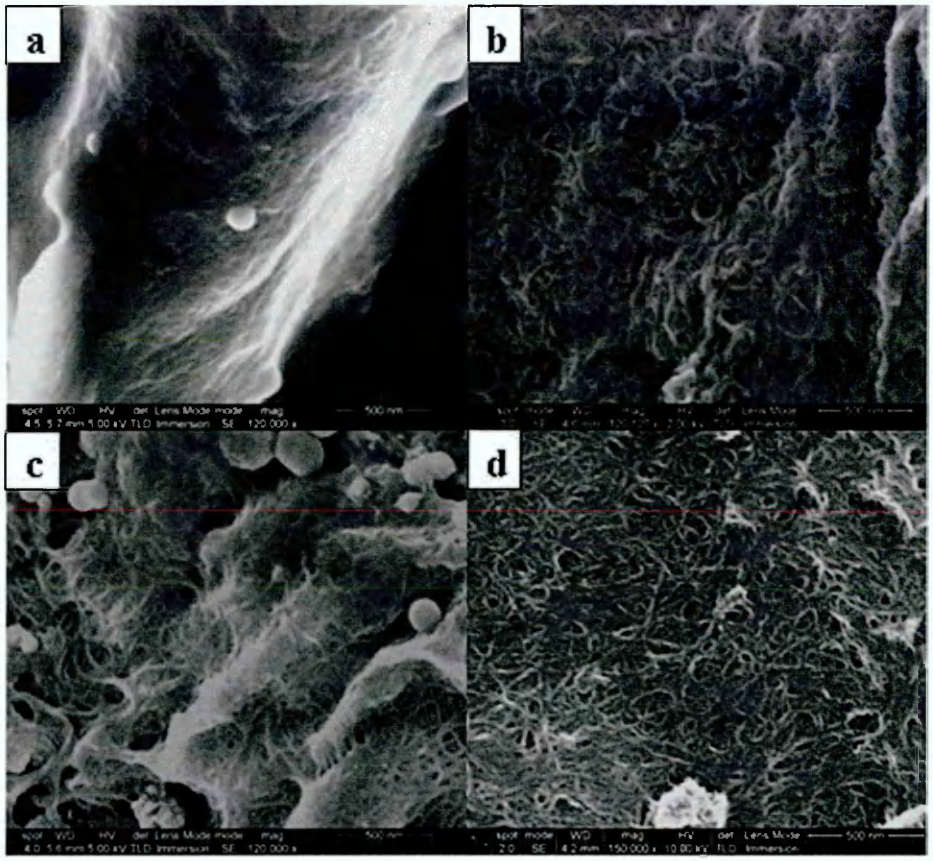

Figure 6. SEM images for (a) pristine (b) Acid-treated SWCNT, (c) hybrid 1 and (d) hybrid 2 thin film deposited on silicon substrates.

where L, W and n are as defined in section 2.4, R is the film's resistance as derived for the I–V curves (not given) and t is the film's thickness. Values of conductivity obtained for all films studied are summarised in Table I. From this table it can be seen that the conductivity increases by three orders of magnitude in the case of hybrid 2 film in comparison with the pure $CuPcR_4$ films. The large increase in conductivity of the hybrid films can be ascribed to the large SWCNT/CuPc conjugated π–π system.[80,81] Consequently, charge can favorably transfer from CuPc molecules to SWCNTs resulting in a large increase in conductivity. On the other hand, hybrid 1 exhibited very high conductivity (samples demonstrated short circuit in our measuring system) in almost all prepared samples. Pristine CNTs are typically composed of metallic and semiconducting nanotubes and their separation has been a serious obstacle in many applications and research.[12,82] Yang et al.[83] have reported that the acid treatment of SWCNT separates the semiconducting from the metallic phases. It has been shown that the majority of metallic CNTs with smaller diameters (typically ≤ 1.1 nm) will be etched way as a result of acid treatment, whereas those with larger diameters are significantly reduced leaving the semiconducting nanotubes intact.[83]

3.3. Total Internal Reflection Ellipsometry (TIRE)

Using total internal reflection ellipsometry spectroscopy (TIRE), thin films of the new hybrid have been examined as an optical sensing membrane for the detection of benzo[a]pyrene in water to demonstrate the sensing properties of the hybrid. It is known that benzo[a]pyrene is a product derived from incomplete combustion of organic material and is considered responsible for chemically-induced cancer in humans.[84]

The spectra of two ellipsometric parameters Ψ and Δ, representing, respectively, the amplitude ratio $tg(\Psi) = A_p/A_s$ and phase shift $\Delta = \phi_p - \phi_s$ between p- and s-components of polarised light reflected form a surface, were recorded with the M2000V instrument in the 350–1000 nm spectral range using the rotating analyzer principle. Optical parameters of the reflection system, i.e., thicknesses, refractive indices and extinction coefficients of the substrate and adsorbed layers, can be obtained by solving the reverse ellipsometric problem numerically:

$$tg(\Psi)\exp(i\Delta) = R_p/R_s \tag{2}$$

where R_p and R_s are Fresnel reflection coefficients for p- and s-components of polarized light related to the parameters of reflection system, particularly the thickness (d),

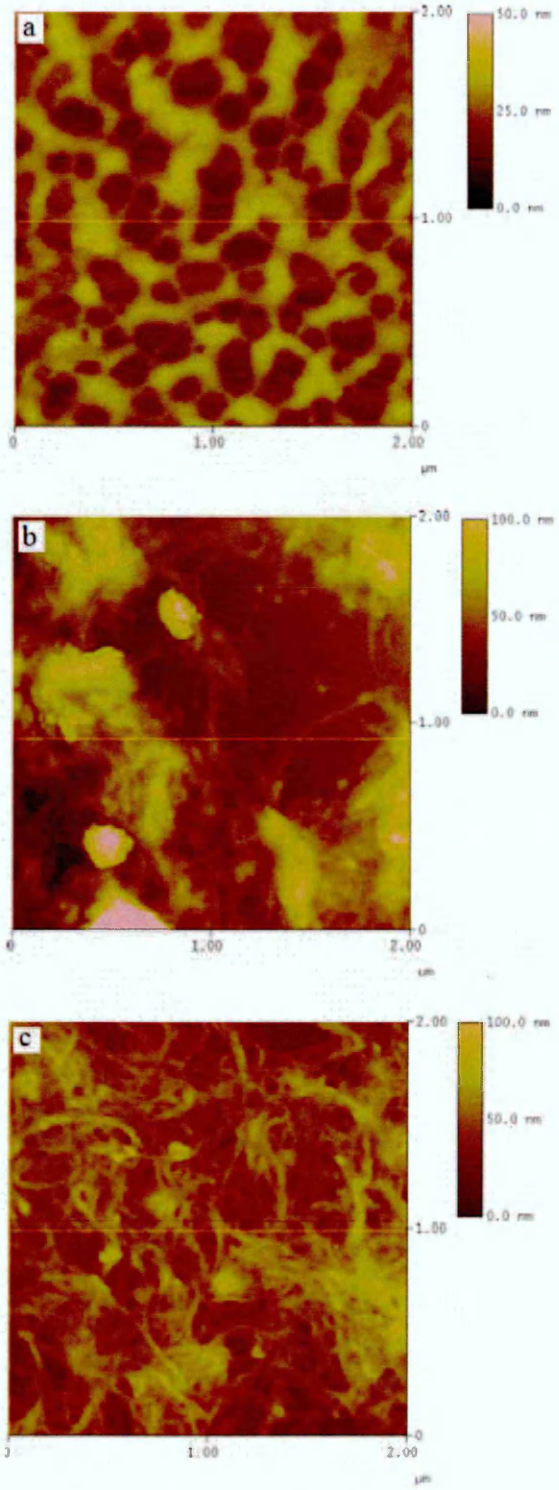

Figure 7. Atomic force microscopy images of (a) $CuPcR_4$, (b) hybrid 1 and (c) hybrid 2 films. Roughness analysis are shown below.

refractive index (n) and extinction coefficient (k) of the adsorbed layers, via Fresnel equations.[85] The fitting is performed by solving Fresnel equations many times for different values of n, k and d and subsequently minimizing

Table I. DC-conductivity, roughness analysis and experimental data fitting (films' thicknesses, refractive indexes and extinction coefficient), the optical properties is at 632.22 nm wavelength.

	$CuPcR_4$	Hybrid 1	Hybrid 2
Electrical conductivity			
σ, Ω^{-1} m^{-1}	1.67×10^{-4}	S/C	7.54×10^{-1}
Roughness parameters			
R_a, nm	1.733	8.213	5.811
RMS, nm	3.501	15.575	9.550
R_{max}, nm	8.461	37.570	20.275
Before exposure			
d, nm	97.86	–	147.73
N	1.532	–	1.334
K	0.373	–	0.133
Ellipsometry fitting parameters			
d, nm	98.1	–	149.49
After exposure			
N	1.542	–	1.359
K	0.377	–	0.135

the error function of the experimental and theoretical (calculated) values of Ψ and Δ using one of least-square techniques. Commercial WVASE32® software is provided by J.A. Woollam Co., Inc. for this task. Figure 8 shows the typical TIRE spectra of Cr/Au films used in the present work. The spectrum of $\Psi(\lambda)$, demonstrating the amplitude ratio of A_p/A_s, resembles very much the conventional surface plasmon resonance (SPR) curve, while the spectrum of $\Delta(\lambda)$ is associated with the phase shift between p- and s-components of polarized light. The latter changes sharply from 270° down to −90° near the plasmon resonance. According to Arwin's modelling,[86] the position of the sharp drop in $\Delta(\lambda)$ spectrum is about 10 times more sensitive to analytes adsorption than $\Psi(\lambda)$ spectrum.

To examine the compatibility of the hybrids prepared in this work with TIRE technique, small volumes of solutions of $CuPcR_4$, hybris 1 and hybrid 2 in DMF were drop-casted onto the gold-coated glass substrates by using microcyrenge. Thereafter, the samples were exposed to

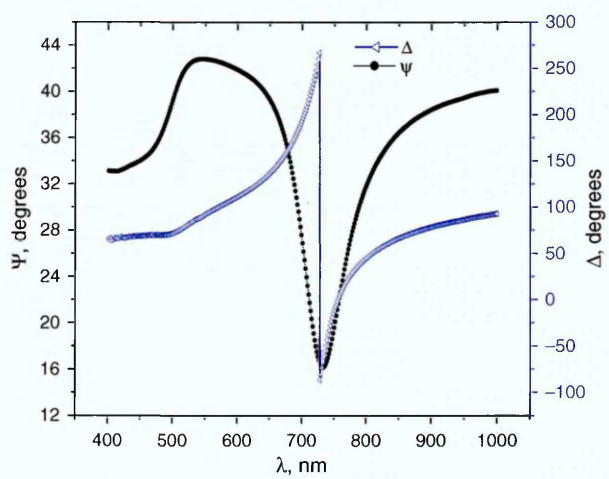

Figure 8. Typical TIRE spectra of Cr/Au film.

deionized water and saturated solution of benzo[a]pyrene in water (6.2 μg/l) to demonstrate the changes of ellipsometry spectra and thus films' optical parameters induced by the adsorption of benzo[a]pyrene onto the films surfaces. It is worthwhile mentioning that the films of hybrid 1 were shown to be rough and inhomogeneous and therefore unsuitable for optical investigation, as it has not given well-resolved spectra when measured by spectroscopic ellipsometry. On the other hand, thin films prepared from hybrid 2 exhibited much smoother surfaces and has therefore shown significant enhancement in the adsorption properties as active optical sensing layer. Figure 9 shows the spectra of $\Psi(\lambda)$ and $\Delta(\lambda)$ of $CuPcR_4$ and hybrid 2 thin films before and after exposure to benzo[a]pyrene. The initial response time of the studied layers was a fraction of minute but the spectra were measured 5 min after injection of contaminated water in order to achieve equilibrium. During exposure to contaminated water, it was difficult to detect shifts in $\Psi(\lambda)$ because of the shape of the curve, however, significantly larger shifts have been observed in $\Delta(\lambda)$ spectra. These are typical features of TIRE method as reported earlier.[29,46,57] The spectra of $\Delta(\lambda)$ were further enlarged and shown at the bottom of Figure 9 to provide better assessment of the effect of benzo[a]pyrene exposures. It can clearly be seen that the adsorption of benzo[a]pyrene on hybrid 2 film has resulted in larger shift (9.55 nm) than that shown by pure $CuPcR_4$ (4.6 nm) under exposure to saturated benzo[a]pyrene solution in water. Carbon nanotubes in general are characterised with uniform surface with delocalised π-electrons of high density, which enhances their adsorption properties, especially for analytes with aromatic molecules.[87] It is necessary to emphasise that the aim of the present work is to investigate the suitability of functionalized CNTs as sensing active layers which are compatible with optical techniques such as TIRE. Therefore the work does not examine effects of different concentrations of this analyte as well as different range of other related analytes. This is the subject of continuing study and the results will be published in a separate article. The parameters of organic films before and after exposure to benzo[a]pyrene solution in water were determined by fitting experimental Ψ and Δ spectra to the theoretical organic model by fixing Cr/Au layer parameters. Table I summarises the thickness of all layers found from theoretical data fitting as well as the values of refractive index and extinction coefficients given at $\lambda = 632$ nm. The data in Table I shows an increase in film thickness as well as optical parameters (n and k) for both films. The increase in films' thickness in the case of hybrid 2 was more significant which is probably due to the predominant surface interaction of the analyte with SWCNT/$CuPcR_4$ films. Further to the data summarised in Table I the variation in refractive index and extinction coefficient as a function of λ for both films in pure water and benzo[a]pyrene solution media are shown in Figure 10.

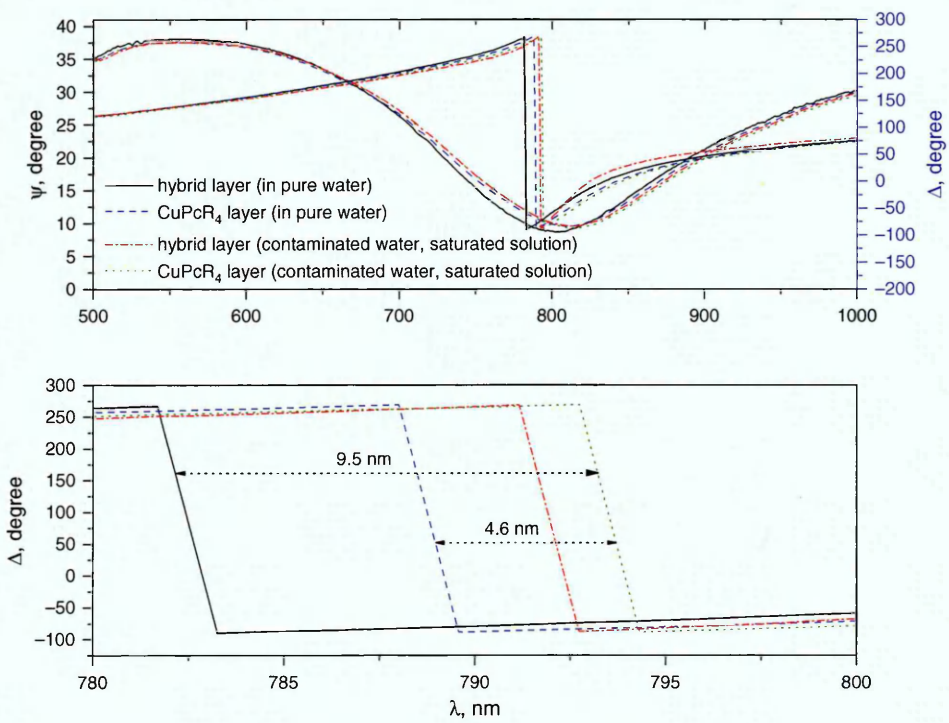

Figure 9. $\Psi(\lambda)$ and $\Delta(\lambda)$ TIRE spectra of $CuPcR_4$ film in water (dashed line); after injection of benzo[a]pyrene saturated solution (dotted line). Hybrid 2 films in water (solid line); after injection of benzo[a]pyrene saturated solution (dashed-dotted line). An enlarged section of $\Delta(\lambda)$ spectra are shown at the bottom of the figure.

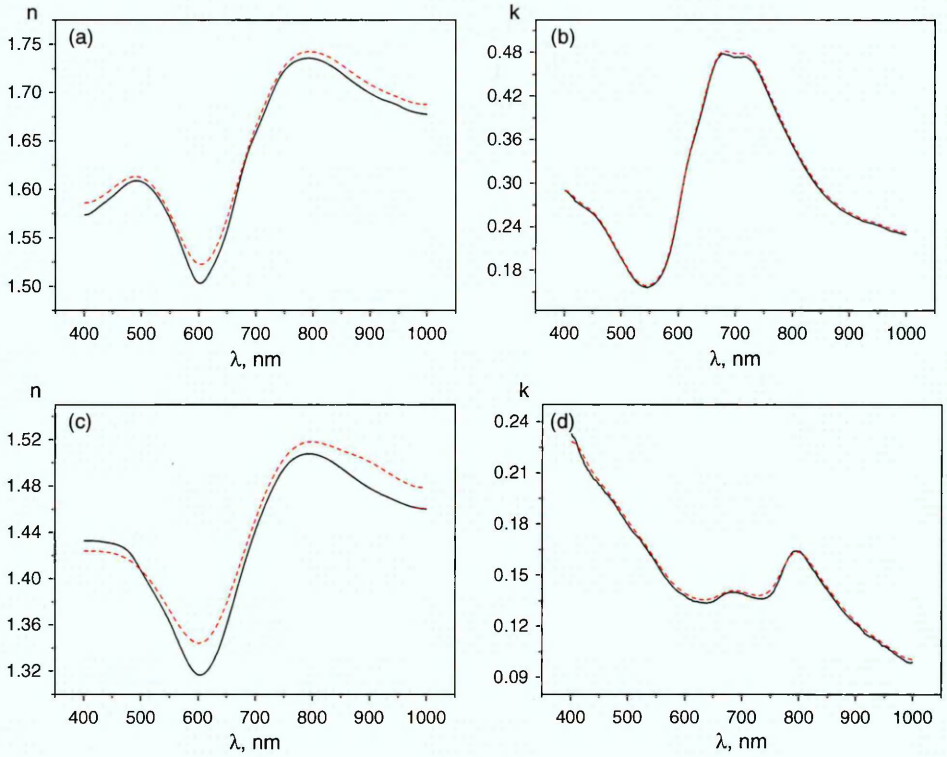

Figure 10. Refractive index (n) and extinction coefficient (k) of $CuPcR_4$ film (a) and (b) and hybrid 2 film (c) and (d) in pure water (solid line) and benzo[a]pyrene solution (dashed line).

4. CONCLUSION

Hybrid structures of single-walled carbon nanotubes and $CuPcR_4$ have been prepared. FTIR and Raman spectra have shown that non-covalent binding between $CuPcR_4$ and SWCNTs has been significantly enhanced as a result of acid treatment of CNTs. Using SEM and AFM measurements morphology of the films is found to be highly dependent on the solubility of the hybrid which is determined by the method used to produce the hybrid structure. The acid-treatment of CNTs is found to result in the separation of bundled carbon nanotubes, leading to enhanced π–π interaction formation in the SWCNT/$CuPcR_4$ system. Thin films of acid-treated SWCNT/$CuPcR_4$ hybrid exhibited much higher conductivity than $CuPcR_4$ and improved films' homogeneity has enabled the use of such hybrids as optically active sensing layers for the detection of pollutants in water. The response of acid-treated SWCNT/$CuPcR_4$ hybrid films to the presence of benzo[a]pyrene in water was shown to be two times larger than that demonstrated by $CuPcR_4$ films. This work is in continuation in order to further examine the interaction of thin films of such hybrids with different analytes, both in water and in ambient air, as well as examining a range of different pollutants' concentrations.

Acknowledgments: Hikmat Banimuslem wishes to acknowledge the financial support from the Higher Committee for Education Development in Iraq (HCED). The authors acknowledge the financial support through the bilateral project between the Scientific and Technological Research Council of Turkey (TUBITAK, Project number: 108M384) and the Russian Foundation of Basic Research (RFBR, Project numbers: 12-03-91372-CT_a).

References and Notes

1. S. Iijima, *Nature* 354, 56 (**1991**).
2. Y. Ji, Y. Y. Huang, and E. M. Terentjev, *Langmuir* 27, 13254 (**2011**).
3. S. E. Khadem, M. Rasekh, and A. Toghraee, *Appl. Math. Model* 36, 2329 (**2012**).
4. J. Liu, Y. Wang, Z. Qu, and X. Fan, *Opt. Laser Technol.* 44, 960 (**2012**).
5. M. P. Siswana, K. I. Ozoemena, and T. Nyokong, *Electrochim. Acta* 52, 114 (**2006**).
6. J. Pillay and K. I. Ozoemena, *Chem. Phys. Lett.* 441, 72 (**2007**).
7. J. Francisco Silva, S. Griveau, C. Richard, J. H. Zagal, and F. Bedioui, *Electrochem. Commun.* 9, 1629 (**2007**).
8. K. I. Ozoemena, D. Nkosi, and J. Pillay, *Electrochim. Acta* 53, 2844 (**2008**).
9. J. Kong, C. Zhou, A. Morpurgo, H. T. Soh, C. F. Quate, C. Marcus, and H. Dai, *Appl. Phys. A* 69, 305 (**1999**).
10. M. F. L. De Volder, S. H. Tawfick, R. H. Baughman, and A. J. Hart, *Science* 339, 535 (**2013**).
11. S. B. Yang, B.-S. Kong, D.-H. Jung, Y.-K. Baek, C.-S. Han, S. K. Oh, and H.-T. Jung, *Nanoscale* 3, 1361 (**2011**).
12. J. L. Blackburn, T. M. Barnes, M. C. Beard, Y.-H. Kim, R. C. Tenent, T. J. McDonald, B. To, T. J. Coutts, and M. J. Heben, *ACS Nano* 2, 1266 (**2008**).

13. A. Kaniyoor and S. Ramaprabhu, *J. Nanosci. Nanotechnol.* 12, 8323 (**2012**).
14. B. A. Gonfa, M. A. E. Khakani, and D. Ma, *Rev. Nanosci. Nanotechnol.* 1, 22 (**2012**).
15. C. G. de Jesus, V. dos Santos, C. G. Canestraro, V. Zucolotto, S. T. Fujiwara, Y. Gushikem, K. Wohnrath, and C. A. Pessoa, *J. Nanosci. Nanotechnol.* 11, 3499 (**2011**).
16. B. Wang, X. Zhou, Y. Wu, Z. Chen, and C. He, *Sensor Actuat. B.-Chem.* 171, 398 (**2012**).
17. G. Cardenas-Jiron, P. Leon-Plata, D. Cortes-Arriagada, and J. M. Seminario, *J. Phys. Chem. C* 115, 16052 (**2011**).
18. H. Li, Z. Xu, K. Li, X. Hou, G. Cao, Q. Zhang, and Z. Cao, *J. Mater. Chem.* 21, 1181 (**2011**).
19. I. Kruusenberg, L. Matisen, and K. Tammeveski, *J. Nanosci. Nanotechnol.* 13, 621 (**2013**).
20. Y. Wang, N. Hu, Z. Zhou, D. Xu, Z. Wang, Z. Yang, H. Wei, E. S. Kong, and Y. Zhang, *J. Mater. Chem.*, 21, 3779 (**2011**).
21. W. Chidawanyika and T. Nyokong, *Carbon* 48, 2831 (**2010**).
22. N. He, Y. Chen, J. Bai, J. Wang, W. J. Blau, and J. Zhu, *J. Phys. Chem. C* 113, 13029 (**2009**).
23. T. Mugadza and T. Nyokong, *Electrochim. Acta* 54, 6347 (**2009**).
24. N. Kilinc, A. S. Ahsen, D. Atilla, A. G. Gürek, S. E. San, Z. Z. Oztürk, and V. Ahsen, *Sens. Lett.* 6, 607 (**2008**).
25. J. Pillay and K. I. Ozoemena, *Electrochim. Acta* 54, 5053 (**2009**).
26. F. C. Moraes, D. L. C. Golinelli, L. H. Mascaro, and S. A. S. MacHado, *Sensor Actuat. B-Chem.* 148, 492 (**2010**).
27. Z. Yang, H. Pu, J. Yuan, D. Wan, and Y. Liu, *Chem. Phys. Lett.* 465, 73 (**2008**).
28. T. Basova, A. Hassan, F. Yuksel, A. G. Gürek, and V. Ahsen, *Sensor Actuat. B.-Chem.* 150, 523 (**2010**).
29. T. Basova, A. Tsargorodskaya, A. Nabok, A. K. Hassan, A. G. Gürek, G. Gümüs, and V. Ahsen, *Mater. Sci. Eng. C-Biomim.* 29, 814 (**2009**).
30. N. Kobayashi, Phthalocyanine: Properties and Applications, edited by C. C. Leznoff and A. B. P. Lever, VCH Publishers Ltd., Cambridge (**1993**), Vol. 2, p. 97.
31. N. Kobayashi, *Curr. Opin. Solid St. M.* 4, 345 (**1999**).
32. L. M. P. C. Centurion, W. C. Moreira, and V. Zucolotto, *J. Nanosci. Nanotechnol.* 12, 2399 (**2012**).
33. D. Atilla, A. G. Gürek, T. V. Basova, V. G. Kiselev, A. Hassan, L. A. Sheludyakova, and V. Ahsen, *Dyes Pigments* 88, 280 (**2011**).
34. T. V. Basova, A. Hassan, M. Durmus, A. G. Gürek, and V. Ahsen, *Synth. Met.* 161, 1996 (**2011**).
35. A. Guchhait, S. Das, S. K. Ray, A. J. Pal, *Nanosci. Nanotechnol. Lett.* 5, 13 (**2013**).
36. H. U. Khan, M. E. Roberts, W. Knoll, and Z. Bao, *Chem. Mater.* 23, 1946 (**2011**).
37. S. Liu, W. M. Wang, A. L. Briseno, S. C. B. Mannsfeld, and Z. Bao, *Adv. Mater.* 21, 1217 (**2009**).
38. P. R. Somani and S. Radhakrishnan, *Mater. Chem. Phys.* 77, 117 (**2003**).
39. B. Mukherjee, A. K. Ray, A. K. Sharma, M. J. Cook, and I. Chambrier, *J. Appl. Phys.* 103, 074507 (**2008**).
40. C. G. Claessens, U. Hahn, and T. Torres, *Chem. Rec.* 8, 75 (**2008**).
41. N. S. Panicker, T. G. Gopinathan, I. Dhanya, and C. S. Menon, *J. Phys.-Condens. Mat.* 405, 4556 (**2010**).
42. T. V. Basova, N. M. Kurochkina, A. Y. Tsivadze, and A. K. Ray, *J. Electron. Mater.* 39 145 (**2010**).
43. T. Torres, D. M. Guldi, J. J. Cid, C. G. Claessens, M. Garcia-Iglesias, I. Lopez-Duarte, M. Martinez-Diaz, D. Mate, A. Medina, M. Rodriguez-Morgade, I. Sanchez, and P. Vazquez, *ECS Meeting Abstracts* 2, 1115 (**2008**).
44. T. V. Basova, A. G. Gürek, D. Atilla, A. K. Hassan, and V. Ahsen, *Polyhedron* 26, 5045 (**2007**).
45. T. Basova, E. Kol'tsov, A. K. Ray, A. K. Hassan, A. G. Gürek, and V. Ahsen, *Sensor Actuat. B-Chem.* 113, 127 (**2006**).
46. A. Hassan, T. Basova, F. Yuksel, G. Gümüs, A. G. Gürek, and V. Ahsen, *Sensor Actuat. B-Chem.* 175, 73 (**2012**).
47. M. A. Hamon, J. Chen, H. Hu, Y. Chen, M. E. Itkis, A. M. Rao, P. C. Eklund, and R. C. Haddon, *Adv. Mater.* 11, 834 (**1999**).
48. Z. Z. Oztürk, R. Zhou, V. Ahsen, O. Bekaroglu, and W. Gopel, *Sensor Actuat. B-Chem.* 36, 404 (**1996**).
49. R. Zhou, F. Josse, W. Göpel, Z. Z. Öztürk, and Ö. Bekaro, *Appl. Organomet. Chem.* 10 557 (**1996**).
50. S. Z. Topal, A. G. Gürek, K. Ertekin, D. Atilla, B. Yenigul, and V. Ahsen, *Mater. Chem. Phys.* 121, 425 (**2010**).
51. L. Valli, *Adv. Colloid Interf. Sci.* 116, 13 (**2005**).
52. R. George and A. Snow, *J. Heterocycl. Chem.*, 32, 495 (**1995**).
53. H. Yanik, D. Aydin, M. Durmuş, and V. Ahsen, *J. Photochem. Photobiol. A*, 206, 18 (**2009**).
54. D. Perrin and W. Armarego, Purification of Laboratory Chemicals, Pergamon Press, Oxford (**1989**).
55. W. Feng, Y. Li, Y. Feng, and J. Wu, *Nanotechnology* 17, 3274 (**2006**).
56. A. Nabok and A. Tsargorodskaya, *Thin Solid Films* 516, 8993 (**2008**).
57. A. V. Nabok, A. Tsargorodskaya, A. K. Hassan, and N. F. Starodub, *Appl. Surf. Sci.* 246 381 (**2005**).
58. F. Patolsky, Y. Weizmann, and I. Willner, *Angew. Chem. Int. Ed.* 43, 2113 (**2004**).
59. J. Liu, A. G. Rinzler, H. Dai, J. H. Hafner, R. K. Bradley, P. J. Boul, A. Lu, T. Iverson, K. Shelimov, C. B. Huffman, F. Rodriguez-Macias, Y. Shon, T. R. Lee, D. T. Colbert, and R. E. Smalley, *Science* 280, 1253 (**1998**).
60. P. Diao and Z. Liu, *J. Phys. Chem. B* 109, 20906 (**2005**).
61. S. Singh, S. K. Tripathi, and G. S. S. Saini, *Mater. Chem. Phys.* 112, 793 (**2008**).
62. L. Piao, Q. Liu, and Y. Li, *J. Phys. Chem. C* 116, 1724 (**2012**).
63. K. A. Wepasnick, B. A. Smith, J. L. Bitter, and D. H. Fairbrother, *Anal. Bioanal. Chem.* 396, 1003 (**2010**).
64. B. Ballesteros, G. De La Torre, C. Ehli, G. M. A. Rahman, F. Agulló-Rueda, D. M. Guidi, and T. Torres, *J. Am. Chem. Soc.* 129, 5061 (**2007**).
65. T. Mugadza and T. Nyokong, *Electrochim. Acta* 55, 6049 (**2010**).
66. C. Casiraghi, A. Hartschuh, H. Qian, S. Pliscanec, C. Georgia, A. Fasoli, K. S. Novoselov, D. M. Basko, and A. C. Ferrari, *Nano Lett.* 9, 1433 (**2009**).
67. C. Dyke and J. Tour, *Nano Lett.* 3, 1215 (**2003**).
68. L. Alvarez, G. de la Fuente, A. Righi, S. Rols, E. Anglaret, J. Sauvajol, E. Munoz, W. Maser, A. Benito, and M. Martinez, *Phys. Rev. B* 63, 153401 (**2001**).
69. D. Huo, L. Yang, C. Hou, H. Fa, X. Luo, Y. Lu, X. Zheng, J. Yang, and L. Yang, *Spectrochim. Acta A* 74, 336 (**2009**).
70. S. Gotovac, H. Honda, Y. Hattori, K. Takahashi, H. Kanoh, and K. Kaneko, *Nano Lett.* 7, 583 (**2007**).
71. Y. Zhang, J. Zhang, H. Son, J. Kong, and Z. Liu, *J. Am. Chem. Soc.* 127, 17156 (**2005**).
72. C. Fantini, M. L. Usrey, and M. S. Strano, *J. Phys. Chem. C* 111, 17941 (**2007**).
73. E. Jubete, K. Elechowska, O. A. Loaiza, P. J. Lamas, E. Ochoteco, K. D. Farmer, K. P. Roberts, and J. F. Biernat, *Electrochim. Acta* 56, 3988 (**2011**).
74. J. Chao, W. Huang, J. Wang, S. Xiao, Y. Tang, and J. Liu, *Biomacromolecules* 10, 877 (**2009**).
75. A. Jha, U. K. Ghorai, D. Banerjee, S. Mukherjee, and K. K. Chattopadhyay, *RSC Adv.* 3, 1227 (**2013**).
76. C. A. Dyke and J. M. Tour, *J. Phys. Chem. A* 108, 11151 (**2004**).
77. P. J. Camp, A. C. Jones, R. K. Neely, and N. M. Speirs, *J. Phys. Chem. A* 106, 10725 (**2002**).
78. R. A. Hatton, N. P. Blanchard, V. Stolojan, A. J. Miller, and S. R. Silva, *Langmuir* 23, 6424 (**2007**).

79. J. J. Hernández, M.-C. García-Gutiérrez, D. R. Rueda, T. A. Ezquerra, and R. J. Davies, *Compos. Sci. Technol.* 72, 421 (**2012**).
80. M. D. Shirsat, T. Sarkar, J. Kakoullis Jr., N. V. Myung, B. Konnanath, A. Spanias, and A. Mulchandani, *J. Phys. Chem. C* 116, 3845 (**2012**).
81. E. B. Barros, A. G. S. Filho, V. Lemos, J. M. Filho, S. B. Fagan, M. H. Herbst, J. M. Rosolen, C. A. Luengo, and J. G. Huber, *Carbon* 43, 2495 (**2005**).
82. D. Rossouw, G. A. Botton, E. Najafi, V. Lee, and A. P. Hitchcock, *ACS Nano* 6, 10965 (**2012**).
83. C. Yang, J. S. Park, K. H. An, S. C. Lim, K. Seo, B. Kim, K. A. Park, S. Han, C. Y. Park, and Y. H. Lee, *J. Phys. Chem. B* 109, 19242 (**2005**).
84. L. J. Casarett, J. Doull, C. D. Klaassen, and M. O. Amdur, Casarett and Doull's Toxicology: The Basic Science of Poisons, Macmillan (**1986**).
85. R. M. A. Azzam, *Thin Solid Films* 519, 2584 (**2011**).
86. H. Arwin, M. Poksinski, and K. Johansen, *Appl. Optics* 43, 3028 (**2004**).
87. M. Kragulj, J. Trickovic, B. Dalmacija, Á. Kukovecz, Z. Kónya, J. Molnar, and S. Roncevic, *Chem. Eng. J.* 225, 144 (**2013**).

Received: 9 July 2013. Accepted: 22 August 2013.

Sensors and Actuators B 190 (2014) 990–998

Contents lists available at ScienceDirect

Sensors and Actuators B: Chemical

journal homepage: www.elsevier.com/locate/snb

ɪpper phthalocyanine/single walled carbon nanotubes hybrid thin ɪs for pentachlorophenol detection

ɪmat Banimuslem[a], Aseel Hassan[a], Tamara Basova[b,*], Asuman Dakoğlu Gülmez[c], ɜem Tuncel[c], Mahmut Durmuş[c], Ayşe Gül Gürek[c], Vefa Ahsen[c,d]

ɜrials and Engineering Research Institute, Sheffield Hallam University, Sheffield S1 1WB, UK
laev Institute of Inorganic Chemistry, Department of chemistry of coordination, cluster and supramolecular compounds, SB RAS, 3 Lavrentiev Ave. 0 Novosibirsk, Russia
ɜe Institute of Technology, Department of Chemistry, Gebze, Kocaeli, Turkey
ITAK-Marmara Research Center, Materials Institute, Gebze, Kocaeli, Turkey

TICLE INFO

ɜe history:
ved 11 June 2013
ved in revised form 29 August 2013
ted 11 September 2013
able online 20 September 2013

ɔrds:
locyanine
ɔn nanotubes
al sensors
chlorophenol
ilms
ɔometry

ABSTRACT

Tetra-substituted copper phthalocyanine ($CuPcR_4$, $R = -S(CH_2)_{15}CH_3$) has been prepared and characterised by UV–Vis, FT-IR and mass-spectrometry. Hybrid materials were produced by mixing $CuPcR_4$ with acidified single-walled carbon nanotubes (SWCNTs) and characterised by UV–Vis absorption spectroscopy, scanning electron microscopy and atomic force microscopy. Thin films of pristine $CuPcR_4$ and SWCNT/$CuPcR_4$ were prepared by spin coating onto gold-coated glass slides and applied as active layers to detect pentachlorophenol (PCP) in water utilizing total internal reflection ellipsometry (TIRE) technique. Different concentrations of PCP in water ranging from 0.5 to 10 μg/l have been examined in the current work. It is revealed that the phase shift ($\Delta(\lambda)$) spectra of SWCNT/$CuPcR_4$ films were two times larger than the shifts produced by the pristine $CuPcR_4$ films with clear recovery in the $\Delta(\lambda)$ spectra after flushing the cell with water. The adsorption of PCP on both types of films is discussed and films' sensitivity was determined using the change in films' refractive index.

ntroduction

'he worldwide use of pesticides and herbicides for agricultural oses is classified as a global environmental pollution problem. icides used in agriculture can easily take way to surface or nd waters, possibly causing adverse ecotoxicological effects on tic life and changing drinking water quality [1]. Chlorophenols esent a major group of pollutants of environmental concern. to their wide spreading and toxic properties, some chlorinated ols, such as pentachlorophenol (PCP), 2-chlorophenol, 2,4-lorophenol, and 2,4,6-trichlorophenol (2,4,6-TCP) have been idered as priority pollutants. PCP is the most toxic represen-e of the chlorophenols and an important organic chemical for ronmental studies because of its common application in agri-re, industry and commercial product synthesis [2]. It is highly c and persistent in water and soil. Concentrations of PCP ran- from trace levels to 10,500 μg/l in various surface waters from rent countries have been reported by the World Health Orga-tion [3]. Furthermore, it can accumulate in living organisms and result in negative effects, including carcinogenicity and acute toxicity.

Different analytical procedures based on liquid chromatography–mass spectrometry (LC–MS) [4–6], LC–tandem mass spectrometry (LC–MS/MS) [7], high performance liquid chromatography (HPLC) [8], and gas chromatography–mass spectrometry (GC–MS) [9] have been reported to provide efficient determination of these pesticides, according to the present legislation. However these methods, although highly sensitive and specific, are quite laborious, time-consuming, and expensive, and not suitable for on-site applications. There is therefore continuous demand for highly sensitive, cost-effective, rapid and portable detection methods which at the same time can meet international legislation allowed levels of PCP and other toxic compounds.

Ellipsometry can be used in total internal reflection (TIRE) mode and in combination with the surface plasmon resonance phenomenon for sensing aspects [10–12]. There has been extensive work in applying TIRE as a technique for the detection of biomolecules [13,14]. It was established that TIRE is a more suitable technique than SPR method for the registration of low molecular weight toxins such as simazine, atrazine and T2 mycotoxin [15]. TIRE technique has attracted substantial attention because of its fast response, simple instrumentation, being non-destructive

orresponding author. Tel.: +7 383 3302814; fax: +7 383 3309489.
-mail addresses: basova@niic.nsc.ru, tbasova@mail.ru (T. Basova).

-4005/$ – see front matter © 2013 Elsevier B.V. All rights reserved.
//dx.doi.org/10.1016/j.snb.2013.09.059

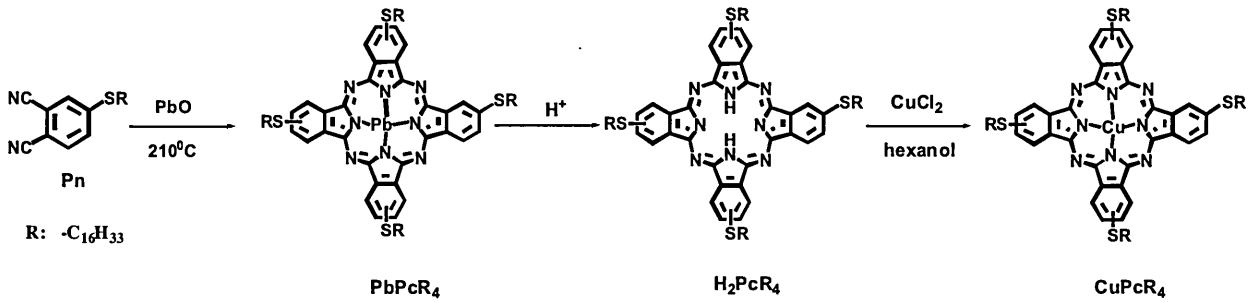

Fig. 1. Synthesis of 2(3),9(10),16(17),23(24)-tetrakis(hexadecylthio) phthalocyaninato copper(II) ($CuPcR_4$).

ethod and its ability of performing measurements in non-ansparent media [16].

Many research studies have shown the ability of carbon nano-bes (CNTs) to adsorb different pollutants [17–22]. This ability is e to the strong interaction between the CNTs surface and the pol-tants caused by the unique structure of CNTs resulting from the localised π-electrons on the hexagonal arrays of carbon atoms graphene sheets or CNTs surface. However, almost all sensor plications using CNTs as active layer are either electrical or elec-ochemical based sensors and because CNTs are optically inert they e not incorporated in optical based sensors such as surface plas-on resonance or total internal reflection ellipsometry techniques. n the other hand, phthalocyanines (Pcs), especially, their readily luble peripherally substituted derivatives, possess a wide range chemical and physical properties that make them interesting uilding blocks for a number of applications and new materials 3–26]. Among these properties are the presence of highly con-gated π-electron systems and high absorptivity in the near-IR gion. Pcs have been extensively used as active layers to detect rge variety number of pollutants using TIRE and SPR techniques 7–30].

This work reports for the first time the use of single-walled car-on nanotubes (SWCNT) hybridised with tetrasubstituted copper hthalocyanine $CuPcR_4$ (Fig. 1) as an optical active layer to detect entachlorophenol in water using TIRE technique. The morphology d optical properties of the SWCNT/$CuPcR_4$ hybrid films are also iscussed.

. Experimental

1. Materials

4-(*n*-Hexadecylthio) phthalonitrile (Pn) was synthesised cording to reported procedure [31]. SWCNTs were commercially urchased from Sigma-Aldrich. Pentachlorophenol (PCP) were btained from Sigma-Aldrich with 98% purity and its solution in eionised water in the concentration range 0.5–10 μg/l was used this study. After detection, deionised water was injected into the ll to remove adsorbed PCP molecules from film surface. All other agents and solvents of reagent grade quality were obtained from mmercial suppliers and were dried as described in Perrin and marego [32].

. Measurements

The IR spectra were recorded between 4000 and 650 cm^{-1} using Perkin Elmer Spectrum 100 FT-IR spectrometer with an atten-ated total reflection (ATR) accessory, featuring a zinc selenide nSe) crystal. Optical spectra in the UV–visible region were corded with Shimadzu UV-Vis-2101 spectrophotometer using 1 cm path length cuvette at room temperature. Matrix-assisted laser desorption/ionisation time-of-flight mass spectrometry (MALDI-TOF-MS) measurements were performed on a Bruker Daltonics micrOTOF by using 2,3-dihydroxybenzoic acid as matrix. The surface morphology of the films was investigated by SEM and AFM using FEI-nova nanosem 200 and Nanoscope IIIa multimode atomic force microscope, respectively.

The experimental set-up for TIRE measurements was built on M2000V (J.A. Woollam Co., Inc.) spectroscopic ellipsometer, operating in the 350–1000 nm wavelength range, as shown in the schematic diagram presented in Fig. 2. The set-up comprises a white light source (1), monochromator (2), polariser (3), analyser (4) and a photodetector array (5). Additional elements, which allow performing TIRE measurements, are a BK7 glass prism (6) with a gold-coated glass slide (7) brought into optical contact via index matching fluid, and the reaction cell (8) sealed to the top of the Au-coated slide through a rubber O-ring (9). The choice of the prism was dictated by conditions of total internal reflection of light on the glass/water interface; the prism used in this case is 68° BK7 glass prism with an index of refraction $n = 1.515$. Further details of TIRE method and the experimental set-up are found in previous publications [15,33]. The cell has a volume of 2 ml and contains inlet and outlet tubes to allow injection of different gases or fluids into the cell in order to perform different chemical interactions. Elements 6–9 were fixed on the ellipsometer sample stage using vacuum suction.

The spectra of the two ellipsometric parameters Ψ and Δ, representing, respectively, the amplitude ratio $tg(\Psi) = A_p/A_s$ and phase shift $\Delta = \varphi_p - \varphi_s$ between *p*- and *s*-components of polarised light, were recorded with the M2000V instrument in the 350–1000 nm spectral range using the rotating analyzer principle. Optical parameters of the reflection system, i.e. thicknesses, refractive indices and extinction coefficients of the substrate and adsorbed layers, can be obtained by solving the reverse ellipsometric problem numerically:

$$tg(\psi)\exp(i\Delta) = \frac{R_p}{R_s} \quad (1)$$

where R_p and R_s are Fresnel reflection coefficients for *p*- and *s*-components of polarised light related to the parameters of reflection system, particularly the thickness (d) and refractive index (n) of the adsorbed layers, via Fresnel equations [34]. The fitting is performed by solving Fresnel equations many times for different values of n and d and subsequently minimizing the error function of the experimental and theoretical (calculated) values of Ψ and Δ using one of least-square techniques. Commercial WVASE32® software is provided by J.A. Woollam Co., Inc. for this task. The samples for TIRE study were prepared by the evaporation of 3–5 nm of chromium on microscopic glass slides followed by the evaporation of 25–30 nm of gold layer.

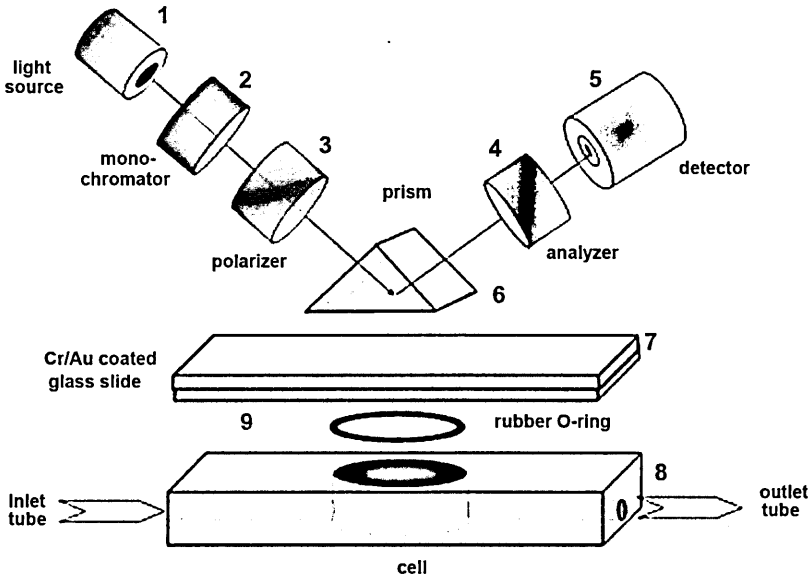

Fig. 2. Total internal reflection ellipsometry experimental set-up.

Synthesis of CuPcR4

-(*n*-Hexadecylthio) phthalonitrile (Pn) (0.50 g, 1.30 mmol) and d PbO (0.145 g, 0.65 mmol) were stirred at 210 °C for 5 h under n atmosphere in solvent-free conditions as we described in previous paper [25]. The reaction mixture was then dissolved :1/dichloromethane:acetic acid mixture to remove lead metal the cavity and obtain metal-free derivative (H_2PcR_4) of PbPcR4 1). This acidic mixture was extracted with water and organic e was dried over anhydrous sodium sulfate. It is known from literature that PbPcs can easily lose their central metal ion especially in acidic media and transform into the correspond- metal-free analogues. The formation of metal-free derivative confirmed by the formation of splitted Q band in the UV–Vis trum of this complex. H_2PcR_4 (0.20 g, 0.18 mmol) was refluxed er argon atmosphere with anhydrous $CuCl_2$ (34 mg, 0.25 mmol) ried *n*-hexanol (2 ml) for 2 h and the reaction mixture was red into ethanol. The precipitates were filtered and washed ethanol. The crude product was purified over silica gel column sing 100:1/dichloromethane:hexane as eluent. Yield: 260 mg, (from H_2PcR_4 to CuPcR4). IR [(ATR) ν_{max} (cm^{-1})]: 3066 (C_{ar}–H), 7–2850 (C–H), 1602 (C=C), 1508, 1466, 1389, 1341, 1313, 1261, 3, 1102, 1086 (C–S–C), 1070, 1038. UV–Vis (THF): λ_{max} (nm) ε) 349 (5.06), 622 (4.79), 689 (5.45). MALDI-TOF-MS *m/z*: Calcd. $C_{96}H_{144}CuN_8S_{16}$: 1602.06, found 1602.50 $[M]^+$ (100), 1637.69 $Cl]^+$.

Preparation of SWCNTs–CuPcR4 hybrid

/CNTs were first acidified and cut into short and uncapped otubes according to a multi-step procedure developed by lley and co-workers [36]. This was carried out by refluxing nanotubes in 2.6 M HNO_3 for 48 h followed by stir- in a mixture of concentrated H_2SO_4 and HNO_3 (3:1, at 40 °C for 12 h. The mixture was centrifuged and hed thoroughly in deionised water and dried at 70 °C for .

e acidified SWCNTs (0.5 mg) were added to a solution of cR4 (1.5 mg/ml) in chloroform and ultrasonicated for 15 min. films were produced by spin-casting the obtained solution onto gold-coated slides and onto silicon substrates using a photoresist spinner (Microsystem model 4000) at 2000 rpm. Similarly, thin films were produced from a solution of pristine CuPcR4 in chloroform (2 mg/ml) for comparison.

3. Results and discussion

3.1. Characterisation of SWCNT/CuPcR4 hybrid films

3.1.1. UV–Vis absorption spectra

Fig. 3 shows the UV–visible absorption spectra of solutions of SWCNTs, CuPcR4 and SWCNT/CuPcR4 hybrid in DMF. CuPcR4 exhibits typical electronic absorption spectrum with two strong absorption regions, one in the wavelength range 640–695 nm (Q-band) arising from the electron transitions from the highest occupied molecular orbital (HOMO) a_{1u} to the lowest unoccupied molecular orbital (LUMO) e_g and one in the range 300–450 nm

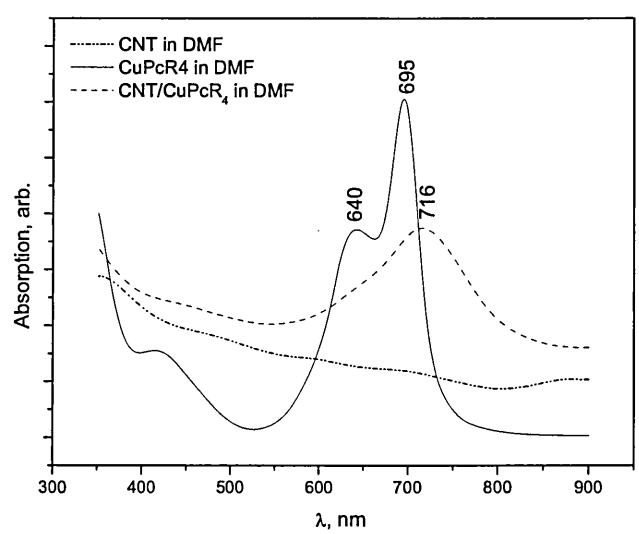

Fig. 3. Optical absorption spectra of pristine SWCNT (dotted line), CuPcR4 (solid line) and SWCNT/CuPcR4 hybrid (dashed line) in DMF.

ble 1
ughness analysis of $CuPcR_4$ and SWCNT/$CuPcR_4$ films.

Film	R_a (nm)	RMS (nm)	R_{max} (nm)
$CuPcR_4$	0.837	1.204	4.186
SWCNT/$CuPcR_4$	2.727	3.812	11.906

--band) which is attributed to the electron transitions from the OMO) a_{2u} to the (LUMO) e_g [23]. Furthermore, absorption within e Q-band is split into two absorption peaks, one with much igher intensity than the other at $\lambda = 695$ and 640 nm, respectively. his can be ascribed to dominant monomer absorption with the tter being ascribed to molecular aggregation in DMF solution. The sorption spectrum of SWCNT is featureless as reported elsewhere 37] and is attributed to the poor exfoliating ability of DMF.

The maximum of the Q-band in the absorption spectrum of the 'CNT/$CuPcR_4$ hybrid is broadened and red-shifted by ~21 nm in mparison with $CuPcR_4$ spectrum. It can also be seen that the Q- and splitting has disappeared in the hybrid absorption spectrum, hich indicates dominant monomer absorption. These changes are ggested to take place due to the strong π–π interaction between rbon nanotubes and phthalocyanine molecules, where phthalo- anines are usually considered as electron donors, while carbon anotubes as acceptors [38]. This interaction has been frequently scribed to the reduced aggregation in the MPc/CNT composites 39,40].

.1.2. Morphology

Fig. 4 shows SEM images of pristine SWCNTs, acid-treated WCNTs and SWCNT/$CuPcR_4$ hybrid deposited as thin film from loroform solution onto silicon substrate. Pristine CNTs typically nd to bundle together (Fig. 4a) and to aggregate due to Van er Waals attraction between individual tubes [41] as well as the igh length to diameter ratio; this makes them hard to disperse common organic solvents. Chemical modification has been per- rmed to achieve enhanced interaction between SWCNTs and uPcR$_4$ molecules leading to the formation of a composite with uch improved solubility in chloroform. The obtained solution is onveniently used for thin film deposition using spin-coating tech- ique. Fig. 4b shows that the intrinsic quality of SWCNTs structure is till preserved after the acid treatment. However, after mixing with hthalocyanine (Fig. 4c), the composite dispersion was significantly proved to form a uniformly suspended solution in chloroform; ence smoother films were obtained to perform optical investiga- ion, using TIRE experiments.

Fig. 5a and b shows AFM images of $CuPcR_4$ and SWCNT/$CuPcR_4$ lms spun onto silicon substrates with the roughness analy- is presented at the bottom of the figures. The films of $CuPcR_4$ Fig. 5a) demonstrate fibrous-like porous morphology. Fig. 5b on e other hand shows that phthalocyanine molecules are attached the surface of carbon nanotubes confirming the formation of etworks of $CuPcR_4$ and SWCNT. Similar morphology was observed r poly(3-hexylthiophene) (P3HT)/multi-walled carbon nanotube WCNT) films [42] and MWCNTs and SWCNTs with lead tetra- o-pentyloxyphthalocyanine (PbPc) [22]. The main roughness (R_a), tandard deviation (RMS) and maximum height (R_{max}) are summ- rised in Table 1. The inset to Fig. 5b represents an enlarged AFM age of SWCNT/$CuPcR_4$ deposited on silicon, showing individ- al and shortened nanotubes with approximate length of 250 nm urrounded by phthalocyanine molecules.

.2. Total internal reflection ellipsometry (TIRE)

The adsorption of PCP onto the surface of $CuPcR_4$ and CNT/$CuPcR_4$ thin films in water solutions has been stud- d using TIRE method. $CuPcR_4$ and SWCNT/$CuPcR_4$ hybrid films

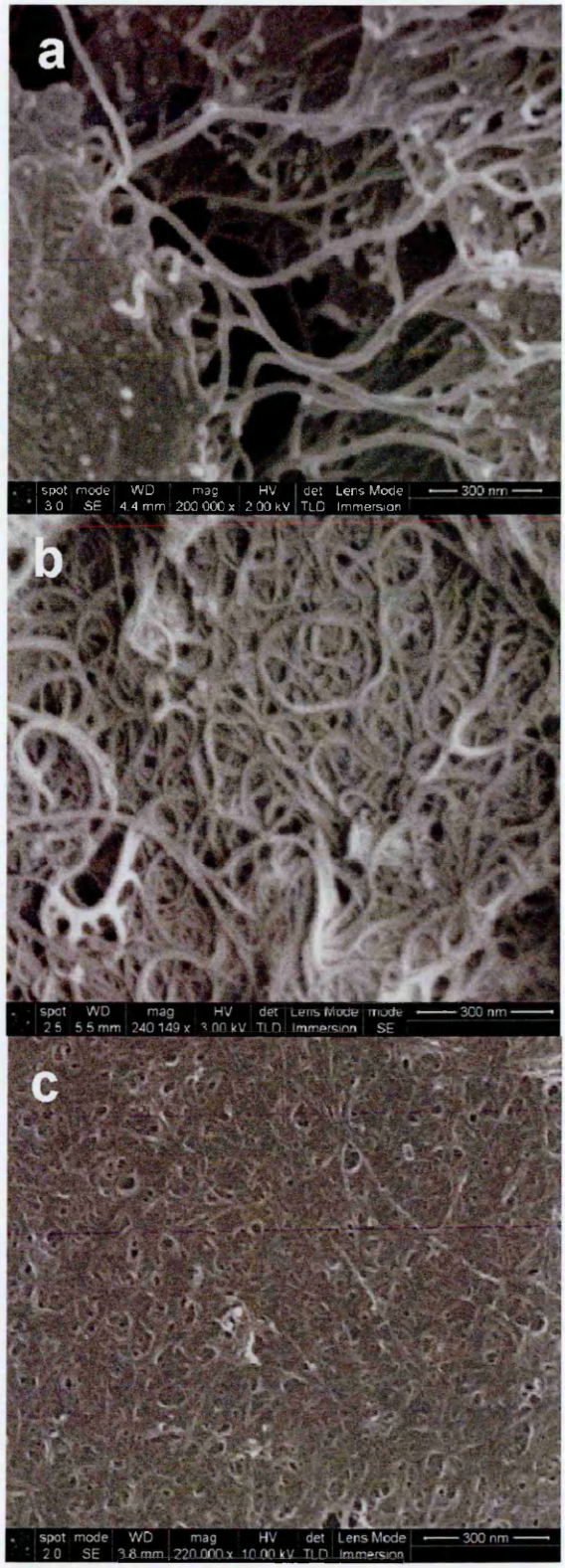

Fig. 4. SEM images of (a) pristine SWCNT, (b) acidified SWCNT and (c) SWCNT/$CuPcR_4$ hybrid in thin film form.

were spun onto gold-coated glass substrates as described in Section 2. Fig. 6 shows the typical TIRE spectra of Cr/Au films used in the present work. The spectrum of $\Psi(\lambda)$, demonstrating the amplitude ratio of A_p/A_s, resembles very much the conventional surface plasmon resonance (SPR) curve, while the spectrum of $\Delta(\lambda)$ is

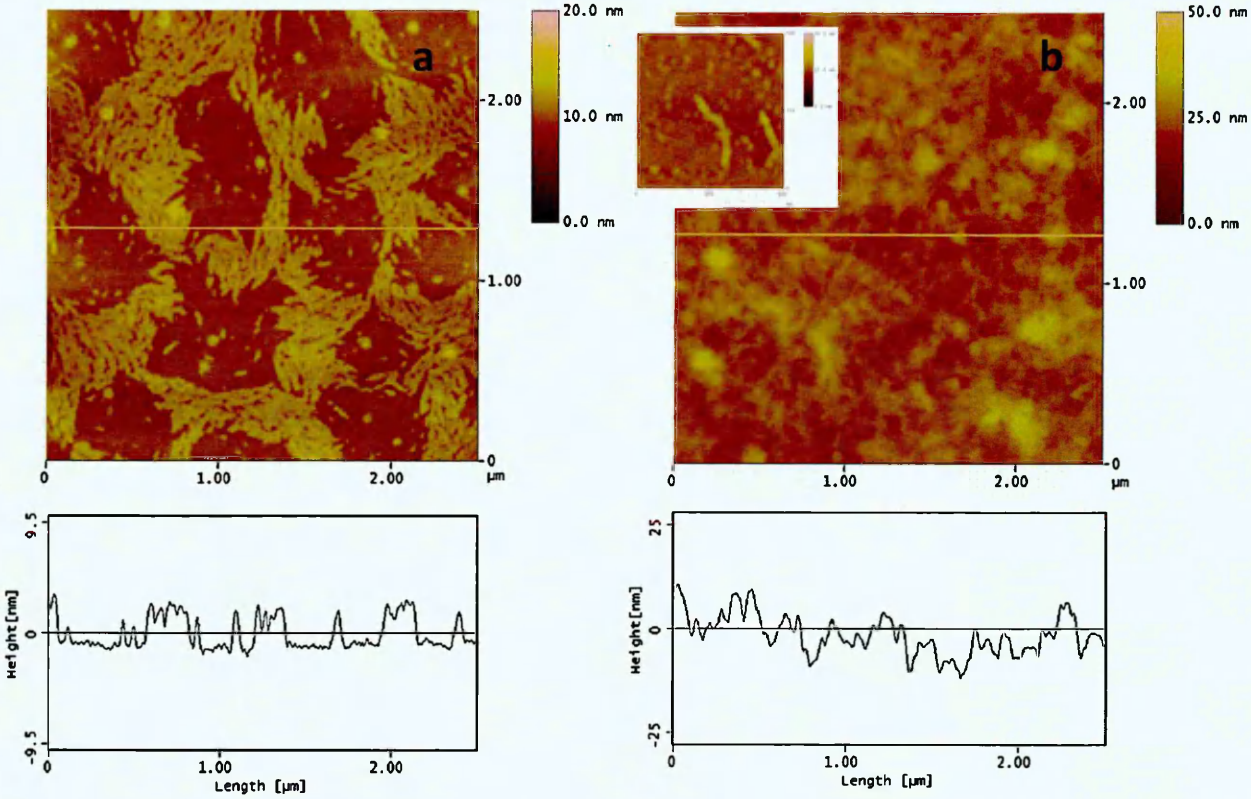

. AFM images of (a) $CuPcR_4$, (b) SWCNT/$CuPcR_4$ hybrid in thin film form. Inset to Fig. 5b is a higher resolution AFM image of SWCNT/$CuPcR_4$ deposited on silicon.

ciated with the phase shift between *p*- and *s*-components olarised light. The latter changes sharply from 270° down to ° near the plasmon resonance. According to Arwin's modelling , the position of the sharp drop in $\Delta(\lambda)$ spectrum is about 10 s more sensitive to analytes adsorption than $\Psi(\lambda)$ spectrum. 7 represents the spectra of $\Psi(\lambda)$ and $\Delta(\lambda)$ of $CuPcR_4$ and NT/$CuPcR_4$ hybrid thin films before and after exposure to PCP. concentration of PCP was varied from 0.5 to 10 µg/l in deionised er. The initial response time of the sensors was fraction of a ute but the spectra were measured 5 min after injection of

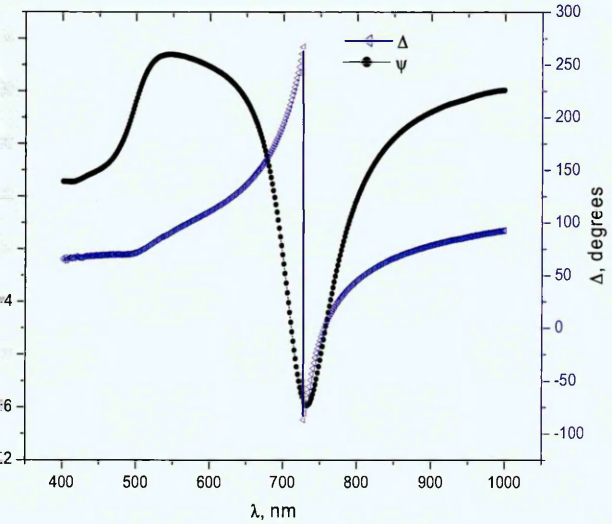

Fig. 6. Typical TIRE spectra of Cr/Au film.

contaminated water or pure water to achieve the equilibrium response or recovery, respectively. Furthermore, longer exposure time has been examined to establish the recovery of the sensors.

During exposure to contaminated water, it was difficult to detect shifts in $\Psi(\lambda)$ because of the shape of the curve, however, significantly larger shifts have been observed in $\Delta(\lambda)$ spectra. These are typical features of TIRE method as reported earlier [15,16,28]. The spectra of $\Delta(\lambda)$ were further enlarged and shown at the bottom of Fig. 7 to provide better assessment of the effect of PCP exposures. It can clearly be seen that the adsorption of PCP on hybrid film has resulted in larger shifts (6.41, 10.98 and 14.19 nm) than pure $CuPcR_4$ (3.05, 4.67 and 7.82 nm) under PCP exposures of concentrations 1, 2 and 5 µg/l in water, respectively. Carbon nanotubes in general are characterised with uniform surface with delocalised π-electrons of high density, which enhances their adsorption properties, especially for analytes with oxygen-containing aromatic molecules such as PCP [43]. The adsorption of PCP can also be ascribed to the π–π interactions between the π electrons of the aromatic ring of PCP and the π electron system of the aromatic rings of the SWCNTs [44]. Complete recovery of $\Delta(\lambda)$ spectra are observed after flushing the cell with deionised water as previously established for films of metal phthalocyanines with other types of substituents [27]. However, when exposure to 5 µg/l PCP-contaminated water continued for 30 min, $CuPcR_4$ exhibited further shift but did not show complete recovery after flushing with water; in contrast to SWCNT/$CuPcR_4$ layer which remained stable with time under repeated exposures to 5 µg/l PCP-contaminated water and exhibited complete reversibility. It is expected that the presence of SWCNT in the composite film inhibits the diffusion of PCP molecules inside the film and most interaction takes place on the surface of the film.

Theoretical fitting to experimental Ψ and Δ spectra was carried out by applying a four-layer model consisting of water solution,

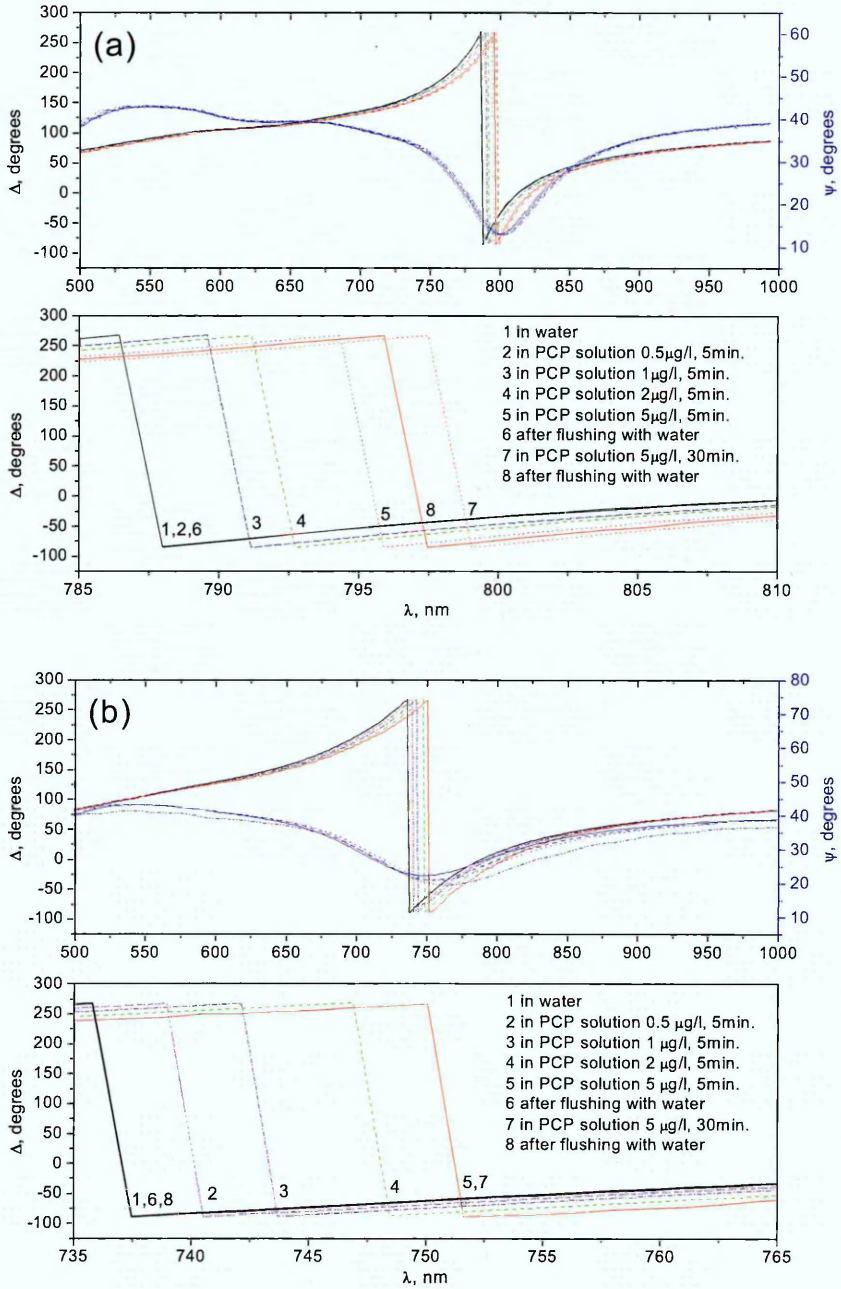

ig. 7. $\Psi(\lambda)$ and $\Delta(\lambda)$ TIRE spectra of (a) $CuPcR_4$ coated Cr/Au and (b) SWCNT/$CuPcR_4$ hybrid films in water (1); after injection of PCP solution of 0.5 μg/l (2); 1 μg/l (3); 2 μg/l); 5 μg/l (5) for 5 min; after flushing with water (6) and after injecting with PCP solution 5 μg/l for 30 min (7); after flushing with water (8). An enlarged section of $\Delta(\lambda)$ pectra are shown at the bottom of the figure.

rganic layer, Au layer and BK7 glass. The optical parameters (film hickness d, refractive index n and extinction coefficient k) of all yers are summarised in Table 2.

able 2
arameters of four-layer model in TIRE fitting.

Layer	n	k	d (nm)
BK7	1.51	0	Ambient
Cr/Au	0.36	2.86	27.43
Active layer	See Table 3		
Aqueous solution	1.34	0	–

The parameters of the organic films after exposure to PCP solutions in water were determined by fitting experimental Ψ and Δ spectra to the theoretical organic model by fixing Cr/Au layer parameters. Table 3 summarises the thickness of all layers found from theoretical data fitting for multiple samples as well as the values of refractive index and extinction coefficients given at $\lambda = 632$ nm. It is worthy to mention that no apparent difference was found between optical parameters and thickness of the initial films deposited on Si and on Au-coated glass substrates. The data in Table 3 show an increase in film thickness as well as optical parameters (n and k) for both films; the only exception was in k value which exhibited a small decrease in the case of $CuPcR_4$ film as a result of PCP adsorption. The decrease in k value may be a result of

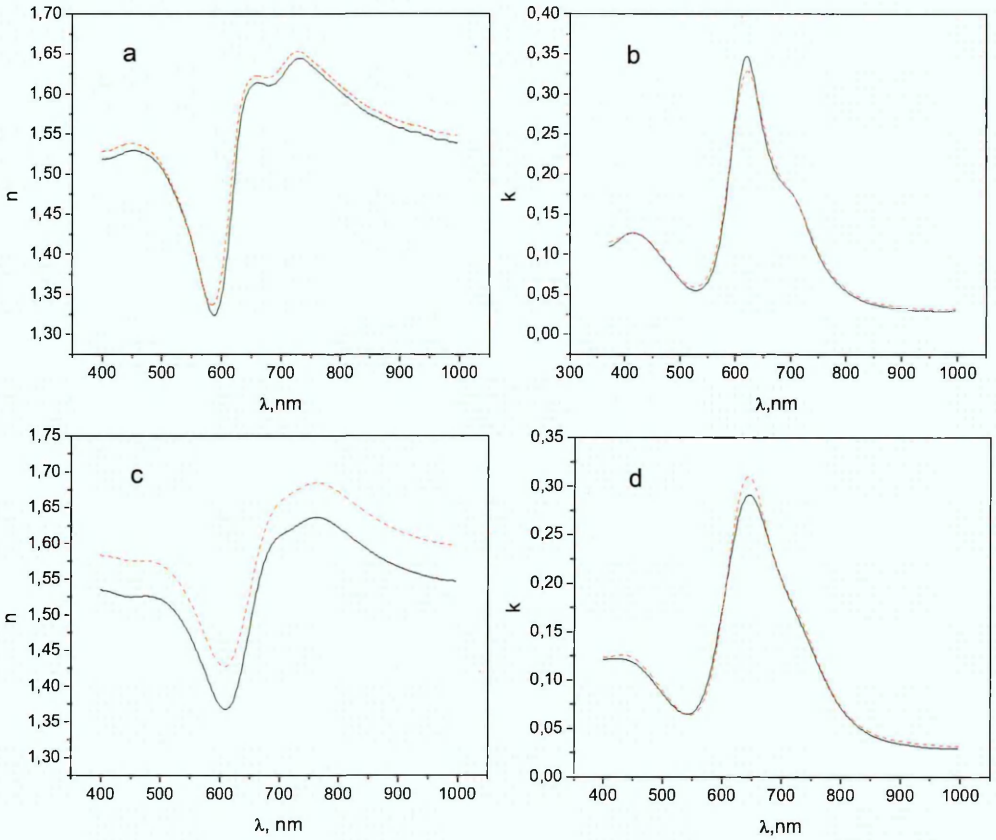

... Refractive index (n) and extinction coefficient (k) of $CuPcR_4$ film ((a) and (b)) and SWCNT/$CuPcR_4$ film ((c) and (d)) in pure water (solid line) and PCP solution of 10 μg/l ...ed line).

...3
...ges in the optical parameters of $CuPcR_4$ and SWCNT/$CuPcR_4$ films caused by adsorption of PCP from its solution with concentration of 10 μg/l.

	$CuPcR_4$			SWCNT/$CuPcR_4$		
	n (632 nm)	k (632 nm)	d (nm)	n (632 nm)	k (632 nm)	d (nm)
...ial film	1.56 ± 0.01	0.32 ± 0.01	37.4 ± 0.3	1.41 ± 0.02	0.28 ± 0.02	54.2 ± 0.9
...osed film	1.59 ± 0.01	0.31 ± 0.01	38.1 ± 0.6	1.47 ± 0.02	0.29 ± 0.02	57.5 ± 0.7

...ge of film structure due to chemical reaction on the surface of ...alocyanine film and perhaps film swelling due to penetration ...P molecules into this film. The investigated $CuPcR_4$ exhibits ...id crystalline properties and the film structure of LC phthalo...ine films is very sensitive to different types of interactions, ...as discussed in a previous publication [45]. The increase in ...s' thickness in the case of SWCNT/$CuPcR_4$ composite was more ...ificant which is probably due to the predominant surface inter...on of the analyte with SWCNT/$CuPcR_4$ films. Further to the data ...marised in Table 3 the variation in refractive index and extinc... coefficient as a function of λ for both films in pure water and solution media (concentration of 10 μg/l) are shown in Fig. 8. ...urther studies are under way in order to provide a full compar... of SWCNT/MPc hybrid films response to unsubstituted phenol its chlorosubstituted derivatives. In an earlier publication it was ...onstrated that exposure of $ZnPcR_8$ films to low concentrations ...enzene and toluene in water has not resulted in any significant ...onse. As for other halosubstituted phenol derivatives, it has shown that layers of $ZnPcR_8$ demonstrate a good response to ...lorophenol, 4-bromophenol and 4-iodophenol using QCM and ...-FTIR difference spectroscopy [46].

...ig. 9 shows the dependence of the phase shift change ($\delta\Delta$) on concentration in the range 0.5–10 μg/l in water for $CuPcR_4$

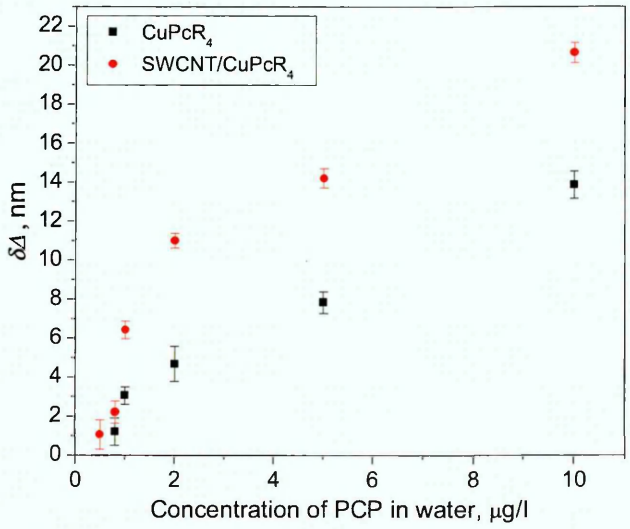

Fig. 9. Phase shift changes ($\delta\Delta$) in $\Delta(\lambda)$ spectra of SWCNT/$CuPcR_4$ hybrid and $CuPcR_4$ films on treatments with PCP solutions in water in the concentration range 0.5–10 μg/l.

nd SWCNT/CuPcR$_4$ layers. Reproducibility of the sensors' response as been examined for the two types of layers, and experimen- l errors in the spectral shifts are potted in Fig. 9. The minimum etection limit of PCP was 0.8 μg/l for CuPcR$_4$ layer, which is sim- ar to that determined in our previous publication where films f octatosylamido substituted zinc phthalocyanine were used as ctive layers for PCP detection using TIRE technique [11]. In the case f SWCNT/CuPcR$_4$ layers the minimum detection limit of PCP was und to be 0.5 μg/l. This is a higher concentration than that deter- ined in the literature where different analytical methods based on quid chromatography–mass spectrometry [47] and liquid chro- atography with electrochemical detection [48] were used, in hich the detection limit can reach some nanograms per litre. How- ver the obtained detection limit in our work is lower than that btained by traditional spectrophotometric techniques [49]. Fur- ermore, resolution of the ellipsometer used in this work is very w (~0.06 nm), however the detection limit depends not only on llipsometer resolution, but also on the reproducibility of the mea- ured signal obtained from several samples. Fig. 9 represents the hift in $\Delta(\lambda)$ taking into account measurement errors from multi- le samples. No reproducible shift in $\Delta(\lambda)$ was observed for PCP oncentrations below 0.5 μg/l, while reproducibility in the mea- ured $\Delta(\lambda)$ started to occur at 0.5 μg/l concentration in the case of he hybrid films. In the case of the pure CuPcR4 films reproducibility the measured $\Delta(\lambda)$ started to occur at 0.8 μg/l concentration.

In order to evaluate the response of the two types of layers the verage sensitivity has been calculated based on changes in films' efractive indices using the following equation:

$$= \frac{1}{n_0}\frac{1}{m}\sum_{i=1}^{m}\frac{\delta n}{C_i} \quad (2)$$

here δn is the change in the film refractive index under ana- te concentration C_i, m is the number of different concentrations sed in the study, and n_0 is the initial film refractive index (before xposure to PCP). Similar principle for evaluation of the aver- ge sensitivity was used in Ref. [50] where nickel phthalocyanine erivatives were studied as sensitive materials for the detection f organic solvent vapours using quartz crystal and capacitance ransducers.

Changes in extinction coefficients of the films as well as hanges in their thickness as a result of interaction with PCP ere not as consistent as those deduced for films' index of efraction. The average sensitivities were estimated as 2.18×10^{-3} nd 1.52×10^{-2} RIU/(μg/l) for CuPcR$_4$ and CuPcR$_4$/SWCNT lay- rs, respectively. The method of layer preparation as well as the btained layer structure are known to influence the layer sensitiv- ty to the detected analytes [51]. The observed larger sensitivity in he case of hybrid films was thought to be determined by the larger umber of adsorption sites made available to the analyte molecules n the film surface due the large surface to volume area compared o pure CuPcR$_4$ film.

. Conclusion

Thin films of single-walled carbon nanotubes (SWCNT) ybridised with tetrasubstituted copper phthalocyanine (CuPcR$_4$) ave been used as optical active layers to detect pentachlorophenol PCP) in water using Total Internal Reflection Ellipsometry (TIRE) echnique. The morphology and optical properties of the hybrid lms were studied and the interaction between the two materials as ascribed to π–π interaction as well as van der Waals forces. e interaction of PCP solution in water at concentrations between .5–10 μg/l with SWCNT/CuPcR$_4$ hybrid films as well as with ristine CuPcR$_4$ was studied. Changes in the phase shift ($\Delta(\lambda)$) pectra of SWCNT/CuPcR$_4$ films were found to be two times larger than those demonstrated by the pristine CuPcR$_4$ films with clear recovery after flushing the cell with water even for the highest examined PCP concentration. Films' sensitivities of 2.18×10^{-3} and 1.52×10^{-2} RIU/(μg/l) were found for CuPcR$_4$ and SWCNT/CuPcR$_4$ layers, respectively, as were estimated using changes in film's index of refraction values. The SWCNT/CuPcR$_4$ hybrid films have demonstrated detection limit of about 0.5 μg/l, whereas CuPcR$_4$ exhibited higher concentration detection limit of 0.8 μg/l. The principle aim of the present work was to demonstrate for the first time the use of SWCNT/CuPcR$_4$ hybrid films as optical active layers to detect toxic analytes in water using optical method. Sensor selectivity was not addressed in the current work and it will be the subject of future investigation.

Acknowledgements

The authors acknowledge the financial support through the bilateral project between the Scientific and Technological Research Council of Turkey (TUBITAK, Project number: 108M384) and the Russian Foundation of Basic Research (RFBR, Project numbers: 12-03-91372-CT_α). Hikmat Banimuslem wishes to acknowledge the financial support from the Higher Committee for Education Development in Iraq (HCED). The help in performing SEM measurements by Mr Vinay Patel is gratefully acknowledged.

References

[1] L.G. Freitas, H. Singer, S.R. Müller, R.P. Schwarzenbach, C. Stamm, Source area effects on herbicide losses to surface waters—a case study in the Swiss Plateau, Agric. Ecosyst. Environ. 128 (2008) 177–184.
[2] Y. Lin, C.A. Timchalk, D.W. Matson, H. Wu, K.D. Thrall, Integrated microfluidics/electrochemical sensor system for monitoring of environmental exposures to lead and chlorophenols, Biomed. Microdevices. 3 (2001) 331–338.
[3] World Health Organization (WHO), Pentachlorophenol; Environmental Health Criteria 71, World Health Organization, International Programme on Chemical Safety, Geneva, Swizerland, 1987.
[4] A. Di Corcia, C. Crescenzi, E. Guerriero, R. Samperi, Ultratrace determination of atrazine and its six major degradation products in water by solid-phase extraction and liquid chromatography–electrospray/mass spectrometry, Environ. Sci. Technol. 31 (1997) 1658–1663.
[5] R. Koeber, C. Fleischer, F. Lanza, K. Boos, B. Sellergren, D. Barcelót, Evaluation of a multidimensional solid-phase extraction platform for highly selective on-line cleanup and high-throughput LC–MS analysis of triazines in river water samples using molecularly imprinted polymers, Anal. Chem. 73 (2001) 2437–2444.
[6] S. Rodriguez-Mozaz, M.J. López De Alda, D. Barceló, Monitoring of estrogens, pesticides and bisphenol A in natural waters and drinking water treatment plants by solid-phase extraction–liquid chromatography–mass spectrometry, J. Chromatogr. A 1045 (2004) 85–92.
[7] R. Jeannot, H. Sabik, E. Sauvard, E. Genin, Application of liquid chromatography with mass spectrometry combined with photodiode array detection and tandem mass spectrometry for monitoring pesticides in surface waters, J. Chromatogr. A 879 (2000) 51–71.
[8] G. Gervais, S. Brosillon, A. Laplanche, C. Helen, Ultra-pressure liquid chromatography–electrospray tandem mass spectrometry for multiresidue determination of pesticides in water, J. Chromatogr. A 1202 (2008) 163–172.
[9] T. Dagnac, S. Bristeau, R. Jeannot, C. Mouvet, N. Baran, Determination of chloroacetanilides, triazines and phenylureas and some of their metabolites in soils by pressurised liquid extraction, GC–MS/MS, LC–MS and LC–MS/MS, J. Chromatogr. A 1067 (2005) 225–233.
[10] J.D. Wright, J.V. Oliver, R.J.M. Nolte, S.J. Holder, N.A.J.M. Sommerdijk, P.I. Nikitin, The detection of phenols in water using a surface plasmon resonance system with specific receptors, Sens. Actuators, B 51 (1998) 305–310.
[11] T. Basova, A. Hassan, F. Yuksel, A.G. Gürek, V. Ahsen, Optical detection of pentachlorophenol in water using thin films of octa-tosylamido substituted zinc phthalocyanine, Sens. Actuators, B 150 (2010) 523–528.
[12] H. Arwin, M. Poksinski, K. Johansen, Total internal reflection ellipsometry: principles and applications, Appl. Opt. 43 (2004) 3028–3036.
[13] P. Westphal, A. Bornmann, Biomolecular detection by surface plasmon enhanced ellipsometry, Sens. Actuators, B 84 (2002) 278–282.
[14] B. Lassen, M. Malmsten, Competitive protein adsorption studied with TIRF and ellipsometry, J. Colloid Interface Sci. 179 (1996) 470–477.
[15] A.V. Nabok, A. Tsargorodskaya, A.K. Hassan, N.F. Starodub, Total internal reflection ellipsometry and SPR detection of low molecular weight environmental toxins, Appl. Surf. Sci. 246 (2005) 381–386.
[16] A. Hassan, T. Basova, F. Yuksel, G. Gümüş, A.G. Gürek, V. Ahsen, Study of the interaction between simazine and metal-substituted phthalocyanines using spectral methods, Sens. Actuators, B 175 (2012) 73–77.

L. Dumée, M.R. Hill, M. Duke, L. Velleman, K. Sears, J. Schütz, N. Finn, S. Gray, Activation of gold decorated carbon nanotube hybrids for targeted gas adsorption and enhanced catalytic oxidation, J. Mater. Chem. 22 (2012) 9374–9378.
C. Gao, Z. Guo, J. Liu, X. Huang, The new age of carbon nanotubes: an updated review of functionalized carbon nanotubes in electrochemical sensors, Nanoscale 4 (2012) 1948–1963.
T. Mugadza, Y. Arslanoğlu, T. Nyokong, Characterization of 2,(3)-tetra-(4-oxo-benzamide) phthalocyaninato cobalt(II)—single walled carbon nanotube conjugate platforms and their use in electrocatalysis of amitrole, Electrochim. Acta 68 (2012) 44–51.
A.L. Ndiaye, C. Varenne, P. Bonnet, E. Petit, L. Spinelle, J. Brunet, A. Pauly, B. Lauron, Elaboration of single wall carbon nanotubes-based gas sensors: evaluating the bundling effect on the sensor performance, Thin Solid Films 520 (2012) 4465–4469.
A.P. Terzyk, A. Pacholczyk, M. Wiśniewski, P.A. Gauden, Enhanced adsorption of paracetamol on closed carbon nanotubes by formation of nanoaggregates: carbon nanotubes as potential materials in hot-melt drug deposition-experiment and simulation, J. Colloid Interface Sci. 376 (2012) 209–216.
B. Wang, X. Zhou, Y. Wu, Z. Chen, C. He, Lead phthalocyanine modified carbon nanotubes with enhanced NH_3 sensing performance, Sens. Actuators, B 171–172 (2012) 398–404.
T.V. Basova, M. Çamur, A.A. Esenpinar, S. Tuncel, A. Hassan, A. Alexeyev, H. Banimuslem, M. Durmuş, A.G. Gürek, V. Ahsen, Effect of substituents on the orientation of octasubstituted copper(II) phthalocyanine thin films, Synth. Met. 162 (2012) 735–742.
S. Tuncel, H.A.J. Banimuslem, M. Durmuş, A.G. Gürek, V. Ahsen, T.V. Basova, A.K. Hassan, Liquid crystalline octasubstituted lead(II) phthalocyanines: effects of alkoxy and alkylthio substituents on film alignment and electrical properties, New J. Chem. 36 (2012) 1665–1672.
D. Atilla, A.G. Gürek, T.V. Basova, V.G. Kiselev, A. Hassan, L.A. Sheludyakova, V. Ahsen, The synthesis and characterization of novel mesomorphic octa- and tetra-alkylthio-substituted lead phthalocyanines and their films, Dyes Pigm. 88 (2011) 280–289.
T.V. Basova, A. Hassan, M. Durmuş, A.G. Gürek, V. Ahsen, Orientation of the liquid crystalline nickel phthalocyanine films confined between electrodes, Synth. Met. 161 (2011) 1996–2000.
A. Hassan, T. Basova, S. Tuncel, F. Yuksel, A.G. Gürek, V. Ahsen, Phthalocyanine films as active layers of optical sensors for pentachlorophenol and simazine detection, Procedia Eng. 25 (2011) 272–275.
T. Basova, A. Tsargorodskaya, A. Nabok, A.K. Hassan, A.G. Gürek, G. Gümus, V. Ahsen, Investigation of gas-sensing properties of copper phthalocyanine films, Mater. Sci. Eng., C 29 (2009) 814–818.
T. Basova, V. Plyashkevich, A. Hassan, Spectral characterization of thin films of vanadyl hexadecafluorophthalocyanine $VOPcF_{16}$, Surf. Sci. 602 (2008) 2368–2372.
T. Basova, E. Kol'tsov, A.K. Ray, A.K. Hassan, A.G. Gürek, V. Ahsen, Liquid crystalline phthalocyanine spun films for organic vapour sensing, Sens. Actuators, B 113 (2006) 127–134.
I. Gürol, V. Ahsen, Ö. Bekaroğlu, Synthesis of tetraalkylthio-substituted phthalocyanines and their complexation with Ag(I) and Pd(II), J. Chem. Soc., Dalton Trans. (1994) 497–500.
D. Perrin, W. Armarego, Purification of Laboratory Chemicals, Second ed., Pergamon Press, Oxford, 1989.
A. Nabok, A. Tsargorodskaya, The method of total internal reflection ellipsometry for thin film characterisation and sensing, Thin Solid Films 516 (2008) 8993–9001.
R.M.A. Azzam, The intertwined history of polarimetry and ellipsometry, Thin Solid Films 519 (2011) 2584–2588.
S. Tuncel, T.V. Basova, V.G. Kiselev, S.A. Gromilov, I.V. Jushina, M. Durmuş, A.G. Gürek, V. Ahsen, Tetraoctylthio- and tetraoctyloxy-substituted lead phthalocyanines: synthesis, characterization, liquid-crystalline properties, and thin film studies, J. Mater. Res. 26 (2011) 2962–2973.
J. Liu, A.G. Rinzler, H. Dai, J.H. Hafner, R.K. Bradley, P.J. Boul, A. Lu, T. Iverson, K. Shelimov, C.B. Huffman, F. Rodriguez-Macias, Y. Shon, T.R. Lee, D.T. Colbert, R.E. Smalley, Fullerene pipes, Science 280 (1998) 1253–1256.
T. Mugadza, T. Nyokong, Synthesis and characterization of electrocatalytic conjugates of tetraamino cobalt(II) phthalocyanine and single wall carbon nanotubes, Electrochim. Acta 54 (2009) 6347–6353.
N. He, Y. Chen, J. Bai, J. Wang, W.J. Blau, J. Zhu, Preparation and optical limiting properties of multiwalled carbon nanotubes with conjugated metal-free phthalocyanine moieties, J. Phys. Chem. C 113 (2009) 13029–13035.
Z. Yang, H. Pu, J. Yuan, D. Wan, Y. Liu, Phthalocyanines-MWCNT hybrid materials: fabrication, aggregation and photoconductivity properties improvement, Chem. Phys. Lett. 465 (2008) 73–77.
Y. Wang, N. Hu, Z. Zhou, D. Xu, Z. Wang, Z. Yang, H. Wei, E.S. Kong, Y. Zhang, Single-walled carbon nanotube/cobalt phthalocyanine derivative hybrid material: preparation, characterization and its gas sensing properties, J. Mater. Chem. 21 (2011) 3779–3787.
J.J. Hernández, M. García-Gutiérrez, D.R. Rueda, T.A. Ezquerra, R.J. Davies, Influence of single wall carbon nanotubes and thermal treatment on the morphology of polymer thin films, Compos. Sci. Technol. 72 (2012) 421–427.
F. Boon, S. Desbief, L. Cutaia, O. Douhéret, A. Minoia, B. Ruelle, S. Clément, O. Coulembier, J. Cornil, P. Dubois, R. Lazzaroni, Synthesis and characterization of nanocomposites based on functional regioregular poly(3-hexylthiophene) and multiwall carbon nanotubes, Macromol. Rapid. Commun. 31 (2010) 1427–1434.
[43] M. Salam, Effect of oxidation treatment of multi-walled carbon nanotubes on the adsorption of pentachlorophenol from aqueous solution: kinetics study, Arabian J. Chem. 5 (2012) 291–296.
[44] P.E. Diaz-Flores, R. Leyva-Ramos, R.M. Guerrero-Coronado, J. Mendoza-Barron, Adsorption of pentachlorophenol from aqueous solution onto activated carbon fiber, Ind. Eng. Chem. Res. 45 (2006) 330–336.
[45] T. Basova, S. Paul, D. Paul, P. Vadgama, A.G. Gürek, V. Ahsen, A. Ray, Liquid crystalline phthalocyanine thin films as nanoscale substrates for protein adsorption, J. Bionanosci. 2 (2008) 114–118.
[46] L. Giotta, G. Giancane, D. Mastrogiacomo, T. Basova, P. Metrangolo, L. Valli, Phenol chemisorption onto phthalocyanine thin layers probed by ATR-FTIR difference spectroscopy, Phys. Chem. Chem. Phys. 11 (2009) 2161–2165.
[47] A. Kovács, A. Kende, M. Mörtl, G. Volk, T. Rikker, K. Torkos, Determination of phenols and chlorophenols as trimethylsilyl derivatives using gas chromatography–mass spectrometry, J. Chromatogr. A 1194 (2008) 139–142.
[48] M.N. Sarrión, F.J. Santos, M.T. Galceran, Determination of chlorophenols by solid-phase microextraction and liquid chromatography with electrochemical detection, J. Chromatogr. A 947 (2002) 155–165.
[49] A.M. Awawdeh, H.J. Harmon, Spectrophotometric detection of pentachlorophenol (PCP) in water using water soluble porphyrins, Sens. Actuators, B 106 (2005) 234–242.
[50] Z.Z. Öztürk, R. Zhou, U. Weimar, V. Ahsen, Ö. Bekaroğlu, W. Göpel, Soluble phthalocyanines for the detection of organic solvents: thin film structures with quartz microbalance and capacitance transducers, Sens. Actuators, B 26–27 (1995) 208–212.
[51] A. Nooke, U. Beck, A. Hertwig, A. Krause, H. Krüger, V. Lohse, D. Negendank, J. Steinbach, Ellipsometric detection of gases with the surface plasmon resonance effect on gold top-coated with sensitive layers, Thin Solid Films 519 (2011) 2659–2663.

Biographies

Hikmat Banimuslem is a Ph.D. student in the Material and Engineering research Institute, Sheffield Hallam University, UK. He is currently investigating functional materials, which include the hybrids of CNT and substituted phthalocyanine molecules for sensor applications.

Aseel Hassan B.Sc., M.Sc., Ph.D. in Physics, is a Senior Lecturer at the Faculty of Arts, Computing Engineering and Sciences of Sheffield Hallam University, UK. He carries out his research within the Materials and Engineering Research Institute and his interest lies in thin film technology mainly for application in chemical and biosensing, as well as for electronic device application. He uses optical techniques such as surface plasmon resonance and spectroscopic ellipsometry, as well as quartz crystal microbalance detection techniques, employing organic thin films such as metallophthalocyanines and calix-resorcinarenes as the sensing layers.

Tamara Basova received her Ph.D. (1999) and D.Sc. (2011) in Physical Chemistry from Nikolaev Institute of Inorganic Chemistry, Novosibirsk, Russia. Now, she is a leading researcher in the institute. Her research interests are mainly directed towards the synthesis and characterisation of various phthalocyanines and the investigation of the sensor and electrical properties of their oriented films.

Asuman Dakoğlu Gülmez received the B.Sc. degree from Department of Chemistry of Karadeniz Technical University, Turkey. She received M.Sc. degree from Chemistry Department, Gebze Institute of Technology, Turkey. Her research interest lies in the synthesis, characterisation and liquid crystalline properties of phthalocyanines and their transition metal complexes.

Sinem Tuncel B.Sc., M.Sc., Ph.D. is a Research Assistant at Chemistry Department, Gebze Institute of Technology, Turkey. Her research interests are the synthesis and characterisation of phthalocyanines and the investigation of their liquid crystalline, photophysical and photochemical properties.

Mahmut Durmuş B.Sc., M.Sc., PhD is an Associated Professor at Gebze Institute of Technology, Department of Chemistry in Turkey. His research interests are the design, synthesis and characterisation of advanced materials such as phthalocyanines, borondipyrromethenes (BODIPY), coumarins and phosphazenes for different applications including photodynamic therapy (PDT) of cancer, liquid crystals, energy transfer dyes, chemosensors *etc.*

Ayşe Gül Gürek B.Sc., M.Sc., Ph.D. is a professor at Department of Chemistry of Gebze Institute of Technology Turkey. Her research interests are: the synthesis of stable ligands, e.g. phthalocyanines, *vic*-dioximes with such functional groups as crown ether, aza ether, and thia ether, the synthesis of transition metal complexes and the investigation of their liquid crystal, semiconductor, and chemical sensor properties by enlightening the structure of these macrocyclic compounds.

Vefa Ahsen B.Sc., M.Sc., Ph.D. is a professor at the Chemistry Department of Science Faculty at Gebze Institute of Technology Turkey. His research interest lies in the synthesis of stable ligands, e.g. phthalocyanines, *vic*-dioximes with such functional group as crown ether, aza ether, and thia ether, the synthesis of their alkaline and transition metal complexes as nanomaterials. The main application areas of these materials (gas sensors, photodynamic therapy, catalysis, liquid crystals, semiconductors and NLO) are investigated.

Dalton Transactions

PAPER

View Article Online
View Journal | View Issue

Distribution of single-walled carbon nanotubes in pyrene containing liquid crystalline asymmetric zinc phthalocyanine matrix†

Cite this: Dalton Trans., 2014, 43, 4689

Sinem Tuncel,[a] Esra Nur Kaya,[a,b] Mahmut Durmuş,*[a] Tamara Basova,*[c] Ayşe Gül Gürek,[a] Vefa Ahsen,[a] Hikmat Banimuslem[d] and Aseel Hassan[d]

A novel pyrene containing asymmetric Zn(II) phthalocyanine (AB3 type) was synthesized and characterized by various spectroscopic techniques as well as elemental analysis. A symmetric polyoxyethylene substituted Zn(II) phthalocyanine (B4 type) derivative was also prepared in order to compare the properties and determine the effect of the pyrene group on the phthalocyanine molecule. Composites of synthesized zinc(II) phthalocyanine–single wall carbon nanotubes (ZnPc–SWCNTs) containing 1 and 2 wt% carbon nanotubes were prepared by mixing these two components in dichloromethane followed by removal of the solvent and drying under vacuum. The liquid crystalline properties of the pure compounds and their composites were investigated in comparison with symmetric polyoxyethylene substituted Zn(II) phthalocyanine (B4 type) by using polarized optical microscopy, differential scanning calorimetry and X-ray diffraction analysis. The distribution of the SWCNTs in the ordered matrix of the columnar mesophase of these derivatives was studied by the method of polarized Raman spectroscopy and scanning electron microscopy (SEM). It was shown that the nature of the mesophases was not altered in these composites. The I(v) dependencies for the films deposited onto interdigitated electrodes were measured and it was shown that the lateral conductivity tends to increase with increasing SWCNT concentration.

Received 1st October 2013,
Accepted 3rd December 2013
DOI: 10.1039/c3dt52736k
www.rsc.org/dalton

Introduction

In order to satisfy the demands of the rapid growth in nanotechnology, it is necessary to develop different types of functional materials possessing outstanding electrical, optical, or mechanical properties. Among these, composite materials play a central role in these new technologies, due to their synergetic combination of two or more components.[1] A thriving area of relevant research has focused on the smart integration of carbon nanotubes (CNTs) with phthalocyanine (Pc) complexes for enhancing optoelectronic,[2] electro-catalytic[3] and sensing[4] properties. The results have shown that these hybrids can be more efficient in improving the relative responses compared to the individual CNT or Pc species. In these hybrids, CNTs are functionalized with metallophthalocyanine derivatives either *via* covalent[5–7] or non-covalent[5,8,9] interactions. These hybrids are currently receiving thorough investigation by several research groups in order to enhance the optoelectronic, electro-catalytic and sensing properties of MPc films.[5–10] The evidence so far has shown that these hybrids can be more efficient in improving the relative response of hybrid films compared to the individual CNT or MPc species.[5–10]

Another type of functional materials is composite materials which can be obtained by the dispersion of small amounts (0.1–10 wt%) of carbon nanotubes in a phthalocyanine matrix. In this combination, liquid crystalline (LC) materials have attracted increasing attention for their formation of composites with CNTs,[11–14] as LC materials have the potential to orient CNTs for anisotropic electrical conduction. On one hand, the flexible orientational order of LC materials provides a facile approach to efficiently align CNTs. On the other hand, CNTs could induce distinctive changes in the physical properties of the LC matrix, leading to enhanced performances of the LC materials. Some examples of the alignment of nanotubes in nematic LC materials are given in the literature.[15] Patrick and Lynch[16] reported a variety of methods for the post-synthesis organization of single- and multi-walled carbon nanotubes (SWCNTs and MWCNTs) using thermotropic

Gebze Institute of Technology, Department of Chemistry, P.O. Box: 141, 1400 Gebze, Kocaeli, Turkey. E-mail: durmus@gyte.edu.tr; Fax: (+)90(262)60531 01
Marmara University, Faculty of Art and Science, Department of Chemistry, 34722 Kadikoy-Istanbul, Turkey
Nikolaev Institute of Inorganic Chemistry SB RAS, Novosibirsk, 630090, Russia
Materials and Engineering Research Institute, Sheffield Hallam University, Sheffield S1 1WB, UK

† Electronic supplementary information (ESI) available: The mass, FT-IR and ^{1}H-NMR spectra of compound 3, DSC spectra of compounds 3, 4 and their composites, polarizing optical microscope images of 3/SWCNT composites and I(v) characteristics of pure 3 and 4 and their composite films. See DOI: 10.1039/c3dt52736k

matic LC media in the presence of an external alignment rce (magnetic or electric field, substrate grooves, *etc*). Lager- ll and co-workers[17,18] utilized the lyotropic nematic LC ases with rod-shaped and disk-shaped micelles to induce e alignment of SWCNTs. The functionalization of 'CNT-COCl with a discotic moiety, notably hydroxy-termi- ted triphenylene, and their alignment in the supramolecular der of a columnar mesophase were investigated by Kumar d Bisoyi.[19] Octadecylamine functionalized single walled rbon nanotubes in triphenylene and rufigallol-based room mperature monomeric and polymeric discotic liquid crystals ere investigated by the same group.[20] Discotic ionic liquid stals of triphenylene derivatives bearing six imidazolium n pendants were reported to serve as excellent dispersants r pristine SWCNTs.[21]

Liquid crystalline (LC) phthalocyanines self-organize from mmon solvents into columnar aggregates and become of terest as potential solution processed materials for appli- tion in molecular electronics.[22–26] The columnar stacks of iscotic Pc molecules with efficient overlap of π-orbitals along e stacking direction and low reorganization energy[27] provide icient anisotropic electronic transport channels along the olecular columns in the liquid crystalline mesophases with ole mobilities in the order of 10^{-1} cm^2 V s^{-1}.[28]

While the hybrids of SWCNTs with metal phthalocyanines ave been studied in detail,[5–10,29] the experimental data on the istribution and alignment of CNTs in the matrix of liquid rystalline phthalocyanines are rather scarce.

The main target of this work was to investigate the dis- ersion of single-walled carbon nanotubes in novel liquid crys- lline asymmetrically substituted Pc bearing one pyrene and ix polyoxy groups as side chains. The effect of nanotubes on e phase behavior of this zinc phthalocyanine derivative and n the structural and functional properties of the SWCNT- hthalocyanine composite thin films was investigated. The olyoxy groups were chosen to exhibit the liquid crystalline roperties of the target materials. The pyrene group was also hosen to enhance the interaction of phthalocyanines with the NTs. The pyrenyl group is known to interact strongly with 'CNTs *via* π-stacking interactions.[30–32] This has been used, or example, in the production of SWCNT-nanoparticle ybrids,[30] the grafting of proteins and other biological mole- ules to SWCNTs[30] and to immobilize light harvesting groups n the SWCNTs, as well as in the design of new photoelectric evices.[32]

The composites of symmetrically substituted zinc phthalo- anine bearing eight polyoxy groups as side chains are also tudied for a comparison.

xperimental

aterials

-Nitrophthalonitrile,[33] 4,5-dichlorophthalonitrile,[34] 4-(1-pyrenyl- ethoxy)phthalonitrile (1)[35] and 4,5-bis(4,7,10-trioxaundecan- -sulfanyl)phthalonitrile (2)[36] were synthesized and purified according to reported procedures. All reaction solvents were dried and purified as described by Perrin and Armarego.[37] All other reagents were obtained from commercial suppliers. The SWCNTs were purchased from Sigma-Aldrich and used without further purification or chemical treatment.

Equipment

FT-IR spectra were recorded between 4000 and 650 cm^{-1} using a Perkin Elmer Spectrum 100 FT-IR spectrometer with an attenuated total reflection (ATR) accessory featuring a zinc selenide (ZnSe) crystal. Matrix-assisted laser desorption/ionization time-of-flight mass spectrometry (MALDI-TOF-MS) measurements were performed on a Bruker Daltonics micrOTOF (Bremen, Germany) using 2,5-dihydroxybenzoic acid as a matrix. ^{1}H NMR spectra were recorded in DMSO-d_6 solutions on a Varian 500 MHz spectrometer. Optical spectra in the UV-visible region were recorded with Varian 50 scan, Shimadzu UV-Vis-3101 and Shimadzu UV-Vis-2101 spectrometers using a 1 cm pathlength cuvette at room temperature.

The phase transition behaviors of the Pcs were observed by means of a polarizing optical microscope (POM) (Leitz Wetzlar Orthoplan-pol.) equipped with a hot stage (Linkam TMS 93) and a temperature controller (Linkam LNP). Thermogravimetric analysis (TGA) was carried out on a Mettler Toledo Stare Thermal Analysis System at a rate of 10 °C min^{-1} in a nitrogen flow (50 mL min^{-1}). Transition temperatures were determined at a scan rate of 10 °C min^{-1} using a Mettler Toledo Star Thermal Analysis System/DSC 822. The differential scanning calorimeter (DSC) system was calibrated with 3 mg indium samples under a nitrogen atmosphere. X-ray diffraction measurements (XRD) (Cu-Kα-radiation) were performed using a Bruker Advanced D8 diffractometer.

Raman spectra were recorded with a Triplemate, SPEX spectrometer equipped with CCD detector in back-scattering geometry. The 488 nm, 40 mW line of an Ar-laser was used for the spectral excitation.

Scanning electron microscopy (SEM) images were obtained using a FEI-nova nanosem 200.

Spectroscopic ellipsometry was used to determine the thickness of the films using a Woolam M-2000 V^{TM} rotating analyser spectroscopic ellipsometer in the spectral range of 400–800 nm. DC-conductivity measurements were carried out using a Keithley 4200 semiconductor characterization system.

Synthesis

2,3,9,10,16,17-Hexakis(4,7,10-trioxaundecan-1-sulfanyl)-23(24)-(1-pyrenylmethoxy) phthalocyaninato zinc(II) (3). 4-(1-Pyrenylmethoxy)phthalonitrile (1) (100 mg, 0.28 mmol), 4,5-bis(4,7,10-trioxaundecan-1-sulfanyl)phthalonitrile (2) (405.7 mg, 0.84 mmol), 1,8-diazabicyclo[5.4.0] undec-7-ene (DBU) (0.08 mL, 0.56 mmol) and $Zn(OAc)_2$ (102 mg, 0.56 mmol) were refluxed in dry *n*-pentanol (5 mL) for 24 h under an argon atmosphere. Then, the reaction mixture was cooled to room temperature and poured into *n*-hexane. The green solid product was precipitated and collected by filtration. The solid

s dissolved in dichloromethane and filtered in order to remove any inorganic impurities then concentrated. Firstly, B2 type phthalocyanine was eliminated over a silica gel column using a 50 : 1 dichloromethane–ethanol mixture, then symmetrical AB3 type phthalocyanine **3** was obtained using a : 1 dichloromethane–ethanol mixture and finally symmetric A4 type phthalocyanine **4** was obtained using a 10 : 1 dichloromethane–ethanol mixture as the eluent.

Compound **3**: FT-IR [(ATR) ν_{max}/cm^{-1}]: 3190–3040 (Ar–CH), 60–2855 (CH), 1602 (Ar–C=N), 1459 (C=C), 1358 (C–N), 60 (C–O–C), 1084 (–OCH_3). UV–Vis (DMF): λ_{max} nm (log ε) 1 (4.35), 624 (3.63), 373 (3.98), 344 (3.95). ^{1}H-NMR 00 MHz, DMSO-d_6) δ ppm: 8.97–7.64 (br, m, 18H, Ar–H), 90 (bs, 2H, OCH_2), 4.00–3.94 (m, 12H, OCH_2), 3.75–3.68 (m, 2H, OCH_2), 3.68–3.60 (m, 24H, SCH_2, OCH_2), 3.57–3.47 (m, 2H, OCH_2), 3.40–3.34 (m, 12H, OCH_2), 3.15 (s, 18H, OCH_3). lemental analysis: calcd (%) for $C_{91}H_{110}N_8O_{19}S_6Zn$: C 58.21, 5.90, N 5.97; found: C 58.56, H 6.01, N 5.71. MS (MALDI-F), *m/z* (%): Calcd 1877.69, found 1878.30 $[M + H]^+$.

Preparation of phthalocyanine-SWCNT composite materials. ZnPc/SWCNT dispersion was prepared by adding a small mount (1–2 wt%) of the SWCNTs to the zinc phthalocyanine lution in dichloromethane and subjected to sonication uring 1–2 hours to enhance the nanotube solubility. Then the lms of composites of **3–SWCNT** and **4–SWCNT** were deposited spin coating or drop-casting of the dispersion in dichloroethane onto the glass slides for further investigation.

Results and discussion

Synthesis and characterization

The synthesis of the phthalonitrile derivatives (**1** and **2**, Scheme 1) has been previously reported.[35,36] The synthesis of unsymmetrical phthalocyanines is complicated compared to symmetrically substituted Pcs as they often require extensive purification methods to obtain the desired products. Scheme 1 shows the chemical structure and the synthetic route of compound **3**. The statistical condensation method of two phthalonitriles **1** and **2** was employed in this work.

The reaction for the formation of **3** was performed by a statistical method using a 1 : 3 ratio of phthalonitrile **1** (A): phthalonitrile **2** (B). As a result, the AB3 (**3**), A2B2 and B4 (**4**) isomers were obtained in different amounts during the synthesis of compound **3**. The three main phthalocyanine isomers (A2B2, AB3 and B4), displaying different polarities, were readily separated on silica-gel column chromatography. Firstly the elution of the A2B2 derivative (eluent: dichloromethane–ethanol 50/1) followed by the desired AB3 phthalocyanine **3** (eluent: dichloromethane–ethanol 25/1), and finally symmetric B4 phthalocyanine **4** (eluent: dichloromethane–ethanol 10/1) were obtained as pure samples after purification by column chromatography. The synthesis and characterization of the B4 type Zn(II) phthalocyanine derivative (**4**) was also previously reported by us.[38]

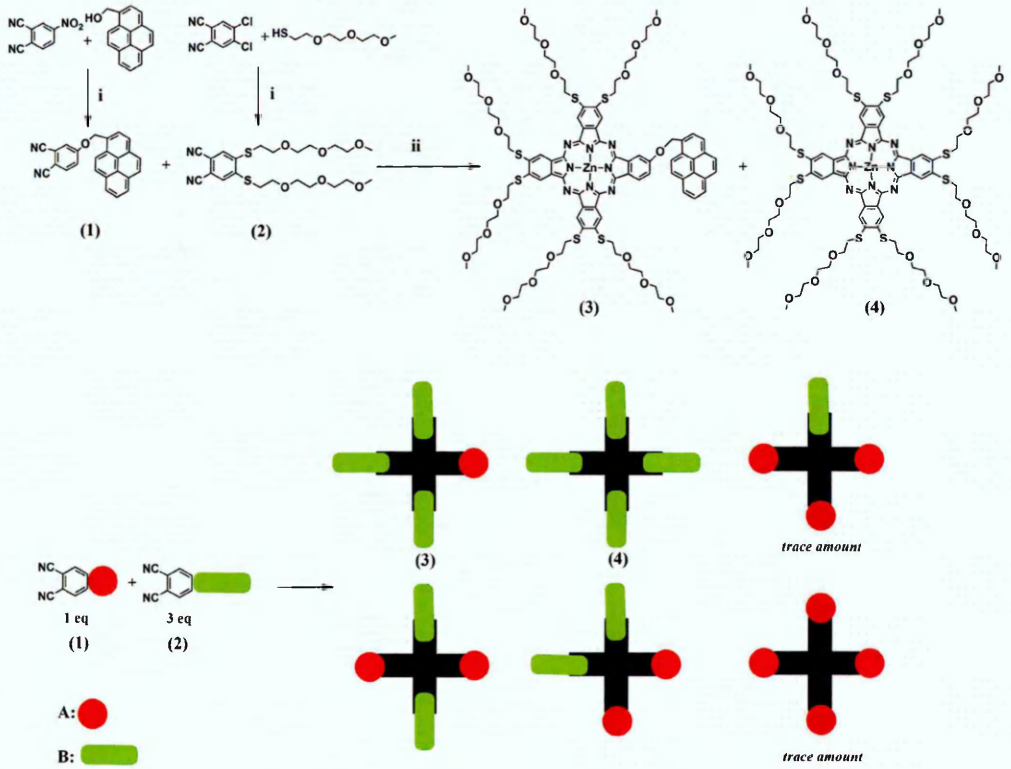

Scheme 1 Synthesis of target zinc(II) phthalocyanine compounds. Reagents: (i) K_2CO_3, DMF. (ii) $Zn(OAc)_2$, *n*-pentanol, DBU.

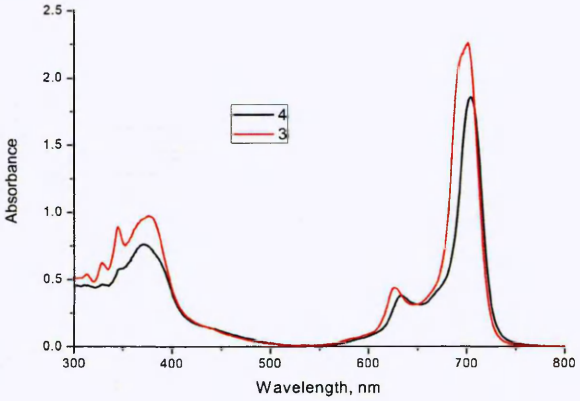

Fig. 1 UV-vis optical absorption spectra of **3** and **4** in DMF (1×10^{-5} M).

The characterization of complex **3** was achieved using matrix-assisted laser desorption/ionization-time of flight (MALDI-TOF) (Fig.S1, ESI†), FT-IR (Fig. S2, ESI†), and proton nuclear magnetic resonance (^{1}H-NMR) (Fig. S3, ESI†) spectroscopies and elemental analysis.

The optical absorption spectra of the solutions of compounds **3** and **4** in DMF are shown in Fig. 1. The absorption spectrum of ZnPc **4** in DMF consists of a Soret band at 372 nm and a Q-band at 704 nm. The introduction of one pyrene moiety leads to a small shift in the Soret band to 371 nm and the Q-band to 698 nm.

Liquid crystalline properties of zinc phthalocyanines. According to the thermogravimetric analysis (TGA) results, it was observed that compounds **3** and **4** both start to decompose above 200 °C. In order to avoid decomposition, DSC measurements were performed in the temperature range of 25–200 °C. The differential scanning calorimeter (DSC) measurements of compound **3** did not show any significant peak corresponding to any phase transition (Fig. S4, ESI†). This may be the result of interrupting the heating cycle before reaching the clearing point. However, in the polarized optical microscope (POM) measurements it was observed that compound **3** became an isotropic liquid at about 230 °C accompanying decomposition. When we cooled this sample from isotropic melt, a typical hexagonal texture was formed at about 200 °C. This hexagonal texture remained constant until 130 °C during cooling. A fingerprint texture of the rectangular phase was observed below 130 °C as can seen in Fig. 2 confirming the transition from hexagonal phase to rectangular phase. Similar transitions have been observed in the literature.[39]

In the DSC measurements, compound **4** shows a transition at about 100 °C for all the heating cycles and at 80 °C for all cooling cycles (Fig. S5, ESI†). However, if the sample was prepared by evaporating a dichloromethane solution of compound **4** on one glass slide, a mosaic texture typical for planar alignment was obtained at room temperature without annealing. In the POM measurements it was observed that compound became an isotropic liquid at about 236 °C accompanying decomposition.

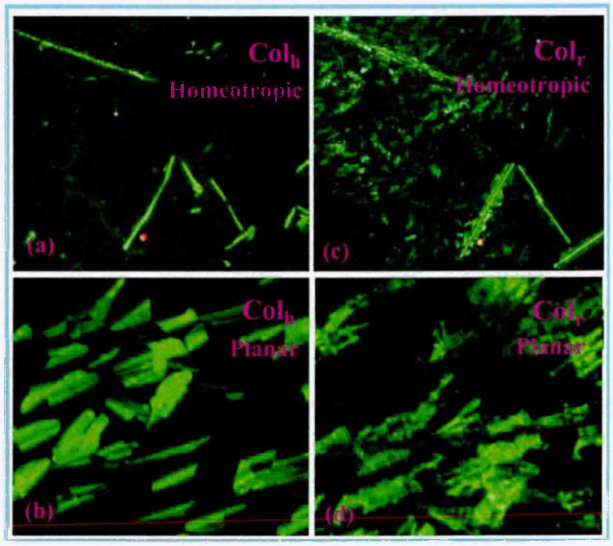

Fig. 2 POM measurements for compound **3**. (a) Homeotropic alignment in the Col$_h$ mesophase, 200 °C. (b) Planar alignment in the Col$_h$ mesophase, 200 °C. (c) Homeotropic alignment in the Col$_r$ mesophase, 25 °C. (d) Planar alignment in the Col$_r$ mesophase, 25 °C. Magnification: 40x. Heating–cooling rate: 20 °C min^{-1}.

The identification of mesophases was carried out by X-ray diffraction (XRD) measurements at room temperature. Dichloromethane solutions of **3** and **4** were dropped on glass slides and left for the solvent to evaporate at room temperature. The powder diffraction patterns of **3** and **4** contain typical reflections of a columnar mesophase of substituted Pcs (Fig. 3 and 4, Table 1). In the low angle region (2θ = 4°–6°), the phthalocyanine derivatives produce a sharp peak with either a shoulder or a small additional peak. In the literature, it is observed that, in the case of the rectangular columnar phase, the (10) peak of the Col$_h$ mesophase splits in the (11) and (20) reflections of the Col$_r$ phase.[39] Additionally, it is known that the lattice constants a and b can be calculated from the equation: $1/d^2_{hkl} = h^2/a^2 + k^2/b^2$. Based on this information, possible indexation of the Col$_r$ mesophase can be proposed as in Table 1. These results suggest a two-dimensional rectangular lattice with disc-like molecules stacked in columns in a rectangular arrangement. Both XRD patterns of **3** and **4** show a Col$_r$ phase with *P2gg* symmetry.

ZnPc–SWCNT composites. Binary mixtures of SWCNTs with phthalocyanine were prepared by mixing the two components in dichloromethane followed by removal of solvent and drying under vacuum. Four composites of ZnPc–SWCNT (compounds **3** and **4**) containing 1 and 2 wt% carbon nanotubes were prepared and analyzed by polarizing optical microscopy. All ZnPc–SWCNT composites containing 1 and 2 wt% were found to be liquid crystalline in nature. Similar to the pure ZnPcs, they show textures of columnar mesophases at room temperature (Fig. 5). Fig. 5a and 5d show the typical mosaic textures of pure phthalocyanine derivatives. For the SWCNT composites (Fig. 5b, c, e, f), the texture is obviously different, especially in

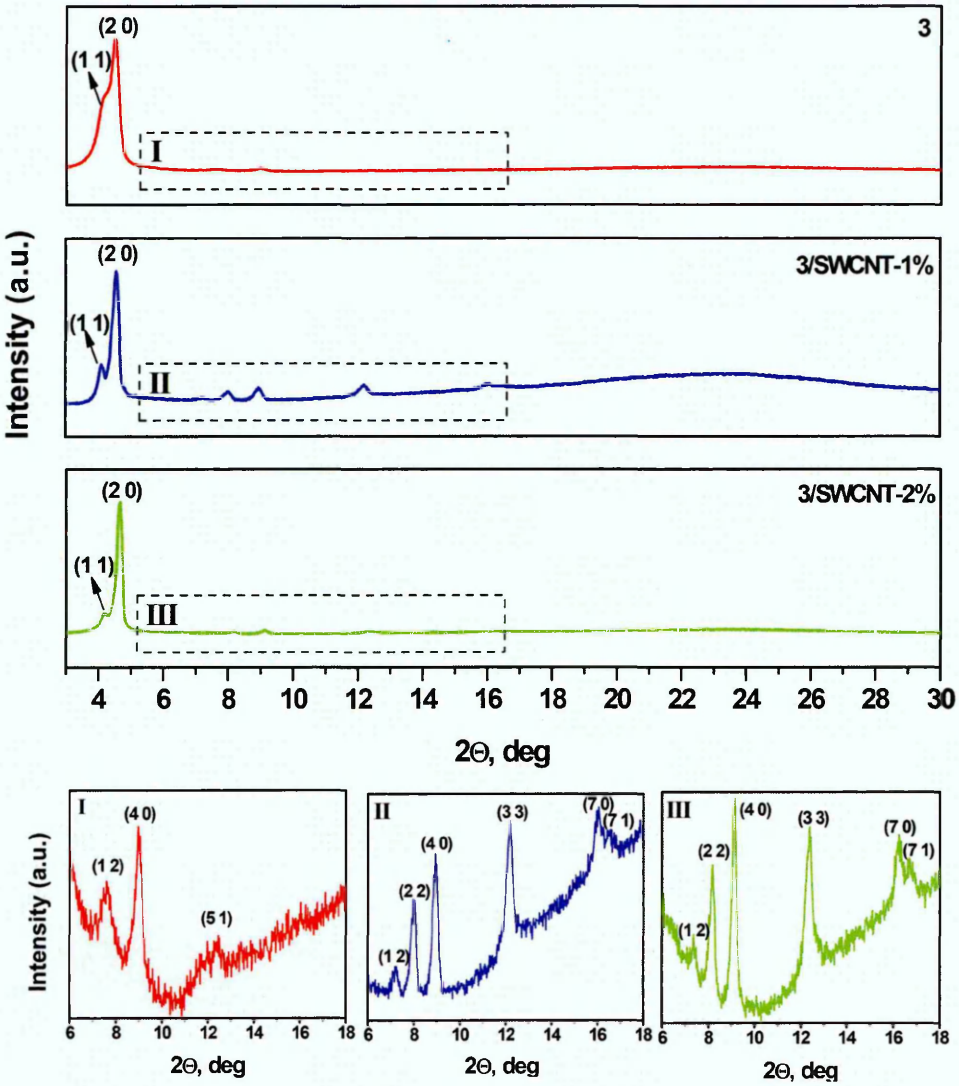

Fig. 3 XRD patterns of compound **3** and its composites at room temperature.

the case of **3–SWCNT** (Fig. 5b, c), to that of the pure materials. Inclusion of carbon nanotubes into the columnar matrix leads to an increase in the domain size, especially in the case of the composite **3–SWCNT**. We can suggest that SWCNTs dispersed in the LC matrix can act as seeds for oriented domain growth as was observed in the case of nematic liquid crystals.[40–42]

In the case of composite **3–SWCNT**-1% the fan-shaped texture is still persistent whereas a star-like layered structure is clearly seen for composite **3–SWCNT**-2%. It is necessary to mention that when we tried to insert more than 2 wt% SWCNTs in the columnar liquid crystal we observed small black aggregates of CNTs under the polarizing microscope, which meant that the CNTs were not homogeneously dispersed in the liquid crystal matrix of the composites with such high CNT additive concentration. In the case of composite **SWCNT** the formation of inhomogeneous films containing a small amount of black aggregates of CNTs starts to be observed even at 2 wt% SWCNTs.

In addition to microscopic analysis, we also examined the effect of SWCNTs on the phthalocyanine phase transitions using differential scanning calorimetry. No additional phase transition peaks from the phthalocyanines without SWCNTs characteristic of a phase separated system were detected in the calorimetric studies. However, it is necessary to mention that when we annealed the **3–SWCNT** composites between two glass slides, we also observed by POM the same rectangular-hexagonal phase transitions as was observed for pure **3** (Fig. S6, ESI†). If we compare the transitions, we can conclude that the transition temperature from rectangular to hexagonal mesophase increases with the addition of SWCNTs (Table 2).

The X-ray diffraction patterns of the composites at room temperature show similar features to those of compounds **3** and **4** confirming the rectangular columnar mesophase of the

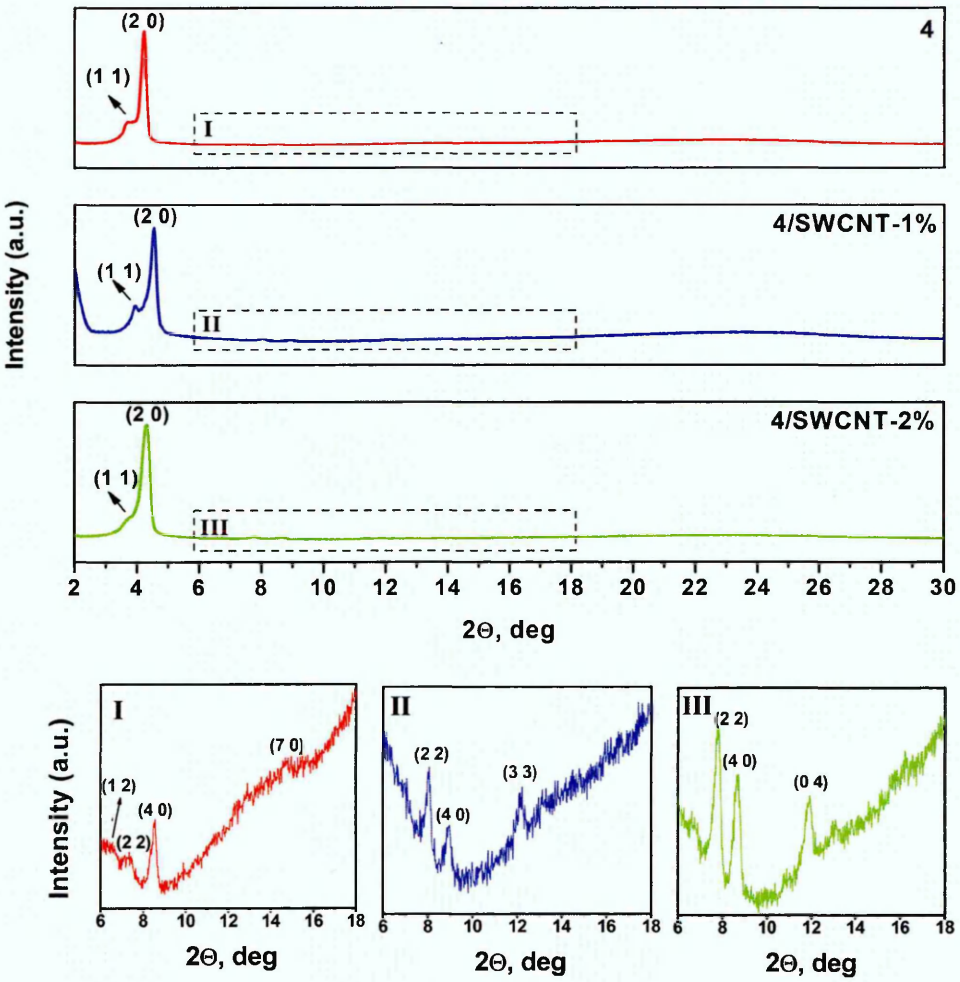

Fig. 4 XRD patterns of compound **4** and its composites at room temperature.

composites as shown in Fig. 3 and 4. The columnar mesophase structure is not destroyed by the inclusion of the SWCNTs, however a shift of the corresponding XRD peaks is observed. The XRD patterns of compound **3** at 20 °C display the most intensive diffraction peak at $2\theta = 4.52°$ corresponding to an intercolumnar distance of 19.53 Å (Fig. 3). This peak shifts to 4.56° (d = 19.36 Å) in the XRD pattern of the composite **3–SWCNT** containing 1 wt% SWCNTs and to 4.66° (d = 18.95 Å) in that of the composite **3–SWCNT** containing 2 wt% SWCNTs. This indicates that the inclusion of carbon nanotubes into the columnar matrix leads to a decrease in the intercolumnar distance. In the case of compound **4** the corresponding diffraction peak at $2\theta = 4.22°$ (d = 20.91 Å) shifts to $2\theta = 4.54°$ (d = 19.45 Å) upon addition of 1 wt% of SWCNT, however the addition of more amount of SWCNT (2 wt%) leads back to an increase in the intercolumnar distance to 20.44 Å which can be associated with the formation of an inhomogeneous material as was already revealed by POM.

The XRD patterns of the **3–SWCNT** composites also show the Col_r phase with *P2gg* symmetry, however it is obvious that the number of diffraction peaks increases after the addition of SWCNTs to compound **3**. This appears to be explained by the formation of domains with different orientations. As opposed to the Col_r phase with *P2gg* symmetry in the case of **4**, the XRD patterns of **4–SWCNT-1%** and **4–SWCNT-2%** show a Col_r phase with *C2 mm* symmetry (*hk*: $h + k = 2n$, *h*0: $h = 2n$, 0*k*: $k = 2n$ for *C2 mm*; *hk*: no conditions, *h*0: $h = 2n$, 0*k*: $k = 2n$ for *P2gg*).

Thin films of the composites **3–SWCNT** and **4–SWCNT** were deposited by drop-casting of their solutions in dichloromethane onto interdigitated electrodes to examine the conductivity as well as molecule orientations in the films.

The orientation of the phthalocyanine molecules in the films of the pure ZnPc derivatives and their composites were studied by the method of polarized Raman spectroscopy. The principles of Polarized Raman spectroscopy for investigation of molecular film orientation are described in detail in earlier publications.[43–48] This method is based on the measurement of the ratio of intensities of the bands for each symmetry type of vibrations in the Raman spectra measured in the parallel (I_{ii}) and cross (I_{ij}) polarizations of incident and scattering light

Table 1 X-Ray diffraction data for compounds **3** and **4** and their composites at room temperature

Compound	Phase	Observed spacings (Å)	Calculated spacings (Å)	Lattice parameters (Å)	Miller indices (h k)
	Col_r	21.2744	21.2744	a = 39.07	(1 1)
		19.5346	19.5346	b = 24.80	(2 0)
		11.5901	11.8231		(1 2)
		9.8400	9.7675		(4 0)
		7.1438	7.4531		(5 1)
3–SWCNT-1%	Col_r	21.5296	21.5296	a = 38.73	(1 1)
		19.3624	19.3624	b = 25.90	(2 0)
		12.2971	12.2721		(1 2)
		11.0661	10.7583		(2 2)
		9.8821	9.6824		(4 0)
		7.2490	7.1722		(3 3)
		5.5144	5.5329		(7 0)
		5.3312	5.4105		(7 1)
3–SWCNT-2%	Col_r	21.1194	21.1194	a = 37.90	(1 1)
		18.9504	18.9504	b = 25.43	(2 0)
		12.0079	12.0576		(1 2)
		10.8004	10.5604		(2 2)
		9.6508	9.4750		(4 0)
		7.1435	7.0403		(3 3)
		5.4542	5.4143		(7 0)
		5.2993	5.2957		(7 1)
	Col_r	23.8566	23.8566	a = 41.84	(1 1)
		20.9197	20.9197	b = 29.04	(2 0)
		13.4669	13.7052		(1 2)
		12.0379	11.9203		(2 2)
		10.3243	10.4600		(4 0)
		6.0294	5.9772		(7 0)
4–SWCNT-1%	Col_r	22.2990	22.2990	a = 38.90	(1 1)
		19.4491	19.4491	b = 27.21	(2 0)
		10.9620	11.1553		(2 2)
		9.8643	9.7250		(4 0)
		7.2392	7.4369		(3 3)
4–SWCNT-2%	Col_r	23.6689	23.6689	a = 40.88	(1 1)
		20.4402	20.4402	b = 29.03	(2 0)
		11.3251	11.3251		(2 2)
		10.2258	10.2258		(4 0)
		7.4191	7.4191		(0 4)

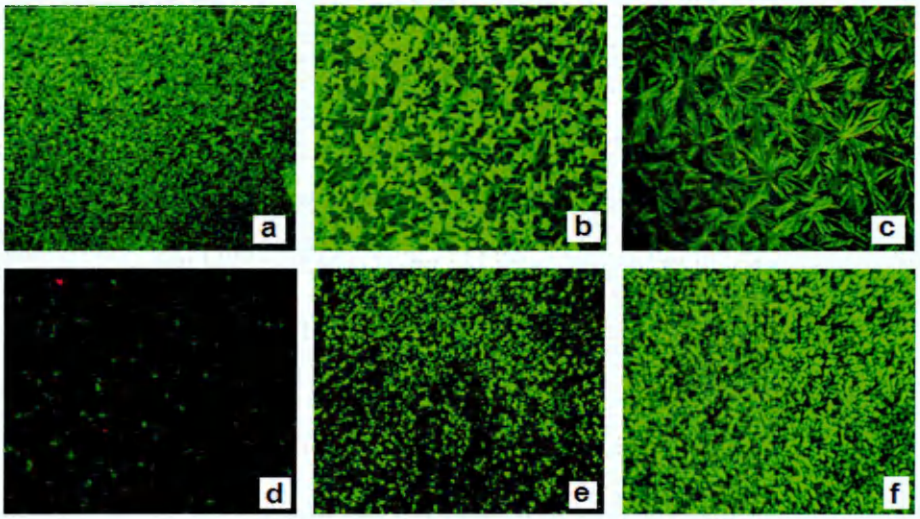

Fig. 5 Polarizing optical microscopy images of the films of pure **3** (a) and its composites containing 1 wt% (b), 2 wt% (c) SWCNTs; pure **4** (d) and its composites containing 1 wt% (e), and 2 wt% (f) SWCNTs, obtained under crossed polarized light.

and allows estimation of the angle of molecule inclination relative to the substrate surface. A phthalocyanine molecule is characterized by D_{4h} group symmetry where A_{1g}, B_{1g}, B_{2g}, E_g modes are Raman active.[46,47] The detailed analysis of the Raman tensors for the D_{4h} symmetry group and the determination of the molecular orientation are described in ref. 43.

able 2 Transitions from rectangular phase to hexagonal phase bserved during heating and cooling under POM for compound 3 and composites

ompound	Transition temperatures (°C)
	$Col_r \underset{130}{\overset{135}{\rightleftharpoons}} Col_h$
-SWCNT-1%	$Col_r \underset{167}{\overset{173}{\rightleftharpoons}} Col_h$
-SWCNT-2%	$Col_r \underset{177}{\overset{180}{\rightleftharpoons}} Col_h$

ate: 20 °C min^{-1}, Col_r: columnar rectangular phase, Col_h: hexagonal olumnar phase.

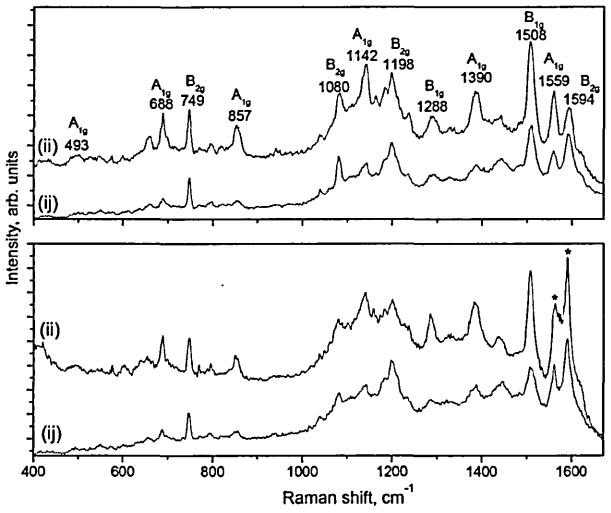

Fig. 6 Polarized Raman spectra of 3 and 3–SWCNT-2% films in parallel (ii) and cross (ij) polarizations of incident and scattered light. The Raman bands labelled with an asterisk correspond to the SWCNTs.

The Raman spectra of the films of the pure 3 and 4 derivatives and their composites deposited on glass substrates in parallel (ii) and cross (ij) polarizations are shown in Fig. 6 and 7, respectively. The intensities of the strongest lines with known symmetry types are measured. It has already been shown that there are no intensive bands belonging to organic substituents in the range from 300 to 1650 cm^{-1} in Raman spectra of substituted phthalocyanines due to the resonance character of the Raman spectra excited by the lasers of the visible region.[44]

Thus, all bands in the Raman spectrum belong to the bending and stretching vibrations of the phthalocyanine macrocycle. The determination of the symmetry types of all observed modes was made on the basis of the polarized spectra of ZnPc solutions in $CHCl_3$ and by analogy with the Raman spectra of the metallophthalocyanines with similar substituents.[49] The symmetry types of the most intensive bands used for the determination of film orientation are indicated in Fig. 6 and 7. The average values of I_{ii}/I_{ij} ratios for each symmetry type of vibration are listed in Table 3.

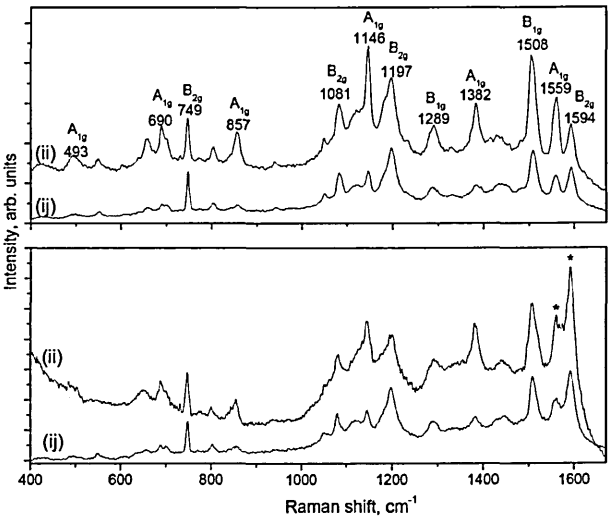

Fig. 7 Polarized Raman spectra of 4 and 4–SWCNT-2% films in parallel (ii) and cross (ij) polarizations of incident and scattered light. The Raman bands labelled with an asterisk correspond to SWCNT.

Table 3 Measured I_{ii}/I_{ij} ratios for A_{1g}, B_{1g} and B_{2g} modes in the Raman spectra of the ZnPc and their composite films and calculated angles of the ZnPc molecule inclination relative to the substrate surface

Film	I_{ii}/I_{ij} ratios for A_{1g}, B_{1g} and B_{2g} modes			Angle (°)
	A_{1g}	B_{1g}	B_{2g}	α
3	3.7	3.6	1.4	85
3–SWCNT-2%	3.9	3.2	1.4	82
4	4.0	2.9	1.3	76
4–SWCNT-2%	4.1	1.3	1.3	Disordered film

The angles of inclination of the molecules relative to the substrate surface (α) in the film of pure 3 and 4 derivatives were calculated to be 85° and 76°, respectively. The inclusion of carbon nanotubes into the columnar matrix of 3–SWCNT doesn't lead to big changes in the inclination angle of the ZnPc molecules relative to the substrate surface. On the contrary, the film of 4–SWCNT is disordered because the ratio of intensities of the corresponding vibrations in the (ii) and (ij) spectra were close to that in the spectra of solution.

SEM images of the films of the composites 3–SWCNT containing 1 wt% and 2 wt%, and 4–SWCNT containing 2 wt% of SWCNTs are given in Fig. 8(a,b) and 8(c), respectively. The films consist of thicker nanotubes of 10–30 nm in diameter. These nanotubes appear to consist of bundles of SWCNTs wrapped by layers of LC phthalocyanine molecules. We suggest that the core part of the phthalocyanine LC molecules anchors around the SWCNT walls, meanwhile the tail part repels sideways to enhance the π–π stacking by maximizing the hexagon–hexagon interactions between the two species. A similar scheme of interaction between the porphyrin derivative ZnP $(alkyl)_4$ and the surface of the semiconducting SWCNTs was visualized by performing DFT calculations in ref. 50.

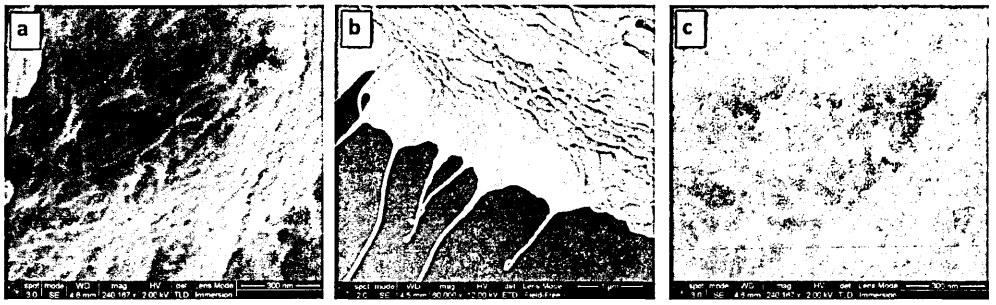

ig. 8 SEM images of the films of the composites 3–SWCNT (a - surface view, b - edge view) containing 2 wt% of SWCNTs and 4–SWCNT (c) containing 2 wt% of SWCNTs.

able 4 Calculated conductivity of pure 3 and 4 derivatives and their omposites 3–SWCNT and 4–SWCNT containing 1 and 2 wt% of WCNTs

ilm	Conductivity (Ω^{-1} m^{-1})
	8.2×10^{-6}
-SWCNT-1%	1.9×10^{-2}
-SWCNT-2%	3.6×10^{-2}
	4.4×10^{-6}
-SWCNT-1%	4.6×10^{-3}
-SWCNT-2%	8.6×10^{-3}

In the case of 3–SWCNT-2% these thicker nanotubes have a tendency to lie stretched mainly in one direction in the LC matrix (Fig. 8(a)), while in 4–SWCNT-2% they are more tangled and disordered (Fig. 8(c)). The edge view of the 3–SWCNT-2% film (Fig. 8(b)) shows that the films of 3–SWCNT-2% have a layered structure with the layers aligning parallel to each other and with the phthalocyanine molecules perpendicular to the layers according to the data of polarized Raman spectroscopy. The more ordered structure of the 3–SWCNT films appears to be connected to the presence of the pyrene groups in compound 3 which are known to interact strongly with SWCNTs *via* π-stacking interactions.[29–32] Meanwhile, discotic LC materials derived from triphenylene have been reported to orient CNTs.[19,20] However, owing to their rather low miscibility with pristine CNTs, the use of CNTs covalently modified with triphenylene was essential.

The I(v) dependencies for the films deposited onto interdigitated electrodes are given in Fig. S7 (ESI†). The calculated conductivities are summarized in Table 4. The lateral conductivity tends to increase with increasing SWCNT concentration. For example, the conductivity of the 3–SWCNT-2% composite films is about 4 orders of magnitude higher than that of the pure films. It is necessary to mention that an increase in SWCNT concentration above 2% leads to the formation of non-homogeneous composite films containing small particles of aggregated nanotubes. The larger electrical conductivity of the nanocomposites arises due to the highly delocalized π electron density of phthalocyanine molecules bonded to SWCNTs which provide a facile path for electronic conduction. An increase in conductivity in the region of 2–4 orders of magnitude in dependence on the orientations of the LC columns and SWCNTs has been observed in the case of discotic ionic liquid crystals of triphenylene derivatives bearing six imidazolium ion pendants.[21]

Conclusions

In this study, the investigation of the dispersion of single-wall carbon nanotubes in liquid crystalline asymmetric Zn(II) phthalocyanine bearing one pyrene and six polyoxy units (AB3 type) and symmetric Zn(II) phthalocyanine bearing eight polyoxy units (B4 type) was carried out. The phthalocyanine derivatives were synthesized by using a statistical method with two different substituted phthalonitriles (A and B). Both pure compounds and their composites with SWCNTs showed liquid crystalline properties with rectangular columnar stacking at room temperature. POM, Raman spectra and conductivity investigations indicate intercalation of the SWCNTs into the matrix of discotic liquid crystalline zinc phthalocyanines. The dispersion of SWCNTs in the liquid crystalline phthalocyanine matrix provide a route for synthesizing novel materials with interesting properties useful for applications in many devices such as photoconductors, light emitting diodes, solar cells, sensors, optical data storage, thin film transistors and so on. The nature of the mesophases is not altered in these composites. On the other hand, the films of composites exhibit enhanced electrical conductivity of about four orders of magnitude compared to the corresponding pure phthalocyanines.

The inclusion of carbon nanotubes into the columnar matrix leads to an increase in the domains size, especially in the case of composite 3–SWCNT. The films of 3–SWCNT have a layered structure with the layers aligning parallel to each other and with the phthalocyanine molecules perpendicular to the layers according to the data of polarized Raman spectroscopy.

Acknowledgements

This work was supported by a bilateral project between The Scientific and Technological Research Council of Turkey

TUBITAK, Project number: 111M699) and the Russian Foundation of Basic Research (RFBR, Project number: 12-03-91372-T_a).

Notes and references

1 T. M. McEvoy, J. W. Long, T. J. Smith and K. J. Stevenson, *Langmuir*, 2006, **22**, 4462.
2 U. Hahn, S. Engmann, C. Oelsner, C. Ehli, D. M. Guldi and T. Torres, *J. Am. Chem. Soc.*, 2010, **132**, 6392.
3 T. Mugadza and T. Nyokong, *Electrochim. Acta*, 2010, **55**, 6049.
4 F. C. Moraes, D. L. C. Golinelli, L. H. Mascaro and S. A. S. Machado, *Sens. Actuators, B*, 2010, **148**, 492.
5 G. Bottari, J. A. Suanzes, O. Trukhina and T. Torres, *J. Phys. Chem. Lett.*, 2011, **2**, 905.
6 T. Mugadza and T. Nyokong, *Polyhedron*, 2011, **30**, 1820.
7 T. Mugadza and T. Nyokong, *J. Colloid Interface Sci.*, 2011, **354**, 437.
8 Y. Wang, N. Hu, Z. Zhou, D. Xu, Z. Wang, Z. Yang, H. Wei, E. S.-W. Kong and Y. Zhang, *J. Mater. Chem.*, 2011, **21**, 3779.
9 X. Wang, Y. Liu, W. Qiu and D. Zhu, *J. Mater. Chem.*, 2002, **12**, 1636.
10 W. Feng, Y. Li, Y. Feng and J. Wu, *Nanotechnology*, 2006, **17**, 3274.
11 Y. Ji, Y. Y. Huang and E. M. Terentjev, *Langmuir*, 2011, **27**, 13254.
12 M. Rahman and W. Lee, *J. Phys. D: Appl. Phys.*, 2009, **42**, 063001.
13 G. Scalia, *ChemPhysChem*, 2010, **11**, 333.
14 H. Qi and T. Hegmann, *J. Mater. Chem.*, 2008, **18**, 3288.
15 I. Dierking, G. Scalia and P. Morales, *J. Appl. Phys.*, 2005, **97**, 044309.
16 M. D. Lynch and D. L. Patrick, *Nano Lett.*, 2002, **2**, 1197.
17 J. Lagerwall, G. Scalia, M. Haluska, U. Dettlaff-Weglikowska, S. Roth and F. Giesselmann, *Adv. Mater.*, 2007, **19**, 359.
18 J. P. E. Lagerwall, G. Scalia, M. Haluska, U. Dettlaff-Weglikowska, F. Giesselmann and S. Roth, *Phys. Status Solidi B*, 2006, **243**, 3046.
19 S. Kumar and H. K. Bisoyi, *Angew. Chem., Int. Ed.*, 2007, **46**, 1501.
20 H. K. Bisoyi and S. Kumar, *J. Mater. Chem.*, 2008, **18**, 3032.
21 J. J. Lee, A. Yamaguchi, Md. A. Alam, Y. Yamamoto, T. Fukushima, K. Kato, M. Takata, N. Fujita and T. Aida, *Angew. Chem., Int. Ed.*, 2012, **51**, 8490.
22 J. Simon and P. Bassoul, in *Phthalocyanines: Properties and Applications*, ed. C. C. Leznoff and A. B. P. Lever, VCH, New York, 1993, vol. 2, p. 223.
23 A. M. van de Craats, N. Stutzmann, O. Bunk, M. M. Nielsen, M. Watson, K. Müllen, H. D. Chanzy, H. Sirringhaus and R. Friend, *Adv. Mater.*, 2003, **15**, 495.
24 L. Schmidt-Mende, A. Fechtenkötter, K. Müllen, E. Moons, R. H. Friend and J. D. MacKenzie, *Science*, 2001, **293**, 1119.
25 S. Wang, Y. Q. Liu, X. B. Huang, S. L. Xu, J. R. Gong, X. H. Chen, L. Yi, Y. Xu, G. Yu, L. J. Wan, C. L. Bai and D. B. Zhu, *Appl. Phys. A*, 2004, **78**, 553.
26 C. Chu, V. Shrotriya, G. Li and Y. Yang, *Appl. Phys. Lett.*, 2006, **88**, 153504.
27 J.-L. Bredas, D. Beljonne, V. Coropceanu and J. Cornil, *Chem. Rev.*, 2004, **104**, 4971.
28 A. M. van de Craats and J. M. Warman, *Adv. Mater.*, 2001, **13**, 130.
29 R. O. Ogbodu, E. Antunes and T. Nyokong, *Dalton Trans.*, 2013, **42**, 10769.
30 L. Bogani, C. Danieli, E. Biavardi, N. Bendiab, A.-L. Barra, E. Dalcanale, W. Wernsdorfer and A. Cornia, *Angew. Chem., Int. Ed.*, 2009, **48**, 746.
31 R. J. Chen, Y. Zhang, D. Wang and H. Dai, *J. Am. Chem. Soc.*, 2001, **123**, 3838.
32 F. D'Souza, R. Chitta, A. S. D. Sandanayaka, N. K. Subbaiyan, L. D'Souza, Y. Araki and O. Ito, *J. Am. Chem. Soc.*, 2007, **129**, 15865.
33 J. G. Young and W. Onyebuagu, *J. Org. Chem.*, 1990, **55**, 2155.
34 D. Wöhrle, M. Eskes, K. Shigehara and Y. Yamada, *Synthesis*, 1993, 194.
35 I. Özçeşmeci, A. Gelir and A. Gül, *Dyes Pigm.*, 2012, **92**, 954.
36 S. Dabak, V. Ahsen, F. Heinemann and P. Zugenmaier, *Mol. Cryst. Liq. Cryst.*, 2000, **348**, 111.
37 D. D. Perrin and W. L. F. Armarego, *Purification of Laboratory Chemicals*, Pergamon Press, Oxford, 2nd edn, 1989.
38 D. Atilla, N. Saydan, M. Durmuş, A. G. Gürek, T. Khan, A. Rueck, H. Walt, T. Nyokong and V. Ahsen, *J. Photochem. Photobiol., A*, 2007, **186**, 298.
39 J. Tant, Y. H. Geerts, M. Lehmann, V. De Cupere, G. Zucchi, B. Wegge Laursen, T. Bjørnholm, V. Lemaur, V. Marcq, A. Burquel, E. Hennebicq, F. Gardebien, P. Viville, D. Beljonne, R. Lazzaroni and J. Cornil, *J. Phys. Chem. B*, 2005, **109**, 20315.
40 J. M. Russell, S. Oh, I. LaRue, O. Zhou and E. T. Samulski, *Thin Solid Films*, 2006, **509**, 53.
41 I. Dierking, G. Scalia, P. Morales and D. LeClere, *Adv. Mater.*, 2004, **16**, 865.
42 R. A. Mrozek, B. Kim, V. C. Holmberg and T. A. Taton, *Nano Lett.*, 2003, **3**, 1665.
43 T. V. Basova and B. A. Kolesov, *Thin Solid Films*, 1998, **325**, 140.
44 T. V. Basova, B. A. Kolesov, A. G. Gürek and V. Ahsen, *Thin Solid Films*, 2001, **385**, 246.
45 T. Basova, A. G. Gürek and V. Ahsen, *Mater.Sci. Eng., C*, 2002, **22**, 99.
46 C. Jennings, R. Aroca, A.-M. Hor and R. O. Loutfy, *J. Raman Spectrosc.*, 1984, **15**, 34.
47 R. Aroca, Z. Q. Zeng and J. Mink, *J. Phys. Chem. Solids*, 1990, **51**, 135.
48 T. V. Basova, M. Durmuş, A. G. Gürek, V. Ahsen and A. Hassan, *J. Phys. Chem. C*, 2009, **113**, 19251.

9 T. V. Basova, M. Çamur, A. A. Esenpınar, S. Tuncel, A. Hassan, A. Alexeyev, H. Banimuslem, M. Durmuş, A. G. Gürek and V. Ahsen, *Synth. Met.*, 2012, **162**, 735.

50 F. D'Souza, S. K. Das, A. S. D. Sandanayaka, N. K. Subbaiyan, D. R. Gollapalli, M. E. Zandler, T. Wakahara and O. Ito, *Phys. Chem. Chem. Phys.*, 2012, **14**, 2940.

Sensors and Actuators B 199 (2014) 277–283

Contents lists available at ScienceDirect

Sensors and Actuators B: Chemical

journal homepage: www.elsevier.com/locate/snb

Effect of pyrene substitution on the formation and sensor properties of phthalocyanine-single walled carbon nanotube hybrids

Esra Nur Kaya[a,b], Sinem Tuncel[a], Tamara V. Basova[c,d], Hikmat Banimuslem[e], Aseel Hassan[e], Ayşe Gül Gürek[a], Vefa Ahsen[a], Mahmut Durmuş[a,*]

[a] Gebze Institute of Technology, Department of Chemistry, P.O. Box: 141, 41400, Gebze, Kocaeli, Turkey
[b] Marmara University, Faculty of Art and Science, Department of Chemistry, 34722 Kadikoy-Istanbul, Turkey
[c] Nikolaev Institute of Inorganic Chemistry SB RAS, Novosibirsk 630090, Russia
[d] Novosibirsk State University, Pirogova Str. 2, Novosibirsk, Russia
[e] Materials and Engineering Research Institute, Sheffield Hallam University, Sheffield S1 1WB, UK

ARTICLE INFO

Article history:
Received 30 January 2014
Received in revised form 23 March 2014
Accepted 27 March 2014
Available online 4 April 2014

Keywords:
Phthalocyanine
Carbon nanotubes
Chemical sensors
Ammonia vapour
Conductivity

ABSTRACT

The hybrids of single walled carbon nanotubes (SWCNTs) with symmetrically octasubstituted zinc phthalocyanine (**2**) bearing eight polyoxyethylene groups and asymmetrically substituted zinc phthalocyanine (**1**) bearing one pyrene and six polyoxyethylene groups as side chains have been prepared and characterized by Raman and fluorescence emission spectroscopies, scanning electron and transmission electron (SEM and TEM) microscopies, and thermogravimetric analysis. The pyrene group was chosen to enhance the interaction of phthalocyanine molecules with SWCNTs. Thin films of pristine SWCNTs and SWCNT/ZnPc hybrids were prepared by drop casting onto interdigitated electrodes and employed as active layers to detect ammonia vapour (1–200 ppm) by measuring electrical resistance changes. A comparative analysis of sensors' response of pristine SWCNTs and SWCNT/ZnPc hybrid films to ammonia vapour was carried out to demonstrate the synergic effect between SWCNTs and ZnPc derivatives. Influence of pyrene substituent in the phthalocyanine ring on the hybrid formation and their sensor response has also been discussed.

1. Introduction

Hybrid and composite materials play more important role in nanoelectronics due to the synergic effects on the electrical, optical, or mechanical properties of two or more components [1–3]. The use of carbon nanotubes (CNTs) and their hybrids in sensing has been extensively studied in recent years and progress in CNT-based sensor development for gas detection has been the subject of several reviews [4–6]. The use of nanostructured materials for gas sensing has been of great interest due to their unique and interesting properties including high surface-to-volume ratio and sensitive electronic structures [7–10]. Upon exposure to gas molecules, the electrical resistance of single-walled carbon nanotubes (SWCNTs) changes and the threshold voltage is shifted due to charge transfer between the semiconducting SWCNT and electron-withdrawing and electron-donating molecules.

It is well known that defect sites on SWCNTs play an important role in the electrical response for the binding of chemical vapor molecules [11]. It was found that the chemical sensitivity of SWCNTs could be significantly increased by controllably introducing a low density of defects along the sidewalls of the tubes [11,12]. The other way to increase sensitivity of SWCNTs is achieved through introduction of some functional groups [13] or by producing hybrids with different compounds [14,15].

As ammonia is a low boiling point compound and volatile, it is very important to develop sensitive devices to detect the gaseous NH_3 molecules. Chemical sensing application of SWCNTs for NO_2 and NH_3 gases was first reported by Kong et al. [16]. Other studies have revealed that semiconducting SWCNTs could detect small concentrations of NH_3 and NO_2 with high sensitivity at room temperature [17].

On the other hand, metal phthalocyanine derivatives possess high sensitivity, fast response, ease of processability, as well as a scope of operation at room temperature; they have therefore been studied extensively as thin films for chemical detection [18]. Jiang et al. have described the process of interaction between copper tetra-4-(2,4-di-*tert*-amylphenoxy)phthalocyanine (tapCuPc) and

* Corresponding author. Tel.: +90 262 6053019; fax: +90 262 6053005.
E-mail address: durmus@gyte.edu.tr (M. Durmuş).

http://dx.doi.org/10.1016/j.snb.2014.03.101
0925-4005/

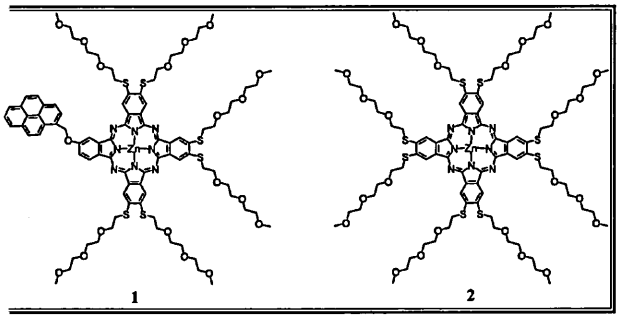

ig. 1. Asymmetrical (**1**) and symmetrical (**2**) zinc phthalocyanine derivatives.

I_3 [19]. Two different types of amphiphilic phthalocyanines have en compared for their sensing properties to NH_3 [20]. Sensor sponse of spin-casted films of copper, lead and nickel 1,8,15,22-tra-iso-pentyloxyphthalocyanine (Cu, Pb and NiPc(iso-PeO)$_4$) to ımonia vapour was studied by Wang et al. [21].

The combined excellent properties of carbon nanotubes and thalocyanines were demonstrated for the development of sentive NH_3 sensors based on CNT/phthalocyanine hybrids [22,23]. e evidence so far has shown that these hybrids are expected to more efficient in improving the relative response of hybrid films mpared to the pristine CNT or phthalocyanine species. There are o different routes for hybridising metal phthalocyanines and rbon nanotubes; in the first type CNT are functionalized with etallophthalocyanine derivatives through formation of covalent nding [24–26] while in the second type the hybrid can be rmed through non-covalent interaction between the two mateals [27–29].

In this work, hybrids of SWCNTs with symmetrically octabstituted ZnPc bearing eight polyoxyethylene groups (**2**) and ymmetrically substituted ZnPc bearing one pyrene and six polyyethylene groups (**1**) as substituents (Fig. 1) were prepared and aracterized. The pyrene group was chosen to enhance the intertion of the phthalocyanine molecules with the CNTs. This class f organic molecules is known to interact strongly with SWCNTs ia π-stacking interactions [30–33]. To demonstrate the potential pplications of the SWCNT/ZnPc hybrids in gas sensing, a conducmetric gas sensor device based on these hybrid materials has een fabricated. A comparative analysis of sensor response of prisne SWCNTs and SWCNT/ZnPc hybrid films to ammonia vapour –200 ppm) was carried out to demonstrate the synergic effect etween SWCNTs and ZnPc derivatives. Influence of pyrene group s substituent in the phthalocyanine ring on the hybrids formation nd their sensor response is discussed.

. Experimental

.1. Materials

Synthesis and characterization of zinc(II) phthalocyanine erivatives **1** and **2** (Fig. 1) have already been described in an earlier ublication [34]. SWCNTs were purchased from Sigma-Aldrich and sed without further purification and chemical treatment.

.2. Equipment

Optical spectra in the UV–visible region were recorded with himadzu UV–vis-3101 and 2101 spectrometers using 1 cm path ngth cuvette at room temperature. Fluorescence emission spectra ere recorded on a Varian Eclipse spectrofluorometer. Thermoavimetric analysis (TGA) was carried out on a Mettler Toledo STARe Thermal Analysis System at a rate of 10 °C min^{-1} in nitrogen flow of 50 mL min^{-1}.

Raman spectra were recorded with a Triplemate, SPEX spectrometer equipped with CCD detector in back-scattering geometry. The spectral excitation was achieved using 488 nm line Ar laser with the power of 40 mW.

Scanning electron microscopy (SEM) images were obtained using FEI-nova nanosem 200. Transmission electron microscopic (TEM) images were obtained using JEM-2010 instrument at an accelerating voltage of 200 kV. A thin film sample was prepared by dispensing a droplet of the hybrids dispersed in dichloromethane on a 200 mesh copper grid covered with a "holey" carbon film and allowing the solvent to evaporate.

Spectroscopic ellipsometry measurements were carried out to determine the thickness of the films using a Woolam *M*-2000*V*™ rotating analyser spectroscopic ellipsometer in the spectral range of 400–800 nm. DC-conductivity measurements were carried out using Keithley 236 semiconductors characterization system.

2.3. Preparation of SWCNT-phthalocyanine hybrids

5 mg of zinc phthalocyanines (**1** or **2**) have been dissolved in 1 mL DMF and sonicated for 15 min. At the same time 1.0 mg SWCNTs was suspended in 3 mL DMF and sonicated for 30 min. After sonication the suspension was stirred and the solution of phthalocyanines **1** or **2** was added drop wise to the SWCNTs suspension during stirring to obtain the hybrids **SWCNT/1** and **SWCNT/2**, respectively. Addition of zinc phthalocyanine solution was stopped when the green phthalocyanine solution became colorless due to phthalocyanine adsorption onto the SWCNT. The stirring was continued for another 1 h before the mixture was centrifuged. The obtained solid was washed with DMF several times, centrifuged again and finally dried in vacuum.

2.4. Sensor properties study

The sensing performance was studied at the relative humidity of 50% RH under exposures to low-concentration of NH_3 in the range 1–200 ppm. Pure commercial NH_3 gas ("Dioksid", Russia) was used as the NH_3 source. Air was used as the diluent gas, and NH_3 was diluted by a syringe static volumetric method. Diluted NH_3 was injected into the container using a microsyringe. The test chamber was degassed by turning a heating element on at 80 °C immediately after the removal of NH_3 gas.

Thin films of hybrids SWCNT/**1** and SWCNT/**2** were deposited by drop-casting their solutions in DMF (0.5 mg/mL) onto interdigitated electrodes which were used as substrates for the electrical characterization of the films. The electrical resistance of the sensors was measured using a Keithley 236 electrometer by applying a constant DC voltage of 3 V. The response and recovery times of the films were defined as the times needed to reach 90% of the steady state resistance.

3. Result and discussion

3.1. Characterization of SWCNT/phthalocyanine hybrids

3.1.1. Raman spectra

The non-covalent attachment of phthalocyanine molecules to SWCNTs can be confirmed by Raman spectroscopy. Raman spectra for pristine SWCNTs and both hybrids are shown in Fig. 2. The radial breathing modes (RBM), disorder (D) mode and tangential/graphite mode (G-band) are monitored as indicators of functionalization with phthalocyanine molecules [35]. The spectra were normalized to the tangential G band at ~1590 cm^{-1}. Both spectra of pristine SWCNTs before and after hybridization contained the following

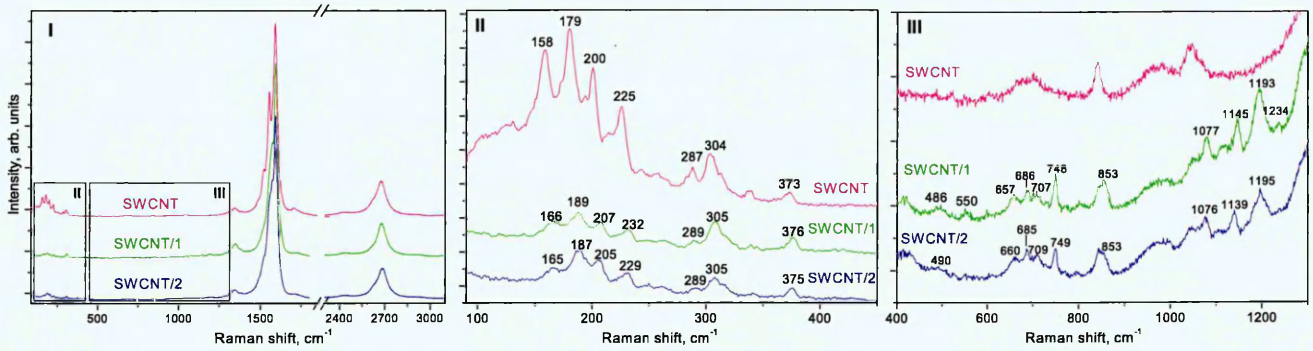

Fig. 2. Raman spectra of pristine SWCNT, hybrids SWCNT/**1** and SWCNT/**2** in the range 90--3200 cm^{-1} (I), in the range of radial breathing modes 90–450 cm^{-1} (II), in the range of phthalocyanine vibrations 400–1300 cm^{-1} (III).

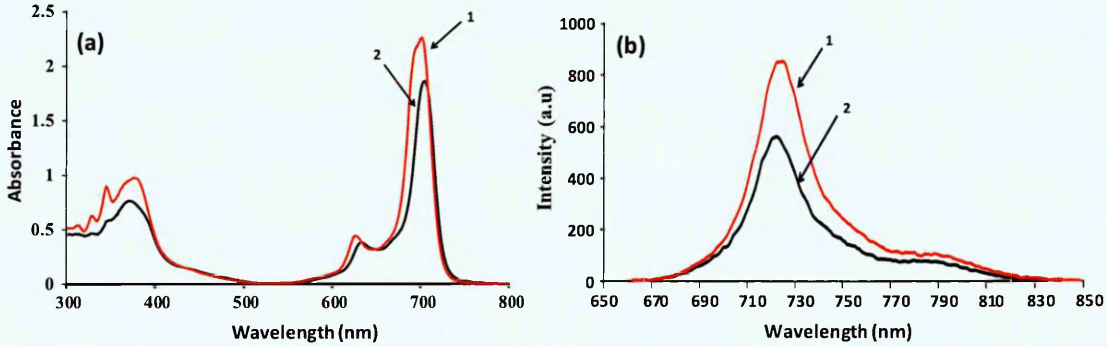

Fig. 3. (a) UV–vis optical absorption spectra of **1** and **2** in DMF ($C = 1 \times 10^{-5}$ M) (b) fluorescence emission spectra of **1** ($\lambda_{em} = 719$) and **2** ($\lambda_{em} = 721$) in DMF ($C = 1 \times 10^{-6}$ M). Excitation wavelength = 650 nm.

characteristic peaks: the D band located at about 1340 cm^{-1} (disorder mode), which is due to breathing modes of sp^2 atoms in the rings [2,36,37] and the G band centered at 1590 cm^{-1} (tangential mode), due to bond stretching of all pairs of sp^2 atoms in both rings and chains [38].

In Fig. 2 (region III), which is an enlarged part of the spectrum from 400 to 1350 cm^{-1}, we can see that the characteristic vibrations of phthalocyanine macrocycle [34] have been affected noticeably by interaction with SWCNTs. Comparing SWCNTs and hybrid spectra, only little variation of the ratio of the D band to the G band (I_D/I_G) can be observed, which suggests that ZnPc derivatives are attached to the surface of SWCNTs through a non-covalent modification. Moreover, the multiple peaks observed in the radial breathing mode (RBM) of SWCNTs in the range 158–304 cm^{-1} (Fig. 2 (region II)) could be ascribed to a distribution of diameters in the SWCNT samples [39,40]. They correspond to nanotube diameters in the range from 0.7 to 1.4 nm. The Raman spectra of the non-covalently functionalized SWCNT/**1** and SWCNT/**2** revealed significant shift in the peak positions located in the range 158–225 cm^{-1}. For example, the RBMs at 158, 179, 200, 225 cm^{-1} of SWCNTs have shifted to 165, 187, 205, 229 cm^{-1} and to 166, 189, 207, 232 cm^{-1} after the adsorption of ZnPc **2** and ZnPc **1**, respectively. It was shown that the radial breathing modes of the Raman spectrum are sensitive to the adsorption coating of the nanotubes with polynuclear aromatic hydrocarbon molecules [41]. The π–π stacking interaction between SWCNTs and phthalocyanine aromatic rings induced a higher frequency shift of RBM and gave rise to a kind of mode "hardening effect" [42]. In particular, the higher frequency shift indicates that SWCNTs become stiffer after coating with the aromatic rings. Adsorption of **1** containing an additional pyrene group is shown to induce a more remarkable shift in comparison with **2** due to the enhanced ZnPc molecule-SWCNT interaction.

3.1.2. *Optical absorption and fluorescence emission spectra*

The optical absorption and fluorescence emission spectra of the zinc phthalocyanines **1** and **2** solutions in DMF are shown in Fig. 3. The absorption spectrum of ZnPc **2** in DMF consists of a Soret band at 372 nm and a Q-band at 704 nm. Introduction of one pyrene moiety leads to a small shift of the Soret band to 371 nm and Q-band to 698 nm. The fluorescence emission peaks were observed at 719 nm for **1** and 721 nm for **2** in DMF. Because of the pyrene substitution, **1** showed higher emission intensity than **2** as shown in Fig. 3b. The formation of the SWCNT/ZnPc hybrids can also be confirmed by the fluorescence measurements. The addition of sonicated SWCNT solution to a solution containing either **1** or **2** in DMF quenched the emission of both macrocycles as shown in Figs. 4 and 5, respectively. However, the fluorescence intensity of **1** was found to be more quenched than **2** suggesting that pyrene

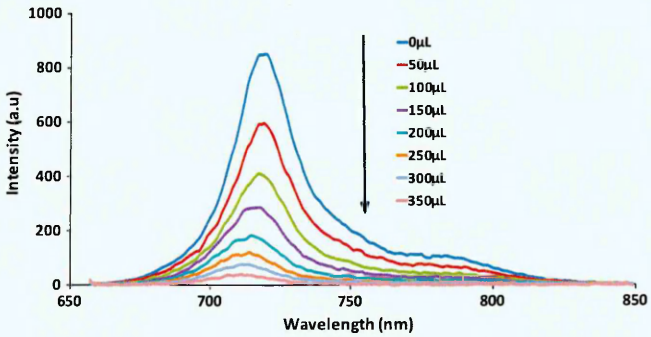

Fig. 4. Fluorescence emission changes of **1** observed during the titration of SWCNT (0–350 µl) in DMF ($C = 1 \times 10^{-5}$ M). Excitation wavelength = 650 nm.

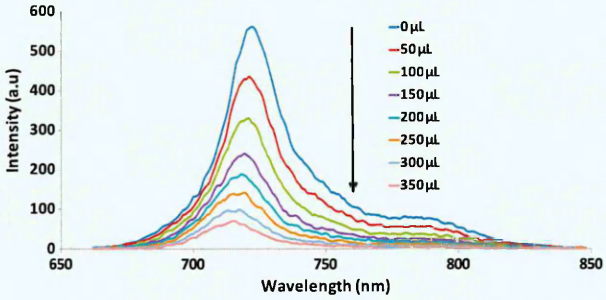

5. Fluorescence emission changes of **2** observed during the titration of SWCNT 350 µl) in DMF ($C = 1 \times 10^{-5}$ M). Excitation wavelength = 650 nm.

bstituted Pc **1** has interacted with SWCNT more efficiently an **2**.

1.3. Thermogravimetric analysis

A loss of weight of about 5.79% for pristine SWCNTs can be served (Fig. 6). It is also revealed that the thermogram of **1** ig. 6a) presents a loss of weight of 51.2% and the thermogram **2** (Fig. 6b) presents a loss of weight of 56.3%. When SWCNT-Pc hybrids are heated to 900 °C in an inert atmosphere, 22.2% ass loss for **1** and 14.7% mass loss for **2** were observed in the TGA periment.

Considering the weight loss of the pristine SWCNTs, the cor-cted weight loss due to ZnPc on nanotubes was then estimated be 16.3% for **1** and 8.8% for **2.** Concerning the amount of ZnPc olecules anchored on the surface of the nanotubes, a real ratio 31.8% (16.3%/51.2%) for **1** and 15.6% (8.8%/56.3%) for **2** have en calculated, taking into account the weight loss of both ZnPcs d SWCNTs. As a result, the number of functional groups in the hybrid was therefore estimated as one ZnPc derivative (**1**) per 336 [(68.2% × 1877.69)/(31.8% × 12)] carbon atoms and one ZnPc derivative (**2**) per 904 [(84.4% × 2003.93)/(15.6% × 12)] carbon atoms. This result also confirms that **1** has interacted to SWCNTs almost 2.7 times more efficiently than **2**.

3.1.4. Microscopy characterization

Indirect evidence for SWCNT/ZnPc interactions can be reached from transmission electron microscopy (TEM) and scanning electron microscopy (SEM). Both techniques assist in the visualization of SWCNT [35]. Inspection of the TEM images of pristine SWCNT shows the presence of large aggregates of nanotubes. Fig. 7 shows SEM images of pristine SWCNT (a), SWCNT/**1** hybrid (b) and SWCNT/**2** hybrid (c) as powders. Compared with the pristine SWCNTs (Fig. 7(a)), the SEM images of SWCNT/**2** hybrid show an appreciable decrease in stacking as seen in Fig. 7(c), but some increases in thickness were also observed, confirming the formation of nanohybrids, probably due to the intermolecular alkyl–π and π–π interactions between the ZnPc molecules and SWCNTs. After treatment with **1,** nanoparticles of phthalocyanine with a diameter from several to tens of nanometers are clearly resolved on SWCNT walls. Fig. 7(b) obviously shows the bundles of nanotubes in hybrid and the clusters of phthalocyanine attached on the surfaces of CNTs.

Fig. 8 shows the TEM images of SWCNT/**1** (a) and SWCNT/**2** (b) hybrids. From these figures, we can observe the coverage of phthalocyanines on the sidewall of SWCNTs. Furthermore the SWCNT/ZnPc nanohybrid appears to be made of bundles composed of tubes with specific rugged surface and a layer of about 1.5–2 nm in thickness immobilized onto the sidewall of SWCNTs. Energy-dispersive X-ray (EDX) spectroscopy study proves the presence of zinc in the area of the grafted objects.

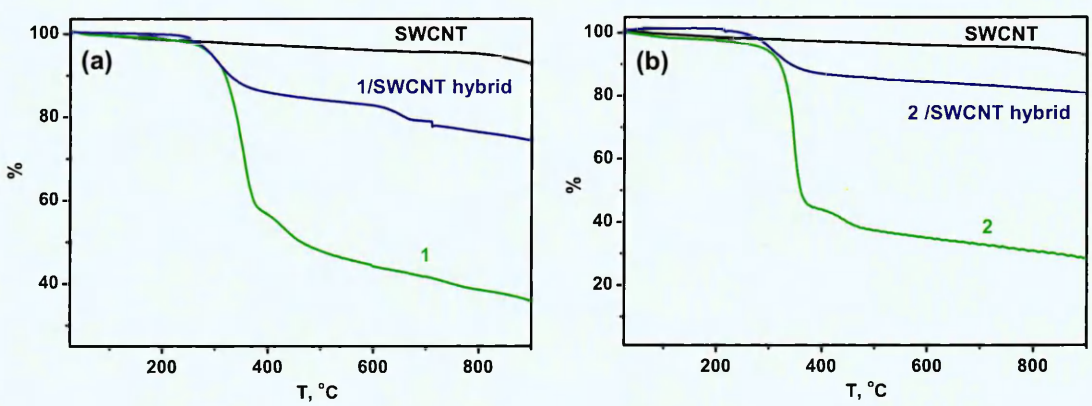

Fig. 6. (a) TGA of pristine SWCNT, **1** and SWCNT/**1** hybrid; (b) TGA of pristine SWCNT, **2** and SWCNT/**2** hybrid.

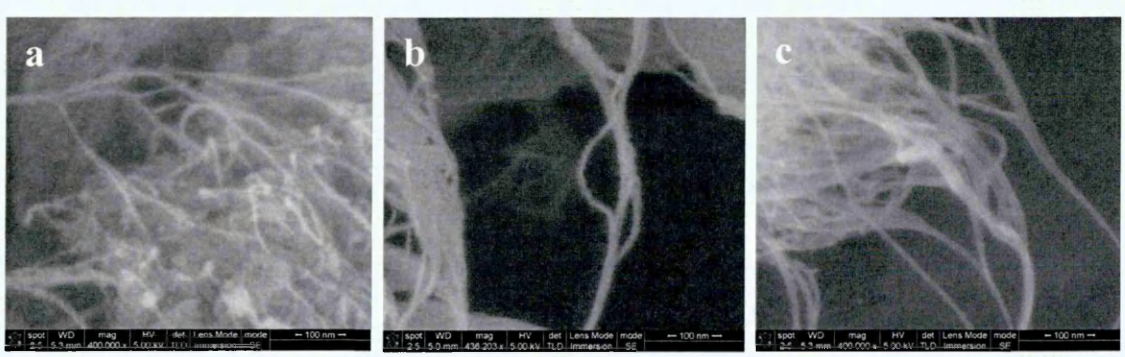

Fig. 7. SEM images of pristine SWCNT (a), SWCNT/**1** hybrid (b) and SWCNT/**2** hybrid (c).

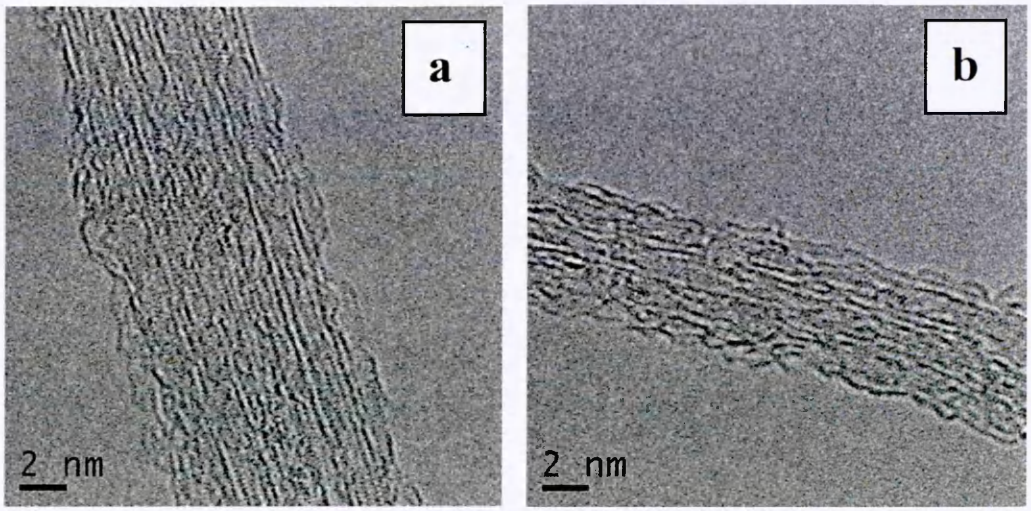

Fig. 8. TEM images of SWCNT/**1** hybrid (a) and SWCNT/**2** hybrid (b).

Using DFT calculations applied to a closely similar molecules the intermolecular alkyl–π and π–π interactions and relative orientation of porphyrin derivative ZnP(alkyl)$_4$ on the surface of semiconducting SWCNTs were visualized [43]. The results show that the aromatic macrocycle interacts with the surface of the nanotubes and that the alkyl chains also surround the nanotubes to some extent.

3.2. Study of electrical and sensor properties of SWCNT/ZnPc hybrids

Fig. 9 shows the normalized sensor response R ($R = (R_c - R_o)/R_o$; where R_c is the steady state resistance of the sensor at certain concentration of ammonia and R_o is the baseline resistance of the sensor) of the films of pristine SWCNTs and SWCNT hybrids with ZnPc **1** and **2** on exposure to ammonia of the concentrations 5, 20, 40, 60 and 80 ppm. In order to degas the sample, heating was immediately applied at 80 °C after turning the NH_3 gas off. A temperature higher than room temperature was chosen following published results in the literature, which demonstrated that the sensor resistance of SWCNT films did not return to baseline value for a long time after NH_3 was replaced by fresh air at room temperature [44–46].

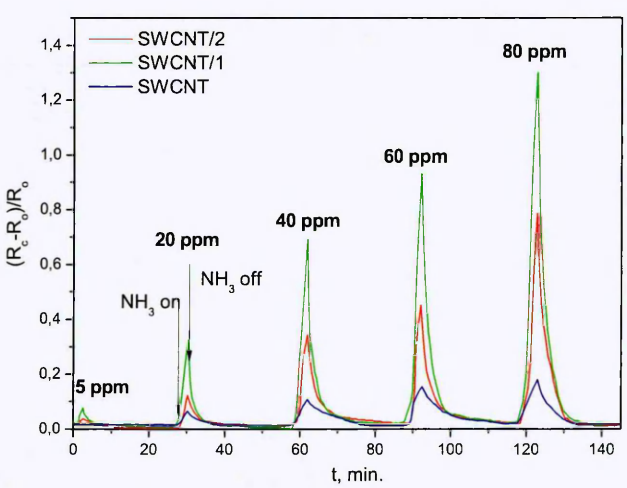

Fig. 9. The response curve of pristine SWCNT, SWCNT/**1** and SWCNT/**2** films to ammonia vapor at concentrations of 5–80 ppm.

The resistance of the sensor increased following 3 min exposure to NH_3; this is the result of adsorption of electron donating NH_3 molecules on pristine SWCNTs causing charge transfer between the SWCNTs and the analyte molecules. This result shows that the pristine SWCNT exhibits p-type behavior. Similar results were observed for films of both studied hybrids.

The proposed mechanism of sensor response of the modified carbon nanotubes to ammonia and other reducing analytes has already been discussed in the literature [23,27]. The theoretical studies indicate a weak interaction between pristine SWCNTs and NH_3, with little charge transfer [47,48]. It is also known that surface charge transfer interaction occurs upon adsorption of strong electron donor molecules like ammonia [21] onto the surface of phthalocyanine derivative in hybrids leading to electron transfer from NH_3 to the phthalocyanine molecule; the formed charge-transfer complexes trap holes leading to the observed increase in the resistance. Since SWCNT/MPc conjugates can form an excellent charge transfer complexes [36,49], the charge can favorably travel from MPc derivatives to SWCNTs rapidly, resulting in a large and fast variation in the films' resistance. The combination of the useful properties of SWCNTs (namely, high conductivity and extremely high surface area), and the properties of MPc derivatives (specifically, appropriate binding sites for ammonia resulting in charge transfer complexes) provides grounds for synergic effect between SWCNTs and ZnPc derivatives as active layers for sensor applications.

Both hybrids SWCNT/**1** and SWCNT/**2** exhibited an enhanced response to NH_3 compared to that of pristine SWCNT film, with the largest response observed in the case of SWCNT/**1** hybrid. The response of pristine SWCNT and SWCNT/ZnPc hybrid films towards different NH_3 concentrations is depicted in Fig. 10. The results show that the response values for SWCNT/ZnPc hybrids are much higher than that of pristine SWCNT sensor. The SWCNT/**1** sensor can detect about 1 ppm of NH_3 gas, which indicates relativity higher sensitivity compared to that demonstrated by pristine SWCNT. Meanwhile, the SWCNT sensor can detect 10 ppm of NH_3. Response linearity for all three films towards ammonia was observed for concentrations in range up to 100 ppm with a trend to saturate at concentrations higher than 100 ppm. The response value of SWCNT/**1** film is higher than the SWCNT/**2** hybrid films. This result can be explained by the presence of larger number of active sites (ZnPc with pyrene substituents) in SWCNT/**1** hybrid since derivative **1** was shown to interact with SWCNTs almost 2.7 times more efficiently than **2**.

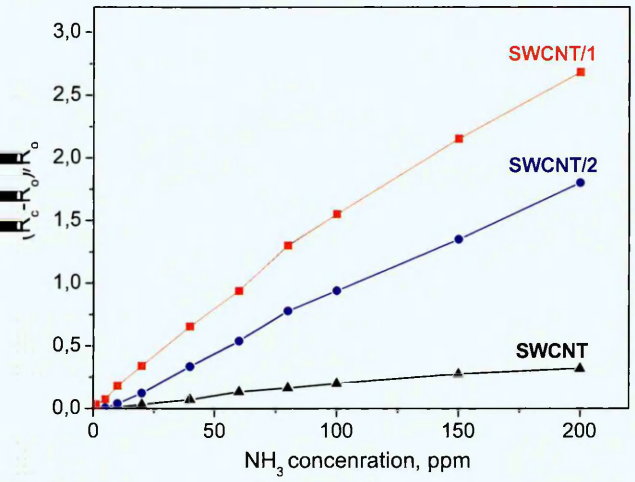

10. Response curves of pristine SWCNT and SWCNT/ZnPc hybrid films vs NH_3 ncentration.

Conclusions

Hybrid structures of single-walled carbon nanotubes with symetrically octasubstituted ZnPc bearing eight polyoxy groups d asymmetrically substituted ZnPc bearing one pyrene and six lyoxy groups as side chains have been prepared and characterred by spectral methods and microscopy. It was shown by the ethods of Raman spectroscopy, fluorescence spectroscopy and ermogravimetry that pyrene containing ZnPc has interacted with /CNTs more efficiently than zinc phthalocyanine without pyrene bstituent. The amount of pyrene-containing ZnPc anchored on e surface of nanotubes was almost 2.7 times more than ZnPc withut pyrene substituent. To demonstrate the potential applications the SWCNT/ZnPc hybrids towards gas sensing, a conductometric s sensor device based on the hybrid materials has been fabcated. The comparative analysis of sensor response of pristine /CNTs and films of the SWCNT/ZnPc hybrids to ammonia vapour –200 ppm) was carried out to demonstrate the synergic effect etween SWCNTs and ZnPc derivatives. It has also been shown that e response of the hybrid films with pyrene containing ZnPc to e ammonia vapour is two times larger than that demonstrated y hybrid films with ZnPc without pyrene substituents.

cknowledgements

The authors are very thankful to Dr. V.I. Zaikovsky (Boreskov stitute of Catalysis, Siberian Branch, Russian Academy of ciences) for the measurements of TEM images. This work as supported by bilateral project between The Scientific and echnological Research Council of Turkey (TUBITAK, Project numr: 111M699) and the Russian Foundation of Basic Research FBR, Project number: 12-03-91372-CT_a). Hikmat Banimuslem cknowledges the financial support from the Higher Committee for ducation Development in Iraq (HCED). Tamara Basova acknowldges the financial support from the Ministry of Education and cience of the Russian Federation.

eferences

1] U. Hahn, S. Engmann, C. Oelsner, C. Ehli, D.M. Guldi, T. Torres, Immobilizing water-soluble dendritic electron donors and electron acceptors-phthalocyanines and perylenediimides-onto single wall carbon nanotubes, J. Am. Chem. Soc. 132 (2010) 6392–6401.
2] T. Mugadza, T. Nyokong, Synthesis, characterization and the electrocatalytic behaviour of nickel (II) tetraamino-phthalocyanine chemically linked to single walled carbon nanotubes, Electrochim. Acta 55 (2010) 6049–6057.
[3] F.C. Moraes, D.L.C. Golinelli, L.H. Mascaro, S.A.S. Machado, Determination of epinephrine in urine using multi-walled carbon nanotube modified with cobalt phthalocyanine in a paraffin composite electrode, Sensors Actuators B: Chem. 148 (2010) 492–497.
[4] T. Zhang, S. Mubeen, N.V. Myung, M.A. Deshusses, Recent progress in carbon nanotube-based gas sensors, Nanotechnology 19 (2008) 332001.
[5] P. Bondavalli, P. Legagneux, D. Pribat, Carbon nanotubes based transistors as gas sensors: state of the art and critical review, Sensors Actuators B: Chem. 140 (2009) 304–318.
[6] M. Bouvet, P. Gaudillat, J.-M. Suisse, Phthalocyanine-based hybrid materials for chemosensing, J. Porphyrins Phthalocyanines 17 (2013) 913–919.
[7] J. Beheshtian, M. Kamfiroozi, Z. Bagheri, A.A. Peyghan, B12N12 nano-cage as potential sensor for NO_2 detection, Chin. J. Chem. Phys. 25 (2012) 60–64.
[8] A.L. Verma, S. Saxena, G.S.S. Saini, V. Gaur, V.K. Jain, Hydrogen peroxide vapor sensor using metal-phthalocyanine functionalized carbon nanotubes, Thin Solid Films 519 (2011) 8144–8148.
[9] A.A. Peyghan, A. Omidvar, N.L. Hadipour, Z. Bagheri, M. Kamfiroozi, Can aluminum nitride nanotubes detect the toxic NH_3 molecules? Physica E 44 (2012) 1357–1360.
[10] Y.-F. Hu, Z.-H. Zhang, H.-B. Zhang, L.-J. Luo, S.-Z. Yao, Sensitive and selective imprinted electrochemical sensor for p-nitrophenol based on ZnO nanoparticles/carbon nanotubes doped chitosan film, Thin Solid Films 520 (2012) 5314–5321.
[11] J.A. Robinson, E.S. Snow, S.C. Badescu, T.L. Reinecke, F.K. Perkins, Role of defects in single-walled carbon nanotube chemical sensors, Nano Lett. 6 (2006) 1747–1751.
[12] M.A. Turabekova, T.C. Dinadayalane, D. Leszczynska, J. Leszczynski, Comprehensive study on the dissociative chemisorption of NH_3 on the sidewalls of stone-wales defective armchair (5,5) single-walled carbon nanotubes, J. Phys. Chem. C 116 (2012) 6012–6021.
[13] K.-Y. Dong, J. Choi, Y.D. Lee, B.H. Kang, Y.-Y. Yu, H.H. Choi, B.-K. Ju, Detection of a CO and NH_3 gas mixture using carboxylic acid-functionalized single-walled carbon nanotubes, Nanoscale Res. Lett. 8 (2013) 12.
[14] K. Datta, P. Ghosh, M.A. More, M.D. Shirsat, A. Mulchandani, Controlled functionalization of single-walled carbon nanotubes for enhanced ammonia sensing: a comparative study, J. Phys. D: Appl. Phys. 45 (2012) 355305.
[15] M.-R. Yu, G. Suyambrakasam, R.-J. Wu, M. Chavali, Preparation of organic–inorganic (SWCNT/TWEEN–TEOS) nano hybrids and their NO gas sensing properties, Sensors Actuators B: Chem. 161 (2012) 938–947.
[16] J. Kong, N. Franklin, C. Zhou, M. Chapline, S. Peng, K. Cho, H. Dai, Nanotube molecular wires as chemical sensors, Science 287 (2000) 622–625.
[17] L. Valentini, I. Armentano, J.M. Kenny, C. Cantalini, L. Lozzi, S. Santucci, Sensors for sub-ppm NO_2 gas detection based on carbon nanotube thin films, Appl. Phys. Lett. 82 (2003) 961–963.
[18] A.W. Snow, W.R. Barger, Phthalocyanine films in chemical sensors, in: C.C. Leznof, A.B.P. Lever (Eds.), Phthalocyanines, Properties and Application, vol. 1, John Wiley and Sons, New York, 1989, p. P341.
[19] D.P. Jiang, A.D. Lu, Y.J. Li, X.M. Pang, Y.L. Hua, Interaction between copper tetra-4(2 4-ditert-amylphenoxy) phthalocyanine Langmuir–Blodgett films as a gas sensitive sensor and NH_3, Thin Solid Films 199 (1991) 173–179.
[20] X.M. Ding, H.J. Xu, L.G. Zhang, D.P. Jiang, A.D. Lu, A novel amphiphilic zinc phthalocyanine LB films as gas sensor material and its interaction with NH_3, Mol. Cryst. Liq. Cryst. 337 (1999) 481–484.
[21] B. Wang, X. Zhou, Y. Wu, Z. Chen, C. He, X. Zuo, Preparation, characterization and NH_3-sensing of 1,8,15,22-tetra-iso-pentyloxyphthalocyanine copper, nickel and lead spin-coating films, Sensors Actuators B: Chem. 161 (2012) 498–503.
[22] B. Wang, X. Zhou, Y. Wu, Z. Chen, C. He, Lead phthalocyanine modified carbon nanotubes with enhanced NH_3 sensing performance, Sensors Actuators B: Chem. 171–172 (2012) 398–404.
[23] B. Wang, Y. Wu, X. Wang, Z. Chen, C. He, Copper phthalocyanine noncovalent functionalized single-walled carbon nanotube with enhanced NH_3 sensing performance, Sensors Actuators B: Chem. 190 (2014) 157–164.
[24] W. Chidawanyika, C. Litwinski, E. Antunes, T. Nyokong, Photophysical study of a covalently linked quantum dot-low symmetry phthalocyanine conjugate, J. Photochem. Photobiol. A Chem. 212 (2010) 27–35.
[25] N. He, Y. Chen, J. Bai, J. Wang, W.J. Blau, J. Zhu, Preparation and optical limiting properties of multiwalled carbon nanotubes with pi-conjugated metal-free phthalocyanine moieties, J. Phys. Chem. C 113 (2009) 13029–13035.
[26] T. Mugadza, T. Nyokong, Electrochemical, microscopic and spectroscopic characterization of benzene diamine functionalized single walled carbon nanotube-cobalt (II) tetracarboxy-phthalocyanine conjugates, J. Colloid Interf. Sci. 354 (2011) 437–447.
[27] Y. Wang, N. Hu, Z. Zhou, D. Xu, Z. Wang, Z. Yang, H. Wei, E.S.-W. Kong, Y. Zhang, Single-walled carbon nanotube/cobalt phthalocyanine derivative hybrid material: preparation, characterization and its gas sensing properties, J. Mater. Chem. 21 (2011) 3779–3787.
[28] S. Khene, T. Nyokong, Electrooxidation of chlorophenols catalyzed by nickel octadecylphthalocyanine adsorbed on single-walled carbon nanotubes, Electroanalysis 23 (2011) 1901–1911.
[29] X. Wang, Y. Liu, W. Qiu, D. Zhu, Immobilization of tetra-*tert*-butylphthalocyanines on carbon nanotubes: a first step towards the development of new nanomaterials, J. Mater. Chem. 12 (2002)1636–1639.
[30] L. Bogani, C. Danieli, E. Biavardi, N. Bendiab, A.-L. Barra, E. Dalcanale, W. Wernsdorfer, A. Cornia, Single-molecule-magnet carbon-nanotube hybrids, Angew. Chem. Int. Ed. 48 (2009) 746–750.

[31] F. D'Souza, R. Chitta, A.S.D. Sandanayaka, N.K. Subbaiyan, L. D'Souza, Y. Araki, O. Ito, Supramolecular carbon nanotube-fullerene donor-acceptor hybrids for photoinduced electron transfer, J. Am. Chem. Soc. 129 (2007) 15865–15871.
[32] J. Bartelmess, B. Ballesteros, G. de la Torre, D. Kiessling, S. Campidelli, M. Prato, T. Torres, D.M. Guldi, Phthalocyanine-pyrene conjugates: a powerful approach toward carbon nanotube solar cells, J. Am. Chem. Soc. 132 (2010) 16202–16211.
[33] R.O. Ogbodu, E. Antunes, T. Nyokong, Physicochemical properties of a zinc phthalocyanine–pyrene conjugate adsorbed onto single walled carbon nanotubes, Dalton Trans. 42 (2013) 10769–10777.
[34] S. Tuncel, E.N. Kaya, M. Durmuş, T. Basova, A.G. Gürek, V. Ahsen, H. Banimuslem, A. Hassan, Distribution of single-walled carbon nanotubes in pyrene containing liquid crystalline asymmetric zinc phthalocyanine matrix, Dalton Trans. 43 (2014) 4689–4699.
[35] K.A. Wepasnick, B.A. Smith, J.L. Bitter, D. Howard Fairbrother, Chemical and structural characterization of carbon nanotube surfaces, Anal. Bioanal. Chem. 396 (2010) 1003–1014.
[36] B. Ballesteros, G. De La Torre, C. Ehli, G.M.A. Rahman, F. Agulló-Rueda, D.M. Guidi, T. Torres, Single-wall carbon nanotubes bearing covalently linked phthalocyanines—photoinduced electron transfer, J. Am. Chem. Soc. 129 (2007) 5061–5068.
[37] C. Casiraghi, A. Hartschuh, H. Qian, S. Pliscanec, C. Georgia, A. Fasoli, K.S. Novoselov, D.M. Basko, A.C. Ferrari, Raman spectroscopy of graphene edges, Nano Lett. 9 (2009) 1433–1441.
[38] C. Dyke, J. Tour, Unbundled and highly functionalized carbon nanotubes from aqueous reactions, Nano Lett. 3 (2003) 1215–1218.
[39] L. Alvarez, G. de la Fuente, A. Righi, S. Rols, E. Anglaret, J. Sauvajol, E. Munoz, W. Maser, A. Benito, M. Martinez, Diameter dependence of Raman intensities for single-wall carbon nanotubes, Phys. Rev. B 63 (2001) 153401.
[40] D. Huo, L. Yang, C. Hou, H. Fa, X. Luo, Y. Lu, X. Zheng, J. Yang, L. Yang, Molecular interactions of monosulfonate tetraphenylporphyrin (TPPS1) and meso-tetra(4-sulfonatophenyl)porphyrin (TPPS) with dimethyl methylphosphonate (DMMP), Spectrochim. Acta A 74 (2009) 336–343.
[41] S. Gotovac, H. Honda, Y. Hattori, K. Takahashi, H. Kanoh, K. Kaneko, Effect of nanoscale curvature of single-walled carbon nanotubes on adsorption of polycyclic aromatic hydrocarbons, Nano Lett. 7 (2007) 583–587.
[42] Y. Zhang, J. Zhang, H. Son, J. Kong, Z. Liu, Substrate-induced Raman frequency variation for single-walled carbon nanotubes, J. Am. Chem. Soc. 127 (2005) 17156–17157.
[43] F. D'Souza, S.K. Das, A.S.D. Sandanayaka, N.K. Subbaiyan, D.R. Gollapalli, M.E. Zandler, T. Wakahara, O. Ito, Photoinduced charge separation in three-layer supramolecular nanohybrids: fullerene-porphyrin-SWCNT, Phys. Chem. Chem. Phys. 14 (2012) 2940–2950.
[44] J. Li, Y. Lu, Q. Ye, M. Cinke, J. Han, M. Meyyappan, Carbon nanotube sensors for gas and organic vapor detection, Nano Lett. 3 (2003) 929–933.
[45] E. Bekyarova, M. Davis, T. Burch, M.E. Itkis, B. Zhao, S. Sunshine, R.C. Haddon, Chemically functionalized single-walled carbon nanotubes as ammonia sensors, J. Phys. Chem. B 108 (2004) 19717–19720.
[46] K.-Y. Dong, D.-J. Ham, B.H. Kang, K. Lee, J. Choi, J.-W. Lee, H.H. Choi, B.-K. Ju, Effect of plasma treatment on the gas sensor with single-walled carbon nanotube paste, Talanta 89 (2012) 33–37.
[47] C.W. Bauschlicher Jr., A. Ricca, Binding of NH_3 to graphite and to a (9,0) carbon nanotubes, Phys. Rev. B 70 (2004) 115409.
[48] S. Peng, K. Cho, Chemical control of nanotube electronics, Nanotechnology 11 (2000) 57–60.
[49] W. Chidawanyika, T. Nyokong, Characterization of amine-functionalized single-walled carbon nanotube-low symmetry phthalocyanine conjugates, Carbon 48 (2010) 2831–2838.

Biographies

Esra Nur Kaya received the BSc and MSc degree from Department of Chemistry of Marmara University, Turkey. Her research interests are the synthesis and characterization of coumarin, phthalocyanines and the investigation of their photophysical and photochemical properties.

Sinem Tuncel BSc, MSc, PhD is a research assistant at Chemistry Department, Gebze Institute of Technology, Turkey. Her research interests are the synthesis and characterization of phthalocyanines and the investigation of their liquid crystalline, photophysical and photochemical properties.

Tamara Basova received her PhD in physical chemistry from Nikolaev Institute of Inorganic Chemistry, Novosibirsk, Russia, in 1999 and then DSc degree in 2011. Now, she is a leading scientist in the institute. Her research interests are mainly directed towards the synthesis and characterization of various phthalocyanines and the investigation of the sensor and electrical properties of their oriented films.

Hikmat Banimuslem is a PhD student in the Material and Engineering Research Institute, Sheffield Hallam University, UK. He is currently investigating functional materials, which include the hybrids of CNT and substituted phthalocyanine molecules for sensor applications.

Aseel Hassan BSc, MSc, PhD, CPhys, MInstP, is a senior lecturer at Sheffield Hallam University and a member of the Materials and Engineering Research Institute. His research interests lie in thin film technology, mainly for application in chemical and biosensing, as well as for electronic device application. He uses optical techniques such as surface plasmon resonance and spectroscopic ellipsometry, as well as quartz crystal microbalance detection techniques, employing organic thin films such as metallophthalocyanines and calix-resorcinarene as sensing elements.

Ayşe Gül Gürek BSc, MSc, PhD is a professor at Department of Chemistry of Gebze Institute of Technology Turkey. Her research interests are mainly directed towards the synthesis and characterization of the stable ligands, e.g. phthalocyanines, vic-dioximes with such functional groups as crown ether, aza ether, and thia ether, and the investigation of their liquid crystal, semiconductor, NLO, photodynamic therapy (PDT) of cancer and chemical sensor properties by enlightening the structure of these macrocyclic compounds.

Vefa Ahsen BSc, MSc, PhD is a professor at the Chemistry Department of Science Faculty at Gebze Institute of Technology Turkey. His research interest lies in the synthesis of stable ligands, e.g. phthalocyanines, vic-dioximes with such functional group as crown ether, aza ether, and thia ether, the synthesis of their alkaline and transition metal complexes as nanomaterials. The main application areas of these materials (gas sensors, photodynamic therapy, catalysis, liquid crystals, semiconductors and NLO) are investigated.

Mahmut Durmuş BSc, MSc, PhD is an associate professor at Gebze Institute of Technology, Department of Chemistry in Turkey. His research interests are the design, synthesis and characterization of advanced materials such as phthalocyanines, borondipyrromethenes (BODIPY), coumarins and phosphazenes for different applications including photodynamic therapy (PDT) of cancer, liquid crystals, energy transfer dyes, chemosensors, etc.

Online available since 2014/Apr/03 at www.scientific.net
© (2014) Trans Tech Publications, Switzerland
doi:10.4028/www.scientific.net/KEM.605.461

Copper phthalocyanine functionalized single-walled carbon nanotubes: thin film deposition and sensing properties

Hikmat Banimuslem[1,a], Aseel Hassan[1,b], Tamara Basova[2,c], Irina Yushina[2,d], Mahmut Durmuş[3,e], Sinem Tuncel[3,f], Aliye Aslı Esenpınar[4,g], Ayse Gül Gürek[3,h], Vefa Ahsen[5,i]

[1]Materials and Engineering Research Institute, Sheffield Hallam University, Sheffield S1 1WB, UK
[2]Nikolaev Institute of Inorganic Chemistry SB RAS, 3 Lavrentiev Ave., Russia
[3]Gebze Institute of Technology, Department of Chemistry, Gebze, Kocaeli, Turkey
[4]Kırklareli University, Department of Chemistry, 39100, Kırklareli, Turkey
[5]TUBITAK-Marmara Research Center, Materials Institute, Gebze, Kocaeli, Turkey
[a]hikmatadnan@gmail.com, [b]a.hassan@shu.ac.uk, [c]basova@niic.nsc.ru, [d]yushina@niic.nsc.ru, [e]durmus@gyte.edu.tr, [f]stuncel@gyte.edu.tr, [g]aliesenpinar@gmail.com, [h]gurek@gyte.edu.tr, [i]ahsen@gyte.edu.tr

Keywords: Hybrid; SWCNT; metal phthalocyanine; thin films; SEM; TIRE.

Abstract. Thin films of non-covalently hybridised single-walled carbon nanotubes (SWCNT) and tetra-substituted copper phthalocyanine ($CuPcR_4$) molecules have been produced. The π-π interaction between SWCNTs and $CuPcR_4$ molecules has been revealed by using different characterisation techniques. Scanning electron microscopy (SEM) measurements have shown that films obtained from the acid-treated SWCNTs/$CuPcR_4$ hybrids demonstrated more homogenous surface. Using total internal reflection ellipsometry spectroscopy (TIRE), thin films of the new hybrid have been examined as an optical sensing membrane for the detection of benzo[a]pyrene in water to demonstrate the sensing properties of the hybrid.

Introduction

Since their discovery by Iijima in 1991 [1], carbon nanotubes (CNTs) have attracted significant interest by researchers around the globe due to their unique electronic, metallic and structural properties [2]. The modification of CNT network surface by subjecting them to different chemical treatment and through hybridization with various organic materials has enabled their use in applications such as photovoltaic application [3] and chemical detection [4]. Among these hybrids, the smart integration of carbon nanotubes (CNT) with metallophthalocyanine (MPc) complexes has gained increasing attention over the past few years. The evidence so far has shown that these hybrids are expected to be more efficient in improving the relative response of hybrid films compared to the individual CNT or MPc species [5-7]. On the other hand, the Application of different phthalocyanine films as active layers in surface plasmon resonance (SPR) and total internal reflection ellipsometry (TIRE) techniques have been widely reported in the literatures [8,9]. In this work hybrid thin films have been prepared from SWCNT functionalised with tetra-substituted copper phthalocyanine $CuPcR_4$ with R= $S(CH_2CH_2O)_3CH_3$ molecules. The interaction between the two materials was investigated by using different characterisation methods. The aim of current study is to examine the compatibility of thin films produced from SWCNT/MPc hybrids with optical detection techniques, using TIRE method.

Experimental

1(4), 8(11), 15(18), 22(25)- Tetrakis- [2-(2-(2-methoxyetoxy) ethoxy) ethylthio] phthalocyaninato copper (II) was synthesized and the preparation and characterization will be published in a separate work. All other materials used in this work were purchased from commercial suppliers. 5 mg of $CuPcR_4$ has been dissolved in 1 ml DMF and sonicated for 15

minutes. At the same time 1mg of SWCNTs was suspended in 3 ml DMF and sonicated for 40 minutes. After sonication, the suspension was stirred and the $CuPcR_4$ solution was added drop wise to the CNTs suspension during stirring. The stirring was continued for another 5 hours before the mixture was centrifuged, washed with DMF several times, centrifuged again and finally dried resulting in hybrid 1. Similar procedure has been followed to prepare hybrid 2 but SWCNTs was acid treated before use according to the literature [10]. Gold-coated glass substrate has been prepared by sequentially evaporating 3-5 nm of chromium onto microscopic slides followed by the evaporation of 25-30 nm of gold layer under vacuum of about $3x10^{-5}$ $mbar$. Other slides used for hybrid films deposition in this work are rigorously cleaned glass slides for spectroscopic measurements.

Results and discussion

UV-Vis absorption spectra of SWCNT (Fig. 1a) are featureless as it was frequently reported in the literature [11], whereas, $CuPcR_4$ exhibited typical electronic absorption spectra with two characteristic regions of peaks: the Q-band in the wavelength range 600-750 nm and the Soret (B) band in the wavelength range of 300-450 nm. The peak maxima of the Q-bands shifted to the red in the absorption spectra of hybrid 1 and hybrid 2 suggesting strong π-π interactions between SWCNTs and $CuPcR_4$ derivative [7]. Raman spectra normalized to the tangential G band at ~1580 cm^{-1} for pristine SWCNT, acid treated SWCNT and both hybrids are shown in Fig. 2. Comparing curve (a) with curve (b) in Fig. 2, little variation of the ratio of the D band [12] at ~1340 cm^{-1} to the G band (I_D/I_G) can be observed, which suggests that $CuPcR_4$ molecules are attached to the surface of SWCNT through non-covalent bond. The D/G peak intensity ratio increases from 0.04 for pristine SWCNT to 0.30 for acid treated SWCNT (Fig. 2c) which indicates the formation of covalent bonds at the surface of the carbon nanotube through conversion of sp^2-hybridized carbon atoms to sp^3-hybridized carbons on the nanotube surface. Further increase I_D/I_G to 0.47 was also observed in the spectrum of acid treated SWCNT hybrids with $CuPcR_4$ (Fig. 2d).

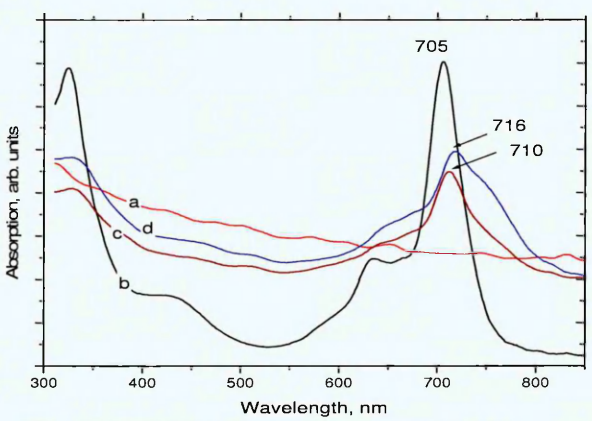

Fig. 1. UV-Vis absorption spectra of (a) SWCNTs, (b) $CuPcR_4$, (c) hybrid 1 and (d) hybrid 2 in DMF

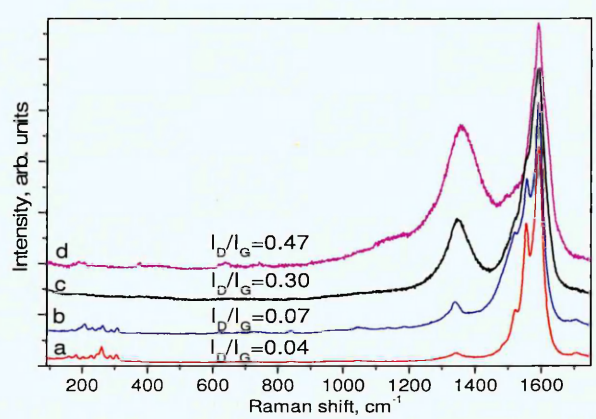

Fig. 2. Raman spectra of pristine SWCNT (a), hybrid 1 (b), acid-treated SWCNT (c) and hybrid 2 (d).

The Raman spectra of the noncovalently functionalized SWCNT-$CuPcR_4$ also revealed significant shift on the radial breathing modes (RBM) [13] located in the range 158-225 cm^{-1}. The π-π stacking interaction between SWCNT and phthalocyanine rings induced a higher frequency shift of RBM and give a kind of mode "hardening effect" [14]. In the Raman spectrum of the acid-treated SWCNTs, the RBMs have disappeared when compared to the spectrum of pristine SWCNTs (Fig. 2c). Fig. 3a, b, c and d shows SEM images of pristine SWCNT, acid-treated SWCNT, hybrid 1 and hybrid 2, respectively. Pristine CNTs typically tend to bundle together (Fig. 3a and c) and to aggregate due to van der Waals attraction between individual tubes [15]; this makes them hard to disperse in common organic solvents. Acid treatment of the nanotubes provides the de-bundling

effect (Fig. 3b and d) disrupting the van der Waals interactions and leading to the formation of a composite with much improved solubility in organic solvents and hence smoother films were obtained.

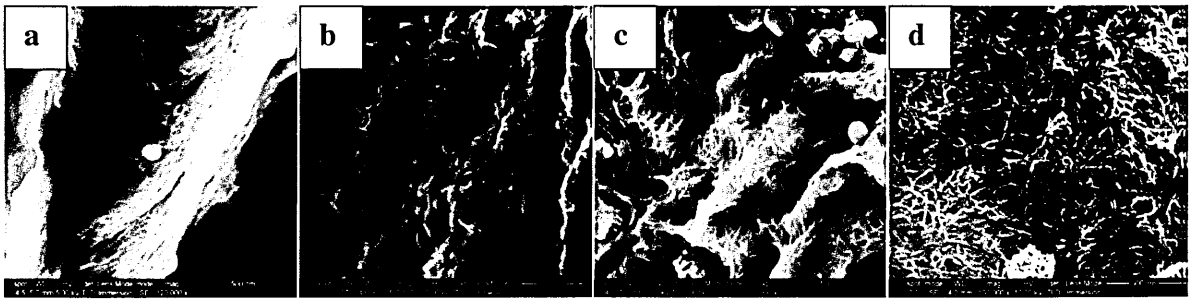

Fig. 3. SEM images for (a) pristine, (b) acid-treated SWCNT, (c) hybrid 1and (d) hybrid 2 thin film deposited on silicon substrates.

Using total internal reflection ellipsometry spectroscopy (TIRE), thin films of the new hybrid have been examined as an optical sensing membrane for the detection of benzo[a]pyrene in water. It is known that benzo[a]pyrene is a product derived from incomplete combustion of organic material and is considered responsible for chemically-induced cancer in humans [16]. Full details of TIRE method, experimental set-up and typical TIRE spectra of Cr/Au films are reported in previous publications [9,17]. To examine the compatibility of the hybrids prepared in this work with TIRE technique, small volumes of solutions of $CuPcR_4$, hybrid 1 and hybrid 2 in DMF were drop-casted onto the gold-coated glass substrates by using microsyringe. Thereafter, the samples were exposed to deionized water and saturated solution of benzo[a]pyrene in water (6.2 μg/l) to demonstrate the changes of ellipsometry spectra and thus films' optical parameters induced by the adsorption of benzo[a]pyrene onto the films surfaces. It is worthwhile mentioning here that the films of hybrid 1 were shown to be rough and inhomogeneous and therefore unsuitable for optical investigation, as it has not given well-resolved spectra when measured by spectroscopic ellipsometry. On the other hand, thin films prepared from hybrid 2 exhibited much smoother surfaces and has therefore shown significant enhancement in the adsorption properties as active optical sensing layer. Fig. 4 shows the spectra of $\Psi(\lambda)$ and $\Delta(\lambda)$ of $CuPcR_4$ and hybrid 2 thin films before and after exposure to benzo[a]pyrene.

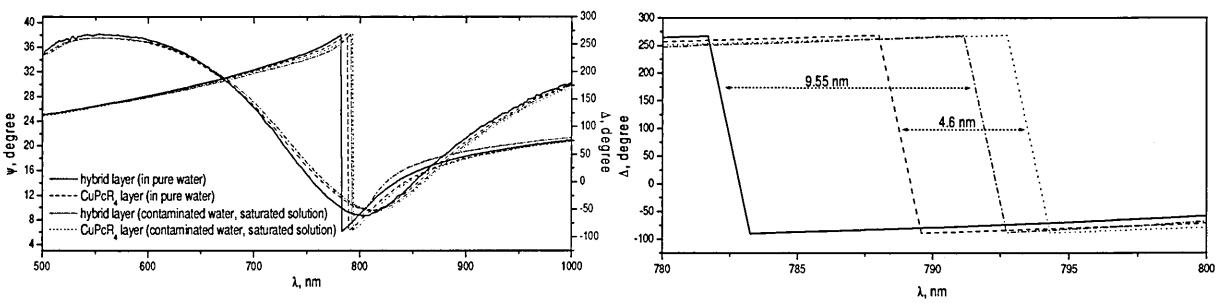

Fig. 4. $\Psi(\lambda)$ and $\Delta(\lambda)$ TIRE spectra of $CuPcR_4$ film in water (dashed line); after injection of benzo[a]pyrene saturated solution (dotted line). Hybrid 2 films in water (solid line); after injection of benzo[a]pyrene saturated solution (dashed-dotted line). An enlarged section of $\Delta(\lambda)$ spectra are shown at the right of the figure to provide better assessment.

The adsorption of benzo[a]pyrene on hybrid 2 film has resulted in larger shift (9.55 nm) than that shown by pure $CuPcR_4$ (4.6 nm) under exposure to saturated benzo[a]pyrene solution in water. Carbon nanotubes in general are characterised with uniform surface with delocalised π-electrons of high density, which enhances their adsorption properties, especially for analytes with aromatic molecules [18]. Table 1 summarises the thickness, refractive index and extinction coefficients given

at λ=632 nm of all layers found from theoretical data fitting. The changes in optical parameters in the case of hybrid 2 were more significant which is probably due to the predominant surface interaction of the analyte with SWCNT/$CuPcR_4$ films.

Table 1. Experimental data fitting (films' thicknesses, refractive indexes and extinction coefficients)

	Before exposure			After exposure		
	d, nm	**n**	**k**	**d, nm**	**n**	**k**
$CuPcR_4$	97.86	1.532	0.373	98.1	1.542	0.377
Hybrid 2	147.73	1.334	0.133	149.49	1.359	0.135

Conclusion

The acid-treatment of CNTs is found to result in the separation of bundled carbon nanotubes, leading to enhanced π-π interaction in the SWCNT/$CuPcR_4$ system. The improved films' homogeneity has enabled the use of such hybrids as optically active sensing layers for the detection of pollutants in water. The response of acid-treated SWCNT/$CuPcR_4$ hybrid films to the presence of benzo[a]pyrene in water was shown to be two times larger than that demonstrated by $CuPcR_4$ films.

References

[1] S. Iijima: Nature Vol. 354 (1991), p. 56

[2] J. Liu, Y. Wang, Z. Qu and X. Fan: Opt. Laser Technol. Vol. 44 (2012), p. 960

[3] S. Yang, B. Kong, D. Jung, Y. Baek, C. Han, S.Oh and H. Jung: Nanoscale Vol. 3 (2011), p.1361

[4] B. Wang, X. Zhou, Y. Wu, Z. Chen and C. He: Sensor. Actuat. B-Chem. Vol. 171-172 (2012), p.398

[5] J. Lee, H. Jung, J. Choi, T. An, G. Lim and S. Kong: Sensor Letters Vol. 11 (2013), p.452

[6] A. Babaei, M. Aminikhah and A. Taheri: Sensor Letters Vol. 11(2013), p.413

[7] Z. Yang, H. Pu, J. Yuan, D. Wan and Y. Liu: Chem. Phys. Lett. Vol. 465 (2008), p.73

[8] T. Basova, E. Kol'tsov, A.K. Ray, A.K. Hassan, A.G. Gürek and V. Ahsen: Sensor. Actuat. B-Chem. Vol.113 (2006), p.127

[9] A. Hassan, T. Basova, F. Yuksel, G. Gümüş, A.G. Gürek and V. Ahsen: Sensor. Actuat. B-Chem. Vol.175 (2012), p.73

[10] J. Liu, A.G. Rinzler, H. Dai, J.H. Hafner, R.K. Bradley, P.J. Boul, A. Lu, T. Iverson, K. Shelimov, C.B. Huffman, F. Rodriguez-Macias, Y. Shon, T.R. Lee, D.T. Colbert and R.E. Smalley: Science Vol.280 (1998), p.1253

[11] T. Mugadza and T. Nyokong: Electrochim. Acta Vol.54 (2009), p.6347

[12] K.A. Wepasnick, B.A. Smith, J.L. Bitter and D.H. Fairbrother: Analyt. Bioanalyt. Chem. Vol.396 (2010), p.1003

[13] D. Huo, L. Yang, C. Hou, H. Fa, X. Luo, Y. Lu, X. Zheng, J. Yang and L. Yang; Spectrochim. Acta Mol. Biomol. Spectros. Vol.74 (2009), p.336

[14] Y. Zhang, J. Zhang, H. Son, J. Kong and Z. Liu: J. Am. Chem. Soc. Vol.127 (2005), p.17156

[15] J.J. Hernández, M. García-Gutiérrez, D.R. Rueda, T.A. Ezquerra and R.J. Davies: Composites Sci. Technol. Vol.72 (2012), p.421

[16] L.J. Casarett, J. Doull, C.D. Klaassen, M.O. Amdur, Casarett and Doull's Toxicology: The Basic Science of Poisons, Macmillan, 1986.

[17] A. Nabok and A. Tsargorodskaya: Thin Solid Films Vol. 516 (2008), p.8993

[18] M. Kragulj, J. Trickovic, B. Dalmacija, Á. Kukovecz, Z. Kónya, J. Molnar and S. Roncevic: Chem. Eng. J. Vol.225 (2013) p.144

Materials and Applications for Sensors and Transducers III
10.4028/www.scientific.net/KEM.605

Copper Phthalocyanine Functionalized Single-Walled Carbon Nanotubes: Thin Film Deposition and Sensing Properties
10.4028/www.scientific.net/KEM.605.461

AIP | The Journal of Chemical Physics

Formation of ordered films of axially bridged aluminum phthalocyanine [(tBu)4PcAl]2O via magnetic field-induced reaction

Tamara Basova, Aleksei Berezin, Vladimir Nadolinny, Heiko Peisert, Thomas Chassé et al.

Citation: J. Chem. Phys. **139**, 204710 (2013); doi: 10.1063/1.4832875
View online: http://dx.doi.org/10.1063/1.4832875
View Table of Contents: http://jcp.aip.org/resource/1/JCPSA6/v139/i20
Published by the AIP Publishing LLC.

THE JOURNAL OF CHEMICAL PHYSICS 139, 204710 (2013)

Formation of ordered films of axially bridged aluminum phthalocyanine $[(tBu)_4PcAl]_2O$ via magnetic field-induced reaction

Tamara Basova,[1,a)] Aleksei Berezin,[1] Vladimir Nadolinny,[1] Heiko Peisert,[2] Thomas Chassé,[2] Hikmat Banimuslem,[3] and Aseel Hassan[3]
[1]*Nikolaev Institute of Inorganic Chemistry, Russian Academy of Sciences, Lavrentiev Pr., 3, 630090 Novosibirsk, Russia*
[2]*Institute for Physical and Theoretical Chemistry, Auf der Morgenstelle 18, 72076 Tübingen, Germany*
[3]*Materials and Engineering Research Institute, Sheffield Hallam University, Sheffield S1 1WB, United Kingdom*

(Received 19 September 2013; accepted 7 November 2013; published online 27 November 2013)

The μ-(oxo)bis[tetra-*tert*-butylphthalocyaninato] aluminum(III) $[(tBu)_4PcAl]_2O$ films with the crystallites oriented preferably in one direction were obtained via chemical transformation of tetra-*tert*-butylsubstituted chloroaluminum(III) phthalocyanine $(tBu)_4PcAlCl$ film upon its annealing in magnetic field. A comparative analysis of the influence of post-deposition annealing process without and under applied magnetic field of 1 T, on the orientation and morphology of $(tBu)_4PcAlCl$ and $[(tBu)_4PcAl]_2O$ films, has been carried out by the methods of UV-vis, Infrared and Raman spectroscopies, XRD as well as atomic force microscopy. The formation of $[(tBu)_4PcAl]_2O$ films with elongated crystallites having preferential orientation was observed upon heating of the films in magnetic field while annealing without magnetic field under the same conditions does not demonstrate any effect on the structure and morphology of these films. The reasons of the sensitivity of this reaction to the presence of such magnetic field is discussed and studied by electronic paramagnetic resonance spectroscopy. © *2013 AIP Publishing LLC*. [http://dx.doi.org/10.1063/1.4832875]

I. INTRODUCTION

Thin films of metal phthalocyanines, especially those having gallium, aluminum, and indium central metal atoms, possess remarkable optoelectronic characteristics which makes them and their various derivatives of interest as active layers in optoelectronic device applications.[1–4] Among those derivatives are the peripherally unsubstituted gallium and aluminum phthalocyanines with axial chloro, fluoro, or hydroxyl ligands (PcMX, X = Cl, F, OH) that were investigated for their optical third-order nonlinearity.[5] Optical limiting materials usually rely on their nonlinear optical response. As an example of those materials are the μ-oxo-bridged dimers $[(PcM)_2O]$, where M = Ga or Al have been shown to exhibit good photoreceptor properties.[6]

Substituted metal phthalocyanine molecules have long been shown to be suitable for deposition as thin films using simple solution processed methods such as spin coating and Langmuir-Blodgett techniques due to their largely improved solubility in common solvents. For instance, tetra-*tert*-butyl substituted phthalocyaninates were shown to exhibit very good optical limiting properties making them useful in practical device applications;[7,8] this was shown to be partly due to the large nonolinear absorption coefficient of these materials. Furthermore, it was demonstrated that photophysical and photochemical properties of substituted phthalocyanine complexes are very useful for photodynamic therapy (PDT) applications.[9,10] The non-peripherally substituted Al(III), Ga(III), and In(III) phthalocyanines showed higher singlet oxygen quantum yields in comparison to peripherally substituted analogues which was explained by red-shift in the Q-band of the UV-Vis absorption spectra in DMSO.[9]

Ordered phthalocyanine thin films are of crucial importance in real device application, especially in photovoltaic and chemical detection applications. The study of the physical properties of these films including their morphology and molecular structure and long-range order, is necessitated by the requirement to establish a relationship between these properties and the films' performance in such devices. The photoelectrochemical efficiency of ordered films of aluminum tetraphenylporphyrin produced by thermal vacuum deposition was shown to be higher than that exhibited by polycrystalline films.[11] The photocurrent quantum yield of uniform AlPcCl thin film with epitaxial orientation was 25 times as high as that of the rugged and cracked polycrystalline film.[12] This enhancement in the photocurrent has been ascribed to the molecular orientation, in which the planar molecules stay perpendicular to the substrate surface.

Molecules possessing dipole moment are expected to offer a route to controlling the growth of the molecules in thin films in the presence of an external field. Several studies were carried out to investigate the effects of externally applied electric or magnetic field on film growth of different metal phthalocyanines.[13–18] The growth of vacuum evaporated copper phthalocyanine films in the presence of magnetic field of 6 mT has resulted in a new stacking behavior and thus different orientation relative to the substrate surface.[15] It was also shown that the presence of electric and magnetic fields influences the molecular orientation, the polymorphism, and the

a)Author to whom correspondence should be addressed. Electronic mail: basova@niic.nsc.ru

surface morphology of the films of TiOPc,[19] AlClPc[20], and VOPc.[21]

The hydrolysis of AlClPc upon immersion in KCl water solutions at different pH was shown to lead to the formation of hydroxyaluminum phthalocyanine Al(OH)Pc and then to the formation of μ-(oxo)bis[phthalocyaninato] aluminum(III), $(PcAl)_2O$.[2,22,23] In a recent publication we have demonstrated the transformation of AlClPc to $(PcAl)_2O$ by applying magnetic field of 1 T during post-deposition of the vacuum sublimed PcAlPc thin films.[24] This transformation of AlClPc to $(PcAl)_2O$ on the substrate surface upon annealing under ambient conditions was monitored by UV/vis, IR, Raman, X-ray photoelectron spectroscopy (XPS), as well as atomic force microscopy (AFM). We have observed two interesting effects upon heating the AlClPc films in such magnetic field; firstly, the temperature of the chemical transformation of AlClPc to $(AlPc)_2O$ was seen to decrease from 300 °C to 200 °C, and secondly, $(AlPc)_2O$ films with elongated crystallites and with preferential orientation were formed. The reason behind the effect of magnetic fields on the growth and structure of aluminum phthalocyanine films remains unclear and, therefore, further studies are required in order to fully explain it.

This study is a continuation of the work published earlier.[24] In this work, we are aiming to demonstrate another example of formation of ordered films of axially bridged tetra-*tert*-butylsubstituted aluminum phthalocyanine $[(tBu)_4PcAl]_2O$ via magnetic field-induced reactions. This is especially important for the phthalocyanines with sterically demanding substituents such as tetra-*tert*-butyl which usually form films with low degree of ordering because of reduced intermolecular interaction.[25] Furthermore, we are aiming to investigate the reasons of the sensitivity of this reaction to the presence of such magnetic field by electronic paramagnetic resonance spectroscopy. Besides, the method of polarized Raman spectroscopy is used to estimate the orientation of the molecules relative to the substrate surface in the films annealed with and without magnetic field.

II. EXPERIMENTAL DETAILS

$(tBu)_4PcAlCl$ was prepared via reaction of 4-*tert*-butylphthalonitrile (Sigma-Aldrich) and anhydrous aluminum(III) chloride in quinoline media at the temperature of about 230 °C.[15] The synthesized phthalocyanine was purified by vacuum gradient sublimation at a residual pressure of 10^{-4} Torr at the temperature of 360 °C. $[(tBu)_4PcAl]_2O$ was prepared following a similar method described for $[PcAl]_2O$ in Ref. 26. First, $(t\text{-}Bu)_4PcAl(OH)$ was precipitated from its solution in sulphuric acid with ammonia water solution and then filtered and washed with water. $(t\text{-}Bu)_4PcAl(OH)$ was sublimed in vacuum of 10^{-4} Torr at the temperature of 450 °C and $[(tBu)_4PcAl]_2O$ was obtained as a result.

Thin films of $(tBu)_4PcAlCl$ and $[(tBu)_4PcAl]_2O$ were prepared via organic molecular beam deposition (OMBD) under high vacuum of 1×10^{-7} mbar at the evaporation rate of 10 Å/min and substrate temperature of 25 °C. Film thickness was controlled using a quartz crystal microbalance; the obtained films have a nominal thickness of about 50-60 nm. Quartz slides, polished Si wafers, and KBr substrates were used as substrates. The annealing of thin films of $(tBu)_4PcAlCl$ was performed under ambient conditions with and without applied magnetic field of 1 T using the same heating plate with precise temperature controller. For films annealed under applied magnetic field, the heating plate was put between permanent magnets as shown in Ref. 24.

Raman spectra of all samples were recorded with a SPEX Triplemate spectrometer equipped with CCD spectrometric detector and microscope attachment for backscattering experimental geometry. The 488 nm (40 mW) line of an argon ion laser was used for spectral excitation. The laser beam with the diameter of $\sim$1 μm was focused onto the sample via a microscope objective with 100-fold magnification (numerical aperture NA = 0.9). The spectral resolution was about 2 cm^{-1}.

Infrared spectra of powders in KBr pellets and of the deposited films on KBr substrates were recorded using a Vertex 80 FTIR spectrometer.

AFM measurements were performed under ambient conditions in tapping mode using a Nanoscope IIIa (Digital Instruments; now Veeco Instruments, Plainview, U.S.A.) scanning probe microscope. The oscillation frequency was around 300 kHz and the scan rate was about 1 Hz. The tip radius was typically in the range 4–7 nm. UV-vis spectra of thin films deposited on quartz substrates were recorded with a UV-VIS-NIR scanning spectrophotometer (UV-VIS-3101PC «Shimadzu») in the range of 400-1000 nm. X-Ray diffraction measurements were performed using an automatic diffractometer DRON-3M (R = 192 mm, CuK_α-irradiation, Ni-filter, scintillation detector with amplitude discrimination, Soller slits with aperture of 2.5° on primary and reflected beams) in the region of 2θ from 5° to 60° with the scanning step of 0.03°. All measurements were carried out under ambient conditions.

EPR experiments were performed by a modified Varian EPR spectrometer E-109 in X-band of frequency at room temperature. Spin trap in experiment for the study of short living radicals was C-phenyl-*tert*-butyl nitron (PBN).

III. RESULTS AND DISCUSSION

A. Film characterisation by spectral methods and XRD

UV-vis absorption spectra of as-deposited $(tBu)_4PcAlCl$ film and the films underwent gradual annealing with temperature step of 10 °C are shown in Figure 1. It can be seen that the UV-vis absorption spectrum of the as-deposited $(tBu)_4PcAlCl$ film (Figure 1) on a glass slide consists of a wide characteristic absorption band with two maxima at 655 and 703 nm. The XRD pattern of the as-deposited $(tBu)_4PcAlCl$ film is shown in Figure 2(a). According to XRD data the as-deposited $(tBu)_4PcAlCl$ film is amorphous or consists of the nanoislands which are insufficient to yield sharp diffraction features and a large number of defects. A similar broad spectrum was also observed for the amorphous films of unsubstituted AlClPc.[27]

As-deposited $(tBu)_4PcAlCl$ films were annealed with and without magnetic field in air under ambient conditions.

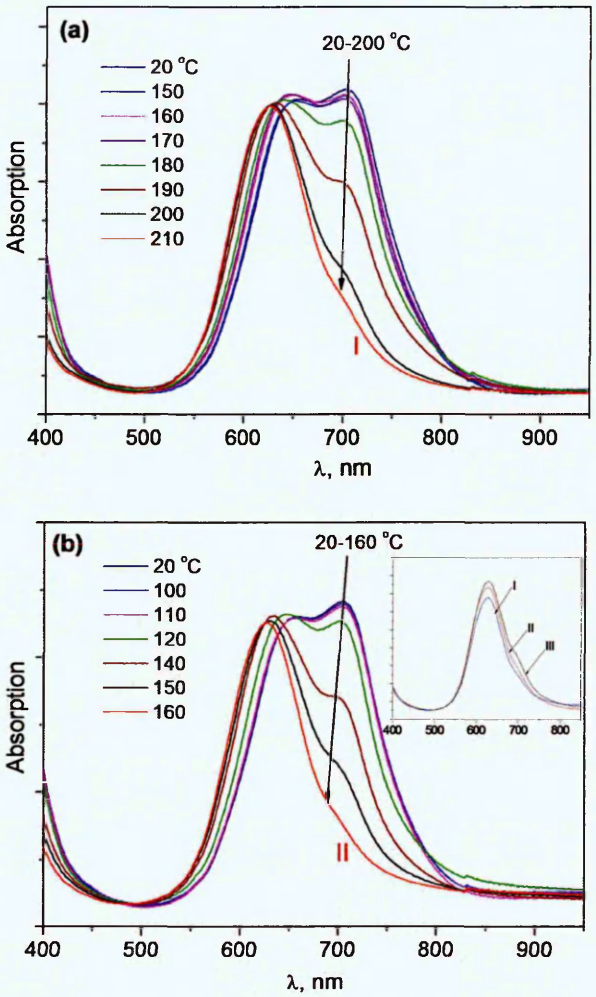

FIG. 1. UV-vis spectra of aluminum phthalocyanine thin films during annealing in the temperature range 20 °C-210 °C without (a) and under (b) magnetic field (1 T). The inset in Fig. (b) shows the spectra of $(tBu)_4PcAlCl$ film after annealing under ambient conditions at 210 °C (I), $(tBu)_4PcAlCl$ film after annealing under magnetic field of 1 T at 160 °C (II), and $[(tBu)_4PcAl]_2O$ film deposited by OMBD (III).

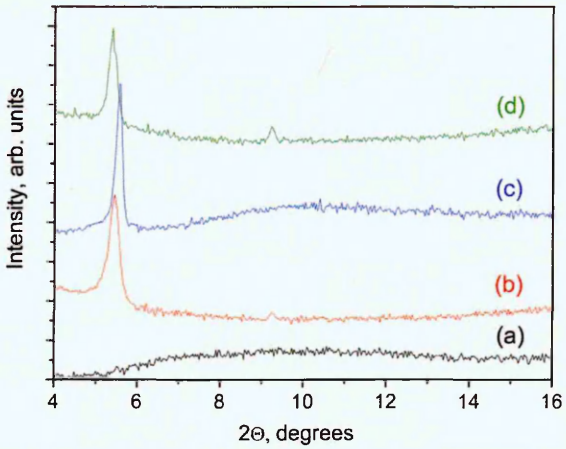

FIG. 2. X-ray diffraction patterns of aluminum phthalocyanine thin films on glass: $(tBu)_4PcAlCl$ as-deposited film (a); $(tBu)_4PcAlCl$ film after annealing under ambient conditions at 210 °C (b); $(tBu)_4PcAlCl$ film after annealing under magnetic field of 1 T at 160 °C (c); $[(tBu)_4PcAl]_2O$ film deposited by OMBD (d).

No changes were observed in the UV-vis spectra of the $(tBu)_4PcAlCl$ films heated without magnetic field up to temperatures below 150 °C (Figure 1(a)). When the $(tBu)_4PcAlCl$ films were heated to temperatures above 150 °C in air, the intensity of the band at 703 nm started to decrease, while the shoulder at 655 nm is shifted to 647 nm without changing its intensity (Figure 1(a)). The spectra of the annealed $(tBu)_4PcAlCl$ films agree well with the spectrum of a $[(tBu)_4PcAl]_2O$ film deposited at similar conditions by thermal evaporation of $[(tBu)_4PcAl]_2O$ powder (see the inset of Fig. 1(b)). The first changes in the spectra of the $(tBu)_4PcAlCl$ films heated under applied magnetic field become noticeable at annealing temperatures above 110 °C. The heating to temperatures larger than 160 °C or annealing at 160 °C for longer time does not lead to any additional spectral changes. This can be interpreted by complete transformation of $(tBu)_4PcAlCl$ to $[(tBu)_4PcAl]_2O$ taking place at 160 °C which is 50 °C lower than that in the case of $(tBu)_4PcAlCl$ films heated without magnetic field.

We may suggest that as in the case of unsubstituted AlClPc[24] annealing of $(tBu)_4PcAlCl$ film under ambient conditions both in magnetic field and without magnetic field leads to chemical transformation of $(tBu)_4PcAlCl$ to the corresponding μ-oxo-dimer $[(tBu)_4PcAl]_2O$. The temperature of this chemical transformation decreases from 210 °C to 160 °C, when magnetic field was applied during post-deposition annealing.

The XRD patterns of $(tBu)_4PcAlCl$ films after annealing both with and without magnetic field are presented in Figures 2(b) and 2(c), respectively. The XRD patterns of $[(tBu)_4PcAl]_2O$ film deposited by OMBD with the subsequent annealing at 210 °C are also given for comparison (Figure 2(d)). The annealing of $(tBu)_4PcAlCl$ films with magnetic field leads to notable changes in the XRD pattern. The new peaks at $2\theta = 5.45°$ (d = 16.2 Å) and $2\theta = 9.26°$ (d = 9.5 Å) appeared after film annealing without magnetic field (Figure 1(b)), while the XRD pattern of the film heated under applied magnetic field (Figure 2(b)) has exhibited one intensive peak at $2\theta = 5.54°$ corresponding to a lattice spacing of 15.9 Å. The crystal structures of $(tBu)_4PcAlCl$ and $[(tBu)_4PcAl]_2O$ were not resolved, however, the peak position at $2\theta = 5.54°$ agrees with the position of the diffraction peaks in films of other tetra-*tert*-butyl metal phthalocyanines, i.e., $2\theta = 5.51°$ (d = 16.04 Å) in the case of $CuPc(tBu)_4$ films deposited on glass and gold substrates.[28] The presence of only one XRD peak suggests that the film annealed in the presence of magnetic field is characterized by preferential ordering. It is necessary to point out that the XRD pattern of the $[(tBu)_4PcAl]_2O$ film deposited by OMBD (Figure 2(d)) is similar to that of the $(tBu)_4PcAlCl$ film heated without applied magnetic field (Figure 2(d)) and contains two peaks at $2\theta = 5.42°$ and $2\theta = 9.25°$.

For further understanding, the vibrational spectra (IR and Raman) of as-deposited and annealed $(tBu)_4PcAlCl$ films were measured. The IR spectrum of as-deposited $(tBu)_4PcAlCl$ film is presented in Fig. 3(a). The positions and relative intensities of the main vibrations corresponding to phthalocyanine macrocycle and *tert*-butyl substituents are in good agreement with those published for $(tBu)_4PcZn$

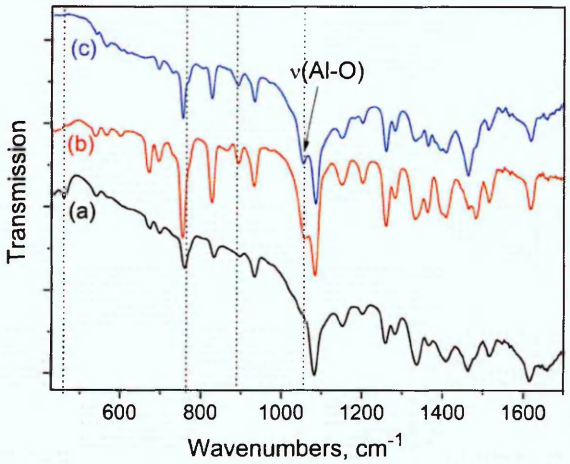

FIG. 3. IR spectra of aluminum phthalocyanine thin films on KBr substrates: $(tBu)_4PcAlCl$ as-deposited film (a); $(tBu)_4PcAlCl$ film after annealing under ambient conditions at 210 °C (b), $(tBu)_4PcAlCl$ film after annealing under magnetic field (1 T) at 160 °C (c).

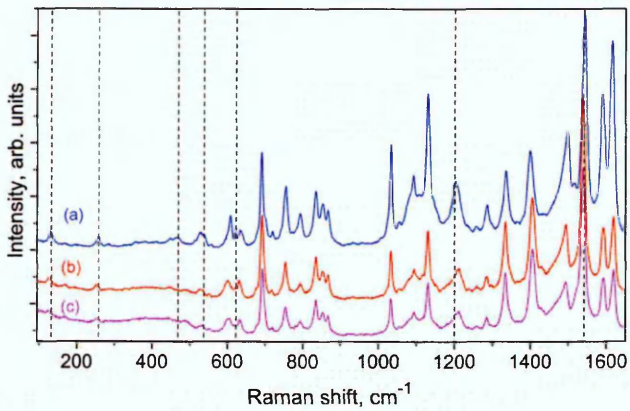

FIG. 4. Raman spectra of aluminum phthalocyanine thin films on glass substrates: $(tBu)_4PcAlCl$ as-deposited film (a); $(tBu)_4PcAlCl$ film after annealing under ambient conditions at 210 °C (b); $(tBu)_4PcAlCl$ film after annealing under magnetic field of 1 T at 160 °C (c).

in Ref. 29. Introduction of four *tert*-butyl substituents in the $(tBu)_4PcAlCl$ molecule leads to a change of the intensity and position of some bands and to the appearance of some new bands in comparison with unsubstituted PcAlCl.[20] Undoubtedly, the appearance of new bands at 670-690 and 1258 cm^{-1} in the spectrum of $(tBu)_4PcAlCl$ in comparison with that of PcAlCl is associated with bending vibrations of peripheral *tert*-butyl groups. The annealing of $(tBu)_4PcAlCl$ films leads to remarkable changes in the IR spectra. The IR-spectra of the films after annealing (Figures 3(b) and 3(c)) contain a comparatively intensive band at 1050 cm^{-1} which can be assigned to the asymmetrical stretching of the Al–O bond[24] which was not observed in the spectrum of the as deposited film. At the same time band at 459 cm^{-1} corresponding to stretching vibration of Al–Cl completely disappears after the annealing of the films. The two bands located at 760 and 894 cm^{-1} corresponding to the vibrations of inner phthalocyanine macrocycle in the IR spectrum of as-deposited film shift to 753 and 890 cm^{-1}, respectively, after heating (Figures 3(b) and 3(c)).

Raman spectra of $(tBu)_4PcAlCl$ and $[(tBu)_4PcAl]_2O$ appear to be very similar to each other at first glance, however, some changes are also visible in the Raman spectra upon transformation of $(tBu)_4PcAlCl$ to $[(tBu)_4PcAl]_2O$ (Figure 4). The assignment of the vibration bands in the spectra has been reached by analogy with unsubstituted aluminium phthalocyanines.[20,23] The experimentally found vibrations with considerable contribution of ν(Al-Cl) are located at 258, 465, and 537 cm^{-1}. They exhibit very low intensity compared to other vibrations because of small changes in the polarizability and, therefore, they might be partly overlapped by vibrations of the Pc ring system. In Figures 4(b) and 4(c) these bands of Al–Cl have nearly vanished in the spectra corresponding to the films after the reaction and new modes close to the wavenumbers of Al–Cl are assigned to Al–O–Al vibrations. The central atom specific mode for AlPc is found at 1542 cm^{-1}. The main contribution to this vibration is given by displacements of the C_α-N_β-C_α bridge bonds of the phthalocyanine macrocycle. The shift of 5 cm^{-1} to lower wavenumbers indicates a change in the central atom surrounding.

To get deeper insight into the structural transformations of the aluminum phthalocyanine films, we also studied their morphology using AFM technique. Figure 5 shows the morphology of the as-deposited $(tBu)_4PcAlCl$ (Figure 5(a)) films and the $[(tBu)_4PcAl]_2O$ films formed after heating of the as-deposited $(tBu)_4PcAlCl$ with and without magnetic field at 180 °C and 220 °C, respectively. It is seen from Figure 5(a) that the as-deposited films consist of very small grains with RMS film roughness of 0.74 nm. Remarkable changes in morphology are observed after film annealing; the film annealed at 220 °C without magnetic field consists of larger disordered domains (Figure 5(b)). Note that the RMS roughness of the samples increased to 4.11 nm. The AFM image of the thin film heated at 160 °C under magnetic field (Figure 5(c)) revealed elongated well-formed crystallites (r.m.s. roughness is 6.02 nm) which mostly tend to be oriented in one direction and lying parallel to each other. It is necessary to mention that the long axes of the crystallites are

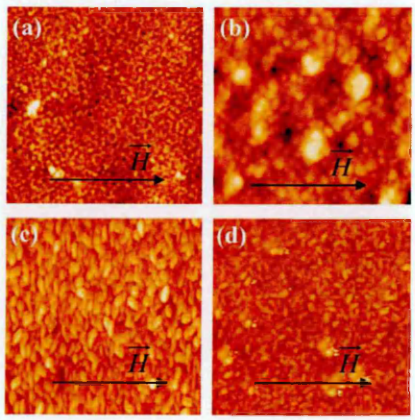

FIG. 5. AFM images (2 μm × 2 μm) of aluminum phthalocyanine thin films on glass substrates: as-deposited $(tBu)_4PcAlCl$ film (a); $[(tBu)_4PcAl]_2O$ films obtained by annealing of $(tBu)_4PcAlCl$ under ambient conditions at 210 °C (b) and of $(tBu)_4PcAlCl$ after annealing under magnetic field of 1 T at 160 °C (c); $[(tBu)_4PcAl]_2O$ film deposited by OMBD (d). The orientation of the magnetic field lines ($\vec{H}$) is shown in each image.

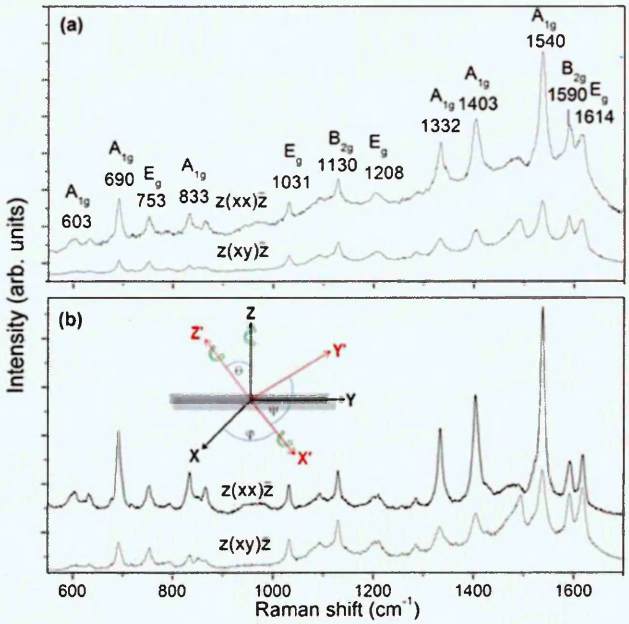

FIG. 6. Polarized Raman spectra of $[(tBu)_4PcAl]_2O$ films obtained by annealing of $(tBu)_4PcAlCl$ film under ambient conditions at 210 °C (a) and by annealing $(tBu)_4PcAlCl$ film after annealing under magnetic field of 1 T at 160 °C (b). The inset shows the Euler coordinates employed: φ corresponds to the rotation around the substrate Z-axis, θ – to the rotation around the molecular X'-axis (the tilt angle between Z and Z′), and ψ – to the rotation around the molecular Z′-axis.

oriented perpendicular to the field lines of the applied magnetic field. For the sake of comparison it is important to point out that the $[(tBu)_4PcAl]_2O$ film obtained by physical vapour deposition of $[(tBu)_4PcAl]_2O$ powder is characterized by disordered randomly shaped smaller crystallites.

Non-polarized spectra of films of $(tBu)_4PcAlCl$ before and after heating provide qualitative evidence of their chemical transformation to $[(tBu)_4PcAl]_2O$, as shown in Figures 1, 3, and 4. This technique however, does not give quantitative understanding to the films' orientation. This issue is further clarified here using polarization dependent Raman spectroscopy and to present a comparison between the orientation of $[(tBu)_4PcAl]_2O$ films obtained by annealing $(tBu)_4PcAlCl$ both without and under applied magnetic field.

B. Investigation of the films orientation by polarized Raman spectroscopy

Polarized Raman spectroscopy was used to investigate the orientation of the studied aluminum phthalocyanine molecules relative to the substrate surface. This method is based on the analysis of the depolarization ratio $\rho = I(z(xy)\bar{z})/I(z(xx)\bar{z})$ of the modes of the corresponding symmetry type in the Raman spectra registered in parallel and perpendicular polarizations of the incident and scattered light. It allows the determination of a preferential angle of the molecules inclination (θ) relative to the substrate surface (cf. the inset of Figure 6). The details of this technique have already been described in Refs. 30–33.

Figure 6 shows the polarized Raman spectra of the $[(tBu)_4PcAl]_2O$ films obtained by annealing of $(tBu)_4PcAlCl$ films without (a) and under (b) magnetic field, recorded in the parallel ($z(xx)\bar{z}$) and cross ($z(xy)\bar{z}$) polarizations of incident and scattered light. The annealing temperature was 210 °C (a) and 160 °C (b), i.e., above the reaction temperature in both cases. The symmetry types of some Raman modes are indicated in Figure 6. They were determined on the basis of comparison with the Raman spectra of the unsubstituted $(PcAl)_2O$ derivative.[23] The depolarization ratios of the selected A_{1g}, B_{2g}, and E bands in the spectra of $[(tBu)_4PcAl]_2O$ films and the corresponding Euler angles θ are given in Table I. The $[(tBu)_4PcAl]_2O$ films annealed without magnetic field were disordered because the depolarization ratio $\rho = I_{ii}/I_{ij}$ were similar to that of solutions. Analysis of the depolarization ratio in the Raman spectra of $[(tBu)_4PcAl]_2O$ film

TABLE I. Experimental depolarization ratios $\rho = I_{ii}/I_{ij}$ for the A_{1g}, E, and B_{2g} modes obtained from polarization dependent Raman spectra of the $[(tBu)_4PcAl]_2O$ films obtained by annealing without and under applied magnetic field of 1 T as well as by OMBD.

		Depolarization ratio $\rho_{(ij/ii)}$		
Symmetry irrep	Raman shift (cm^{-1})	Film annealed without magnetic field	Film annealed with magnetic field	Film deposited by OMBD
A_{1g}	690	0.25	0.33	0.23
	833	0.25	0.32	0.22
	1332	0.30	0.29	0.29
	1403	0.26	0.33	0.25
	1540	0.31	5	0.31
Mean		**0.29**	**0.32**	**0.26**
E	753	0.70	1.0	0.68
	1031	0.75	1.0	0.78
	1208	0.79	1.0	0.80
	1614	0.70	1.1	0.74
Mean		**0.74**	**1.0**	**0.75**
B_{2g}	1130	0.75	1.0	0.77
	1590	0.75	1.0	0.74
Mean		**0.75**	**1.0**	**0.76**

deposited by OMBD with the subsequent annealing at 210 °C did not reveal any preferential orientation of the molecules relative to the substrate surface. Films annealed in the presence of magnetic field lead to a visible difference in the depolarization ratio ρ and thus to a difference in the film crystallites orientation. The angle of inclination relative to the substrate surface in the films annealed in the presence of the magnetic field was equal to 85 ± 5° suggesting a nearly *perpendicular* orientation of the phthalocyanine macrocycles to the substrate surface. Therefore, it may be clearly seen that the external magnetic field applied during post-deposition annealing has a pronounced influence on the molecular orientation in the aluminum phthalocyanine thin films.

Similar to the case of unsubstituted PcAlCl[24] two effects were observed during post-deposition annealing of $(tBu)_4PcAlCl$ films in magnetic field of 1T; these are: (i) the temperature of the chemical transformation of $(tBu)_4PcAlCl$ to $[(tBu)_4PcAl]_2O$ decreases from 210 °C to 160 °C and (ii) the $[(tBu)_4PcAl]_2O$ films with preferentially oriented elongated crystallites and phthalocyanine macrocycles were formed.

C. Investigation of the transformation of $(tBu)_4PcAlCl$ to $[(tBu)_4PcAl]_2O$ by EPR spectroscopy

In order to explain the sensitivity of the investigated films to the application of magnetic field during heat treatment a possible mechanism of the reaction of transformation of $(tBu)_4PcAlCl$ to $[(tBu)_4PcAl]_2O$ was studied by electron paramagnetic resonance spectroscopy using the method of spin traps.[34,35] As a spin trap we used PBN with the melting point of 78 °C. The samples were prepared in the following way: $(tBu)_4PcAlCl$ powder was mixed with PBN in a ratio ~1:1. Then the mixture was kept at 78 °C for a period of 30 min at different conditions: (i) in vacuum of 10^{-4} Torr and (ii) at atmospheric pressure. Further, the mixtures were cooled down to room temperature and dissolved in acetone. Afterwards, the solution was purged with helium gas for oxygen removal and EPR spectra were recorded.

The first sample heated in vacuum did not show any EPR signal. The second mixture heated at atmospheric pressure with the presence of water vapour exhibited a characteristic EPR spectrum (Figure 7). This signal is related to the adducts of short-lived OH radicals with the PBN spin trap. The obtained experimental value is in good agreement with that of the constant of hyperfine interaction for adduct of PBN with OH radicals. Similar results were also obtained for unsubstituted PcAlCl. Therefore, we can conclude that the reaction of $(tBu)_4PcAlCl$ and PcAlCl with water with the formation of the corresponding μ-oxodimers proceeds according to a radical mechanism involving the metal phthalocyanine AlPc· and OH· radicals.

On the basis of the data obtained the process of dimerization in the films can be described as a sequence of the following reactions. We suggest that upon heating water molecules penetrate between phthalocyanine layers. H_2O molecules interact with $(tBu)_4PcAlCl$ molecules producing HCl, MPc^+, HO^-. As the electron transfer in the solid state is faster than the OH^- diffusion, the electron is transferred from HO^-

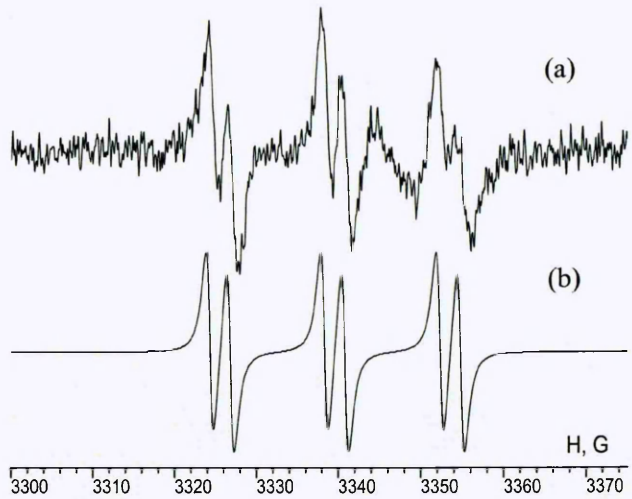

FIG. 7. EPR spectra of the adducts of OH radicals with PBN: experimental (a); calculated (b).

to MPc^+ and radicals OH· and MPc· are formed. Further, OH· radical substitutes chlorine giving $(tBu)_4PcAlOH$. Then, $(tBu)_4PcAlOH$ reacts with $(tBu)_4PcAlCl$ liberating HCl and producing the μ-oxo-dimer $(tBu)_4PcAlOAlPc(tBu)_4$.

In this manner the results of the EPR investigations shed some light on the role of magnetic field. Due to the radical state of the phthalocyanine molecule it gains magnetic moment capable of interaction with external magnetic field. This may explain the significant decrease of the transformation temperature upon annealing in magnetic field. It is well known that chemical reactions that involve radical intermediates can be influenced by magnetic fields, which act to alter their rate, yield, or product distribution.[36–38]

Systematic investigations of the chemical transformation of $(tBu)_4PcAlCl$ to $[(tBu)_4PcAl]_2O$ on the substrate surface using complementary methods such as optical spectroscopies, X-ray diffraction, and electron spin resonance allowed us to conclude that the presence of a magnetic field parallel to the substrate surface during annealing of the film improves substantially the azimuthal order of crystalline domains with the phthalocyanine molecules oriented perpendicular to the substrate surface and are turned so that their dipole moments oppose the magnetic field direction (Figure 8).

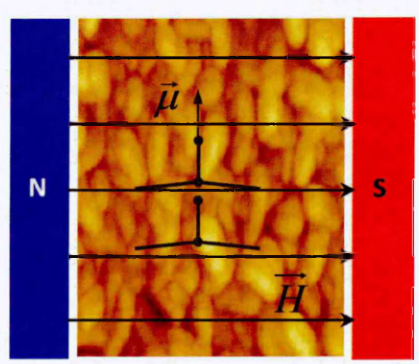

FIG. 8. Scheme of orientation of the crystallites and the phthalocyanine molecules in the films relative to the magnetic field direction.

IV. CONCLUSIONS

In this work, the influence of post-deposition annealing without and under applied magnetic field on the chemical transformation of $(tBu)_4PcAlCl$ to $[(tBu)_4PcAl]_2O$ on the substrate surface was studied using complementary methods such as optical spectroscopies, X-ray diffraction, and atomic force microscopy. Combination of these methods with polarized Raman spectroscopy technique allowed to conclude that the presence of a magnetic field parallel to the substrate surface during annealing of the film improves the azimuthal order of crystalline domains with the phthalocyanine molecules oriented perpendicular to the substrate surface and are turned so that their dipole moments oppose the magnetic field direction. Study by electron paramagnetic resonance spectroscopy using the method of spin traps has shown that the reaction of transformation of $(tBu)_4PcAlCl$ to $[(tBu)_4PcAl]_2O$ proceeds according to radical mechanism with formation of the metal phthalocyanine $AlPc^{\cdot}$ and $OH^{\cdot}$ radicals. Due to the radical state of the phthalocyanine it gains magnetic moment capable of interaction with external magnetic field.

ACKNOWLEDGMENTS

Financial support by the German Research Council (PE 546/5-1 and CH 132/23-1) is gratefully acknowledged.

[1]R. O. Loutfy, A. M. Hor, and A. Rucklidge, J. Imaging Sci. **31**, 31 (1987).
[2]F. Santerre, R. Côté, G. Veilleux, R. G. Saint-Jacques, and J. P. Dodelet, J. Phys. Chem. **100**, 7632 (1996).
[3]A. Ioannidis and J. P. Dodelet, J. Phys. Chem. B **101**, 901 (1997).
[4]Y. Sakakibara, R. N. Bera, T. Mizutani, K. Ishida, M. Tokumoto, and T. Tani, J. Phys. Chem. B **105**, 1547 (2001).
[5]Z. Z. Ho, C. Y. Ju, and W. M. Hetherington III, J. Appl. Phys. **62**, 716 (1987).
[6]K. Yamasaki, O. Okada, K. Inami, K. Oka, M. Kotani, and H. Yamada, J. Phys. Chem. B **101**, 13 (1997).
[7]J. W. Perry, K. Mansour, I. Y. S. Lee, X. L. Wu, P. V. Bedworth, C. T. Chen, D. Ng, S. R. Marder, P. Miles, T. Wada, M. Tian, and H. Sasabe, Science **273**, 1533 (1996).
[8]J. S. Shirk, R. G. S. Pong, S. R. Flom, H. Heckmann, and M. Hanack, J. Phys. Chem. A **104**, 1438 (2000).
[9]H. Yanık, D. Aydın, M. Durmuş, and V. Ahsen, J. Photochem. Photobiol., A **206**, 18 (2009).
[10]T. Nyokong, Coord. Chem. Rev. **251**, 1707 (2007).
[11]H. Yanagi, M. Ashida, Y. Harima, and K. Yamashita, Chem. Lett. **19**(3), 385 (1990).
[12]H. Yanagi, S. Douko, Y. Ueda, M. Ashida, and D. Wöhrle, J. Phys. Chem. **96**, 1366 (1992).
[13]S. Zhu, C. E. Banks, D. O. Frazier, B. Penn, H. Abdeldayem, R. Hicks, H. D. Burns, and G. W. Thompson, J. Cryst. Growth **211**, 308 (2000).
[14]K. Hayashi, S. Kawato, Y. Fujii, T. Horiuchi, and K. Matsushige, Appl. Phys. Lett. **70**, 1384 (1997).
[15]Z. G. Ji, K. W. Wong, P. K. Tse, R. W. M. Kwok, and W. M. Lau, Thin Solid Films **402**, 79 (2002).
[16]W. P. Hu, Y. Q. Liu, S. Q. Zhou, J. Tao, D. F. Xu, and D. B. Zhu, Thin Solid Films **347**, 299 (1999).
[17]A. Cristadoro, G. Lieser, H. J. Räder, and K. Müllen, ChemPhysChem **8**, 586 (2007).
[18]A. Cristadoro, M. Ai, H. J. Räder, J. P. Rabe, and K. Müllen, J. Phys. Chem. C **112**, 5563 (2008).
[19]B. E. Schuster, T. V. Basova, H. Peisert, and T. Chasse, ChemPhysChem **10**, 1874 (2009).
[20]T. V. Basova, V. G. Kiselev, V. A. Plyashkevich, P. B. Cheblakov, F. Latteyer, H. Peisert, and T. Chassè, Chem. Phys. **380**, 40 (2011).
[21]V. Kolotovska, M. Friedrich, D. R. T. Zahn, and G. Salvan, J. Cryst. Growth **291**, 166 (2006).
[22]F. Santerre, R. Cote, G. Lalande, L. Gastonguay, D. Guay, and J. P. Dodelet, J. Phys. Chem. **99**, 17198 (1995).
[23]F. Latteyer, H. Peisert, J. Uihlein, T. Basova, P. Nagel, M. Merz, S. Schuppler, and T. Chassé, Anal. Bioanal. Chem. **405**, 4895 (2013).
[24]T. Basova, V. Plyashkevich, F. Petraki, H. Peisert, and T. Chassé, J. Chem. Phys. **134**, 124703 (2011).
[25]I. Biswas, H. Peisert, T. Schwieger, D. Dini, M. Hanack, M. Knupfer, T. Schmidt, and T. Chassé, J. Chem. Phys. **122**, 064710 (2005).
[26]J. E. Owen and M. E. Kenney, Inorg. Chem. **1**, 334 (1962).
[27]D. Guay, G. Veilleux, R. G. Saint-Jacques, R. Côté, and J. P. Dodelet, J. Mater. Res. **4**, 651 (1989).
[28]Y.-L. Lee, W.-C. Tsai, C.-H. Chang, and Y.-M. Yang, Appl. Surf. Sci. **172**, 191 (2001).
[29]N. S. Lebedeva, E. V. Parfenyuk, and E. A. Malkova, Spectrochim. Acta A **68**, 491 (2007).
[30]T. V. Basova, V. G. Kiselev, I. S. Dubkov, F. Latteyer, S. A. Gromilov, H. Peisert, and T. Chassè, J. Phys. Chem. C **117**, 7097 (2013).
[31]R. Aroca, C. Jennings, R. O. Loutfy, and A. M. Hor, J. Phys. Chem. **90**, 5255 (1986).
[32]D. R. T. Zahn, G. N. Gavrila, and G. Salvan, Chem. Rev. **107**, 1161 (2007).
[33]F. Latteyer, H. Peisert, U. Aygül, I. Biswas, F. Petraki, T. Basova, A. Vollmer, and T. Chassè, J. Phys. Chem. C **115**, 11657 (2011).
[34]E. G. Janzen, D. E. Nutter Jr., E. R. Davis, B. J. Blackburn, J. L. Poyer, and P. B. McCay, Can. J. Chem. **56**, 2237 (1978).
[35]B. E. Zubarev, *Method of Spin Traps. Application in Chemistry, Biology and Medicine* (Moscow State University, 1984).
[36]H. Hayashi, *Introduction to Dynamic Spin Chemistry: Magnetic Field Effects on Chemical and Biochemical Reactions* (World Scientific: Singapore, 2004).
[37]C. T. Rodgers, Pure Appl. Chem. **81**, 19 (2009).
[38]H. Fischer, *Magnetic Properties of Free Radicals: Molecules and Radicals* (Springer Verlag, 1987), Vol. 17.

Synthetic Metals 162 (2012) 735–742

Contents lists available at SciVerse ScienceDirect

Synthetic Metals

journal homepage: www.elsevier.com/locate/synmet

Effect of substituents on the orientation of octasubstituted copper(II) phthalocyanine thin films

Tamara V. Basova[a,*], Meryem Çamur[b], Aliye Aslı Esenpınar[b], Sinem Tuncel[c], Aseel Hassan[d], Alexey Alexeyev[a], Hikmat Banimuslem[d], Mahmut Durmuş[c], Ayşe Gül Gürek[c], Vefa Ahsen[c,e]

[a] Nikolaev Institute of Inorganic Chemistry SB RAS, 3 Lavrentiev Ave., Novosibirsk 630090, Russia
[b] Kırklareli University, Department of Chemistry, 39100 Kırklareli, Turkey
[c] Gebze Institute of Technology, Department of Chemistry, P.O. Box: 141, 41400 Gebze, Kocaeli, Turkey
[d] Faculty of Arts, Computing, Engineering and Sciences, Sheffield Hallam University, Furnival Building, 153 Arundel Street, Sheffield S1 2NU, United Kingdom
[e] TUBITAK-Marmara Research Center, Materials Institute, P.O. Box: 21, 41470 Gebze, Kocaeli, Turkey

ARTICLE INFO

Article history:
Received 24 November 2011
Received in revised form 30 January 2012
Accepted 7 February 2012
Available online 30 March 2012

Keywords:
Phthalocyanine
Thin films
Liquid crystals
Molecular alignment

ABSTRACT

Octasubstituted copper(II) phthalocyanines containing alkylthio-, alkyloxy-, (trioxyethylene)thio- and (trioxyethylene)oxy- substituents in peripheral positions have been synthesized and characterized using UV–vis, IR, and mass spectroscopies. The mesogenic properties of the copper(II) phthalocyanines have been studied by differential scanning calorimetry, polarizing optical microscopy, and X-ray diffraction. The effect of the nature of substituents in the phthalocyanine ring on the liquid crystalline properties and the orientation of the molecules in thin films have also been investigated using a range of spectral methods as well as by X-ray diffraction analysis. Visible absorption spectroscopy yielded an evidence of a thermally induced molecular reorganization in the films. Polarized Raman spectroscopy was used to study the preferential orientation of molecules relative to the substrate surface. Influence of the nature of substituents in the phthalocyanine molecule in the thin films conductivity was also investigated.

1. Introduction

Phthalocyanine (Pc) and its derivatives constitute one of the most studied classes of organic functional materials in nonlinear optics [1,2], liquid-crystalline electronic charge carriers [3,4], exciton-transport materials [5], optical data storage [6], photodynamic cancer therapy [7], solar cells [8], catalysis [9] and as the active layers of gas sensors [10].

Substitutions of long alkyl, alkyloxy and alkylthio substituents into the aromatic ring leads to the enhancement of the solubility and liquid-crystalline behavior in which the aromatic rings assemble into columnar stacks [11–13]. Columnar liquid crystals such as discotic liquid crystals with high order materials are good candidates as organic semiconductors for electronic devices due to their potential to possess high mobility of charge carriers as well as the anisotropic property of conduction along the columns [14–17].

The alignment of discotic liquid crystals becomes a crucial point for high conductivity in different electronic devices. There are two typical alignments of discotic liquid crystals; homeotropic and homogeneous (planar) ones. In the former the discs lie on a plate horizontally, and in the latter the discs stand on a plate perpendicularly. Generally, liquid crystals are so flexible that they can be spread uniformly on a plate and between two plates. Homeotropic alignment can be generated by thermal annealing, that is, upon slow cooling of the isotropic melt confined between two substrates. Homeotropic alignment has been reported for some hexabenzocoronene (HBC) [10], phthalocyanine [11,12] and triphenylene mesogens [13–15]. It has been concluded that the intercolumnar packing dimensions of the polycyclic aromatic hydrocarbons are strongly dependent on the aromatic core size, the side chain length, and the number of side chains [18]. Low isotropic melt viscosity associated with the presence of oxygen atoms in the flexible side chains have been postulated as key parameters for the homeotropic alignment of phthalocyanine mesogens [19–24].

Although many different side-chain-modified Pcs and other discotic molecules have been synthesized, the thin film properties for only limited number of phthalocyanines were reported. The exploitation of the desirable optical and electrical or electrochemical properties of phthalocyanines relies on the precise control over the molecular packing and ordering in the solid phase. Many Pc derivatives with flexible side-chains make excellent candidates for Langmuir–Blodgett (LB) film fabrication as well as films produced by spin coating, and self-assembly [19].

In this article, the effect of different substituents on the orientation of the film of octasubstituted copper(II) phthalocyanines with alkylthio-, alkyloxy-, (trioxyethylene)thio- and

* Corresponding author.
E-mail address: basova@niic.nsc.ru (T.V. Basova).

0379-6779/$ – see front matter © 2012 Elsevier B.V. All rights reserved.
doi:10.1016/j.synthmet.2012.02.006

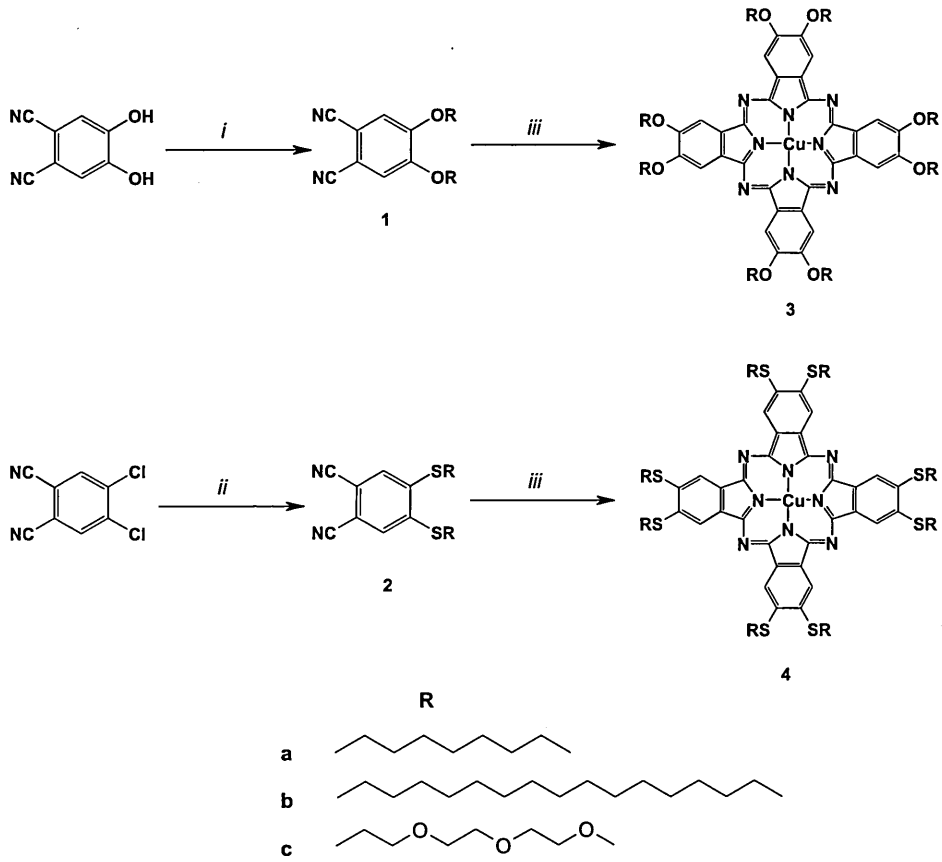

ig. 1. Synthesis of octa-substituted copper(II) phthalocyanines. Reagents and conditions: (*i*) RBr, K_2CO_3, DMF, rt, 3 days; (*ii*) RSH, K_2CO_3, DMF, rt, 3 days; (*iii*) $CuCl_2$ nhydrous), DBU, *n*-hexanol, reflux, 24 h.

rioxyethylene)oxy-substituents in peripheral positions (Fig. 1) is udied by the method of X-ray phase analysis, polarized Raman ectroscopy and polarized optical microscopy (POM). The effect f nature of substituents in phthalocyanine ring on the liquid crys- lline properties and the orientation of the molecules in thin films ave been investigated using a range of spectral methods as well as ' X-ray diffraction (XRD) analysis. Polarized Raman spectroscopy as used to study the preferential orientation of molecules relative the substrate surface.

Experimental part

1. Materials

All used reagents were purchased from commercial suppliers. ıPcR$_8$ derivatives (Fig. 1) were synthesized and characterized cording to the literature procedures [25–28]. 4,5-Dihydroxy- ıthalonitrile [29], 4,5-dichlorophthalonitrile [30], 4,5-bis(octyl- io)phthalonitrile (**2a**) [31], 4,5-bis(hexadecylthio)phthalonitrile **b**) [32], and 4,5-bis(1-tia-4,7,10-trioxaundecanyl)phthalonitrile **c**) [33] were synthesized according to reported procedure. 5-Bis(octyloxy)phthalonitrile (**1a**) [34], 4,5-bis(hexadecyloxy)- ıthalonitrile (**1b**) [34] and 4,5-bis(1,4,7,10-tetraoxaundeca- l)phthalonitrile (**1c**) [35] were synthesized according to the mod- ed reported procedure by using 4,5-dihydroxyphthalonitrile as ecursor which has previously been described by Torres and co- orkers [29]. Hexanol, *n*-hexane, THF, DMF and dichloromethane CM) were dried as described by Perrin and Armarego [36] before e.

2.2. Equipment

The IR spectra were recorded on a Shimadzu Fourier Transform FTIR-8300 using KBr pellets. The mass spectra were acquired on a Bruker Daltonics (Bremen, Germany) MicroTOF mass spectrometer using 2,5-dihydroxybenzoic acid as matrix. Absorption spectra of sample solutions in the UV–vis region were recorded with a Shimadzu 2001 UV spectrophotometer using 1 cm path-length cuvettes at room temperature. Electronic absorption spectra of films deposited on glass and KBr substrates were recorded with a UV–vis–NIR scanning spectrophotometer (Shimadzu, UV-VIS-3101PC) in the range from 400 to 900 nm. Thermogravimetric analyses were carried out on a Mettler Toledo Star^e Thermal Analysis System at a rate of 10 °C min^{-1} in a nitrogen flow (50 mL min^{-1}). Transition temperatures were determined using a Mettler Toledo Star Thermal Analysis System/DSC 822 differential scanning calorimeter (DSC) system at the scan rate of 10 °C min^{-1}. DSC was calibrated with 3–4 mg indium samples under nitrogen atmosphere. Optical textures were observed with the POM Biomed MMR-3. X-ray diffraction measurements were performed using automatic diffractometer DRON-3M (R = 192 mm, CuKα-irradiation, Ni-filter, scintillation detector with amplitude discrimination, Soller slits with aperture of 2.5° on primary and reflected beams) in the region of 2θ from 5° to 60° with the scanning step of 0.03°. All measurements were carried out under ambient conditions.

2.3. Film preparation and characterization

Small volume (3–4 μL) of solutions of the CuPcR$_8$ derivatives in chloroform (10 mg/mL) was dispensed via a glass pipette onto

Table 1
Initial decomposition and main decomposition temperatures of $CuPcR_8$ complexes.

Compound	Initial decomposition temperature (°C)	Main decomposition temperature (°C)
3a	300	420
3b	300	424
3c	300	406
4a	330	378
4b	330	384
4c	285	337

an ultrasonically cleaned substrate held onto photoresist spinner (Microsystem model 4000). The speed of substrate rotation was 2000 rpm. Spinning was continued for 30 s during which time the solvent had evaporated to generate a film of the phthalocyanine derivative. The films were then heated to a temperature 10–20 °C above the isotropic transition temperature or to the maximal possible temperature lower than temperature of decomposition (Table 1) and then slowly cooled down to room temperature at the rate of 10 °C min^{-1} for comparison with as-deposited layers. Glass slides, gold-coated slides and KBr plates were used as substrates. For conductivity measurements interdigitated electrodes were used as substrates.

The thickness of the films deposited on one substrate was measured by ellipsometry. Spectroscopic ellipsometric measurements were performed on films deposited on silicon substrates using a Woolam M-2000V™ rotating analyzer spectroscopic ellipsometer in the spectral range of 400–800 nm. Raman spectra were recorded with a Triplemate, SPEX spectrometer equipped with CCD detector in back-scattering geometry. The 488 nm, 20 mW line of an Ar-laser was used for the spectral excitation.

2.4. Synthesis

2.4.1. 2,3,9,10,16,17,23,24-Octakis(octyloxy)phthalocyaninato copper(II) (3a)

4,5-Bis(octyloxy)phthalonitrile (**1a**) (0.50 g, 1.30 mmol), anhydrous $CuCl_2$ (0.088 g, 0.65 mmol), anhydrous *n*-hexanol (3 mL) and DBU (0.10 mL, 0.65 mmol) were stirred at reflux temperature during 24 h under argon atmosphere. The reaction mixture was then cooled and poured into acetone. The resulting precipitates were filtered and washed with ethanol. The green product was purified by column chromatography on silica gel using dichloromethane as eluent [25]. Yield: 0.090 g (17%). IR [(KBr) υ_{max}/cm^{-1}]: 3079 (Ar—CH), 2920–2851 (CH_2), 1607 (C=N), 1505 (Ar—C=C), 1458, 1418, 1384 (deformation C—H), 1276, 1202 (C—O—C), 1101, 1069, 853. UV-vis (THF): λ_{max} nm (log ε): 343 (4.54), 608 (4.23), 673 (5.01). MALDI-TOF-MS *m/z*: Calcd. for $C_{96}H_{144}CuN_8O_8$: 1601.77, Found 1601.76 $[M]^+$.

2.4.2. 2,3,9,10,16,17,23,24-Octakis(hexadecyloxy)phthalocyaninato copper(II) (3b)

3b was prepared by the same procedure as described for **3a** by starting with 4,5-bis(hexadecyloxy)phthalonitrile (**1b**) (0.50 g, 0.82 mmol), anhydrous $CuCl_2$ (0.055 g, 0.41 mmol), anhydrous *n*-hexanol (3 mL) and DBU (0.07 mL, 0.45 mmol). The green product was purified by column chromatography on silica gel using hexane:dichloromethane (1:10) as eluent [25]. Yield: 0.110 g (21%). IR [(KBr) υ_{max}/cm^{-1}]: 3065 (Ar—CH), 2918–2850 (CH_2), 1608 (C=N), 1505 (Ar—C=C), 1463, 1386 (deformation C—H), 1272, 1203 (C—O—C), 1073, 875. UV-vis (THF): λ_{max} nm (log ε): 343 (4.67), 606 (4.28), 673 (5.02). MALDI-TOF-MS *m/z*: Calcd. for $C_{160}H_{272}CuN_8O_8$: 2499.55, Found 2499.15 $[M]^+$.

2.4.3. 2,3,9,10,16,17,23,24-Octakis-[2-(2-(2-methoxyethoxy)ethoxy)ethoxy]phthalocyaninato copper(II) (3c)

3c was prepared by the same procedure as described for **3a** by starting with 4,5-bis(1,4,7,10-tetraoxaundecanyl)phthalonitrile (**1c**) (0.50 g, 1.00 mmol), anhydrous $CuCl_2$ (0.07 g, 0.50 mmol), anhydrous *n*-hexanol (3 mL) and DBU (0.07 mL, 0.45 mmol). The oily green product was purified by column chromatography on neutral Al_2O_3 using dichloromethane as eluent [26]. Yield: 0.325 g (60%). IR [(KBr) υ_{max}/cm^{-1}]: 3080 (Ar—CH), 2920–2872 (CH_2), 1608 (C=N), 1508 (Ar—C=C), 1460, 1412, 1352 (deformation C—H), 1280, 1200 (C—O—C), 1096, 1064. UV-vis (THF): λ_{max} nm (log ε): 343 (4.64), 610 (4.49), 673 (4.93). MALDI-TOF-MS *m/z*: Calcd. for $C_{88}H_{128}CuN_8O_{32}$: 1873.58, Found 1873.18 $[M]^+$.

2.4.4. 2,3,9,10,16,17,23,24-Octakis(octylthio)phthalocyaninato copper(II) (4a)

4a was prepared and purified by the same procedure as described for **3a** by starting with 4,5-bis(octylthio)phthalonitrile (**2a**) (0.50 g, 1.20 mmol), anhydrous $CuCl_2$ (0.081 g, 0.60 mmol), anhydrous *n*-hexanol (3 mL) and DBU (0.09 mL, 0.60 mmol) [27]. Yield: 0.300 g (58%). IR [(KBr) υ_{max}/cm^{-1}]: 3068 (Ar—CH), 2952–2850 (CH_2), 1595 (C=N), 1504 (Ar—C=C), 1468, 1408, 1376 (deformation C—H), 1088 (C—S—C), 956. UV-vis (THF): λ_{max} nm (log ε): 326 (4.63), 634 (4.39), 704 (5.03). MALDI-TOF-MS *m/z*: Calcd. for $C_{96}H_{144}CuN_8S_8$: 1730.33, Found 1730.84 $[M]^+$.

2.4.5. 2,3,9,10,16,17,23,24-Octakis(hexadecylthio)phthalocyaninato copper(II) (4b)

4b was prepared by the same procedure as described for **3a** by starting with 4,5-bis(hexadecylthio)phthalonitrile (**2b**) (0.50 g, 0.78 mmol), anhydrous $CuCl_2$ (0.053 g, 0.39 mmol), anhydrous *n*-hexanol (3 mL) and DBU (0.06 mL, 0.40 mmol). The green product was purified by column chromatography on silica gel using hexane:dichloromethane (1:10) as eluent [28]. Yield: 0.120 g (23%). IR [(KBr) υ_{max}/cm^{-1}]: 3044 (Ar—CH), 2917–2849 (CH_2), 1595 (C=N), 1504 (Ar—C=C), 1468, 1412, 1377 (deformation C—H), 1088 (C—S—C), 956. UV-vis (THF): λ_{max} nm (log ε): 326 (4.65), 634 (4.41), 704 (5.04). MALDI-TOF-MS *m/z*: Calcd. for $C_{160}H_{272}CuN_8S_8$: 2628.06, Found 2627.94 $[M]^+$.

2.4.6. 2,3,9,10,16,17,23,24-Octakis-[2-(2-(2-methoxyethoxy)ethoxy)ethylthio]phthalocyaninato copper(II) (4c)

4c was prepared by the same procedure as described for **3a** by starting with 4,5-bis(1-tia-4,7,10-trioxaundecanyl)phthalonitrile (**2c**) (0.70 g, 1.40 mmol), anhydrous $CuCl_2$ (0.09 g, 0.70 mmol), anhydrous *n*-hexanol (3 mL) and DBU (0.1 mL, 0.70 mmol). The oily green product was purified by column chromatography on neutral Al_2O_3 using dichloromethane as eluent. Yield: 0.364 g (52%). IR [(KBr) υ_{max}/cm^{-1}]: 3067 (Ar—CH), 2915–2871 (CH_2), 1602 (C=N), 1505 (Ar—C=C), 1450, 1391 (deformation C—H), 1308, 1195, 1085 (C—S—C), 1033. UV-vis (THF): λ_{max} nm (log ε): 324 (4.59), 634 (4.59), 704 (4.93). MALDI-TOF-MS *m/z*: Calcd. for $C_{88}H_{128}CuN_8O_{24}S_8$: 2002.10, Found 2001.95 $[M]^+$.

3. Results and discussion

3.1. Synthesis and characterization

The synthetic route of $CuPcR_8$ complexes is shown in Fig. 1. 4,5-Bis(octyloxy)phthalonitrile (**1a**), 4,5-bis(hexadecyloxy)phthalonitrile (**1b**) and 4,5-bis(1,4,7,10-tetraoxaundecanyl)phthalonitrile (**1c**) were synthesized via nucleophilic substitution of 4,5-dihydroxyphthalonitrile with

Table 2
Temperatures of phase transitions of $CuPcR_8$ complexes.

Compound	Temperature of phase transition (°C)
3a	$C \underset{45}{\overset{100(123^{[25]})}{\rightleftarrows}} Col_h \overset{300(300^{[25]})}{\longrightarrow}$ dec
3b	$C_1 \underset{41}{\overset{50}{\rightleftarrows}} C_2 \underset{102}{\overset{117(93^{[25]})}{\rightleftarrows}} Col_h \underset{260}{\overset{270(300^{[25]})}{\longrightarrow}}$ dec.
3c	$C \underset{10}{\overset{50(62^{[26]})}{\rightleftarrows}} Col_h \overset{290(260^{[26]})}{\longrightarrow}$ dec.
4a	$C \underset{-15}{\overset{77(77^{[28]})}{\rightleftarrows}} Col_h \overset{300(350^{[28]})}{\longrightarrow}$ dec.
4b	$C \underset{-18}{\overset{-34}{\rightleftarrows}} C_2 \underset{31}{\overset{43(26^{[28]})}{\rightleftarrows}} Col_h \underset{270}{\overset{274(263^{[28]})}{\rightleftarrows}} IL$
4c	$C \underset{-}{\rightleftarrows} Col_h \underset{285}{\overset{(285^{[29]})}{\rightleftarrows}} IL$

C: crystal; Col_h: columnar hexagonal; dec.: decomposition; IL: isotropic liquid.

corresponding alkyl bromides in the presence of K_2CO_3 in anhydrous DMF. 4,5-Bis(octylthio)phthalonitrile (**2a**), ,5-bis(hexadecylthio)phthalonitrile (**2b**) and 4,5-bis(1-tia-,7,10-trioxaundecanyl)phthalonitrile (**2c**) were synthesized via ucleophilic substitution of 4,5-dichlorophthalonitrile with cor-esponding alkyl thiols in the presence of K_2CO_3 in anhydrous MF. The synthesis of Cu(II) phthalocyanine complexes (**3a–c** and **a–c**) were attempted by treatment of corresponding substituted hthalonitriles with anhydrous $CuCl_2$ in the presence of DBU as ase in freshly distilled *n*-hexanol. All synthesized complexes ere identified by MALDI-TOF mass spectroscopy using 2,5-ihydroxybenzoic acid as matrix (Supporting Information), FT-IR nd UV–vis spectroscopy.

.2. Mesogenic properties of the $CuPcR_8$ complexes

$CuPcR_8$ derivatives were chosen for this research because they xhibit a hexagonal columnar (Col_h) structure over a wide tempera-ure range. The thermal stability of the $CuPcR_8$ complexes has been vestigated by thermal gravimetric analysis (TGA). Initial decom-osition and main decomposition temperatures of Pcs are given in able 1. It is obvious that alkyloxy substituted derivatives are more table than alkylthio substituted Pc at high temperatures. The tem-eratures of phase transitions of $CuPcR_8$ complexes are presented Table 2. Investigation of liquid crystalline properties of some $uPcR_8$ has already been described in the literature [25,26,28]. The rresponding phase transition temperatures reported in the liter-ure are given in parentheses in Table 2. The phase transitions of me compounds were measured only during heating cycle in pre-ous papers [25,26,28]. The clearing and melting points for liquid ystalline compounds measured during heating stage can differ om those measured during cooling stage. The phase transition mperatures measured during cooling stage are more important r the preparation of ordered films, therefore they were also mea-red during cooling stage for $CuPcR_8$ derivatives in this work able 2).

It was reported in the corresponding literature that **3c** shows phase transition at 62 °C, before its melting at 260 °C, which is companied by decomposition. It was also reported that, a crys-lline state has been observed at room temperature [26]. However, is compound was heated to melting point and cooled down to om temperature and six Bragg reflections were observed at 25 °C om XRD in this study (see Supporting Information). Additionally, a uid crystal–crystal transition was observed at 10 °C in DSC mea-rements during the cooling confirming that **3c** is liquid crystal ove 10 °C (see Supporting Information).

3.3. Films characterization

It was shown earlier that the spin-coating method provides a simple and convenient procedure for formulating ordered films of the phthalocyanines which can be heated to form thin liquid-crystalline films [37–39]. The electronic absorption spectra of the films of $CuPcR_8$ before and after heating are presented in Fig. 2. The Q-band structure is more complex than that observed in the solution phase where non-aggregated phthalocyanines give rise to a single main band assigned to the doubly degenerate transition a_{1u}–e_g. In the optical spectra of $CuPcR_8$ films the main absorption bands are broadened through exciton coupling effects which also lead to shifts in the band positions. These are dependent upon molecular packing [40].

Splitting of Q-band in the spectra of the films of **3a**, **3b**, **3c** and **4a** before heating indicate the herring-bone arrangement of phthalocyanine molecules which is typical for many crystalline phthalocyanines [41]. Films give rise to both a red- and a blue-shifted band consistent with exciton splitting arising from the presence of translationally non-equivalent molecules in the 'unit cell', as in a herringbone arrangement of molecules within adjacent columns. After heating the spectra of films **3a** and **3b** change, however the Q-band splitting does not disappear confirming the persistence of herring-bone arrangement.

The spectra of the films of **3c** and **4a** after heating are blue shifted relative to the spectra of the monomers. From these spectral changes it can be deduced that on passing from crystal to mesophase, changes into parallel (face-to-face) dimer stacking are observed. This type of re-organization is analogous to that undergone by the octaalkyl analogues upon transition from the crystal phase to the hexagonal discotic mesophase [42–44].

The Q-bands in the spectra of **4b** and **4c** films are blue-shifted both before and after thermal treatment. The **3c**, **4a**, **4b** and **4c** derivatives are liquid crystalline at room temperature (Table 2).

The X-ray diffraction data obtained for the films before and after thermal treatment are presented in Fig. 3. The X-ray patterns of **3a** film before thermal treatment (Fig. 3) contain two peaks related to the layer spacings of 23.9 Å and 20.6 Å, while only one peak related to the spacing of 24.5 Å is observed after thermal treatment. The as-deposited films of **3b**, **3c** and **4c** were amorphous while the films after thermal treatment reveal the reflections from layer spacings of 30.9, 24.6 and 22.1 Å in the X-ray pattern, respectively. Therefore the main tendency to form more ordered films after thermal treatments is observed for all investigated films.

The polarized optical microscope images of the **3c**, **4a**, **4b** and **4c** films deposited on glass slide were obtained in parallel and crossed polarizers (Fig. 4). The typical birefringent texture between crossed polarizers is the signature of planar alignment with the random distribution of columnar axes orientation. Between parallel polarizers, digitated star-like structures were observed, which are typical of Col_h phases [45]. The polarized optical microscope images of the **3a** and **3b**, crystalline films do not exhibit any specific texture.

The Raman spectroscopy was used to study the preferential orientation of molecules relative to the substrate surface. The principles of polarized Raman spectroscopy for investigation of the molecular film orientation were described in details in earlier publications [43,44]. This method allows estimating the angles of molecule inclination relative to the substrate surface. In terms of the phthalocyanine molecule, the designation of its molecular axes is presented in Fig. 5, where the molecular *z*-axis coincides with the main axis of rotation (C_4). Rotating the $CuPcR_8$ molecule around *x*- and *y*-axis with the angle α and β, respectively, the resulting molecular orientation exhibits an inclination angle of the molecule plane with respect to the substrate plane (Fig. 5). By averaging the Raman tensor components obtained by rotation around *x*, *y* and *z* axes, the dependence of the I_{ii}/I_{ij} ratio for each symmetry

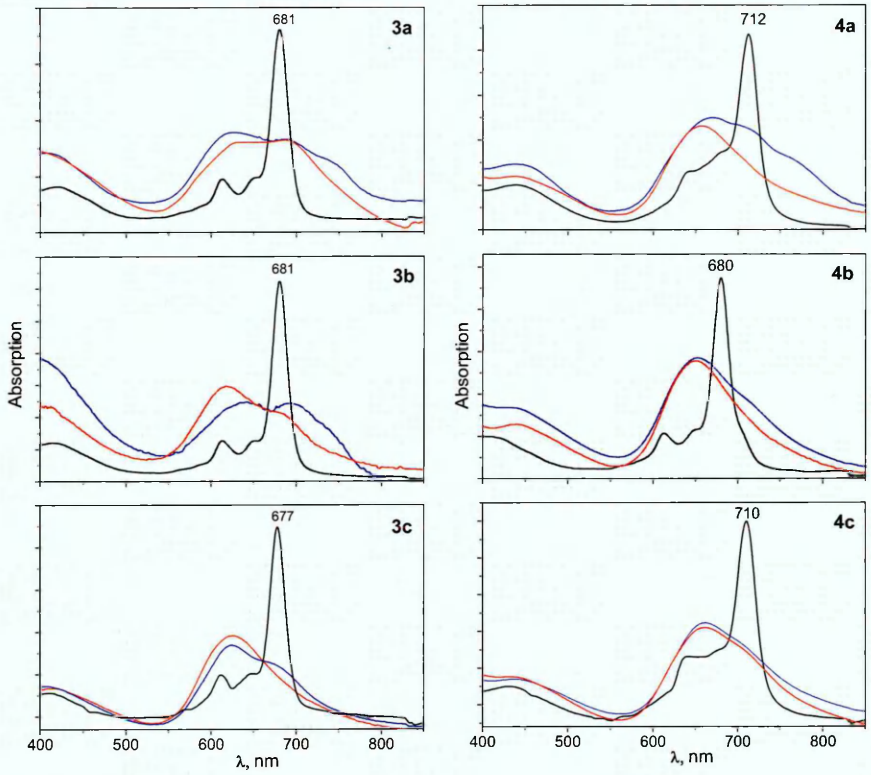

Fig. 2. Electronic absorption spectra of **3a**, **3b**, **3c**, **4a**, **4b** and **4c** solutions in chloroform (black lines); as-deposited films on glass (blue lines); films after heating (red lines). (For interpretation of the references to color in this figure legend, the reader is referred to the web version of the article.)

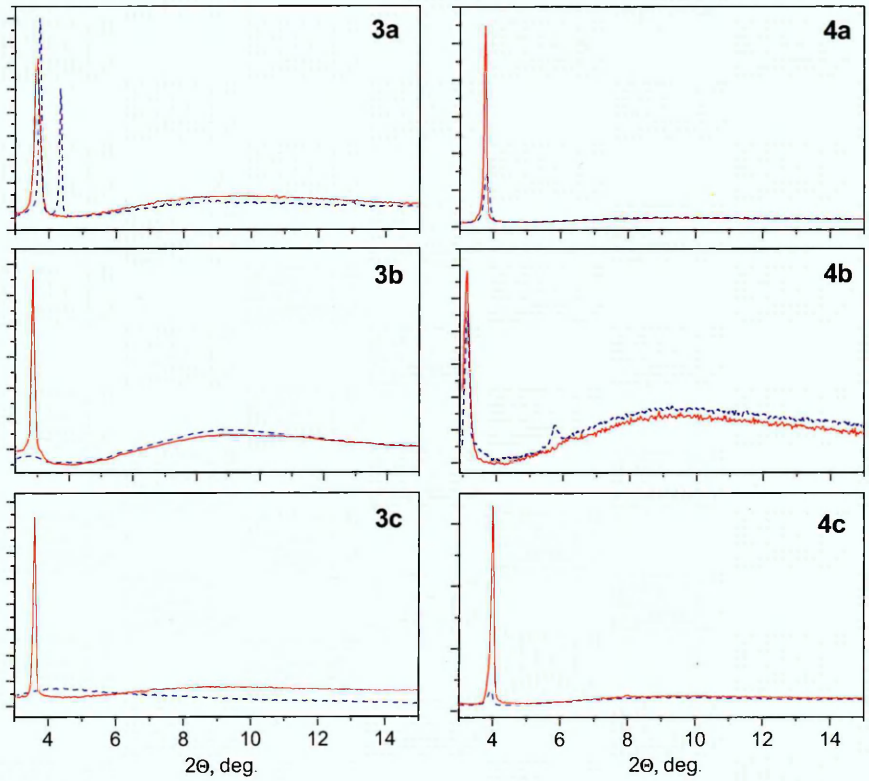

Fig. 3. X-ray diffraction data for the films of **3a**, **3b**, **3c**, **4a**, **4b** and **4c** as-deposited films on glass slides (dashed lines) at room temperature; films after thermal treatment (solid lines).

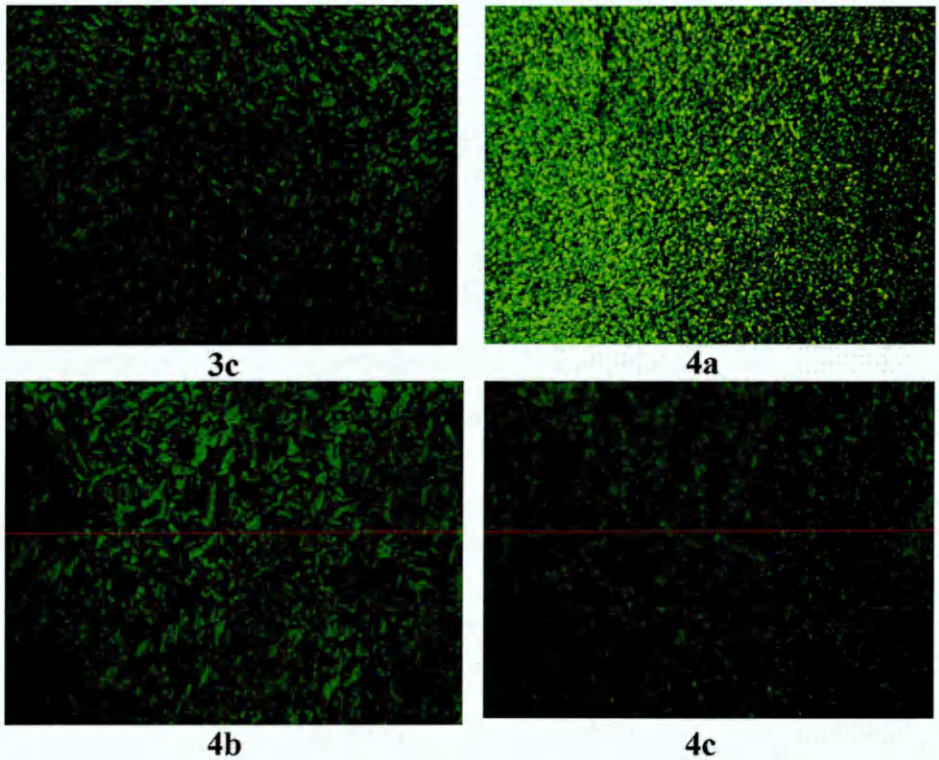

Fig. 4. Optical texture of the films of **3c**, **4a**, **4b** and **4c** at room temperature after thermal treatment. Magnification 40×.

pe of vibrations on the angle α and β (i.e. molecular orientation) ay be deduced. Thereby, regarding the rotation around the z-axis, n averaging in the range from 0 to $\pi/2$ has to be carried out. The xpressions for I_{ii} or I_{ij} have the following overall form:

$$_{ii} = \frac{2}{\pi} \cdot \int_0^{\pi/2} f_{ii}^2(\alpha, \beta, \gamma)\, d\gamma \quad (1)$$

$$_{ij} = \frac{2}{\pi} \cdot \int_0^{\pi/2} f_{ij}^2(\alpha, \beta, \gamma)\, d\gamma \quad (2)$$

where $f_{ii}(\alpha, \beta, \gamma)$ and $f_{ij}(\alpha, \beta, \gamma)$ denote the Raman tensor components (ii) and (ij) of a specific Raman mode obtained by their rotation around x, y and z axes on α, β and γ, respectively. Knowing the experimental ratios of intensities I_{ii}/I_{ij} for A_{1g}, B_{1g} and B_{2g} modes and using Eqs. (1) and (2), the α and β angles may be derived.

The symmetry types of the most intensive bands used for the determination of film orientation are indicated in Fig. 6. The bands assignment was carried out on the basis of comparison with similar phthalocyanine molecules [46].

The polarized Raman spectra of **3a** and **4b** films deposited on glass substrates are shown in Fig. 7 (for **3a** and **4b**) as examples.

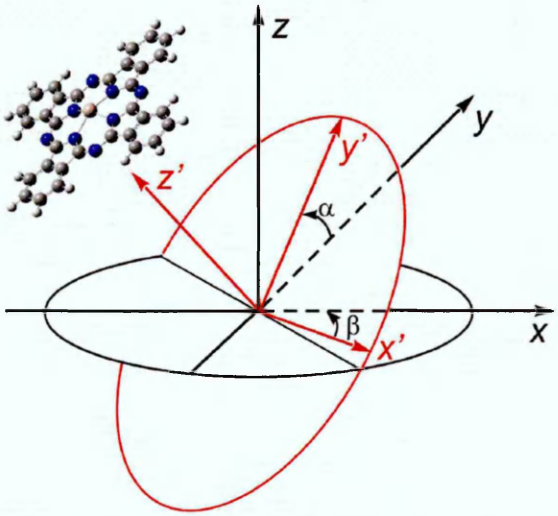

g. 5. Designation of molecular axes of $CuPcR_8$ molecule and scheme of its sug-sted orientation with respect to the substrate surface.

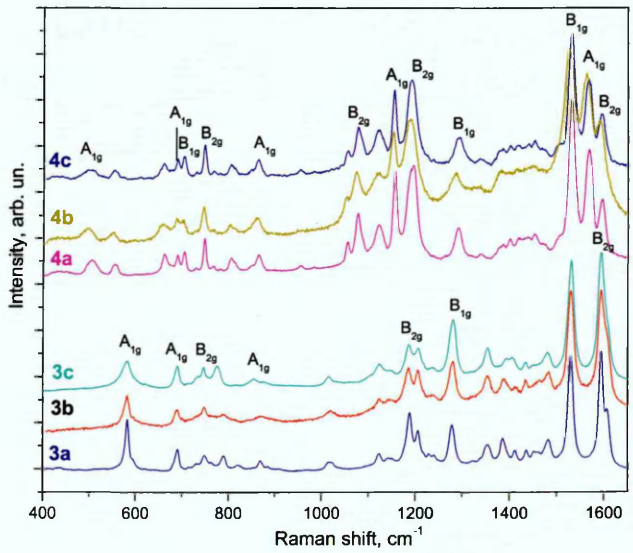

Fig. 6. Raman spectra of **3a**, **3b**, **3c**, **4a**, **4b** and **4c** derivatives.

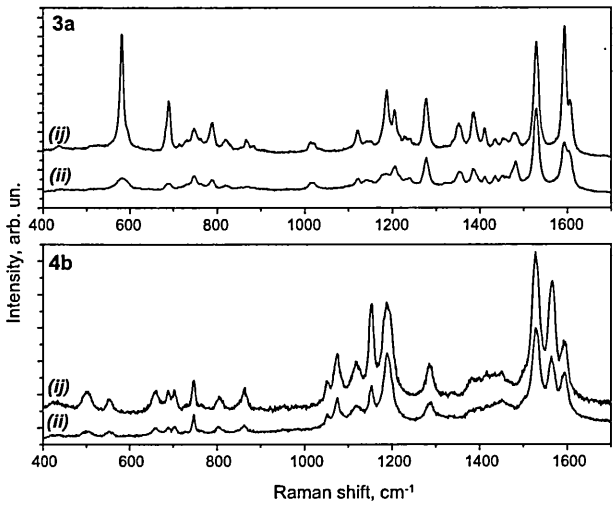

Fig. 7. Polarized Raman spectra of **3a** and **4b** films after heating in parallel (*ii*) and cross (*ij*) polarizations of incident and scattered light.

The average values of I_{ii}/I_{ij} ratios for each symmetry type of vibrations in the polarized spectra of the films of all $CuPcR_8$ derivatives are listed in Table 3. The α angle is 42–45° for the films of **3a** and **3b** derivatives deposited on the surface of glass slides. The molecules in the film have the same inclination angles but they are azimuthally disordered. As was shown above these compounds are crystalline at room temperature. Similar angle (~48°) between molecular plane and normal to the substrate was estimated by Wang and co-author [47] in the films of $CuPcR_8$ ($R = -OC_8H_{17}$). A herringbone arrangement of molecules within adjacent columns is observed for both unsubstituted and substituted phthalocyanines [47–50]. Interestingly, this type of arrangement is also observed for the horizontally lifted LB films of the peripherally substituted octaalkyl phthalocyanines [51,52].

The inclination angle α of molecules in the films of the other four derivatives (**3c**, **4a**, **4b**, **4c**) deposited on the surface of glass slides was calculated to be 85–90°. According to DSC data, these phthalocyanines are liquid crystalline at room temperature.

The formation of the films of **3c**, **4a**, **4b**, **4c** derivatives with planar alignment is due to the ability of discotic mesogens to self-assemble in columnar superstructures. It is known that discotic molecules can adopt two characteristic orientations (planar and homeotropic) of columnar superstructures on surfaces, which are required for electronic devices with different geometries [14]. In the films with planar (homogeneous) alignment the edge-on orientation of the discotic molecules and columns parallel to the substrate surface is observed [53,54]. These results are in a good agreement with the data of polarized microscopy exhibiting typical birefringent texture between crossed polarizers which is typical for planar alignment with the random distribution of columnar axes orientation. It has been shown that planar alignment can be obtained for the films of different discotic mesogens deposited on the surface of slides with an air interface [55]. The planar alignment with a random distribution of the columnar director in the plane parallel to the air interface has been observed for films of two tetra-substituted nickel phthalocyanines ($NiPcR_4$, $R = -OCH(CH_2OC_{12}H_{25})_2$ and $R = -SCH(CH_2(OCH_2CH_2)_2OC_2H_5)_2$) deposited on KBr, Si and quartz surfaces [39].

Table 3
Measured I_{ii}/I_{ij} ratios for A_{1g}, B_{1g} and B_{2g} modes in the Raman spectra of the annealed $CuPcR_8$ films and calculated angles of molecule inclination.

Compound	I_{ii}/I_{ij} ratios for A_{1g}, B_{1g} and B_{2g} modes			Angle (°)	
	A_{1g}	B_{1g}	B_{2g}	α	β
3a	11	1.3	2.8	42	45
3b	10	1.5	2.9	45	45
3c	3.4	3.4	1.2	90	5
4a	3.5	3.4	1.2	90	5
4b	3.7	3.6	1.4	85	8
4c	3.6	3.5	1.3	85	6

Table 4
Film thickness and calculated conductivity of $CuPcR_8$ films.

Compound	Thickness (nm)	$\sigma_{//}$ (Ω^{-1} m^{-1})
3a	198	5.1×10^{-9}
3b	150	2.6×10^{-8}
3c	139	4.2×10^{-8}
4a	120	6.7×10^{-8}
4b	116	5.0×10^{-8}
4c	156	2.0×10^{-7}

For spin-coated films of octasubstituted phthalocyanines there is a contest between π–π attractive interaction and steric effect which results in different types of molecular arrangements depending on the electronic influence of side chains on the phthalocyanines core [41]. For **3a** and **3b**, alkoxysubstituted phthalocyanines containing the smaller size of the oxygen atom which is bridging the Pc macrocycle to the alkyl chain, there is a steric obstruction to the side-chains resting in the same plane as the aromatic ring in comparison with alkylthiosubstituted phthalocyanines. This leads to a higher phase transition temperature of **3a** and **3b** to the mesophase and formation of crystalline phases at room temperature with a herringbone arrangement which is believed to maximize the attractive interactions between Pc cores (H-bonding and π–π interaction) [41,56].

The current–voltage (*I–V*) characteristics of $CuPcR_8$ films were measured in the direction parallel to the films plane using interdigitated electrode structures. Film thicknesses were determined by spectroscopic ellipsometry and were used in the calculation of conductivities of $CuPcR_8$ complexes; the results are summarized in Table 4. The lateral conductivity tends to decrease slightly with the increase of chain length (films **3a** and **3b**; **4a** and **4b**). A similar behavior was observed by Nakahara and co-workers for in-plane conductivity as a result of increasing chain length in phthalocyanine molecules [57]. The observed decrease in conductivity with increasing length of the alkyl chain was related to an increase in the hopping distance between localized sites [58]. The conductivity of alkylthio-substituted (**4a–4c**) phthalocyanines is higher than that of alkyloxy-substituted derivatives (**3a–3c**). The Q-bands of alkylthio-substituted phthalocyanines are red-shifted, compared with the Q-bands of alkyl- and/or alkyloxy-substituted phthalocyanines. The red-shift means that the energy gap between the HOMO and LUMO narrows on changing from alkyl or alkyloxy groups to alkylthio groups [28]. This was found to result in an increased electroconductivity, as was previously reported by van de Craats and his co-workers for alkylthio-substituted phthalocyanines, both for the metal free and copper complexes [59]. Furthermore, it was suggested that the larger size of the sulphur atom which is bridging the Pc macrocycle to the alkyl chain is the cause for hindering the structural disorder in the molecular stacks during the melting of the hydrocarbon chain when transition from crystalline to hexagonal mesophase (D_h) takes place [60]. This was found to enhance the electron mobility of charge carriers between stacks by one order of magnitude and thus leading to higher conductivity as compared to the alkyloxy-substituted derivatives.

4. Conclusions

In this work, the synthesis of octa-substituted copper(II) phthalocyanines containing alkylthio-, alkyloxy-, (trioxyethylene)thio- and (trioxyethylene)oxy-substituents in

peripheral positions has been described. The CuPcs were characterized using UV–vis and FT-IR spectroscopies, as well as mass spectrometry. The phase transition temperatures of the complexes have been determined by the POM and DSC experimental techniques. The formation of the columnar-hexagonal (Col_h) mesophase over a wide temperature range has been confirmed using a range of methods. The temperature of phase transitions depends on the type of substituents.

Thermally induced molecular reorganization within spun CuPc films was studied by visible absorption spectroscopy and XRD. The polarized Raman spectroscopy was used to study the preferential orientation of molecules relative to the substrate surface. It was shown that the type of substituent in the phthalocyanine molecule has a significant effect on the films' orientation and electrical properties. The inclination angles α of molecules in the films of $CuPcR_8$ (**3a** and **3b**) with alkyloxy-substituents ($-OC_8H_{17}$ and $-OC_{16}H_{33}$) were about 45°. These compounds are crystalline at room temperature. The inclination angles in the films of the other four derivatives (**3c**, **4a**, **4b**, **4c**) deposited on the surface of glass slides were found to be 85–90°. According to obtained DSC data, these phthalocyanines are liquid crystalline at room temperature. The higher conductivity values were found for the films of phthalocyanines with the molecules oriented perpendicular to the substrate surface. The lateral conductivity tends to decrease slightly with the increasing of chain length, and the higher conductivity in the alkylthio-derivatives is thought to be caused by the reduced structural disorder during phase transition which is caused by the presence of sulphur atoms.

cknowledgements

This work was supported by bilateral project between The Scintific and Technological Research Council of Turkey (TUBITAK, roject number: 108M384) and the Russian Foundation of Basic esearch (RFBR, Project numbers: 09-03-91219 and 12-03-91372).

ppendix A. Supplementary data

Supplementary data associated with this article can be found, in he online version, at doi:10.1016/j.synthmet.2012.02.006.

eferences

[1] N.B. McKeown, Phthalocyanine Materials: Synthesis, Structure, Function, Cambridge Univ. Press, Cambridge, 1998.
[2] J. Simon, P. Bassoul, Design of Molecular Materials: Supramolecular Engineering, Wiley-VCH, Weinheim, Germany, 2000.
[3] S. Ambily, F.P. Xavier, C.S. Menon, Mater. Lett. 41 (1999) 5–8.
[4] F. Yuksel, M. Durmuş, V. Ahsen, Dyes Pigments 90 (2011) 191–200.
[5] J.A. Jiménez Tejada, K.M. Awawdeh, J.A. López Villanueva, J.E. Carceller, M.J. Deen, N.B. Chaure, T. Basova, A.K. Ray, Org. Electron. 12 (2011) 832–842.
[6] H. Donker, A. van Hoek, W. van Schaik, R.B.M. Koehorst, M.M. Yatskou, T.J. Schaafsma, J. Phys. Chem. B 109 (2005) 17038–17046.
[7] E.I. Yslas, L.N. Milla, S. Romanini, E.N. Durantini, M. Bertuzzi, V.A. Rivarola, Exp. Ther. Med. 1 (2010) 713–718.
8] A. Varotto, C-Y. Nam, I. Radivojevic, J.P.C. Tome, J.A.S. Cavaleiro, C.T. Black, C.M. Drain, J. Am. Chem. Soc. 132 (2010) 2552–2554.
9] W.M. Li, A.P. Yu, D.C. Higgins, J. Am. Chem. Soc. 132 (2010) 17056–17058.
0] M. Passard, C. Maleysson, A. Pauly, S. Dogo, J.-P. Germain, J.-P. Blanc, Sens. Actuators B 18–19 (1994) 489–492.
1] K. Ohta, L. Jacquemin, C. Sirlin, L. Bosio, J. Simon, New J. Chem. 12 (1988) 751–754.
[12] M.K. Engel, P. Bassoul, L. Bosio, H. Lehmann, M. Hanack, J. Simon, Liq. Cryst. 15 (1993) 709–722.
[13] J.F. van der Pol, E. Neeleman, J.W. Zwikker, R.J.M. Nolte, W. Drenth, J. Aerts, R. Visser, S.J. Picken, Liq. Cryst. 6 (1989) 577–592.
[14] A.M. van de Craats, J.M. Warman, M.P. de Haas, Adv. Mater. 8 (1996) 823–826.
[15] N. Boden, R.J. Bushby, J. Clements, B. Movaghar, Phys. Rev. B 52 (1995) 13724–13780.
[16] J. Piris, M.G. Debije, N. Stuzmann, et al., Adv. Mater. 15 (2003) 1736–1740.
[17] R.E. Hughes, S.P. Hart, D.A. Smith, et al., J. Phys. Chem. B 106 (2002) 6638–6645.
[18] W. Pisula, Z. Tomovic, B. El Hamaoui, et al., Chem. Mater. 17 (2005) 4296–4303.
[19] K. Hatsusaka, M. Kimura, K. Otha, Bull. Chem. Soc. Jpn. 76 (2003) 781–787.
[20] H. Lino, J.I. Hanna, R.J. Bushby, et al., J. Appl. Phys. Lett. 87 (2005), 132102-1–132102-3.
[21] N. Terasawa, H. Monobe, K. Kiyohara, Y. Shimizu, Chem. Commun. 14 (2003) 1678–1679.
[22] J.C. Gêminard, P. Oswald, J. Phys. II 4 (1994) 959–974.
[23] S.K. Prasad, D.S. Shankar Rao, S. Chandrasekhar, S. Kumar, Mol. Cryst. Liq. Cryst. 396 (2003) 121–139.
[24] K. Ohta, T. Watanabe, S. Tanaka, et al., Liq. Cryst. 10 (1991) 357–368.
[25] J. Sleven, T. Cardinaels, C. Görller-Walrand, K. Binnemans, ARKIVOC (2003) 68–82.
[26] T. Toupance, P. Bassoul, L. Mineau, J. Simon, J. Phys. Chem. 100 (1996) 11704–11710.
[27] H. Eichhorn, D. Wöhrle, D. Pressner, Liq. Cryst. 22 (1997) 643–653.
[28] K. Ban, K. Nishizawa, K. Ohta, H. Shirai, J. Mater. Chem. 10 (2000) 1083–1090.
[29] B. Cabezon, E. Quesada, S. Esperanza, T. Torres, Eur. J. Org. Chem. (2000) 2767–2775.
[30] D. Wöhrle, M. Eskes, K. Shigehara, A. Yamada, Synthesis 2 (1993) 194–196.
[31] B. Del Rey, U. Keller, T. Torres, G. Rojo, F. Agullo-Lopez, S. Nonell, C. Marti, S. Brasselet, I. Ledoux, J. Zyss, J. Am. Chem. Soc. 120 (1998) 12808–12817.
[32] B. Del'Rey, M.V. Martinez-Diaz, J. Barbera, T. Torres, J. Porphyrins Phthalocyanines 4 (2000) 569–573.
[33] S. Dabak, V. Ahsen, F. Heinemann, P. Zugenmaier, Mol. Cryst. Liq. Cryst. 348 (2000) 111–127.
[34] J. Sleven, C. Gorller-Walrand, K. Binnemans, Mater. Sci. Eng. C, Biomim. Supramol. Syst. C18 (2001) 229–238.
[35] T. Toupance, V. Ahsen, J. Simon, J. Am. Chem. Soc. 116 (1994) 5352–5361.
[36] D.D. Perrin, W.L.F. Armarego, Purification of Laboratory Chemicals, 2nd ed., Pergamon Press, Oxford, 1989.
[37] M.J. Cook, D.A. Mayes, R.H. Poynter, J. Mater. Chem. 5 (1995) 2233–2238.
[38] T. Basova, E. Kol'tsov, A.G. Gürek, D. Atilla, V. Ahsen, A.K. Hassan, Mater. Sci. Eng. C 28 (2008) 303–308.
[39] T.V. Basova, M. Durmuş, A.G. Gürek, V. Ahsen, A. Hassan, J. Phys. Chem. C 113 (2009) 19251–19257.
[40] M.J. Cook, in: R.J.H. Clark, R.E. Hester (Eds.), Spectroscopy of New Materials, Wiley, Chichester, 1993, pp. 87–88.
[41] B.M. Hassan, H. Li, Neil B. McKeown, J. Mater. Chem. 10 (2000) 39–45.
[42] K. Hatsusaka, K. Ohta, I. Yamamoto, H. Shirai, J. Mater. Chem. 11 (2001) 423–433.
[43] T.V. Basova, B.A. Kolesov, A.G. Gürek, V. Ahsen, Thin Solid Films 385 (2001) 246–251.
[44] T. Basova, A.G. Gürek, V. Ahsen, Mater. Sci. Eng. C 22 (2002) 99–104.
[45] I. Dierking, Texture of Liquid Crystal, Wiley-VCH, Weinheim, Germany, 2003.
[46] T.V. Basova, V.G. Kiselev, B-E. Schuster, H. Peisert, T. Chasse, J. Raman Spectrosc. 40 (2009) 2080–2087.
[47] M. Wang, Y.-L. Yang, K. Deng, C. Wang, Chem. Phys. Lett. 439 (2007) 76–80.
[48] S.M. Critchley, M.R. Willis, M.J. Cook, J. McMurdo, Y. Maruyama, J. Mater. Chem. 2 (1992) 157–159.
[49] M.J. Cook, J. McMurdo, D.A. Miles, R.H. Poynter, J.M. Simmons, S.D. Haslam, R.M. Richardson, K. Welford, J. Mater. Chem. 4 (1994) 1205–1213.
[50] R.H. Poynter, M.J. Cook, M.A. Chesters, D.A. Slater, J. McMurdo, K. Welford, Thin Solid Films 243 (1994) 346–350.
[51] H. Nakahara, K. Fukuda, K. Kitahara, H. Nishi, Thin Solid Films 178 (1989) 361–366.
[52] M.J. Cook, J. Mater. Chem. 6 (1996) 677–689.
[53] S. Sergeyev, W. Pisula, Y.H. Geerts, Chem. Soc. Rev. 36 (2007) 1902–1929.
[54] V. de Cupere, J. Tant, P. Viville, R. Lazzaroni, W. Osikowicz, W. Salaneck, Y.H. Geerts, Langmuir 22 (2006) 7798–7806.
[55] P. Smolenyak, R. Peterson, K. Nebesny, M. Törker, D.F. O'Brien, N.R. Armstrong, J. Am. Chem. Soc. 121 (1999) 8628–8636.
[56] P. Weber, D. Guillon, A. Skoulios, Liq. Cryst. 9 (1991) 369–382.
[57] H. Nakahara, K.Z. Sun, K. Fukuda, N. Azuma, H. Nishi, H. Uchida, T. Katsube, J. Mater. Chem. 5 (1995) 395–399.
[58] D. Atilla, N. Kilinç, F. Yuksel, A. Gürek, Z. Öztürk, V. Ahsen, Synth. Met. 159 (2009) 13–21.
[59] A.M. van de Craats, P.G. Shouten, J.M. Warman, Ekisho 2 (1998) 12–27.
[60] K. Ban, K. Nishizawa, K. Ohta, A.M. van de Craats, J.M. Warman, I. Yamamoto, H. Shirai, J. Mater. Chem. 11 (2001) 321–331.

NJC

View Article Online / Journal Homepage / Table of Contents for this issue
Dynamic Article Links

Cite this: *New J. Chem.*, 2012, **36**, 1665–1672

www.rsc.org/njc

PAPER

Liquid crystalline octasubstituted lead(II) phthalocyanines: effects of alkoxy and alkylthio substituents on film alignment and electrical properties†

Sinem Tuncel,[a] Hikmat A. J. Banimuslem,[b] Mahmut Durmuş,*[a] Ayşe Gül Gürek,[a] Vefa Ahsen,[ac] Tamara V. Basova[d] and Aseel K. Hassan[b]

Received (in Montpellier, France) 29th March 2012, Accepted 30th May 2012
DOI: 10.1039/c2nj40247e

Octasubstituted lead(II) phthalocyanines containing alkylthio- and alkoxy- groups in peripheral positions have been synthesized and characterized using ^{1}H and ^{13}C NMR, UV-Vis, IR and mass spectroscopies as well as elemental analysis. The mesogenic properties of the octasubstituted lead(II) phthalocyanines have been investigated by differential scanning calorimetry, polarizing optical microscopy, and X-ray diffraction. The sandwich structures ITO/PbPc/In were prepared to investigate the $J(V)$ characteristics of thin films of these molecules. The dissimilar behavior of the films before and after heat-treatment is expected to result in changing the alignment inside the columnar stacking of the molecules in the films.

Introduction

With the advent of nanotechnology and the availability of new materials, the fabrication of electronic device, especially field effect transistors, photovoltaic cells and light emitting diodes (LEDs) has gained new momentum in recent years. Discotic liquid crystalline materials have attracted recent attention in these fields due to their molecular alignment. These promising materials may form efficient π–π columnar stacks that produce high charge-carrier mobilities, the magnitude of which is fundamentally determined by the degree of order and π–π molecular orbital overlap within the columnar stacks.[1]

Phthalocyanines (Pcs) are attractive materials since their physical and chemical properties can be improved both by the substituents in the periphery and by the central metal ion in the cavity. Pcs bearing long alkyl, alkoxy and alkylthio substituents are known to exhibit discotic columnar liquid crystalline behavior.[2]

One of the main advantages of mesomorphic phthalocyanines over many other discotic macrocycles is their strong absorption in the visible and NIR regions,[3–5] which makes them good candidates for optoelectronic applications.[6]

Lead is of particular interest among the metal ions which form complexes with Pcs since its diameter (2.4 Å) is larger than the phthalocyanine cavity (1.6 Å). The Pb atom deviates by 0.37–0.40 Å from the plane of the phthalocyanine ring. This non-planar geometry results in a strong electrical dipole moment oriented normally to the plane of the molecule as well as low transition temperatures among the other metallated phthalocyanine derivatives.[7–13]

For unsubstituted phthalocyanines, the electrical switching effect was found for films of PbPc in the monoclinic phase.[14] The switching effect was observed only in films consisting of a mixture of monoclinic grains and the amorphous phase but not in films having a triclinic phase structure. In connection with this, there have been some works that were devoted to structural studies of evaporated PbPc films.[15,16] However, the nature of the switching effect has yet not been clearly understood. Some works have also explored the potential of some octasubstituted lead phthalocyanines as an active material for memory devices.[11,17]

Films of substituted lead phthalocyanines have not been as thoroughly investigated as those of unsubstituted PbPc. Nonperipheral 1,4,8,11,15,18,22,25-octakis(hexylsulfanyl) phthalocyanines have been synthesized and characterised by X-ray crystallography in the work of Cook and co-workers.[18] Furthermore, nonperipheral tetraalkoxy substituted,[19] tetra- and octadiethoxymalonyl substituted,[20] tetrakis(cumylphenoxy)[21] tetranitro- and tetraaminosubstituted[22] lead phthalocyanines were synthesised and characterized. The first mesomorphic lead phthalocyanines

[a] *Gebze Institute of Technology, Department of Chemistry, P.O. Box: 141, 41400, Gebze, Kocaeli, Turkey. E-mail: durmus@gyte.edu.tr; Fax: +902626053101; Tel: +902626053075*
[b] *Faculty of Arts, Computing, Engineering and Sciences, Sheffield Hallam University, Furnival Building, 153 Arundel Street, Sheffield S1 2NU, United Kingdom. E-mail: a.hassan@shu.ac.uk; Tel: 0114 225 6904*
[c] *TUBITAK-Marmara Research Center, Materials Institute, P.O. Box: 21, 41470, Gebze, Kocaeli, Turkey. E-mail: ahsen@gyte.edu.tr; Fax: +902626412309; Tel: +902626772000*
[d] *Nikolaev Institute of Inorganic Chemistry SB RAS, 3 Lavrentiev Ave, Novosibirsk 630090, Russia. E-mail: basova@niic.nsc.ru; Fax: +7 383 3309489; Tel: +7 383 3302814*

† Electronic supplementary information (ESI) available. See DOI: 10.1039/c2nj40247e

were reported in 1987.[8,10] Simon *et al.* showed that alkoxymethyl substituted phthalocyaninato lead(II) complexes ($PbPcR_8$, with R = $-CH_2OC_nH_{2n+1}$ (n = 8, 12, 18)) form a hexagonal columnar mesophase, which is stable at room temperature when n = 8 and 12,[8] and since then Ford *et al.* pointed out that octa-(2-ethylhexyloxy) lead phthalocyanines exist in mesophases from −100 to +200 °C.[9] These derivatives were alkoxy[9,23–24] and alkoxy methyl[8] octasubstituted mesogens with side chains substituted at the 2,3-positions on the benzene ring but mesomorphic alkylthio-substituted lead Pc compounds have not been synthesized except those discussed in our recently published work.[13] Furthermore, a comparative analysis of the mesogenic and spectral properties of tetrakis PbPc derivatives has been performed in terms of different heteroatoms and the effect of substituent position.[25]

We report here on the mesogenic properties of novel lead(II) Pcs octasubstituted with octylthio, octyloxy and hexadecyloxy groups ($PbPcR_8$). The hexadecylthio substituted lead(II) phthalocyanine derivative was synthesized according to our earlier work.[13] The preparation of thin films of these phthalocyanines and their investigation by the methods of spectral ellipsometry and polarized microscopy are reported. The current–voltage characteristics and electrical switching behavior in sandwich structures of ITO/$PbPcR_8$/In are also studied.

Results and discussion

Synthesis and characterization

The synthetic route of octasubstituted lead(II) phthalocyanine complexes ($PbPcR_8$) is shown in Fig. 1. 4,5-bis(octyloxy) phthalonitrile (**1a**) and 4,5-bis(hexadecyloxy)phthalonitrile (**1b**) were synthesized *via* nucleophilic substitution of 4,5-dihydroxyphthalonitrile with corresponding octyl or hexadecylbromide groups in the presence of K_2CO_3 in dried DMF. 4,5-bis(octylthio)phthalonitrile (**2a**) and 4,5-bis(hexadecylthio)-phthalonitrile (**2b**) were synthesized *via* nucleophilic substitution of 4,5-dichlorophthalonitrile with corresponding octylthiol or hexadecylthiol groups in the presence of K_2CO_3 in dried DMF. The synthesis of Pb(II) phthalocyanine complexes (**3a, b** and **4a, b**) was carried out by melting of the corresponding substituted phthalonitriles in the presence of dried PbO.

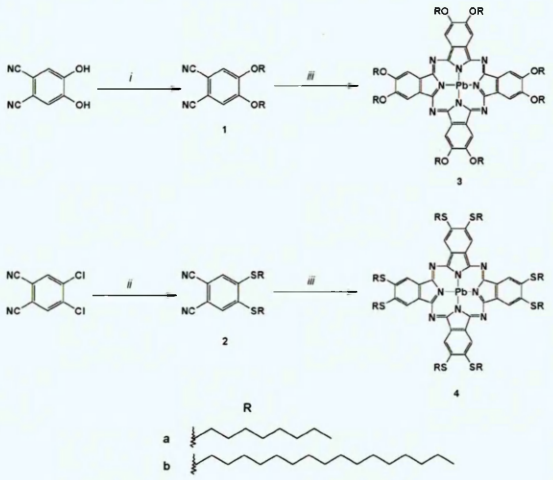

Fig. 1 The synthesis of octa-substituted lead(II) phthalocyanines. Reagents and conditions: (i) RBr, K_2CO_3, DMF, rt, 3 days; (ii) RSH, K_2CO_3, DMF, rt, 3 days; (iii) PbO (dried), 210 °C, solvent-free, 5 h.

All synthesized complexes were fully identified by elemental analysis, FT-IR, UV-Vis, ^{1}H-NMR, ^{13}C-NMR and MALDI-TOF mass spectroscopy, and the analyses were consistent with the predicted structures. In the IR spectra, the absence of the characteristic C≡N stretches at ~2300 cm^{-1} for phthalonitriles (**1a, b** and **2a, b**) are indicative of metallophthalocyanine formation. Pb(II) phthalocyanine complexes (**3a, b** and **4a, b**) showed characteristic vibrations for aromatic CH stretching at *ca.* 3050–3080 cm^{-1} and aliphatic CH stretching at *ca.* 2844–2956 cm^{-1}.

The Pb(II) complexes were found to be pure by ^{1}H-NMR spectra with all the substituents and ring protons observed in their respective regions. The resonances belonging to ring protons were observed as singlets at 8.73 ppm for **3a**, 8.79 ppm for **3b**, 8.87 ppm for **4a** and 8.99 ppm for **4b** integrating 8 aromatic protons for each complex. While SCH_2 signals were observed at 3.27 ppm for **4a** and 3.37 ppm for **4b** as triplets, OCH_2 protons were shifted downfield due to the greater electronegativity of the oxygen atom and observed between 4.33–4.43 ppm for **3a** and 4.41–4.54 ppm for **3b** as two sets of quartet of doublets (dq) in a 1 : 1 ratio instead of one triplet (Fig. 2). This indicates the non-equivalent nature of protons (H_a, H_b) on OCH_2 groups, similar to that observed for the rare earth sandwich phthalocyanines as reported in the literature.[26a] It is known that the lead ion is unable to completely enter the central cavity of the phthalocyanine ring due to its large ionic size, resulting in the out-of-plane structure of Pb(II) phthalocyanine bearing C_4 symmetry,[19] as well as Pb(II) porphyrins.[26b] It has also been reported that X-ray diffraction analysis of Pb(II) phthalocyanines has revealed the unusual aza coordination of phthalocyanine in a pseudo-double decker supramolecular structure.[18,19,27] Molecular interactions in solution can lead to dimerization similar to pseudo-doubledecker structures, which can result in the differentiation of the hydrogen atoms depending on whether they are displaced out of the inter-phthalocyanine space or in the interphthalocyanine space. However, the SCH_2 protons are equivalent in SR substituted compounds (**4a** and **4b**) in contrast to OR substituted compounds (**3a** and **3b**) and the two sets of quartet of doublets could not be observed in ^{1}H-NMR spectra of SR derivatives (**4a, 4b**) (Fig. 2). It can be suggested that the sulphur atom, being larger compared to the oxygen atom, can limit the molecular interactions in solution, which prevents dimerization.

Moreover, the resonances belonging to methyl protons were observed as triplets at 0.85 ppm for **3a**, 0.80 ppm for **3b**, 0.90 ppm for **4a** and 0.89 ppm for **4b**, integrating 24 protons for each complex. Furthermore, the ^{13}C-NMR spectra of Pb(II) complexes (**3a, b** and **4a, b**) showed all carbon shifts of Pc ring and aliphatic chains, confirming the predicted structures.

The electronic absorption spectra of **3a, b** and **4a, b** in THF (1×10^{-5} M) are presented in Fig. 3. In common with other Pc derivatives, PbPc complexes have two intensive bands in the UV–vis spectra: the Soret band (B-band) and the Q-band. The Q-band absorption has been assigned to a π–π^* transition from the highest occupied molecular orbital (HOMO) of a_{1u} symmetry

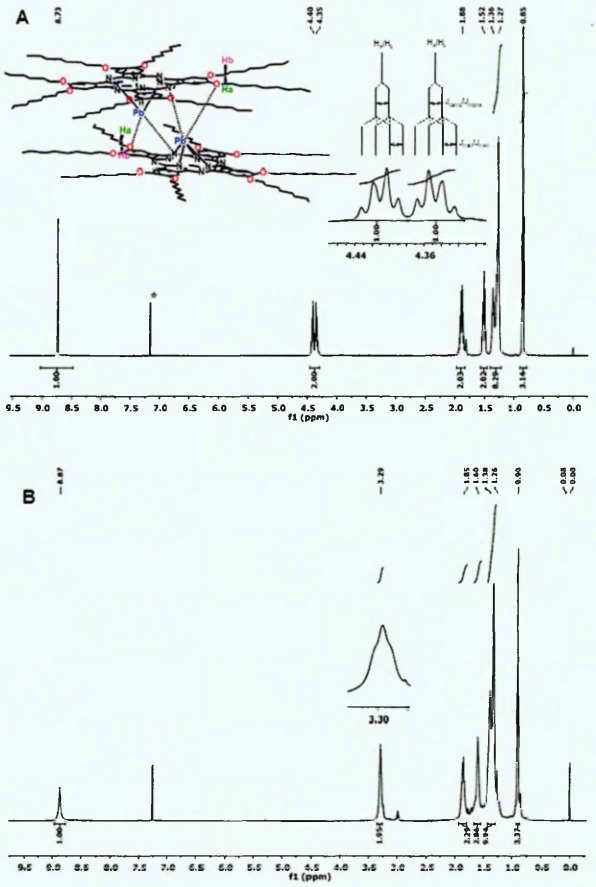

Fig. 2 ^{1}H-NMR spectra of **3a** (A) and **4a** (B).

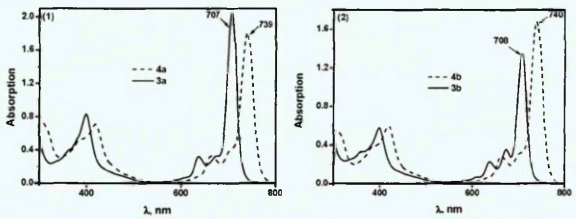

Fig. 3 Electronic absorption spectra of **3a, 4a** (1) and **3b, 4b** (2) in tetrahydrofuran (THF) ($C = 1 \times 10^{-5}$ M).

to the lowest unoccupied molecular orbital (LUMO) of e_g symmetry. In THF, the Q bands were observed at 707 nm for **3a**, 708 nm for **3b**, 739 nm for **4a** and 740 nm for **4b**. The red-shift *ca.* 30 nm in the spectra of SR-substituted derivatives (**4a**, **4b**) compared to OR-substituted derivatives (**3a**, **3b**) can be ascribed to the greater electron donating nature of SR groups in comparison with OR groups; this is due to the higher electron donating ability of sulphur atoms compared to that of oxygen atoms. The increase of electron density in the phthalocyanine ring results in the narrowing of the highest occupied molecular orbital (HOMO)–lowest unoccupied orbital (LUMO) gap.[28] Furthermore, the presence of Pb ions leads to an additional shift to longer wavelengths in comparison with planar Pc analogues. For instance, the Q bands of Pb(II) phthalocyanine complexes (**3a, b** and **4a, b**) were red-shifted by ~30 nm compared to their Cu(II) counterparts in THF.[29] The observed red spectral shift is due to the non-planar structure of Pb(II) phthalocyanine complexes. MALDI-TOF-MS spectra of the compounds were obtained without using any matrix and the protonated molecular ion peaks were observed at 1746.46, 2644.37, 1874.05 and 2772.70 for complexes **3a, b, 4a, b**, respectively. The Pb(II) phthalocyanine complexes were converted to metal-free counterparts using a matrix such as 2,3-dihydroxybenzoic acid (DHB) in MALDI-TOF-MS studies.

Mesogenic properties of the $PbPcR_8$ complexes

The thermal stability of the $PbPcR_8$ complexes has been investigated by TGA. Decomposition starts at 300 °C for each complex. The main decomposition temperatures are 410 °C for **3a**, 409 °C for **3b**, 388 °C for **4a** and 393 °C for **4b**. It is obvious that alkoxy substituted lead(II) Pcs (**3a** and **3b**) are more thermally stable than alkylthio lead(II) Pcs (**4a** and **4b**). However, there is not any significant change in the main decomposition temperatures depending on the chain length. The phase transition temperatures of $PbPcR_8$ complexes were determined by differential scanning calorimetry (DSC). DSC measurements were performed on the virgin materials with a scanning rate of 10 °C min^{-1}. Phase transition temperatures of the PbPc complexes upon second heating and cooling runs are summarized in Table 1. The clearing temperatures of studied PbPcs complexes decreased with increasing chain length. The clearing temperatures of the octakis(alkylthio)-substituted PbPcs (**4a**, **4b**) were lower in comparison with those of their oxygen analogues (**3a**, **3b**). Pb(II) sterically destabilizes the co-facial columnar structure and drastically reduces both the crystal-to-mesophase and mesophase-to-isotropic transition temperatures.[30] Clearing points of Pb(II) phthalocyanine compounds were observed at lower temperatures compared to metal-free and other planar metallophthalocyanine counterparts, such as Cu(II), Zn(II), and Ni(II) complexes.[29,31,32–34] Moreover, clearing points could not be observed for metal-free and Cu(II), Zn(II), Ni(II) metallophthalocyanine bearing octyl chain as they undergo decomposition before reaching their clearing temperature.

The textures of the $PbPcR_8$ derivatives were obtained by heating of a sample of the $PbPcR_8$ derivatives to the isotropic temperature and then cooling from isotropic melt; characteristic features of the columnar phase are revealed, as shown in Fig. 4.

Table 1 Phase transition temperatures, °C (corresponding enthalpy changes in parentheses, kJ mol^{-1}) for lead(II) Pc compounds (**3a, 3b, 4a** and **4b**) determined by DSC. Heating and cooling rates: 10 °C min^{-1}, Phase nomenclature: Cr and Cr′: crystal phases, Col_h: discotic hexagonal columnar mesophase, I: isotropic phase[a]

Compound	Phase transition temperatures, °C
3a	$Cr \xrightarrow{-3.7(3.16)} Col_h \xrightarrow{300^*} I$
3b	$Cr \underset{23.5(8.67)}{\overset{35.0(18.77)}{\rightleftharpoons}} Cr' \underset{38.2(42.71)}{\overset{48.5(34.47)}{\rightleftharpoons}} Col_h \underset{185^{**}}{\overset{190^{**}}{\rightleftharpoons}} I$
4a	$Cr \underset{-3.2(5.92)}{\overset{6.7(1.95)}{\rightleftharpoons}} Col_h \underset{222.9(2.42)}{\overset{240.0(1.44)}{\rightleftharpoons}} I$
4b[13]	$Cr \underset{22.8(104.97)}{\overset{31.2(108.33)}{\rightleftharpoons}} Col_h \underset{184.7(3.65)}{\overset{204.5(7.43)}{\rightleftharpoons}} I$

[a] *Only observed under the optical polarizing microscope with accompanying decomposition. **Only observed under the optical polarizing microscope.

The identification of mesophases was carried out by X-ray diffraction (XRD) measurements. All XRD data are summarized in Table 2. The powder diffraction patterns of **3a**, **3b** and **4a** contain typical reflections of a columnar mesophase of substituted Pcs.[2] These features were also observed for **4b** and were reported in an earlier publication.[13] In the low angle region, the phthalocyanine derivatives produce sharp peaks with the ratio of $1:\sqrt{3}:\sqrt{4}:\sqrt{7}$. These results suggest a two-dimensional hexagonal lattice with disc-like molecules stacked in columns in the hexagonal arrangement.

The fact that the alkylthio derivatives have smaller lattice constants can be connected with the sulphur–sulphur interactions arising from the high polarizability of the sulphur atoms. Consequently, the structural disorder in the columnar structure will be reduced in the stacked alkylthio molecules, leading to a decrease in the intermolecular distance. Although, the S···S interaction is a weak attractive force in gases and solutions, it plays an important role in the packing of molecules in crystals. Some examples of S···S interactions, which are one of the major forces that influence the structures of organic conductors, are described in the literature.[35–38]

Table 2 X-Ray diffraction data for lead(II) Pc compounds (**3a**, **3b**, **4a** and **4b**)

Compound	Observed spacings (Å)	Theoretical spacings (Å)	Lattice constant (Å)	Ratio	Miller indices
3a	23.77	23.77	27.4	1	(100)
	14.02	13.72		$\sqrt{3}$	(110)
	12.20	11.88		$\sqrt{4}$	(200)
	9.26	8.98		$\sqrt{7}$	(210)
3b	30.46	30.46	35.2	1	(100)
	18.23	17.59		$\sqrt{3}$	(110)
	15.60	15.23		$\sqrt{4}$	(200)
	12.09	11.51		$\sqrt{7}$	(210)
4a	20.63	20.63	23.8	1	(100)
	11.84	11.91		$\sqrt{3}$	(110)
	10.57	10.31		$\sqrt{4}$	(200)
	7.78	7.80		$\sqrt{7}$	(210)
4b[13]	25.97	25.97	30.02	1	(100)
	15.01	14.99		$\sqrt{3}$	(110)
	12.97	12.98		$\sqrt{4}$	(200)
	9.85	9.81		$\sqrt{7}$	(210)

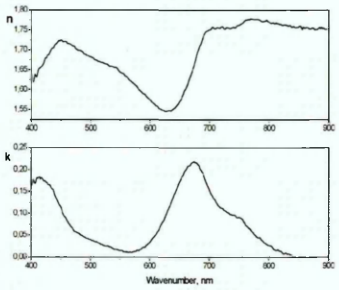

Fig. 5 Variation of refractive index and extinction coefficient of **4a** film deposited at 2000 rpm. with incident photon wavelength.

Film investigation

Spectroscopic ellipsometry measurements were carried out for the characterization of thickness, refractive index (n) and extinction coefficient (k) of the $PbPcR_8$ films. Using the Levenberg–Marquardt multivariate regression algorithm, the measured ellipsometric data were fitted to the model for organic films. A detailed description of the principles of ellipsometry can be found in ref. 39. The resulting variation of refractive index and extinction coefficient of **4a** film deposited at 2000 rpm with incident photon wavelength are shown in Fig. 5 as an example. The thicknesses, refractive indices and extinction coefficients (at λ = 633 nm) obtained from ellipsometry fitting procedures for the other lead phthalocyanines are listed in Table 3.

Table 3 Thicknesses, refractive indices and extinction coefficients (at λ = 633 nm) obtained in accordance with ellipsometry fitting procedures and DC conductivity for $PbPcR_8$ films deposited at 2000 rpm

Comp.	n	k	Thickness/nm	DC conductivity (σ)/$\Omega^{-1}m^{-1}$ Before heating	After heating
3a	1.50	0.15	38.4	1.7×10^{-10}	5.5×10^{-8}
3b	1.44	0.08	40.12	1.9×10^{-10}	4.1×10^{-9}
4a	1.55	0.12	46.66	2.5×10^{-10}	7.8×10^{-7}
4b	1.51	0.09	47.73	3.3×10^{-10}	2.3×10^{-7}

The current–voltage characteristics of thin films of **4a** are presented in Fig. 6. As shown in the inset to Fig. 6, the conduction was found to be ohmic at low voltages due to thermal generation of charge carriers, but exhibits power-law dependence at higher voltages (V > 0.5 V). The room temperature conductivities are summarized in Table 3. The conductivity was determined from the linear (Ohmic) region of the measured $I(V)$ curves, *i.e.*, in the voltage range 0–0.5 V. The obtained results demonstrate an increase in electronic conduction after heat treatment. Increase of conductivity is found to be larger for **4a** and **4b** films compared to **3a** and **3b**.

The $J(V)$ characteristics are shown to be mainly dependant on the type of electrodes used. In the case of Al bottom and top electrodes, all junctions have shown open-circuit, probably due to a naturally grown insulating Al_2O_3 layer formed onto

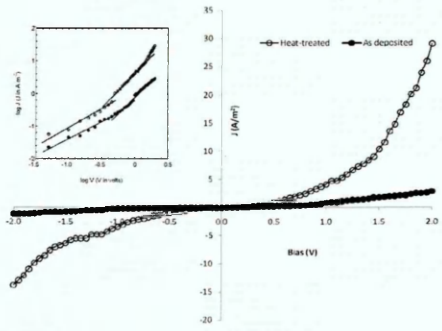

Fig. 6 $J(V)$ characteristics of thin films of **4a** deposited between ITO and In electrodes. The inset shows the same data of the forward bias characteristics plotted on a log-log scale.

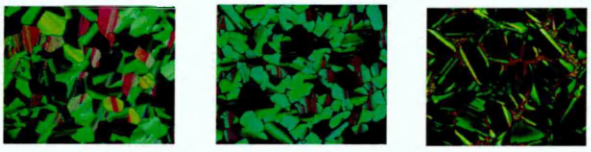

I II III

Fig. 4 Optical textures of $PbPcR_8$ complexes for **3a** (I) at room temperature, **3b** (II) at 100 °C and **4a** (III) at room temperature; magnification 40×.

the surface of the bottom Al electrode.[40] Evaporation of gold electrodes has always led to short circuit in all of our produced samples. AFM micrographs have revealed the bumpy surface morphology of the evaporated gold film.[40] This confirms the aggregation of Au atoms, leading to the formation of large grains on both the organic film and the glass substrate. Furthermore, due to the high melting point of Au it appears to cause damage to the $PbPcR_8$, which is in liquid crystalline form at about room temperature.

The ITO/PbPc/In structures, on the other hand, have exhibited interesting $J(V)$ behavior. Fig. 6 shows the $J(V)$ curves of **4a** before and after heat treatment as an example. Both curves demonstrate asymmetric characteristics over the two bias polarities, however, after heat treatment, the studied structure demonstrates clear rectification characteristics, typical of diode behavior. Similar characteristics were observed for the other PbPc analogues studied here. The dissimilar behavior before and after heat-treatment can be explained by the effect of thermal treatment on the films, which is expected to result in changing the alignment inside the columnar stacking of the molecules in the films. $PbPcR_8$ derivatives exhibit a hexagonal columnar structure over a wide temperature range. It was shown in previous works[41,42] that the ordered films of liquid crystalline metal phthalocyanines can be obtained upon slow cooling from isotropic melt or by heating at the temperature of liquid crystalline phase for some time. Moreover, it has been shown earlier that the heat treatment of films of LC nickel phthalocyanines deposited between two electrodes is found to result in hexagonal homeotropic alignment of molecules in the films.[43] The conduction mechanism at higher voltages ($V >$ 0.5 V) is not discussed here because this is a subject of separate work. Charge transport properties of similar phthalocyanine discotic liquid crystals were studied earlier in the works of Geerts and co-authors.[44,45]

POM has been used to check the alignment of the $PbPcR_8$ films. Electrical measurements and POM investigations were carried out at room temperature (25 °C). The POM images recorded between crossed polarizers for the films of $PbPcR_8$ deposited between ITO and metal electrodes after heat-treatment are presented in Fig. 7. At this temperature, **3a** and **4a** are in the mesophase, but **3b** is in the crystalline phase. The temperature of transition to crystalline phase for **4b** (22.8 °C, Table 1) is close to room temperature, however, according to POM and X-ray phase investigations crystallization was not observed under this experimental conditions. The **4a** and **4b** films deposited between ITO and metal electrodes do not exhibit any birefringence over a large area when observed between cross-polarizers during POM measurements (Fig. 7(c, d)). The lack of birefringence is characteristic of the hexagonal homeotropic phase, which has a face-on arrangement of discs, as illustrated schematically in Fig. 7(c, d).[46,47] In other words, the molecules rotate in the direction of face-on to the substrate plane after thermal treatment. The films of **4b** (Fig. 7(d)) deposited between ITO and indium electrodes looks more homogeneous than those of **4a** (Fig. 7(c)) in which polydomains are evident. The occurrence of homeotropic alignment is thus related to the presence of the upper electrode, which induces a confinement of the liquid crystal film and plays the same role as a top substrate in the case of the films confined between two substrates.[46,48,49]

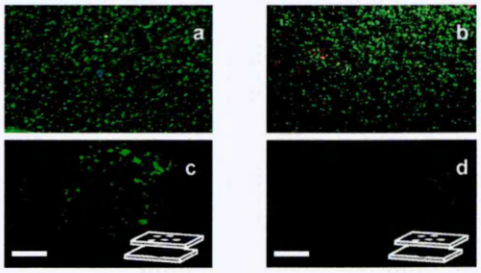

Fig. 7 Polarizing optical microscopy images with cross polarizers of the **3a** (a), **3b** (b), **4a** (c), **4b** (d) films deposited between ITO and metal electrode. Schematic illustrations of the macroscopic alignments are also given. The sample is placed perpendicular to the incident light beam. The scale bar indicates 50 μm.

At the same time the films of $PbPcR_8$ with alkoxysubstituents (**3a** and **3b**) do not show homeotropic alignment between ITO and In at room temperature (Fig. 7(a, b)). Such behavior of alkoxy substituted phthalocyanines may be connected with their higher viscosity at room temperature and higher temperature of phase transition to LC phase in the case of **3b**.

The obvious increase of the conductivity for heat-treated **4a** and **4b** films can be ascribed to the increasing of π–π interaction in the columnar homeotropic alignment as opposed to the disordered structure of as deposited films.[50] Sulphur atoms in **4a** and **4b** positively affect the electrical conductivity in comparison with oxygen in the substituent chains of **3a** and **3b** (see Table 3). As the sulphur is larger than oxygen, the rotational and translational movements of the molecules are hindered within the cores of the columns. Consequently, the structural disorder will be reduced in the stacked alkylthio molecules, leading to rapid charge transport.[51] The lowest value of conductivity for **3b** films may also be explained by the formation of crystalline phase at room temperature. According to previous publications,[52,53] the molecules in the crystal are arranged in tilted stacks, which are widely spaced, with the contacts between the aromatic cores bigger than in the mesogenic phase.

Among all studies only $PbPcR_8$ analogues **4a** and **4b** have exhibited switching behavior (Fig. 8).

The films of these compounds have been shown as switching loops of memory cells, which can be utilised in applications as memory or logic elements.[54] This effect, however, was found to degrade after a few cycles of $I(V)$ tests, and has completely disappeared after the samples were subjected to heat treatment. On the first measured $I(V)$ loop, the on state current was found to be larger than the off state by nearly three orders of magnitude giving a high ON/OFF ratio (see inset to Fig. 8). The possible explanation of this molecular switching effect is that the freshly deposited PbPc film is composed of clusters of different structures within the column stacks before heating. The variation in the film substructure may result in the occurrence of potential barriers, which have to be surmounted by the charge carriers, thus giving rise to the highly conducting ON state. Furthermore, in the ON state, the external electric field is possibly able to turn some of the stacks into equal orientations, resulting in equal lead ion separation, which would enhance the highly conductive channels.[55] Several other metal phthalocyanines, both substituted[11,17,56] and unsubstituted[57,58] have demonstrated electrical switching, which was explained by the existence of potential barriers that

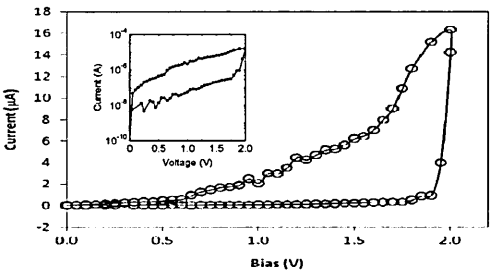

Fig. 8 Switching characteristics of **4a** films deposited between ITO and In electrodes. The inset shows the same data produced on a log-linear scale for clarity.

control charge transport and thus switching between the ON and OFF states. Thin films of unsubstituted PbPc of the monoclinic structure have shown switching behaviour, which was explained by an electric field-induced order–disorder transition mechanism in the stacking direction.[57] In a printed memory device which utilises a water soluble CuPc derivative and conductive polymer layers sandwiched between two metal electrodes, switching from the OFF state to the ON state was ascribed to increased crystallinity of the CuPc film.[56] This change in crystallinity was confirmed by SEM study, and was found to be responsible for the conductivity after switching. Mukherjee and co-workers[17] have attributed the bistable effect in ITO/PbPc/Al devices to a combination of the presence of a hole-injection barrier at the ITO/PbPc interface and space charge limited hole transport across the undepleted region of the PbPc film to the counter electrode. Thermally deposited thin films of unsubstituted copper phthalocyanine (CuPc) have exhibited bistable effects with an increased ON/OFF ratio when the film deposition rate was increased.[58] It was argued that the conductive switching behaviour of the CuPc bistable devices involves a bulk trap-controlled space charge limited mechanism and that the carrier transport could be ascribed to a field-induced arrangement of structural defects.[58]

In the current study the disappearance of the switching effect in heat-treated samples can be further supported by the POM images, which clearly reveal film transformation to a hexagonal homeotropic phase, which results in the disappearance of the potential barriers between clusters within the stacks that were thought to be present in the freshly prepared samples. In the present study our initial investigation of electrical switching in sandwich devices involving the new LC crystalline $PbPcR_8$ molecules has shown some encouraging results, which will certainly require extensive and dedicated research in this subject in order to establish the occurrence of this interesting phenomenon and to further elucidate the bistable effect mechanism itself.

Conclusions

In this work, the synthesis of new mesomorphic octasubstituted alkylthio- and alkoxy- Pb(II) phthalocyanines has been described. The Pb(II) phthalocyanines were characterized using different spectroscopic techniques (^{1}H and ^{13}C-NMR, UV-Vis, FT-IR, and mass spectroscopies) and elemental analysis. The alkoxy-substituted lead Pcs exhibited higher stability due to thermal variation than the alkylthio-substituted lead Pcs, and clearing points of all prepared Pb(II)Pc complexes were found to be lower in comparison with metal-free phthalocyanine and other planar metallophthalocyanines. The XRD analysis indicates the formation of the columnar-hexagonal (Col_h) mesophase, which is further established by the lack of birefringence in POM measurement. The films of the synthesized compounds exhibited an increase in electronic conduction after heat treatment. A typical switching effect was also observed in **4a** and **4b** films with high ON/OFF ratios, making them promising candidates for memory applications.

Experimental

Materials

4,5-dihydroxyphthalonitrile,[59] 4,5-dichlorophthalonitrile,[60] 4,5-bis(octylthio)phthalonitrile (**2a**)[61] and 4,5-bis(hexadecylthio) phthalonitrile (**2b**)[62] were synthesized according to reported procedure. 4,5-bis(octyloxy)phthalonitrile (**1a**)[31] and 4,5-bis(hexadecyloxy)phthalonitrile (**1b**)[31] were synthesized according to the modified reported procedure by using 4,5-dihydroxyphthalonitrile as a precursor, which has previously been described by Torres and co-workers.[59] All other reagents and solvents of reagent-grade quality were obtained from commercial suppliers and were dried as described in Perrin and Armarego.[63]

Instrumentation

The IR spectra were recorded between 4000 and 650 cm^{-1} using a Perkin Elmer Spectrum 100 FT-IR spectrometer with an attenuated total reflection (ATR) accessory, featuring a zinc selenide (ZnSe) crystal. Optical spectra in the UV-visible region were recorded with Shimadzu UV-Vis-3101 and 2101 spectrometers using 1 cm pathlength cuvette at room temperature. Matrix-assisted laser desorption/ionization time-of-flight mass spectrometry (MALDI-TOF-MS) measurements were performed on a Bruker Daltonics micrOTOF (Bremen, Germany). ^{1}H and ^{13}C NMR spectra were recorded in $CDCl_3$ solutions on a Varian 500 MHz spectrometer. The phase transition behaviors of Pcs were observed by means of a polarizing optical microscope (POM) (Leitz Wetzler Orthoplan-pol.) equipped with a hot stage (Linkam TMS 93) and a temperature controller (Linkam LNP). Thermogravimetric analysis (TGA) was carried out on a Mettler Toledo Star^e Thermal Analysis System at a rate of 10 °C min^{-1} in a nitrogen flow (50 mL min^{-1}). Transition temperatures were determined at a scan rate of 10 °C min^{-1} using a Mettler Toledo Star Thermal Analysis System/DSC 822. The differential scanning calorimeter (DSC) system was calibrated with 3 mg indium samples under a nitrogen atmosphere. X-ray diffraction measurements (XRD) (Cu-Kα-radiation) were performed using a Bruker Advanced D8 diffractometer.

Synthesis

2,3,9,10,16,17,23,24-Octakis(octyloxy)phtalocyaninato lead(II) (3a). 4,5-bis(octyloxy)phthalonitrile (**1a**) (0.50 g, 1.30 mmol) and dried PbO (0.145 g, 0.65 mmol) were stirred at 210 °C for 5 h under an argon atmosphere in solvent-free conditions. The reaction mixture was then dissolved in dichloromethane and filtered to eliminate inorganic impurities. The solvent was evaporated and the crude product was purified

through a Bio Beads column (Bio Rad Laboratories) using dichloromethane as an eluent. The green product was further purified by preparative thin layer chromatography on silica gel using dichloromethane/*n*-hexane, 20 : 1 (v/v). Yield: 0.150 g (26%). IR [(ATR) ν_{max}/cm^{-1}]: 3077 (Ar C–H), 2952–2855 (aliphatic C–H), 1603 (C=C), 1495, 1450, 1370, 1262, 1188, 1075, 1041, 871, 741. UV-Vis (THF): λ_{max} nm (log ε) 359 (4.59), 399 (4.92), 638 (4.55), 707 (5.31). ^{1}H NMR (500 MHz, $CDCl_3$): δ = 0.85 (t, 24H, CH_3), 1.22–1.39 (m, 64H, CH_2), 1.48-1.54 (m, 16H, CH_2), 1.84–1.95 (m, 16H, CH_2), 4.33–4.43 (dq, 16H, OCH_2), 8.73 (s, 8H, CH_{ar}). ^{13}C NMR (125 MHz, $CDCl_3$): δ = 14.17 (CH_3), 22.75 (CH_2), 26.24 (CH_2), 29.38 (CH_2), 29.48 (CH_2), 29.53 (CH_2), 31.92 (CH_2), 69.74 (OCH_2), 105.80 ($C_{ar}H$), 131.72 (C_{ar}), 152.02 (C_{ar}–O), 153.51 (C_{ar} C=N). Calc. for $C_{96}H_{144}N_8O_8Pb$: %C 66.06, %H 8.32, %N 6.42; Found: %C 66.43, %H 8.87, %N 6.04. MS (MALDI-TOF), *m*/*z* (%): Calcd. for $C_{96}H_{144}N_8O_8Pb$: 1745.45, found 1746.46 [M + H]$^+$ (100).

2,3,9,10,16,17,23,24-Octakis(hexadecyloxy)phtalocyaninato lead(II) (3b). **3b** was prepared by the same procedure as described for **3a** by starting with 4,5-bis(hexadecyloxy)-phthalonitrile (**1b**) (0.50 g, 0.82 mmol) and dried PbO (0.092 g, 0.41 mmol). The green product was purified by preparative thin layer chromatography on silica gel using dichloromethane/*n*-hexane, 10 : 1 (v/v). Yield: 0.100 g (18%). IR [(ATR) ν_{max} cm^{-1}]: 3077 (Ar C–H), 2918–2844 (aliphatic C–H), 1603 (C=C), 1495, 1455, 1376, 1274, 1200, 1086, 1041, 865, 752, 712. UV-Vis (THF): λ_{max} nm (log ε) 359 (4.52), 399 (4.77), 638 (4.36), 708 (5.14). ^{1}H NMR (500 MHz, $CDCl_3$): δ = 0.80 (t, 24H, CH_3), 1.12–1.38 (m, 176H, CH_2), 1.39–1.46 (m, 16H, CH_2), 1.55–1.65 (m, 16H, CH_2), 1.95–2.04 (m, 16H, CH_2), 4.41–4.54 (dq, 16H, OCH_2), 8.79 (s, 8H, CH_{ar}). ^{13}C NMR (125 MHz, $CDCl_3$): δ = 13.10 (CH_3), 21.68 (CH_2), 25.29 (CH_2), 28.37–28.77 (CH_2), 30.93 (CH_2), 68.92 (OCH_2), 104.75 ($C_{ar}H$), 130.72 (C_{ar}), 151.11 (C_{ar}–O), 152.48 (C_{ar} C=N). Calc. for $C_{160}H_{272}N_8O_8Pb$: %C 72.71, %H 10.37, %N 4.24; Found: %C 73.08, %H 10.79, %N 4.11. MALDI-TOF-MS *m*/*z*: Calcd. for $C_{160}H_{272}N_8O_8Pb$: 2643.17, found 2644.37 [M + H]$^+$ (100).

2,3,9,10,16,17,23,24-Octakis(octylthio)phtalocyaninato lead(II) (4a). **4a** was prepared and purified by the same procedure as described for **3a** by starting with 4,5-bis(octylthio)phthalonitrile (**2a**) (0.50 g, 1.20 mmol) and dried PbO (0.134 g, 0.60 mmol). Yield: 0.200 g (36%). IR [(ATR) ν_{max} cm^{-1}]: 3050 (Ar C–H), 2956-2852 (aliphatic C–H), 1592 (C=C), 1460, 1364, 1312, 1080, 1064. UV-Vis (THF): λ_{max} nm (log ε) 384 (4.73), 418 (4.86), 663 (4.52), 739 (5.26). ^{1}H NMR (500 MHz, $CDCl_3$): δ = 0.90 (t, 24H, CH_3), 1.26–1.45 (m, 64H, CH_2), 1.54–1.68 (m, 16H, CH_2), 1.79–1.95 (m, 16H, CH_2), 3.27 (t, 16H, SCH_2), 8.87 (s, 8H, CH_{ar}). ^{13}C NMR (125 MHz, $CDCl_3$): δ = 14.15 (CH_3), 22.74 (CH_2), 28.77 (CH_2), 29.32 (CH_2), 29.40 (CH_2), 29.45 (CH_2), 31.95 (CH_2), 33.96 (SCH_2), 121.01 ($C_{ar}H$), 135.00 (C_{ar}), 140.09 (C_{ar}–S), 153.57 (C_{ar} C=N). Calc. for $C_{96}H_{144}N_8PbS_8$: %C 61.53, %H 7.75, %N 5.98; Found: %C 61.98, %H 7.56, %N 5.48. MALDI-TOF-MS *m*/*z*: Calcd. for $C_{96}H_{144}N_8PbS_8$: 1873.98, found 1874.05 [M]$^+$ (100).

2,3,9,10,16,17,23,24-Octakis(*n*-hexadecylthio)phtalocyaninato lead(II) (4b). **4b** was prepared by the same procedure as described in our previous work[13] by starting with 4,5-bis(hexadecylthio)phthalonitrile (**2b**) (0.369 g, 0.576 mmol) and dried PbO (0.064 g, 0.288 mmol) Yield: 0.075 g (19%). IR [(ATR) ν_{max} cm^{-1}]: 3055 (Ar C–H), 2955–2849 (aliphatic C–H), 1591 (C=C), 1467, 1404, 1363, 1310, 1059. UV-Vis (THF): λ_{max} nm (log ε) 384 (4.60), 419 (4.78), 663 (4.47), 740 (5.23). ^{1}H-NMR (500 MHz, $CDCl_3$): δ = 0.89 (t, 24H, CH_3), 1.22-1.51 (m, 192H, CH_2), 1.59–1.74 (m, 16H, CH_2), 1.84–2.00 (m, 16H, CH_2), 3.37 (t, 16H, SCH_2), 8.99 (s, 8H, CH_{ar}). ^{13}C-NMR (125 MHz, $CDCl_3$): δ = 14.36 (CH_3), 22.94 (CH_2), 29.05 (CH_2), 29.63 (CH_2), 29.67 (CH_2), 29.78 (CH_2), 29.94–30.07 (CH_2), 32.17 (SCH_2CH_2), 34.24 (SCH_2), 121.34 ($C_{ar}H$), 135.30(C_{ar}), 140.44 (C_{ar}–S), 153.84 (C_{ar} C=N). Calc. for $C_{160}H_{272}N_8PbS_8$: %C 69.33, %H 9.89, %N 4.04; Found: %C 69.76, %H 9.46, %N 3.97. MALDI-TOF-MS *m*/*z*: Calcd. for $C_{160}H_{272}N_8PbS_8$: 2771.71, found 2772.70 [M + H]$^+$ (100).

Film preparation and characterization

Thin films of $PbPcR_8$ were prepared in sandwich forms using spin coating. Solutions in dichloromethane in the concentration 10 mg mL^{-1} were spun at 2000 rpm onto ITO coated slides and were left to dry for a few hours. Two sandwich structures (ITO/PbPc/In, Al/PbPc/Al) were prepared to investigate the current density–voltage (*J*(*V*)) characteristics of thin films of these molecules. Indium and aluminum as electrodes were evaporated under vacuum pressure of about 2 × 10^{-5} mbar using vacuum thermal deposition. The rate of film deposition was controlled by a film thickness monitor at the rate 0.1 nm s^{-1}, and the obtained thickness was 40 nm.

Thickness of the spin coated $PbPcR_8$ films was measured by spectroscopic ellipsometry. The measurements were performed on films deposited on silicon substrates using a Woolam M-2000 V^{TM} rotating analyser spectroscopic ellipsometer in the spectral range of 400–800 nm. Optical textures were observed with the polarizing microscope Leitz Wetzler Orthoplan–pol equipped with the hot stage Linkam TMS 93 and temperature-controller Linkam LNP.

The *J*(*V*) characteristics of the devices produced in this work were investigated before and after heat treatment at 70 °C using semiconductor characterisation system (Keithly 4200). The measurements were performed by applying a cyclic bias regime in the range ±2 V (starting from −2 V up to +2 V and then back to −2 V). All electrical measurements were performed in air and at room temperature.

Acknowledgements

This work was supported by bilateral project between The Scientific and Technological Research Council of Turkey (TUBITAK, Project number: 108M384) and the Russian Foundation of Basic Research (RFBR, Project number: 09-03-91219). One the authors (HB) acknowledges the financial support of the Higher Committee for Education Development in the Iraqi government as well as the University of Babylon.

Notes and references

1 B. R. Kaafarani, *Chem. Mater.*, 2011, **23**, 378.
2 J. Simon and P. Bassoul, in *Phthalocyanine Based Liquid Crystals: Towards Submicronic Devices,Phthalocyanines, Properties and Application*, ed. C. C. Leznof and A. B. P. Lever, VCH Weinheim, Germany, 1993, vol. 2, p. 22.

3 M. K. Engel, P. Bassoul, L. Bosio, H. Lehmann, M. Hanack and J. Simon, *Liq. Cryst.*, 1993, **15**, 709.
4 J. Simon and C. Sirlin, *Pure Appl. Chem.*, 1989, **61**, 1625.
5 M. J. Cook, *Chem. Rec.*, 2002, **2**, 225.
6 S. Laschat, A. Baro, N. Steinke, F. Giesselmann, C. Hagele, G. Scalia, R. Judele, E. Kapatsina, S. Sauer, A. Schreivogel and M. Tosoni, *Angew. Chem., Int. Ed.*, 2007, **46**, 4832.
7 P. Weber, D. Guillon and A. Skoulios, *J. Phys. Chem.*, 1987, **91**, 2242.
8 C. Piechocki, J. C. Boulou and J. Simon, *Mol. Cryst. Liq. Cryst.*, 1987, **149**, 115.
9 W. T. Ford, L. Sumner, W. Zhu, Y. H. Chang, P. J. Um, K. H. Choi, P. A. Heiney and N. C. Maliszewskyj, *New J. Chem.*, 1994, **18**, 495.
10 M. Hanack, A. Beck and H. Lehmann, *Synthesis*, 1987, **8**, 703.
11 T. Basova, A. G. Gürek, D. Atilla, A. K. Hassan and V. Ahsen, *Polyhedron*, 2007, **26**, 5045.
12 M. Hanack, A. Gül, A. Hirsch, K. Braja, L. R. Subramanian and E. Witke, *Liq. Cryst.*, 1990, **187**, 365.
13 D. Atilla, A. G. Gürek, T. V. Basova, V. G. Kiselev, A. Hassan, L. A. Sheludyakova and V. Ahsen, *Dyes Pigm.*, 2011, **88**, 280.
14 Y. Machida, Y. Saito, A. Taomoto, K. Nichogi, K. Waragai and S. Asakawa, *Jpn. J. Appl. Phys.*, 1989, **28**, 297.
15 A. Miyamoto, K. Nichogi, A. Taomoto, T. Nambu and M. Murakami, *Thin Solid Films*, 1995, **256**, 64.
16 L. Ottaviano, L. Lozzi, A. R. Phani, A. Ciattoni, S. Santucci and S. Di Nardo, *Appl. Surf. Sci.*, 1998, **136**, 81.
17 B. Mukherjee, A. K. Ray, A. K. Sharma, M. J. Cook and I. Chambrier, *J. Appl. Phys.*, 2008, **103**, 074507.
18 P. M. Burnham, M. J. Cook, L. A. Gerrard, M. J. Heeney and D. L. Hughes, *Chem. Commun.*, 2003, 2064.
19 Y. Bian, L. Li, J. Dou, D. Y.Y. Cheng, R. Li, C. Ma, D. K. P. Ng, N. Kobayashi and J. Jiang, *Inorg. Chem.*, 2004, **43**, 7539.
20 H. A. Dinçer, H. Çerlek, A. Gül and M. B. Koçak, *Main Group Chem.*, 2005, **4**, 209.
21 A. W. Snow and N. L. Jarvis, *J. Am. Chem. Soc.*, 1984, **106**, 4706.
22 B. N. Achar, T. M. M. Kumar and K. S. Lokesh, *J. Porphyrins Phthalocyanines*, 2005, **9**, 872.
23 C. Piechocki, J. Simon, A. Skoulios, D. Gullion and P. Weber, *J. Am. Chem. Soc.*, 1982, **104**, 5245.
24 J. F. Wan der Pol, E. Neeleman, J. W. Zwikker, R. J. M. Nolte, W. Drenth, J. Aerts, R. Wissers and S. J. Picken, *Liq. Cryst.*, 1989, **5**, 577.
25 S. Tuncel, T. V. Basova, V. G. Kiselev, S. A. Gromilov, I. V. Jushina, M. Durmuş, A. G. Gürek and V. Ahsen, *J. Mater. Res.*, 2011, **26**, 2962.
26 (*a*) T. Toupance, V. Ahsen and J. Simon, *J. Am. Chem. Soc.*, 1994, **116**, 5352; (*b*) C. M. Lemon, P. J. Brothers and B. Boitrel, *Dalton Trans.*, 2011, **40**, 6591.
27 Y. Gao, Y. Chen, R. Li, Y. Bian, X. Li and J. Jiang, *Chem.–Eur. J.*, 2009, **15**, 13241.
28 T. Nyokong, in *Structure and Bonding,Functional Phthalocyanine Molecular Materials*, ed. J. Jiang, Springer, New York, 2010, vol. 135, pp. 45–88.
29 T. V. Basova, M. Çamur, A. A. Esenpınar, S. Tuncel, A. Hassan, V. Plyashkevich, A. Alekseev, M. Durmuş, A. G. Gürek and V. Ahsen, *Synthetic Metals*, 2012, **162**, 735.
30 N. B. McKeown, *Phthalocyanine Materials: Synthesis, Structure, Function*, Cambridge University Press, Cambridge, 1998.
31 J. Sleven, C. Görller-Walrand and K. Binnemans, *Mater. Sci. Eng., C*, 2001, **C18**, 229.
32 J. Sleven, T. Cardinaels, C. Görller-Walrand and K. Binnemans, *ARKIVOC*, 2003, 68.
33 K. Ban, K. Nishizawa, K. Ohta and H. Shiraiohta, *J. Mater. Chem.*, 2000, **10**, 1083.
34 H. Eichhorn, D. Wöhrle and D. Pressner, *Liq. Cryst.*, 1997, **22**, 643.
35 J. J. Novoa, M. C. Rovira, C. Rovira, J. Veciana and J. Tarrés, *Adv. Mater.*, 1995, **7**, 233.
36 P. Hudhomme, S. L. Moustarder, C. Durand, N. G. Planas, N. Mercier, P. Blanchard, E. Levillain, M. Allain, A. Gorgues and A. Riou, *Chem.–Eur. J.*, 2001, **7**, 5070.
37 K. Kobayashi, R. Shimaoka, M. Kawahata, M. Yamanaka and K. Yamaguchi, *Org. Lett.*, 2006, **8**, 2385.
38 D. B. Werz, R. Gleiter and R. Frank, *J. Am. Chem. Soc.*, 2002, **124**, 10638.
39 H. Arwin and D. E. Aspnes, *Thin Solid Films*, 1986, **138**, 195.
40 J.-R. Koo, H.-S. Lee, Y. Ha, Y.-H. Choi and Y. K. Kim, *Thin Solid Films*, 2003, **438–439**, 123.
41 T. V. Basova, A. G. Gürek and V. Ahsen, *Mater. Sci. Eng., C*, 2002, **22**, 99.
42 T. V. Basova, M. Durmuş, A. G. Gürek, V. Ahsen and A. Hassan, *J. Phys. Chem. C*, 2009, **113**, 19251.
43 T. V. Basova, A. Hassan, M. Durmuş, A. G. Gürek and V. Ahsen, *Synth. Met.*, 2011, **161**, 1996.
44 C. Deibel, D. Janssen, P. Heremans, V. De Cupere, Y. Geerts, M. L. Benkhedir and G. J. Adriaenssens, *Org. Electron.*, 2006, **7**, 495.
45 S. Sergeyev, W. Pisula and Y. H. Geerts, *Chem. Soc. Rev.*, 2007, **36**, 1902.
46 V. de Cupere, J. Tant, P. Viville, R. Lazzaroni, W. Osikowicz, W. Salaneck and Y. H. Geerts, *Langmuir*, 2006, **22**, 7798.
47 I. Dierking, *Texture of Liquid Crystal*, Wiley-VCH: Weinheim, Germany, 2003.
48 S. Sergeyev, W. Pisula and Y. H. Geerts, *Chem. Soc. Rev.*, 2007, **36**, 1902.
49 H. Einchhorn, *J. Porphyrins Phthalocyanines*, 2000, **4**, 88.
50 K. Ohta, K. Hatsusaka, M. Sugibayashi, M. Ariyoshi, K. Ban, F. Maeda, R. Naito, K. Nishizawa, A. M. Van De Craats and J. M. Warman, *Mol. Cryst. Liq. Cryst.*, 2003, **397**, 25.
51 K. Ban, K. Nishizawa, K. Ohta and A. Craats, *J. Mater. Chem.*, 2001, **11**, 321.
52 M. Helliwell, S. J. Teat, S. J. Coles and W. Reeve, *Acta Crystallogr., Sect. B: Struct. Sci.*, 2003, **B59**, 617.
53 K. Hatsusaka, K. Ohta, I. Yamamoto and H. Shirai, *J. Mater. Chem.*, 2001, **11**, 423.
54 J. R. Heath, C. P. Collier, G. Mattersteig, F. M. Raymo, J. F. Stoddart and E. Wong, *U.S. Patent*, No. 6198655 B1, 10 Mar. 2001.
55 C. Hamann and A. Mrwa, *Int. J. Electronics*, 1992, **73**, 1039.
56 K. Lian, R. Li, H. Wang, J. Zhang and D. Gamota, *Mater. Sci. Eng., B*, 2010, **167**, 12.
57 T. Frauenheim, C. Hamann and M. Muller, *Phys. Status Solidi A*, 1984, **86**, 735.
58 K. Onlaor, B. Tunhoo, P. Keeratithiwakorn, T. Thiwawong and J. Nukeaw, *Solid-State Electron.*, 2012, **72**, 60.
59 B. Cabezon, E. Quesada, S. Esperanza and T. Torres, *Eur. J. Org. Chem.*, 2000, 2767.
60 D. Wöhrle, M. Eskes, K. Shigehara and Y. Yamada, *Synthesis*, 1993, 194.
61 B. Del Rey, U. Keller, T. Torres, G. Rojo, F. Agullo-Lopez, S. Nonell, C. Marti, S. Brasselet, I. Ledoux and J. Zyss, *J. Am. Chem. Soc.*, 1998, **120**, 12808.
62 B. Del'Rey, M. V. Martinez-Diaz, J. Barbera and T. Torres, *J. Porphyrins Phthalocyanines*, 2000, **4**, 569.
63 D. D. Perrin and W. L. F. Armarego, *Purification of Laboratory Chemicals*, Pergamon Press, Oxford, 2nd edn, 1989.

